

Assessing the thermal performance of green infrastructure on urban microclimate

Author:

Bartesaghi Koc, Carlos

Publication Date:

2018

DOI:

<https://doi.org/10.26190/unsworks/20913>

License:

<https://creativecommons.org/licenses/by-nc-nd/3.0/au/>

Link to license to see what you are allowed to do with this resource.

Downloaded from <http://hdl.handle.net/1959.4/61202> in <https://unsworks.unsw.edu.au> on 2024-04-24

Assessing the thermal performance of green infrastructure on urban microclimate

by

Carlos Antonio Alonso Bartesaghi Koc

A thesis submitted for the degree of
Doctor of Philosophy



Australian Graduate School of Urbanism
Faculty of Built Environment

The University of New South Wales

Supervisors

A/Prof Paul Osmond; Prof Alan Peters

Co-supervisor

Dr Matthias Irger

November 2018

THE UNIVERSITY OF NEW SOUTH WALES
Thesis/Dissertation Sheet



Australia's
Global
University

Surname/Family Name : **Bartesaghi Koc**
Given Name/s : **Carlos Antonio Alonso**
Abbreviation for degree as give in the University calendar : **PhD**
Faculty : **Built Environment**
School : **Australian Graduate School of Urbanism**
Thesis Title : **Assessing the thermal performance of green infrastructure on urban microclimate**

Abstract 350 words maximum:

The urban heat island (UHI) is one of the most documented manifestations of urbanisation and the subject of intensive research over recent decades. Australia, as many other highly urbanised countries, has developed policies and strategies to promote more compact settlements; however, new urban development is characterised by higher urban densities and larger proportion of impervious surfaces that can potentially intensify UHIs. Among mitigation strategies, green infrastructure (GI) has proved effective in reducing urban temperatures. However, more research is needed to determine which compositions, amounts and spatial distributions are more effective in providing cooling benefits. This PhD research responds to this need by proposing a new taxonomy of green infrastructure typologies (GITs) to classify urban landscapes into 34 standard classes. Very high-resolution thermal, spectral imagery and LiDAR data were employed to examine the relationships between functional, structural and configurational descriptors of GI and the diurnal and nocturnal thermal patterns across the Sydney metropolitan area. Remote sensing data were collected by aircraft in February 2013 (summer) and August 2012 (winter) in calm, clear and dry conditions. This study demonstrates the applicability of the proposed methodological framework and classification scheme in urban climatology by analysing the inter- and intra-variability of land surface temperatures (LSTs) among typologies. Results show that water bodies, well irrigated grasses and aligned and clustered trees provide the largest cooling effects at daytime. However, at night well irrigated grasses are much cooler than forested areas, while water features are among the warmest GITs. It was also found that: (1) the composition and abundance of land covers is more influential in LSTs than the spatial distribution; (2) the lack of irrigation significantly affects the cooling capacity of vegetation, and (3) the cooling effect of vegetation is significantly outweighed by the warming effect of surrounding impervious surfaces. Several statistical models were produced for an accurate prediction of LSTs based on the individual contributions of derived GI parameters. Resulting estimates were employed to propose key principles, mitigation strategies and guidelines that can be implemented by researchers, governments and practitioners to prioritise greening interventions, improve urban microclimates and mitigate the urban heat more effectively.

Declaration relating to disposition of project thesis/dissertation

I hereby grant to the University of New South Wales or its agents the right to archive and to make available my thesis or dissertation in whole or in part in the University libraries in all forms of media, now or here after known, subject to the provisions of the Copyright Act 1968. I retain all property rights, such as patent rights. I also retain the right to use in future works (such as articles or books) all or part of this thesis or dissertation. I also authorise University Microfilms to use the 350 word abstract of my thesis in Dissertation Abstracts International (this is applicable to doctoral theses only).

.....
Signature

.....
Witness Signature

.....
Date

The University recognises that there may be exceptional circumstances requiring restrictions on copying or conditions on use. Requests for restriction for a period of up to 2 years must be made in writing. Requests for a longer period of restriction may be considered in exceptional circumstances and require the approval of the Dean of Graduate Research.

**FOR OFFICE USE
ONLY**

Date of completion of requirements for Award:

ORIGINALITY STATEMENT

‘I hereby declare that this submission is my own work and to the best of my knowledge it contains no materials previously published or written by another person, or substantial proportions of material which have been accepted for the award of any other degree or diploma at UNSW or any other educational institution, except where due acknowledgement is made in the thesis. Any contribution made to the research by others, with whom I have worked at UNSW or elsewhere, is explicitly acknowledged in the thesis. I also declare that the intellectual content of this thesis is the product of my own work, except to the extent that assistance from others in the project's design and conception or in style, presentation and linguistic expression is acknowledged.’

INCLUSION OF PUBLICATIONS STATEMENT

UNSW is supportive of candidates publishing their research results during their candidature as detailed in the UNSW Thesis Examination Procedure.

Publications can be used in their thesis in lieu of a Chapter if:

- The student contributed greater than 50% of the content in the publication and is the “primary author”, ie. the student was responsible primarily for the planning, execution and preparation of the work for publication
- The student has approval to include the publication in their thesis in lieu of a Chapter from their supervisor and Postgraduate Coordinator.
- The publication is not subject to any obligations or contractual agreements with a third party that would constrain its inclusion in the thesis

Please indicate whether this thesis contains published material or not.

☐

This thesis contains no publications, either published or submitted for publication.

☒

Some of the work described in this thesis has been published and it has been documented in the relevant Chapters with acknowledgement.

☐

This thesis has publications (either published or submitted for publication) incorporated into it in lieu of a chapter and the details are presented below.

CANDIDATE'S DECLARATION

I declare that:

- I have complied with the Thesis Examination Procedure
- where I have used a publication in lieu of a Chapter, the listed publication(s) below meet(s) the requirements to be included in the thesis.

Name Carlos Bartesaghi Koc	Signature	Date (dd/mm/yy) 30/08/2018
--------------------------------------	------------------	--------------------------------------

COPYRIGHT STATEMENT

'I hereby grant the University of New South Wales or its agents the right to archive and to make available my thesis or dissertation in whole or part in the University libraries in all forms of media, now or here after known, subject to the provisions of the Copyright Act 1968. I retain all proprietary rights, such as patent rights. I also retain the right to use in future works (such as articles or books) all or part of this thesis or dissertation.

I also authorise University Microfilms to use the 350 word abstract of my thesis in Dissertation Abstract International (this is applicable to doctoral theses only). I have either used no substantial portions of copyright material in my thesis or I have obtained permission to use copyright material; where permission has not been granted I have applied/will apply for a partial restriction of the digital copy of my thesis or dissertation.'

AUTHENTICITY STATEMENT

'I certify that the Library deposit digital copy is a direct equivalent of the final officially approved version of my thesis. No emendation of content has occurred and if there are any minor variations in formatting, they are the result of the conversion to digital format.'

Abstract

The urban heat island (UHI) is one of the most documented manifestations of urbanisation and the subject of intensive research over recent decades. Australia, as many other highly urbanised countries, has developed policies and strategies to promote more compact settlements; however, new urban development is characterised by higher urban densities and larger proportion of impervious surfaces that can potentially intensify UHIs. Among mitigation strategies, green infrastructure (GI) has proved effective in reducing urban temperatures. However, more research is needed to determine which compositions, amounts and spatial distributions are more effective in providing cooling benefits. This PhD research responds to this need by proposing a new taxonomy of green infrastructure typologies (GITs) to classify urban landscapes into 34 standard classes. Very high-resolution thermal, spectral imagery and LiDAR data were employed to examine the relationships between functional, structural and configurational descriptors of GI and the diurnal and nocturnal thermal patterns across the Sydney metropolitan area. Remote sensing data were collected by aircraft in February 2013 (summer) and August 2012 (winter) in calm, clear and dry conditions. This study demonstrates the applicability of the proposed methodological framework and classification scheme in urban climatology by analysing the inter- and intra-variability of land surface temperatures (LSTs) among typologies. Results show that water bodies, well irrigated grasses and aligned and clustered trees provide the largest cooling effects at daytime. However, at night well irrigated grasses are much cooler than forested areas, while water features are among the warmest GITs. It was also found that: (1) the composition and abundance of land covers is more influential in LSTs than the spatial distribution; (2) the lack of irrigation significantly affects the cooling capacity of vegetation, and (3) the cooling effect of vegetation is significantly outweighed by the warming effect of surrounding impervious surfaces. Several statistical models were produced for an accurate prediction of LSTs based on the individual contributions of derived GI parameters. Resulting estimates were employed to propose key principles, mitigation strategies and guidelines that can be implemented by researchers, governments and practitioners to prioritise greening interventions, improve urban microclimates and mitigate the urban heat more effectively.

To God, my dearest family and beloved wife

Acknowledgements

First and foremost, I would like to deeply thank to my dearest parents and family for their endless love and encouragement to pursue this challenge, and especially to my loving wife Aida for her enduring patience, support, kindness and good humour throughout this journey.

Special thanks to my PhD supervisors, Dr Paul Osmond and Prof Alan Peters who challenged me to overcome my limitations, inspired me with their boundless wisdom, motivated me with their passion, and enlightened me with honest and humorous perspectives on scholarly life. Their generosity, friendship, sounding advice and guidance contributed enormously to make this journey an enjoyable and remarkable experience. I am indebted also to my second supervisor, Dr Matthias Irger, whose research work served as the main source of inspiration for this dissertation. His breadth of expertise and insightful feedback enhanced all aspects of my research. I extend my gratitude to my mentor Lic.rer.reg. (MSc.) Dora Guillen who instilled in me the passion for the environment and guided me in the selection of my research topic.

This thesis has relied extensively on a variety of valuable and costly instrumentation, software and datasets, generously provided by my supervisors, Dr Paul Hackney from City of Parramatta Council, the Commonwealth Scientific and Industrial Research Organisation (CSIRO), and the New South Wales Land Registry Services (LPI). My research has benefitted enormously from the feedback and assistance of many experts and professionals who committed directly or indirectly to this task. My gratitude is owed especially to Prof Mat Santamouris for helping me interpret the evidence and introducing me to the fascinating world of deep learning, and to Dr Iain D. Stewart and Prof Nektarios Chrysoulakis for their valuable comments and suggestions on how to improve my methodological framework. I extend my gratitude to the members of my progress review committee: AProf Linda Corkery and Prof Chris Pettit.

I am also thankful to Natalya De Pooter for her assistance and expertise in the statistical analysis, Lisa Evans for her valuable help with the editing and formatting, my thesis examiners and the anonymous reviewers of several publications associated to this research for their valued recommendations and comments. I warmly acknowledge the community of peers of the Faculty of Built Environment UNSW and close friends who enriched my experience as higher degree researcher.

This research would not have been possible without the support of the UNSW Graduate Research School and the Faculty of Built Environment through the provision of a University International Postgraduate Award (UIPA). I want to also thank the Australian Government Research Training Program Scholarship and the Cooperative Research Centre for Low Carbon Living (CRC-LCL) who provided additional support through a postgraduate top-up scholarship.

Table of contents

Abstract	i
Acknowledgements	v
Table of contents	vii
List of figures	xi
List of tables	xvii
List of publications	xxi
Abbreviations and symbols	xxiii
Chapter 1 – Introduction	1
1.1 Statement of the problem	1
1.2 Research gaps and contributions	6
1.3 Research aims, objectives and questions	8
1.4 Thesis structure	11
Chapter 2 – Theoretical background	15
2.1 Introduction	15
2.2 Definitions, principles and importance of green infrastructure	15
2.3 Climate change, population growth, urban densification and the loss of vegetation ..	21
2.4 The urban climate	24
2.4.1 Scales of climatic study	25
2.4.2 The energy balance of urban surfaces	28
2.4.3 The energy balance of vegetated surfaces	32
2.4.4 The energy balance of water systems	34
2.4.5 The urban heat island: definition and types	36
2.4.6 Responding to the urban heat island	41
2.5 Benefits of green infrastructure on urban microclimate	43
2.5.1 The urban cool island and the park cool island	44
2.5.2 Shading	46
2.5.3 Evapotranspirative cooling	48
2.5.4 Wind flow modification	50
2.5.5 Benefits to human thermal comfort	51
2.5.6 The impacts of vegetation on energy savings	53
2.6 Urban morphology and green infrastructure performance	54
2.6.1 Urban morphology: definition and characteristics	54
2.6.2 Factors influencing the thermal performance of green infrastructure	55

2.6.3	Classification of urban morphology: the local climate zone scheme for urban heat island studies	62
2.7	Summary	67

Chapter 3 – Assessing the cooling effects of green infrastructure: A systematic review 69

3.1	Introduction	69
3.2	Methods.....	70
3.3	Overview of existing evidence.....	73
3.4	Geographic patterns and climate zones.....	75
3.5	Research focus and topics	79
3.6	Green infrastructure types and scale of analysis	81
3.7	Common parameters of analysis	83
3.8	Methods, data sources, data acquisition and data processing	86
3.8.1	On-site observations	86
3.8.2	Remote sensing	89
3.8.3	Experimental methods.....	98
3.8.4	Numerical modelling and simulation	99
3.9	Investigation period.....	102
3.10	Summary	103

Chapter 4 – Developing a green infrastructure typology for climate studies..... 107

4.1	Introduction	107
PART I: Towards a comprehensive green infrastructure typology: <i>A systematic review</i> ..		109
4.2	Methods.....	109
4.3	Analysis of geographic patterns	110
4.4	Analysis of approaches, methods and parameters.....	113
4.4.1	Functional-configurational classification	113
4.4.2	Structural-contextual classification	119
4.5	Identification of categories and typologies	126
4.5.1	Tree canopy	126
4.5.2	Green open spaces and water bodies.....	127
4.5.3	Green roofs.....	128
4.5.4	Vertical greenery systems	132
4.5.5	Other classifications	135
4.6	Summary of findings.....	137
PART II: Establishing a classification framework and typologies to support climate studies		139
4.7	Need for a new classification scheme	139
4.8	Classification criteria	140

4.9 Classification by logical division	141
4.10 Conceptual green infrastructure typology (GIT) matrix.....	144
4.11 Streamlined green infrastructure typology for remotely sensed applications.....	146
4.12 Summary.....	155
Chapter 5 – Research methodology	157
5.1 The methodological framework.....	157
5.1.1 Dependent and independent variables	157
5.1.2 Data sources.....	158
5.1.3 Airborne-based data acquisition protocols	160
5.1.4 Workflow and implementation	162
5.2 Summary.....	166
Chapter 6 – Data collection and data processing	167
6.1 Case study area	167
6.1.1 Geographic location and climate	169
6.1.2 Vegetation conditions	170
6.1.3 Case study 1: Summer	171
6.1.4 Case study 2: Winter.....	174
6.2 Airborne data collection and pre-processing	176
6.2.1 Summer data collection	176
6.2.2 Winter data collection.....	185
6.3 Computation of variables	192
6.3.1 Surface covers.....	192
6.3.2 Landscape metrics	201
6.3.3 Altitude	201
6.3.4 Computation of variables per each spatial unit.....	204
6.4 Classification of green infrastructure typologies (GITs)	207
6.5 Summary.....	211
Chapter 7 – Data analysis and results	213
7.1 Introduction	213
7.2 Green infrastructure typologies classifications.....	215
7.2.1 Classification results at different spatial scales	215
7.2.2 Classification results at the local scale (50m grid)	217
7.2.3 Accuracy and quality evaluation.....	230
7.3 Land surface temperature differences and cooling capacity of green infrastructure typologies	237
7.3.1 Thermal differentiation of GITs	237
7.3.2 Assessing the cooling effects of GITs	254
7.4 Prediction of land surface temperatures	261
7.4.1 Multiple linear regressions	262
7.4.2 Spatial regression models	268

7.5 Summary	281
-------------------	-----

Chapter 8 – Discussion.....285

8.1 Introduction	285
8.2 Airborne remote sensing for mapping green infrastructure and thermal conditions..	286
8.3 Classification of green infrastructure for climate-related studies	288
8.3.1 Identifying an optimal grid size for classifications	289
8.3.2 Defining relevant classification descriptors and cut-off values	290
8.3.3 Evaluating the accuracy of classifications.....	293
8.3.4 Assessing the predictability of the classification scheme.....	297
8.4 Thermal performance of green infrastructure typologies at local-scale.....	300
8.4.1 Understanding the thermal profiles and cooling effects of GITs	300
8.4.2 Understanding the factors that influence the thermal performance of GITs at local-scale	307
8.4.3 Defining SUHI mitigation strategies based on GITs.....	311
8.4.4 Caveats	316
8.5 Prediction of land surface temperatures	317
8.6 Implications of the evidence in planning and design	325
8.6.1 Guiding principles of climate-sensitive green infrastructure interventions...	325
8.6.2 SUHI mitigation: strategies and design guidelines at the local scale	328

Chapter 9 – Conclusive summary.....333

9.1 Summary of findings.....	334
9.2 Significance of research	341
9.3 Limitations and potential directions for further research	342

References345

Appendices.....371

Appendix A – List of questions used for the systematic review of studies analysing the cooling effects of green infrastructure	371
Appendix B – Key extracted information from reviewed studies assessing the cooling effects of green infrastructure (<i>ordered by author and year</i>).....	372
Appendix C – Metadata statement of LiDAR data	382
Appendix D – Data processing workflow.....	385
Appendix E – Datasheets for Green Infrastructure Typologies (GITs)	397
Appendix F – Performance assessment of selected machine learning classifiers.....	431
Appendix G – Summary statistics and results of normality tests and cluster analysis of GIT classifications	436
Appendix H – Results of regression models.....	444

List of figures

Figure 2.1	Conceptual diagram of a green infrastructure network showing core areas, hubs and corridors.	17
Figure 2.2	Conceptual view of the different atmospheric layers and their relationship with the climatological scales and the natural and artificial elements of the built environment. (Redrawn from Grimmond (2006); Harris and Coutts (2011); Oke (1988b); Oke (1997) and Roth, 2012).....	27
Figure 2.3	(a) Schematic volume showing the surface energy balance components of an urban area and (b) a section of the net radiation exchanges of outdoor surfaces. (Redrawn based on Oke, 1988b).	30
Figure 2.4	Schema of the energy exchanges involved in a soil-plant-air volume. (Redrawn based on Oke, 1992).	32
Figure 2.5	Schematic view of the daytime energy fluxes between an isolated tree and the environment of a street canyon. (T_l and T_a , temperatures of leaf and air respectively). (Redrawn based on Oke et al., 1989).	33
Figure 2.6	Schematic representation of the heat fluxes involved in the energy balance of a water volume.	35
Figure 2.7	(a) Schematic cross-section of a typical urban heat island, its corresponding diurnal and nocturnal air/surface temperature traverses and different types of urban heat island. (b) Isotherms map of a typical CLUHI. (Redrawn based on Erell et al., 2011; Roth, 2012 and Voogt, 2002).....	37
Figure 2.8	Schema of the climate-related functions that vegetation provides to the environment.	44
Figure 2.9	General proportions of reflected, absorbed and transmitted radiation through a deciduous canopy in summer and winter. (Redrawn based on Hunter et al., 2012).....	47
Figure 2.10	Schematic representation of the evapotranspiration process.	49
Figure 2.11	Schematic representation of energy exchanges between a pedestrian and the surrounding urban environment; and the influence of green infrastructure (GI) on human thermal comfort.	52
Figure 2.12	Schematic views of a (a) symmetrical urban canyon (b) one-sided open space, (c) circular plaza, and (d) rectangular courtyard, its geometric descriptors, and SVF parameters.	56

Figure 2.13 Common effects of urban geometry on the penetration, absorption and reflection of solar radiation at noon and in different seasons in (a) shallow and (b) deep urban canyons oriented E-W.....	57
Figure 2.14 Air-flow regimes over different arrays of buildings with increasing H/W ratio.	59
Figure 3.1 List of thematic aspects identified in the reviewed literature that are fundamental for investigating the climatic effects of green infrastructure.	72
Figure 3.2 Geographic distribution of reviewed literature based on affiliations, study locations, and climate zones.....	78
Figure 3.3 Venn diagram depicting the percentage distribution, interactions and overlaps of main research topics and sub-topics investigated by the reviewed literature on thermal performance of green infrastructure.....	80
Figure 3.4 Main methodological approaches and methods used to investigate the cooling effects of green infrastructure. Based on Hunter et al. (2014); Motazedian and Leardini (2012); Ng et al. (2012); Völker et al. (2013) and Zhao-wu et al. (2015).....	85
Figure 3.5 Combination of different methods employed in the literature. Note: sizes are proportional to the number of studies.	85
Figure 3.6 The electromagnetic spectrum and differentiation of bands for spectral analyses.	89
Figure 3.7 Differences between multispectral and hyperspectral imagery. (Redrawn based on Irger, 2014)	94
Figure 3.8 Estimation of SVF from a DSM using RVT software: (a) value is determined as a proportion of visible sky (Ω) above certain point (pixel), and (b) the algorithm computes the horizon angle (γ) for 'n' directions (eight in the image) in a specific search radius (R).	98
Figure 4.1 An environmentally-based and hierarchical classification system for urban greenspaces combining several functional aspects (Redrawn based on Hough, 2002).	114
Figure 4.2 Typical cross-sections of intensive and extensive green roofs.....	132
Figure 4.3 Several typologies of green facades organised according to the type of anchor system and planter.....	134
Figure 4.4 Different typologies of living walls differentiated in terms of the type of fixings and planter.....	135
Figure 4.5 Logical division of urban green infrastructure according to the climatic function, structural properties and spatial relationship of its elements for the formulation of typologies.....	142
Figure 4.6 Spatial conceptualisation of five high level categories of green infrastructure resulting from the combination of vegetation layers, ground surfaces and building structures.....	143

Figure 4.7 Proposed conceptual green infrastructure typology (GIT) as a double-entry matrix.....	145
Figure 4.8 Streamlined green infrastructure typology (GIT) for remotely sensed applications.....	147
Figure 5.1 Schematic overview of dependent (red) and independent (green) variables derived from their corresponding data sources (dark grey). Complementary ground-based data (blue) may be incorporated if available or necessary.....	159
Figure 5.2 Schematic representation of the implementation of the methodological framework and list of relevant data sources and variables.....	163
Figure 6.1 Map of main geographical features, location of case studies and spatial coverage of the datasets within the Sydney metropolitan area.....	168
Figure 6.2 Location, extent, and main morphological characteristics of case study 1.....	172
Figure 6.3 Location, extent, and main morphological characteristics of case study 2.....	175
Figure 6.4 Extent of the airborne diurnal and nocturnal thermal images acquired in summer.....	177
Figure 6.5 Diurnal thermal imagery of representative sites in summer captured around 1pm on 8 February 2013.....	178
Figure 6.6 Nocturnal thermal imagery of representative sites in summer captured around 1am on 9 February 2013.....	179
Figure 6.7 Extent of the airborne-based multispectral imagery acquired in summer 2013 presented as a NDVI image.....	181
Figure 6.8 Digital surface model (DSM) depicting the spatial extent of LiDAR data acquired for the case study 1.....	183
Figure 6.9 Examples of three-dimensional representations of LiDAR point cloud data of representative sites.....	184
Figure 6.10 Extent of the airborne diurnal and nocturnal thermal images acquired in winter.....	186
Figure 6.11 Diurnal thermal imagery of representative sites in winter captured around 12pm on 6 August 2012.....	188
Figure 6.12 Nocturnal thermal imagery of representative sites in winter captured around 12am on 4 August 2012.....	189
Figure 6.13 Extent of the airborne-based hyperspectral imagery acquired in winter 2012 presented as a NDVI image.....	190
Figure 6.14 Digital surface model (DSM) depicting the spatial extent of LiDAR data acquired for the case study 2 and three-dimensional representations of LiDAR point cloud data of exemplary sites.....	191
Figure 6.15 Workflow for the computation of variables, automated classification of GITs, and statistical and spatial analysis based on airborne-based data.....	193
Figure 6.16 Identification of surface covers from reclassified NDVI images.....	195

Figure 6.17 Comparison of building footprints extracted from LiDAR data using LP360 software and the results after the splitting and squaring process.	198
Figure 6.18 Differentiation between impervious ground and impervious building coloured according to the average building height.	199
Figure 6.19 Identification of vegetation layers (based on height and irrigation regimes) and water surfaces using a refinement method combining spectral-derived imagery and LiDAR data.	202
Figure 6.20 Examples of landscape metrics (CIRCLE_AM and NLSI) calculated for each grid cell to determine the compactness and linearity of tree arrangements.	203
Figure 6.21 Examples of computed surface fractions and other independent variables per spatial unit using <i>Zonal statistics</i> in ArcMap.....	205
Figure 6.22 Examples of mean diurnal and nocturnal temperature calculated per spatial unit using <i>Zonal statistics</i> in ArcMap.	206
Figure 6.23 Datasheet containing all variables and classification parameters calculated in summer for the green infrastructure typology IM4: Mostly impervious with aligned trees.	209
Figure 6.24 Datasheet containing all variables and classification parameters calculated in winter for the green infrastructure typology PV9: Mostly non-irrigated grasses with clustered trees.	210
Figure 7.1 Extent of the (a) diurnal and (b) nocturnal data analyses conducted for the summer and winter case studies.....	214
Figure 7.2 Extent of the pilot study and results of classifications using spatial units of 25 x 25m, 50 x 50m and 100 x 100m. Note: See comparison of detailed portion in Figure 7.3.	216
Figure 7.3 Comparison of classification results of a small portion of the pilot study area into 25x25m, 50x50m and 100x100m grid resolutions.....	217
Figure 7.4 Automated GIT classification for the Case study 1: Summer (above) and a detailed fraction (below) using spatial units of 50 x 50m.	218
Figure 7.5 Comparison of the total number of grids, percentage of total area, distribution of surface fractions, and mean values of independent and dependent variables estimated for each GIT identified for the case study 1.....	219
Figure 7.6 Degree of imperviousness and proportion of tree canopy measured for GITs identified for the case study 1.	221
Figure 7.7 Automated GIT classification for the Case study 2: Winter (above) and a detailed fraction (below) using spatial units of 50 x 50m.	226
Figure 7.8 Comparison of the total number of grids, percentage of total area, distribution of surface fractions, and mean values of independent and dependent variables estimated for each GIT identified for the case study 2.....	227
Figure 7.9 Degree of imperviousness and proportion of tree canopy measured for GITs identified for the case study 2.	228

Figure 7.10 Box-plots, number of samples and frequency distribution of mean diurnal LSTs recorded in summer. Average mean LSTs estimated per each GIT are presented in bold.	240
Figure 7.11 Box-plots, number of samples and frequency distribution of mean nocturnal LSTs recorded in summer. Average mean LSTs estimated per each GIT are presented in bold.	241
Figure 7.12 Box-plots, number of samples and frequency distribution of mean diurnal LSTs recorded in winter. Average mean LSTs estimated per each GIT are presented in bold.	244
Figure 7.13 Box-plots, number of samples and frequency distribution of mean nocturnal LSTs recorded in winter. Average mean LSTs estimated per each GIT are presented in bold.	245
Figure 7.14 Binary matrix showing the results of the Games-Howell post hoc tests for all pairwise comparisons of mean diurnal and nocturnal LSTs in summer. Points in cells indicate pairs of GITs for which mean LSTs were not significantly different ($p > 0.05$).	250
Figure 7.15 Percentage of significant diurnal and nocturnal LST differences in summer ($p < 0.05$) achieved by each GIT as a result of multiple comparison tests. Dotted lines represent average values for both times of the day.	250
Figure 7.16 Binary matrix showing the results of the Games-Howell post hoc tests for all pairwise comparisons of mean diurnal and nocturnal LSTs in winter. Points in cells indicate pairs of GITs for which mean LSTs were not significantly different ($p > 0.05$).	251
Figure 7.17 Percentage of significant diurnal and nocturnal LST differences in winter ($p < 0.05$) achieved by each GIT as a result of multiple comparison tests. Dotted lines represent average values for both times of the day.	251
Figure 7.18 Cooling effect of GITs in summer relative to the base case (IM1 <i>Highly impervious</i>).	252
Figure 7.19 Cooling effect of GITs in winter relative to the base case (IM1 <i>Highly impervious</i>).	253
Figure 7.20 TVX matrix with scatterplots of mean NDVI versus mean diurnal and nocturnal LSTs for summer and winter times. Sequential colours represent each GIT subgroup.	257
Figure 7.21 Results of simple linear regressions between vegetation abundance descriptors and diurnal and nocturnal LST reductions of terrestrial GITs in summer and winter. Clusters identified through hierarchical analysis are represented by distinct colours.	260
Figure 7.22 Main types of spatial dependence applied to spatial regression models.	270
Figure 8.1 Examples of common errors identified in the pre-classified LiDAR points cloud data.	294
Figure 8.2 Examples of errors and inaccuracies on the surface cover extractions related to spectral issues and spatial resolution of images.	295

Figure 8.3	Example of misclassifications related to the limitations of FRAGSTATS metrics.....	296
Figure 8.4	Comparison of the number of levels (binary splits) and overall accuracies calculated by the fine, medium, and coarse decision trees classifiers.....	298
Figure 8.5	Example of class discrimination applied by linear and non-linear support vector machines classifiers (SVM) classifiers.	299
Figure 8.6	Examples of the combinatory effect of ground surface covers and spatial configuration of trees on diurnal LSTs.	306
Figure 8.7	Interpretation of the TVX scatterplot of mean NDVI versus mean diurnal LSTs for summer.	308
Figure 8.8	Diurnal and nocturnal thermal performance of GITs defined by the results of cluster analysis.....	311
Figure 8.9	Example of potential SUHI mitigation measures and their individual and cumulative effect on average diurnal and nocturnal LSTs in a <i>Mostly impervious with grasses</i> (IM2) typology during summer.	328
Figure 8.10	Example of potential SUHI mitigation measures and their individual and cumulative effect on average diurnal and nocturnal LSTs in a <i>Mostly impervious with scattered trees</i> (IM5) typology during summer.....	329
Figure 8.11	Example of potential SUHI mitigation measures and their individual and cumulative effect on average diurnal and nocturnal LSTs in a <i>Mostly impervious with aligned trees</i> (IM4) typology during winter.	329
Figure 8.12	Example of potential SUHI mitigation measures and their individual and cumulative effect on average diurnal and nocturnal LSTs in a <i>Mixed surfaces with aligned trees</i> (MX5) typology during winter.	330

List of tables

Table 1.1	Synthesis of the thesis structure and the links between research phases, chapters, objectives, questions, gaps, employed methods and outcomes.....	13
Table 2.1	Ecosystem service categories to measure green infrastructure effectiveness.....	19
Table 2.2	Comparison of atmospheric layers, climatological scales and typical urban scales.	28
Table 2.3	Classification of UHI types according to their underlying processes, spatial coverage, timing and magnitude and methods of observation. Adapted from Roth (2012).....	38
Table 2.4	Mitigation approaches for urban heat island.	42
Table 2.5	Characteristics of urban/park cool islands attributed to vegetation.....	45
Table 2.6	Typical albedo values for common urban surfaces. (Based on Akbari 2009; Oke 1992)	61
Table 2.7	Summary of LCZ classes, their definitions, visual description, and main geometric and surface cover cut-off values as defined by Stewart and Oke (2012).	64
Table 3.1	List of journals and disciplines containing most papers that investigated the cooling effects of green infrastructure. Disciplines based on Roy et al. (2012) categorisation.	77
Table 3.2	Distribution of different green infrastructure types studied by literature according to their scale of analysis.....	81
Table 3.3	List of common dependent (DEP), independent (IND) and intervening (INT) variables analysed by studies.....	84
Table 3.4	List of common instruments used for ground-based observations.	88
Table 3.5	List of main remote sensing data sources utilised by studies.	92
Table 4.1	Number and type of articles per geographic location.....	110
Table 4.2	Different terminology organised into four main categories of green infrastructure.	111
Table 4.3	Number and origin of studies focusing on different green infrastructure categories.....	112
Table 4.4	List of methods, approaches and parameters used by ' <i>functional-configurational</i> ' classifications.	117
Table 4.5	List of methods, approaches and parameters used by studies under 'structural-configurational' classifications.	119
Table 4.6	Example of the characterisation of patches using HERCULES parameters.	122

Table 4.7 Summary of the 13 main categories and 57 urban vegetation structure types (UVSTs) including their proportion of vegetated layers and specific green volume.....	123
Table 4.8 Example of a typical urban vegetation structure type matrix (Type 1.1) showing a list of structural attributes (horizontal axis) and the three height classes of vegetation layers (vertical axis).	124
Table 4.9 List of tree canopy typologies identified by studies. <i>Spatial scales: Me=Meso; Lo=local; Mi=Micro</i>	126
Table 4.10 List of green open spaces and water bodies typologies identified by studies.	129
Table 4.11 List of green roof typologies identified by studies.	131
Table 4.12 List of vertical greenery systems typologies identified by studies.	133
Table 4.13 List of other types of classification of green infrastructure.	136
Table 4.14 Overview of quantitative and qualitative descriptors for all the 34 green infrastructure typologies (GITs) proposed.	150
Table 5.1 List of dependent and independent variables selected for the present research	158
Table 5.2 Summary of protocols for the acquisition of airborne remotely sensed and ground-based data.	161
Table 6.1 Standard point classification of LiDAR data based on LPI protocols. (Modified after Land Property Information, 2015).	182
Table 6.2 NDVI thresholds defined for the identification of surface covers in summer and winter.	194
Table 6.3 Distribution of ‘classifiable’ and ‘unknown’ number of grids per case study.	208
Table 7.1 Confusion matrix of the GIT classification results for the pilot study at 50m grid resolution showing user accuracy (UA), producer accuracy (PA), overall accuracy (OA) and Kappa index.	231
Table 7.2 Summary of selected and excluded predictors and responses for the supervised machine learning models performed for each case study.	233
Table 7.3 Summary of model’s accuracy achieved for each dataset accompanied by a description of classifiers. Models with highest accuracies (in bold) were selected for further assessment. Descriptions based on MathWorks (2018b).	234
Table 7.4 Frequency distribution of mean diurnal LSTs in summer for each GIT with a fitted normal distribution and results of the Kolmogorov-Smirnov test (N=sample size; standard deviations are in parenthesis, <i>p</i> -values <0.05 indicates a non-normal distribution, * This is a lower bound of the true significance).	247
Table 7.5 Bivariate correlations between mean NDVI and vegetation abundance indicators.	259

Table 7.6 Summary statistics of Ordinary Least Square (OLS) regression models for the prediction of diurnal and nocturnal LSTs in summer and winter using all independent variables.	264
Table 7.7 Summary statistics of revised OLS regression models for the prediction of diurnal and nocturnal LSTs in summer and winter using a selection of independent variables.	268
Table 7.8 Diagnostics for spatial dependence for revised OLS models 1B, 2B, 3B, and 4B.	271
Table 7.9 LISA results (Moran scatterplot, cluster and significance maps) for the dependent variable and residuals of Model 1B showing the presence of spatial clusters (hot-/coldspots) and spatial outliers.	273
Table 7.10 Summary of the Maximum Likelihood Estimation of SEMs for the prediction of diurnal and nocturnal LSTs in summer and winter, in comparison with the performance of revised OLS models.	275
Table 7.11 Comparison of regression coefficients (β) for all variables included in SEM versus revised OLS.	276
Table 7.12 Global Moran's I of residuals for SEM 1C, 2C, 3C and 4C.	276
Table 7.13 Summary of the Maximum Likelihood Estimation of revised SEMs for the prediction of diurnal and nocturnal LSTs in summer and winter that are applicable separately to aquatic and terrestrial locations.	278
Table 7.14 Summary of regression coefficients (β) for all variables included in the revised SEM applicable for aquatic and terrestrial contexts.	279
Table 8.1 Summary of diurnal SUHI mitigation strategies for summer using GITs. Typologies are ordered and organised in groups according to similar thermal performance.	312
Table 8.2 Summary of diurnal SUHI mitigation strategies for winter using GITs. Typologies are ordered and organised in groups according to similar thermal performance.	313
Table 8.3 Summary of nocturnal SUHI mitigation strategies for summer using GITs. Typologies are ordered and organised in groups according to similar thermal performance.	314
Table 8.4 Summary of nocturnal SUHI mitigation strategies for winter using GITs. Typologies are ordered and organised in groups according to similar thermal performance.	315
Table 8.5 Summary of equations for the prediction of diurnal and nocturnal LSTs for aquatic and terrestrial locations in Sydney metropolitan area derived from revised SEMs.	320
Table 8.6 Relative effect of each individual independent variable on mean LSTs at local scale in summer.	321
Table 8.7 Relative effect of each individual independent variable on mean LSTs at local scale in winter.	321

List of publications

Versions of several chapters of this thesis have been published –or have been submitted for publication– in the following journals and conference proceedings:

Refereed journals:

- Bartesaghi Koc, C., Osmond, P., Peters, A. (2019), Mapping and classifying green infrastructure typologies for climate-related studies based on remote sensing data, *Urban Forestry and Urban Greening*, doi: 10.1016/j.ufug.2018.11.008.
- Bartesaghi Koc, C., Osmond, P., & Peters, A. (2018). Evaluating the cooling effects of green infrastructure: A systematic review of methods, indicators and data sources. *Solar Energy*, 166, 486–508. doi:10.1016/j.solener.2018.03.008.
- Bartesaghi Koc, C., Osmond, P., & Peters, A. (2017). Towards a comprehensive green infrastructure typology: A systematic review of approaches, methods and typologies. *Urban Ecosystems*, 20, 15-35. doi:10.1007/s11252-016-0578-5.
- Bartesaghi Koc, C., Osmond, P., Peters, A., & Irger, M. (2018). Understanding land surface temperature differences of Local Climate Zones based on airborne remote sensing data. *Journal of Selected Topics in Applied Earth Observations and Remote Sensing (JSTARS)*, 10 (11). doi: 10.1109/JSTARS.2018.2815004.

Refereed conference papers:

- Bartesaghi Koc, C., Osmond, P., & Peters, A. (2016). A Green Infrastructure Typology Matrix to Support Urban Microclimate Studies. *Procedia Engineering*, 169, 183–190. doi:10.1016/j.proeng.2016.10.022.
- Bartesaghi Koc, C., Osmond, P., Peters, A., & Irger, M. (2017a). A methodological framework to assess the thermal performance of green infrastructure through airborne remote sensing. *Procedia Engineering*, 180, 1306–1315. Doi: 10.1016/j.proeng.2017.04.293.
- Bartesaghi Koc, C., Osmond, P., Peters, A., & Irger, M. (2017b). Mapping Local Climate Zones for urban morphology classification based on airborne remote sensing data. In *2017 Joint Urban Remote Sensing Event (JURSE)* (pp. 1–4). IEEE. Thursday, June 01, 2017. doi: 10.1109/JURSE.2017.7924611.

Refereed abstracts and oral presentations:

- Bartesaghi Koc, C., Osmond, P., Peters, A. (2017), 'Mapping and classifying green infrastructure typologies for climate-related studies based on airborne remote sensing data', *Oral presentation at GreenInUrbs Conference 2017: Nature based solutions for sustainable and resilient cities*, 4-7 April 2017, Orvieto – Italy.
- Bartesaghi Koc, C., Osmond, P. and Peters, A. (2016), 'Evaluating the thermal performance of urban green infrastructure at local scale: A methodological framework'. *Oral presentation and proceedings at 11th Australian Climate Change Adaptation Research Network for Settlements and Infrastructure (ACCARNSI) and ECR Conference*, 15-17 February. Canberra, Australia.
- Bartesaghi Koc, C., Osmond, P., Peters, A. & Irger, M. (2016), A Green Infrastructure Typology Matrix to Support Urban Microclimate Studies, *Oral presentation and proceedings at the 4th International Conference on Countermeasures to Urban Heat Island*, National University of Singapore, Singapore. May 2016.
- Bartesaghi Koc, C., Osmond, P., Peters, A. and Irger, M. (2016), A methodological framework to assess the thermal performance of green infrastructure through airborne remote sensing, *Oral presentation and proceedings at International High- Performance Built Environment Conference (iHBE) – A Sustainable Built Environment Conference 2016 Series (SBE16)*, November 2016, Sydney, Australia.
- Bartesaghi Koc, C., Osmond, P., Peters, A. & Irger, M. (2016), Application of a green infrastructure typology and airborne remote sensing to classify and map urban vegetation for climate adaptation, *Oral presentation and proceedings at the Climate Adaptation Conference 2016*, Adelaide, Australia.

Abbreviations and symbols

ABS	Australian Bureau of Statistics
AIC	Akaike information criterion
ASHRAE	American Society of Heating Refrigerating and Air-conditioning engineers
Alt	Altitude
BLUHI	Boundary layer urban heat island
BOM	Bureau of Meteorology
°C	Degrees Celsius
CIRCLE_AM	Related circumscribing circle (area-weighted mean)
CLUHI	Canopy layer urban heat island
cm	Centimetres
CSIRO	Commonwealth Scientific and Industrial Research Organisation
DAY_T _s	Diurnal surface temperature
DEM	Digital elevation model
DSM	Digital surface model
DTM	Digital terrain model
EDT	Eastern daylight time
ET	Evapotranspiration
EVI	Enhanced vegetation index
ft	Feet
Fr_High_Veg	Fraction of high vegetation
Fr_Imp_Bld	Fraction of impervious building
Fr_Imp_Grnd	Fraction of impervious ground
Fr_Low_IRR	Fraction of irrigated low vegetation
Fr_Low_NIR	Fraction of non-irrigated low vegetation
Fr_Med_Veg	Fraction of medium vegetation
Fr_Tot_Imp	Fraction of total impervious
Fr_Tot_Wat	Fraction of total water
GI	Green infrastructure
GIT	Green infrastructure typology
GIS	Geographic information systems
GOS	Green open spaces
GPS	Geographic positioning system
GR	Green roofs
HTC	Human thermal comfort
IPCC	Intergovernmental panel on climate change
K	Kelvin
km ²	Square kilometres
kn	Knots
KNN	<i>K</i> -nearest neighbour
LAI	Leaf area index
LAD	Leaf area density
LAG	Spatial lag model
LCZ	Local climate zone

LGA	Local government area
LID	Low impact development
LiDAR	Light detection and ranging
LM	Lagrange multiplier
LPI	Land and Property Information
LST	Land surface temperature
LULC	Land-use/Land-covers
m	Metres
m ²	Square metres
MASL	Metres above sea level
MEA	Millennium ecosystem assessment
MLR	Multiple linear regression
mm	Millimetres
MRT	Mean radiant temperature
NDVI	Normalized difference vegetation index
NIG_T _s	Nocturnal surface temperature
NIR	Near infrared
nLSI	Normalised landscape shape index
NSW	New South Wales
OEH	Office of Environment and Heritage
OLS	Ordinary least squares
PAN	Panchromatic
PCC	Parramatta City Council
PCI	Park cool island
SC	Spatial configuration
SEM	Spatial error model
SST	Sub-surface temperature
SUHI	Surface urban heat island
SSUHI	Sub-surface urban heat island
SVF	Sky view factor
SVM	Support vector machine
SWIR	Shortwave infrared
T _a	Air temperature
T _s	Surface temperature
TC	Tree canopy
TIR	Thermal infrared
UAV	Unmanned aerial vehicle
UBL	Urban boundary layer
UCI	Urban cool island
UCL	Urban canopy layer
UCM	Urban canopy models
UHI	Urban heat island
USU	Urban structural units
UV	Ultraviolet
UVST	Urban vegetation structure types
VIS	Visible light
VGS	Vertical greenery systems
WB	Water bodies
WV	Water vapour

Chapter 1

Introduction

1.1 Statement of the problem

Cities are centres of cultural and economic activity that over the last century have uninterruptedly welcomed newcomers migrating from rural areas in search of a better life and economic growth (United Nations, 2012; Zupancic et al., 2015). This incremental changes to the urban population have resulted in an unprecedented urbanisation that has led to the radical territorial expansion of urban settlements, especially in developing countries (UN, 2012). The so-called urban sprawl has caused the loss of natural habitats, biodiversity, vegetation and permeable soils that have been irremediably replaced by sealed surfaces, buildings and roads (Forest Research, 2010a; Lehmann, 2014; Motazedian & Leardini, 2012; Zupancic et al., 2015). Furthermore, rapid urbanisation has considerably altered the natural balance through significant changes in land-uses causing serious environmental and climatic impacts such as land degradation, soil erosion, air and water pollution, noise, habitat loss and temperature increase (Roy et al., 2012; Santamouris, 2015; Stewart, 2011b).

This thesis specifically focuses on the context of Australia, which is one of the most urbanised countries in the world with nearly 85% of its population residing in major urban centres; expected to grow up to 93% by 2050 (UN, 2012). Urbanisation exacerbates heat extremes, which makes Australian cities extremely vulnerable to climate change (CSIRO & BOM, 2015; IPCC, 2013). In response to urban sprawl, Australia –like many other countries– has developed policies and strategies to promote more compact cities (Irger, 2014). Through this vision, authorities intended to concentrate infrastructure, services and resources; however, they failed in decreasing car dependency because of a poor public transport provision.

Hence, major Australian cities are still characterised by sparsely built precincts of detached houses, large plot sizes, extensive parking areas, paved driveways, and a large proportion

of wide roads (Irger, 2014). To some extent, densification policies have succeeded as the average plot size has decreased and the number of apartments per hectare have grown in recent years. However, larger and denser urban developments have been erected at the expense of private and public greenspaces and under-utilised brownfields; consequently, these new neighbourhoods are characterised by impervious surfaces, higher local temperatures and greater energy consumption and carbon emissions associated with cooling (Irger, 2014; Newton et al., 2013). Despite these facts, there is scant research conducted in Australian cities analysing the interplay between vegetation loss, changes in land surface properties and the rise of urban temperatures (Coutts et al., 2007; Hunter et al., 2012; Norton et al., 2013).

In terms of the urban climate, the combined effects of urbanised land, densification of cities and human activities raises the amount of anthropogenic heat liberated to the atmosphere, lowers evaporative cooling, affects natural ventilation, and alters the urban heat balance by increasing the available sensible heat emerging from pavements and buildings (Santamouris, 2015). As a consequence, urban cores experience higher ambient temperatures compared to their natural surroundings, a phenomenon known as the urban heat island (UHI) (Gill, 2006; Oke, 1982, 1988b; Oke et al., 1989; Oke, 1992; Stewart, 2011b; Voogt & Oke, 2003). However, UHIs are influenced by both local and regional aspects including the urban morphology and structural parameters of cities, synoptic weather conditions, thermal properties of materials, and the presence and magnitude of the heat sources and sinks (Santamouris et al., 2017). The interest in UHI has considerably grown in the last decades as it addresses two major environmental problems: global warming and human over-population (Stewart & Oke, 2012). Hence, it is one of the most documented phenomenon associated with climate change (Santamouris, 2014). In fact, many cases have been documented in which the magnitude of the climatic effects of UHI equalled or exceeded those of the global climate changes, a situation that alarms the scientific community worldwide (Grimmond, 2006; Santamouris, 2015).

In this context, primary concerns of current climate studies are the extremely high urban temperatures and the increase in the intensity, frequency and duration of heatwaves that cause significant impacts on different spheres of human life and cities' economy (Bowler et al., 2010b; Hunter et al., 2012; Steffen et al., 2011; Völker et al., 2013). It has been demonstrated that higher urban temperatures have serious consequences on indoor and outdoor thermal comfort (Coutts et al., 2012; Santamouris et al., 2017). In fact, UHI has been pointed out as a major threat to human health and well-being due to the inability of urban populations, especially vulnerable sectors such as the elderly and children, to adapt

and respond effectively to severe thermal stress (Coutts et al., 2015; Norton et al., 2013; Norton et al., 2015; Tzoulas et al., 2007). Hence, there is a strong connection between increased mortality and extreme heat (Baccini & Schindler, 2008; Zupancic et al., 2015). Moreover, numerous studies have indicated the remarkable impact of UHI on the urban economy and the environment as it increases the energy consumption and peak electricity demand used for cooling purposes, rises carbon and greenhouse gas emissions, and facilitates the concentration of certain air pollutants and tropospheric ozone (Lehmann, 2014; Santamouris, 2015; Santamouris et al., 2017; Wang, Z.-H. et al., 2016; Zupancic et al., 2015).

Among several mitigation technologies and strategies, *green infrastructure* –including parks, trees, water bodies, green roofs and vertical greenery systems– has been identified as a nature-based and efficient solution for reducing urban temperatures and mitigating the negative effects of UHI (Erell et al., 2011; Gill et al., 2007; Santamouris, 2014, 2015; Spronken-Smith et al., 2000). Also referred to as *urban greenery* or *urban greenspaces*, urban green infrastructure has been defined as the interconnected network of natural and engineered features and spaces capable of providing a broad range of ecological, economic and social functions and services, maintaining natural processes, and protecting the biodiversity of urban and rural settings (Benedict & McMahon, 2002, 2006; European Environment Agency, 2011; Faehnle, 2014; Naumann et al., 2011; Roy et al., 2012; Williamson, 2003). Therefore, green infrastructure networks –as opposed to grey (or conventional) infrastructure– play a key role in delivering more sustainable and resilient settlements as they can be implemented to reduce carbon emissions and remedy the negative consequences of urban warming and climate change at lower capital, maintenance and operational costs, and with fewer negative impacts on the environment (Gill, 2006; Pakzad, 2017).

Four high level categories of (1) provisioning, (2) regulating, (3) supporting, and (4) cultural have been proposed to organise different ecosystem services (ESS) provided by green infrastructure and measure their effects on human health and well-being (Mazza et al., 2011; Millennium Ecosystem Assessment, 2005). Among *regulating* services, urban greenery is capable of modifying urban microclimates, reducing extreme weather conditions and mitigating urban warming by: (1) providing protection and shading from solar radiation, (2) cooling ambient air through evapotranspiration, and (3) modifying air movement and heat exchange throughout the city (Bowler et al., 2010b; Coutts & Harris, 2012; Forest Research, 2010b; Hunter et al., 2012; Norton et al., 2013; Oke et al., 1989; Santamouris, 2015). Simultaneously, urban greenery can help to reduce noise, filter

ambient pollutants, reduce erosion and facilitate soil stabilisation, decrease human stress, increase property values and cities attractiveness (Mazza et al., 2011; Santamouris, 2015). In terms of climate modification, shading potential is mostly associated with the biophysical and morphological characteristics of vegetation (Hunter et al., 2012). However, evapotranspiration is usually an overlooked parameter since its estimation is laborious, costly and mostly conducted for agricultural purposes (Nouri et al., 2015). Indeed, little research has focused on estimating evapotranspiration in highly heterogeneous urban contexts and exploring the relationships between evaporative cooling, water availability (irrigation regimes), vegetation abundance and temperature reductions (Nouri, Beecham et al., 2013).

Numerous studies have demonstrated –through observational, experimental and simulated methods– that an increase in vegetation cover corresponds with lower ambient temperatures within and near to vegetation features (parks, trees, green roofs, green walls, etc.); which corresponds with the moderation of the canopy layer urban heat island (CLUHI) (Bowler et al., 2010b; Santamouris, 2015, 2015; Taha et al., 1991). Furthermore, remote sensing studies suggest that greater vegetation cover results effective in attenuating the surface urban heat island (SUHI) and reducing land surface temperatures (LST) (Coutts et al., 2016; Harris & Coutts, 2011; Huang et al., 2015).

Additionally, studies on park cool island (PCI) and urban cool island (UCI) reported significant temperature differences between greenspaces and their urban surroundings either during night and day periods (Skoulika et al., 2014; Spronken-Smith & Oke, 1998; Yang et al., 2017). Existing evidence suggests that cooling benefits of trees and greenspaces vary as a function of the bio-physical, morphological and spatial arrangement of green infrastructure (*i.e.* size and shape of parks, crown width and arrangement of trees and greenspaces) (Bartesaghi Koc, Osmond, & Peters, 2017; Bowler et al., 2010a; Cao et al., 2010; Motazedian & Leardini, 2012; Santamouris, 2015; Zhou et al., 2011). Studies also indicate that the intensity, magnitude and extent of these temperature reductions are affected by several factors such as prevailing weather conditions, season, irrigation and maintenance, distance from the vegetation or water body, the surrounding urban morphology, local anthropogenic heat, and distance to coast (sea breeze effect) (Al-Gretawee et al., 2016; Cao et al., 2010; Hiemstra et al., 2017; Manteghi et al., 2015; Yang et al., 2017).

Despite the current evidence on the positive climatic benefits of green infrastructure, more research is still required to determine the most efficient typologies, amounts, composition and spatial configuration necessary to provide an optimal thermal cooling of urban

environments using empirical data and predictive models with higher accuracy and precision (Bowler et al., 2010b; Coutts & Harris, 2012; Kong et al., 2013; Motazedian & Leardini, 2012; Zupancic et al., 2015). Moreover, no commonly agreed typologies and protocols have been proposed yet to confidently compare, report and predict the combinatory climatic effects of distinct types of green infrastructure (parks, trees, green roofs, etc.) across multiple locations and spatial scales. Therefore, it is necessary to develop a standardised classification system for green infrastructure dedicated to climate-related studies (Bowler et al., 2010b). Such system should be based on a holistic approach embracing the fundamental principles of green infrastructure, namely multi-functionality, connectivity and spatio-temporal heterogeneity and should combine functional, morphological and configurational attributes of vegetation and water bodies into one single scheme (Ahern, 2007; Bartesaghi Koc, Osmond, & Peters, 2017; Cadenasso et al., 2013; Pickett et al., 2017).

Oke (2006, 2009) and Erell et al. (2011) have defined three main spatial scales for climate studies, namely the meso- (city-wide), local- (neighbourhoods/precincts) and the micro- (street canyons, buildings) scales. Among these, the local scale corresponds to the level in which urban planning and design mostly occurs and that concerns local governments, planning authorities, developers and practitioners (Norton et al., 2013). Nonetheless, most of the literature has concentrated on meso and micro scales; while studies at local scale are less numerous since these are costly, challenging and laborious (Motazedian & Leardini, 2012; Norton et al., 2013). In this respect, there is a lack of assessment frameworks for a more detailed and comprehensive evaluation of the thermal performance of green infrastructure at a local level using a combination of empirical (in-situ and remote sensing) and inferential methods (numerical modelling). Furthermore, more attention should be put on defining the appropriate indicators, measurements, data sources and optimal spatio-temporal resolutions necessary to achieve a more accurate and precise analysis of urban precincts or neighbourhoods.

Current urban developments in Australia and around the world do not fully incorporate climate sensitive considerations at the local level, not because of lack of evidence, but because of the extreme complexity that requires multi-disciplinary approaches and due to the lack of specific guidelines and climatological information (Coutts & Harris, 2012; Hunter et al., 2012; Irger, 2014; Norton et al., 2015; Oke, 2006). There are still enormous communication gaps between climate scientists and planners, designers and policy makers that have to be bridged (Coutts et al., 2016). To address this problem, it is imperative to develop frameworks and predictive models for faster mapping, evaluation, and estimation

of the best types and amounts of green infrastructure required for a specific place. In addition, there is an urgent need for evidence-based guidelines to inform policy and support practitioners on the best strategies to design and implement green infrastructure into new and retrofitted urban precincts for a more effective mitigation of urban warming (Bowler et al., 2010b; Buchholz, 2013; Hunter et al., 2012; Irger, 2014; Lehmann, 2014; Norton et al., 2015; Zupancic et al., 2015).

1.2 Research gaps and contributions

A critical look at the previous section and the reviewed literature (extensively discussed in Chapters 2, 3 and 4) highlights the urgent necessity to better understand the thermal performance of green infrastructure on urban microclimate, in particular the analysis of the underlying factors influencing LST reductions and SUHI mitigation at the local level (precinct/neighbourhood scale).

The relationship between green infrastructure and both air and surface temperatures reductions has been well established in the literature; however, more research is needed to determine which types, compositions, abundance and spatial arrangement of greenery and water bodies are more effective in providing cooling benefits (Bowler et al., 2010b; Coutts & Harris, 2012; Kong et al., 2013; Morakinyo & Lam, 2016; Norton et al., 2013; Shashua-Bar & Hoffman, 2000; Zupancic et al., 2015).

The present dissertation responds to this gap by proposing a more comprehensive and holistic methodological framework to analyse the interplay and cumulative thermal effects of natural and artificial features of green infrastructure over large urban areas. Spaceborne remote sensing has been commonly employed to undertake such analysis; however, satellite imagery currently has a spatial resolution of several metres, which is not always suitable for microclimatic modelling of urban precincts and buildings (Coutts et al., 2016; Gaitani et al., 2017; Irger, 2014).

Therefore, the present research explores the capacity of airborne remote sensing to perform microclimatic analyses with a high level of detail, precision and accuracy. Accordingly, airborne-based imagery in very high resolution is employed to analyse the influence of the bio-physical and configurational characteristics of green infrastructure on the seasonal variation and spatial patterns of diurnal and nocturnal LSTs of several precincts across the Sydney metropolitan area.

The lack of robust and widely accepted green infrastructure typologies to support climate research has forced researchers to adopt terminology from related disciplines, a situation that hinders the comparability of climatic results. Thus, improvements in collecting and reporting temperature data on several types of green infrastructure and at various spatial scales and sites are urgently needed. To address this issue, current green infrastructure terminology and classification approaches were systematically reviewed. As a result, a new taxonomy of green infrastructure based on three key principles: dynamic spatial and temporal heterogeneity, connectivity, and multi-functionality was introduced to classify vegetation and water bodies according to physical and spatial parameters. This scheme is critically evaluated as a standardised classification system intended for climate-related studies; also, it is practically tested and validated in the Australian context. The implementation of this new scheme provided the opportunity to develop an innovative GIS-based methodology for the automated classification and thermal mapping of green infrastructure and built surfaces; a workflow that can be easily implemented by researchers and practitioners with different skill levels.

Presently, there is lack of technical guidance on how to design, plan and implement urban greenery to provide a maximum thermal cooling and mitigate urban warming more effectively. In this regard, the successful application of the abovementioned classification scheme and workflow within the proposed methodological framework has facilitated the development of a statistical model for a more precise and accurate prediction of LSTs at local scale; and consequently, a better estimation of the cooling effects of green infrastructure.

Overall, this research contributes to advancing the knowledge of how neighbourhoods and urban precincts should be planned and designed to incorporate green infrastructure for SUHI amelioration. The present study also compares the thermal profiles of different urban precincts with attention to vegetation (and its spatial distribution), water bodies and other urban surface characteristics. This analysis identifies which characteristics and factors are more influential on the modification of the local microclimate, particularly on elevated surface temperatures.

Additionally, a set of design guidelines and recommendations are provided as a crucial step towards better communication between climate scientists, policy makers and practitioners. Ideally, this technical guidance can provide valuable information to help city planners, urban designers and landscape architects inform their decisions, identify critical areas, prioritise interventions and deliver more sustainable, climate-resilient and cooler cities with greater confidence. It is expected that these changes in policy and design will trigger

positive impacts on communities in terms of human health and wellbeing as well as on the reduction of carbon emissions, pollutants and electricity consumption. It is also anticipated that studies from related disciplines would benefit from the contributions of this thesis.

1.3 Research aims, objectives and questions

This research aims, firstly, to explore and understand the interplay and cumulative effects of different types of green infrastructure on urban microclimate; and secondly, to identify the optimal types, amount, compositions and arrangements of green infrastructure necessary to provide maximum thermal cooling and mitigate urban warming more effectively.

To achieve these aims, the following objectives and research questions were defined:

Objective 1. To propose an assessment framework to examine the relationships between green infrastructure, urban characteristics and land surface temperatures at local scale; and to test and validate this framework using very high-resolution data for the automated classification of green infrastructure and thermal assessment of a large urban area of Sydney in summer and winter.

Questions to be answered in Chapter 3:

- 1.1 What are the different methods, indicators, data sources, data collection requirements (duration, seasons and times), spatial scales, type of measurements, and instruments that are commonly used to study the cooling effects of green infrastructure on the urban climate?
- 1.2 What are the advantages and disadvantages of available methods, approaches and indicators of one over another?

Question to be answered in Chapter 5:

- 1.3 What is the most adequate methodological framework for a precise and accurate analysis of the thermal profiles of green infrastructure at local scale using very high-resolution data?

Question to be answered in Chapters 8 and 9:

- 1.4 What are the strengths and limitations of the proposed assessment framework?
- 1.5 Which improvements or modifications are necessary to implement the proposed assessment framework in other climate conditions and locations?

Objective 2. To advance taxonomies of green infrastructure by proposing a standardised classification scheme dedicated to climate-related studies. This is intended to assist in the analysis, comparability and reporting of the seasonal and spatial variability of diurnal and nocturnal land surface temperatures of different urban precincts of the Sydney metropolitan area.

Questions to be answered in Chapter 4:

- 2.1 What are the available methods, approaches, parameters and terminology currently used to catalogue green infrastructure?
- 2.2 What are the principles and criteria for designing a green infrastructure classification scheme that can be applied in climate research?

Questions to be answered in Chapters 5 and 6:

- 2.3 What are the typologies and their structural and configurational parameters and threshold values to classify green infrastructure using remotely sensed data?

Questions to be answered in Chapter 7:

- 2.4 Which green infrastructure typologies, compositions, abundance and spatial configurations are the most and least efficient in reducing surface temperatures at local scale?
- 2.5 What are the spatio-temporal patterns and variability of diurnal and nocturnal land surface temperatures among typologies?
- 2.6 Is there any statistically significant difference among typologies?

Objective 3. To develop a statistical model for a precise and accurate prediction of land surface temperatures in different urban contexts, times of the day and seasons. This model is intended to quantify the relationships between land surface temperatures and different green infrastructure parameters, as well as to determine which urban design interventions or aspects can help reducing land surface temperatures of neighbourhoods more effectively.

Questions to be answered in Chapters 7 and 8:

- 3.1 What are the relationships between land surface temperatures and different functional, structural and configurational attributes of green infrastructure?
- 3.2 What is the extent and magnitude of the contributions of green infrastructure in the urban microclimate, and which variables and factors are more influential in modifying land surface temperature conditions of urban precincts?
- 3.3 How much vegetation cover and what type of changes in surface covers are necessary for reducing surface temperatures more effectively?

Objective 4. To explore the implications of the evidence in urban planning and design by developing cooling scenarios from predictive models and proposing general guidelines and recommendations on the most effective strategies to implement green infrastructure for heat mitigation and climate adaptation.

Questions to be answered in Chapters 8 and 9:

- 4.1 What principles, strategies, and practical guidance can be derived from the evidence to incorporate green infrastructure in urban planning and design to moderate urban microclimates and mitigate SUHI more effectively?
- 4.2 How can the thermal differentiation and statistical analysis of typologies be utilised to improve the communication of evidence by proposing different heat mitigation scenarios?

1.4 Thesis structure

This dissertation involves four fundamental phases that are structured into nine chapters and 8 appendices [Table 1.1]. The first part – ‘*Context*’ – corresponds to [Chapter 1](#), which presents a brief overview of the topic and provides background information necessary to understand the problem and the significance of this research. It also outlines the aims and objectives, defines the gaps and questions, and describes the thesis structure.

The second part – ‘*Literature review*’ – encompasses Chapters 2, 3 and 4. [Chapter 2](#) provides a theoretical overview of the interdisciplinary contexts relevant to green infrastructure, its modifying effect on the urban microclimate and its relationship with urban morphology and the design and planning of cities. The chapter begins with a review of overarching definitions and principles of green infrastructure, followed by a brief discussion of the impacts of climate change, and urbanisation on vegetation loss and land use changes. The chapter also describes basic theory around urban climatology with special attention to the scales of study, the energy balance of built and vegetated surfaces and the characterisation of UHIs. Finally, it concentrates on the main benefits of green infrastructure on urban microclimate and human life and discusses the effects of urban morphology on vegetation performance.

[Chapter 3](#) presents a comprehensive systematic review of studies that quantified and reported on the relationship between vegetation-related characteristics and their effect on human thermal comfort, air and surface temperatures. It takes a critical look at methodological aspects to identify gaps, capabilities and limitations of the reviewed studies and determine the most adequate approaches, methods and variables that can serve this research.

[Chapter 4](#) focuses on developing a new taxonomy of green infrastructure that can be applied in climate research. It starts with a systematic review and evaluation of the existing evidence on how green infrastructure is being categorised and characterised worldwide. It then defines the classification criteria, approaches and indicators, and proposes a new conceptual matrix to classify green infrastructure from a climate-oriented perspective. Finally, it presents a streamlined typology, parameters and threshold values for remotely sensed classifications.

The third part – ‘*Methodology*’ – encompasses Chapters 5 and 6. [Chapter 5](#) introduces the proposed methodological framework (based on the literature review) and explains the research methods employed in different sections of this dissertation. [Chapter 6](#) describes

the case study area and gives a full account of the equipment, data sources, and data collection protocols and measurements. It finally discusses the methods and procedures for the estimation of variables and presents the workflow for the automated mapping and classification of green infrastructure based on remote sensing data.

The fourth part – ‘*Empirical analysis*’– is composed by Chapters 7, 8 and 9. [Chapter 7](#) provides the statistical analysis of data and results from both seasons, summer and winter. It begins with an assessment of the quality of classifications (from Chapter 6) followed by a detailed statistical and spatial analysis of diurnal and nocturnal surface temperature patterns. This section also describes the correlations between variables and estimates of the cooling capacity of all identified typologies. Furthermore, it presents, compares and analyses the results of several multivariate linear regression and spatial autocorrelation models formulated to predict surface temperatures for the study area.

[Chapter 8](#) interprets and discusses the significance of the evidence and evaluates the relevance and applicability of the proposed assessment framework, the introduced classification system and findings of this research for policy making, and urban design and planning. It further provides a list of guidelines and recommendations on the most effective strategies to implement green infrastructure for urban warming adaptation and mitigation.

Finally, [Chapter 9](#) concludes with a summary of the main research outcomes and contributions to knowledge, discusses the limitations of the present study and proposes suggestions, improvements and recommendations for further research. [Table 1.1](#) provides a synthesis of the thesis structure and the links between research phases, chapters, objectives, questions, gaps, employed methods and outcomes.

Table 1.1 Synthesis of the thesis structure and the links between research phases, chapters, objectives, questions, gaps, employed methods and outcomes.

Part	Chapter	Obj.*	Quest.*	Gaps	Methods	Outcomes
Context	1. Introduction	-	-	-	Literature review	Defined context, research gaps, aims & questions.
	2. Theoretical Background	-	-	-		Understood theories & concepts related to the topic.
Literature review	3. Assessing the cooling effects of GI	OB1	Q1.1, Q1.2	G1 - Need for a holistic framework to assess the thermal profiles of GI at local level.	Systematic literature review	Reviewed & determined the most appropriate methods, indicators & data for the research.
	4. Developing a GI typology for climate studies	OB2	Q2.1, Q2.2	G2 - Lack of adequate taxonomies of GI to assess, compare and report climatic data		Identified key classification principles & criteria. Defined a new GI typology.
Methodology	5. Research methodology	OB1	Q1.3, Q2.3	G1	Airborne remote sensing	Defined the assessment framework based on the literature.
	6. Data collection & Data processing	OB2	Q2.3	G1 G2	Systematic literature review	Selected the case study. Collected data & computed required variables.
Empirical Analysis	7. Data analysis & results	OB2, OB3	Q2.4, Q2.5, Q2.6, Q3.1, Q3.2, Q3.3	G1 G2	Statistical analysis & modelling	Tested & validated the proposed classification scheme & framework. Developed a predictive model. Addressed objectives and questions.
	8. Discussion	OB3, OB4	Q1.4, Q1.5, Q3.2, Q3.3, Q4.1, Q4.2	G3 - Lack of technical guidance on how to design, plan and implement GI to provide a maximum thermal cooling		Proposed set of guidelines and recommendations. Discussed implications on planning, design and future research.
	9. Conclusive summary	OB1, OB4	Q1.4, Q1.5, Q4.1, Q4.2			

A: Aim, OB: Objective, Q: Question, G: gap, GI: Green Infrastructure

* See section 1.3 for specific objectives and questions

Chapter 2

Theoretical background

2.1 Introduction

This chapter provides a review of the theoretical background and interdisciplinary contexts relevant to green infrastructure, its modifying effect on the urban microclimate and its relationship with urban morphology and the design and planning of cities.

Initially, the chapter describes the main definitions, approaches and principles that have been formulated around green infrastructure and summarises the multiple benefits and services that can be obtained from the implementation of green infrastructure in cities.

The chapter further discusses the negative impacts of climate change, population growth, urban development and the loss of vegetation influencing urban climates and the rising of urban temperatures. It also analyses the importance of spatial scales in climate research, defines and classifies the different types of UHIs, and summarises the multiple benefits of green infrastructure on urban microclimate, human thermal comfort and buildings.

Finally, it reviews the effect of urban morphology on both the local climate and green infrastructure performance. It additionally presents a detailed analysis of the local climate zones (LCZ) (Stewart & Oke, 2012), as it is an important approach currently used to characterise, examine and compare UHIs in a standardised way and is the basis of our conceptual-methodological framework.

2.2 Definitions, principles and importance of green infrastructure

Green infrastructure is a relatively new concept –historically rooted in a long line of thinking– that in recent decades has concentrated the attention of researchers and practitioners of multiple disciplines as it offers a contemporary approach to conceptualise,

plan, design and manage natural and built resources in a sustainable way (Ahern, 2007; Mell, 2010; Youngquist, 2009). The concept originated in the United States in the 1990s, and rapidly developed in the UK and Europe as a result of the opportunities that provided for spatial and landscape planning and for the development, maintenance and enhancement of environments (Mell, 2010; Mell, 2013).

The intrinsic multi-dimensionality –in time, space and perceptions– of green infrastructure has led to variability and subjectivity in its discussion and application; limiting to some extent, a consensual understanding of its implications at both local and global levels (Mell, 2014; Pauleit et al., 2014). As an evolving and contested term, the conceptualisation of green infrastructure depends on particular approaches, research scopes, priorities and people's interests (Davies et al., 2006; Mell, 2010; Naumann et al., 2011). Initially, green infrastructure was described in terms of ecology and conservation goals and the role it plays in the management of natural landscapes and biodiversity (Benedict & McMahon, 2002, 2006).

In recent years, research has brought together aspects from human geography, urban planning and landscape ecology into the green infrastructure concept (Mell, 2008). These approaches include the protection of natural life and biodiversity (Williamson, 2003), the benefits to human health and well-being (Tzoulas et al., 2007), the capacity for water management and run-off control, also known as the Low Impact Development (LID) approach (Buchholz, 2013; United States Environmental Protection Agency, 2011), the connectivity capacity (Benedict & McMahon, 2002; TEP, 2005; Williamson, 2003), and the multi-functionality of 'green' resources (Davies et al., 2006; Office of the Deputy Prime Minister, 2002a, 2002b; TEP, 2005).

While there is no single definition, green infrastructure is generally recognised as 'the interconnected network of natural, semi-natural and engineered features and spaces capable of providing a broad range of ecological, economic and social ecosystem services. These networks provide functions and benefits capable of maintaining natural processes and protecting the biodiversity of urban and rural settings' (Benedict & McMahon, 2002, 2006; Davies et al., 2006; East Midlands Green Infrastructure Network, 2006; EEA, 2011; Faehnle, 2014; MEA, 2005; Naumann et al., 2011; Tzoulas et al., 2007; Williamson, 2003).

According to Benedict and McMahon (2006), green infrastructure comprises a conglomerate of natural and man-made elements (core areas) organised in 'hubs' which provide the space for plant and animal species to develop, acting as the ecological building blocks for the network (Pakzad, 2017). These hubs are spatially connected and integrated

through corridors that facilitate the interrelation and communication among species, and the interchange of nutrients and information. These linkages are determined by the morphological composition and spatial configuration of natural systems and are essential to prevent the fragmentation of habitats and enhance the resilience of the network (Benedict & McMahon, 2006; Pickett et al., 2017; Weber & Allen, 2010) [Figure 2.1].

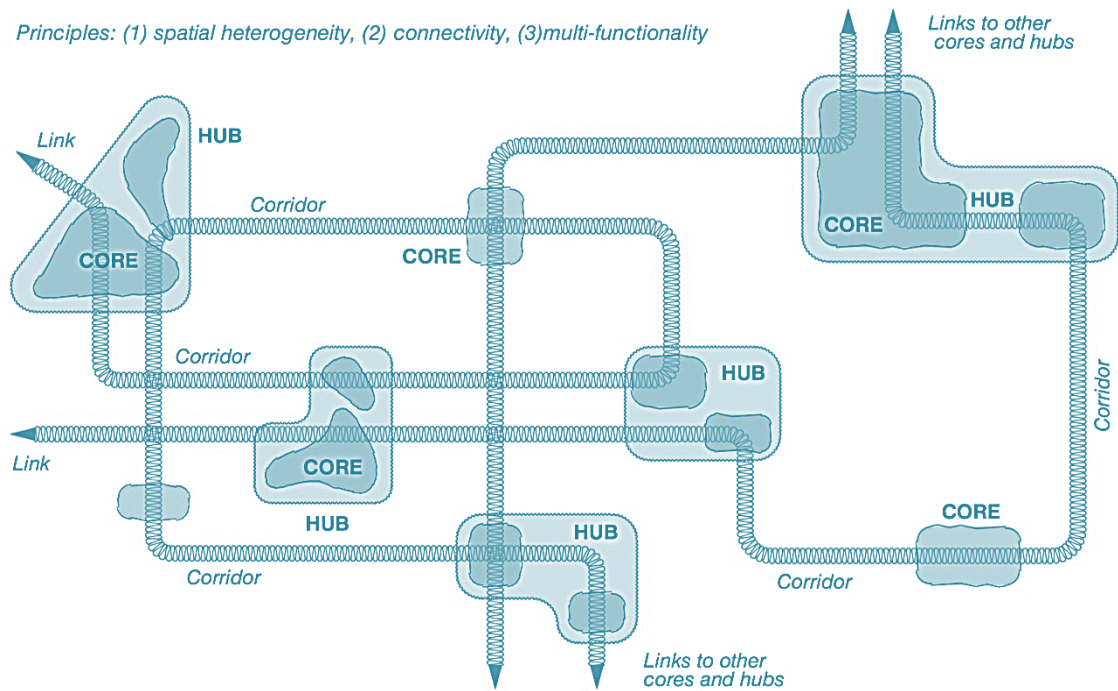


Figure 2.1 Conceptual diagram of a green infrastructure network showing core areas, hubs and corridors. (Adapted from Benedict & McMahon, 2002 and Weber & Allen, 2010).

From a holistic view, there are three overarching principles underpinning the concept of green infrastructure as a ‘life support system’ that should be understood under a multi-scale approach (Ahern, 2007). These principles are: (a) dynamic spatial and temporal heterogeneity (Cadenasso et al., 2007; Cadenasso et al., 2013; Pickett et al., 2017), (b) spatial interconnectivity or integration (blue-green-grey continuum) (Benedict & McMahon, 2006; Davies et al., 2006; Mazza et al., 2011; Mell, 2008; Pauleit et al., 2014), and (c) multi-functionality (Davies et al., 2006; European Commission, 2012; Landscape Institute, 2009; Mell, 2008; Pauleit et al., 2014; TEP, 2005; The Mersey Forest, 2011).

Green infrastructure, as an urban system, should be conceived and studied as a spatially heterogeneous and temporally dynamic phenomenon encompassing a combination of natural, semi-natural and engineered landscape elements (Cadenasso et al., 2013; Pickett et al., 2017). For instance, urban parks comprise different pavements and types of vegetation. Heterogeneity can appear at all spatial scales; however, finer scales are usually

characterised by a large number of features so exhibit highly heterogeneous conditions compared to coarse scales that may be made up of more homogenous elements. Urban design plays a key role in determining these levels of heterogeneity by defining the amount and configuration of those elements, for example in the case of the uniformity of a streetscape (Cadenasso et al., 2013). Furthermore, the concept of dynamic heterogeneity is extremely important both as a driver and an outcome of a mosaic of biophysical (ecological) and social processes, and is a key feature defining temporal changes, spatial patterns, hierarchical organisations and the ecological functioning of urban landscapes (Cadenasso et al., 2013; Pickett et al., 2017).

The maintenance and enhancement of ‘ecological connectivity’ is a key aim of green infrastructure that is crucial to support ecosystems’ functioning and ensure the connectivity of habitats and wildlife (Mazza et al., 2011; Naumann et al., 2011; Weber & Allen, 2010). Connectivity has two main components; the ‘structural connectivity’ which refers to the physical interactions among elements within an ecological network, and secondly, the ‘functional connectivity’ that relates to the behavioural responses between the species and the landscape structure (Mazza et al., 2011). These structural and functional interrelationships are meant to create valuable linkages to maintain the ecological balance between natural and built environments (East Midlands Development Agency, 2010; Lehmann, 2014; Williamson, 2003). Therefore, the provision of green infrastructure networks is increasingly valued in a variety of planning contexts since they can serve multiple functions and to deliver a broad range of human and environmental services (Davis, 2010; Ely & Pitman, 2014; EMDA, 2010; Forest Research, 2010b; Natural Economy Northwest, 2010; Pakzad & Osmond, 2016; Szulczewska, 2012).

The multiple benefits that people can obtain from natural ecosystems and from the transformation of resources into essential goods are called ‘ecosystem services’ (ESS) (Ely & Pitman, 2014; MEA, 2005; Pitman et al., 2015). These benefits include recreation, stress relief, increased property values, noise attenuation, stormwater retention, air purification, heat reduction, aesthetic enhancement and protection of biodiversity among many others (Naumann et al., 2011; Norton et al., 2013). These ESS have been organised into the four main categories of (a) provisioning, (b) supporting, (c) regulating and (d) cultural services (Ely & Pitman, 2014; Mazza et al., 2011; MEA, 2005). Researchers have found a strong linkage between green infrastructure, ESS and different components of human well-being such as security, health, good social relations and high quality of life (Groot et al., 2010; Tzoulas et al., 2007). Therefore, ESS can be used as performance indicators of the magnitude and extent of the impacts and effectiveness of green infrastructure (MEA, 2005;

Naumann et al., 2011). A summary of main ecosystem categories and services is presented in Table 2.1.

The benefits and contributions of green infrastructure are vast and concern economic, social and environmental aspects (Davis, 2010; EMDA, 2010; Forest Research, 2010b; Groot et al., 2002; NEN, 2010; Szulczewska, 2012). For instance, green infrastructure can potentially reduce the capital, operational and maintenance costs for climate change mitigation and adaptation by increasing urban resilience, providing healthy environments, preventing natural disasters, reducing carbon emissions and ameliorating the effects of the UHI (Benedict & McMahon, 2006; European Environment Agency, 2013; Pakzad & Osmond, 2016).

Table 2.1 Ecosystem service categories to measure green infrastructure effectiveness.
Based on Gómez-Baggethun and Barton (2013); Mazza et al. (2011) and Pakzad and Osmond (2016).

Categories	Ecosystem services	Examples
<i>Provisioning services</i>	Food supply	- Production of vegetables and livestock - Area of agricultural land
	Water provision	- Total of freshwater resources - Water storage capacity
	Raw materials	- Provision of fuel - Forest growing stock - Resources production (i.e. paper, cotton, wood, etc.) - Biomass and bioenergy production
	Genetic resources (for food security)	- Increase of crop varieties - Livestock and fish variety
	Medical resources	- Species for natural and homeopathic medicine
	Ornamental resources	- Handcraft work - Ornamental plant species from sustainable sources
<i>Supporting services</i>	Nutrient cycling	- Soil organisms/functional groups - Nutrient retention, circulation and removal
	Primary production	- Net primary production
	Provision of habitats	- Conservation of biodiversity and habitats of birds, insects and other animals - Animal sighting - Species connectivity
	Maintenance of genetic diversity	- Enhancement of species diversity - Phylogenetic diversity - Gene conservation
<i>Regulating services</i>	Air quality regulation	- Air purification/avoided emissions - Removal and fixation of pollutants
	Climate modification	- Urban temperature regulation (Evaporative cooling and shading) - Wind flow alteration
	Climate change mitigation/adaptation	- Carbon sequestration and exchange - Reduced energy-related emissions
	Moderation of extreme events	- Storm, wave, and floods attenuation and prevention - Heat absorption during severe heatwaves

Categories	Ecosystem services	Examples
	Water management	<ul style="list-style-type: none"> - Water flow regulation and mitigation - Run-off control - Water infiltration capacity - Soil water storage capacity
	Waste treatment	<ul style="list-style-type: none"> - Effluent filtering - Water quality control - Nutrient fixation, circulation and removal
	Erosion prevention	<ul style="list-style-type: none"> - Soil erosion reduction - Enhancement of soil quality and compactness
	Maintenance of soil fertility	<ul style="list-style-type: none"> - Regulation of soil-carbon content - Soil formation
	Pollination	<ul style="list-style-type: none"> - Pollination of plants and seed dispersal through birds and insects
	Biological control	<ul style="list-style-type: none"> - Changes in disease burden - Control of species richness (i.e. predators) - Control of biological agents and species
	Noise control	<ul style="list-style-type: none"> - Noise absorption by vegetation barriers
<i>Cultural services</i>	Landscape and amenity values	<ul style="list-style-type: none"> - Change of number of residents and visitors - Real state economic valuation - Cultural identity
	Recreation and cognitive development	<ul style="list-style-type: none"> - Opportunities for recreation, community engagement, meditation and pedagogy - Increase or nature tourism
	Cultural values, educational and inspirational services	<ul style="list-style-type: none"> - Sense of place and belonging - Human health benefits - Research improvements

Researchers from the United States (US) reveal a particular interest in water management and LID projects since the provision of green infrastructure can also help to reduce the costs related to soil erosion, run-off control and rainwater management, and to mitigate the negative effects of extreme weather events such as storms, floods, landslides and bushfires (Beauchamp & Adamowski, 2013; Buchholz, 2013; EPA, 2011). Similarly, Australian experts have concentrated on water management and climatic benefits of greenspaces, green roofs and vertical greenery from a Water Sensitive Urban Design (WSUD) perspective (Coutts et al., 2012, 2012; Coutts et al., 2013; Hunter et al., 2014; Norton et al., 2015; Williams et al., 2010).

Among all ESS, the regulating services including the climate modification, climate change mitigation and adaptation, air quality regulation and reduction of carbon emissions (carbon sequestration and energy savings) have attracted an enormous interest from researchers given the unparalleled effects of climate change, particularly the increment of urban temperatures, and the severity, duration and frequency of heat waves (Forest Research, 2010a, 2010b; Gill, 2006; Hunter et al., 2012; Motazedian & Leardini, 2012; Norton et al., 2013; Norton et al., 2015; Willemsen & Pardyjak, 2012).

Increasing and implementing green infrastructure networks in urban areas, including vegetation and water features¹, is regarded as an effective strategy to substantially reduce air and surface temperatures by shading people and surfaces from high solar radiation, reducing UV exposure, increasing evaporative cooling and altering wind patterns (Bowler et al., 2010b; Coutts & Harris, 2012; Norton et al., 2013; Norton et al., 2015; Oke et al., 1989; Taha, 1997). Since this dissertation particularly focuses on the climate regulation services and benefits of green infrastructure, a more detailed discussion on these aspects is provided in following sections of this chapter.

2.3 Climate change, population growth, urban densification and the loss of vegetation

It is widely recognised that human influence has been the dominant cause of the accelerating increase of the observed global temperature since mid-20th century; that according to the Intergovernmental Panel on Climate Change (IPCC) has risen by around 0.85°C from 1880 to 2012 and 0.12°C every ten years since 1951 (CSIRO & BOM, 2015; IPCC, 2013). The influence of human activities and economic growth cannot only be detected in the warming of the atmosphere and oceans, but also in the global change of water and nutrients cycles, the decrease of snow and polar ice, in the global mean sea level rise and the increasing number of extreme weather events (CSIRO & BOM, 2015; IPCC, 2013). Compared to the climate of 1986-2005, the IPCC has not only projected a significant change on temperatures, but has also indicated that warming will be stronger over land than oceans; hotter days and stronger heatwaves will become more frequent; cold weather and snowfall is expected to decline; and extreme rainfall and drought events will become more intense in the following decades (IPCC, 2013).

The Australian continent possesses extensive arid and semi-arid areas, highly variable rainfall cycles and weather patterns dominated by El Niño-Southern Oscillation (ENSO) that make the country extremely vulnerable to global warming (Irgler, 2014). Indeed, Australia has experienced a substantial warming since last century, evidenced by the increment of the mean, daily minimum and daily maximum temperatures, the recurrent anomalous warm seasons and the more frequent number of heat-related records broken very recently (Bureau of Meteorology, 2018; Bureau of Meteorology & Commonwealth Scientific and Industrial Research Organisation, 2016; CSIRO & BOM, 2015).

¹ Also referred as ‘blue infrastructure’ or ‘urban blue spaces’ (Völker et al. (2013).

Extreme heat conditions were experienced in Australia during the summer of 2012-2013 – the so-called ‘angry summer’ – in which near-surface air and sea-surface temperatures were the highest ever recorded for Australia (Bureau of Meteorology, 2013; CSIRO & BOM, 2015). Furthermore, annual average temperatures have increased by 0.9°C since 1910 and are expected to rise up to 2°C by 2030 and up to 5°C by 2070 (BOM & CSIRO, 2016; Bureau of Meteorology, 2016; CSIRO & BOM, 2015). Furthermore, it is projected that major capital cities across Australia will experience significant rise in the already elevated temperatures and the number of consecutive hot days as a consequence of the combined effects of climate change and existing UHIs (BOM, 2016; BOM & CSIRO, 2016). The ability of Australian cities to adapt and mitigate the impacts of climate change and urban warming are likely to be challenged by the rapid urban development and substantial population growth that is currently experiencing.

Australia is one of the most highly urbanised countries in the world with nearly 85% of residents living in urban areas (Australian Bureau of Statistics, 2017). In 2012, 66% of Australians resided in major capital cities, a proportion that will substantially grow to a projected 74% by 2061 (ABS, 2017). According to the ABS (2017), Sydney is expected to remain as the most populous city in the country with predicted 8.0 million people in 2061, closely followed by Melbourne with 7.6 million. Perth is projected to experience the highest growth (187%) increasing from 1.9 million in 2012 to 5.5 million in 2061; while the second highest growth (118%) will be experienced by Brisbane increasing from 2.2 million to 4.8 million over the same period.

Australia has experienced significant population growth over the last 20 years at an average rate of 1.3% per year, and in the last two years at a rate of 1.6% per year as a consequence of higher fertility and immigration rates (ABS, 2017). The estimated resident population (ERP) at September 2017 reached 24.7 million and is projected to increase up to 48.3 million by 2061 and 70.1 million people by 2101 (ABS, 2017). Similarly, the ageing of Australia's population is expected to continue. The proportion of people aged 65 years and over is projected to increase from 14 percent in 2012 to 22% in 2061 and to 25% in 2101. People aged 85 years or older making up 2% of the total population in 2012 are predicted to grow up to 5% by 2061 and up to 6% by 2101 (ABS, 2017). Under these demographic conditions, more people will live in urbanised areas in the next decades. Additionally, a more elderly population is likely to be affected by elevated urban temperatures and global warming who may experience severe discomfort, health issues and premature death.

During the 20th century, the planning policies in Australia were mainly influenced by the desire of affordable housing, cheap fuel prices and the rise of car ownership which favoured

the urban sprawl of major cities. This led to the development of dispersed and unsustainable urban patterns with a lack of efficient public transport and community services, segregated land-uses, large proportion of roads, traffic congestion and pollution, economic disadvantage and social inequity (Irger, 2014). In response, current development strategies in Australia promote urban densification as an alternative to accommodate new residents and promote better standards of life, economic growth, affordable housing, and the provision of better infrastructure services (water, energy, and transportation). Accordingly, new urban development has reduced plot sizes and accommodated larger numbers of dwellings per hectare, so typical suburban dwellings are steadily being replaced by larger residential complexes (Irger, 2014; Newton et al., 2013).

However, as urban density increases, the proportion of vegetation decreases as public and private open spaces are eventually replaced by hard surfaces (*i.e.* bitumen, concrete, bricks and tiles) of high thermal conductivity, low albedo values and high heat storage capacity (Erell et al., 2011; Hunter et al., 2012; Oke, 1982). The lack of pervious surfaces and the removal of tree canopy cause a dramatic decrease of available shading, evapotranspiration and water infiltration rates, resulting in drier and hotter conditions for urban environments (Coutts et al., 2007). After a period of rain, impervious surfaces tend to dry/evaporate much faster than natural soils contributing to a rapid evaporative cooling of the air for a short period of time. However, over the following days, a significant increment of air temperature is often registered since the absence of available moisture contributes to a rapid increase in sensible heat near surfaces (Coutts et al., 2007; Erell et al., 2011).

Also, densely developed urban areas possess distinctive urban geometries (urban canyons) that contribute to further urban warming by facilitating the creation and intensification of UHIs (Coutts et al., 2007; Hunter et al., 2012) (see Section 2.4.5). Large quantities of solar radiation are absorbed and stored during the day due to large proportion of horizontal and vertical urban surfaces including building facades and multiple reflections from glazing. All this heat is released at night and remains trapped in between deep and narrow street canyons that inhibit the dissipation of long-wave radiation to the sky and prevent natural ventilation by reducing the rate of air-flow (wind speeds) through building spaces (Erell et al., 2011; Hunter et al., 2012).

There is not enough evidence to demonstrate that urban compactness is necessarily sustainable (Neuman, 2005); in fact, a move towards denser urban morphologies extends the time that cities and residents are exposed to unfavourable climatic conditions which demand a higher consumption of energy and resources (Coutts et al., 2007). Since the local microclimate is highly dependent on the presence of vegetation and building density,

compact cities should be planned and designed in the future to mitigate urban warming and climate change more effectively. This implies the adoption of climate-sensitive measures including the strategic provision of green infrastructure and ESS, appropriate design of the urban form, and the thorough selection of building materials (*i.e.* lighter-coloured roofs and facades with higher albedo) to reduce heat storage (Santamouris, 2014, 2015).

2.4 The urban climate

The climatic conditions of urban areas should be understood as the combination of different physical phenomena such as temperature, humidity, wind, precipitation, radiation, cloudiness and general air quality (pollutants and particulate matter). The urban climate at a macro level is mainly influenced by geographical and meteorological factors (*i.e.* topography, latitude, longitude, prevailing winds) (Oke, 1992). Conversely, the urban microclimate, which refers to the unique conditions of a given location, is predominantly affected by the highly heterogeneous nature of urban environments, specifically the physical structure of the urban form such as height and shape of buildings, the presence of vegetation, and the orientation of streets (Erell et al., 2011; Oke, 1988b).

The relationship between climates, the outside urban environments and the indoor thermal conditions has been the topic of study of a large number of investigations since last century. However, only in recent decades have investigations undertaken appropriate systematic research given the interest in understanding and mitigating global warming and climate change (Erell et al., 2011). The climate of London by Luke Howard (1818) can be considered the first scientific study in urban climate that identified and analysed the UHI in London based on empirical measurements (Erell et al., 2011; Grimmond, 2006). Given the widespread availability of meteorological instruments, subsequent research analysed the differences in energy fluxes between urban areas and their rural surroundings by comparing the records of different weather stations or mobile traverses (Erell et al., 2011; Irger, 2014; Oke, 1988b).

Since the 1970s the discipline of urban climatology has progressed significantly. Investigations have focused on observing the atmospheric processes such as the radiant energy budget and understanding the mechanisms behind the creation of particular urban climates (Erell et al., 2011; Grimmond, 2006; Oke, 1988b). In recent decades, the advent of spaceborne (satellite) and airborne (aircrafts and drones) imagery has enabled analysis of the spatial and temporal variability of surface temperatures, particularly the evolution of UHI, in relation to vegetation and the urban form (Amiri et al., 2009; Voogt & Oke, 2003; Weng, 2009, 2012).

The UHI is considered the most compelling focus of urban climate research in the last decades as it has been well documented in most large and medium cities around the world (Grimmond, 2006; Santamouris, 2015). Thermal remote sensing has also been used to determine the biophysical properties of surfaces (*i.e.* emissivity, albedo, roughness, land cover fractions), and to study surface-atmosphere exchanges including evapotranspiration, net radiation, and sensible heat flux (Grimmond, 2006; Weng, 2009).

2.4.1 Scales of climatic study

Urban climates are characterised by particular processes and phenomena occurring at varying scales imposed by the biophysical characteristics of cities and the layered stratification of the atmosphere (Erell et al., 2011; Roth, 2012). Recognition of the impact of scale is crucial to understand the functioning and the genesis of particular climatic phenomena such as heat islands (Roth, 2012). Scale is also important for the study of the interactions among different atmospheric layers and for the discernibility of the elements of the urban surface (Arnfield, 2003; Roth, 2012).

Urban features, either natural or artificial, possess distinctive energy budgets that generate significant modifying effects both within urbanised areas, and in the atmospheric volume of air above and beyond its boundaries (Erell et al., 2011). For instance, the thermal budgets of horizontal ground-level surfaces result from the combination of paved areas, irrigated and non-irrigated greenspaces with contrasting thermal, spectral, radiative, and aerodynamic and moisture characteristics. Furthermore, building surfaces (walls and roofs) are unevenly exposed to solar radiation, net long-wave radiation, humidity and ventilation at varying times. (Arnfield, 2003; Oke, 1988a).

The distinction of atmospheric layers has been a guiding principle and fundamental in urban climate research to fully understand the issues of scale, and more importantly, to investigate the causality of urban climate modifications (Arnfield, 2003; Oke, 1982). Accordingly, the portion of the troposphere affected by the terrestrial surface is known as the ‘*planetary boundary layer*’ (PBL) that comprises the *urban boundary layer* (UBL) and the *urban canopy layer* (UCL) (Erell et al., 2011; Oke, 1976, 1982, 1988b, 1992, 1997) [Figure 2.2].

The UBL is defined as the lowest portion of the atmosphere that is affected by the surface characteristics of urban areas and the activities within it (Erell et al., 2011; Oke, 1988b). As depicted in Figure 2.2, the UBL situates directly above the UCL and extends upward up to approximately ten times the height of the buildings or up to where the influence of

urban surfaces no longer exists (Erell et al., 2011; Hunter et al., 2012; Oke, 1988b). Overall, the conditions within the UBL are relatively homogeneous since they are principally influenced by local- to meso-scale processes such as rainfall, prevailing winds or major land uses which operate at larger spatial and temporal scales (Arnfield, 2003; Hunter et al., 2012; Irger, 2014; Oke, 1988b).

The UBL can be additionally divided into a number of sub-layers with distinctive characteristics (Oke, 1992). The upper part of the UBL corresponds to the ‘*mixed layer*’ which presents homogeneous conditions and is less likely to be influenced by urban surfaces. Immediately below, the ‘*surface layer*’ is composed by the ‘*inertial or constant flux sub-layer*’ that develops because of the passing air above buildings and the heat generated within the city. Since this sub-layer is characterised by a turbulent mixing of air, it is not affected by individual urban elements (*i.e.* single buildings or trees), but rather by the urban texture as a whole (Erell et al., 2011; Oke, 1992). The transition between the relatively homogeneous conditions of upper sub-layers and the highly variable air-flow conditions (wakes and plumes) generated by buildings of different heights, vegetation and open spaces of various dimensions occur in the ‘*roughness sub-layer*’ [Figure 2.2].

The very lowest part of the atmosphere within the *roughness sub-layer* corresponds to the UCL which extends from the ground to about roof-level of buildings, trees and other objects [Figure 2.2] (Oke, 1988b, 1997). In comparison to the UBL, the conditions in the UCL are highly heterogeneous and widely vary from place to place. The UCL presents a mosaic of individual microclimates whose character is determined by the physical characteristics of the immediate surroundings such as height and shape of buildings, amount of vegetation, proportion of open space and the thermal and spectral attributes of materials (Erell et al., 2011).

Within the atmospheric layers, the natural and artificial elements of the urban surface can be hierarchically aggregated into different spatial scales which possess distinctive climates, energy balances and climatic interactions (Arnfield, 2003; Oke, 1992). In fact, the spatial variability of urban elements is likely to be reduced as spatial scale becomes coarser (Ahern, 2007; Arnfield, 2003, 2003; Erell et al., 2011; Mell, 2010; Oke et al., 1989). For instance, there is less thermal difference between larger areas across the city (*i.e.* large forested areas) than between individual features of a street such as trees or buildings (Arnfield, 2003; Oke et al., 1989; Stewart & Oke, 2009).

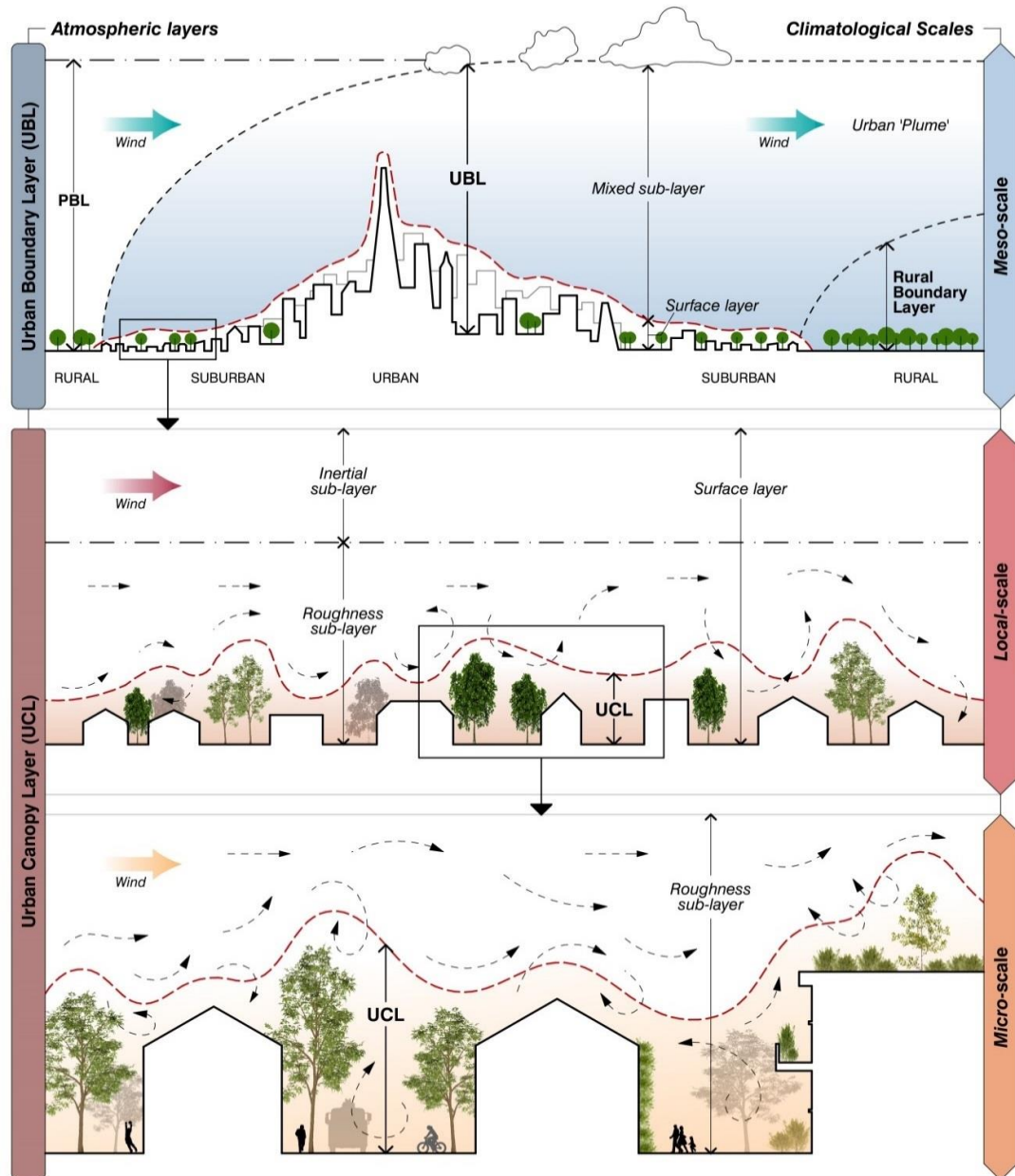


Figure 2.2 Conceptual view of the different atmospheric layers and their relationship with the climatological scales and the natural and artificial elements of the built environment. (Redrawn from Grimmond (2006); Harris and Coutts (2011); Oke (1988b); Oke (1997) and Roth, 2012).

Experts recognise three spatial scales that can be used for the study of climatological phenomena, namely the *meso*-, the *local*- and the *micro*-scale (Erell et al., 2011; Harris & Coutts, 2011; Hunter et al., 2012; Oke et al., 1989; Oke, 1992, 2006, 2009; Roth, 2012) [Table 2.2]. The *meso-scale* refers to climate processes of extensive areas, usually over tens of kilometres, which encompass entire regions or city-wide networks of green and grey infrastructure. The *local-scale* is appropriate for describing the climatic profiles of a portion of the city, usually a neighbourhood or array of buildings covering a horizontal area of hundreds to a thousand metres. The *microscale* is the smallest spatial scale which refers to surface energy balances and the surrounding climate of individual structures and spaces

such as streets, buildings, facets, courtyards, green roofs and green walls (Erell et al., 2011; Hunter et al., 2012; Oke et al., 2017; Roth, 2012). It is at the *local*- and *micro*- scales within the UCL where people mostly experience the thermal effects of climate change and UHI and where most design intervention occurs (Hunter et al., 2012; Roth, 2012). Hence, these are the more pertinent scales to measure the potential benefits and effectiveness of green infrastructure on human beings (Hunter et al., 2012).

Urban climatologists are required to deal with the complexity and heterogeneity of urban landscapes when interpreting the observations at a particular spatial scale (Arnfield, 2003; Cadenasso et al., 2013; Harris & Coutts, 2011). [Figure 2.2](#) and [Table 2.2](#) shows the relationship between the atmospheric layers, the climatological scales and the typical urban scales by incorporating a description of common features and dimensional ranges as reference. It should be noted that these dimensional ranges may sometimes overlap due to the variability of terrain conditions and climatic phenomena (Erell et al., 2011).

As scale is an important consideration for studying the urban climate, abovementioned climatological scales are also applicable to the study and discernibility of the so-called ‘urban forest’ (Oke et al., 1989). This research will particularly focused on analysing the cooling effects of green infrastructure at local scale. This focus corresponds to a comprehensive review of the literature, and reasons and justifications are presented and discussed in Chapter 3.

Table 2.2 Comparison of atmospheric layers, climatological scales and typical urban scales. Adapted from Oke et al. (2017); Oke (2006); Oke et al. (1989) and Erell et al. (2011).

Atmosph. layers	Climatic scales	Urban units	Green/water features	Built features	Dimensional ranges
UBL	Meso	Region	City plus surrounding countryside		25 - 100 km
		City	Complete urban forest	Large urban areas and several districts	10 - 100 km
UCL	Local	Neighbourhoods, LCZs, precincts	Greenbelt, forest, lake, swamps, ocean	City centres, residential areas, suburban zones, etc.	1 - 10 km
		Block	Park, wood, storage pond, streams	City blocks: several buildings and open spaces	100 - 1000 m
	Micro	Street canyon	Line of street trees or gardens, river, canals	Building facades, streets, roads, trees, gardens, etc.	5 - 50 m
		Building	Tree, fountain	Single buildings	10 - 100 m
		Facets	Leaf, lawn, pond	Roof, wall, road	1 - 10 m

2.4.2 The energy balance of urban surfaces

To understand the meteorology of the boundary layer and the climatology of any site (commonly referred as microclimate) is crucial to analyse the energy balance of urban and

vegetated surfaces as these are responsible for the thermodynamic behaviour of air and surface temperatures, humidity, airflow and concentration of pollutants (Oke, 1988b). The concept of ‘energy balance’ is derived from the first law of thermodynamics, which states that energy can never be created or lost, just converted; therefore, the energy input must equal the sum of stored energy and the energy output (Erell et al., 2011). When applied to urban systems, this means that the sum of the heat from the sun and anthropogenic processes must equal the heat that is stored in materials, transferred to the atmosphere or has been taken up by the evaporation process (Irger, 2014).

The surface energy balance of an urban area can be expressed in an equation (Oke, 1988b) which describes the heat exchanges between different surfaces (Erell et al., 2011), and it is written as follows:

$$Q^* + Q_F = Q_H + Q_E + \Delta Q_S + \Delta Q_A \quad [\text{Eq. 2.1}]$$

where Q^* represents the *net all-wave radiation (short- and long-wave)*; Q_F is the *anthropogenic heat flux* that is usually generated by buildings and human activities; Q_H is the *convective (or turbulent) sensible heat flux* which is the energy transferred from surfaces to the air; Q_E is the *latent heat flux* resulting from evaporation; ΔQ_S is the *net storage heat flux* or heat stored in materials and ΔQ_A is the *net horizontal heat advection* which is the energy required for air velocity (Erell et al., 2011; Oke, 1988b). To illustrate and evaluate the energy fluxes within an urban area, Oke (1988b) suggested an imaginary volume which extends from a depth in the substrate where energy exchanges are negligible to a level in the atmosphere near the limits of the UCL (Grimmond, 2006) [Figure 2.3a].

The *net exchange of radiation* occurring over any outdoor surface in the urban canopy can be described with the following balance equation (Oke, 1988b):

$$Q^* = (K_{dir} + K_{dif}) - K\uparrow + L\downarrow - L\uparrow \quad [\text{Eq. 2.2}]$$

where Q^* is the *net radiative balance*, K_{dir} represents the *direct short-wave radiation* coming directly from the sun, K_{dif} is *diffuse short-wave radiation* scattered by the atmosphere (*i.e.* clouds, aerosols), $K\uparrow$ is *short-wave reflected* by surfaces, and $L\downarrow$ and $L\uparrow$ are the long-wave radiation received and emitted by a surface, respectively (Erell et al., 2011; Oke, 1988b).

Figure 2.3b illustrates the surface radiation budget of an urban area which depends on seasonal aspects (time of the day and year), amount of suspended particulate matter such as dust, pollutants, water vapour, and the albedo and emissivity of surfaces. Hence, the

amount of reflected, absorbed and emitted *short-* and *long-wave* radiation within the UCL is the direct result of the combined effects of the urban geometry and the properties of natural (vegetation and water features) and man-made materials (Erell et al., 2011; Irger, 2014).

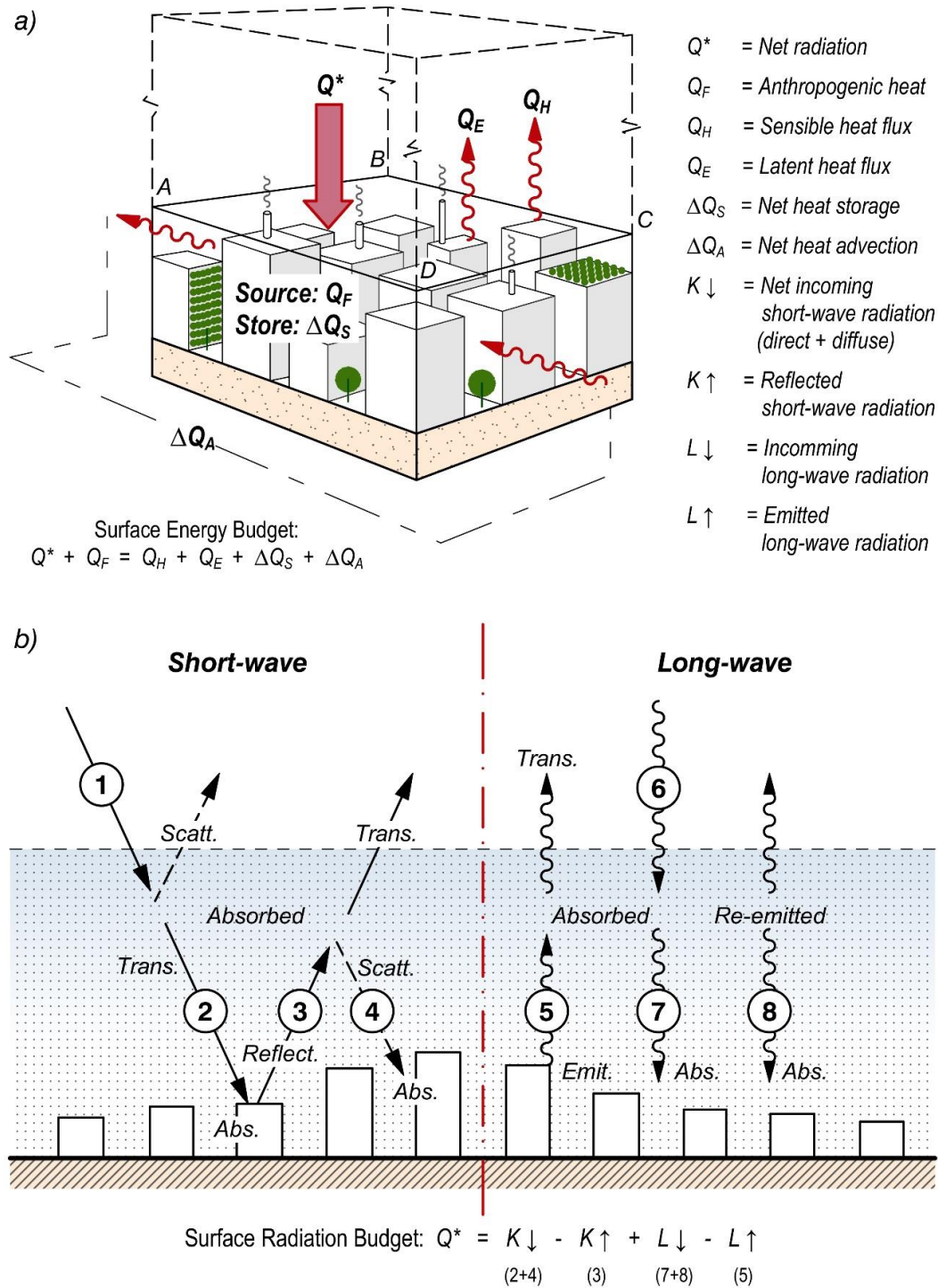


Figure 2.3 (a) Schematic volume showing the surface energy balance components of an urban area and (b) a section of the net radiation exchanges of outdoor surfaces. (Redrawn based on Oke, 1988b).

The *anthropogenic heat* (Q_F) is the amount of energy produced by human processes which basically comprises (a) the heat from vehicular traffic, (b) the waste heat from buildings (mainly heating and cooling) and industrial activities, and (c) the heat released from human metabolism (*i.e.* large-scale movements of people) (Erell et al., 2011; Oke, 1988b). The magnitude of anthropogenic heat largely varies among cities, and between rural and urban areas as depends on population density and per capita energy consumption. The latter also depends on multiple factors including the local climate, the degree and type of industrial activity, the transport system, etc. (Arnfield, 2003; Oke, 1988b).

The portion of energy transferred from surfaces to the adjacent air is known as the *convective sensible heat* (Q_H) (Oke, 1988b). The size of this convection depends on two factors, the resistance to heat transfer and the magnitude of the temperature difference between surfaces and the surrounding air, both affected by air velocity (Erell et al., 2011). Thus, sensible heat transfer is constrained by the roughness of urban surfaces (density and height of trees and buildings) that modifies wind flows (Oke et al., 1989; Oke, 1997).

The *latent heat flux* (Q_E) represents the amount of energy that has been taken up during evaporation and transpiration commonly associated with natural surfaces such as permeable soils, vegetation and water bodies. The urban water budget affects the magnitude of the latent heat flux which in turns affects the available radiant energy, causing air temperature fluctuations (Erell et al., 2011). In-depth discussions on evapotranspiration and its influence on urban microclimates are presented in Section 2.5.3.

The *net storage heat flux* (Q_S) describes the continual change in the amount of heat available in the urban fabric which depends on the ability of materials to emit, reflect, absorb and store radiant energy (Erell et al., 2011). The rate of these changes is determined by the thermal conductivity (capacity of dispersion) and the heat capacity of surfaces; however, their size and spatial arrangement are also influential factors (Erell et al., 2011). Therefore, the replacement of vegetation and pervious surfaces with man-made materials is the main reason for the increment of heat storage within urban areas, and a major contributor to the formation of UHIs (Oke, 1988b).

Finally, the *net horizontal heat advection* (Q_A) represents the energy required for the transport of moisture and heat from one to another location (air velocity). Advection is affected by differences in latent and sensible heat that depend on the geometry and density of the urban form (Erell et al., 2011; Oke, 1988b). Since cities are highly heterogeneous, advection is variable and influenced by local features (roughness) such as the extent of planted areas and building density (Erell et al., 2011). For instance, the irrigated grass and

tree cover of a local park can influence the advection of paved streets in its vicinity, resulting in site-specific microclimatic characteristics (Oke, 1988b; Oke et al., 1989).

2.4.3 The energy balance of vegetated surfaces

To analyse the cooling effects of green infrastructure on urban microclimate, a basic understanding of the fluxes involved in the energy balance of vegetated and aquatic surfaces is necessary. The energy balance of vegetated surfaces requires defining a soil-plant-air system as a volume which extends from the top of plants to a depth in the soil where there are no significant vertical heat fluxes [Figure 2.4] (Oke, 1992). These energy exchanges can be expressed in following equation (Oke, 1992):

$$Q^* = Q_H + Q_E + \Delta Q_S + \Delta Q_P \quad [\text{Eq. 2.3}]$$

where ΔQ_S represents the net rate of *physical heat storage* which results from the absorption or release of heat by the plant biomass (*i.e.* leaves, stems), the soil and air, and ΔQ_P is the net rate of *biochemical heat storage* as a consequence of plant photosynthesis (Oke, 1992). Depending on the characteristics of the surrounding environment, heat advection (ΔQ_A) may be also considered to account for the loss and gain of energy due to latent and sensible heat transport (Erell et al., 2011; Oke, 1992).

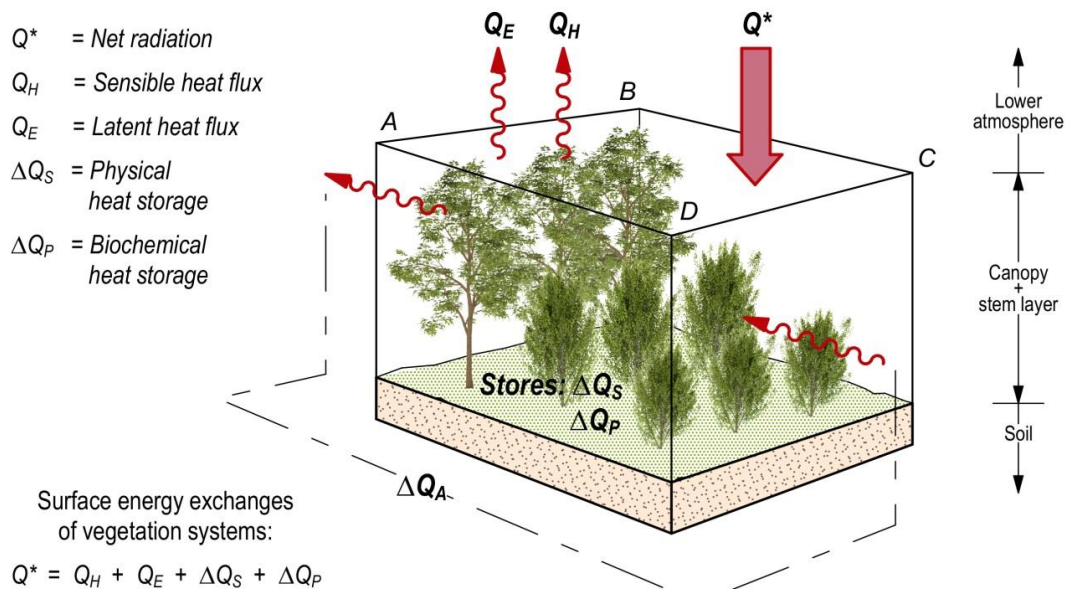


Figure 2.4 Schema of the energy exchanges involved in a soil-plant-air volume. (Redrawn based on Oke, 1992).

The energy balance of vegetation is complex and deserves further study (Oke et al., 1989). In urban landscapes, the non-homogeneity of vegetated surfaces results in unequal radiative, sensible and latent heat fluxes that are spatially variable (Erell et al., 2011; Oke,

1992). For instance, greater foliage density may cause a reduced penetration of short-wave solar radiation, the interception of long-wave radiation emitted by ground surfaces, reduced advection, lower air velocity and increased surface water infiltration compared to impervious surfaces or bare soil that might modify existing thermal conditions (Erell et al., 2011).

Figure 2.5 illustrates the daytime energy fluxes of a single street tree affecting the micrometeorology of an urban canyon (Oke et al., 1989). The heat gains mainly correspond to direct short-wave radiation from the sun, long-wave radiation from the atmosphere, and large amounts of reflected short-wave and long-wave radiant energy from surrounding walls and floor. In cases in which the air temperature in the street canyon exceeds the temperature of leaves, trees are also subject to the advection of sensible heat (Oke et al., 1989).

This considerable heat load is dissipated through transpiration as part of the photosynthesis, a process that is fundamentally dependent upon the water content and wind balance of the tree (Oke et al., 1989). Well irrigated vegetated surfaces increase evaporation from soil and transpiration from plants, resulting in an increment of the latent heat flux and a simultaneous reduction of the sensible heat flux to the atmosphere; this is perceived as a temperature drop (Erell et al., 2011; Oke et al., 1989; Oke, 1992). For many years, the study of these aspects has been the subject of agricultural and forest meteorology; however, these are also of great importance for urban planning and the mitigation of UHI given their influence on the thermal efficiency of green infrastructure (Erell et al., 2011).

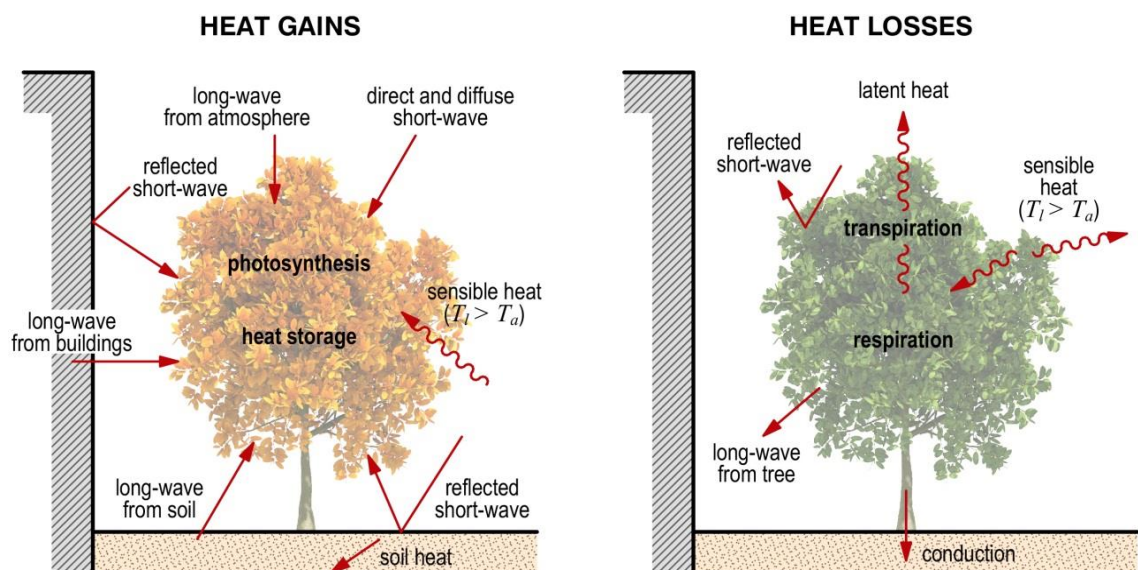


Figure 2.5 Schematic view of the daytime energy fluxes between an isolated tree and the environment of a street canyon. (T_l and T_a , temperatures of leaf and air respectively). (Redrawn based on Oke et al., 1989).

2.4.4 The energy balance of water systems

The thermal capacities of water bodies (*i.e.* oceans, rivers, lakes, etc.) should be also considered when examining the microclimatic effects of green infrastructure as they are significant transporters and stores of energy (Oke, 1992). Given that water is fluid, the thermal behaviour and heat exchanges between aquatic surfaces and the air are complicated as these occur not only by conduction and radiation, but also by advection and convection. As with vegetated surfaces, the energy balance of the surface layer of a water body can be represented through a hypothetical volume [Figure 2.6] that extends to the depth where there are no more vertical heat transfers, and can be expressed in the following equation:

$$Q^* = Q_H + Q_E + \Delta Q_S + \Delta Q_A \quad [\text{Eq. 2.4}]$$

where ΔQ_S represents the change of heat storage in the layer and ΔQ_A corresponds to the net horizontal heat transfer due to water currents (Oke, 1992). In Figure 2.6, it can be observed that ΔQ_A is a form of horizontal heat flux divergence and convergence. Depending on the amount of rainfall and depth of the water surface, the net heat transfer (Q_R) and the heat conduction from the underlying soil (Q_G) should also be added to the equation (Oke, 1992).

Water bodies are excellent heat absorbers due to their low albedo values and because the short-wave absorption occurs within a considerable volume, while most of the long-wave radiation from the atmosphere is absorbed with no significant reflection (Oke, 1992). Accordingly, a large body of water (*i.e.* ocean, lake) acts as a major heat sink (ΔQ_S) during the day, absorbing most of the incoming solar radiation and leaving little energy to be transported into the atmosphere until late afternoon. Conversely, a large volume of water becomes a major heat source at night as the energy stored (approx. 300 W m^{-2}) generates an upward flow of heat towards the atmosphere (Oke, 1992). However, differences from the above patterns and observed surface temperatures may arise due to localised advection currents, the effect of waves, the presence of organic components (*i.e.* plankton) and turbidity (Oke, 1988b, 1992).

Although all water bodies are good absorbers of radiation, they may exhibit very little thermal response which is generally attributable to four aspects:

- a. penetration of short-wave radiation to considerable depths, so the absorbed energy is diffused through a large volume;

- b. mixing of heat gain/losses throughout a large volume due to convection and mass transport by fluid motions;
- c. evaporative cooling tends to destabilise surfaces which further enhance the mixing effect;
- d. the exceptionally large thermal capacity of water, which requires enormous amounts of heat to raise its temperatures to the same level as most dry soils.

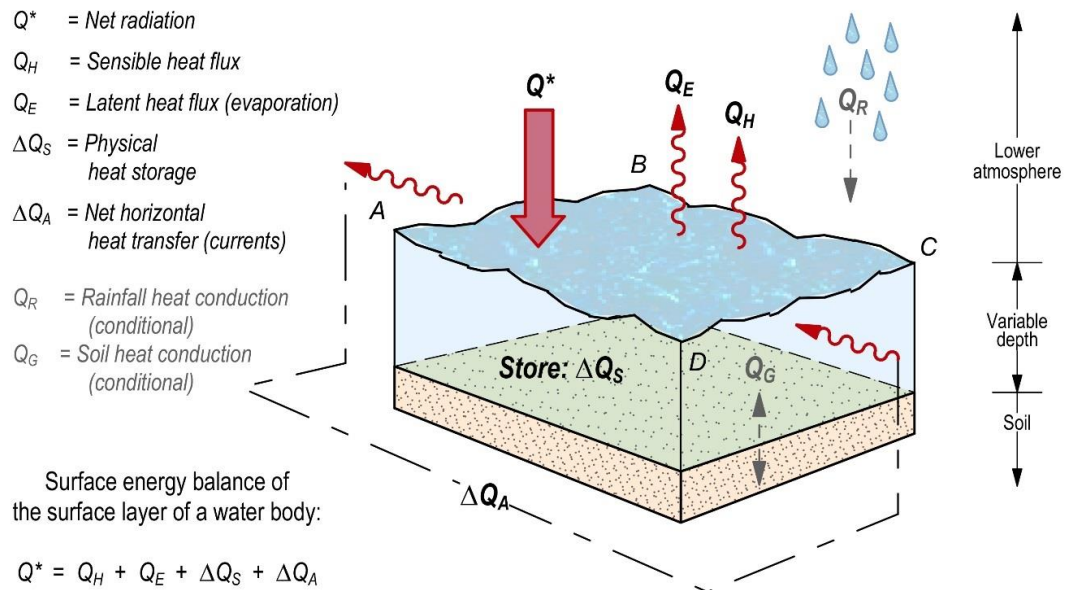


Figure 2.6 Schematic representation of the heat fluxes involved in the energy balance of a water volume. (Redrawn based on Oke, 1992).

Since these properties clearly contrast with those of land (terrestrial) surfaces, their thermal performance/behaviour are evidently different. Indeed, aquatic surface temperatures tend to exhibit less spatial variability than soils (Oke, 1992). Most of the previous discussion refers to relatively large bodies of water and may differ for smaller systems (*i.e.* rivers, ponds) since the latter present a reduced thermal inertia due to a smaller volume of water involved.

Oke (1992) has also pointed out that edge-effects (*i.e.* in riversides or coastline areas) must be considered when examining the thermal profiles of shallow water because short-wave radiation can penetrate to the floor, warming up the lower part of the aquatic system. The presence of vegetation in water surfaces –like in creeks or swamps– further enhance the warming process due to the additional heat absorption of plants. All the aspects mentioned in this section were taken into account for developing both the new classification system for green infrastructure and the assessment framework presented in Chapters 4 and 5, respectively.

2.4.5 The urban heat island: definition and types

The UHI is one of the most important and well-documented manifestations of climate change that has been the subject of research since it was first described for the city of London by Luke Howard in the early 19th century (Erell et al., 2011; Howard, 1818; Oke, 1982; Santamouris, 2015). The UHI has been commonly defined as the phenomenon in which urban areas experience higher temperatures compared to their undeveloped surroundings (Erell et al., 2011; Gartland, 2008; Oke, 1982; Roth, 2012). When isotherms are drawn over a city as a series of concentric lines, it can be observed an island-like pattern of urban temperatures increasing from city's edge towards the densest areas (Erell et al., 2011) [Figure 2.7b]. The same schematic pattern of the UHI structure can be seen in the corresponding cross-section of the city that starts with a large gradient ('cliff') at the city's periphery, continues steadily across suburban areas ('plateau') and reaches its maximum ('peak') at the city centre [Figure 2.7a].

The conventional way to measure the UHI intensity (ΔT_{u-r}) is by calculating the temperature difference between representative locations of rural and urban conditions (Erell et al., 2011). However, the urban-rural dichotomy provides a coarse description of cities that it is not adequate for an accurate analysis of the UHI as it is a continuum and dynamic phenomenon (Erell et al., 2011; Stewart & Oke, 2012). Although the UHI has been mostly reported during the daytime, this is more typically experienced at night (Oke, 1979). As air temperatures decline after sunset, rural areas release radiative energy to the sky more rapidly than the urban counterparts, resulting in a sharp temperature contrast. Conversely, the trend is shortly reversed after sunrise when urban areas warm at a slower rate than the rural surroundings (Erell et al., 2011; Oke, 1982).

UHIs are primarily driven by urban development, rather than climate change; however, they both have a compounding effect upon each other (Harris & Coutts, 2011). The causes of the formation of heat islands can be mainly attributed to the following factors: reduced evaporation and convection, and increased net radiation², heat storage and anthropogenic heat (Gartland, 2008).

The presence of the city entails a multitude of man-made modifications to the natural environment by replacing vegetation with dark-coloured surfaces of low albedo and high heat capacity (Harris & Coutts, 2011; Oke, 1982). This alters the individual components of the radiative and energy exchanges of the built environment as such type of hard surfaces

² According to Gartland (2008), *Net radiation* consists of four separate radiation processes taking place at the Earth's surface: incoming solar radiation, reflected solar radiation, atmospheric radiation and surface radiation.

absorb and retain large amounts of thermal energy that are slowly emitted at night (Gartland, 2008; Harris & Coutts, 2011; Oke, 1982; Roth, 2012). Furthermore, the removal of vegetation increases the exposure of impervious surfaces to direct short-wave radiation from the sun and decreases water infiltration, soil moisture and evapotranspiration (Gartland, 2008; Oke, 1979; Roth, 2012).

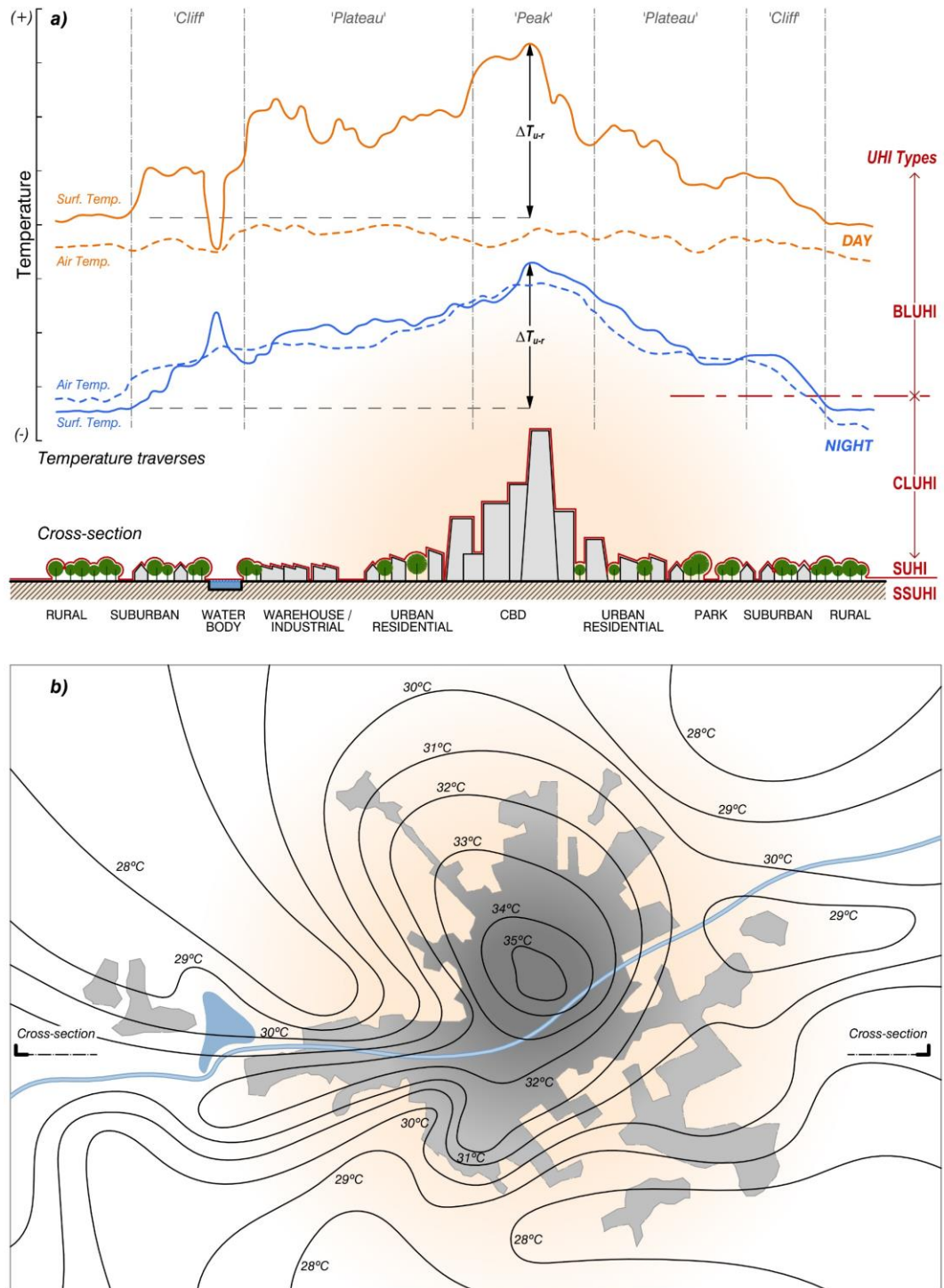


Figure 2.7 (a) Schematic cross-section of a typical urban heat island, its corresponding diurnal and nocturnal air/surface temperature traverses and different types of urban heat island. (b) Isotherms map of a typical CLUHI. (Redrawn based on Erell et al., 2011; Roth, 2012 and Voogt, 2002).

Moreover, complex and dense urban geometries reduce air-flow, generate multiple reflections from the incoming short-wave radiation and trap the emitted long-wave radiation in deep and narrow street canyons (Oke, 1988b; Roth, 2012). Urban air pollution and anthropogenic heat released to the atmosphere also affects considerably the net long-wave radiation balance of cities (Erell et al., 2011; Gartland, 2008; Roth, 2012).

UHIs are better understood and measured as either a surface (surface urban heat island – SUHI and sub-surface urban heat island - SSUHI) or atmospheric (atmospheric urban heat island) phenomena. The latter type can be additionally subdivided into boundary-layer urban heat island (BLUHI) and canopy-layer urban heat island (CLUHI) (Erell et al., 2011; Oke, 1976, 1979, 1982) (Figure 2.7b).

Table 2.3 Classification of UHI types according to their underlying processes, spatial coverage, timing and magnitude and methods of observation. Adapted from Roth (2012).

UHI type / spatial coverage	Underlying processes	Timing: Magnitude	Observation methods
BLUHI / Meso-scale	<i>Day:</i> bottom-up sensible heat flux through top of roughness sub-layer, top-down heat entrainment into the UBL, and radiative flux divergence due to polluted air	<i>Day/night:</i> small and positive, decreasing with height in UBL.	Vertical sensing: tall buildings, radiosondes, tethered balloons, aircraft-mounted instrumentation;
	<i>Night:</i> Similar to day, but intensity of processes is reduced Anthropogenic heat under special conditions		Regional numerical modelling
CLUHI/ Local- & micro-scales	<i>Day:</i> strong positive sensible heat flux at surface; sensible heat flux convergence in canyon.	<i>Day:</i> small, sometimes negative if shading is extensive	Fixed stations; Mobile traverses; Urban flux towers
	<i>Night:</i> often positive sensible heat flux from the release of stored heat, long-wave radiative flux convergence and anthropogenic heat	<i>Night:</i> large and positive, increases from sunset; maximum between a few hours after sunset to predawn hours	
SUHI / Meso-, local- & micro-scales	<i>Day:</i> strong radiation absorption and heating by exposed dry and dark surfaces; surface energy balance	<i>Day:</i> very large and positive	Remote sensing: ground-based, spaceborne, and airborne (including unmanned aerial vehicles- UAV)
	<i>Night:</i> larger cooling at roofs (large sky view) compared to canyon facets (restricted sky view); surface energy balance	<i>Night:</i> large and positive	
SSUHI Micro-scale	Sub-surface energy balance; heat diffusion into the ground	<i>Day/night:</i> small, follows the patterns of SUHI	Underground in-situ probes

Although they are related, these main UHI types differ in terms of properties, intensity, genesis, spatial distribution, temporal behaviour and level of homogeneity (Roth, 2012).

Hence, they are not necessarily studied concurrently (in space and time) and their distinction is sometimes introduced according to the observation method (Erell et al., 2011; Roth, 2012). For instance, heat islands identified from fixed weather stations are different from those measured by car traverses, or obtained from remote sensing imagery (Roth, 2012). [Table 2.3](#) lists the main types of UHIs and their main characteristics, processes, spatial coverage, and methods of observation.

2.4.5.1 Subsurface urban heat island (SSUHI)

SSUHI refers to temperatures under the city which results from the conductive properties of substrates, soils and underground infrastructure (if any) (Harris & Coutts, 2011; Irger, 2014). The spatial variability of SSUHIs depend on the ability of particular surfaces to reflect and emit energy as well as the interaction of radiative energy with the ground (Harris & Coutts, 2011).

2.4.5.2 Surface urban heat island (SUHI)

SUHI describes the temperature differences of the entire three-dimensional urban surface interface of a city and its surroundings (streets, walls, roofs, greenspaces, trees, etc.) (Oke, 1982; Roth, 2012). However, the distinction between the energy exchanges of horizontal (roofs, roads, grass and top of trees) and vertical (walls) facets is important as their processes contribute differently to the duration and magnitude of the SUHI (Harris & Coutts, 2011; Voogt & Oke, 2003).

The SUHI is governed by the physical properties of surfaces such as emissivity, reflectivity, conductivity, absorptivity and sensible heat storage capacity, and their orientation to the sun (Roth, 2012; Voogt & Oke, 2003). SUHIs are usually strongest in summer and during daytime just after noon when solar heating reaches its maximum and creates large thermal differences between dry and wet, and built and vegetated surfaces (Roth, 2012). Relating surface and ambient temperature differences is complex; hence, misinterpretations may occur when using surface measurements to analyse CLUHIs (Roth, 2012).

Remote sensing has been commonly used to capture the spatio-temporal patterns of SUHI since large areas can be monitored and analysed simultaneously and continuously (Arnfield, 2003; Gartland, 2008; Weng, 2009). While spaceborne and airborne imagery provide a bird's eye view of horizontal surfaces due to the view angle of sensors, surface temperatures of walls and facades have been captured through hand-held thermal cameras (Voogt & Oke, 2003). However, studies of complete three-dimensional surface temperatures are scarce (Voogt & Oke, 1997). In comparison to ground-based

measurements, the remotely sensed SUHI is an indirect measurement requiring the consideration of the intervening atmosphere and radiative properties of surfaces within specific spectral wavelengths (Gartland, 2008; Voogt & Oke, 2003). The accuracy and precision of remotely sensed SUHI is generally constrained by spatial resolution since the interpretation and analysis of the data mainly depends on the camera resolution and its relevance to the scale where the processes occur. The literature around the application of remote sensing to investigate green infrastructure and its effects on SUHI is further described in Chapters 3 and 6.

2.4.5.3 Canopy layer urban heat island (CLUHI)

The CLUHI refers to the air temperature differences observed in the volume of the air closest to the ground surface that extends upwards to the roof-top level of buildings and tree canopy (Erell et al., 2011; Oke, 1976, 1988a). The overall morphology of CLUHIs can be related to the shape, geography of cities (*i.e.* topography, water bodies, trees, etc.) and the meso-scale background climate (air intermixes with the UBL) of the urban region (Oke, 1979, 1982). Its internal pattern, however, is an expression of the surface energy transfers occurring inside urban canyons, which are strongly influenced by micro-scale factors such as urban form, building density, convection, evapotranspiration, and radiative properties of nearby surfaces (Oke, 1979; Roth, 2012).

CLUHI intensity is typically more pronounced at night when the volume of the air is affected by the sensible heat transferred from buildings and roads into urban canyons. Conversely, during daytime, the urban-rural difference is less prominent, especially in dense areas, because tall buildings promote shading of surfaces (Roth, 2012). However, recently developed schemes such as the LCZ have demonstrated that these differences may vary depending on the time of the day and the areas that are compared (see Section 2.6.3) (Stewart, 2011b). The CLUHI has been the most investigated type of UHI as it is the most relevant to human health, well-being and energy consumption (Roth, 2012); and because it is generally inexpensive and easier to measure. Typical methods to measure CLUHI include a network of fixed weather stations (in-situ sensors and flux towers) at standard (screen-level³) meteorological heights and mobile traverses (usually cars) (Oke, 1988b; Voogt & Oke, 2003) (see Section 3.8.1). The collected weather data from two or more locations is then compared by using scatterplots or UHI transects (Gartland, 2008).

³ Air temperature that is normally measured at 2m above the ground surface in correspondence to the human height (Steenveld et al. (2011)).

2.4.5.4 Boundary layer urban heat island (BLUHI)

BLUHI describes the urban warmth of entire cities and regions that extends into the UBL up to a height of hundreds of metres (Oke, 1982; Roth, 2012). BLUHIs result from the cumulative effects of the climatic condition of the UCL below. Indeed, the BLUHI is a phenomenon that extends from local to meso-scales and whose intensity is comparatively less than the CLUHIs (Roth, 2012). Depending on wind conditions, BLUHIs form domes of hot air that extend downwind above and beyond cities and that may influence and exacerbate CLUHIs due to the air exchanges with the canopy layer below (Oke, 1982).

The BLUHI has been investigated with the aid of vertical sensing including tall towers, radiosondes, tethered balloon flights and aircraft-mounted instruments (Gartland, 2008; Oke, 1979; Roth, 2012). Nonetheless, it has not received the same attention as its UCL counterpart given the difficulties of probing the air at large heights (Oke, 1979; Roth, 2012). Regional climate models such as the NCAR-MM5 (Fifth-Generation Penn State/NCAR Mesoscale Model) (Grell et al., 1994) have been employed to evaluate the large-scale effects of the BLUHI and its mitigation measures (Gartland, 2008; Oke, 1982).

2.4.6 Responding to the urban heat island

To compensate for urban warming is necessary to apply appropriate mitigation strategies to increase thermal losses and decrease thermal gains in cities (Santamouris, 2015). Managing extreme heat and reducing its associated morbidity and mortality is an enormous challenge for communities, state and local governments (Harris & Coutts, 2011). So far, the most common response has been the use of air conditioning; however, this entails a higher consumption of energy, larger greenhouse gas emissions as well as additional urban warming through anthropogenic heat (Harris & Coutts, 2011). Furthermore, relying on air conditioning reduces the adaptation capacity of populations to warm environments and propitiates the dependency to assisted cooling technologies that may fail in some instances (Harris & Coutts, 2011; Lam et al., 2016; Spagnolo & Dear, 2003b).

The most effective and common countermeasures to mitigate UHI include: (a) increasing the use of reflective, high-albedo, surface wetness and cool materials in pavements, roofs and building envelopes; (b) increasing the use of low temperature natural sinks for heat dissipation; (c) decreasing the generation of anthropogenic heat; and (d) expanding green infrastructure networks through additional greenspaces, street trees, green roofs, green walls and water features (Santamouris, 2015). These and other UHI mitigation approaches are summarised in [Table 2.4](#).

Table 2.4 Mitigation approaches for urban heat island.

(Summarised from Coutts et al., 2010; Harris & Coutts, 2011; Irger, 2014; Osmond & Sharifi, 2017 and Santamouris, 2014, 2015).

Mitigation approach	How it works
Increase green infrastructure (trees and green open spaces)	<ul style="list-style-type: none"> Vegetation is a natural cooling system as it provides evapotranspiration and dissipates heat through latent heating instead of sensible heating. Vegetated open spaces and tree canopy provide cooling for areas downwind and through park/urban cool islands.
Use of green roofs/walls	<ul style="list-style-type: none"> Green roofs/walls reduce heat transfers into buildings and encourage evapotranspiration. Green roofs can help to collect rainwater and to decrease stormwater intensities and nutrients loads.
Increased evaporative cooling	<ul style="list-style-type: none"> Active systems (<i>i.e.</i> evaporative spray coolers and misting fans) located in public spaces and passive cooling systems such as vegetation and water features can be used to increase evaporation and remove heat from the atmosphere.
Water sensitive urban design (WSUD)	<ul style="list-style-type: none"> Enhancing evapotranspiration and heat dissipation by improving irrigation, water infiltration and retention.
Increased shading & reduce solar exposure	<ul style="list-style-type: none"> Strategic location of vegetation (east, west and north in Australia) and shading devices can reduce solar exposure and heat storage of buildings in summertime.
Increased reflectivity & albedo	<ul style="list-style-type: none"> Highly reflective and light-coloured materials (<i>i.e.</i> cool roofs) limit heat transfer into buildings and heat storage by reflecting great amounts of solar radiation. This reduces the need for summertime indoor cooling.
High thermal emittance surfaces	<ul style="list-style-type: none"> Albedo can be increased by covering existing materials (cool pavements) with coatings that reflect in the near infrared.
Streetscape design	<ul style="list-style-type: none"> Increasing the sky-view factor up to a certain point by widening streets as building heights increase enables better ventilation and cooling. Defining an appropriate orientation of streets and buildings can help to control the exposure to incoming solar radiation.
Energy efficiency	<ul style="list-style-type: none"> Waste heat production can be minimised by using more products with excellent energy efficiency ratings.
Building design	<ul style="list-style-type: none"> Appropriate insulation in walls and roofs and the use of double glazing can reduce the need for assisted cooling and heating which in turns reduces the amount of anthropogenic heat. Non-technical design solutions of facades and buildings such as proper orientation, façade treatment, shading, cooling surface materials, etc.
Mass transport	<ul style="list-style-type: none"> Shifting commuter travel to public transport helps reducing anthropogenic heat produced by private vehicle usage.

Among all mitigation strategies, green infrastructure has concentrated the attention of many researchers given its demonstrated capacity to lower urban air and surfaces temperatures and because of the multiple benefits and ecosystem services (ESS) that provides to nature and human populations (Bowler et al., 2010b; Harris & Coutts, 2011; McPherson et al., 2011). Notwithstanding the existing evidence, there is not enough guidance on how best to plan, implement and design green infrastructure to provide maximum cooling benefits (Bowler et al., 2010b; Harris & Coutts, 2011; Kong et al., 2013; Motazedian & Leardini, 2012; Zupancic et al., 2015). An in-depth discussion on the specific benefits and effects of green infrastructure on urban microclimates is provided in Section 2.5 of this chapter.

Researchers, policy-makers and practitioners require better methodological frameworks and tools to inform their decisions about the best approaches, priority locations,

distributions and combinations of green infrastructure for a more effective mitigation of different types of UHI at different spatial scales (Bartlesghi Koc, Osmond, Peters, & Irger, 2017a; Beauchamp & Adamowski, 2013; Buchholz, 2013; Harris & Coutts, 2011; Newton et al., 2013).

Remote sensing and geographical information systems (GIS) have been identified as potential tools for monitoring and understanding the cooling effects of green infrastructure on the spatio-temporal variability of SUHIs (Harris & Coutts, 2011). Compared to satellite remote sensing, airborne remote sensing (from aircrafts or UAVs) can provide a more accurate and detailed information of SUHIs across large urban areas. Since SUHIs have a large influence on the adjoining air, remotely sensed observations can be used to analyse its relationship with CLUHIs (Harris & Coutts, 2011; Weng, 2009). Further discussion on the application of remote sensing on climate and green infrastructure research is presented in Chapter 3.

2.5 Benefits of green infrastructure on urban microclimate

Urban green infrastructure also known as ‘*urban greening*’ or ‘*urban vegetation*’ is capable of providing multiple benefits and improve the microclimate conditions of urban areas and its surroundings (Erell et al., 2011; Irger, 2014; Oke et al., 1989). Nonetheless, the cooling mechanisms and climate-relevant functions of vegetation and water features are complex as they largely vary with the type, size, composition, structure, and spatial distribution of their elements [Figure 2.8] (Bowler et al., 2010b; Erell et al., 2011; Mathey et al., 2011).

In contrast to urban surfaces, vegetated areas are characterised by distinctive thermal, morphological, aerodynamic and physiological features that can significantly alter urban microclimates by: (a) lowering the penetration of short-wave solar radiation to the ground through shading, (b) blocking the upwelling long-wave radiation emitted by the ground, (c) providing evapotranspiration, (d) reducing surface run-off, (e) increasing water infiltration and storage in soils, biomass and natural surfaces (leaves), and (f) altering wind patterns, speed and advection [Figure 2.8] (Arlt et al., 2005; Erell et al., 2011; Hunter et al., 2012; Mathey et al., 2010; Mathey et al., 2011). However, the cooling effects of urban greenery are quite complex and are affected by external (intervening or confounding) factors including wind speed and direction (especially the sea breeze), the surrounding built-up structures and orientation, the overall meteorological conditions, the season, and time of day (Erell et al., 2011; Mathey et al., 2011).

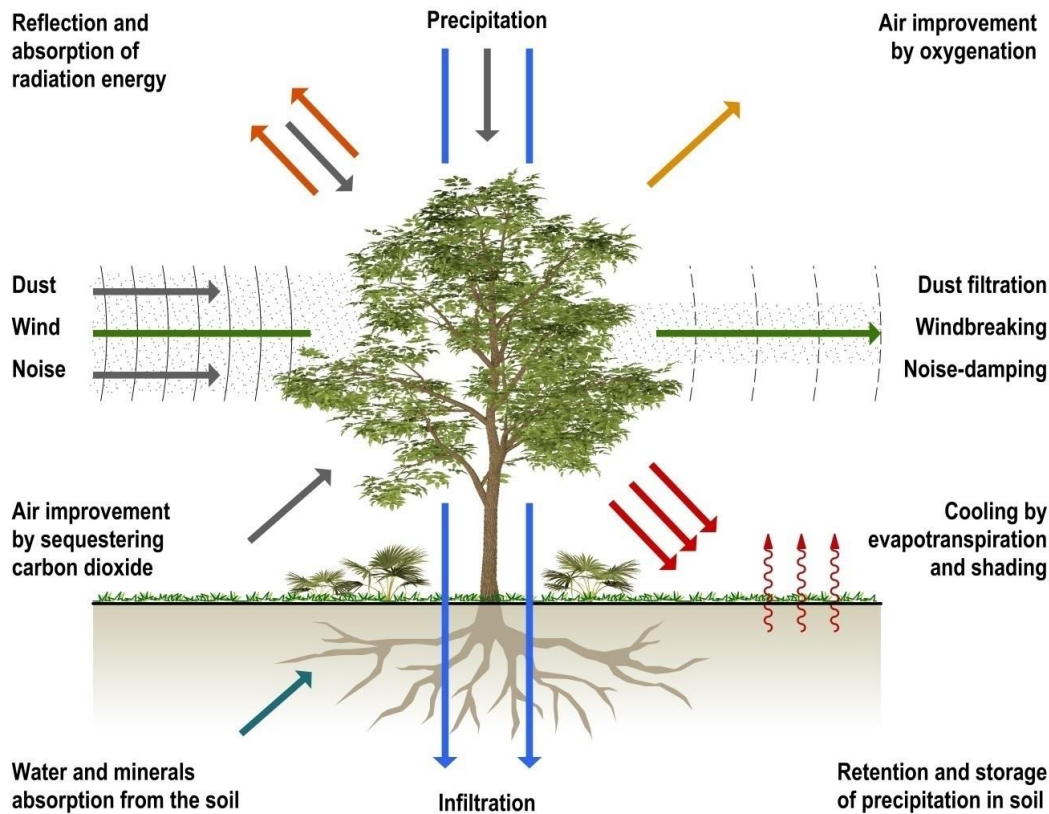


Figure 2.8 Schema of the climate-related functions that vegetation provides to the environment. (Modified and translated from Arlt et al., 2005 and Mathey et al., 2011).

2.5.1 The urban cool island and the park cool island

Contrary to the UHI, the ‘urban cool islands’ (UCIs) and ‘park cool islands’ (PCIs) refer to the phenomena where greenspaces and water bodies establish a zone of larger advective influence beyond its borders, resulting in lower temperatures than those of the immediate impervious surfaces (Chen et al., 2014; Oke et al., 1989; Spronken-Smith & Oke, 1998); however unlike PCIs, UCIs can also be attributed to urban morphology descriptors (Yang et al., 2017).

Several studies on the cooling benefits of urban parks have demonstrated that air temperatures of greenspaces can be from 1 to 4°C cooler than those of the surrounding built-up areas, with the greatest ‘zone of influence’ extending downwind from parks (Bowler et al., 2010a, 2010b; Chen & Wong N. H., 2006; Hunter et al., 2012; Oke et al., 1989; Potchter et al., 2006; Shashua-Bar & Hoffman, 2000; Spronken-Smith & Oke, 1998). As with heat islands, cool islands can be classified into two types: ‘atmospheric cool islands’ which are calculated from air temperature measurements and ‘surface cool islands’ that are derived from thermal remote sensing imagery (Chen et al., 2014).

It is not appropriate, however, to assume that all parks are cooler than their surrounding area at all times, as cooling intensities are the result of a number of factors (Erell et al., 2011). For instance, if a park is well irrigated, day-time PCIs typically develop due to the combined effects of shading and soil moisture, whereas night-time PCIs form in relatively dry and sparse tree canopy conditions. A comparison of the characteristics of diurnal and nocturnal UCIs/PCIs attributed to vegetation is presented in Table 2.5.

Table 2.5 Characteristics of urban/park cool islands attributed to vegetation.
(Adapted from Erell et al., 2011).

Characteristics	Diurnal UCIs/PCIs	Nocturnal UCIs/PCIs
Type of park	Irrigated park with substantial tree canopy	Dry parks with sparse tree canopy
Mechanism involved	Evaporation and shading: trees shade the surface, while well irrigated grass is typically cooler than paved surfaces	Long-wave radiant cooling: sky view factor is close to one
Duration: Time of max. intensity	Afternoon (forest type) or early evening (garden, savannah and multi-use types)	Several hours after sunset
Comments	Masked by anthropogenic heat and heat from nearby materials	Warmer during the night than neighbouring areas

Furthermore, evidence suggests that cool islands are more likely to be observed during calm and clear nights as day-time cool islands might be masked by anthropogenic heat and the continued supply of warm air from nearby artificial materials (Chen et al., 2014; Hunter et al., 2012; Jansson et al., 2007; Shashua-Bar & Hoffman, 2000; Spronken-Smith & Oke, 1998; Spronken-Smith et al., 2000). Other aspects affecting the magnitude of cool islands include the geographic latitude, canyon geometry and orientation, and the urban thermal mass (Erell et al., 2011).

The presence or absence of tree canopy, is also a crucial factor influencing the UCIs/PCIs formation (Erell et al., 2011; Spronken-Smith & Oke, 1998). For instance, parks with dense tree coverage may exhibit cooler temperatures in the afternoon because of shading and warmer conditions at night due to the heat trapped under the canopy and the reduced advection. Conversely, parks with sparse canopy cover are typically warmer during the day since most surfaces are exposed to short-wave solar radiation and are cooler at night due to long-wave radiation losses (Hunter et al., 2012; Spronken-Smith & Oke, 1998).

Other critical aspects affecting the cooling benefits of greenspaces are the characteristics of vegetated surfaces and the water availability –mainly conditioned by changes in irrigation and rainfall– as these properties govern the surface energy balance, the water balance and the evaporative cooling processes of vegetation (Erell et al., 2011; Spronken-

Smith & Oke, 1998). The study of the role of irrigation and evapotranspiration in cooling the built environment remains a knowledge gap and a critical research issue (Hunter et al., 2012). These aspects are discussed in detail in Section 2.5.3 of this chapter.

The cooling effects from parks are highly localised and rapidly decline as the distance from parks' edge increases (Hunter et al., 2012; Upmanis et al., 1998). Moreover, park size, composition and distribution also cause a significant effect on the magnitude of UCIs/PCIs (Cao et al., 2010; Erell et al., 2011; Kong, Yin, Wang et al., 2014; Upmanis et al., 1998). For example, the cooling effect of a small and isolated park is usually limited to its boundaries, so may be negligible in its surroundings (Bowler et al., 2010b; Erell et al., 2011; Hunter et al., 2012). Nonetheless, the relationship between park sizes and cool island intensity is non-linear and not fully understood yet (Cao et al., 2010; Spronken-Smith & Oke, 1998). Up to now, research suggests that larger single parks may have more pronounced climatic effects than small parks distributed throughout urban areas, but the critical size is a question that remains unresolved (Bowler et al., 2010b; Cao et al., 2010; Hunter et al., 2012). Since large vegetated areas are increasingly less frequent in inner city areas, future studies should concentrate on how to maximise the cooling potential of fine-meshed network of small greenspaces (Mathey et al., 2011).

2.5.2 Shading

Plants provide shade for buildings, pedestrian spaces and heat-absorbing surfaces by intercepting incoming solar radiation; a crucial aspect to reduce air and surface temperatures (Erell et al., 2011; Hunter et al., 2012). Additionally, vegetation on buildings such as green roofs and vertical greenery systems contribute to reduce the heat transfer to buildings, resulting in improved indoor thermal conditions and lower overall energy consumption used for cooling (Hunter et al., 2012; Pérez et al., 2014; Santamouris, 2014). Nevertheless, greenery can also trap the upwelling long-wave heat reflected or emitted from horizontal and vertical surfaces to the sky, situation which may alter the heat fluxes and inhibit convective cooling of urban areas and buildings, especially at night (Akbari, 2002; Hunter et al., 2012).

The quality, effectiveness and amount of shade is determined by factors such as placement, form/shape, size, type and angle of leaves, density, height, clumpiness, and continuity of canopy layers (Arlt et al., 2005; Hunter et al., 2012). The reflection of short-wave solar radiation to the atmosphere is also greatly influenced by the size, structure, angle and epidermal properties of leaves. On the other hand, absorption of radiation is determined by the chlorophyll and water content on leaves as heat is dissipated as part of the

photosynthesis process (Hunter et al., 2012). For instance, a recent study found that small-leaved species tend to be more effective at cooling than broad-leaved species, since the former exhibit lower crown temperatures (Kong et al., 2016). Another important factor is the effect of vegetation arrangement as the amount and distribution of shading over the ground varies between single, clusters and rows of trees (Erell et al., 2011).

The provision of ideal shading conditions [Figure 2.9] is a difficult task as several spatial- and time-specific factors come into play. For example, trees may not always shade desired areas, deciduous plants might lose their foliage in a season when it is not required, and in winter, branches may partially obstruct sun's rays in a given location where solar penetration is required (Erell et al., 2011). Hence, the selection of plant species and specific type of foliage (deciduous and evergreen) is crucial to achieve desirable microclimatic effects (Erell et al., 2011).

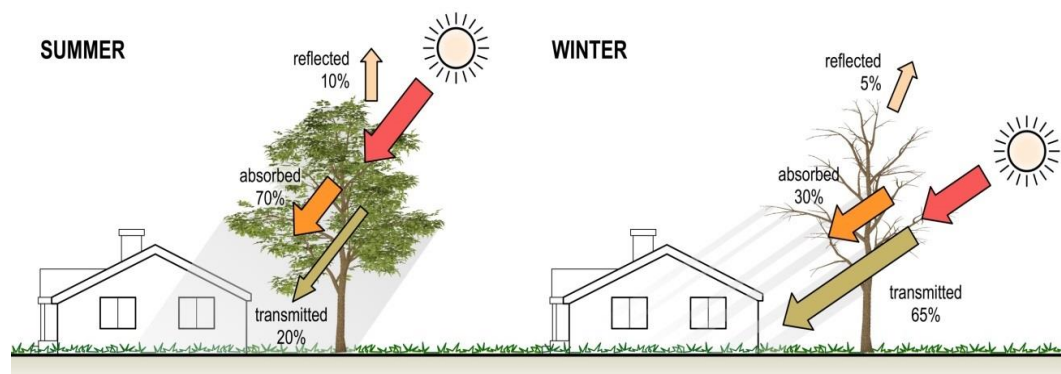


Figure 2.9 General proportions of reflected, absorbed and transmitted radiation through a deciduous canopy in summer and winter. (Redrawn based on Hunter et al., 2012).

The vegetation canopy consists of branches and twigs that are opaque to sunlight which either absorb or reflect almost all the incident radiation. On the other hand, leaves are translucent at different degrees, allowing radiation to penetrate mainly in the near infrared part of the solar spectrum (Erell et al., 2011). Transmissivity is a dimensionless parameter that allows quantifying the amount or proportion of total solar radiation passing through branches and leaves to the ground or other surfaces below; values that largely vary among plants species (Erell et al., 2011; Hunter et al., 2012).

The Leaf Area Index (LAI) is another key dimensionless variable that has been widely used as an indicator of ecological function and as a factor for controlling energy exchanges, transpiration and photosynthetic activity (Osmond & Zakiur Rahman, 2016). LAI has been defined by Kjelgren and Montague (1998) as:

$$\frac{\text{the total 'single-sided' leaf area of canopy (m}^2\text{)}}{\text{the ground area (m}^2\text{) directly under the crown}} \quad [\text{Eq. 2.5}]$$

LAI has also emerged as a metric providing areal estimation of the shading potential of vegetation canopies. Accordingly, vegetation with multiple foliage layers and thick, large and dense leaves exhibit high LAI values; while plants with few branches and sparse and thin leaves have low LAI values (Hunter et al., 2012). Nonetheless, the use of LAI raises some issues. Firstly, it is a highly dynamic index depending on multiple factors such as vegetation phenology, season, species composition and maturity, management regimes (water availability), meteorological conditions (*i.e.* vapour pressure deficit and temperature) and site conditions (soil nutrient availability) (Hunter et al., 2012; Osmond & Zakiur Rahman, 2016). Secondly, LAI cannot fully represent the physiological functionality and morpho-anatomical features of plants (such as stomatal conductance and photosynthetic activity) influencing the overall capacity of vegetation to provide evaporative cooling and withstand dry conditions (Hunter et al., 2012). Other common vegetation-related indices and indicators employed in climatic research are reviewed in Chapter 3.

2.5.3 Evapotranspirative cooling

Urban greenery is capable of modifying air and surface temperatures through the combined effects of evaporation and transpiration; a phenomenon which is commonly referred to as evapotranspirative cooling (Allen et al., 1998; Erell et al., 2011; Hunter et al., 2012). Evaporation refers to the process in which liquid water present in soil and other surfaces (*i.e.* water bodies, wet vegetation, pavement, etc.) is converted to water vapour. On the other hand, transpiration consists of the conversion of liquid water contained in plant tissues into water vapour. This vapour is released to the atmosphere through leaf stomata which also enable the exchange of carbon dioxide and oxygen as part of the photosynthesis process (Allen et al., 1998). Evaporation and transpiration occur at the same time; hence, it is difficult to differentiate and analyse both processes separately (Allen et al., 1998) [Figure 2.10].

Since energy is required to change the state of water from liquid to vapour, sensible heat from direct solar radiation and the surrounding air is absorbed and transformed into latent heat (Hunter et al., 2012). This is perceived as a temperature reduction in the portion of the atmosphere adjacent to natural surfaces (Allen et al., 1998; Erell et al., 2011; Oke et al., 1989). In response to external heat, transpiration enables plants to keep a moderate surface temperature and avoid overheating which may cause permanent physiological damage

(Hunter et al., 2012; Oke et al., 1989). Plants also cool their leaves through two other mechanisms: conduction and convection. Conduction is the process of transferring the absorbed heat to the air mass in direct contact to the leaf; and convection refers to heat transfer by mass motion of the air (wind movement) passing around leaves (Hunter et al., 2012; Oke et al., 1989).

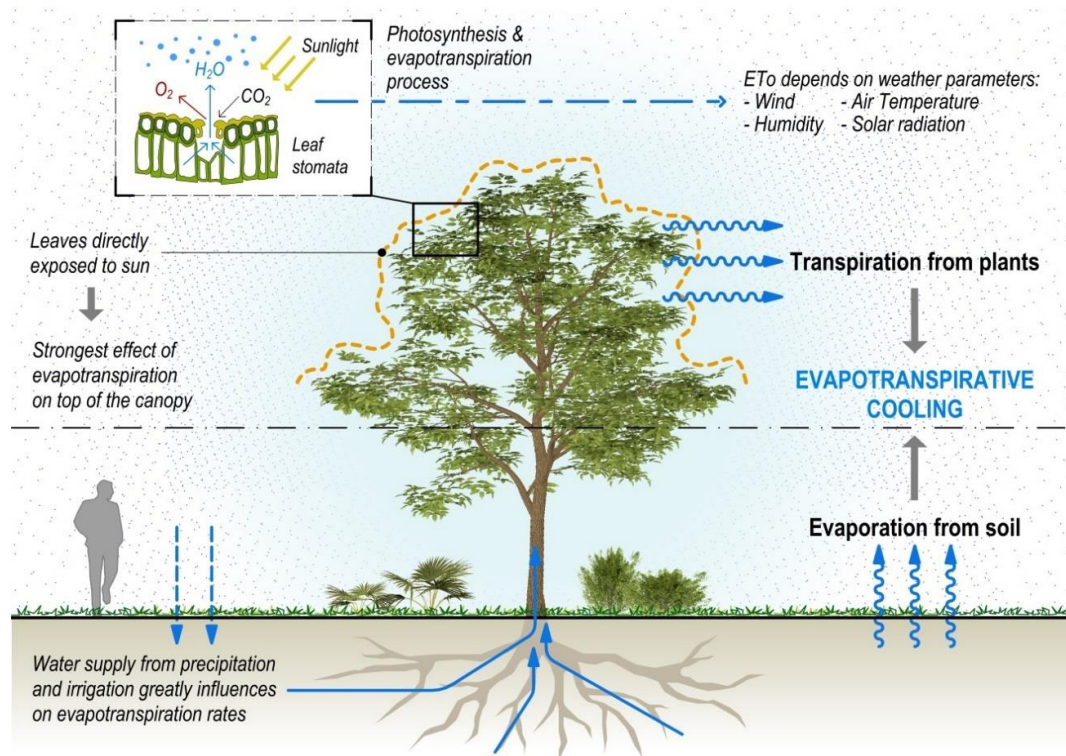


Figure 2.10 Schematic representation of the evapotranspiration process.

Evapotranspiration is a complex phenomenon that varies greatly from place to place as it depends on factors such as plant species/physiology, energy supply (radiation), vapour pressure gradient, available water, wind speed, prevailing meteorological conditions, season, and time of day (Allen et al., 1998; Irger, 2014). As photosynthesis is only possible in the presence of sunlight, transpirative cooling can only occur during the day. In fact, as most of the vapour transfer occurs on the portion of the plant directly exposed to sunlight, the cooling of air temperatures is usually strongest at the top of the vegetation canopy with a lesser effect on the air near the ground (Erell et al., 2011; Oke et al., 1989).

The dissipation of heat through evapotranspiration greatly depends on the wind conditions and water balance (Arlt et al., 2005; Erell et al., 2011). As evapotranspiration increases, the surrounding air gradually saturates up to a point of equilibrium in which no more vapour can be transferred to the atmosphere. Wind is responsible for the replacement of this

saturated air with drier air; hence, evapotranspiration rates greatly depends on wind speed and air humidity (Allen et al., 1998).

Furthermore, in the presence of unrestricted water, the cooling potential of plants is noticeably enhanced; however, evaporative cooling can be significantly affected by restricted water supply, poor irrigation conditions and scarce precipitation. Leaf stomata may also be blocked by the presence of particulates or be closed as a response to excessive heat stress as a result of UHIs, hot weather, heatwaves or severe droughts (Irger, 2014).

The response of plants to heat stress largely varies in terms of the species, the amount of exposed vegetated surface and humidity. For instance, plant species from hot and arid climates are usually more tolerant to drought and high temperatures by dissipating heat through their small leaves or by closing their stomata to prevent extreme water loss (Erell et al., 2011; Hunter et al., 2012). However, evapotranspiration rates from such species can be sometimes negligible or minimal compared to those of broad-leaved plants, resulting in a reduced cooling effects (Chen et al., 2014; Erell et al., 2011; Hunter et al., 2012).

2.5.4 Wind flow modification

Wind conditions in urban areas are complex and depend on several factors including the presence of vegetation, and the morphology and orientation of streets and buildings (Erell et al., 2011; Pitman et al., 2015). Winds provide multiple benefits to urban environments such as decreasing air temperatures and improving the air quality by transporting pollutants away from the city. However, winds may also contribute to increased ‘wind-chill’ factor, compromise comfort and safety, and carry dust, smoke and other harmful particulate emissions (Erell et al., 2011; Pitman et al., 2015).

Vegetation can contribute to the modification of wind patterns and advection in two ways. On one hand, greenery influences wind speeds and funnel cool breezes towards open spaces, streets and buildings, which can help reduce air temperatures and remove air pollutants. On the other hand, vegetation used as windbreaks and shelterbelts can obstruct cooling breezes, reduce wind velocity, trap excess heat under their canopy and reduce cold air infiltration into buildings, resulting in higher air temperatures in both indoor and outdoor spaces (Caborn, 1965; Hunter et al., 2012; Miller et al., 2015; Pitman et al., 2015; Stathopoulos et al., 1994).

The alteration of wind patterns by vegetation imply advantages and disadvantages at various times of the year (Miller et al., 2015). For instance, the wind-shielding effect of trees and vegetative walls may result in reduced building space heating costs in winter,

while the energy consumption through air-conditioning can significantly increase in summer as beneficial cooling breezes are restricted (Akbari & Taha, 1992; Heisler, 1986; Huang et al., 1990; Hunter et al., 2012; Pitman et al., 2015; Stathopoulos et al., 1994).

The effect of greenery on wind direction and velocity depends on various characteristics of vegetation including height, type of species, porosity of branches, type and density of foliage, number of rows, spacing between rows and dispersion between features (Heisler & Dewalle, 1988; Miller et al., 2015; Stathopoulos et al., 1994). Accordingly, small and localised trees in a single row may not provide a substantial channelling, deflection or obstruction of wind compared to dense rows of trees (Erell et al., 2011; Heisler & Dewalle, 1988).

2.5.5 Benefits to human thermal comfort

Human thermal comfort (HTC) can be defined as the physiological and perceptual condition of the body that expresses satisfaction with the thermal qualities of a specific place and at a given time, (ASHRAE, 2017; Erell et al., 2011; Hiemstra et al., 2017; Norton et al., 2013). HTC largely depends on individual perception since the underlying basis for this subjective sensation lies in the way that person's body absorbs and dissipates heat to the surrounding environment (ASHRAE, 2017; Erell et al., 2011; Norton et al., 2013).

People's perception of HTC is influenced by four microclimatic conditions, namely (1) air temperature, (2) mean radiant temperature (MRT), (3) relative humidity, and (4) air velocity; as well as by personal factors such as the person's level of activity or '*metabolic rate*', and the amount of clothing (Hiemstra et al., 2017; Hunter et al., 2012; Irger, 2014; Miller et al., 2015; Norton et al., 2013; Spagnolo & Dear, 2003b).

While the relative humidity and air determine the ability of the body to cool through transpiration and ventilation, the MRT represents the amount of radiation perceived by a person –so it can be considered as the result of the radiative exchange of energy between the human body and the environment (ASHRAE, 2017). There is a large variability in the limits of temperature, humidity and other microclimatic factors that define a comfort zone, since different populations and individuals are acclimatised to various set of conditions. Nonetheless, it is widely accepted that thermal discomfort is caused when thermal gain or loss occurs very rapidly (Erell et al., 2011; Pearlmutter et al., 2014).

Several indices combining thermo-physiological and meteorological parameters have been developed to evaluate HTC for both indoor and outdoor spaces. Among an extensive list, the physiologically equivalent temperature (PET) model is one of the most commonly used

(Mayer & Höppe, 1987). PET values ranging between 18 and 23°C are considered as comfortable, while values of 29, 35 and 41°C are defined as moderate (*warm*), great (*hot*) and extreme (*very hot*) heat stress (*thermal perception*) thresholds respectively (Hiemstra et al., 2017; Matzarakis & Mayer H., 1996). Other common indices are the Outdoor Standard Effective Temperature (OUT-SET*) (Spagnolo & Dear, 2003b) and predicted mean vote (PMV) (Fanger, 1972).

At the microscale, the body of standing person can be influenced in various ways by different types of vegetation which may help to moderate thermal stress under hot outdoor conditions (Erell et al., 2011). The impact of trees on pedestrian's energy balance is mainly radiative as they prevent a body from overheating by limiting the exposure to short-wave radiation from the sun and reducing the long-wave radiation reflected by surrounding surfaces (primarily impervious ground and buildings). The latter occurs due to the lower surface temperatures of shaded areas [Figure 2.11] (Emmanuel & Loconsole, 2015; Erell et al., 2011; Hiemstra et al., 2017; Hunter et al., 2012; Norton et al., 2013).

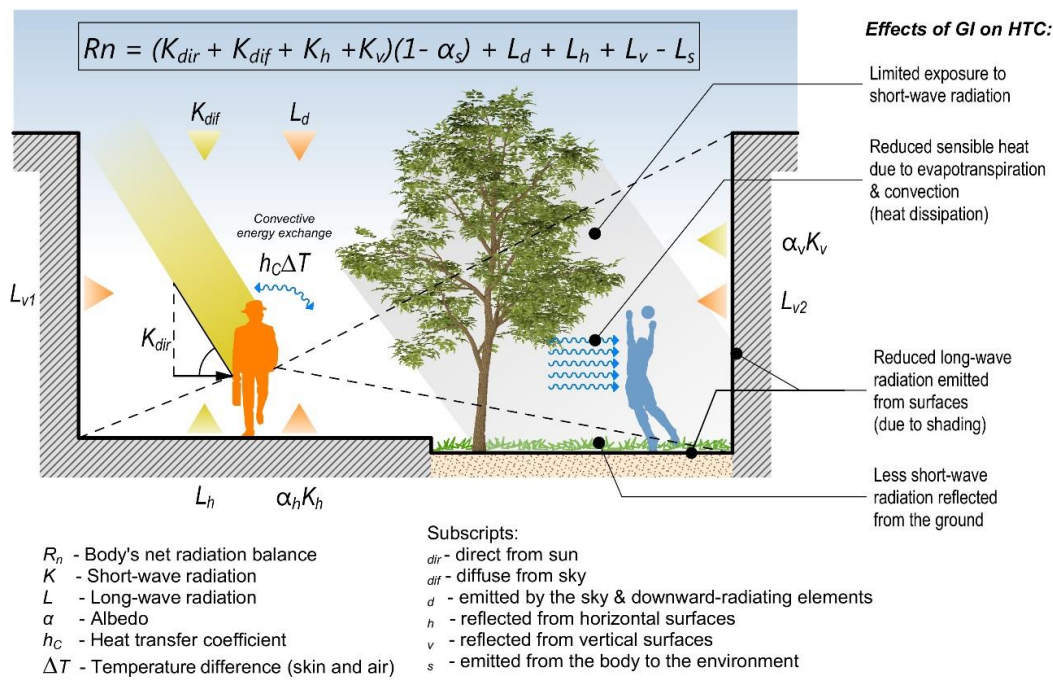


Figure 2.11 Schematic representation of energy exchanges between a pedestrian and the surrounding urban environment; and the influence of green infrastructure (GI) on human thermal comfort. (Modified after Pearlmutter et al., 2014)

The other important determinant of pedestrian comfort is the rate at which each body dissipates heat by both evaporation (sweating) and convection (wind); factors that can be significantly modified by the amount and arrangement of transpiring trees (Erell et al., 2011; Shashua-Bar et al., 2011). For instance, dense clusters of trees may trap significant

radiant heat and limit air-flows underneath their canopies; which may be perceived by pedestrians as warmer air temperature conditions, especially at night (Erell et al., 2011).

Contrastingly, vegetated ground covers moderate pedestrian's thermal stress in a different way. A typical well-irrigated lawn or grass exhibits low albedo and reflect considerably less short-wave radiation onto pedestrians than paved ground. Additionally, ground vegetation transforms most of the absorbed energy into latent heat through evapotranspiration. This does not only contribute to reduce the sensible heat of the adjacent air, but it also features a much lower surface temperature than hard surfaces (Erell et al., 2011; Norton et al., 2013; Pearlmutter et al., 2009; Shashua-Bar et al., 2011).

However, the irrigation of vegetative surfaces places a significant burden on water resources, that in some regions may be restricted in terms of quality and quantity. Hence, under hot weather conditions, the potential effects of low vegetation can be enhanced when used in combination with shrubs and trees, which in turn, may help to moderate the rate of water loss and improve water savings (Erell et al., 2011; Shashua-Bar et al., 2011).

2.5.6 The impacts of vegetation on energy savings

It has been demonstrated that green infrastructure can be effectively used as passive energy saving systems in buildings due to their cooling effects on outdoor surface temperatures and indoor air temperatures (Akbari, 2002; Pérez et al., 2014; Wang, Z.-H. et al., 2016). This is possible because adjacent and integrated vegetation to buildings –such as green roofs/walls and green facades– enable the interception of solar radiation, provide thermal insulation and evaporative cooling, and alter wind velocities or change wind patterns (if necessary) (Ottelé et al., 2011; Pérez et al., 2011b).

A review of recent studies has demonstrated that the thermal performance of extensive and intensive green roofs can reduce the dependence on air-conditioning and energy consumption of the whole building, resulting in energy savings ranging between 40% and 110% (Hunter et al., 2012; Santamouris, 2014). Nonetheless, most of the energy savings attributed to green roofs correspond to summer cooling rather than winter heating (Hunter et al., 2012).

Similarly, studies on vertical greenery systems have reported significant improvements on the thermal performance and reduced energy consumption of buildings in summer periods, with less emphasis on winter seasons (Hunter et al., 2012; Olivieri et al., 2014; Ottelé et al., 2011; Pérez et al., 2011b; Pérez et al., 2014). Reported energy savings differ between greening systems, climates and for heating and cooling (Ottelé et al., 2011). For instance,

direct and indirect green facades⁴ can reduce up to 1.2% of the energy consumption of the whole building required for heating and up to 43% for cooling in a Mediterranean climate (Alexandri & Jones, 2008). While the percentage of energy savings for cooling remains the same for planter boxes and felt layers living wall systems, the energy savings for heating can be increased up to 4% and 6.3% respectively in the same climate conditions (Alexandri & Jones, 2008; Ottelé et al., 2011).

Although the number of available observational studies is high, comparability of results is hindered by a lack of consistency between studies in terms of parameters measured, design, functionality and the construction system used, the type of plant species used, differences in building's construction and operational mechanisms, and the variability of external micro-climatic conditions and air-conditioning and heating systems installed (Hunter et al., 2012; Pérez et al., 2014). Furthermore, most studies and measurements have been conducted at the building scale; hence, empirical analyses of energy saving potentials at local and meso-scale are scarce or results have been mostly estimated through simulation (Hunter et al., 2012).

2.6 Urban morphology and green infrastructure performance

2.6.1 Urban morphology: definition and characteristics

Urban morphology refers to a set of natural and man-made objects, their arrangements, interrelationships, classifications, and dynamic variations that shape the built environment and cities (Kropf, 1993; Osmond, 2008). Also referred as *urban form*, it comprises buildings, city blocks or plots, streets and open spaces, different surface covers, vegetation and water features; which combination and distribution (in different patterns) generate and support distinct land uses, characters, appearance and functioning (Irger, 2014).

From a holistic view, urban morphologies should be conceived and studied not as deterministic objects, but as living systems encompassing multiple and dynamic economic, socio-cultural, and environmental processes (Osmond, 2008). Precisely, these metabolic processes and energy fluxes govern the urban ambience, microclimate, vegetation performance and human activities (Irger, 2014; Osmond, 2008); aspects that are the key focus of the present research. Under this *systemic approach*, green infrastructure's features can be influenced by other elements and aspects of urban form and vice versa. These

⁴ Direct green facades refer to climbing vegetation that uses the wall as supporting system while indirect green facades employ an additional structure such as trellis, cables or meshes affixed to walls (see Section 4.5.4).

interrelationships should be understood and interpreted at different levels of hierarchical organisation: building → lot → block → city → region, as each level exhibits distinct climates, physical characteristics and metabolic processes (Kropf, 1993; Osmond, 2008).

Based on above-mentioned facts, a series of urban morphology aspects that influence and affect the thermal performance of green infrastructure were identified. A discussion of these aspects is presented in next sections as this can help understand the complex bio-physical and climatological processes and interpret the results that will be analysed in subsequent chapters.

2.6.2 Factors influencing the thermal performance of green infrastructure

2.6.2.1 Urban geometry: the urban canyon

The urban canyon is the most widely used model for describing and quantifying the physical properties of the urban fabric and the open spaces between buildings that influence the microscale climate of a place (Erell et al., 2011). A typical urban canyon refers to a three-dimensional linear space (*i.e.* a street) between two adjacent buildings that comprises a horizontal surface flanked on both sides by vertical walls (Nunez & Oke, 1977) [Figure 2.12]. Although this model cannot accurately and universally represent the highly heterogeneous characteristics of the real world, the principles and descriptors can be generally applied in most urban contexts, including one-sided and non-linear shapes (Erell et al., 2011).

The generation of UHIs and promotion of urban warmth is mostly governed by urban geometry and urban compactness since they determine the amount of admitted and reflected short-wave radiation and radiative loss (long-wave) emitted to the sky, the amount of energy stored, and the dispersion of heat and pollutants through wind (Nunez & Oke, 1977; Oke, 1988a; Oke et al., 1989). The geometry of an urban canyon can be described by three main parameters: the *height-width ratio* (H/W), the *sky view factor* (SVF), and the *canyon axis orientation* (θ). Their study is crucial to understand the energy balance of the natural and artificial components and surfaces within the urban canyon.

Height-width ratio (H/W)

The H/W ratio –also known as aspect ratio– refers to the proportion between the average height of the adjacent vertical walls (H) and the average width of the space between them (W) that controls the amount of shade, short-wave, and long-wave radiation available for increasing air and surface temperatures (Erell et al., 2011; Oke, 1981). Although this ratio

mostly applies to symmetrical canyons with continuous heights, the averaging of both H and W enables a general categorisation of most streets (Erell et al., 2011); and can be also applied to courtyards, parks, circular and irregular spaces [Figure 2.12].

However, the relevant limit for solar access to street canyons does not only depend on the H/W ratio, but also on the latitude, season and time of the day when it is measured (Oke, 1988a) [Figure 2.13]. For instance, shading in shallow canyons is mostly likely if solar altitude is low; therefore, daytime UCIs are more likely to occur in high-latitude locations (Erell et al., 2011).

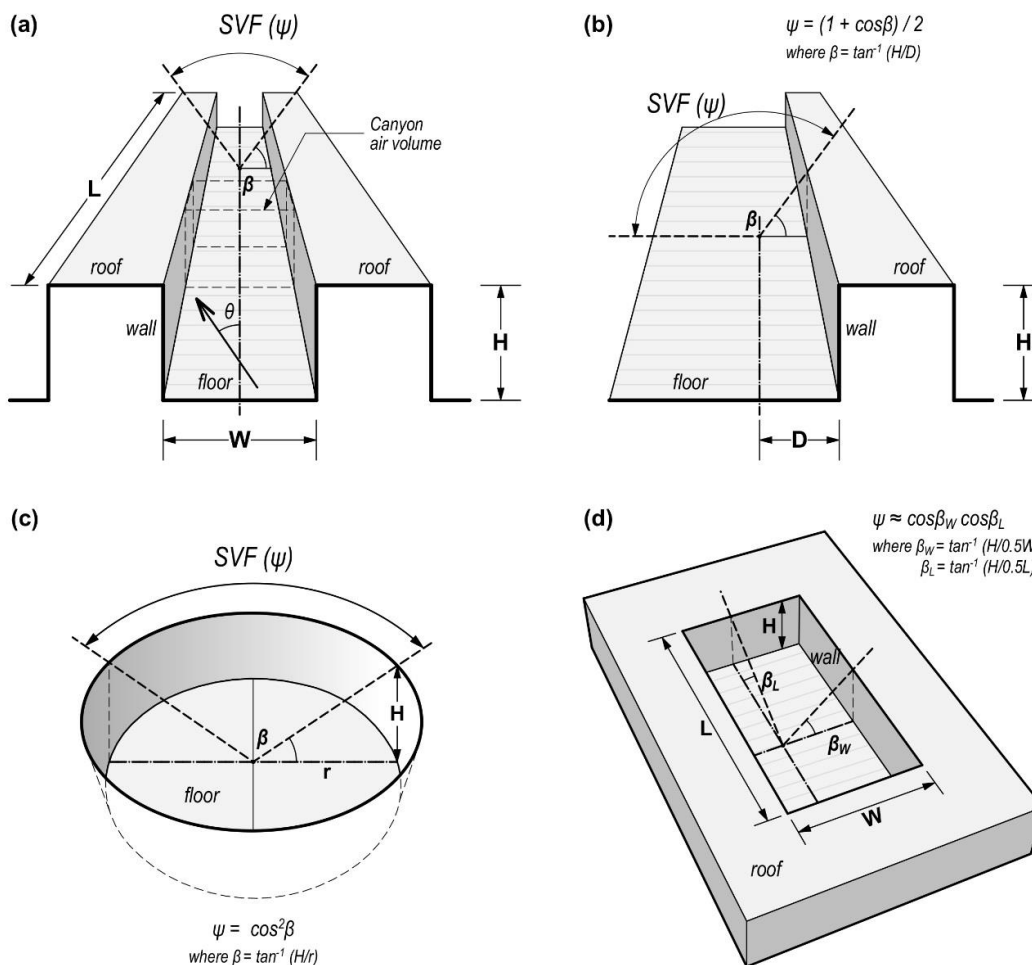


Figure 2.12 Schematic views of a (a) symmetrical urban canyon (b) one-sided open space, (c) circular plaza, and (d) rectangular courtyard, its geometric descriptors, and SVF parameters. (Redrawn based on Erell et al., 2011 and Nunez & Oke, 1977).

The sky view factor (SVF)

The ability of any surface to cool is determined by the magnitude of its long-wave radiative loss –usually occurring at night–, that is proportional to the extent to which a surface is exposed to the sky (Oke, 1988a). The sky view factor, $SVF(\psi)$, is a unitless parameter that

can help quantifying the cooling of a space by measuring the proportion of the viewing hemisphere occupied by the sky in a specific point or over the entire area of a horizontal surface (Oke, 1988a). When measured from the centre line on a horizontal surface in a symmetrical and infinitely long canyon [Figure 2.12], the SVF can be expressed as:

$$\psi = \cos\beta \quad [\text{Eq. 2.6}]$$

where $\beta = \tan^{-1}(H/0.5W)$, and where H and W corresponds to the height and width of the canyon respectively. Accordingly, both, SVF and H/W ratio can be correlated to each other (Erell et al., 2011; Oke, 1988a). As depicted in Figure 2.12, the SVF may also be estimated for other types of space (*i.e.* a large plaza or a courtyard) whose geometries are non-linear; in which case, variations of the above equation are required.

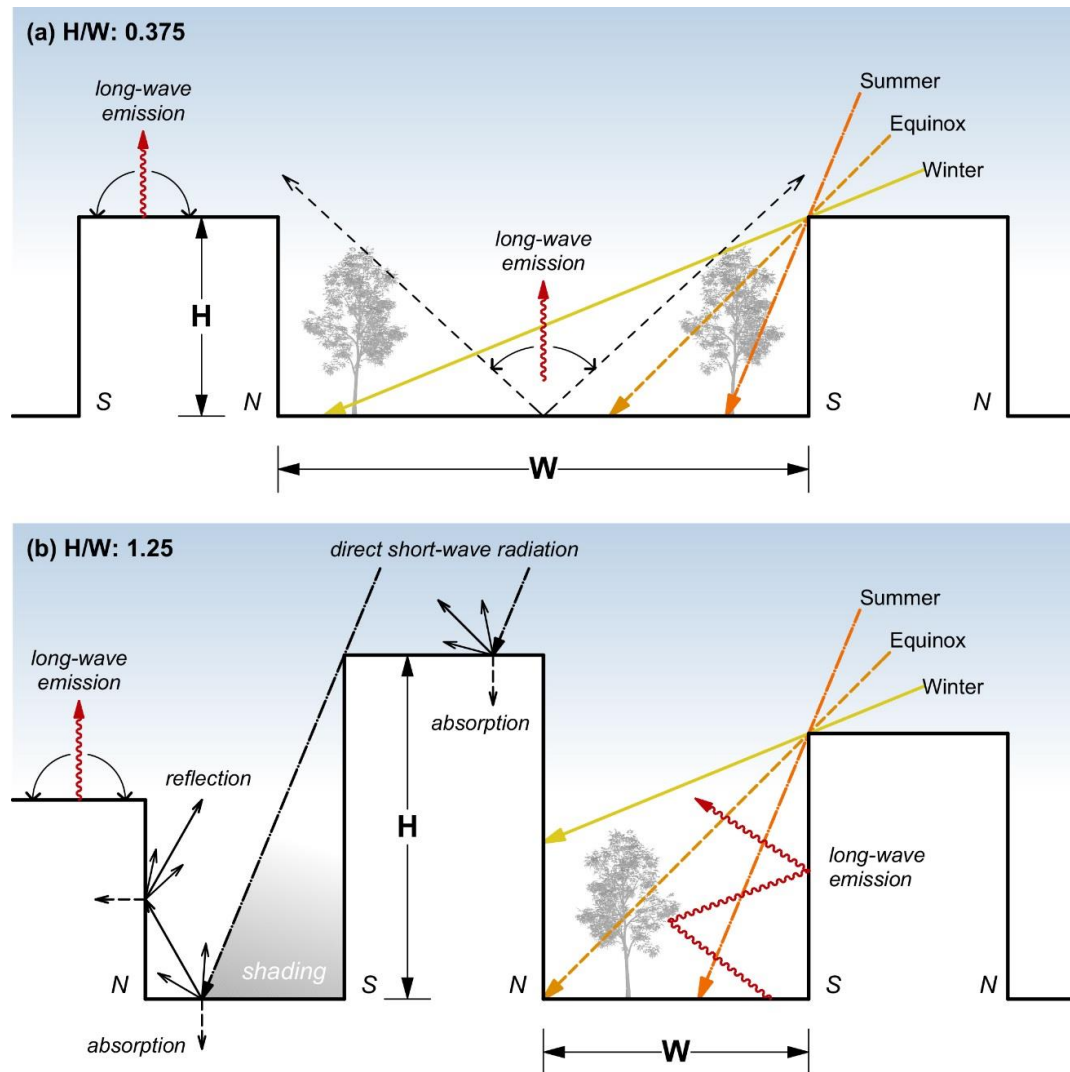


Figure 2.13 Common effects of urban geometry on the penetration, absorption and reflection of solar radiation at noon and in different seasons in (a) shallow and (b) deep urban canyons oriented E-W. (Redrawn based on Erell et al., 2011 and Oke, 1988a)

SVF values range between 0 and 1, where 1 represents an unobstructed horizon that is completely open to the sky. Lower SVF values indicate a larger proportion of the sky occupied by obstacles with a radiative emission greater than the portion of the sky they obstruct. This usually corresponds with an enhanced long-wave emission from the overlying hemisphere and reduced radiative losses from surfaces (Oke, 1988a).

The interpretation of SVF values varies among types of UHIs. For example, taller buildings create deeper urban canyons (with low SVFs) that increase the mutual reflection and absorption of radiation among building facets; so, the heat trapped within the canyon is one of the main causes of daytime peak values of *net radiation* (Q^*) and the generation of nocturnal CLUHIs (Oke, 1981, 1982) [Figure 2.13]. On the other hand, a flat, unobstructed and poorly irrigated vegetated surface exposed to the sun throughout the day may exhibit higher LST than a narrow street canyon where individual facets are sequentially exposed to the sun for a couple of hours and shaded most of the remaining time (Erell et al., 2011). Conversely, the same flat natural surface may exhibit lower surface temperatures at night, as most of the radiative heat is released to the sky at a faster pace than its urban counterpart.

Estimation methods, and other applications of SVF in climate research are further discussed in Chapter 3.

The canyon axis orientation (θ)

This parameter describes the direction or cardinal orientation (*i.e.* N-S, NW-SE) of an elongated space measured as the angle (expressed in degrees) between a line running from north to south and the main axis (or centre line) running the length of a street or linear space, measured in a clock-wise direction (Erell et al., 2011) [Figure 2.12]. As well as previous geometric descriptors, street orientation has a significant impact on air-flows (discussed in next section), the degree of shading at street level, and the exposure of horizontal and vertical surfaces to direct solar radiation, [Figure 2.13] (Erell et al., 2011; Oke, 1988a). However, the significance of these impacts may vary according to seasonal and diurnal patterns, and the specific location of a city (Oke, 1988a).

2.6.2.2 Air-flow

Wind speed and wind direction are extremely variable within the UCL as these are affected by the built form, the patterns and orientation of streets and open spaces, the presence of vegetation, the local topography and other meteorological factors; hence, its measurement and inclusion in microclimatic models is extremely complex (Erell et al., 2011). Oke (1988a) defined distinct types of air-flows within the UCL, that largely depend on the array

of buildings, so at closer spacings the wakes are highly disturbed compared to well separated buildings where flows do not interact with each other [Figure 2.14].

Moreover, the surface roughness of an urban environment –defined by the H/W ratio, the orientation of streets and the configuration of buildings– affects wind patterns, the degree of wind penetration into the urban fabric and the amount of shelter provided from intense winds (Oke, 1988a). Thus, compact urban form inhibits the exchange and infiltration of air at both pedestrian level and the mixing layer above roofs, leading to a large concentration of pollutants and heat between buildings; factors affecting the thermal comfort of pedestrians, the cooling performance of vegetation and the electricity demand used for cooling (Oke, 1988a).

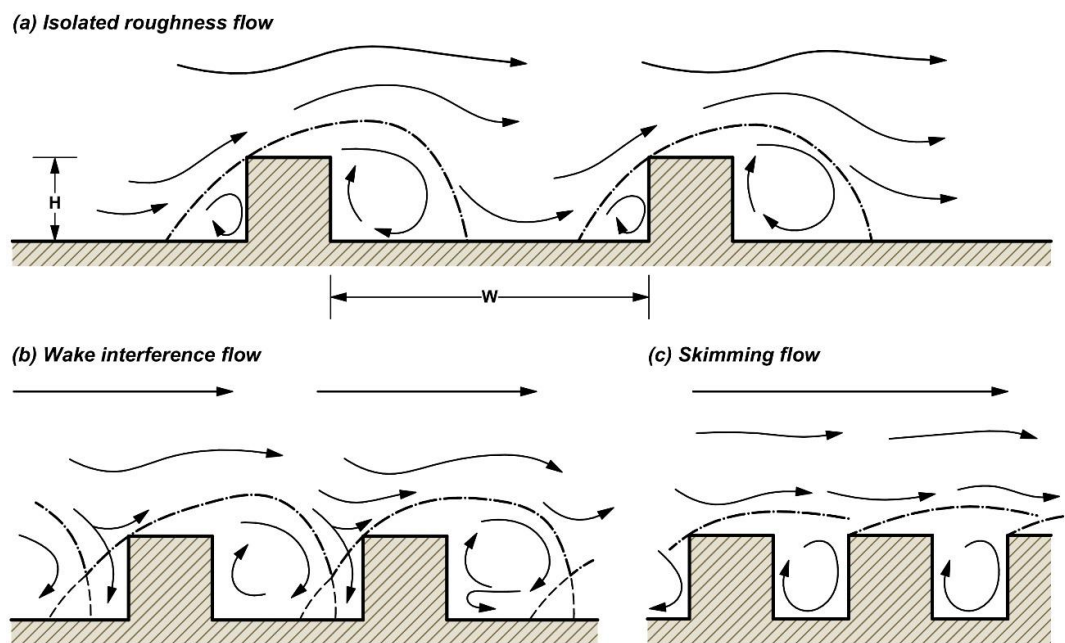


Figure 2.14 Air-flow regimes over different arrays of buildings with increasing H/W ratio. (Redrawn from Oke, 1988a)

2.6.2.3 Properties of urban surfaces: Albedo

Man-made structures of the urban environment, such as buildings and impervious surfaces (*i.e.* pavements, asphalt, concrete) exhibit thermal and optical properties that differ considerably from those of natural features and surfaces. These differences are of special significance for studying the thermal conditions of a given location due to the substantial heterogeneity and variation of conditions at local and micro scales (Oke et al., 1989). According to Erell et al. (2011), two characteristics determine the differences between natural and artificial surfaces:

- a. The moisture content of pervious surfaces –absorbed from precipitation or irrigation– leads to changes in thermal conductivity, thermal diffusivity and admittance, and volumetric heat capacity of ground surfaces. Thus, in the absence of available moisture, a positive net radiant balance contributes to a rapid increase of sensible heat near built surfaces, so this is reflected in a higher air temperature. In contrast, the evapotranspiration provided by vegetated surfaces leads to reduced sensible heat which is registered as lower air temperatures during daytime. Additionally, the albedo of natural ground surfaces decreases at the time that moisture content increases because of the air-water interactions between soil particles and the inter-space between them.
- b. Seasonal changes in vegetation cause variations in surface albedo of a given area, since the albedo of full foliage is typically lower than that of most soils.

Although the precise effect of urban materiality on UHI intensity is laborious and difficult to quantify, it has been identified that highly absorptive and dark-coloured materials tend to exacerbate SUHIs compared to lighter and highly reflective materials. This is possible due to the lower absorption of short-wave radiation and increased infrared emission of the latter, that help release sensible heat to the atmosphere and decrease surface temperatures (Santamouris, 2015). Similarly, whereas the effects of built surfaces on urban microclimate are well-established, the interactions between natural and artificial surfaces are not fully understood yet.

Another crucial factor of the surface energy balance influencing the local- and micro-climate is the amount of heat stored in materials that depends on the *thermal capacity* (C) and *thermal conductivity* (k) of materials (Erell et al., 2011). The relationship between both is referred as *thermal diffusivity* ($\alpha = k/C$) and represents the heat dispersion rate of a material. The higher the thermal diffusivity, the more constant and evenly distributed its temperature over time (Gartland 2008). This is considered a key factor in the creation of CLUHIs and SUHIs as urban landscapes are characterised by a large variation of natural and artificial materials with different thermal diffusivity characteristics (Oke, 1992).

Albedo

One property of materials is their hemispherically and wavelength-integrated capacity to reflect incoming short-wave radiation (Akbari, 2009; Taha, 1997). This is commonly referred as *albedo* (α) and is calculated through the following equation:

$$\alpha = \frac{K_{dir} + K_{dif}}{K_{\uparrow}} \quad [\text{Eq. 2.7}]$$

where K_{dir} represents the direct incoming short-wave radiation from the sun, K_{dif} is the incoming diffuse short-wave radiation and K_{\uparrow} is the total amount of short-wave radiation reflected by the surface⁵. Albedo values range from 0 representing surfaces that absorb all the radiation (*i.e.* dark-coloured surfaces), to 1 for surfaces reflecting all the radiation (*i.e.* light-coloured materials) (Akbari, 2009).

In the context of climatology, there exists two types of albedo, the *surface albedo* which refers to values of individual materials and the *urban albedo* that responds to diverse combinations of multiple surfaces and the geometric aspects of urban form at larger urban scales. According to Taha (1997), typical urban albedo of most North-American and European cities range between 0.15 to 0.20 due to the high proportion of pavements and roads, compared to North African towns with urban albedos of 0.30 to 0.45. Similar differences were found between city cores and their surroundings given the presence of extensive vegetated areas which normally exhibit higher albedos than hard surfaces (Taha, 1997).

Regarding surface albedos, the capacity of materials to reflect solar radiation is determined by their physical (*i.e.* roughness) and chemical properties, as well as the angle of solar incidence (Akbari, 2009). A list of typical albedo values for common urban surfaces is presented in Table 2.6. Since the emissivity of materials defines its ability to emit radiative heat, the consideration of surface albedo is key to understand the modification of air and surface temperatures within the UCL. For instance, rough and dark-coloured surfaces like asphalt have low albedo, so they absorb almost all the solar energy throughout the day. This combined with their low moisture content and inability to evaporate water, significantly raises surface temperatures of streets and parking lots in sunny summer afternoons (Akbari, 2009).

Table 2.6 Typical albedo values for common urban surfaces. (Based on Akbari 2009; Oke 1992)

Man-made materials	Albedo	Natural materials	Albedo
Asphalt	0.05 – 0.20	Trees	0.15 – 0.20
Concrete	0.10 – 0.35	Grass	0.25 – 0.30
Brick/stone	0.20 – 0.40	Wet soil	0.10 – 0.25
Corrugated iron	0.10 – 0.16	Dry soil	0.20 – 0.40
Tar & gravel	0.08 – 0.18		
Red/Brown tile	0.10 – 0.35		
Coloured paint	0.15 – 0.35		
Highly reflective roof	0.60 – 0.70		
Fresh white paint	0.70 – 0.90		

⁵ Albedo differs from 'reflectivity' since the former is measured across all wavelengths instead of just the visible spectrum (Akbari (2009)).

Generally, pervious surfaces exhibit low albedos compared to impervious materials as they absorb most of the radiation in the visible and ultra-violet spectrums, so this energy is taken up for the photosynthesis process (Erell et al., 2011). However, this hampers a clear correlation between the average surface albedo of a given area and its mean temperatures as the energy balance of natural and artificial surfaces are considerably different. Accordingly, Irger (2014) demonstrated that two spatial units with a completely different proportion of vegetation cover and thermal profiles may display similar average urban albedos and vice versa.

In addition, it has been found that higher air temperatures inside parks can be attributed to a decreased albedo of vegetated surfaces along with other bio-physical aspects such as lack of water content, the heat released by grass decomposition, or photosynthesis midday depression (Chang et al., 2007; Santamouris, 2015). Furthermore, in highly urbanised contexts, the cooling benefits that vegetation provides at night may be outweighed or masked by the thermal impact of surrounding paved areas and low albedo materials (Erell et al., 2011; Santamouris, 2015).

2.6.3 Classification of urban morphology: the local climate zone scheme for urban heat island studies

The ambiguity around the classification of urban form to support various analyses has been identified as an important gap in the literature (Osmond, 2008). From a spatial perspective, the study of climate-related phenomena such as the UHI also requires the subdivision and description of distinct urban morphologies for a multi-temporal, multi-scale and meaningful comparison of their thermal profiles (Irger, 2014; Stewart, 2011b).

The *urban structural units* (USU) scheme developed by German ecologists Pauleit, Duhme and Wickop is an attempt to define urban areas with physiognomically homogeneous characteristics based on built-up form, open spaces and human activities (Pauleit & Duhme, 1998; Wickop, 1998). Originally developed for German cities, the USU framework has been successfully applied for the comparative assessment of urban patterns against economic, social and ecological performance indicators (Pauleit & Duhme, 2000).

Osmond (2008) developed a broader framework and tested the USU in the Australian context for a robust and comprehensive examination of the interrelationships between various aspects of urban form, ambience and metabolism (material flows). However, despite the potential applications and expandable nature of the USU scheme, this has not yet been embraced by climate scientists as there have not been defined universal qualitative and quantitative descriptors for a clearer differentiation of classes and for its application in

non-German contexts or by urban mapping disciplines such as remote sensing (Heldens, 2010; Irger, 2014; Osmond, 2008).

The local climate zones (LCZ) scheme

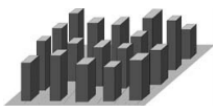





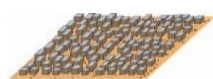


More recently, the *local climate zones* (LCZ) scheme introduced by Stewart and Oke (2012) has attracted the attention of the urban climate community as it enables a standardised classification of urban areas with uniform land cover, structures, materials and human activity that span hundreds of metres to several kilometres and display similar thermal regimes. Originally based on Oke's *urban climate zones* (UCZs) (Oke, 2006); the LCZ system was developed for a generic and universal description and classification of observation sites for UHI studies based on the thermal and physical properties of the built environment, rather than the traditional and ambiguous *urban-rural* characterisation (Stewart & Oke, 2012).


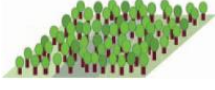
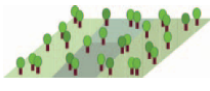
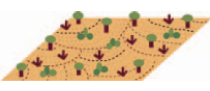

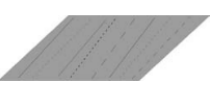
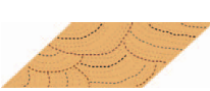
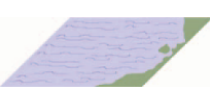
This classification system targets investigations at local scale; and requires the estimation of key indicators such as building and vegetation height and density, H/W ratio, SVF, surface fractions and vegetation content (pervious, built and impervious ground), surface properties (albedo, thermal admittance), and anthropogenic heat. The unique combination of these properties defines the thermal regimes of each class, particularly the characteristic air temperature at pedestrian level and observed surface temperature from a bird's eye view (Stewart & Oke, 2012).

The scheme comprises 17 LCZs distinguished between two groups: *built zones* numbered from 1 to 10 and *natural zones* named with letters from A to G. It also enables the combination of classes from both groups if necessary. [Table 2.7](#) provides a summary of LCZ classes, their definitions and main geometric and surface cover cut-off values as defined by Stewart and Oke (2012).

The system shows potential for universal applicability, so the interest from other disciplines has recently grown as the spatial and temporal variability of air and surface temperatures within and among classes has become a key research question (Geletič et al., 2016; Geletič & Lehnert, 2016; Irger, 2014). For example, LCZs have been extensively implemented in climate research to (a) define the magnitude of UHIs by examining the correspondence between air temperatures and LCZ types (Alexander & Mills, 2014; Bokwa et al., 2015; Emmanuel & Krüger, 2012; Irger, 2014; Leconte et al., 2015; Ng., 2015; Stewart, 2011b; Stewart et al., 2014; Stewart & Oke, 2010; Wang, Z. et al., 2016), (b) identify and classify meteorological sites (Lehnert et al., 2015; Lelovics et al., 2014), and (c) for modelling purposes (Alexander et al., 2015; Bokwa et al., 2015; Irger, 2014).

Table 2.7 Summary of LCZ classes, their definitions, visual description, and main geometric and surface cover cut-off values as defined by Stewart and Oke (2012).

LCZ	Definition	SVF	Aspect ratio	Impervious fractions (%)		Pervious fraction (%)	Height elements (m)
				Built	Ground		
BUILT ZONES							
<div>1 – Compact high-rise</div> 	Dense mix of tall buildings to tens of stories. Few or no trees. Land cover mostly paved. Concrete, steel, stone, and glass	0.2-0.4	>2	40-60	40-60	<10	>25
<div>2 – Compact mid-rise</div> 	Dense mix of mid-rise buildings (3–9 stories). Few or no trees. Land cover mostly paved. Stone, brick, tile, and concrete construction	0.3-0.6	0.75-2	40-70	30-50	<20	10-25
<div>3 – Compact low-rise</div> 	Dense mix of low-rise buildings (1–3 stories). Few or no trees. Land cover mostly paved. Stone, brick, tile, and concrete construction	0.2-0.6	0.75-1.5	40-70	20-50	<30	3-10
<div>4 – Open high-rise</div> 	Open arrangement of tall buildings to tens of stories. Abundance of pervious land cover (low plants, scattered trees). Concrete, steel, stone, and glass construction materials.	0.5-0.7	0.75-1.25	20-40	30-40	30-40	>25
<div>5 – Open mid-rise</div> 	Open arrangement of mid-rise buildings (3–9 stories). Abundance of pervious land cover (low plants, scattered trees). Concrete, steel, stone,	0.5-0.8	0.3-0.75	20-40	30-50	20-40	10-25
<div>6 – Open low-rise</div> 	Open arrangement of low-rise buildings (1–3 stories). Abundance of pervious land cover (low plants, scattered trees). Wood, brick, stone, tile, and concrete	0.6-0.9	0.3-0.75	20-40	20-50	30-60	3-10
<div>7 – Lightweight low-rise</div> 	Dense mix of single-story buildings. Few or no trees. Land cover mostly hard-packed. Lightweight construction materials (e.g., wood, thatch,	0.2-0.5	1-2	60-90	<20	<30	2-4
<div>8 – Large low-rise</div> 	Open arrangement of large low-rise buildings (1–3 stories). Few or no trees. Land cover mostly paved. Steel, concrete, metal, and stone	>0.7	0.1-0.3	30-50	40-50	<20	3-10
<div>9 – Sparsely built</div> 	Sparse arrangement of small or medium-sized buildings in a natural setting. Abundance of pervious land cover (low plants, scattered trees).	>0.8	0.1-0.25	10-20	<20	60-80	3-10

LCZ	Definition	SVF	Aspect ratio	Impervious fractions (%)		Pervious fraction (%)	Height elements (m)
				Built	Ground		
10 – Heavy industry 	Low-rise and mid-rise industrial structures (towers, tanks, stacks). Few or no trees. Land cover mostly paved or hard-packed. Metal,	0.6-0.9	0.2-0.5	20-30	20-40	40-50	5-15
NATURAL ZONES							
A – Dense trees 	Heavily wooded landscape of deciduous and/or evergreen trees. Land cover mostly pervious (low plants). Zone function is natural	<0.4	>1	<10	<10	>90	3-30
B – Scattered trees 	Lightly wooded landscape of deciduous and/or evergreen trees. Land cover mostly pervious (low plants). Zone function is natural	0.5-0.8	0.25-0.75	<10	<10	>90	3-15
C – Bush, scrub 	Open arrangement of bushes, shrubs, and short, woody trees. Land cover mostly pervious (bare soil or sand). Zone function is natural	0.7-0.9	0.25-1.0	<10	<10	>90	<2
D – Low plants 	Featureless landscape of grass or herbaceous plants/crops. Few or no trees. Zone function is natural grassland, agriculture, or urban	>0.9	<0.1	<10	<10	>90	<1
E – Bare rock or paved 	Featureless landscape of rock or paved cover. Few or no trees or plants. Zone function is natural desert (rock) or urban transportation.	>0.9	<0.1	<10	>90	<10	<0.25
F – Bare soil or sand 	Featureless landscape of soil or sand cover. Few or no trees or plants. Zone function is natural desert or agriculture.	>0.9	<0.1	<10	<10	>90	<0.25
G – Water 	Large, open water bodies such as seas and lakes, or small bodies such as rivers, reservoirs, and lagoons.	>0.9	<0.1	<10	<10	>90	–

LCZs were designed specifically for air temperature observations since geometric and surface cover parameters defining each class were selected because of their immediate influence on the thermal conditions at pedestrian level. Accordingly, few studies have applied the approach to examine SUHIs since classification values require further modifications for its implementation based on remotely sensed data (Bartasaghi Koc, Osmond, Peters et al., 2018). From the urban mapping perspective, these improvements should also address problems related to the optical and thermal mapping of urban surfaces such as the correct standardisation of the classification procedure; adequate image

resolutions (pixel size) and collection times; the temporal variability of physical properties, and the appropriate quantity and quality of images for time series analyses (Bechtel et al., 2015; Cai et al., 2017; Geletič et al., 2016; Geletič et al., 2017; Gémes et al., 2016; Irger, 2014; Skarbit et al., 2015).

Beyond its primary function, LCZs have also been used to map intra-urban land covers, so several GIS-based and remotely sensed classification methodologies were introduced and tested based on satellite data (Bechtel et al., 2016; Bechtel & Daneke, 2012; Kaloustian & Bechtel, 2016; Kotharkar & Bagade, 2016; Lelovics et al., 2014; Mitraka et al., 2015; Skarbit et al., 2015; Wicki & Parlow, 2017; Zheng, Y. et al., 2016). In fact, the World Urban Database and Access Portal Tools (WUDAPT) initiative (Bechtel et al., 2016) has emerged as a global cooperative effort to develop a widely available classification method that can be easily replicated in different cities using open-source data and software.

Despite the latest advances in the application of LCZs to urban mapping and thermal remote sensing, some methodological issues have arisen such as the standardisation of classification methods for different research purposes, the definition of appropriate spatial units for observations, the need for very high-resolution imagery and the temporal changes in the surface properties (*i.e.* vegetation phenology) (Bartesaghi Koc, Osmond, Peters, & Irger, 2017b; Bechtel & Daneke, 2012; Geletič & Lehnert, 2016; Lehnert et al., 2015; Zhongli & Hanqiu, 2016).

Although the LCZ system is well suited for the generic classification of urban form, its classification parameters have not been specifically developed for the differentiation of green infrastructure in terms of its abundance, composition and spatial arrangement. Thus, the application of this construct to the present dissertation is unsuitable and limited as it requires further modifications and improvements. These include the combination of several types of pervious surfaces (grasses, shrubs, deciduous/evergreen trees) within the same spatial unit, the consideration of the effect of water availability (rain and irrigation) and the incorporation of three-dimensional descriptors (*i.e.* derived from LiDAR) to consider the effects of vertical surfaces, the size of buildings and vegetation height (Bartesaghi Koc, Osmond, Peters et al., 2018).

However, in the absence of internationally agreed classification standards for green infrastructure (as demonstrated in Chapter 3), the conceptual and methodological frameworks proposed by Stewart and Oke (2012) for the development of LCZs have been adopted by the present thesis for the formulation of a new categorisation system enabling the analysis of the thermal regimes of green infrastructure at local scale. This new

taxonomic framework, typologies and specific value ranges are presented in Chapter 4; the methodological aspects for its implementation based on remote sensing data are discussed in Chapters 5 and 6; and the testing and validation results described in Chapter 7.

2.7 Summary

The intent of this chapter is to provide an overview of key interdisciplinary concepts, principles and aspects relevant to green infrastructure and the urban microclimate. These are necessary to achieve clarity in relation to the spatial scales and the climatic and physical phenomena governing the cooling effects of natural and artificial elements and surfaces in urban contexts.

From a *systemic* or *holistic* view, green infrastructure should be conceived and studied as a multi-scale, multi-temporal, highly heterogeneous and dynamic system comprising natural, semi-natural and man-made features; and their integrated flows of material and energy. Accordingly, three fundamental principles: (a) dynamic spatio-temporal heterogeneity, (b) spatial interconnectivity, and (c) multi-functionality are adopted for the development of new taxonomic and assessment frameworks that are presented in subsequent chapters.

Fundamental concepts and ideas about climatological scales, energy balance of surfaces and the types of UHI are also presented as these are crucial to define the classification framework for green infrastructure and the most adequate methods for the assessment of the thermal regimes of different typologies. Scientists recognise three main spatial scales for the study of the urban climate: the meso-, the local- and the micro-scale. Since a limited number of studies have been conducted at local-scale (as argued in Chapter 3), this thesis will particularly focus on this level as it is the most appropriate for planning and implementing green infrastructure cooling strategies. Furthermore, this is an intermediate level that corresponds to the urban planning and design of cities that is the concern of most local governments, planning authorities, developers and practitioners.

The study of thermal regimes of green infrastructure at the local scale also requires defining the type of climatological phenomena (particularly UHI) that will be targeted, as they differ in terms of physical properties and interactions, observational methods and data requirements. In this sense, this research specifically concentrates on studying the effects of green infrastructure on SUHIs. A systematic literature review on different methodological aspects is presented in Chapter 3 to support this choice. The review of

studies is also intended to identify key methods, indicators and data sources that are incorporated into the proposed assessment framework described in Chapter 5.

Examining the climatic benefits of green infrastructure over large urban areas presupposes a method of classification for a meaningful comparison of multiple sites. The LCZ is evaluated and discussed at the end of this chapter as a potential classification system to achieve this aim. Despite the multiple applications of the LCZs for the study of UHIs and urban mapping, this was designed specifically for heat island observations within the UCL (air temperatures), with less attention to the vegetation content (I. Stewart, personal communication, 2016); therefore, it is not well suited for the purposes of this thesis. However, this research draws on the methodological aspects, and classification criteria and descriptors implemented in the LCZ framework to propose a more targeted categorisation system which is further described in Chapter 4 and will serve to support the empirical investigations discussed in Chapters 7 and 8.

Chapter 3

Assessing the cooling effects of green infrastructure: *A systematic review*⁶

3.1 Introduction

Nowadays, a primary concern of the broad scientific community and, more specifically, of climatologists is the increase in the frequency and intensity of heatwaves and extreme urban temperatures associated with UHIs, which are causing significant impacts on the global economy, and the human health and well-being (Bowler et al., 2010b; Manteghi et al., 2015; Oke et al., 1989; Oke, 1992; Völker et al., 2013). As demonstrated in Chapter 2, green infrastructure can be implemented as an effective heat mitigation strategy as it moderates the negative effects of urban warming through shading, evaporative cooling, and the modification of airflows and heat exchange (Bowler et al., 2010b; Hunter et al., 2012; Oke et al., 1989; Santamouris, 2015; Völker et al., 2013).

Intensive research has been conducted in recent years to understand the impacts of green infrastructure on urban microclimate, and results have been extensively documented in the literature. However, the critique of key methodological aspects (*i.e.* methods, parameters, data collection procedures) and the advantages or disadvantages of one over another remains unattended. The main purpose of this chapter is to identify current knowledge gaps to define the most adequate methodological framework for this research. Furthermore, it is intended to analyse the existing evidence for a more integrated understanding and interpretation of the findings given the disparity of exiting studies in terms of geographic contexts, climates, scales, types of vegetation studied, research methods, needs and resources (data, instrumentation).

⁶ A version of Chapter 3 has been published: Bartesaghi Koc, Osmond, and Peters (2018), Evaluating the cooling effects of green infrastructure: A systematic review of methods, indicators and data sources, *Solar Energy*, 166, p. 486-508.

This chapter begins with an overview of the evidence summarised by most recent literature reviews followed by a systematic review of studies investigating the cooling effects of green infrastructure. Given the extensive number of studies published in recent years, this review is restricted to the most representative research conducted since 2010 comprising air and surface temperatures, CLUHI, SUHI, thermal comfort and heat stress observations.

The results of the review and synthesis of evidence consists of six major sections. The first section analyses the geographic patterns and typical climate zones that have attracted the most attention from climate researchers around the world. In the second section scholarly papers are organised into topics and sub-topics according to their main research focus and interests to examine the interactions among them. The third section describes which green infrastructure types receive most attention in the literature and examines the relationship between climatological scales and green infrastructure types studied.

The fourth section summarises the most common parameters investigated; meanwhile in the fifth section, different methods of investigation, data sources, data acquisition and data processing protocols are discussed followed by an analysis of the advantages and disadvantages of one over another. Finally, the last section focuses on the investigation period of studies, particularly seasons, times of the day and duration of measurements. The remainder of the chapter critically examines the results of this systematic review to provide a summary of key methodological shortcomings, gaps, and suggestions that will be addressed by and incorporated to the proposed frameworks described in Chapters 4 and 5.

3.2 Methods

This chapter applies a systematic literature review following the approaches of Khan et al. (2003), Pickering and Byrne (2013) and Pullin and Stewart (2006). This method differs from typical critical reviews since it integrates a body of literature by methodically extracting specific data from a representative number of studies within a certain period (Pullin & Stewart, 2006; Stewart, 2011a, 2011b). This information is integrated into a single study for the quantitative and qualitative analysis and synthesis of evidence. Moreover, a systematic review must be reproducible by other researchers, explicit in defining specific research questions and selection criteria, and comprehensive in examining the full literature (Khan et al., 2003). In this chapter, a systematic review was conducted to identify geographical patterns⁷, theoretical trends and, more importantly, methodological gaps.

⁷ Affiliations of main authors were used to determine the origin of publications.

In accordance to Khan et al. (2003), Pullin and Stewart (2006) and Stewart (2011a) the present review followed five key stages. Firstly, specific review questions were formulated in terms of the aims and objectives of this thesis and are listed in Appendix A. These were necessary to define the review protocols, the screening criteria and the data to be extracted from each paper. The second stage consisted in identifying relevant publications. This searching process was carried out using three major databases including Google Scholar, Web of Science and Scopus, and combined terms such as *cooling*, *vegetation*, *green infrastructure*, *urban heat island*, *thermal comfort* and *temperature*. The search results were limited to the most recent journal papers using Bowler et al. (2010b) review as a time limit. In the third phase, a representative sample of relevant articles was selected and assessed against the following quality selection criteria:

- a. Publications were peer-reviewed and in English (the exclusion of non-English studies is a limitation that could imply a possible bias in the interpretation of findings).
- b. Studies evaluated any of the following green infrastructure categories: (1) tree canopy; (2) green open spaces; (3) water bodies; (4) green roofs; and (5) vertical greenery (green walls and green facades).
- c. Studies measured or simulated climatic conditions based on a specific geographic location and/or climate zone and compared results against vegetation-related indicators. Studies only measuring or reporting on SUHI, CLUHI or temperature reductions were not included.
- d. Articles reporting on simulations using synthetic data or with unspecified sites were also excluded.
- e. Studies at global scale, over vast regions, or using community land models (Kvalevåg et al., 2010; Lawrence & Chase, 2010; Peng et al., 2014; Shen, M. et al., 2015; Shen, X. et al., 2015; Wang, M. et al., 2015; Xiao, 2014) were not included.
- f. Operational definitions, instrument specifications and data sources were explicitly or implicitly stated.

In the fourth phase, the extraction of information and analysis of evidence was based on a set of thematic aspects corresponding to commonly agreed criteria identified from the literature [Figure 3.1]. These are fundamental aspects to be considered for investigating the climatic effects of green infrastructure. In the last phase, the data synthesis and interpretation of findings was conducted using both qualitative and quantitative analysis with basic statistical methods.

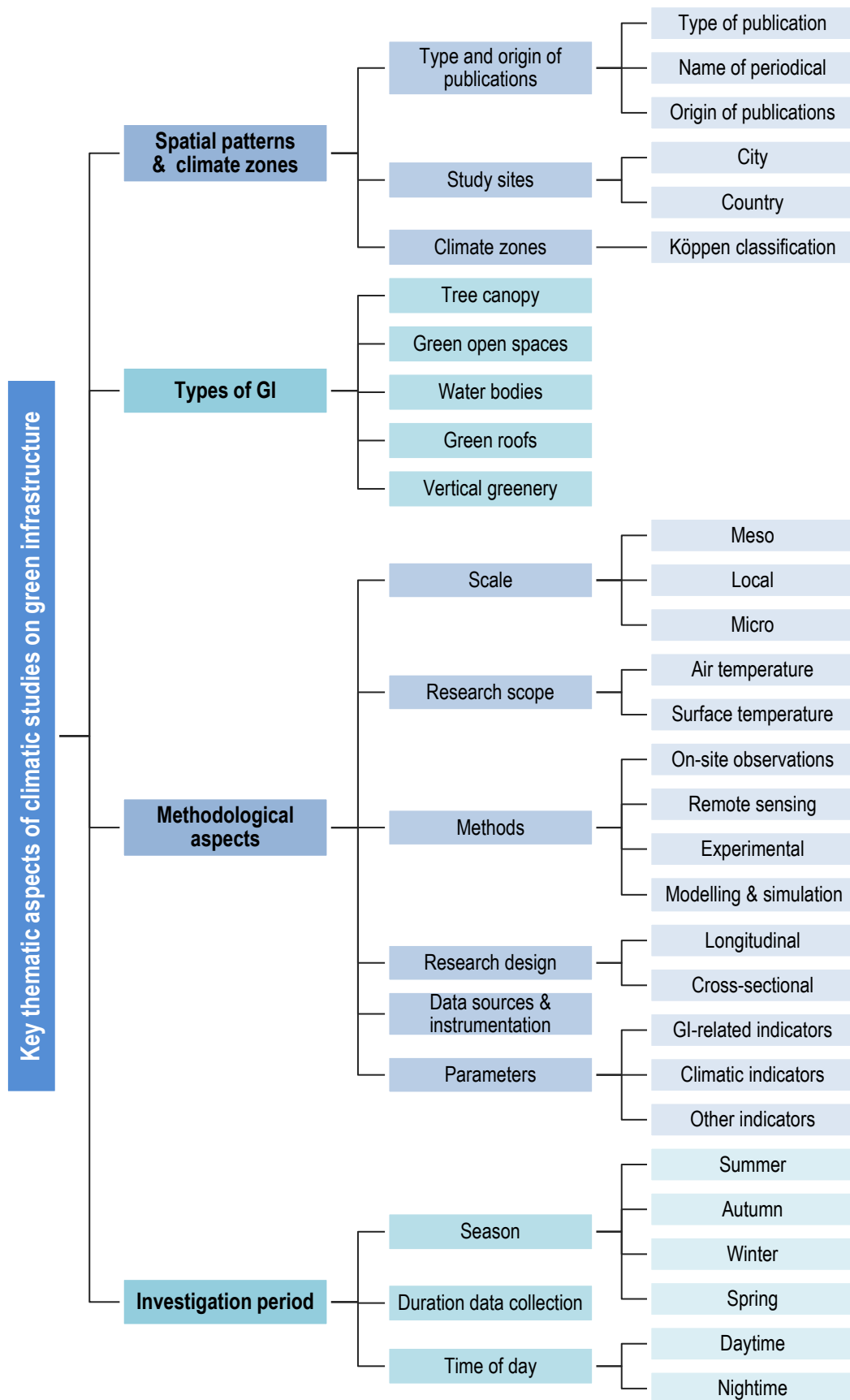


Figure 3.1 List of thematic aspects identified in the reviewed literature that are fundamental for investigating the climatic effects of green infrastructure. (Based on Bartesaghi Koc, Osmond, and Peters (2018))

3.3 Overview of existing evidence

In recent years, intensive research has been carried out to explore and understand the impacts of qualitative and quantitative attributes of green infrastructure on the urban climate; evidence that has been well-documented in previous literature reviews. A comprehensive meta-analysis on the cooling effects of parks, trees and green roofs provided by Bowler et al. (2010b) suggests that an urban park can be up to 1°C cooler on average compared to a non-green site. However, their review was mostly based on air temperature observations of small number of green sites, excluding studies focusing on surface temperature and simulation. The lack of an appropriate description and classification of the urban greenery has been identified as an important barrier hindering the reliability and comparability of studies (Bowler et al., 2010b). Further research is also required to understand the impact of abundance, distribution and type of greenery in the modification of urban microclimates (Bowler et al., 2010b).

Zupancic et al. (2015) presented a review to examine the capacity of greenspaces and urban trees to help mitigate heat and air pollution. Their findings also suggest that the thermal capacities of vegetation are clearly influenced by physical and configurational characteristics and that further research is required on these two particular aspects (Zupancic et al., 2015). They also identified multiple confounding variables that may affect the cooling capacity of urban greenery, especially building density or urban compactness, which deserve more control and attention.

The critical review conducted by Motazedian and Leardini (2012) exclusively focused on studies measuring air temperatures within and near parks by comparing two methodological approaches, on-site measurements and numerical modelling. Since costs and time constraints limit comparative analyses over longer periods, simulations and modelling have been frequently employed to overcome these limitations (Motazedian & Leardini, 2012). Accordingly, Motazedian and Leardini (2012) suggest the combination of both approaches for better, more reliable and comprehensive analyses.

The UCIs and PCIs refer to phenomena where greenspaces and their immediate surroundings have lower temperatures than that of impervious surfaces (Chen et al., 2014; Spronken-Smith & Oke, 1998). Unlike PCIs, UCIs can be also attributed to urban morphology descriptors (*i.e.* H/W ratio and SVF), the properties of materials (*i.e.* albedo, emittance), air flow rates and the presence of anthropogenic heat (Yang et al., 2017). Zhao-wu et al. (2015) summarised current research on UCIs by identifying aspects such as UCI thresholds, cooling intensities, and maximum cooling extents of greenspaces using remote

sensing and simulation. They concluded that future studies should pay more attention to the types of species, location and altitude of greenspaces, and morphological (*i.e.* size, shape, area), and configurational aspects of both vegetation and water bodies (Zhao-wu et al., 2015). Furthermore, long-term observations should be strengthened and more attention should be paid to the spatial scale and image resolution for a more accurate analysis of the spatial and temporal evolution of UCIs (Zhao-wu et al., 2015).

UCIs and PCIs are also important for improving HTC conditions by decreasing mean radiant temperatures. Thus, the quantitative evaluation of the urban greening contributions to HTC and heat stress reduction has been the subject of several reviews (Hiemstra et al., 2017; Jamei et al., 2016; Taleghani, 2017). Hiemstra et al. (2017) presented the main findings of studies from several European and Mediterranean countries by comparing their reported PCI magnitudes. Results show that cooling effects of greenspaces are quite substantial for all studies despite the disparity of climate and physical characteristics, which reported maximum PCI magnitudes between 1.5 and 9.5 °C.

Similarly, Jamei et al. (2016) undertook a review of studies focusing on the effects of vegetation and urban geometry on pedestrian thermal comfort. They found that geographical, structural (*i.e.* Aspect ratio, orientation, SVF) and seasonal factors from each urban context should be considered for the correct choice of vegetation (*i.e.* type of foliage, size, location within the canyon) since this may provide different outdoor thermal effects in summer and in winter. However, planning policies and urban design strategies do not fully incorporate these aspects at the moment of proposing a new settlement (Jamei et al., 2016). Taleghani (2017) reviewed the effect of different heat mitigation strategies on outdoor thermal comfort and concluded that the use of vegetated and artificial surfaces with high albedo (reflective) properties is the most effective solution for reducing MRT and thus, for improving the thermal conditions at pedestrian level.

Santamouris (2014) reviewed simulation studies on reflective and green roofs to evaluate the capacity of meso-scale predictive modelling to inform city scale interventions. Evidence suggests that green roofs, when applied at the city level, may decrease average air temperatures between 0.3 and 3K (Santamouris, 2014). Furthermore, Charoenkit and Yiemwattana (2016), Hunter et al. (2014) and Pérez et al. (2014) evaluated several simulations and experimental studies on vertical greenery used to improve the indoor thermal comfort and energy savings in buildings. These papers mainly focused on climatic conditions, morpho/physiological characteristics, and operability of green facades/walls at microscale, putting aside the methodological aspects. Generally, the application of living

walls and green facades shows a reduction of surface temperatures of building facades between 1 to 15 °C for studies in warm temperate climates (Pérez et al., 2014).

From a remote sensing perspective, Weng (2009) focused on studies examining the influence of vegetation on LST reduction by undertaking a comprehensive review of methods, indicators and data sources. He concluded that most previous work mainly concentrated on understanding the relationships between bio-physical properties of surfaces, vegetation abundance (*i.e.* vegetation indices and land use/land cover types) and their corresponding LST patterns (Weng, 2009). There were also identified gaps for potential research which include the derivation of UHI parameters from LST data and the implementation of remote sensing to calculate surface energy fluxes (Weng, 2009). Although there is an increasing number of remote sensing studies giving special attention to the influence of spatial patterns and configuration of green spaces on LST, reviews on this topic are scarce.

Heat reductions have been broadly attributed to vegetation, but cooling effects have not been established with the same accuracy and precision for water bodies (Völker et al., 2013). Literature has reported on the cooling benefits of water bodies irrespective of vegetation since the thermal properties and cooling mechanism of water differ from those of vegetated surfaces (Manteghi et al., 2015; Oke, 1992; Spronken-Smith et al., 2000; Völker et al., 2013). Although literature on water bodies remains sparse, Gunawardena et al. (2017), Manteghi et al. (2015) and Völker et al. (2013) have presented detailed reviews on this topic, and meta-analyses suggest an air temperature reduction within and near water bodies up to 2.5K (CI 95%, $p < 0.01$) (Völker et al., 2013); and between 2 to 6°C (Manteghi et al., 2015). Until now, evidence on the impacts of water in SUHI mitigation and LST reductions has not been properly reviewed.

3.4 Geographic patterns and climate zones

After the screening process, a total of 165 journal articles from 31 countries and/or territories were identified as eligible for the systematic review of this chapter. In addition, a total of 178 single-studied sites were extracted from the scholarly papers. This number differs from the numbers of articles because many papers investigated more than one location at a time. A complete list of authors, investigated sites, and the extracted data from each study is chronologically presented in Appendix B.

Papers were published in 52 different journals from a wide range of disciplines [Table 3.1], although three journals were dominant – *Building and Environment*, *Landscape and Urban*

Planning and Urban Forestry and Urban Greening. This demonstrates the trans-disciplinary interest of scholars in this topic, with special interest of those in the fields of environment/ecology, urban planning/landscape, arboriculture/forestry, climatology, and energy.

Analysis based on author affiliations shows reviewed papers are predominantly written in Asia (43%), Europe (31.5%) and North America (15.8%), with a strong bias toward three countries: China (18.2%), USA (14.5%) and Hong Kong (7.3%). These figures show the increasing interest of climatologists in developed and industrialised countries in the thermal benefits provided by nature, while these aspects remain unattended by most developing countries [Figure 3.2a, 3.2b]. The geographic distribution of study sites displays an analogous pattern [Figure 3.2c]. From 178 single-studied sites, research is predominantly conducted in Asia ($n=71$, 39.9%), Europe ($n=62$, 34.8%) and North America ($n=26$, 14.6%). Much fewer locations correspond to Oceania ($n=7$, 3.9%), South America ($n=7$, 3.9%) and Africa ($n=5$, 2.8%).

In a country-based analysis, it can be observed a heavy geographic bias toward three countries: China ($n=28$, 15.7%), USA ($n=25$, 14%) and Hong Kong ($n=12$, 6.7%). In a city-based analysis, Beijing ($n=13$), Hong Kong ($n=12$), Phoenix ($n=9$), Athens ($n=6$), Nagoya ($n=6$) and Singapore ($n=6$) are the most investigated. Some other cities are also investigated and include Chicago ($n=4$), Melbourne ($n=4$), Nanjing ($n=4$), Shanghai ($n=4$), Tel Aviv ($n=4$) and Taipei ($n=4$) [Figure 3.2a].

Most studies (83%) corresponds to the northern hemisphere and at higher latitudes, while research within the tropics ($n=28$, 15.7%) and the southern hemisphere ($n=12$, 6.7%) are underrepresented [Figure 3.2a]. According to the updated Köppen-Geiger climate classification (Kottek et al., 2006), studies show a strong bias toward warm, temperate and fully humid climates, particularly the *Temperate oceanic* (*Cfb*) ($n=47$, 26.4%) with warm summers and the *Humid subtropical* (*Cfa*) ($n=36$, 20.2%) and *Cwa* ($n=13$, 7.3%) with hot summers. Studies also concentrate on the *Hot-summer Mediterranean* (*Csa*) ($n=22$, 13.4%), the *Humid continental* (*Dwa*) ($n=15$, 8.4%), and the *Hot desert* (*BWh*) ($n=13$, 7.3%) climates [Figure 3.2d]. Very few studies correspond to *Hot semi-arid* (*Bsh*) ($n=4$, 2.3%), *Cold semi-arid* (*Bsk*) ($n=4$, 2.3%), *Cold desert* (*Bwk*) ($n=3$, 1.7%), *Tropical monsoon* (*Am*) ($n=2$, 1.1%), *Warm summer Mediterranean* (*Csb*) ($n=2$, 1.1%), *Subtropical highland* (*Cwb*) ($n=1$, 0.6%) and *Continental Mediterranean* (*Dsa*) ($n=1$, 0.6%) climates. However, knowledge about these climate zones is crucial as vegetation, irrigation and cooling requirements are considerably different to those proposed for temperate climates [Figure 3.2d].

Table 3.1 List of journals and disciplines containing most papers that investigated the cooling effects of green infrastructure. Disciplines based on Roy et al. (2012) categorisation.

Discipline (# journals per discipline)	Name of journal	# papers per journal	# papers per Discipline
Arboriculture and forestry (3)	Agricultural and Forest Meteorology	2	20
	HortScience	1	
	Urban Forestry & Urban Greening	17	
Architecture (2)	Architectural Science review	5	6
	Building Services Engineering Research and Technology	1	
Climatology (9)	Atmosfera	1	19
	Boundary-Layer meteorology	1	
	Climatic Change	1	
	International Journal of Climatology	4	
	International Journal of Biometeorology	1	
	International Journal of Global Warming	1	
	Journal of Applied Meteorology and Climatology	2	
	Theoretical and Applied Climatology	5	
	Urban Climate	3	
Energy (6)	Applied Energy	2	15
	Energy and Buildings	8	
	Energy Procedia	1	
	Energy Conversion and management	1	
	Renewable Energy	2	
	Solar Energy	1	
Environment and ecology (14)	Asian Journal of Atmospheric Environment	1	62
	Building and Environment	38	
	Ecological Indicators	3	
	Ecological Engineering	1	
	Environmental monitoring and assessment	1	
	Environmental pollution	1	
	Environmental Research letters	1	
	Hydrological Processes	1	
	Indoor and Built Environment	1	
	Landscape ecology	4	
	Science of the total environment	1	
	Sustainability	3	
	Sustainable Cities and Society	4	
	Urban Ecosystems	2	
Geography (6)	Applied Geography	1	7
	Geographical Analysis	1	
	International Journal of Geomate	1	
	Journal of Geophysical Research	2	
	Journal of Geophysical Research	1	
	Progress in Physical Geography	1	
Remote sensing (6)	GIScience & Remote Sensing	1	11
	International Journal of Remote Sensing	4	
	ISPRS Journal of Photogrammetry and Remote Sensing	2	
	Journal of Applied Remote sensing	1	
	Remote Sensing	1	
	Remote Sensing of Environment	2	
Urban planning/landscape (3)	Journal of Urban Planning and Development	2	22
	Landscape and Ecological Engineering	1	
	Landscape and Urban Planning	19	
Other (3)	International Journal of Simulation	1	3
	Natural Hazards	1	
	Procedia Engineering	1	
TOTAL		165	165

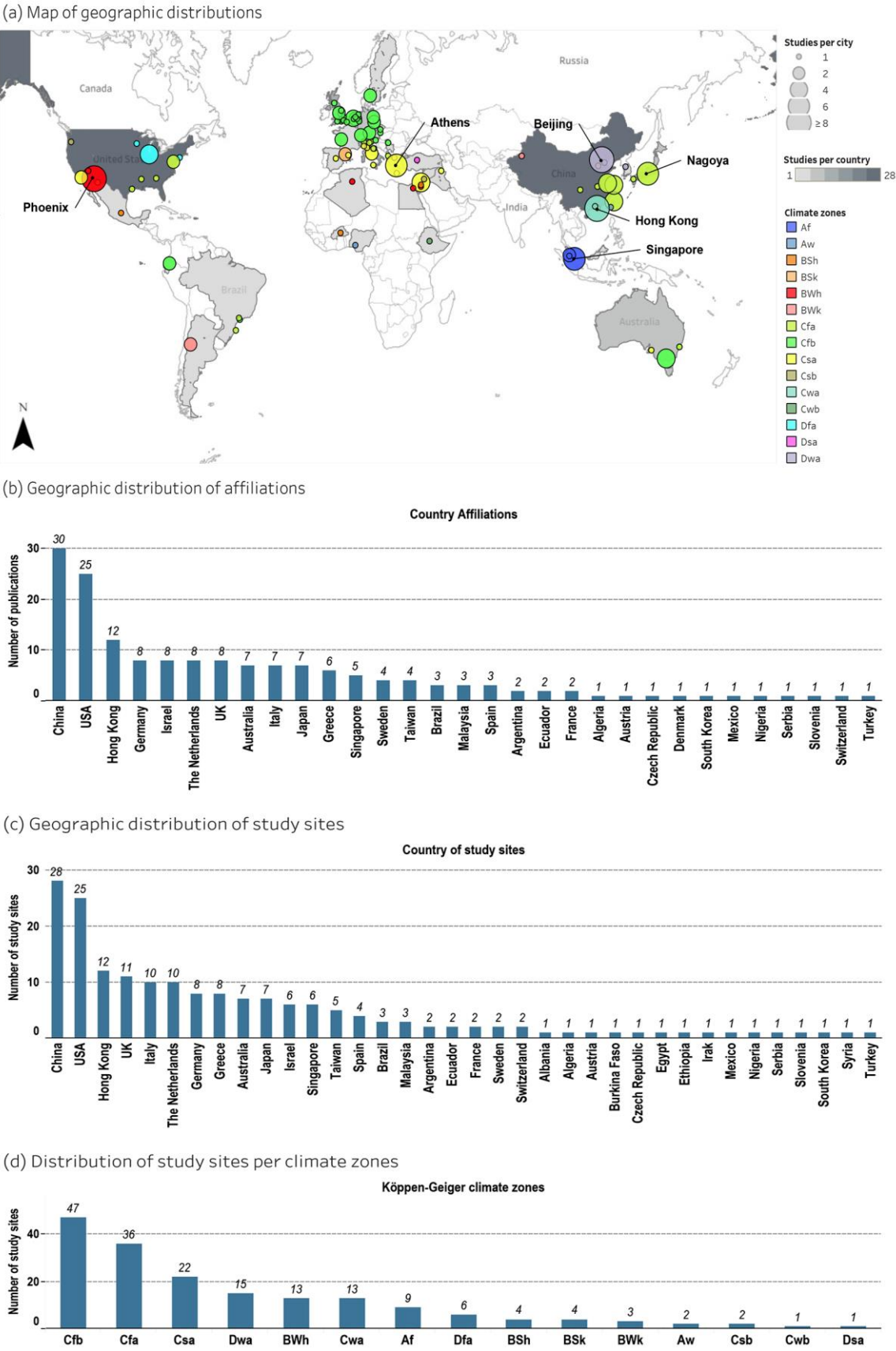


Figure 3.2 Geographic distribution of reviewed literature based on affiliations, study locations, and climate zones.

Factors influencing these geographic patterns may be attributed to: (a) the restriction of the review to publications in English and the limited time and resources to include papers in other languages; (b) the country-based disparity in terms of the number of researchers and available funding; (c) the inability to retrieve and access articles and data from underrepresented regions; (d) the interest of climate researchers in studying cities with severe UHIs (*i.e.* Athens, Beijing, Hong Kong); and (e) research driven by need; for instance, it is not expected temperature-related studies in high latitude cities with low solar intensity or in desert regions with little or no green spaces because of adverse growing conditions.

Previous results demonstrate that more research is necessary regarding the thermal benefits of urban greening in developing countries, southern-hemisphere regions, and many tropical and desert climates. This is particularly important for many cities located in Africa, South America, Oceania, Middle East, South-East Asia and India which are highly urbanised, with large populations, and severely affected by extreme weather conditions.

3.5 Research focus and topics

Generally, researchers study the thermal performance of green infrastructure by analysing the magnitude and intensity of its thermal effects in different types of UHIs (Oke, 2009). In this sense, the papers can be grouped in three main research topics: (a) the regulatory effect of vegetation on air temperatures which is associated to CLUHIs ($n=115$, 69.7%); (b) the reduction of the temperature of urban surfaces which relates to SUHIs ($n=86$, 52.1%); and (c) the analysis of the relationship between air and surface temperature reductions ($n=36$, 21.8%) [Figure 3.3].

Studies can also be divided on specific sub-topics; for example, 42 studies (25.5%) pay attention to HTC, 16 studies (9.7%) focus on evapotranspiration, and 17 studies (10.3%) examine the impact of the spatial configuration of greenspaces on the patterns of SUHIs. Several papers analyse the intensity, extent and spatial variability of PCIs ($n=11$, 6.7%) and UCIs ($n=7$, 4.2%); while very few papers ($n=3$, 1.8%) are interested in thermal sub-surface conditions. Figure 3.3 presents the distribution, interactions and overlaps among reviewed studies within each topic and sub-topic. A full summary of reviewed bibliography is presented in Appendix B.

As can be observed in Figure 3.3, research scopes are diverse, although studies typically examine the cooling effects of green infrastructure on air and surface temperatures separately. HTC is a sub-topic that attracts the attention of most air-temperature studies;

nonetheless, the effect of evapotranspiration on pedestrian thermal comfort is not fully quantified and analysed in the literature. Similarly, the evaluation of human perceptions could be incorporated in or compared against results from simulation and models (*i.e.* ENVI-met). UCI and PCI are commonly used interchangeably among many studies; however, as previously discussed, these are two different phenomena that should properly be differentiated as the former can be also attributed to urban morphology aspects and human activities (*i.e.* building density, street orientation, traffic, abundance of air-conditioning) (Yang et al., 2017). Furthermore, the effect of spatial configuration of vegetation on air temperatures remains relatively unexplored and it mainly concentrates on surface temperature distributions.

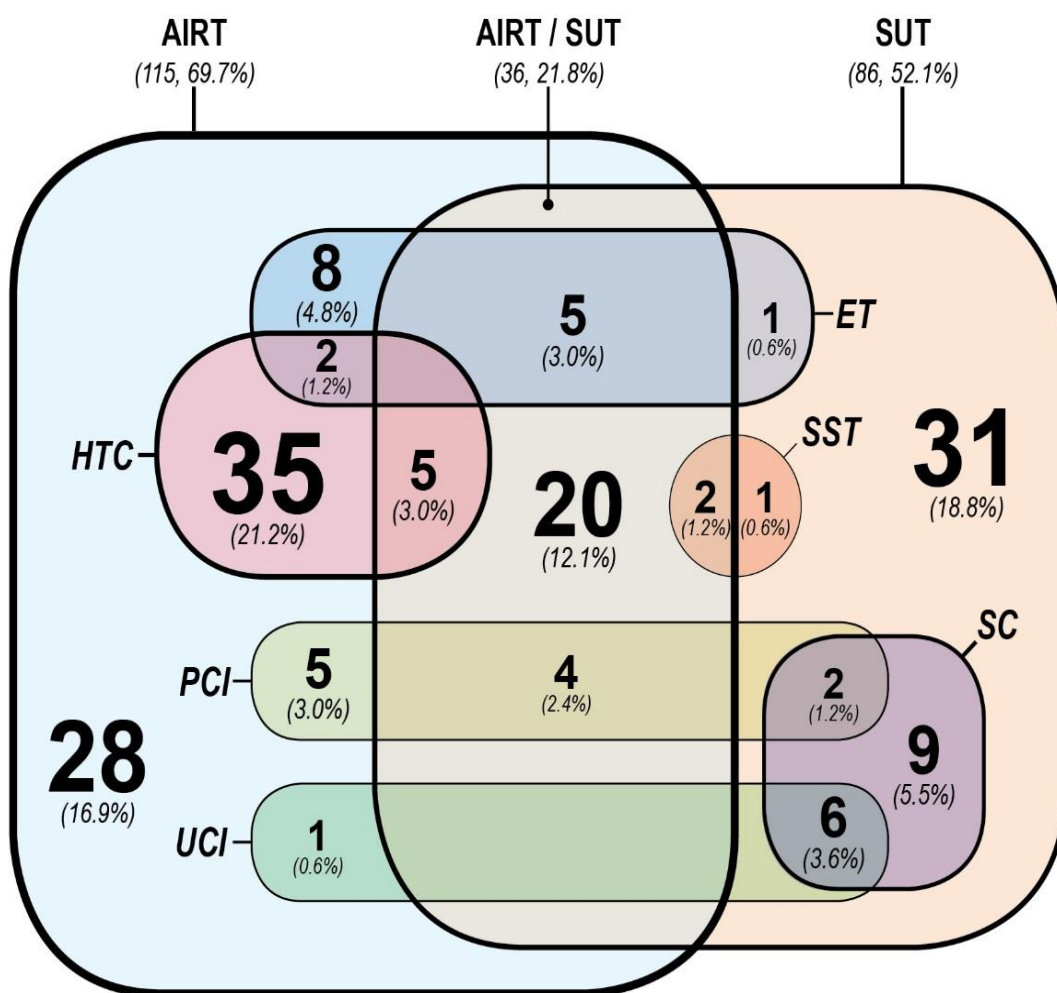


Figure 3.3 Venn diagram depicting the percentage distribution, interactions and overlaps of main research topics and sub-topics investigated by the reviewed literature on thermal performance of green infrastructure.

AIRT Air temperature, *SUT* Surface temperature, *ET* evapotranspiration, *HTC* Human thermal comfort, *UCI* Urban cool island, *PCI* Park cool island, *SC* Spatial configuration, *SST* Sub-surface temperature. Shape sizes and widths of outlines are proportional to level of interest per topic.

3.6 Green infrastructure types and scale of analysis

Due to the lack of robust and widely accepted typologies to support climate research, investigations adopted terms from related disciplines which restrain the comparability of evidence and case studies (Bowler et al., 2010b). To respond to this need, five high level green infrastructure categories are identified in Chapter 4 as a result of a systematic review of classification methods and approaches.

These categories are also employed in this section to identify the interest of studies on particular green infrastructure types; and correspond to (a) tree canopy (TC); (b) green open spaces (GOS); (c) green roofs (GR); (d) vertical greenery systems (VGS); and (e) water bodies (WB) (Bartesaghi Koc et al., 2016, 2017).

Among these categories, two-thirds of papers ($n=113$, 68.5%) studied the cooling benefits of greenspaces ($n=38$, 23.0%) and tree canopies ($n=31$, 18.8%) either individually, or jointly ($n=44$, 26.7%) [Table 3.2]. The latter generally applies when trees are part of a major greenspace (*i.e.* trees within parks) or are analysed at large scales (*i.e.* trees considered as woodland or forest). The increased attention on these two categories responds to the wide-ranging implications and multiple services that both provide to the built environment, especially on outdoor thermal comfort.

Table 3.2 Distribution of different green infrastructure types studied by literature according to their scale of analysis.

GI type	Scale							Grand Total
	Micro	Meso	Local	Meso / Local	Local / Micro	Meso / Micro		
TC-GOS	 13	 12	 16	 1	 1	 1		 44
GOS	 5	 19	 11	 2	 1			 38
TC	 27		 4					 31
VGS	 18		 1					 19
GR	 14	 1				 1		 16
WB	 1	 6	 2					 9
Multi-types	 3	 1	 4					 8
Grand Total	 81	 39	 38	 3	 2	 2		 165

Colour shows details about scale and size shows details about the total number of publications.

Contrastingly, studies examining the thermal profiles of vertical greening ($n=19$, 11.5%), and green roofs ($n=16$, 9.7%) are less numerous [Table 3.2]; and their cooling benefits are typically associated with indoor thermal comfort and energy consumption. It is evident that more research is necessary to evaluate the effects of greenery on buildings at the pedestrian level and to investigate their large-scale cooling potentials beyond simulation.

Studies on water bodies ($n=9$, 5.5%) are very few and usually combined with those of greenspaces [Table 3.2]. Therefore, forthcoming research should focus on understanding the role of geometry and spatial distribution in the thermal performance of water bodies and on examining the diurnal and nocturnal patterns and differences of both surrounding air and surface temperatures.

Few papers conducted analyses of multiple green infrastructure types simultaneously ($n=8$, 4.8%) [Table 3.2]. Indeed, green infrastructure types are commonly analysed individually due to several limitations such as lack of adequate taxonomies and issues related to data collection (deployment, cost, data mismatch, etc.). Hence, the comprehensive study of the combinatory effects of different vegetation surfaces and features, along with other urban characteristics is very challenging, although a very promising area for upcoming research. Nonetheless, as pointed out by Bowler et al. (2010a, 2010b), a confident comparison, reporting and prediction of the thermal regimes of multiple types at once requires universally agreed typologies and protocols. Since the development of such standardised classification scheme is crucial for climate studies, and more especially for this research, this gap is addressed in Chapter 4.

The selection of a specific spatial scale of observation depended on several factors, namely the type of green infrastructure, the extent of the case study area and the type of climatological phenomena targeted. Since the types of measurements, indicators, and methods vary across spatial scales (Erell et al., 2011; Oke, 2006); studies can be categorised according to the three main climatological scales –meso, local and micro– as per section 2.4.1 from Chapter 2.

In accordance, most papers investigated the thermal effects of green infrastructure at the microscale ($n=81$, 49.0%), which include the study of the cooling effects of trees on air temperatures and HTC conditions of street canyons, small and medium courtyards and other outdoor spaces ($n=40$), as well as the thermal benefits and energy savings of green walls/facades ($n=18$) and green roofs ($n=14$) in indoor spaces.

Studies at the meso scale ($n=39$, 23.6%) covered larger areas such as cities and regions and mainly examined the widespread role of greenspaces and tree canopy in reducing LST and mitigating SUHIs. A similar number of studies ($n=38$, 23.0%) evaluated the effects of trees and greenspaces in neighbourhoods and urban precincts, corresponding to the local scale.

Although the local scale is the level at which most urban planning and design occurs (Norton et al., 2013); there is still little knowledge about the most effective types, abundance, composition and arrangement of green infrastructure needed for mitigating heat

and improving thermal comfort at urban precinct, neighbourhood and street canyon levels (Bowler et al., 2010b; Coutts & Harris, 2012; Kong et al., 2013; Morakinyo & Lam, 2016; Norton et al., 2013; Shashua-Bar & Hoffman, 2000; Zupancic et al., 2015). Moreover, comprehensive knowledge on how green infrastructure heterogeneity influences the spatio-temporal variability of temperatures at multiple spatial scales is still missing (Buyantuyev & Wu, 2010). Furthermore, multi-scale analyses were not common among the literature ($n=7$, 4.2%) [Table 3.2].

3.7 Common parameters of analysis

The thermal analysis of green infrastructure typically involves the study of the relationships between quantitative and qualitative descriptors of green infrastructure (considered as *independent variables*) and the climatological conditions (considered as *dependent variables*) of the study site [Table 3.3]. In this review, vegetation-related parameters were categorised into three main groups corresponding to: (a) the functional indicators (*i.e.* photosynthetic activity and evapotranspiration), (b) the structural composition (*i.e.* type, size, height, morphology, area, type of leaf, etc.), and (c) the spatial distribution of vegetation.

In some cases, the abovementioned relationships are also influenced by intervening or confounding variables resulting from morphological, climatological and anthropogenic factors (*i.e.* wind effects, distance to coast, building shade and traffic load) [Table 3.3]. However, this information is often vaguely reported or completely obviated in the literature. Generally, the selection of variables mostly depends on the research focus, scales and types of green infrastructure under study.

Ideally, studies should incorporate indicators from these three categories for a more comprehensive analysis. Nonetheless, it was observed that better data collection and reporting protocols should be established as well as a better control of the effect of intervening variables such as wind, precipitation, topography, surrounding urban form and anthropogenic heat. This could significantly reduce the bias and inaccuracy of results and facilitate the comparability of results among different settings.

The remainder of this section concentrates on describing and analysing the main methods of analysis and their corresponding data sources and data acquisition protocols used for retrieving and estimating the most widely used parameters from Table 3.3. This information is accompanied by a discussion on current shortcomings and potential improvements.

Table 3.3 List of common dependent (DEP), independent (IND) and intervening (INT) variables analysed by studies.

Variable	Type	Focus	Key parameters	
DEP	Climatological	Ambient air, thermal comfort	- Air temperature (T_{air}) - Mean radiant temperature (T_{mrt})	- Relative humidity
		Surfaces	- Surface temperature (T_{surf}) - Soil temperature (sub-surface)	- Short-/long-wave radiation - Heat flux
IND	Functional	Photosynthetic activity	- Normalised difference vegetation index (NDVI) - Enhanced vegetation index (EVI) - Greenness index (VGI)	- Stomatal conductance/resistance - Photosynthetically active radiation (PAR)
		Vegetation abundance / shading	- Leaf area index (LAI) - Leaf area density (LAD)	- Biophysical composition index (BCI)
		Evapotranspirative cooling	- Evapotranspiration rate (ET_o) - Wetness Index (WI)	- Normalised difference water index (NDWI)
	Morphological	Surface fractions	- Land-use/land-covers (LULC) - Vegetation, impervious (ISF), building and water fractions	- Normalised difference built-up index (NDBI) - Local Climate Zones (LCZ)
		Surface properties	- Surface emissivity (ϵ) - Surface albedo - Brightness index (BI) - Thermal conductivity - Solar absorption capacity - Surface permeability	- Substrate type (green roofs) - Depth of substrate (green roofs) - Soil moisture - Soil water content - Soil density - Irrigation rate
		Bio-physical attributes	- Type of foliage - Plant species - Plant solar transmissivity - Leaf colour and thickness	- Leaf absorptivity - Leaf transmittance - Leaf radiation attenuation coefficient
		Formal attributes	- Geometry, size, shape, area & height	
		Supporting structure attributes	- Training system/attachment mode (for green walls/facades)	- Type of supporting material - Dimensions of structures
	Configurational	Spatial distribution	- Vegetation arrangement - Local Moran's I index ¹	- Size-distance index
		FRAGSTATS Landscape metrics ¹	- Percentage of landscape - Landscape shape index - Patch area - Patch density - Largest patch index - Shape Index - Number of patches - Mean patch area/size - Mean patch shape index - Largest patch index - Total edge - Edge density - Class area	- Perimeter area ratio - Mean patch area - Perimeter-area ratio - Aggregation index - Fractal dimension - Contagion - Shannon's diversity - Euclidian nearest-neighbour distance - Neighbourhood green area - Neighbourhood green proportion - Area-weighted mean radius of gyration
INT	Climatological	Air cooling	- Wind direction (V_d) - Wind velocity (V_a)	- Roughness length (Z_o) - Coastal proximity
		Surface cooling, other influencers	- Solar radiation - Air pressure (P_a)	- Rainfall - Cloud cover
	Morphological	Moderating effect of built forms	- Aspect ratio (H/W) - Sky view factor (SVF) - Local climate zones (LCZ) - Volumetric density of buildings	- Altitude and elevation - Solar orientation (aspect) - Topography - Urban vegetation structure types (UVST)
	Other	Human-related factors	- Land-use types - Anthropogenic heat (traffic flow)	- Pollution levels - Socio-economic status

¹ Metrics by McGarigal and Marks (1995) and calculated with FRAGSTATS software (McGarigal et al., 2002)

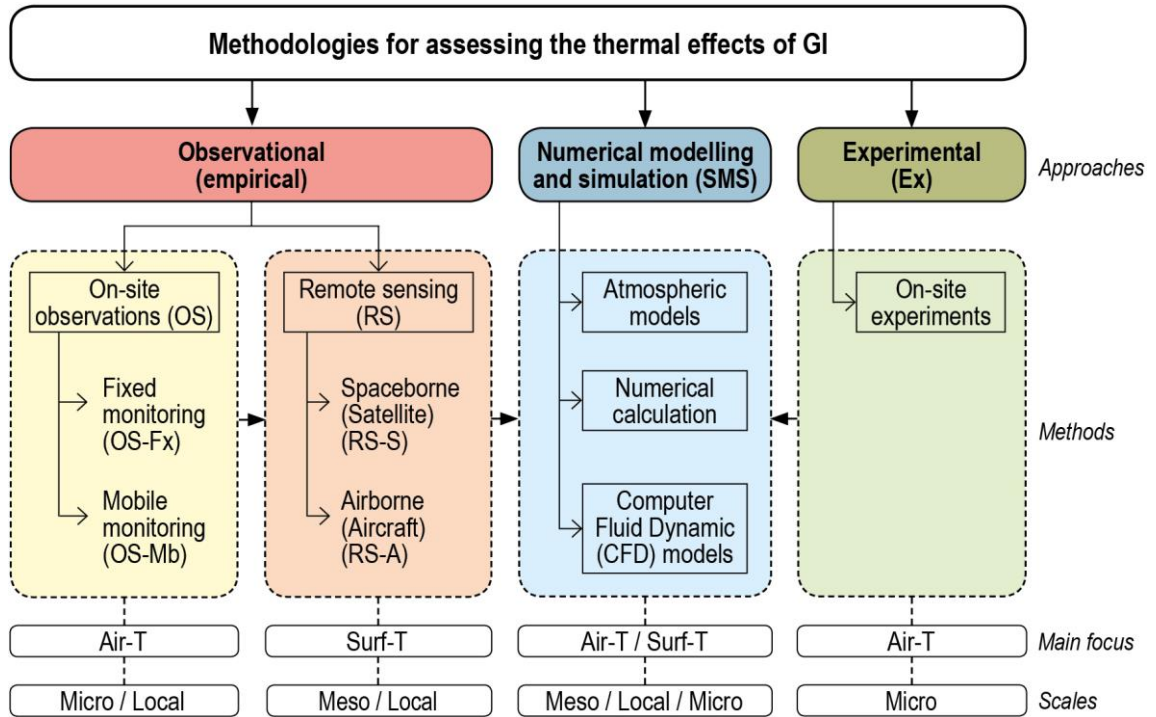


Figure 3.4 Main methodological approaches and methods used to investigate the cooling effects of green infrastructure. Based on Hunter et al. (2014); Motazedian and Leardini (2012); Ng et al. (2012); Völker et al. (2013) and Zhao-wu et al. (2015).

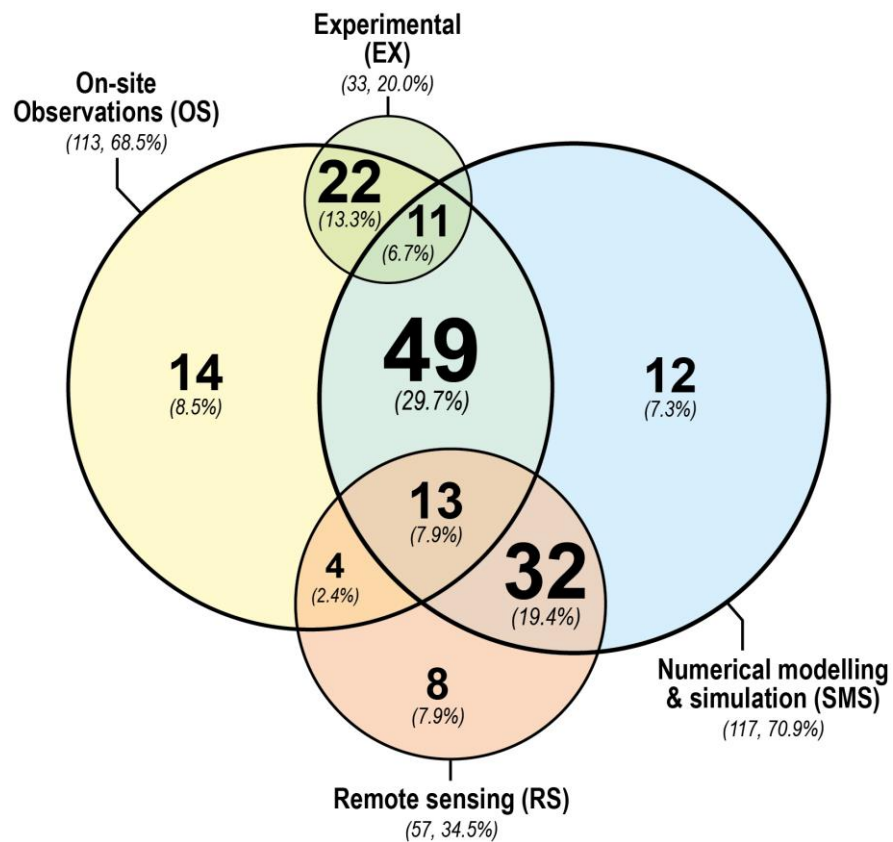


Figure 3.5 Combination of different methods employed in the literature. Note: sizes are proportional to the number of studies.

3.8 Methods, data sources, data acquisition and data processing

The selection of methods to investigate the cooling effects of green infrastructure depend on the research aims, the spatial scale and the green infrastructure types studied. Four main methods of investigation have been identified in this review: (a) on-site observations; (b) remote sensing observations; (c) numerical modelling and simulation; and (c) experimental [Figure 3.4]; and these are applied either separately or in combination [Figure 3.5].

3.8.1 On-site observations

On-site observations are extensively used to study the CLUHI, air temperature and HTC conditions of green sites, street canyons and greenery on buildings and are mainly focused on microscale phenomena ($n=113$, 68.5%) [Figure 3.5]. In this method, microclimatic conditions from representative sites inside greenspaces, beneath trees or near man-made vegetation structures are compared against a control. This method aims at finding correlations between air temperature reductions and vegetation variables such as abundance (*i.e.* NDVI, LAI), bio-physical/geometrical attributes (*i.e.* size, shape, species, foliage and ground substrates) and surface fractions (*i.e.* grass, shrubs, trees, impervious) (Ng et al., 2012).

Empirical in-situ observations require the collection of ground-based climatic data using two distinct techniques; fixed, and mobile stations. Fixed in-situ measurement involves the installation of sensors –for either a short or long term– across representative places (*i.e.* near green facades, within a green space, or across whole cities and regions). The location of instruments depends on the type of research; for instance, climatological parameters related to HTC and air temperatures are typically collected at pedestrian level (1-2m above the ground). In some cases, instruments are mounted at greater heights to avoid vandalism, especially in public spaces. Sensors can also be placed beneath trees, distributed inside greenspaces and the immediate surroundings, fixed to poles in streets, beneath the ground, or near greenery on buildings (*i.e.* green roofs, vertical greenery).

Meteorological conditions across cities and regions are regularly monitored through long term weather stations placed at various heights and locations defined by local meteorological bureaus. Near-surface measurements are collected less than 50cm from the ground, while water content, moisture and sub-surface temperature of soils are measured by probes placed at different depths. To increase the spatial coverage of in-situ measurements, some studies deploy mobile transects across study areas. Sensors are carried

by walking personnel, or installed in bicycles or cars depending on the type, extent and duration of surveys (Motazedian & Leardini, 2012). Mobile transects also include a GPS data logger to record the exact time and location of measurements.

Generally, on-site observations provide high temporal resolutions and accuracy, although they lack good spatial coverage, unless a large number of instruments are deployed. [Table 3.4](#) presents a summary of common instruments employed to conduct in-situ observations.

The geometrical and structural attributes of vegetation (*i.e.* shape, volume, leaf type, height) are usually retrieved from terrestrial data obtained through ground-truthing. For instance, Kong et al. (2013) and Rahman et al. (2017) retrieved three-dimensional tree canopies using terrestrial laser scanning (TLS) while Lehmann et al. (2014) combined aerial views with in-situ inspections to classify urban vegetation structure types (UVST) based on height, green volume, crown shapes and spatial arrangement of trees. As mentioned in Chapter 2, LAI is another indicator associated with the vegetation canopy structure used to describe the amount of foliage, evapotranspiration and the potential interception of solar radiation and wind (Hunter et al., 2012; Kong et al., 2016). LAI is commonly estimated using optical instruments, fish-eye photographs, TLS and spectral imagery with ENVI software (Exelis, 2015).

Aspect ratio (H/W) and SVF are used in UHI research as indicators of built form density and geometry that strongly influence the energy balance of urban areas (Irger, 2014; Konarska, Holmer et al., 2015). Aspect ratio can be calculated from the relationship between building heights and street widths. In contrast, the calculation of SVF requires more sophisticated methods including hemispherical (fish-eye) photographs processed in RayMan software (Cohen et al., 2012; Coutts et al., 2015; Kong et al., 2016; Shashua-Bar et al., 2011; Tan, Z. et al., 2015; Tsiros & Hoffman, 2014) and PIXEL DE CIELO software developed by DELPHI5.0 (Stocco et al., 2015); estimations from digital surface models (DSM) (Steeneveld et al., 2011), and through a simulation available in SOLWEIG software (Konarska, Holmer et al., 2015). More recently, new techniques and software have been developed for the estimation of SVF based on remotely sensed data. These are discussed in the following section.

Table 3.4 List of common instruments used for ground-based observations.

Measurements	Instruments	Models (Manufacturers)
Air temperature	Air temperature sensors, portable thermometers; thermohygrometers	6382OV Davis Funk station / Vantage Pro2 (Davis); DMA 572.1 (LSI-Lastem); DS1921G (Dallas semiconductors); EHT (Decagon); EL-USB-2-LCD (Lascar); HOBO U12-014 / U23-001 / U14-001 / H21 weather station / TMB-M006 (Onset); ibuttons Hygrochron DS1923 (Maxim); iMETOS-ag weather station (Pessl); Kestrel 4000 series; CS215L / HMP45C (Campbell); LM-8000 (Lutron Electronic); Platinum PT100-8160.TFF (Lufft); PT100 (Omega); Q-track 8552 (TSI); RFT-325 (Driesen+Kern); RTR-53 (T&D Co.); SDL310 (Extech); T351-PX1 (Vector); Testo 625 (Testo); TinyTag Plus series (TinyTag); TR-10 (Endress+Hause); TR-72U (A&D Co.); Vaisala Weather Transmitters WXT520 (EcoTech); WatchDog 2550 station (Spectrum)
Geographic location	GPS receiver and data loggers	GPS16X-HVS (Garmin); Holux M-1200E (Holux Technology)
Heat flux	Heat flux plates / gauges	HFP01-03 (Hukseflux); WYP-II (JT Science & Technology Co.)
LAI	LAI meters, hemispherical (fish-eye) camera	LAI-2200 / 3100 (Li-Cor); Nikon Coolpix E4500 and P5100 w/ FC-E8 fisheye converter; Panasonic Lumix DMC-FZ100 w/ fisheye wide-angle lens VLB1658B;
Leaf transmittance	Spectrophotometers	V-570DS w/ integrating sphere INS-470 (Jasco Co.)
Leaf colour/thickness	Colorimeter, thickness gauge	SM-112 (Teclock); MiniScan Plus 4500L (HunterLab)
Mean radiant temper.	Globe thermometer	WBGT-2010SD (Lutron Electronic)
PAR	PAR smart & quantum sensors	PQS1/ PAR lite (Kipp & Zonen); SQ110 (Apogee); S-LIA-M003 (Onset);
Plant evapotranspiration	Sap flow meters; leaf transpiration sensor, lysimeters	Sap flow module EMS 62 (EMS); LI-1600 (Li-Cor); iMETOS-ag station (Pessl); Thermal dissipation probes (TDPs) (Ecomatik)
Plant geometry / height	TLS, Laser canopy & height analyser	Leica ScanStation 2 TLS (Leica); VL400 (Haglof); Riegl LMS-Z420i TLS system.
Rainfall	Weather stations, rain gauges	HOBO RG3 (Onset); iMETOS-ag station (Pessl);
Relative humidity	Relative humidity sensors, hygrometers	6382OV Davis Funk station / Davis weather station Vantage Pro2 (Davis); DMA 572.1 (LSI-Lastem); EHT (Decagon); EL-USB-2-LCD (Lascar); CS215L / HMP45C (Campbell); HOBO U23-001 (Onset); HC2-S3 (Rotronic Messgeräte); ibuttons Hygrochron DS1923 (Maxim); iMETOS-ag station (Pessl); MP100A (Rotronic); RTR-53 (T&D Co.); Testo 625 (Testo); TinyTag Plus series (TinyTag); TR-72U (A&D Co.); WatchDog 2550 station (Spectrum)
Short-/long-wave radiation	Net radiometers, pyranometers, pyrgeometers	CGR3 (Kipp and Zonen); CM7B (Vaisala Oyj); LP02-05 (Hukseflux Thermal Sensors B.V); REBS Q7.1 (Campbell); SP-110 (Apogee);
Soil moisture	Soil moisture probes,	CS616 (Campbell); ECH2O-5 / EC-TCM (Decagon); ML2x ThetaProbe, (Delta-T); MP406 (ICT); TDR 100 (Spectrum); Tensiometer 1 (EcoTech)
Soil temperature	Soil temperature probes	Platinum PT100-8160.TF (Lufft); T107 (Campbell); STP-1, (REBS, Inc.); Thermister (Acorn)
Solar absorption	Spectrophotometers (visible light)	Spectrum Analyser Model 554 / GX 1 / Spectrum One NTS (Spectrum)
Solar radiation	Pyranometers; illumination meters	250A (Li-COR); CM5 / CM11-P / CMP3 / CMP6 (Kipp & Zonen); iMETOS-ag weather (Pessl); MS-601 (Eko); S-LIB-M003 (Onset); SP110 (Apogee);
Stomatal conductance	Open gas-exchange systems	Portable HCM-1000 (Heinz Walz GmbH); SC-1 Sensor (Decagon)
Surface reflectivity/albedo	Spectrophotometer, albedometers	Lambda 950- UV/Vis/NIR (Perkin Elmer); CM7B (Vaisala Oyj);
Surface temperature (ground-based)	Thermocouples, infrared camera/radiometers, thermoresistances, thermistors, laser guns	EL-USB-TC (Lascar); FLIR A615 / FLIR-i5 / AGEMA Thermovision 570 (FLIR Systems); Fluke 572 (Fluke); HOBO U12-014 (Onset); IRTS-P (Campbell); Laser gun PTD1 (Bosch); Laser Temp-Gun 2268-20 (Milwaukee); PT100 (LSI-Lastem); S1-121 / S1-111 (Apogee); Si-111 (Campbell); SKTS 200 U-110K (Umweltanalytische); Testo 830-T1 / 845 (Testo); Thermo Shot F30 (InfRec); Thermo Tracer TH7800 (NEC); Type T copper-constantan (Reotemp); T-type shielded thermocouple (Omega); VarioCam HR inspect 700 (InfraTec).
Sky view factor	Hemispherical camera	Nikon Coolpix E4500 camera with FC-E8 fisheye converter;
Wind speed and direction	Anemometers, 2-D and 3-D ultrasonic anemometers	014A (Campbell); 05103 (Young); 7911 (Davis); 81000 (Young); A100L2 / A100K-Pulse (Vector); CSAT3 (Campbell); LCA501, (TSI); MAX 40+ (Ekipower); Gill WindSonic 2D (Gill); HOBO U30-NRC / H21-001 stations (Onset); HOBO S-WCA-M003 (Onset); iMETOS-ag station (Pessl); SDL310 (Extech); W200 Porton Windvane (Vector); WatchDog 2550 station (Spectrum)

3.8.2 Remote sensing

Remote sensing refers to the acquisition of information of an object or surface from a distance using sensors that capture electromagnetic and thermal properties emitted by them (Brown & Harder, 2016). There are two types of sensors: on one hand, *passive sensors* such as thermal and spectral imagers capture the light and radiation reflected and emitted by a surface across the electromagnetic spectrum [Figure 3.6]. On the other hand, *active sensors* such as LiDAR (Light detection and ranging), radar or sonar technologies, firstly emits energy and then senses the radiation reflected back from the earth's surface or targets (Brown & Harder, 2016).

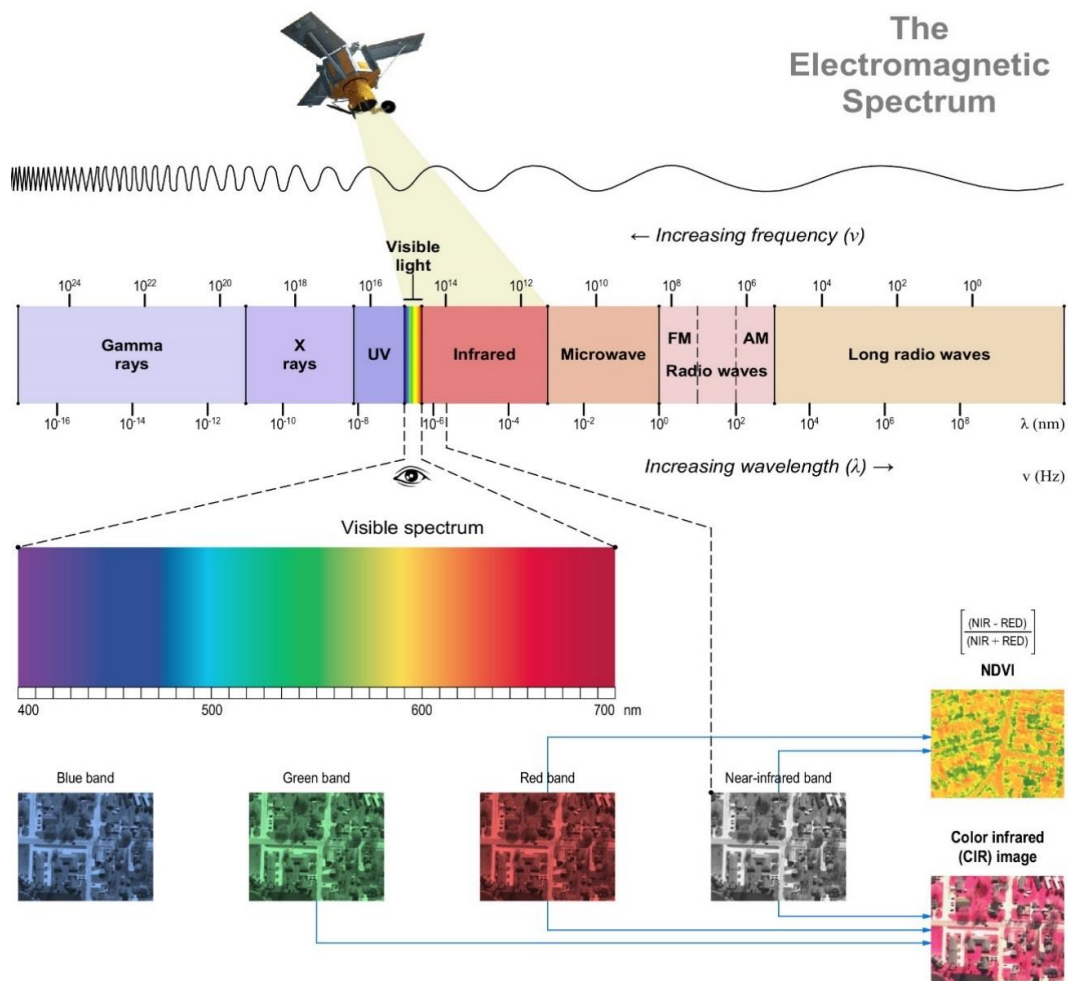


Figure 3.6 The electromagnetic spectrum and differentiation of bands for spectral analyses.

Remotely sensed imagery is based on the *spectral reflectance* of a surface which in turn also depends on *surface roughness*. Since this reflected radiation is unique for every surface in a specific wavelength, with sufficiently high resolution, particular spectral signatures can be distinguished for each material (Brown & Harder, 2016). However, this reflected radiation must travel through the atmosphere before being captured by the sensor, so it is

absorbed and scattered by gases and aerosols in the air. Consequently, there are required atmospheric and radiometric corrections based on the flight altitude, humidity, and other meteorological factors prior to the analysis of images. In addition, to generate accurately georeferenced images it is necessary to apply corrections for optical distortions originated from the sensor system, commonly referred as orthorectification. These corrections require an accurate description of the sensor, the angle of the sensor, the topographic conditions of the surveyed area, the flight path and the orientation of the image (Brown & Harder, 2016).

In urban mapping and climatology, remote sensing has been extensively applied to analyse the relationships between LST and surface-related characteristics –particularly vegetation coverage– of multiple sites or whole cities and regions ($n=57$, 34.5%). Compared to on-site observations, remotely sensed methods offer wider spatial coverage as enable a synchronised capture of conditions over larger areas or across multiple locations (Harris & Coutts, 2011; Weng, 2009). However, remote sensing provides single snapshots of urban surfaces that may not be sufficient for time series analyses, might not be captured at desirable times, and their quality could be affected by poor weather conditions.

Remotely sensed imagery is typically acquired from two main sources. On one hand, satellites (spaceborne remote sensing) continuously orbit the planet and capture images with medium and low resolutions (pixel size) that generally vary between dozens of metres and several kilometres. In recent years, the advent of high-resolution satellite imagery (*i.e.* QuickBird, RapidEye, WorldView-2 and IKONOS) has facilitated the acquisition of highly detailed and accurate images with resolutions of a couple of metres (2-10m).

On the other hand, airborne remote sensing is increasingly utilised to capture high-resolution images (0.5-2m) with sensors mounted in aircrafts (*i.e.* fixed wing, helicopters) that can be deployed at desirable times. More recently, the development of unmanned aerial vehicles (UAVs) and smaller spectral imagers makes possible to obtain images at very high spatial resolutions in a flexible, straightforward and less costly way (Gaitani et al., 2016; Gaitani et al., 2017).

Accordingly, the selection of remotely sensed imagery depends on acquisition costs, scale, extent of analysis, amount of detail (spatial and temporal resolutions), and type of information (number of bands) required. Most remotely sensed studies are conducted at meso-scale employing medium ($n=43$) and low ($n=13$) spatial resolution imagery acquired from Landsat 5TM ($n=18$), Landsat 7ETM+ ($n=12$), ASTER ($n=10$) and MODIS ($n=11$) satellites as this is freely accessible. However, coarse image resolutions have proved inadequate to conduct accurate and reliable analyses of the microclimatic impacts of

vegetation on urban precincts, street canyons and individual buildings (Gaitani et al., 2016; Weng, 2009).

Contrastingly, the use of high-resolution satellite imagery (IKONOS and QuickBird) ($n=13$) and very high resolution airborne-based imagery ($n=11$) offers high levels of flexibility and detail; unfortunately, this is less common due to the complex logistics and prohibitive costs for most users. A summary of the main remote sensing data sources is presented in Table 3.5.

3.8.2.1 Thermal imagery

Remotely sensed thermal infrared (TIR) images retrieved from satellites and aircrafts are largely employed to estimate surface radiant temperatures. An accurate retrieval of LST from TIR data requires corrections for spectral emissivity as sensors do not directly measure the temperature of surfaces, but instead the radiances emitted in the long-wave spectrum. However, it should be noted that emissivity correction methods may differ between satellite and airborne sensors (Coutts et al., 2016; Harris & Coutts, 2011; Weng, 2009).

Alternatively, spectral unmixing techniques (*i.e.* MESMA) can be implemented to estimate the total emissivity of a pixel by assigning emissivity values to each cover type using spectral libraries and estimating their weighting average (N. Chrysoulakis, personal communication, 2017; Kotthaus et al., 2014). However, this technique requires advanced skills and knowledge, as well as hyperspectral data that might not be available in some cases.

The Normalised Emissivity Method (NEM) initially described by Gillespie (1985) and validated by Realmuto (1990) assumes a constant emissivity value in all N channels for a specific pixel to calculate temperatures (T_{si}) from the measured radiances, provided that the atmospheric effects are corrected. The maximum of those N temperature is considered as the LST, as per the following equation:

$$LST = T_{NEM} = \max(T_{si}) \quad \text{with} \quad T_{si} = B^{-1} \left(\frac{R_{gi} - (1 - \varepsilon_{cst}) R_{ati\downarrow}}{\varepsilon_{cst}} \right) \quad [\text{Eq. 3.1}]$$

where B^{-1} is the inverse function of Planck's law, ε_{cst} corresponds to the assumed channel constant emissivity for a given pixel, R_{gi} represents the radiance observed at ground level in channel i , and $R_{ati\downarrow}$ is the downward atmospheric thermal radiance (Gillespie, 1985).

It has been demonstrated that the NEM can be also applied to generate reliable LST estimations for a wide range of materials in a rapid and easily replicable way, therefore, it can be implemented by users with different skill levels (Gillespie, 2015). Moreover, the NEM approach has been tested using high-resolution radiance spectra collected by hyper- and multi-spectral imagers with satisfactory results (Gillespie, 2015; Mushkin et al., 2005; Sobrino et al., 2008; Tang & Li, 2014).

Table 3.5 List of main remote sensing data sources utilised by studies.

Data product	Imagery	Acquisition	Spatial resolution	Temporal resolution
<i>Low resolution satellite imagery (>100 m)</i>				
AVHRR/NOAA	VIS, NIR, SWIR, TIR	Free	1100m	Twice daily
MODIS	VIS, NIR, SWIR, TIR	Free	250, 500, 1000m	Daily at 10h30 & 13h30 (local time)
FY-2C (FengYun-2)	VIS, TIR, WV	Free	1250, 1440, 5000, 5760m	Every 30 minutes
<i>Medium resolution satellite imagery (10-100 m)</i>				
Landsat 5TM	VIS, NIR, SWIR, TIR	Free	30, 120m	Every 16 days at 9h45 (local time)
Landsat 7ETM+	VIS, NIR, SWIR, TIR	Free	15, 30, 60m	Every 16 days at 10h00 (local time)
Landsat 8	VIS, NIR, SWIR, TIR, PAN	Free	15, 30, 60, 100 m	Every 16 days at 10h00 (local time)
SPOT	VIS, NIR, SWIR, PAN	Purchased	2.5, 10, 20m	Every 1-3 days
ASTER	VIS, NIR, SWIR, TIR	Free & purchased	15, 30, 90m	Daily at 10h30 (local time)
Sentinel-2	VIS, NIR, SWIR, WV	Free	10, 20, 60 m	Every 5 days
<i>High resolution satellite imagery (<10 m)</i>				
IKONOS	VIS, NIR, PAN	Purchased	0.8, 4m	Every 3 days
WorldView-2	NIR, TIR, PAN	Purchased	0.5, 1.8, 2.4 m	Every 1-2 days
QuickBird	VIS, NIR, PAN	Purchased	0.6, 2.4, 2.6 m	Every 2-6 days at 10h30 (local time) & on demand
<i>Airborne imagery (resolutions depending on sensors)</i>				
MASTER	VIS, NIR, SWIR, TIR	Purchased	7, 50 m	On demand
AVIRIS	VIS, NIR, SWIR	Purchased	4, 20 m	On demand
ATLAS	VIS, NIR, SWIR, TIR	Purchased	2.5m	On demand
TASI	TIR	Purchased	0.6, 1.25 m	On demand
SASI	SWIR	Purchased	1.25 m	On demand
DAMS	TIR, NIR, UV	Purchased	5 m	On demand
DIMAP	VIS, NIR, SWIR, TIR, LiDAR	Purchased	1, 2m	On demand
Deadalus 1268 ATM	VIS, NIR, SWIR, TIR	Purchased	2.5 – 30m	On demand
HySpex	VIS, NIR	Purchased	0.5, <1m	On demand
HyVista (HyMap)	VIS, NIR, SWIR	Purchased	3 – 10m	On demand
Infratec	TIR	Purchased	0.7 m	On demand
FLIR	TIR	Purchased	0.5 m	On demand
<i>Other airborne-based data</i>				
LiDAR	Point clouds, intensity	Purchased	N/A	On demand

NIR Near infrared, PAN Panchromatic, SWIR Short-wave infrared, TIR Thermal infrared, UV Ultraviolet, VIS Visible light, WV Water vapor. * Some studies used more than one data product at a time, ** Percentage calculate out of 57 remotely-sensed studies

3.8.2.2 Spectral imagery

Spectral sensors can detect electromagnetic radiation reflected and emitted by surfaces in different wavelength ranges or bands across the visible (VIS), near infrared (NIR), shortwave infrared (SWIR) and thermal infrared (TIR) spectrum. One of the most common imagery types collected by remote sensing is the multi-spectral, which is limited to a portion of the whole spectrum and is usually stored in a small number (4-8) of broad bands. Conversely, hyper-spectral sensors provide a high spectral resolution since the information is captured in hundreds of narrow bands that enable the identification of detailed spectral signatures of specific materials (Brown & Harder, 2016) [Figure 3.7].

The use of spectral data is increasingly crucial for urban climatologists as it can facilitate the identification and quantification of surface-derived indices (*i.e.* NDVI, LAI), land-use land-cover (LULC) classes, LCZs, surface fractions, and surface properties (albedo, emissivity, reflectance) (Irger, 2014; Weng et al., 2004; Weng, 2012).

3.8.2.3 Vegetation abundance and coverage: the NDVI

Vegetation abundance and coverage, commonly described by indices such as NDVI and Enhanced Vegetation Index (EVI), have been extensively employed in regression analyses to predict LST (Carlson et al., 1994; Weng et al., 2004). The NDVI is the most common index used to assess plant activity and differentiate general land covers that is estimated from spectral data using the following equation:

$$NDVI = \frac{NIR-RED}{NIR+RED} \quad [Eq. 3.2]$$

where *RED* corresponds to the visible red reflectance band (600-700 nm), and *NIR* is the near infrared reflectance band (750-1300 nm). NDVI values range between 0 and 1, where lower values represent absence of vegetation and higher values correspond to vegetated areas with high chlorophyll density (Gandhi et al., 2015) [Figure 3.6].

A simple threshold NDVI classification analysis can be applied to distinguish different land covers and estimate surface fractions. Typically, negative values indicate the presence of water; values around zero (≤ 0.1) are rock, sand or snow; small values (0.1–0.2) represent impervious surfaces (*i.e.* soils and pavements); moderate values between 0.2 and 0.5 correspond to sparse vegetation usually grasses and shrubs; and high values (> 0.60) represent dense vegetation canopy (Badamasi et al., 2010; Bartesaghi Koc, Osmond, Peters, & Irger, 2017b; Black & Stephen, 2014; Cheng et al., 2008; Gaitani et al., 2016; Gandhi et al., 2015; Irger, 2014).

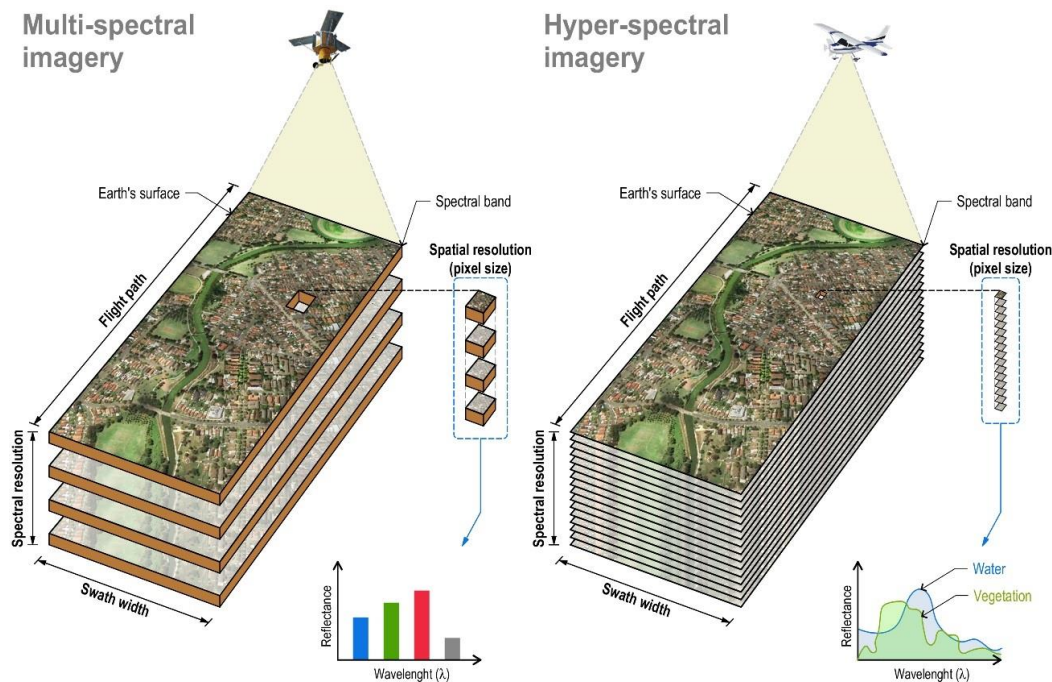


Figure 3.7 Differences between multispectral and hyperspectral imagery. (Redrawn based on Irger, 2014)

Given the differences in radiative temperature between ground surfaces and the vegetation canopy, most remote sensing research has examined the thermal variability of vegetation cover using simple linear correlations. For example, the thermal-vegetation index combines NDVI and LST as a ratio which significantly correlates with surface evapotranspiration and soil moisture (Weng et al., 2004; Weng, 2009). Sun et al. (2015) improved a temperature vegetation index by estimating day-time and night-time air temperatures from MODIS-LST and EVI using a binary linear regression equation. This study identifies evapotranspiration as a crucial factor behind the differences between CLUHI and SUHI that should receive more attention from remote sensing studies (Sun et al., 2015).

Weng (2009) has argued that NDVI-LST models require further calibration since NDVI does not provide areal estimations, but instead it represents the photosynthetic activity or vegetation health. Contrastingly, remotely sensed studies employing LAI and LAD are more scarce (Peters & McFadden, 2010; Shen, M. et al., 2015; Skelhorn et al., 2014; Xiao, 2014). This happens because LAI is typically employed as key input in ENVI-met models by most studies on HTC. Since the use of LAI/LAD has not been fully explored in remote sensing research, more research is required to fully understand the relationships between LAI, NDVI and surface temperature reductions because these have proved to be non-linear (Weng, 2009).

Despite the wide applications of the NDVI, its use has raised concerns as it is sensitive to season, vegetation phenology, irrigation levels, and climatic conditions prior and during

data collection (*i.e.* different values after a heatwave or severe drought than after heavy rainfall). A better understanding of the role of these factors on NDVI values would be useful for a more precise estimation of vegetation fractions and for interpreting the seasonal variability of UHIs.

Evapotranspiration is a key parameter influencing air and surface temperatures that is strongly correlated to NDVI (Nouri, Anderson et al., 2013). The estimation of evapotranspiration is commonly estimated in-situ using lysimeters, sap flow meters and leaf transpiration sensors [Table 3.4]; and primarily conducted for agricultural purposes, and in rural areas. Hence, a promising direction for future research is the estimation of evapotranspiration rates in heterogeneous urban contexts at local and micro-scales, and the study of its role on CLUHI and SUHI mitigation (Nouri et al., 2015). The reviews presented by Nouri et al. (2016) and Nouri, Beecham et al. (2013) evaluate general techniques and remote sensing approaches to predict evapotranspiration from complex vegetated surfaces that could be incorporated by climate scientists.

3.8.2.4 Surface fractions: LULC and LCZs

LULC types originally proposed by Anderson et al. (1976) can be also retrieved from spectral imagery and have been extensively used to analyse the influence of geometrical and physical properties of urban surfaces and built forms on the spatial patterns of LST. Nonetheless, LULC have proved inadequate to analyse certain ecological processes because knowing the purpose (land use) of an area does not necessarily explain its climatic functioning (Cadenasso et al., 2013; Zhou, Cadenasso et al., 2014).

Furthermore, LULC types and typical surface fractions provide areal estimations; thus, they are limited in describing the characteristically fine-scaled, three-dimensional and highly heterogeneous elements of urban landscapes. Since a clear differentiation between biotic and abiotic elements and their spatial distribution is increasingly difficult at coarse scales, LULC may be insufficient to analyse the spatial interrelationships among elements (Bartesaghi Koc, Osmond, & Peters, 2017; Cadenasso et al., 2007; Zhou, Cadenasso et al., 2014). A further discussion on the applications and limitations of LULC is provided in Chapter 4.

Since LCZs provide estimates of surface fraction, some studies employed them to identify and cluster urban areas with similar thermal conditions for the comparison of vegetation's cooling benefits in different contexts (Milošević et al., 2017; Müller et al., 2014; Rasul et al., 2015; Steeneveld et al., 2011; Tan et al., 2017). Although this scheme is specifically

developed for UHI research (as explained in Chapter 2), it can be implemented to standardise observations and analyses (Colunga et al., 2015; Emmanuel & Loconsole, 2015). Nonetheless, the use of LCZs implies several shortcomings: firstly, LCZs lack sufficient detail for microclimatic analysis as they only include general surface/roughness descriptors for vegetation; and secondly, the LCZs scheme requires further calibrations for local contextualisation that would enrich the approach overall.

3.8.2.5 Spatial configuration: FRAGSTATS metrics

Configuration of green infrastructure is an important aspect considered by studies evaluating the spatial patterns of UHIs, UCIs, and PCIs as it is necessary to understand how the cooling efficiency, intensity and magnitude of greenspaces are influenced by geometry, placement or composition (spacing, clumpiness and dispersion), and the type and combination of plant species and other surfaces.

Remote sensing researchers have employed spatial autocorrelation indices such as Local Moran's I (Anselin, 1995) and landscape pattern metrics (McGarigal & Marks, 1995) to analyse the relationship between greenspaces characteristics and the spatio-temporal variability of UCIs, PCIs and SUHIs at city-wide level (Cao et al., 2010; Chen et al., 2014; Fan et al., 2015; Kong, Yin, James et al., 2014; Li et al., 2013; Maimaitiyiming et al., 2014; Zhou et al., 2011).

FRAGSTATS (McGarigal & Marks, 1995) is a computer software program that has been designed to compute a large variety of landscape metrics that has attracted the most attention of researchers (McGarigal et al., 2002; McGarigal, 2015). FRAGSTATS metrics simply quantify the spatial heterogeneity of a landscape; therefore, they have proved useful to assess the composition and configuration of greenspaces that can affect ecological processes such as climate regulation (McGarigal, 2015).

FRAGSTATS normally requires raster images of green patches retrieved from spectral data with a spatial grain or grid (pixel) resolution larger than 0.001m to compute several statistics at three distinct levels, namely *patch*, *class* and *landscape* metrics. Since some metrics quantify landscape composition and others landscape configuration, it is important to understand for each metric which specific aspect of landscape pattern is being analysed. Also, some metrics may be partially or completely redundant as they quantify a similar aspect at various levels. Common FRAGSTATS metrics applied by studies are listed in [Table 3.3](#).

Despite the proved capabilities of FRAGSTATS metrics, studies have mostly applied them at a coarse level to understand the effect of greenspace distribution, overlooking the spatial heterogeneity inside greenspaces. Future studies could equally draw upon the same approach and apply landscape metrics to classify and analyse vegetation features (*i.e.* tree patches) at finer scales.

3.8.2.6 LiDAR data

Current research is not only constrained by the type, quality and resolution of images, but also it is limited in providing sufficient detail of vertical surfaces. Accordingly, the integration of a three-dimensional approach with current methodologies is crucial to examine the interaction of horizontal and vertical surfaces and for a *complete* study of the temperature ranges and spatio-temporal dynamics of urban temperatures, in which cases time-series analyses may be also required (Voogt & Oke, 1997).

Airborne LiDAR has proved useful to provide detailed and accurate three-dimensional information on terrains, building heights and vegetation. Notwithstanding, few studies ($n=5$) utilised LiDAR to generate digital surface models (DSMs) which represents the height elevations of all surfaces and features above the bare earth (trees, buildings and ground), and DEMs (also referred as digital terrain models – DTMs) which only shows the elevation of the ground surface (Brown & Harder, 2016). LiDAR data has been also implemented to generate vector-based Triangular irregular network (TIN), to estimate SVF and aspect ratio, and to identify different types of vegetation covers (*i.e.* grasses, shrubs, tress) by creating raster images (Coutts et al., 2016; Emmanuel & Loconsole, 2015; Konarska, Holmer et al., 2015; Lin et al., 2016; Su et al., 2014).

The continuous development of LiDAR technology has enabled the expansion of its application to other disciplines, such as environmental sciences, archaeology and anthropology; advances that can be equally useful for climatic research. For instance, Kokalj et al. (2011) and Zakšek et al. (2011) proposed a new method of relief mapping which enables a rapid generation of SVF rasters based on remotely sensed DSM images (Kokalj et al., 2017; Zakšek et al., 2011). As a result, a ‘SVF based relief visualisation toolbox (RTV)’ has been successfully developed and is publicly available online (Institute of Anthropological and Spatial Studies, 2018).

This open source and standalone software computes SVF based on diffuse illumination using an imaginary light source that illuminates the relief surface from a celestial hemisphere; so SVF values are calculated using different search radius of the horizon in a

specific number of directions (*i.e.* 8, 16, 32) for each pixel [Figure 3.8]. Hence, the resolution of the resulting GeoTIFF is the same as that of the DSM raster image provided for calculations (Kokalj et al., 2011; Zakšek et al., 2011).

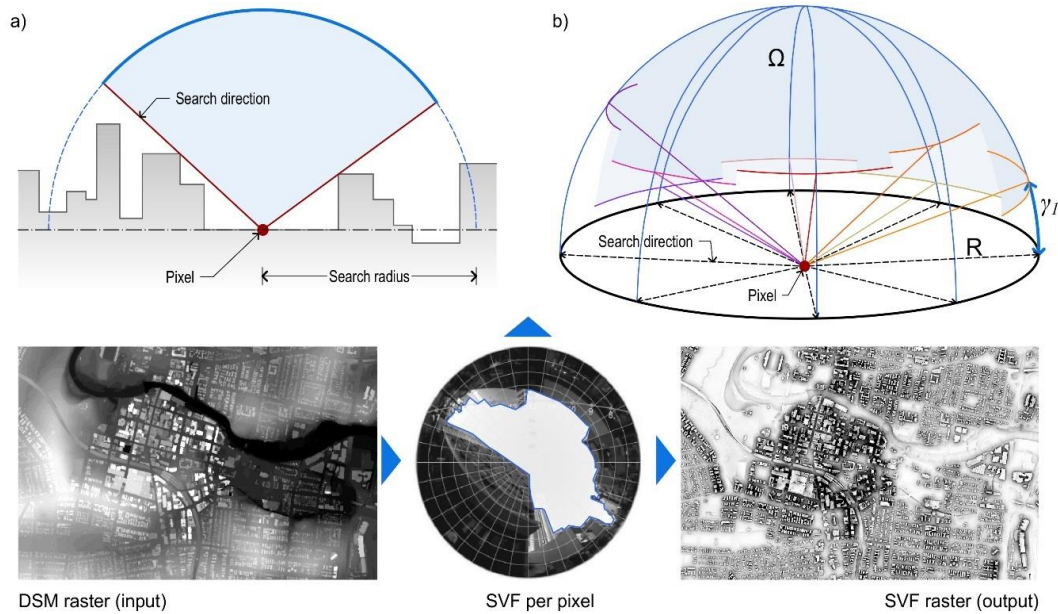


Figure 3.8 Estimation of SVF from a DSM using RVT software: (a) value is determined as a proportion of visible sky (Ω) above certain point (pixel), and (b) the algorithm computes the horizon angle (γ) for 'n' directions (eight in the image) in a specific search radius (R).

3.8.3 Experimental methods

Experimental methods are typically adopted by studies focusing on the thermal performance of greenery on buildings due to logistic limitations for its application across large areas. Experimental studies ($n=33$, 20.0%) involve the manipulation of green features by investigators, enabling measurements under relatively controlled conditions (Bowler et al., 2010b).

The vast majority of experiments used on-site observations to analyse the microscale effects resulting from the variation of foliage density and surface properties of green roofs and vertical greenery. The effect of tree shade and grass on thermal comfort is also investigated through experimental sites, though these studies are very scarce (Shashua-Bar et al., 2011; Snir et al., 2016). Furthermore, measurements collected in experimental sites serve to validate predictive models and to parameterise computer simulations [Figure 3.4].

The thermal performance of green roofs is usually compared against that of conventional and cool roofs. Studies analyse the simple correlations between microclimatic parameters (and indoor thermal comfort) and the properties of substrates (albedo, emissivity,

temperature, moisture, depth) and plant composition (foliage density, species) (Di Giuseppe & D'Orazio, 2014; Jim, 2012, 2015a; Libelle et al., 2011; Lin et al., 2013; Olivieri et al., 2013; Ouldboukhite et al., 2011; Razzaghmanesh et al., 2016).

The thermal profiles of living walls and green façades are contrasted with those of bare concrete walls (control), the immediate surroundings and several simulated scenarios (Hunter et al., 2014). Besides the variation of foliage density and species, studies also quantify the influence of construction materials, training systems, climate, behind-façade air flow and orientation on the cooling effectiveness of vertical greenery systems (Cameron et al., 2014; Chen et al., 2013; Cheng et al., 2010; Djedjig et al., 2015; Kontoleon & Eumorfopoulou, 2010; Koyama et al., 2013; Mazzali et al., 2013; Olivieri et al., 2014; Pérez et al., 2011a; Perini et al., 2011; Susorova et al., 2014; Tan et al., 2014; Wong et al., 2010).

Most of the abovementioned methods emphasise the shading potential of green infrastructure, but fewer concentrate on the evaporative cooling capacities of green roofs (Coutts et al., 2013; Schweitzer & Erell, 2014; Tan, C. L. et al., 2015; Zinzi & Agnoli, 2012), vertical greenery (Davis et al., 2015; Davis & Hirmer, 2015; Hoelscher et al., 2016; Koyama et al., 2013; Koyama et al., 2015) and tree canopy or green open spaces (Gillner et al., 2015; Gromke et al., 2015; Konarska, Uddling et al., 2015; Rahman et al., 2017; Ryu et al., 2015; Shashua-Bar et al., 2011; Wang, Z.-H. et al., 2016).

With some exceptions, experiments lack adequate replication, are conducted during short timeframes or repeated under unidentical conditions. Installation of real-time sensors integrated to facades and roofs of new and retrofitted buildings and urban precincts would facilitate future experimental research of extensive areas.

3.8.4 Numerical modelling and simulation

Compared to empirical methods, numerical modelling, simulations and statistical analysis have been extensively used by most studies ($n=117$, 70.9%) to predict thermal conditions and assess different greening scenarios. In most cases, modelling studies are validated with observational data collected using on-site observations ($n=73$, 44.2%) and remote sensing ($n=45$, 27.3%). In some other cases, simulations are implemented individually ($n=12$, 7.3%) or as part of experimental studies ($n=11$, 6.7%). Only a limited number of articles ($n=13$, 7.9%) combined the three methods, where data from on-site measurements and experiments were used to cross-check remote sensing estimations and calibrate simulations

[Figure 3.5]. Occasionally, model input and output parameters are not clearly distinguished or reported, hindering replication.

Meso-scale atmospheric models such as the Weather Research and Forecasting System (WRF) (Georgescu et al., 2011; Shen, M. et al., 2015) and the coupled WRF-NOAH Land surface model (Zhou & Shepherd, 2010) enable the prediction of climatic impacts of green infrastructure on extensive regions and whole cities. Unlike previous models, the urban climate model MUKLIMO_3 provides a more sophisticated boundary-layer turbulence scheme which is independent of spatial scale (Žuvela-Aloise et al., 2016). The impact of greenspaces on the daytime atmospheric boundary layer conditions has been simulated using a coupled large-eddy simulation-land surface model (Huang et al., 2011). Also employed at city level is the vegetation and atmosphere model HIRVAC-2D (High Resolution Vegetation Atmosphere Coupler) (Lehmann et al., 2014).

At the microscale, urban canopy models (UCM) such as the single-layer Princeton UCM enable the parameterisation of vegetation-related variables and built forms to study the physical processes and heat exchange within the urban canopy (Krayenhoff et al., 2014; Ryu et al., 2015). Another approach includes coupling UCM to the WRF to model the potential large-scale cooling effects of green features on street canyons and buildings through single- and multiple-layer parameterisations (Li & Norford, 2016; Smith & Roebber, 2011; Wang, Z.-H. et al., 2016). However, limitations of UCMs include the advanced mathematical knowledge required for their implementation and their limited application for the study of extensive or large areas.

Several studies have quantified the effects of trees and green open spaces on HTC using several indices and models: the Physiological Equivalent Temperature (PET) biometeorological index, the Temperature of Equivalent Perception (TEP) thermal index, the urban microclimate model Green-CTTC (Shashua-Bar et al., 2012; Shashua-Bar, Potchter et al., 2010; Shashua-Bar, Tsiros et al., 2010), the Outdoor Standard Effective Temperature (OUT-SET*) (Yahia & Johansson, 2014), the COMFA method (Correa et al., 2012; Stocco et al., 2015), the Mediterranean Outdoor Comfort Index (MOCI) (Salata et al., 2017), the index of thermal stress (ITS) (Snir et al., 2016), the Universal Thermal Climate Index (UTCI) (Milošević et al., 2017), the Simulation Platform for Outdoor Thermal Environment (SPOTE) (Hong & Lin, 2015), and the temperature-humidity Index (THI) and relative strain index (RSI) (Morakinyo et al., 2016)

Computational fluid dynamic (CFD) models have been developed to simulate the surface-plant-air interactions based on either monitored data or synthetic microclimatic parameters.

ENVI-met (Bruse, 2011) is a three-dimensional small-scale CFD model extensively used to analyse the thermal comfort regimes of street canyons and greenspaces at fine spatial resolutions (to 0.5m x 0.5m) and short time frames (every 10 seconds) (Bruse, 2011; Ng et al., 2012).

In recent years, ENVI-met has become increasingly popular because it enables scenario testing of different urban design strategies in a variety of contexts; something that is not possible in the real world (Emmanuel & Loconsole, 2015). Nonetheless, ENVI-met poses some limitations as (a) it is relatively limited in calculating the effect of wind speed changes, especially at boundary level, and (b) anthropogenic heat is excluded in canyon-level calculations (Morakinyo & Lam, 2016; Yahia & Johansson, 2014).

Other CFD models utilised at building scale include PHOENICS (Fintikakis et al., 2011; Gaitani et al., 2011), ANSYS FLUENT v.12.4.1 (Gromke et al., 2015; Vidrih & Medved, 2013), the plant-covered wall model, building envelope model, and foliage canopy model (Kontoleon & Eumorfopoulou, 2010). Furthermore, the transient building simulation program (TRNSYS) has recently integrated a heat and moisture transfer model to assess the performance and impacts of green envelopes on buildings' indoor thermal quality (Djedjig et al., 2015).

Simple- and multiple-linear regressions are the most common statistical methods used for the analysis of the relationships between climatological and vegetation-related variables. One- and two-way analysis of variance (ANOVA), *t*-Tests, and other non-parametric methods were carried out to identify significant differences between variables, experiments, locations, samples, seasonal heat patterns and slopes (means) of regression models (Alavipanah et al., 2015; Armson et al., 2012; Cameron et al., 2014; Gillner et al., 2015; Peters & McFadden, 2010, 2010; Rahman et al., 2017, 2017; Scheitlin & Dixon, 2010; Zhang et al., 2013).

A series of spatial autocorrelation models can be applied to calculate the extent and magnitude of cooling effects. For instance, Declet-Barreto et al. (2013) employed the local indicator of spatial autocorrelation (LISA) method which analyses the degree of significant spatial clustering of variables (Anselin, 2005). Publications focusing on spatial configuration performed spatial auto-regression estimations, which include the spatial error model (SEM) that analyses the spatial dependency within error terms across neighbouring locations, and the spatial lag model (LAG) that quantifies the spatial dependency of the same variable in different locations (Anselin, 2005; Connors et al., 2013; Irger, 2014; Li et

al., 2012). Further discussion on these two spatial regression models is presented in Chapter 7 for the analysis of results [Figure 7.22].

3.9 Investigation period

The investigation period includes the season, time of the day and duration of measurements. The vast majority of studies ($n=137$, 83.0%) are typically conducted in summer when UHIs and heatwaves are more frequent and stronger. Investigations during autumn ($n=41$, 24.8%), spring ($n=34$, 20.6%) and winter ($n=32$, 19.4%) are comparably fewer, while only 23 studies (13.9%) were conducted across all seasons. Since SUHI is commonly greatest during the day, 62 studies (37.6%) were performed during late morning and early afternoon (12m–4pm); and only three investigations (1.8%) were exclusively carried out during the evening. Notwithstanding, half the literature ($n=86$, 52.1%) measured diurnal and nocturnal conditions simultaneously to analyse the temperature fluctuations and evolution of UHIs throughout the day.

The duration of measurements varies among studies and depends on the type of research design (longitudinal or cross-sectional). Half the literature was longitudinal ($n=83$), mainly comprised by observational (on-site) and experimental studies employing data (mostly air temperature and humidity) collected by fixed meteorological stations over consecutive days, months or years. The other half of the investigations reported cross-sectional research ($n=82$) that mainly corresponds to remote sensing studies that monitored surface temperatures at specific times of the day and year since satellite- and airborne-based data are not continuously available. Exceptionally, some satellite-based research had access to time-series imagery that enabled the study of thermal variations over longer periods.

In many studies the spatial and temporal mismatch between ground-based and remotely-sensed measurements is very common as datasets are collected for different purposes and at separate times, so air-surface correlations cannot be easily established. It was also found that compared to air temperatures, remotely-sensed estimations tend to be overestimated during the day and underestimated at night. Therefore, simultaneous collection of ground-based and remotely sensed data is strongly recommended for the validation of data and a better understanding of the relationship between air and surface temperatures.

Moreover, longitudinal studies should be strengthened as cooling effects vary between day and night and among seasons as a consequence of vegetation phenology, irrigation levels and the variation of evapotranspiration rates (Cheng et al., 2014; Feyisa et al., 2014; Li et al., 2013; Zhao-wu et al., 2015). In fact, little work has been done to define adequate

timeframes for reassessing sites and to compare the evidence before and after green infrastructure interventions.

In response to previous shortcomings and needs, the advent of UAV technology makes possible to obtain high-resolution and multi-temporal 2D and 3D imagery in a flexible and more affordable way (Gaitani et al., 2017). Despite UAVs representing a promising opportunity for a more precise, accurate and continuous monitoring of green infrastructure implementations, many restrictions in terms of privacy and safety act as barriers for their widespread use in many countries, particularly in urban areas.

3.10 Summary

The aim of this chapter is to systematically review and analyse the most recent and representative peer-reviewed publications investigating the cooling effects of green infrastructure. This review is intended to identify critical knowledge gaps to be incorporated in the research design of this thesis, and to achieve clarity to ensure an integrated understanding and interpretation of findings. In this sense, there have been identified five major gaps in the literature, those that are tackled in the present research.

First, climate scientists should pay attention to developing countries with limited resources and developed countries from the southern hemisphere as we know little about the cooling effects of green infrastructure on these regions. Particularly, this is the case of Australia, a country where green infrastructure strategies are urgently needed, as it is experiencing significant urbanisation and population growth and is severely affected by climate change-related events such as heatwaves, droughts, bushfires and flooding. Furthermore, forthcoming research should also concentrate on defining specific greening recommendations for tropical, semi-arid and desert climates since vegetation, irrigation and cooling strategies are substantially different to those of temperate climates. This gap is addressed in Chapters 6 and 7.

Second, improvements in collecting and reporting temperature data on different green infrastructure typologies and sites are urgently needed. Further research should address this issue by developing standardised protocols and climate-related classification systems for vegetation to facilitate inter-site and inter-typology comparisons at multiple spatial scales. This classification approach should facilitate the three-dimensional analysis of urban areas by incorporating the effect of vertical surfaces and volumetric indicators in current methodologies. The development of a dedicated scheme for vegetation combining approaches such as the LULC (Anderson et al., 1976), the LCZ (Stewart & Oke, 2012) and

the UVST (Lehmann et al., 2014) could help respond to this gap. Thus, a classification framework to respond to this need is proposed in Chapter 4.

Third, most of the literature overlooked the dynamic spatial and temporal heterogeneity, the connectivity, and the multi-functionality principles that govern green infrastructure (as defined in Chapter 2). Accordingly, future research should be strengthened by considering the temporal changes of vegetation (*i.e.* foliage type, phenology, maturity, etc.). It is also recommended a more holistic or integrative approach to examine and understand the interplay and cumulative effects of natural, semi-natural, and artificial surfaces and elements of the built environment.

Moreover, future research should include functional, structural and spatial configuration parameters for a comprehensive thermal analysis of urban vegetation and water features. The use of landscape metrics has been more common in large scale analyses; hence, future studies may explore the possibility of downscaling the use of FRAGSTATS metrics to analyse the fine-scaled composition and distribution inside greenspaces and street canyons. The aspects related to the third gap are considered in the formulation of the green infrastructure typology (GIT) presented in Chapter 4 and in the research methodology and indicators defined in Chapter 5.

Fourth, vegetation abundance, plant structure and shade from trees are aspects that attracted the most attention from researchers; however, the role of water in the provision of optimal cooling has not been fully examined (Coutts et al., 2012; Norton et al., 2013). Accordingly, the study of the influence of irrigation and evapotranspiration rates in air and surface temperature reductions is an interesting area for future research. These considerations are also incorporated in the formulation of the green infrastructure typology (GIT) presented in Chapter 4 and in the definition of the research variables listed in Chapter 5.

Furthermore, minimum irrigation and humidity requirements could be a promising research in the future, as not all vegetated surfaces and plant species are capable of tolerating severe temperatures or providing the same amount of evaporative cooling (Hunter et al., 2012; Norton et al., 2015). The application of remotely sensed techniques for the estimation of evapotranspiration could help reducing the amount of work, time and costs compared to traditional in-situ observations. Advances in the most appropriate selection and spatial distribution of plant species are also crucial to ensure the tolerance of communities to extreme heat events and to maintain or improve ideal climate conditions.

Fifth, a comprehensive methodological framework is required for a more precise and accurate analysis of the thermal profiles of green infrastructure at multiple scales and over large urban areas. Particularly, little is known about the most optimal types, abundance and distribution of green infrastructure necessary to maximise the mitigation of heat at neighbourhood and street canyon levels. This assessment framework is presented in Chapter 5, tested in Chapter 6 and results analysed in Chapter 7.

Key implementations that could be additionally used to tackle this gap include a simultaneous deployment of drone-based technology with in-situ measurements (fixed stations and mobile transects). However, these need to be matched in space and time and should be accompanied by further statistical analysis. Furthermore, UAVs and real-time sensors installed in buildings and across smart precincts/cities are a fantastic opportunity to collect the quantity and quality of data necessary for permanent monitoring of several types of UHIs, and for analysing the effectiveness of green infrastructure interventions at different stages. These suggestions are not implemented in this research due to time and resource constraints.

Finally, despite all the efforts and increasing interest of scientists and governments to mitigate the negative effects of global warming and already increased urban temperatures, future research should focus on translating the existing evidence into an effective set of practical rules and design guidelines for policy makers, industry partners and practitioners in general. This is addressed in Chapters 8 and 9.

Chapter 4

Developing a green infrastructure typology for climate studies

4.1 Introduction

As described in previous chapters, the definition, identification, characterisation and classification of green infrastructure is necessary for the performance-based assessment of green infrastructure across multiple ESS, particularly the climate regulation, and for identifying and delivering more effective planning initiatives and strategies (Jacobs et al., 2014; Naumann et al., 2011).

The development of *typologies* is considered a powerful planning tool and a cross-disciplinary exercise for the holistic comprehension of intricate problems, and for advancing current practices and policies (Mell, 2008, 2010; Young et al., 2014). Hence, the inventory of different types of vegetation and water bodies is crucial to evaluate existing conditions and to develop well-targeted guidelines for designing, planning and managing urban landscapes more effectively (Jacobs et al., 2014; Liu & Yang, 2013; Mell, 2010; Pauleit & Duhme, 2000; Woolley, 2006; Young et al., 2014).

The formulation of a comprehensive classification scheme for green infrastructure, however, requires an understanding of the theoretical basis triggering classifications to be able to distil and organise a whole body of knowledge into standardised terms according to specific goals, subject areas or research focuses (Aldous, 2014; Jacobs et al., 2014; Young et al., 2014). However, existing classification systems offer limited insights on the identification and categorisation of green infrastructure across different urban settings, and are insufficient to support climate studies at fine spatial scales (Bowler et al., 2010b; Young et al., 2014). This represents a significant research gap, in terms of both theory and practice.

Accordingly, the aim of this chapter is to synthesise and evaluate the existing evidence on how green infrastructure is being categorised and characterised worldwide to distil the most relevant approaches and clarify existing typologies. This is intended to provide a conceptual framework which will be applied to propose a classification scheme that can support the mapping and assessment of green infrastructure in the context of this research.

To achieve this, the first part of the chapter integrates evidence from across a broad range of literature by systematically reviewing 85 studies to answer the following questions: (a) what is the geographic location of the key literature dealing with the classification of green infrastructure; (b) what are the different methods, principles, approaches and parameters employed for cataloguing green infrastructure; (d) which high level categories can green infrastructure be classified into; (e) which typologies and terminology can be assigned to each category; and (f) how this knowledge can be translated into a conceptual framework to develop a more comprehensive typology.

The second part of the chapter brings together the conclusions and evidence of this systematic review and defines a conceptual framework and criteria for classifying green infrastructure from a climate-oriented perspective. A new taxonomy (also referred as conceptual matrix) is then proposed consistent with this framework. These taxa are further reduced to streamlined typologies for application based on remote sensing data. The remainder of the chapter presents the definitions, classification parameters and threshold values for all the 34 typologies. The methods for the computation of parameters and the workflow for the automated classification of typologies is presented in Chapter 6.

PART I: Towards a comprehensive green infrastructure typology: A systematic review⁸

4.2 Methods

Similarly to Chapter 3, the present chapter applies a systematic literature review following the approaches and procedures defined by Khan et al. (2003), Pickering and Byrne (2013), Pullin and Stewart (2006) and Stewart (2011b). The searching process was carried out using three major databases including Google Scholar, Web of Science and Scopus, and printed material; and combined terms such as *vegetation*, *green infrastructure*, *urban greening*, *greenery*, *water bodies*, *types*, *taxonomy*, *classification* and *typologies*.

The number of documents identifying or cataloguing different types of green infrastructure is extensive and non-standardised; hence, this systematic review concentrates on the most cited and representative sample of the literature, which includes scholarly papers (conferences and journals), theses, and high-quality grey literature (*i.e.* technical reports, government guidelines). To be included in this review, publications complied with the following selection criteria:

- a. The literature belonged to any of the following fields: urban planning and design, landscape architecture, street design, urban forestry, remote sensing and land surveying, geography and urban climatology or meteorology.
- b. Articles considered any of the following classification aspects: ESS, multi-functionality, morphological and structural attributes, LULC.
- c. The literature studied, described or discerned an identifiable set of typologies, categories, terminology or taxonomies. Literature focusing on specific plant species and types, biological taxonomy, horticultural and gardening classifications were excluded because this are beyond the scope of this research.
- d. Documents were in English, Spanish and German.

The content analysis and interpretation of the findings was based on: (a) type of publication, (b) differing terminology, (c) geographic location of studies under each green infrastructure category identified, (d) classification approaches and parameters, and (d) typologies identified per category. One limitation is the exclusion of other languages which can

⁸ A version of Chapter 4 – Part I has been published: Bartesaghi Koc, Osmond, and Peters (2017), Towards a comprehensive green infrastructure typology: a systematic review of approaches, methods and typologies, *Urban Ecosystems*, 20, p.15-35.

potentially bias interpretation of the findings. The context and the main authors' affiliations are used to determine the geographical origin of studies.

There were identified a total of 100 potential articles that distinguished at least one type of green infrastructure; however, only 85 met the final quality and selection criteria. This systematic review is organised in four main sections including (a) the analysis of the geographic patterns and contextual response; (b) the analysis of classification approaches, methods and parameters; (c) the analysis of categories and typologies and spatial scales identified per category; and (d) a summary of findings that will help in constructing the classification framework proposed in the Part II.

4.3 Analysis of geographic patterns

Geographical context plays an important role on classifying green infrastructure and commonly depends on: (a) the site-related conditions, (b) research objectives, and (c) the country-based geopolitical conditions and regulations (Mell, 2010). This suggests that it is impractical to propose universal and unique classification typologies that can serve for all research purposes and settings since there is a regional bias to particular locations where the classification of green infrastructure concentrates the attention of experts (Davis, 2010; Mazza et al., 2011; Mell, 2014; Naumann et al., 2011).

Table 4.1 Number and type of articles per geographic location.

Type of Publication	UK	Rest of Europe ^a	USA & Canada ^b	Australasia ^c	Asia ^d	Number of papers	Percent of papers
Journal	7	12	11	6	7	44	50.5
Report/Guidelines	14	4	1	8	-	27	31.8
Book/Chapter	2	2	5	-	1	9	11.8
Thesis	1	1	1	-	-	3	3.5
Conference	-	2	-	-	-	2	2.4
Number of papers	24	21	18	14	8	85	100.0
Percent of papers	28.2	24.7	21.2	16.5	9.4	100.0	

Number of studies per country: ^aGermany (n=7), Spain (n=4), European Union-EU (n=3), The Netherlands (n=2), Austria (n=1), Denmark (n=1), Greece (n=1), Italy (n=1). ^bUSA (n=13), Canada (n=5). ^cAustralia (n=12), New Zealand (n=2). ^dHong Kong (n=3), China (n=3), Singapore (n=2).

Table 4.1 presents the number and type of publications grouped according to their geographic location. The review includes publications from 15 countries and/or territories, split fairly evenly between peer reviewed and grey literature. It can be observed that there is a strong geographic bias towards European countries, particularly the United Kingdom (UK) (n=24), followed by other European countries (n=21), especially Germany (n=7) and

Spain ($n=4$), together representing more than half of the reviewed literature ($n=45$). The remaining 50% of publications originate in the USA and Canada ($n=18$) and Australasia ($n=14$) with fewer from Asian countries ($n=8$).

The majority of studies come from peer-reviewed publications (52%); with the exception of the UK, where the discussion on green infrastructure is led by grey literature such as government reports and technical papers. For instance, the Planning Policy Guidance Note 17 (PPG17) produced by the Urban Green Spaces Taskforce (ODPM, 2002a, 2002b), has served as a guideline and benchmark for most reports produced across England since 2002.

The process of identifying and characterising the different assets or components of green infrastructure largely depends on the terminology and definitions employed by each study. In fact, the characterisation of vegetation at different spatial scales and geographical contexts can be performed in a myriad of ways, hindering their standardisation (EEA, 2011; Oke et al., 1989). In a preliminary analysis it was identified that despite the large variety of overlapping terminology, green infrastructure can be generally organised into five main high-level categories: (a) tree canopy (TC), (b) green open spaces (GOS), (c) water bodies (WB), (d) green roofs (GR) and (e) vertical greenery systems (VGS) (green walls/facades) [Table 4.2]. The number and origin of studies concentrated in each category are summarised in Table 4.3.

Table 4.2 Different terminology organised into four main categories of green infrastructure.

Tree canopy (TC)	Green Open Spaces (GOS)	Water bodies (WB)	Green Roofs (GR)	Vertical Greenery Systems (VGS)
Green canopy	Green belts	[Water] features	Eco-roofs	Bio-walls
Green streets	Green corridors	[Open] water	Green	Green façades
Green alleys	Green covers	Blue infrastructure	rooftops	Green walls
[Street]	[Urban] Green spaces	Urban water	Living roofs	Living walls
[Roadside]	Greenways	Aquatic surfaces	Rooftop	Vertical
[Avenue] trees	[Vegetated] Ground	Water-	gardens	landscaping
Shrubs, shrubbery	covers	[courses/ways]		Vertical
Tree cover	Ground surfaces	Waterside		vegetation
Urban forestry	Land covers	[areas/zones]		
Urban tree canopy	[Public] [Urban] open			
Woodland	spaces			
[Forest]land	Urban land			
	[Urban] vegetation			
	structures /			
	Vegetative covers			

Based on: Abunnasr (2013); Ahern (1995); Arlt et al. (2005); Bowler et al. (2010a, 2010b); Brady et al. (1979); Byrne and Sipe (2010); DTLR (2002); Dunnett et al. (2002); English Nature (2003); Foster et al. (2011); Francis and Lorimer (2011); Hunter et al. (2012); Jacobs et al. (2014); Jim (1989, 2015b); Jim and Chen (2003); Landscape Institute (2009); Lehmann et al. (2014); Mathey et al. (2010); Mathey et al. (2011); Norton et al. (2013); Norton et al. (2015); Oberndorfer et al. (2007); Ochoa (1999); ODPM (2002a, 2002b); OEH (2015); Oke et al. (1989); Ottel   et al. (2011); Pauleit et al. (2003); Pauleit and Duhme (2000); P  rez et al. (2014); Peters et al. (2011); Stewart and Oke (2012); Susorova (2015); Tooke et al. (2009); VEAC (2011); Wong (2011); Wong and Chen (2010); Woolley (2006).

Table 4.3 Number and origin of studies focusing on different green infrastructure categories

GI Category	UK	Rest of Europe	USA & Canada	Australia	Asia	Number papers	Percent papers *
GOS	22	13	13	10	5	63	74.1
TC	13	10	13	7	4	47	55.3
WB	17	7	7	3	1	35	29.8
GR	7	3	5	7	1	23	27.1
VGS	2	8	3	7	4	24	28.2
OC ¹	1	-	-	1	-	2	2.4

¹OC=other classification. * Percentage calculated from 85 articles.

Green open spaces and tree canopy attract more attention in European countries where planning strategies are well-established and intervention priorities have focused on the provision of large greenways, corridors and networks at city and regional level. These policy-oriented interests are largely due to the wide implications of green open spaces (including trees) in the quality of life, health and wellbeing of population (Pauleit et al., 2003; Tzoulas et al., 2007); their multi-scale applicability; the rapid inventory process; and the easy multi-sectorial understanding and alignment with existing land-use classes (Davies et al., 2006; Mazza et al., 2011; Mell, 2014; TMF, 2011; Tzoulas et al., 2007).

Studies from Germany can be differentiated from the rest by combining the principle of urban biotopes with the structural characteristics of vegetation (Arlt et al., 2005; Lehmann et al., 2014; Mathey et al., 2010; Pauleit & Duhme, 2000). Furthermore, the study and classification of vertical greenery systems have been the concern of experts from The Netherlands (Ottel   et al., 2011; Perini et al., 2011); and more especially, from Mediterranean countries such as Spain (P  rez et al., 2011a, 2011b; P  rez et al., 2014) and Greece (Kontoleon & Eumorfopoulou, 2010).

Asian countries have also demonstrated a particular interest in green roofs and vertical greenery systems that represent the most suitable solutions in the context of high-density and land scarcity. In Australia, classifications have been triggered by the necessity of prioritising green infrastructure to respond to the UHI phenomenon (Norton et al., 2015), while literature from North America has been more focused on biodiversity conservation and water management implications of green infrastructure, through the notion of low impact development (LID).

4.4 Analysis of approaches, methods and parameters

Literature review (89%), case studies (52%) and remote sensing (including land surveying) (37%) are the most common methods employed to identify and classify green infrastructure. Among these, remote sensing and GIS-based tools have not been fully explored; signifying a great opportunity for a more accurate and time-saving visualisation and analysis of highly complex and heterogeneous settings (Hawken et al., 2014).

The available evidence suggests that green infrastructure can be classified according to (a) *functional* (services); (b) *structural* (form/morphology); and (c) *configurational* (spatial interrelationships) principles; in accordance with the tripartite approaches proposed by Ahern (1995, 2007) and Mell (2008, 2010), and the spatial scales defined by Oke et al. (1989) and Oke (2006). Table 4.4 and 4.5 provide a summary of main principles applied by each study; albeit some classifications are underpinned by more than one principle. Additionally, there are listed different approaches, theoretical concepts and classification parameters that depended on the types of green infrastructure under investigation.

4.4.1 Functional-configurational classification

Green infrastructure is mostly classified from a *functional-configurational* perspective. The *multi-functional network and connectivity* have been widely accepted as the most common classification approach, encompassing aspects such as land uses, purpose, intensity of use, connectivity, spatial scale, spatial configuration, catchment, maintenance, accessibility, values and significance (ecological, cultural, social, political and economic) of functions. For instance, Figure 4.1 depicts an environmentally-based classification system for urban greenspaces as defined by Hough (2002), which combines several functional aspects to define a hierarchical set of greenspace typologies.

Concepts such as ‘*Landscape ecology*’ (Abunnasr, 2013; Ahern, 2007; Jim & Chen, 2003; Li et al., 2005), ‘*Greenspace continuity & Green grid concept*’ (Byrne & Sipe, 2010; Cooper, 2010; Davis, 2010; DEFRA, 2008; Gill et al., 2007; Jim & Chen, 2003; Mazza et al., 2011; Wang, 2001), ‘*Value of public space*’ (Bell et al., 2007), ‘*Patch-corridor-Matrix-Model*’ (Ahern, 2007) and ‘*Need-based approaches*’ (DTLR, 2002; ODPM, 2002a, 2002b) are complementary approaches associated to multi-functionality that are commonly incorporated by studies.

The criteria defined by the Urban Green Space Taskforce (UGST) (DTLR, 2002) and the ‘Planning Policy Guidelines 17 (PPG17)’ (ODPM, 2002a, 2002b) have largely influenced approaches and classifications across the UK. This key literature drew on stakeholder

forums and remote sensing to propose a need-based approach for auditing green spaces, providing the groundwork for most of the later publications. For instance, Gill et al. (2007) updated the PPG17 typology by including urban morphology types (UMT) for the spatial integration of natural processes and human activities. Similarly, the Mersey Forest approach (Landscape Institute, 2009; The Mersey Forest, 2010, 2011), and the East Midlands scoping study (EMDA, 2010; TEP, 2005) utilised the PPG17 to propose a mapping framework to audit green infrastructure for planning development purposes.

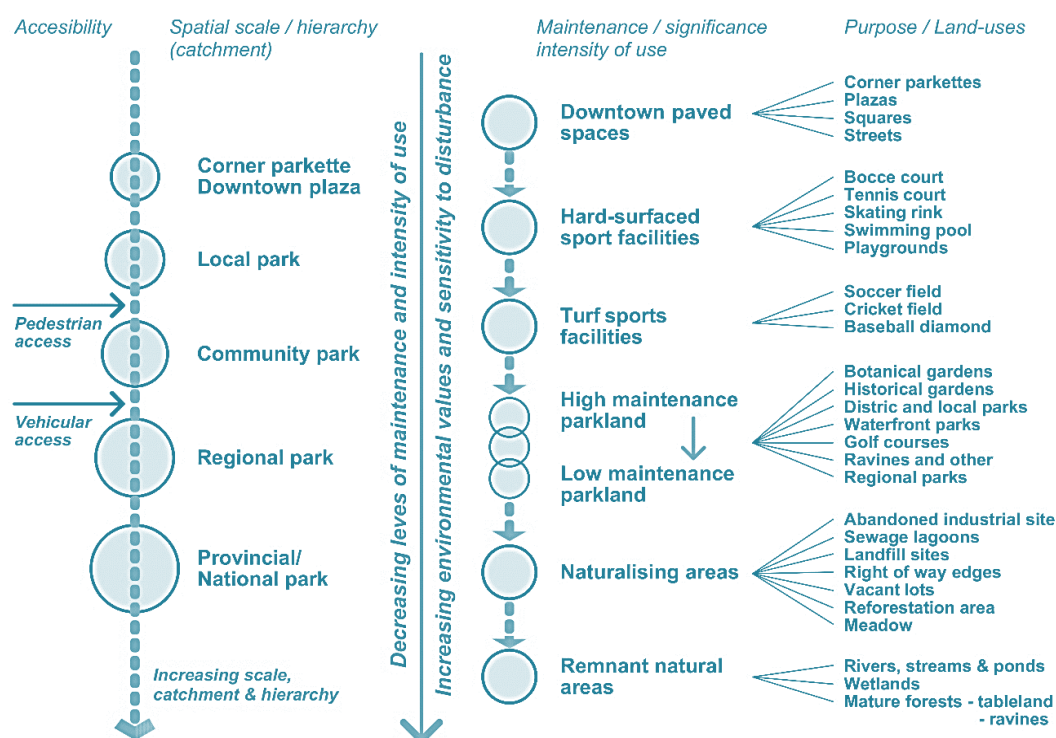


Figure 4.1 An environmentally-based and hierarchical classification system for urban greenspaces combining several functional aspects (Redrawn based on Hough, 2002).

The PPG17 illustrates the strong influence of government planning policies on the identification, characterisation and deliverability of green infrastructure. Its value lies in the broad applicability and flexibility across different geographical settings, ownerships and purposes within the UK (Sheate et al., 2012; Tzoulas et al., 2007). However, government-based taxonomies should be adopted with caution since they are extremely contextualised to particular land uses that reduce their applicability in other geo-political contexts and research scopes.

Indeed, classifications that solely rely on land uses and accessibility (public/private differentiation) are usually constrained in representing the ecological processes of green infrastructure (*i.e.* carbon sequestration, biodiversity or thermal regulation). This is because green infrastructure functionality does not only depend on purpose, but most importantly

on the physiognomic attributes and spatial interdependency of vegetation assets (Ahern, 2007; Cadenasso et al., 2007; Cadenasso et al., 2013; English Nature, 2003; Hawken et al., 2014; Jacobs et al., 2014; Pauleit et al., 2003; Peters et al., 2011; Stewart & Oke, 2012; Tooke et al., 2009; Wilmers, 1988).

In this regard, Mell (2008, 2010) proposes a tripartite approach to classify green infrastructure in terms of *'form'*, *'function'* and *'context'* following Ahern (1995) greenways classification system. Mell's work emphasises the role of green infrastructure beyond land use types, addressing this problem both theoretically and practically by considering the aspects of connectivity, accessibility and multi-functionality (Mell, 2010). On the other hand, Young et al. (2014) proposed a very distinctive categorisation that focuses on the social and ecological aspects of green infrastructure. Both studies attempt to reconcile different overarching classification approaches such as hierarchy (Ahern, 1995; Dunnett et al., 2002), ecological values (Davies et al., 2006), human health (Tzoulas et al., 2007); and valuation of ESS (Dobbs et al., 2011; EEA, 2011; Groot et al., 2002; MEA, 2005).

'Hierarchy and significance' is a concept linked to the principle of multi-functionality that has been pioneered by Ahern (1995). The primary focus of this approach is the importance of landscape contexts and goals across different spatial scales. For example, the hierarchical characterisation introduced in the UK by the London Planning Advisory Committee (LPAC) (Llewelyn-Davies Planning, 1992) has been adopted by a considerable number of studies for the stratified classification of green open spaces at national, regional, metropolitan and local levels (Byrne & Sipe, 2010; Cheltenham Borough Council, 2008; Christchurch City Council, 2010; Dunnett et al., 2002; The Scottish Government, 2008; VEAC, 2011; Wong, 2011).

This has had a great acceptance among local governments and authorities because audit and strategic planning of green infrastructure can be easily assigned to specific jurisdictions (Woolley, 2006). Moreover, the stratified subdivision has the capacity to aggregate or disaggregate categories depending on the level of detail required; nonetheless, there is always the possibility of double counting or overlapping types across scales (Dunnett et al., 2002).

The complexity of the built environment precludes the definition of precise boundaries between the natural and the artificial world. Consequently, there is still no consensus of what can or cannot be considered green infrastructure, which may prove detrimental to understand the discernibility of features (Mell, 2010). To address this limitation, the

accessible natural greenspace standard model (ANGSt) proposed by English Nature (2003) incorporates accessibility, structural complexity and intensity of use as classification parameters based on a gradual progression from grey (artificial) to green (natural) conditions.

Likewise the *abiotic-to-biotic spectrum* proposed by Ahern (2007), the *ANGSt* model conceives green infrastructure as a continuum phenomenon where spatial interrelationships play an important role in supporting bio-physical and ecological processes (Davies et al., 2006; Pauleit et al., 2003). Critically discussed by Pauleit et al. (2003), this model illustrates the difficulties that arise when attempting to reconcile two points of view: the conservation of nature and the public use of greenspaces.

Supporting the *functional* classification principle, the concept of ESS has been employed to differentiate distinctive delivery capacities of vegetation among the high level ESS themes of supporting, providing, regulating, and cultural (Mazza et al., 2011; MEA, 2005). Among these categories, the climate-regulating services have captured the attention of climate change researchers (Bowler et al., 2010b; Hunter et al., 2012; Norton et al., 2013; Norton et al., 2015; Wong & Chen, 2010).

For instance, Bowler et al. (2010b) used an ESS approach to undertake a systematic review of the potential cooling effects of three types of green infrastructure: parks, trees/forests and green roofs. Studies conducted in Australia identified evapotranspiration, albedo, shading and wind flow as key parameters for classification (Coutts et al., 2012; Coutts et al., 2015; Hunter et al., 2012; Norton et al., 2013; Norton et al., 2015).

Returning to ESS as a functional approach, some authors have emphasised the classification of land uses (Cooper, 2010; DEFRA, 2008; Ely & Pitman, 2014; Panduro & Veie, 2013; Sheate et al., 2012), often using remote sensing to inform the spatial distribution of ESS. Reports from the European Union have similarly focused on the use of spatial planning and mapping tools to guide design interventions (Davis, 2010; Mazza et al., 2011; Naumann et al., 2011). In contrast to the holistic overview of ESS proposed by European research, studies from other countries have concentrated on particular services. For instance, Foster et al. (2011) appealed to the low impact development (LID) concept in the USA. In Australia, Ely and Pitman (2014) and Coutts et al. (2012) described the environmental potentialities of green infrastructure appealing to water sensitive urban design (WSUD), while the New South Wales Office of Environment and Heritage (OEH, 2015) addressed green infrastructure from an environmental point of view and Rupprecht et al. (2015) considered biodiversity implications.

Table 4.4 presents a list of the reviewed studies that employ functional and configurational principles to classify green infrastructure by summarising their classification approaches, parameters, and research methods.

Table 4.4 List of methods, approaches and parameters used by ‘functional-configurational’ classifications.

Citation	Classif. Methods	Categories	Classification approaches	Classification parameters
Abunnasr (2013) ^a	LR	TC, GOS, WB, GR, VGS	<ul style="list-style-type: none">• Network approach• Multi-functionality• Landscape ecology	<div>1. Size</div> <div>2. Location & catchment</div> <div>3. Scale & hierarchy</div> <div>4. Spatial configuration & complexity</div> <div>5. Land-use types</div> <div>6. Purpose</div> <div>7. Significance</div> <div>8. Accessibility & ownership</div> <div>9. Management & maintenance</div> <div>10.Intensity of intervention/use</div> <div>11. Functions & values:<div>a. Socio-cultural</div><div>b. Economic</div><div>c. Environmental</div><div>d. Political</div></div> <div>12. Ecosystem services:<div>a. Provisioning</div><div>b. Regulating<ul style="list-style-type: none">- Shading (LAI)- Evapotranspiration- Wind modification- Water supply- Thermal properties- Plant support- Surface properties- Anthropogenic heat- Type of vegetation</div><div>c. Cultural</div><div>d. Supporting</div></div>
Ahern (1995)	LR, CS	GOS, WB	<ul style="list-style-type: none">• Hierarchy & significance• Multi-functionality	
Ahern (2007)	LR	GOS	<ul style="list-style-type: none">• Multi-functional network• Patch-Corridor-Matrix	
Aldous (2014)	LR, GIS, CS	GOS	<ul style="list-style-type: none">• Multi-functionality	
Bell et al. (2007) ^b	LR, RM	GOS	<ul style="list-style-type: none">• Multi-functionality• Value of public space	
Bowler et al. (2010b)	LR	TC, GOS, GR	<ul style="list-style-type: none">• Climate regulating ESS	
Byrne and Sipe (2010)	LR	GOS	<ul style="list-style-type: none">• Hierarchy & significance• Multi-functionality	
CBC (2008) ^b	LR, GIS, APS	GOS		
CCC (2010)	LR, CS	GOS		
Cooper (2010) ^b	CS, NA, GIS, SF	TC, GOS, WB	<ul style="list-style-type: none">• ESS• Network analysis (Green grid)	
Davis (2010)	LR, GIS, CS	TC, GOS	<ul style="list-style-type: none">• ESS• Connectivity	
Davies et al. (2006)	LR, SF	TC, GOS, WB, GR	<ul style="list-style-type: none">• Multi-functionality	
DEFRA (2008) ^b	LR, CS	TC, GOS, WB	<ul style="list-style-type: none">• ESS• Green grid concept	
DTLR (2002) ^b	LR	GOS, WB	<ul style="list-style-type: none">• Multi-functionality• Need-based approach	
Dunnett et al. (2002)	LR, CS, SI	TC, GOS, WB	<ul style="list-style-type: none">• Hierarchy• Multi-functionality	
Ely and Pitman (2014)	LR	TC, GOS, WB, GR, VGS	<ul style="list-style-type: none">• ESS• Water sensitive urban design	
EMDA (2010) ^b	LR, CS	TC, GOS, WB	<ul style="list-style-type: none">• Multi-functional network	
English Nature (2003) ^b	LR, APS, CS	GOS, WB	<ul style="list-style-type: none">• Accessible Natural greenspace standard (ANGSt) model• Multi-functionality	
Foster et al. (2011)	LR, CS	TC/GR	<ul style="list-style-type: none">• ESS• LID	
Gill et al. (2007)	LR, GIS, CS	GOS, WB	<ul style="list-style-type: none">• Multi-functional network• ESS• Urban morphology types	
Hunter et al. (2012)	LR	TC, GR, VGS	<ul style="list-style-type: none">• Climate regulating ESS• Hierarchy	
Jim and Chen (2003)	LR, CS	TC, GOS	<ul style="list-style-type: none">• Multi-functional network• Landscape ecology	
Keeley (2011)	LR	GOS, WB, GR	<ul style="list-style-type: none">• Climate regulating ESS• Green area ratio	

Citation	Classif. Methods	Categories	Classification approaches	Classification parameters
Landscape Institute (2009) ^b	LR, CS	TC, GOS, WB, GR, VGS	<ul style="list-style-type: none"> Multi-functional network ESS 	
Llewelyn-Davies (2000)	LR	TC, GOS, WB	<ul style="list-style-type: none"> Hierarchy & significance Multi-functionality 	
Li et al. (2005)	LR, GIS, CS	TC, GOS, GR, VGS	<ul style="list-style-type: none"> Multi-functional network ESS Landscape ecology 	
Mazza et al. (2011) ^c	LR, CS	TC, GOS	<ul style="list-style-type: none"> ESS Multi-functional network 	
Mell (2010) ^d	LR, SI	Other	<ul style="list-style-type: none"> Multi-functionality 	
Naumann et al. (2011) ^c	LR, CS	TC, GOS	<ul style="list-style-type: none"> ESS Ecosystem habitats 	
Norton et al. (2013); Norton et al. (2015)	LR, GIS	TC, GOS, GR, VGS	<ul style="list-style-type: none"> Climate regulating ESS 	
ODPM (2002a, 2002b) (PPG17)	LR	GOS, WB	<ul style="list-style-type: none"> Multi-functionality Need-based approach 	
OEI (2015)	LR	TC, GOS, GR, VGS	<ul style="list-style-type: none"> Climate regulating ESS Urban green cover 	
Panduro and Veie (2013) ^e	LR, GIS, CS	GOS	<ul style="list-style-type: none"> Hedonic Valuation Model ESS 	
Pauleit et al. (2003) ^f	LR, GIS, SI	GOS, WB	<ul style="list-style-type: none"> Multi-functional network ANGSt model 	
Rupprecht et al. (2015)	LR	TC, GOS, WB, GR, VGS	<ul style="list-style-type: none"> ESS Biodiversity 	
Schilling and Logan (2008)	LR	TC, GOS, WB, GR	<ul style="list-style-type: none"> Multi-functionality 	
Sheate et al. (2012) ^b	LR, NA, GIS	TC, GOS, WB	<ul style="list-style-type: none"> ESS Network analysis 	
TEP (2005) ^b	LR, GIS, SF	TC, GOS, WB	<ul style="list-style-type: none"> Multi-functionality 	
TMF (2010) ^b	LR, CS	TC, GOS, WB, GR		
TMF (2011) ^b	LR, GIS	TC, GOS, WB, GR		
TSG (2008)	LR	GOS	<ul style="list-style-type: none"> Hierarchy & significance Multi-functionality 	
VEAC (2011)	LR	GOS	<ul style="list-style-type: none"> Hierarchy 	
Wang (2001)	LR	GOS, WB	<ul style="list-style-type: none"> Multi-functionality 	
Wong (2011) ^g	LR, GIS, CS	GOS	<ul style="list-style-type: none"> Multi-functional network 	
Wong and Chen (2010)	LR, GIS, CS	TC, GOS, GR, VGS	<ul style="list-style-type: none"> Climate regulating ESS 	
Woolley (2006)	LR, CS	TC, GOS, WB, GR	<ul style="list-style-type: none"> Hierarchy Value of space (home range concept) 	
Young et al. (2014)	LR, CS	Other	<ul style="list-style-type: none"> Multi-functionality (Triple-Bottom-Line) 	

APS=Aerial & photographic survey; CS=Case study; GIS=Geographic information systems; LR=Literature review; NA=Network analysis; RM=Research mapping; SF=Stakeholders forum; SI=Survey & interviews. ESS=Ecosystem Services.

^a Typology after Gill et al. (2007) and Ahern (2007);

^b Classification based on ODPM (2002b) (PPG17);

^c Classification based on Davis (2010);

^d Typology based on Ahern (1995);

^e Typology after Bell et al. (2007);

^f Evaluates English Nature (2003) approach;

^g Urban space typology based on Woolley (2006).

4.4.2 Structural-contextual classification

The identification and study of the structural characteristics of vegetation is another important principle underpinning classifications; nevertheless, it was found that in some cases a functional approach is additionally included to achieve more comprehensive and explanatory typologies. Table 4.5 organises the studies that employed the structural and configurational principles to classify green infrastructure by summarising their classification approaches, parameters, and research methods.

Table 4.5 List of methods, approaches and parameters used by studies under ‘structural-configurational’ classifications.

Citation	Classif. methods	Categories	Classification approaches	Classification parameters
Anderson et al. (1976)	LR, GIS, CS	TC, GOS, WB	<ul style="list-style-type: none"> Land use/land cover (LULC) 	<ol style="list-style-type: none"> 1. LULC types 2. Spatial scale 3. Urban morphology types 4. Vegetation attributes: <ol style="list-style-type: none"> a. Foliage geometry & shape b. Foliage contiguity & distribution c. Foliage density (LAI, NDVI) dimensions / volume d. Foliage type (deciduous, evergreen) e. Extension & orientation f. Segment attributes of trees g. Derived fractions of vegetation h. Thermal properties of plants 5. Surface properties: <ol style="list-style-type: none"> a. Biological b. Physical & thermal c. Structural 6. Supporting structure attributes (only for green roofs and vertical greenery systems): <ol style="list-style-type: none"> a. Construction material b. Installation c. Location & orientation d. Operation & maintenance e. Intensity of use f. Accessibility
Arlt et al. (2005)	LR, GIS, CS	TC	<ul style="list-style-type: none"> Vegetation structure Urban biotopes & land-use 	
Brady et al. (1979) ^b	LR, CS	TC, GOS	<ul style="list-style-type: none"> LULC Urban ecosystem types 	
Cadenasso et al. (2007); Cadenasso et al. (2013)	LR, GIS, CS	TC, GOS, WB	<ul style="list-style-type: none"> LULC 	
Di Gregorio and Jansen (1998)	LR	TC, GOS, WB	<ul style="list-style-type: none"> LULC Hierarchy 	
Dunnett and Kingsbury (2004)	LR, CS	WB, GR, VGS	<ul style="list-style-type: none"> Morphological attributes 	
Francis and Lorimer (2011)	LR	GR, VGS	<ul style="list-style-type: none"> Morphological attributes Urban reconciliation ecology 	
Höfle and Hollaus (2010)	GIS, CS	TC	<ul style="list-style-type: none"> Vegetation edge-based segmentation 	
Hunter et al. (2014)	LR	VGS	<ul style="list-style-type: none"> Morphological attributes Climate regulating ESS 	
Jacobs et al. (2014)	GIS, ITM	TC, GOS, WB	<ul style="list-style-type: none"> Vegetation cover attributes Multi-functionality 	
Jim (1989)	GIS, APS	TC	<ul style="list-style-type: none"> Morphological attributes Spatial configuration 	
Jim (2015b)	LR	VGS		
Kontoleon and Eumorfopoulou (2010)	LR	VGS	<ul style="list-style-type: none"> Morphological attributes 	
La Rosa and Privitera (2013)	LR, CS, GIS	TC, GOS	<ul style="list-style-type: none"> LULC 	
Lehmann et al. (2014) ^a	LR, GIS, CS	TC, GOS, WB	<ul style="list-style-type: none"> Urban vegetation structure types (UVST) Urban biotopes Climate regulating ESS 	
Liu and Yang (2013) ^b	GIS, CS	TC, GOS, WB	<ul style="list-style-type: none"> LULC 	
Mathey et al. (2011) ^a	LR, GIS, CS	TC, GOS, WB	<ul style="list-style-type: none"> UVST 	
Mathey et al. (2010) ^a	LR	TC, GOS, WB	<ul style="list-style-type: none"> Urban biotopes Climate regulating ESS 	

Citation	Classif. methods	Categories	Classification approaches	Classification parameters
Oberndorfer et al. (2007)	LR	GR	<ul style="list-style-type: none"> • Morphological attributes • Provisioning ESS 	
Ochoa (1999)	LR, CS	TC, GOS, WB	<ul style="list-style-type: none"> • Morphological attributes 	
Oke et al. (1989)	LR	TC, GOS	<ul style="list-style-type: none"> • Climate regulating ESS 	
Ottel�� et al. (2011)	LCA, CS	VGS	<ul style="list-style-type: none"> • Morphological attributes • Life cycle analysis (LCA) 	
Pauleit and Duhme (2000)	GIS, CS	TC, GOS	<ul style="list-style-type: none"> • LULC 	
P��rez et al. (2011a, 2011b), P��rez et al. (2014)	LR, CS	VGS	<ul style="list-style-type: none"> • Morphological attributes 	
Perini et al. (2011)	LR, CS	VGS	<ul style="list-style-type: none"> • Morphological attributes • Climate regulating ESS 	
Peters et al. (2011)	GIS, CS	TC, GOS, WB	<ul style="list-style-type: none"> • LULC • Climate regulating ESS 	
Stewart and Oke (2012)	LR, GIS	TC, GOS, WB	<ul style="list-style-type: none"> • LULC • Local climate zones (LCZ) 	
Susorova (2015)	LR	VGS	<ul style="list-style-type: none"> • Morphological attributes • ESS 	
Tooke et al. (2009)	GIS, CS	TC, GOS	<ul style="list-style-type: none"> • Morphological attributes 	
Williams et al. (2010)	LR,CS	GR		
Wilmers (1988)	GIS, APS	TC, GOS, WB	<ul style="list-style-type: none"> • LULC • Morphological attributes 	
Wong et al. (2010)	LR, CS	VGS	<ul style="list-style-type: none"> • Morphological attributes 	
Zhou, Cadenasso et al. (2014)	LR, GIS, CS	TC, GOS	<ul style="list-style-type: none"> • LULC 	

APS=Aerial & photographic survey; CS=Case study; GIS=Geographic information systems; LR=Literature review; NA=Network analysis; RM=Research mapping; SF=Stakeholders forum; SI=Survey & interviews. ESS=Ecosystem Services.

a Approach based on Arlt et al. (2005) vegetation structures classification;

b Classification based on Anderson et al. (1976).

The tremendous importance of spatial configuration for understanding the heterogeneity of green infrastructure, and for discovering how different patterns and physical interactions shape multi-functional networks has been acknowledged by Hawken et al. (2014). The identification of the physical and formal attributes of greenery has been the primary focus of research concerning tree canopy, green roofs and vertical greenery systems categories; whereas land and vegetation cover classifications served for inventorying tree canopy and green open spaces.

In relation to green open spaces and tree canopy, a classification scheme of major LULC types for remote sensing studies in conservation and ecology was initially introduced by Anderson et al. (1976), adopted by Brady et al. (1979) and modified and expanded by Liu and Yang (2013). This classification was originally aimed at studies on natural resource

management at very coarse levels. Over the last decades, Anderson et al. (1976) scheme has become almost a standard for the industry and researchers all over the world, being an influential approach dominating the characterisation of greenspaces and tree canopy (Brady et al., 1979; Jacobs et al., 2014; La Rosa & Privitera, 2013; Liu et al., 2013; Pauleit & Duhme, 2000; Peters et al., 2011).

The LULC scheme has also been adopted by other schemes such as the National Land Cover Characterisation (NLCC) (United States Geological Survey, 2003), the Multi-resolution Land Characteristics (MRLC) [EPA and USGS (1992)], and the global land-cover classification [Food and Agriculture Organisation (FAO) (Di Gregorio & Jansen, 1998)] (Cadenasso et al., 2007; Cadenasso et al., 2013; Di Gregorio & Jansen, 1998).

In some cases, LULC classes have combined vegetated and built-up areas (homes, buildings), derelict land, brownfield land and utilities (*i.e.* roads, power lines) as an effort to integrate engineered and natural elements in a more comprehensive manner (Anderson et al., 1976; Pauleit & Duhme, 2000). However, green roofs and vertical greenery systems are completely excluded from LULC types.







Extensively criticised by Cadenasso et al. (2013) and Cadenasso et al. (2007), Anderson and related approaches have proved to be more suitable for studies at coarse scales as they remain inadequate to capture the spatial interrelationships and heterogeneity of biotic and abiotic elements at fine scales. Cadenasso et al. (2007) also notes that LULC types combine socio-economic functions and purposes (land-uses) with the physical structures of landscapes (land-covers), having left aside the ecological functioning of vegetation and water bodies.

The classification scheme called HERCULES (High Ecological Resolution Classification for Urban Landscapes and Environmental Systems) also relies on land classification, although it separates function (land use) and structure (land cover), and entirely focuses on the latter (Cadenasso et al., 2007; Cadenasso et al., 2013; Zhou, Cadenasso et al., 2014; Zhou & Troy, 2009). This scheme acknowledges the heterogeneity of urban landscapes by proposing the combination of three sets of elements: *buildings*, *surfaces* and *vegetation*, distinguished in terms of *form*, *amount* and *organisation* [Table 4.6]. In contrast to Anderson and related schemes, the HERCULES classification can be applied at medium scales and in varied urban contexts (Cadenasso et al., 2013; Zhou & Troy, 2009).

To amend the deficiencies of urban-rural classifications, and in similar way to the HERCULES approach, Stewart and Oke (2012) proposed LCZs (previously discussed in Chapter 2) as a scheme combining different surface properties, urban morphologies and

human activities. The LCZ characterisation provides a series of standardised land cover types that can be recombined into subclasses, facilitating the investigation of vegetation in particular conditions. Similarly, other studies have used the physical properties of canopy and surface covers as parameters to compare green and non-green open spaces and to differentiate pervious and impervious surfaces (Jacobs et al., 2014; La Rosa & Privitera, 2013; Liu & Yang, 2013; Pauleit & Duhme, 2000; Peters et al., 2011; Wilmers, 1988).

Table 4.6 Example of the characterisation of patches using HERCULES parameters.
(Redrawn based on Cadenasso et al., 2007)

Patch	Coarse vegetation	Fine vegetation	Bare soil	Pavement	Building proportion	Building type
	4	1	0	1	2	S
	4	0	0	0	0	N
	1	2	0	3	2	C
	1	1	4	1	0	N
	1	1	0	3	2	M
	2	4	0	0	0	N

Proportional cover of vegetation, surfaces and buildings is scored using five categories: 0 = none; 1 = present-10%; 2 = 11-35%; 3 = 36-75% and 4 = > 75%. Building types are identified as: N = none; S = single; C = connected; and M = mixed.

In Germany, an approach initially proposed by Arlt et al. (2005) incorporating the *urban biotope theory* and *vegetation structures* has served as the basis for subsequent studies investigating the correlation between tree-derived attributes (*i.e.* volume, size, geometry and height), surface permeability and air temperature differences (Lehmann et al., 2014; Mathey et al., 2010; Mathey et al., 2011). All these parameters interact with existing building structures and land uses to create particular '*urban vegetation structure types*' (UVSTs). Table 4.7 presents a summary of the 13 main categories divided into 57 UVST by considering the specific green volume (m^3/m^2) of each vegetated layer.

Table 4.7 Summary of the 13 main categories and 57 urban vegetation structure types (UVSTs) including their proportion of vegetated layers and specific green volume.
(Based on Arlt et al., 2005 and Mathey et al., 2011)

Category Urban Vegetation Structure Type (UVST)	Proportion of vegetation (%)			Green volume (m ³ /m ²)
	Low	Medium	High	
1. Residential, mixed-uses, industrial, commercial and specialised sites				
1.1 Built-up land with richly structured, park-like gardens	21	16	42	6.2
1.2 Built-up land with richly structured gardens, medium to high proportion of deciduous trees	40	8	23	2.5
1.3 Built-up land with poorly structured, intensively maintained gardens	31	10	11	1.5
1.4 Built-up land with little or no vegetation	16	6	6	0.7
1.5 Built-up land with no or few trees and shrubbery	41	7	13	1.1
1.6 Built-up land with trees and extensive shrubbery	35	19	15	1.5
2. Transport facilities and infrastructure				
2.1 Railway site and facilities, tracks, embankments	36	4	12	1.0
2.2 Road site with bordering greenery	14	0	21	1.4
2.3 Transport facilities and areas largely to completely sealed	0	0	0	0
2.4 Transport areas with greened carparks	9	3	24	1.67
3. Greenspaces				
3.1 Green space with trees and closed canopy	30	8	53	7.6
3.2 Green space with diverse amounts of trees and shrubbery	48	7	25	3.2
3.3 Lawn and sports field	83	1	9	1.2
3.4 Green space with little or no vegetation	14	3	12	1.5
3.5 Green space with young trees and partly with dense woodland	28	16	44	4.6
3.6 Green space with a lot of trees and extensive shrubbery, fruit trees	44	20	14	2.3
3.7 Green space with few trees and shrubbery, primarily decorative function	44	19	12	1.3
3.8 Green space with few trees and shrubbery, primarily lawns	54	10	16	1.4
4. Urban wastelands				
4.1 Urban wasteland with ruderal and other herbaceous plants, early stage of succession	69	8	7	0.7
4.2 Urban wasteland with pioneer trees, groves and woodland, middle stage of succession	76	12	7	1.6
4.3 Urban wasteland with mature trees, groves and woodland, late stage of succession	44	22	18	3.0
5. Landfills and quarries				
5.1 Partly or fully overgrown; restored landfill or quarry	32	61	1	2.1
5.2 Landfill or quarry with little vegetation, partly overgrown	70	19	0	0.6
5.3 Landfill or quarry with no or little vegetation	88	7	1	0.3
6. Agricultural sites				
6.1 Arable land	94	2	0	0.8
6.2 Land for fruit cultivation, orchard	16	77	3	1.4
6.3 Horticultural site, commercial use	40	11	6	0.9
6.4 Horticultural site, private use	64	10	12	1.1
6.5 Vineyard	78	5	13	1.4
7. Grassland				
7.1 Intensive grassland	78	6	7	1.2
7.2 Grassland with little or no trees and shrubbery	92	2	6	1.2
7.3 Grassland with communities of tall herbaceous vegetation	84	4	6	1.4
7.4 Grassland with trees and shrubbery	80	8	8	1.4
8. Trees, shrubs and bushes				
8.1 Bushes; pre-forest shrubbery	1	31	55	5.3
8.2 Hedges; row of shrubs	21	55	21	2.5
8.3 Row of trees; group of trees	25	22	50	6.1
8.4 Meadow with scattered fruit trees	52	33	13	2.6
8.5 Prominent individual tree	0	0	100	9.55
9. Woodland (deciduous, coniferous and mixed)				
9.1 Wood	3	24	73	7.7
9.2 Reforestation; tree nursery	4	81	12	1.8

9.3 Clear-felling; cleared corridor	64	12	23	2.6
9.4 Clearing with herbaceous vegetation	70	16	13	1.8
9.5 Clearing with meadow	96	1	3	0.6
9.6 Developed edge of the wood	19	7	14	10.4
10. Near-natural				
10.1 Near-natural wetland with reed beds, bulrush and sedge-marshland	77	23	0	1
10.2 Near-natural wetland with communities of tall herbaceous vegetation	84	13	3	1
10.3 Near-natural wetland with shrubbery	71	27	2	0.9
10.4 Near-natural wetland with trees	65	12	20	2.3
11. Waterside zones				
11.1 Waterside zone with reeds, bulrushes and sedges	28	37	4	1.0
11.2 Waterside zone with tall herbaceous vegetation, trees and shrubbery	23	18	55	6.3
11.3 Waterside zone with grassy banks	19	2	3	0.3
11.4 Waterside zone with little or no vegetation	15	9	2	0.2
12. Arid grasslands, heathland				
12.1 Arid and semi-arid grassland; heathland	67	28	0	0.5
12.2 Bushy to wooded dry grassland and heathland	35	58	0	1.9
13. Open sites				
13.1 Rocky area	-	-	-	-
13.2 Sandy area	-	-	-	-
13.3 Dune	-	-	-	-

Table 4.8 Example of a typical urban vegetation structure type matrix (Type 1.1) showing a list of structural attributes (horizontal axis) and the three height classes of vegetation layers (vertical axis). (Modified after Lehmann et al., 2014 and Mathey et al., 2011)

UVST 1.1 Built-up land with richly structured, park-like gardens												
Height class of vegetated layers		Selected structural characteristics										
		Spatial coverage and arrangement					Intensity & maintenance		Distinctive features		Specific height class of vegetation layer (m)	Proportionate area (%)
		Sparse	Low density	In groups	In rows	Dense	Low	High	Spontaneous vegetation	Border greenery beside roadways, pathways		
Low	Lawn							X				
	Meadow						X					
	Shrubbery and herbs ($\leq 1\text{m}$)											
Medium	Shrubbery and herbs ($> 1\text{m}$)											
	Low hedges ($\leq 1\text{m}$)											
	Medium hedges ($> 1 \leq 2.5\text{m}$)					X	X					
	Tree hedges ($> 2.5\text{m}$)											
	Bushes ($\leq 2\text{m}$)		X									
	Bushes ($> 2\text{m}$)					X						
	Small trees ($\leq 3\text{m}$)	X										
High	Medium trees ($> 3 \leq 10\text{m}$)			X		X						
	Tall trees ($> 10\text{m}$)		X			X						
Other areas within the urban vegetation structure type											Proportionate area (%)	
Areas without vegetation												
Built-up areas												

The novelty of this scheme is that urban greenery is characterised both individually and collectively in terms of the height of vegetated layers (named as *low*, *medium*, and *high* vegetation), selected qualitative characteristics such as spatial coverage, arrangement of vegetation, intensity of use and maintenance, and presence of distinctive features [Table 4.8] (Lehmann et al., 2014; Mathey et al., 2011).

Similar to the LULC and the PPG17, the UVST is a well-established scheme that is extensively applied in the German context for both research and planning policy. Ochoa (1999) has also proposed the study of ground cover characteristics along with the spatial configuration, orientation, geometry and type of vegetation to identify the capacities of green infrastructure for controlling urban microclimate conditions.

Classification systems such as the LCZ, HERCULES and UVST highlight the importance of integrating functional, morphological and configurational aspects of man-made structures, vegetation features, human activities, and surface properties in a holistic way. Despite their broad applicability and versatility across different urban settings, these schemes are primarily aimed for city and district levels (meso-scale) with relatively homogeneous characteristics. Thus, future research should suggest potential improvements for their application in more heterogeneous conditions and finer spatial scales.

To classify tree canopy structures, Höfle and Hollaus (2010), Jim (1989) and Tooke et al. (2009) employed remote sensing approaches such as decision tree classification (spectral mixture analysis) and vegetation edge-based segmentation to discriminate green elements independently from the functions and services provided. Their main focus is the technical and descriptive study of spatial configurations, patterns of distribution and deciduous-evergreen differentiation.

The classification approaches of green roofs and vertical greenery systems are more straightforward in comparison to other categories due to their structural simplicity. Studies primarily divide green roofs into intensive and extensive, depending on substrate depths, roof dimension and intensity of use. In comparison, vertical greenery systems are differentiated according to the location of greening (rooted on the ground or rooted on the wall), the characteristics of the supporting structures and the level of maintenance (Jim, 2015b; Susorova, 2015). Besides structural attributes, Ottel  et al. (2011) incorporated life cycle analysis (LCA) for a comparative study of the functionality of green facades and living walls. Mostly, green roofs and vertical greenery system typologies have supported studies concerning building energy performance, stormwater benefits, and microclimatic effects at fine scales.

4.5 Identification of categories and typologies

4.5.1 Tree canopy

The classification of tree canopy depends on (a) the functional aspects referring to extent, location, hierarchy, land use and purpose; (b) the structural characteristics such as size, geometry, type of foliage; and (c) the spatial arrangements (isolated, dense, and aligned) of vegetation elements. The differentiation of the tree canopy typologies also depends on the geographic context, within or outside the urban boundary, and more importantly, the spatial scale of observation. For instance, at the meso scale tree canopy can be classified as forestland while at local scale a specific area within could include street trees. This situation causes double counting and/or overlapping of typologies across scales. Table 4.9 offers a list of typologies identified in the literature and the corresponding spatial scales.

Table 4.9 List of tree canopy typologies identified by studies. *Spatial scales: Me=Meso; Lo=local; Mi=Micro.*

Citation	Spatial scale	Tree canopy typologies
Abunnasr (2013)	Me, Lo	
Anderson et al. (1976)	Me	
Bowler et al. (2010b)	Lo, Mi	
Cadenasso et al. (2007); Cadenasso et al. (2013)	Me, Lo, Mi	
Cooper (2010)	Me, Lo	
Davies et al. (2006)	Me, Lo, Mi	
DEFRA (2008)	Me, Lo	
Dunnett et al. (2002)	Me, Lo	
Ely and Pitman (2014)	Lo, Mi	
EMDA (2010)	Me, Lo	1. Street trees / green streets / green alleys / road trees / urban tree canopy
Foster et al. (2011)	Lo	
Hunter et al. (2012)	Lo, Mi	
Jacobs et al. (2014)	Me	2. Street greenways / greenbelts
Jim and Chen (2003)	Me, Lo	3. Street verges / hedges / hedgerows
Landscape Institute (2009)	Me, Lo	4. Shrubs / scrub / bushes
Li et al. (2005)	Me, Lo	5. Urban forestry / forest / community forests / forestland / forest reserves
Llewelyn-Davies (2000)	Me, Lo	
Mazza et al. (2011)	Me	
Naumann et al. (2011)	Me	6. Woodlands / community woodlands
Norton et al. (2013); Norton et al. (2015)	Me, Lo, Mi	7. Parkland trees
OEH (2015)	Lo, Mi	
Oke et al. (1989)	Me, Lo, Mi	
Pauleit and Duhme (2000)	Me, Lo	
Rupprecht et al. (2015)	Lo, Mi	
Schilling and Logan (2008)	Me, Lo	
Sheate et al. (2012)	Me, Lo	
TEP (2005)	Me, Lo	
TMF (2010, 2011)	Me	
Wilmers (1988)	Me, Lo	
Woolley (2006)	Me, Lo, Mi	

Citation	Spatial scale	Tree canopy typologies
Wong and Chen (2010)	Lo, Mi	
Zhou, Cadenasso et al. (2014)	Me, Lo, Mi	
Arlt et al. (2005)	Me, Lo	1. Trees (tall vegetation):
Höfle and Hollaus (2010)	Lo	a. Isolated / scattered / sparse / detached / semi-detached
Jim (1989)	Lo, Mi	b. Linear / in rows / aligned / connected
Lehmann (2014)	Me, Lo	c. Dense clusters (high density)
Mathey et al. (2010); Mathey et al. (2011) ^a	Me, Lo	d. Grouped (medium and low density)
Ochoa (1999)	Mi	e. Geometry (ovoid, cylindrical, conical, conical inverted, spherical)
Stewart and Oke (2012)	Me, Lo	2. Shrubs, bushes (medium vegetation) 3. Turf, lawn, meadow (low vegetation)
Arlt et al. (2005)	Me, Lo	
Dunnett et al. (2002)	Me, Lo	1. Evergreen trees / forest
Liu and Yang (2013)	Me	2. Deciduous trees / forest
Ochoa (1999)	Mi	3. Mixed trees / forest
Peters et al. (2011)	Me, Lo	4. Vegetated wetland
Tooke et al. (2009)	Lo	

^a See Table 4.7 for a specific list of typologies.

4.5.2 Green open spaces and water bodies

Green open spaces attract the most research attention due to their importance for defining planning strategies and interventions. Their classification depends on (a) the spatial scale (hierarchy), dimension and location of spaces (urban core versus periphery); (b) their primary purposes (land uses/land covers) and intensities of use; (c) accessibility and ownership (private versus public); and (d) Biophysical surface characteristics (permeability, amount of vegetation cover, thermal attributes). Contrastingly, water bodies are commonly neglected since these are usually considered as typologies of green open spaces. Table 4.10 lists the different green open space and water body typologies identified by studies at different spatial scales.

The major differentiation of green open spaces emerges from the rural-urban dichotomy (criticised by Stewart & Oke, 2012), the identification of land-use types and the different scales of resolution. Green open spaces have primarily been distinguished into those within urban cores and those beyond the urban periphery, both studied at local- and meso-scales (Abunnasr, 2013; Landscape Institute, 2009; Woolley, 2006). Ahern (2007) classifies greenspaces according to their spatial dimension into urban patches, corridors and matrix; meanwhile Davis (2010) appeals to conservationist approaches, identifying spaces in terms

of their connectivity and biodiversity restoration capacities (Mazza et al., 2011; Naumann et al., 2011).

In the UK, the PPG17 guidelines list 17 distinctive types of greenspaces predominantly focused on land uses for the implementation of planning policies and the delivery of government objectives (ODPM, 2002a, 2002b). The majority of subsequent studies based their own typologies on this list, and whether adopting, extending or modifying it, this has facilitated the identification of needs and opportunities to broaden the community benefits of green infrastructure (Cooper, 2010; DEFRA, 2008; EMDA, 2010; Sheate et al., 2012; TMF, 2010). Likewise, the work of Gill et al. (2007) and TEP (2005) applied PPG17 categories to develop a more complete terminology on green open spaces for North West England (Landscape Institute, 2009).

The intensity of use and level of human intervention has served to discriminate natural and designed greenspaces (English Nature, 2003; Lehmann et al., 2014; Mathey et al., 2010; Mathey et al., 2011; Pauleit et al., 2003). Typologies derived from this approximation resulted from land-cover classifications which have mainly distinguished between hard and soft landscapes (pervious and impervious surfaces) (Keeley, 2011; Norton et al., 2013; Ochoa, 1999; OEH, 2015; Peters et al., 2011; Wilmers, 1988).

Likewise, some studies acknowledge the heterogeneity and complexity of built environments by incorporating a mix of biotic, semi-natural and man-made elements to characterise open spaces as an amalgam of uses, urban biotopes and vegetation features (Anderson et al., 1976; Brady et al., 1979; Cadenasso et al., 2007; La Rosa & Privitera, 2013; Lehmann et al., 2014; Mathey et al., 2010; Mathey et al., 2011; Stewart & Oke, 2012; Zhou, Cadenasso et al., 2014). Accessibility and ownership are also applied to discriminate and audit different types of open spaces (CBC, 2008; TSG, 2008).

4.5.3 Green roofs

Green roofs are a relatively simple category to characterise despite the overlapping terminology used by different authors (*i.e.* eco-roofs, green rooftops, living roofs and rooftop gardens) [Table 4.2]. Table 4.11 summarises different studies organised in sub-groups depending on the typologies that were identified at different spatial scales. The identification of typologies depends mainly on spatial extent, dimensions, substrate thickness, intensity of use, level of maintenance and vegetation size (Dunnett & Kingsbury, 2004; Francis & Lorimer, 2011; Oberndorfer et al., 2007; OEH, 2015; Williams et al., 2010).

Table 4.10 List of green open spaces and water bodies typologies identified by studies.*Spatial scales: Me = Meso; Lo = local; Mi = Micro.*

Citation	Spatial scale	Green open spaces / water bodies typologies
Abunnasr (2013)	Me, Lo	
Ahern (1995, 2007)	Me	
Aldous (2014)	Me	
Anderson et al. (1976)	Me	
Bell et al. (2007)	Me	I. According to the purpose:
Bowler et al. (2010b)	Lo, Mi	1. Parks and gardens: country, urban and local parks, public & private gardens, courtyards
Byrne and Sipe (2010)	Me, Lo	2. Natural & semi-natural green spaces: woodlands, forests, reserves, heathlands, grassland, meadow, conservation land
CBC (2008)	Me, Lo	3. Greenways, green corridors, ecological buffers, green streets/alleys, green wedges, cycle paths, pedestrian trails, routes.
CCC (2010)	Me, Lo	4. Wetlands: marshlands, intertidal mudflats.
Cooper (2010)	Me, Lo	5. Brownfield land: quarries, wastelands, landfills, vacant and derelict land
Davies et al. (2006)	Me, Lo, Mi	6. Amenity green spaces: recreation grounds, sport fields/facilities, golf courses, playgrounds, racecourses,
DEFRA (2008)	Me, Lo	7. Community green spaces: allotments, community gardens, orchards
DTLR (2002)	Me, Lo	8. Green links, utility areas: roads, rails, power lines, drainage-ways, transport corridors
Dunnett et al. (2002)	Me, Lo	9. Agricultural land, farms, ranches
Ely and Pitman (2014)	Me, Lo	10. Landscaped and incidental areas
EMDA (2010)	Me, Lo	11. Churchyards, cemeteries, burial grounds
Gill et al. (2007)	Me	12. Institutional grounds
Jim and Chen (2003)	Me, Lo	13. Civic spaces: squares, plazas, malls, foyers
Landscape Institute (2009)	Me, Lo	14. Built-up areas residential land, multistorey buildings, mixed uses, construction sites.
La Rosa and Privitera (2013)	Me	15. Waterbodies and waterside areas: coasts, beaches, seafronts, rivers, canals, ponds, lakes, estuaries, swales, ditches
Li et al. (2005)	Me, Lo	
Llewelyn-Davies (2000)	Me, Lo	
ODPM (2002a, 2002b)	Me, Lo	
Pauleit and Duhme (2000)	Me, Lo	II. According to the scale and location:
Panduro and Veie (2013)	Me, Lo	1. Urban periphery
Rupprecht et al. (2015)	Lo, Mi	a. National-regional
Schilling and Logan (2008)	Me, Lo	• Patches, corridors, matrixes
Sheate et al. (2012)	Me, Lo	2. Urban cores
TEP (2005)	Me, Lo	a. City-district
TMF (2010, 2011)	Me	3. Neighbourhood
TSG (2008)	Me, Lo	a. Local / parcel
VEAC (2011)	Me, Lo	III. According to accessibility/ownership:
Wang (2001)	Me, Lo	1. Unrestricted
Wong (2011)	Me	2. Limited
Wong and Chen (2010)	Lo, Mi	3. Not accessible
Woolley (2006)	Me, Lo	

Brady et al. (1979)	Me	<ol style="list-style-type: none"> 1. Cliff/organic detritus 2. Derelict/weedy grasslands 3. Derelict savannah 4. Mowed grassland 5. Urban savannah 6. Abiotic/weedy complex 7. Urban/forest plantation 8. Rail-highway/grassland 9. Remnant ecosystem/natural island 10. Remnant ecosystem/agricultural island 11. Lake-stream/aquatic complex 12. Dump/organic detritus
Cadenasso et al. (2007); Cadenasso et al. (2013)	Me, Lo, Mi	
Di Gregorio and Jansen (1998)	Me	According to surface characteristics:
English Nature (2003)	Me	<ol style="list-style-type: none"> 1. Pervious surfaces (permeable) <ol style="list-style-type: none"> a. Irrigated green space b. Non-irrigated green space c. Vegetated surfaces (grasslands, pasture, crops, forests, fields, greenspaces) d. Non-vegetated / bare soils / sands / snow e. Porous pavements f. Rain-gardens / biofilters / bioswales 2. Impervious surfaces (impermeable) <ol style="list-style-type: none"> a. Reflective pavements / hard surfaces b. Bare rocks 3. Water bodies <ol style="list-style-type: none"> a. Vegetated wetlands / wet grounds b. Open water / lakes / rivers
Jacobs et al. (2014)	Me, Lo	
Keeley (2011)	Me	
Liu and Yang (2013)	Me, Lo	
Norton et al. (2013); Norton et al. (2015)	Me, Lo, Mi	
Ochoa (1999)	Mi	
OEH (2015)	Lo, Mi	
Pauleit et al. (2003)	Me, Lo	
Peters et al. (2011)	Me, Lo	
Stewart and Oke (2012)	Me, Lo	
Tooke et al. (2009)	Me	
Wilmers (1988)	Me, Lo	
Zhou, Cadenasso et al. (2014)	Me, Lo, Mi	
Davis (2010)	Me	<ol style="list-style-type: none"> 1. Protected areas 2. Restoration ones 3. Sustainable use areas 4. Green urban and peri-urban features 5. Natural connectivity features 6. Artificial connectivity features 7. Multifunctional zones
Mazza et al. (2011)	Me	
Naumann et al. (2011)	Me	
Lehmann et al. (2014) ^a	Me, Lo	<ul style="list-style-type: none"> • Main categories: <ol style="list-style-type: none"> 1. Residential sites, mixed-use sites as well as industrial, commercial and specialized sites 2. Transport facilities and infrastructure 3. Green spaces 4. Urban wastelands 5. Landfills and quarries 6. Agricultural sites 7. Grassland 8. Trees, shrubs and bushes 9. Woodland 10. Near-natural wetlands 11. Waterside zones 12. Arid grasslands, heathlands 13. Open sites
Mathey et al. (2010); Mathey et al. (2011) ^a	Me, Lo	

^a See Table 4.7 for a specific list of typologies.

Table 4.11 List of green roof typologies identified by studies.*Spatial scales: Me = Meso; Lo = local; Mi = Micro.*

Citation	Spatial scale	Green roofs typologies
Abunnasr (2013)	Lo	1. Green roofs
Bowler et al. (2010b)	Lo, Mi	
Davies et al. (2006)	Lo, Mi	
Ely and Pitman (2014)	Lo, Mi	
Keeley (2011)	Lo	
Landscape Institute (2009)	Lo	
Mazza et al. (2011)	Me	
Naumann et al. (2011)	Me	
Schilling and Logan (2008)	Lo	
TMF (2010, 2011)	Lo	
Woolley (2006)	Lo, Mi	
Dunnett and Kingsbury (2004)	Mi	1. Green roofs
Foster et al. (2011)	Lo	a. Intensive green roofs
Francis and Lorimer (2011)	Mi	b. Extensive green roofs <ul style="list-style-type: none"> • Complete • Modular • Pre-cultivated vegetation blanket
Hunter et al. (2012)	Lo, Mi	c. Semi-extensive
Norton et al. (2013); Norton et al. (2015)	Mi	2. Living roofs
Oberndorfer et al. (2007)	Mi	a. Intensive green roofs
OEH (2015)	Lo, Mi	b. Extensive green roofs
Williams et al. (2010)	Mi	3. Brown roofs
		4. Eco-roofs
		5. Cool roofs
		a. White roofs
Wong and Chen (2010)	Lo, Mi	b. Cool coloured roofs
		c. Blue roofs

Intensive and extensive roofs are the two main types recognised by most authors. Intensive roofs have deeper substrates and consequently more capacity to sustain larger plant species than extensive roofs; and their use depends on this differentiation (Francis & Lorimer, 2011; OEH, 2015) [Figure 4.2]. Some studies also consider brown roofs (gravel substrates), blue roofs (water harvesters) and cool roofs (light coloured roofs) as types within this category (Dunnett & Kingsbury, 2004; Francis & Lorimer, 2011; OEH, 2015); although this is disputable. Dunnett and Kingsbury (2004) have additionally identified a third typology, the *semi-extensive roofs* (also called *semi-intensive*), which combines the characteristics of intensive and extensive roofs, requiring occasional irrigation and moderate maintenance levels.

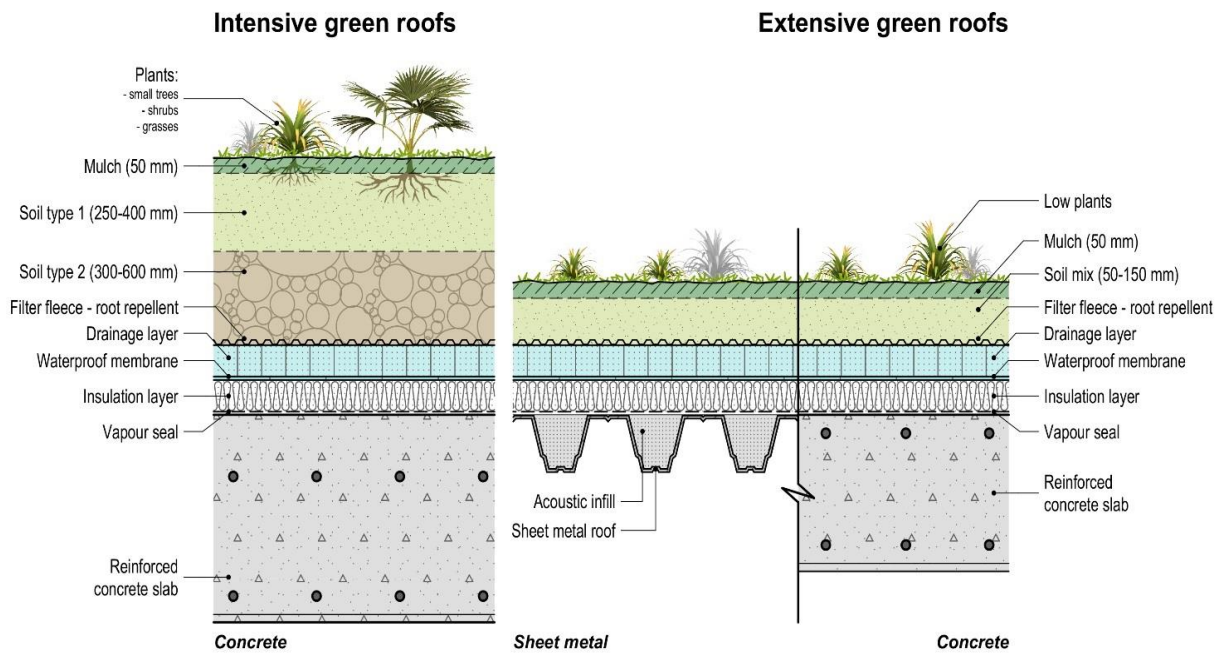


Figure 4.2 Typical cross-sections of intensive and extensive green roofs.
(Redrawn based on Osmond & Sharifi E., 2017).

4.5.4 Vertical greenery systems

Key aspects for the classification of vertical greenery system typologies are the structural characteristics of supporting systems, the selection and types of plants and the level of maintenance required (Jim, 2015b; Susorova, 2015). From a functional perspective, most vertical greenery systems studies relate to their climatic effects and indoor or outdoor thermal performance benefits at micro scales.

Vertical greenery systems are commonly divided into two main types as summarised in [Table 4.12](#); *green facades* and *living walls*. The term *green facades* refers to vegetation rooted on the ground, that make use of either the wall itself for climbing (traditional direct systems) or independent supporting systems such as trellis, wires, cables or meshes (double-skin indirect systems) affixed to walls. [Figure 4.3](#) provides a graphic representation of several typologies of green facades organised according to the type of anchor system and planter.

Conversely, *living walls* have been made of felt, geotextile, pots, panels or boxes where pre-cultivated vegetation has been planted and subsequently suspended and fixed to a larger vertical structure; hence, plants are not in contact with the ground. Living walls demand more complex construction and imply higher installation and maintenance costs in comparison to green facades (Dunnett & Kingsbury, 2004; Francis & Lorimer, 2011; Hunter et al., 2012; Kontoleon & Eumorfopoulou, 2010; Ottelé et al., 2011; Pérez et al.,

2014; Perini et al., 2011; Susorova, 2015; Wong et al., 2010; Wong & Chen, 2010). Figure 4.4 shows two common types of living walls differentiated in terms of the fixings and planter.

Table 4.12 List of vertical greenery systems typologies identified by studies.

Spatial scales: Me = Meso; Lo = local; Mi = Micro.

Citation	Spatial scale	Vertical greenery systems typologies
Abunnasr (2013)	Lo	<ol style="list-style-type: none"> 1. Green facades (rooted on ground / base – extensive) <ol style="list-style-type: none"> a. Traditional direct system (self-climbing) b. Double-skin indirect systems <ul style="list-style-type: none"> • Cable and wire net system • Trellis and container system • Modular trellis panels • Mesh 2. Green walls / living walls (rooted on wall– intensive) <ol style="list-style-type: none"> a. Felt/Mat System (geo-textiles) b. Modular panel system c. Flowerpots (planter boxes) d. Hydroponic systems 3. Bio-walls (indoor)
Dunnett and Kingsbury (2004)	Mi	
Ely and Pitman (2014)	Lo, Mi	
Francis and Lorimer (2011)	Mi	
Hunter et al. (2012); Hunter et al. (2014)	Mi	
Kontoleon and Eumorfopoulou (2010)	Mi	
Landscape Institute (2009)	Lo	
Li et al. (2005)	Lo	
Mazza et al. (2011)	Lo	
Naumann et al. (2011)	Lo	
Norton et al. (2013); Norton et al. (2015)	Mi	
OEH (2015)	Mi	
Ottel�� et al. (2011)	Mi	
P��rez et al. (2011a, 2011b), P��rez et al. (2014)	Mi	
Perini et al. (2011)	Mi	
Susorova (2015)	Mi	
Wong et al. (2010)	Mi	
Wong and Chen (2010)	Mi	
Jim (2015b)	Mi	<ol style="list-style-type: none"> 1. Climber green walls <ol style="list-style-type: none"> a. Wall-toe-substrate <ul style="list-style-type: none"> • In-ground (wall-toe) • Hanging planter-single • Ground planter • Hanging planter-serial b. Training-system <ul style="list-style-type: none"> • Veneer (appressed) • Netting (web) • Trellis (mesh) • Wire rope (cable) 2. Herb-shrub green walls <ol style="list-style-type: none"> a. Substrate-system <ul style="list-style-type: none"> • Box (pot) • Tray (panel) • Bag (pocket) • Absorbent-layer b. Elevated-substrate <ul style="list-style-type: none"> • Containerized soil • Mineral-wool slab • Containerized mix • Geotextile-fabric felt

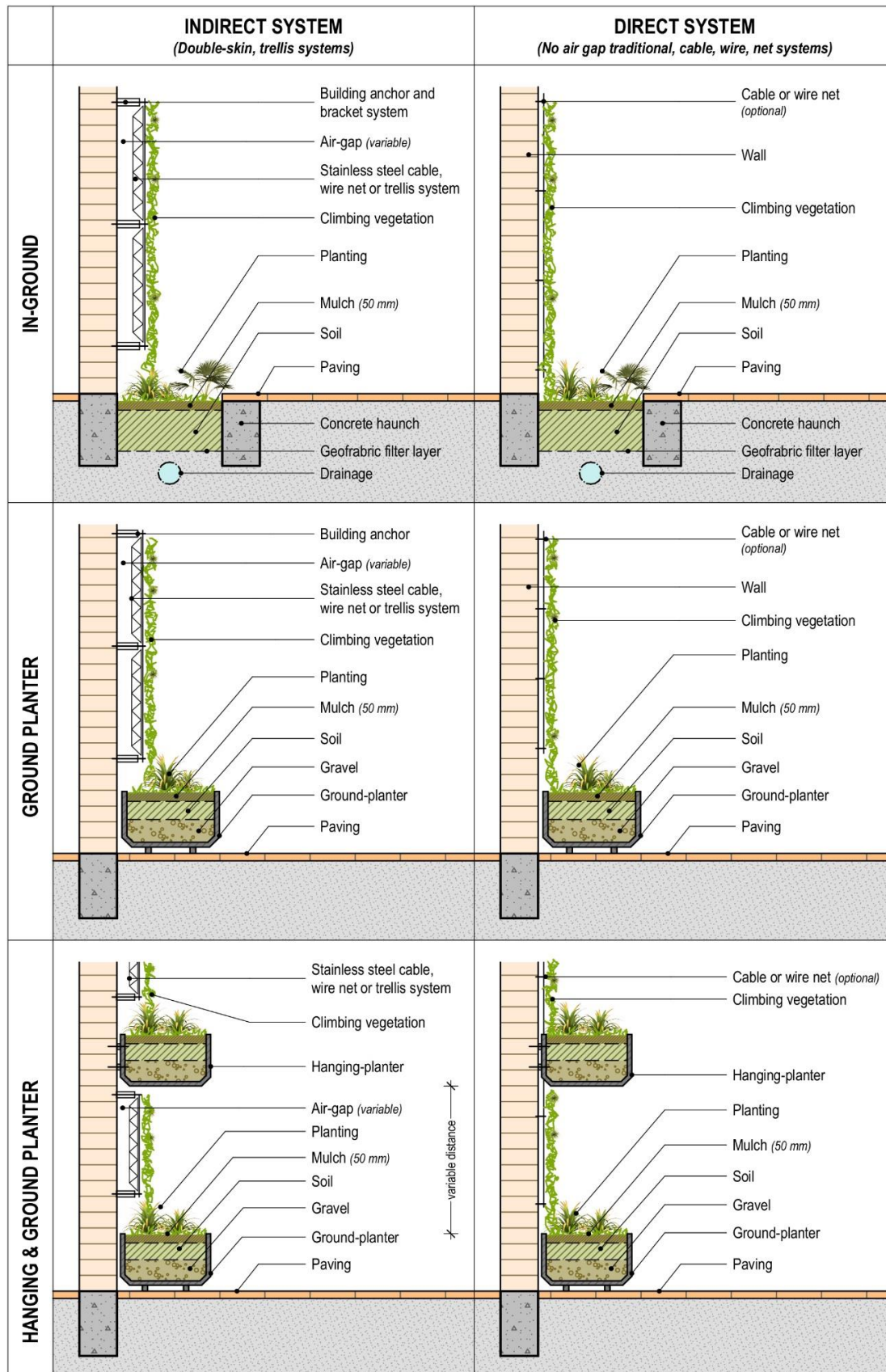


Figure 4.3 Several typologies of green facades organised according to the type of anchor system and planter.
(Redrawn from Osmond & Sharifi, 2017; based on Jim, 2015b; Ottel   et al., 2011 and Susorova, 2015).

Jim (2015b) has proposed a more comprehensive typology based on a triple-criteria scheme: (a) plant growth-forms, (b) the supporting systems and (c) the substrate systems (on ground and elevated) along with wall design factors. The final typology consisted of 24 possible permutations, used for informing designers and researchers about the variations, potentials, and limitations of vertical greenery systems (Jim, 2015b) [Table 4.12].

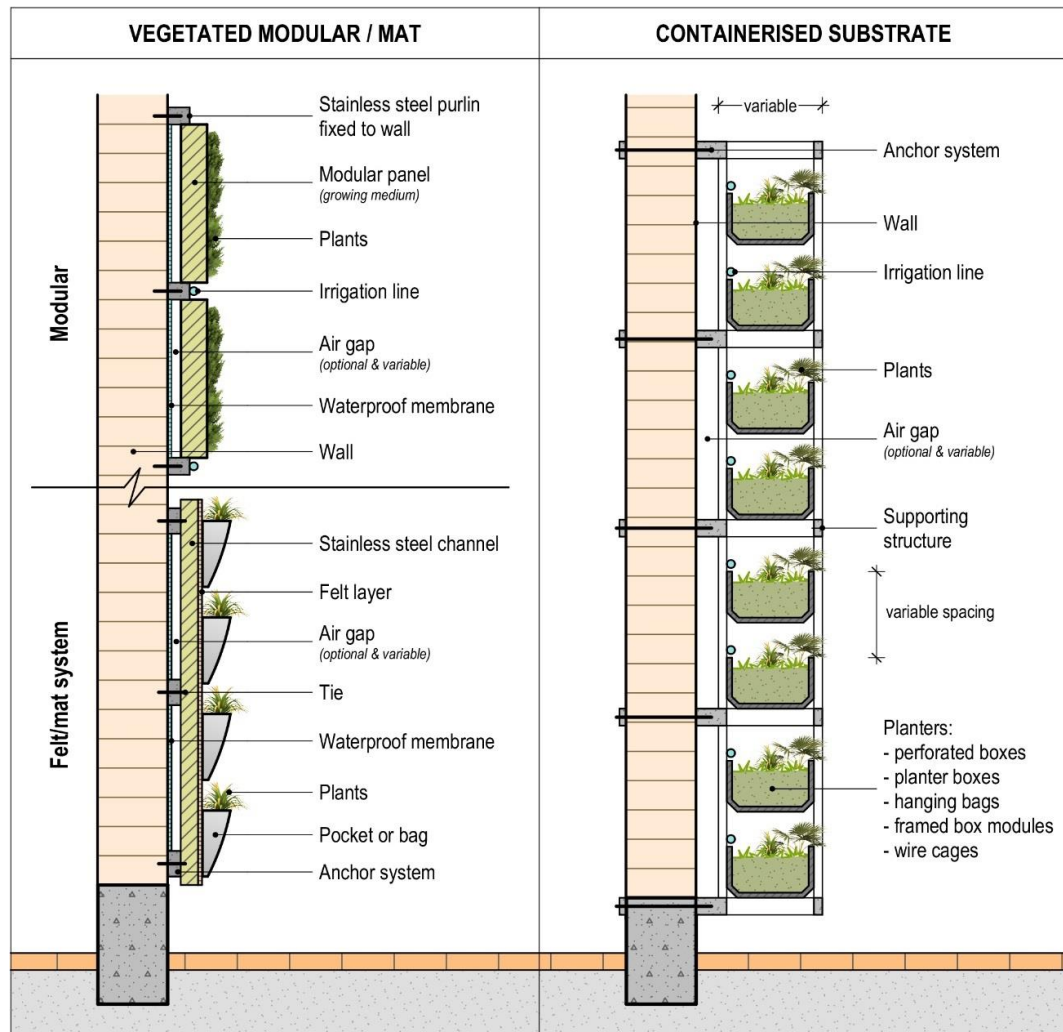


Figure 4.4 Different typologies of living walls differentiated in terms of the type of fixings and planter. (Redrawn from Osmond & Sharifi, 2017; based on Jim, 2015b; Ottelé et al., 2011 and Susorova, 2015).

4.5.5 Other classifications

Mell (2010) and Young et al. (2014) proposed comprehensive classification frameworks instead of focusing on identifying discreet elements and specific typologies [Table 4.13]. Both studies addressed a knowledge gap in terms of understanding the different factors and possibilities of cataloguing green infrastructure not only based on land uses and purposes,

but also in terms of opportunities for intervention (Young et al., 2014), research aims, and planning scenarios (Mell, 2010).

On one hand, Mell (2010) thoroughly analysed Ahern (1995) scale-goal-context approach to propose a refined typology where ecological, economic and social aspects have been translated into *form*, *function* and *context* [Table 4.13]. *Form* refers to the physical characteristics of vegetation elements, *function* to the processes and services provided, and *context* to the different influences on urban landscapes. On the other hand, Young et al. (2014) classification considers the ecological, political and economic triggers for green infrastructure intended to distinguish intervention opportunities based on social and ecological systems. Whereas this typology may be more suitable for strategic planning, it is limited for identifying vegetation assets for performance-based analysis.

Table 4.13 List of other types of classification of green infrastructure.

Spatial scales: Me = Meso; Lo = local; Mi = Micro.

Citation	Spatial scale	Other typologies
Mell (2010)	Me	<p>A typology classification based on vegetation's</p> <ol style="list-style-type: none"> 1. Form: <ol style="list-style-type: none"> a. Ecological element (physical space, connectivity, elements) b. Economic (costs of a space, design) c. Social & cultural (users of a space, aesthetics of a space, motivations) 2. Function: <ol style="list-style-type: none"> a. Ecological element (biodiversity, conservation) b. Economic (industry, business, regeneration) c. Social & cultural (education, recreation, health) 3. Context: <ol style="list-style-type: none"> a. Ecological element (biodiversity, supporting networks, ecological mobility) b. Economic (costs of a space, economic development, sustainability) c. Social & cultural (location, facilitations, motivations, perceptions)
Young et al. (2014)	Me	<ol style="list-style-type: none"> 1. Social system: <ol style="list-style-type: none"> a. Setting: type of social system b. Drivers (social components driving GI) c. Social production units <ul style="list-style-type: none"> • GI production units • GI social configuration of labour d. External relationships <ul style="list-style-type: none"> • Upstream relationship • Downstream relationship 2. Ecological system: <ol style="list-style-type: none"> a. Setting: type of ecological system b. Drivers (ecological components driving GI) c. Cultivated ecosystems <ul style="list-style-type: none"> • GI subparts • System • Ecosystems connection/relation d. External relationships (impact on ESS).

4.6 Summary of findings

A comprehensive classification of green infrastructure is necessary for studying the thermal regimes and cumulative cooling effects of biotic and abiotic elements on urban microclimate. Accordingly, the systematic review presented in the first half of this chapter investigates how different authors identify, characterise and catalogue green infrastructure worldwide.

Present evidence suggests that a universal set of typologies cannot be proposed for all scenarios or research purposes. However, most studies grouped green infrastructure features into five high-level categories of (a) tree canopy; (b) green open spaces; (c) water bodies, (d) green roofs; and (e) vertical greenery systems. In the second half of this chapter, these categories are further disaggregated into specific typologies to support the goals of the present research. A significant amount of overlapping terminology has created ambiguity and loss of clarity when cataloguing green infrastructure. Among the main categories, tree canopy and green open spaces concentrate more interest from researchers and are more difficult to catalogue due to their inherent complexity. In contrast, *living architecture* such as green roofs and vertical greenery systems are more straightforward to classify.

Defining clear boundaries between the natural and the built world is difficult, a gap in knowledge that responds to contrasting views on what constitutes green infrastructure and if typologies should be studied individually or holistically. Hence, there is a necessity to develop a more robust classification system capable of integrating key principles governing green infrastructure, namely (1) dynamic spatio-temporal heterogeneity, (2) connectivity (*blue-green-grey continuum*), and (3) multi-functionality (Ahern, 2007; Bartesaghi Koc, Osmond, & Peters, 2017; Cadenasso et al., 2013; Pickett et al., 2017); tailored according to specific needs and scopes.

It is observed that classification of greenspaces is strongly linked to land uses, purposes, functions, hierarchy and connectivity. However, land use based classifications are insufficient to explain the ecological functioning of vegetated elements and water bodies since knowing the purpose of an area does not necessarily explains its climatic functioning (Cadenasso et al., 2013). In contrast, the categorisation of trees, green roofs and vertical greenery systems is mainly addressed from physical and morphological perspectives. It is strongly suggested that a comprehensive classification scheme should consider a ternary classification approach based on the capacities to provide ESS (functional principle), the bio-physical attributes (structural principle) and the way elements organise and relate to

each other (configurational principle); in line with approaches from Ahern (1995, 2007) and Mell (2008, 2010).

The scope and scale of analysis are crucial when identifying the contribution of different typologies in either urban or natural landscapes. For instance, tree canopy and green open spaces are mostly studied from meso to local scales, while green roofs and vertical greenery systems always concentrate on street canyons and buildings. Moreover, spatial scale is a factor influencing the discernibility of vegetation since at large scales the differentiation of features and their spatial arrangements is hampered by the lack of detail, leading to the homogenisation and generalisation. Hence, sometimes green infrastructure features can be classified into more than one category. That is the case of trees which are typically described as woodland when forming large clusters studied at meso scale, while linear plantations of trees constitute alleys at microscale (Cadenasso et al., 2007; Cadenasso et al., 2013; Oke et al., 1989; Stewart & Oke, 2009).

Accordingly, neglecting or underestimating the influence or hierarchy and scale can lead to an erroneous characterisation of green infrastructure (Lehmann et al., 2014; Oke et al., 1989; Stewart & Oke, 2009). This confirms the necessity of developing a multi-scale and multi-purpose typology that contemplates the heterogeneity of green infrastructure and is suitable for varied contexts and locations. Remote sensing may be suggested as a time-effective method that could help map, classify and evaluate highly complex and diverse geographic settings in a rapid, standardised and automated way.

Most studies emphasise the comparison between tree canopy and green open spaces versus green roofs and vertical greenery systems, because the latter are engineered features with less natural complexity and variability, and because they are partially segregated from larger green infrastructure networks. Furthermore, several researchers consider blue roofs, brown roofs and cool roofs as additional typologies within the green roof category. On one hand, they can provide certain ESS and functions such as climate regulation, while on the other hand their biological content or capacity to sustain complex forms of life is considerably smaller compared to other types of green roofs and green infrastructure. In this sense, future research should concentrate on how to integrate green roofs and vertical greenery systems into natural systems/networks in a more holistic manner. Their inclusion or exclusion may also depend on the scope and intention of a particular research.

The rest of this chapter focuses on developing a classification framework and specific typologies based on the analysis and the evidence from the current and previous (Chapter 3) systematic reviews.

PART II: Establishing a classification framework and typologies to support climate studies⁹

4.7 Need for a new classification scheme

No commonly agreed taxonomies and protocols have been proposed yet to confidently analyse, report and predict the cumulative climatic effects of different categories of green infrastructure (Bartesaghi Koc, Osmond, Peters, & Irger, 2017a, 2017b; Bowler et al., 2010b; Young et al., 2014); a critical knowledge gap identified in the systematic literature reviews presented in Chapters 3 and 4 (Part I). The development of such classification scheme is crucial to determine the optimal typologies, amounts and spatial distributions of green infrastructure for reducing increased urban temperatures more effectively (Bowler et al., 2010b; Zupancic et al., 2015).

In this regard, the second part of this chapter aims: (1) to define the criteria for classifying green infrastructure from a climate-oriented perspective, (2) to formulate a conceptual green infrastructure typology (GIT) matrix, and (3) to propose streamlined typologies for the automated mapping and classification of green infrastructure based on remote sensing data.

The purpose of developing this GIT is to establish order and conventions to perform a faster mapping and classification of large urban areas, facilitate inter-site and inter-typology comparisons, facilitate climate predictions and numerical modelling, and enable the transferability of results and systematisation of acquired knowledge into standardised guidelines. The GIT is also intended to enable a more precise use of terminology and reduce vagueness when describing the vegetation conditions of sites under study.

The new classification system is constructed in four steps: (1) classification criteria are defined combining the approaches proposed by the LULC, the LCZ, the HERCULES and the UVST schemes; (2) green infrastructure elements are divided into appropriately defined classes and sub-classes –based on the procedures defined by Grigg (1965)– for the characterisation of urban landscapes and the observation of thermal conditions; (3) a conceptual typology is presented in a matrix format resulting from the combination of multiple classes and sub-classes; and (4) streamlined typologies are proposed with

⁹ Versions of Chapter 4 – Part II have been published or have been submitted for publication:

- Bartesaghi-Koc et al. (2019), Mapping and classifying green infrastructure typologies for climate-related studies based on remote sensing data. *Urban Forestry and Urban Greening*.
- Bartesaghi Koc et al. (2016), A Green Infrastructure Typology Matrix to Support Urban Microclimate Studies, *Procedia Engineering*, 169, p.183-190.

corresponding qualitative (definitions) and quantitative (spatial and surface) descriptors, and cut-off values for remotely sensed applications.

4.8 Classification criteria

The formulation of a green infrastructure typology (GIT) for climate research entails enormous challenges due to the dynamic spatial and temporal heterogeneity of urban systems, which precludes a clear identification of types (Cadenasso et al., 2013; Mell, 2010; Pickett et al., 2017). According to Grigg (1965) and Stewart (2011b) the formulation of a robust and standardised classification system should also satisfy certain requirements. First, classifications must propose simple and logical nomenclatures for the elements or conditions that are described. Second, the system must facilitate the transferability of information and replicability by other users, so they can perform comparative analyses. Third, the classification system should enable generalisation, so complex objects or conditions can be simplified into classes grouped based on common properties and relations. Hence, the differentiating characteristics should be carefully chosen (Grigg, 1965). Based on the evidence identified and discussed in Chapters 3 and 4, the requirements established by Grigg (1965) and the approaches and criteria applied by the LULC (Anderson et al., 1976), the LCZ (Stewart & Oke, 2012), the HERCULES (Cadenasso et al., 2007) and the UVST (Arlt et al., 2005; Lehmann et al., 2014; Mathey et al., 2011) schemes; the classification system and criteria proposed in this chapter must:

1. Consider the spatio-temporal heterogeneity, connectivity (*blue-green-grey spectrum*), and multi-functionality of green infrastructure by including natural, semi-natural and man-made features.
2. Be sufficiently flexible to allow the optimum number of typologies and the aggregation of additional types in the future.
3. Be broadly accessible for a broad spectrum of users with different skill levels, from novices to experts.
4. Be simple, manageable and easily understood by users from different disciplines.
5. Be repeatable and objectively measurable by incorporating *functional*, *morphological* and *configurational* properties to ensure that classifications can be performed with the same accuracy and consistency by other users and in other contexts.
6. Be generic (standardised) and testable at different spatial scales and urban settings; and not dependent on land uses or socially-constructed factors.
7. Be suitable for use with remote sensing data.

4.9 Classification by logical division

A standardised classification scheme requires the division of green infrastructure into a hierarchy of classes [Figure 4.5]. Each rank (or level) of classes is a set or category where association of elements can be done according to *similarity* and *contiguity* on the basis of common attributes and relationships. These principles were proposed by Grigg (1965) and applied by Stewart (2011b) and Stewart and Oke (2009, 2012) for the development of the LCZ scheme.

For purposes of this research, the association by *similarity* refers to the grouping of individuals from the universe (or objects) based on common inherent bio-physical characteristics. For instance, there exist obvious differences between a plant (*i.e.* tree) and the soil in which it grows. This is the type of association applied in initial stages of classifications. On the other hand, the association by *contiguity* refers to functional and structural relationships (configurations) among assets of the urban landscape; which may be either similar or dissimilar. This type of association is usually established at later stages of classifications (Grigg, 1965).

In accordance with the LCZ, UVST and HERCULES classification schemes, the urban green infrastructure –considered as the universe class– can be divided into three main groups of elements that provide distinct *thermal functions* to the urban climate; namely, *vegetation layers*, *ground surfaces*, and *building structures* (Cadenasso et al., 2007; Cadenasso et al., 2013; Erell et al., 2011; Lehmann et al., 2014; Stewart, 2011b; Zhou, Cadenasso et al., 2014) [Figure 4.5 – Figure 4.6].

The *vegetation layers* comprise a series of stratified natural features such as herbaceous plants, shrubs, trees and climber species of different height and shape (Lehmann et al., 2014; Mathey et al., 2011) that contribute to the modification of airflow, air/surface temperatures, transpiration rates and shading potential. The *ground surfaces* and *building surfaces* comprise a combination of natural and/or man-made objects and surfaces that offer biophysical support for the growth of vegetation and contribute with different values of evaporation, moisture and permeability to the modification of surface temperatures and the microclimate near the ground (Erell et al., 2011; Stewart, 2011b; Stewart & Oke, 2009) [Figure 4.6]. Subsequently, the *vegetation layers* can be divided into *ground vegetation* and *climbing vegetation*; *ground surfaces* into *terrestrial surfaces* and *aquatic surfaces*; and *building structures* into *roof structures* (rooftops of buildings) and *vertical structures* (indoor and outdoor walls) [Figure 4.5].

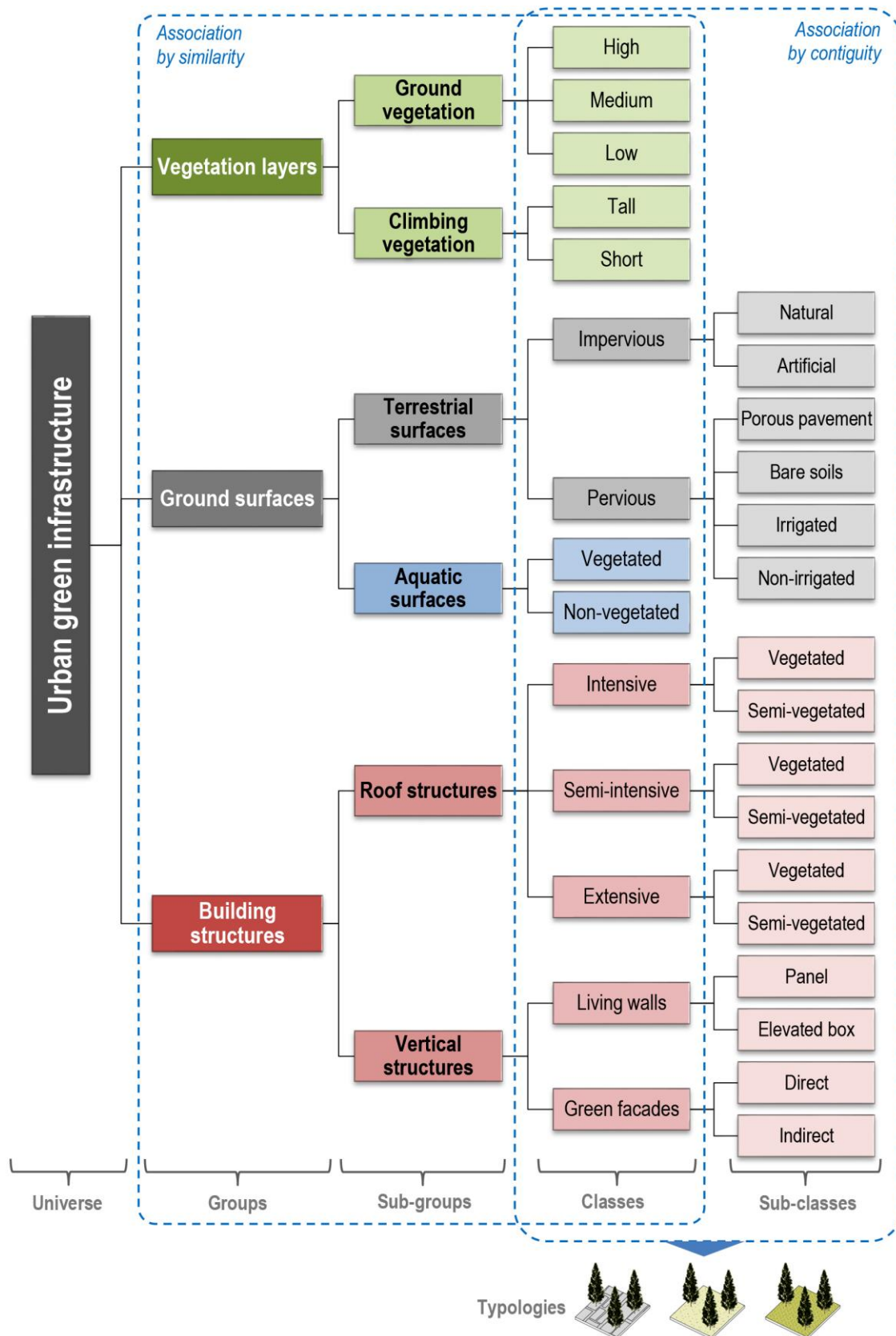


Figure 4.5 Logical division of urban green infrastructure according to the climatic function, structural properties and spatial relationship of its elements for the formulation of typologies.
(Modified after Bartesaghi Koc et al., 2016)

At the next levels of the hierarchy the division into classes and sub-classes (in parenthesis) obeys different morphological factors. *Ground vegetation* can be sub-divided according to vegetation height into *low*, *medium*, and *high*; and *climbing vegetation* can be sub-divided in terms of the length of climbers into *short* and *tall*.

Terrestrial surfaces can be differentiated in terms of permeability, water content and presence of ephemeral and vegetative attributes into *impervious surfaces* (natural and artificial), and *pervious surfaces* (porous pavements, bare soils, non-irrigated and irrigated). Similarly, *aquatic surfaces* can be differentiated in terms of the presence of plants into *vegetated* (wetlands) and *non-vegetated* (open water) surfaces.

Roof structures are sub-divided according to the extension, substrate depth, intensity of use into *intensive*, *semi-intensive*, *extensive* classes; and each of them into *vegetated* and *semi-vegetated* sub-classes. Finally, *vertical structures* are sub-divided in terms of the location of vegetation and type of supporting structure into *living walls* rooted on walls (panel/geo-textile, elevated box) and *green walls* rooted on the ground (direct system, indirect system).

Figure 4.5 depicts all the stages involved in the logical division of green infrastructure.

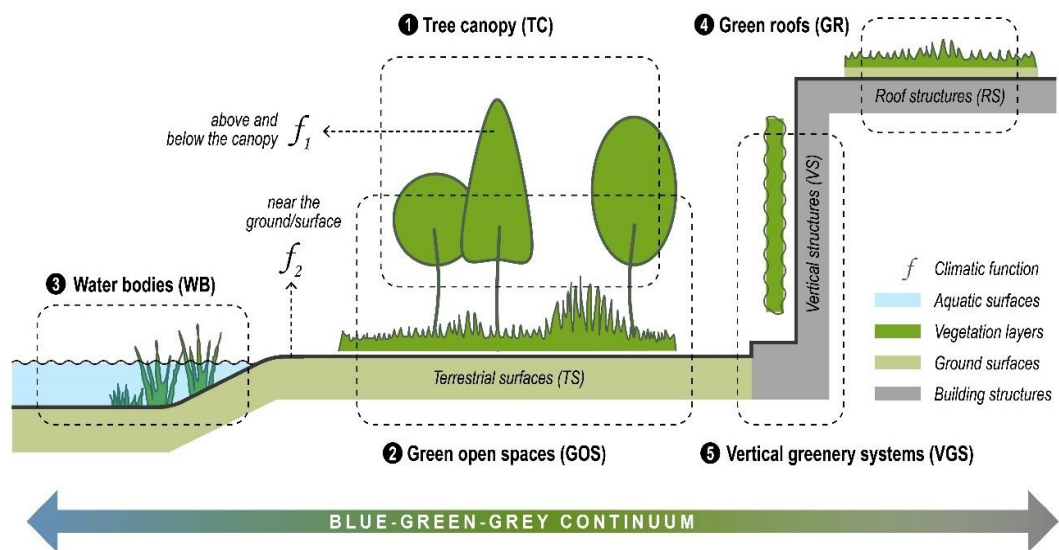


Figure 4.6 Spatial conceptualisation of five high level categories of green infrastructure resulting from the combination of vegetation layers, ground surfaces and building structures.

(Modified from Bartesaghi Koc, Osmond, & Peters, 2017 and Bartesaghi Koc et al., 2016)

When considering the principle of *contiguity* (Grigg, 1965), the resulting classes and sub-classes can be combined in different ways and spatial arrangements to give rise to specific typologies that can be grouped into the five level categories identified in this chapter [Figure 4.6]. These typologies are further defined and described in the following section.

4.10 Conceptual green infrastructure typology (GIT) matrix

Hereafter, all the combinations of classes and sub-classes that emerge from the logical division of green infrastructure is called green infrastructure typology (GIT). The proposed conceptual GIT encompasses a total of 14 classes and 16 sub-classes organised in a double-entry matrix [Figure 4.7]. The *y-axis* comprises five classes corresponding to the *vegetation layers* plus a *no vegetation* class; while the *x-axis* encompasses the remaining 9 classes and 16 sub-classes corresponding to *ground surfaces* and *building structures*.

The matrix allows the combination of classes and subclasses from both axes with a maximum of 108 permutations; however, not all combinations exist in reality. In Figure 4.7 it can be observed the most probable combinations organised like in a periodic table of elements. The matrix also enables the recombination of different permutations aimed at representing the *complex heterogeneity* of urban landscapes. In essence, all proposed typologies are self-explanatory and compatible with existing terminology as per Table 4.2 and the five high level categories previously identified earlier in this chapter.

In detail, *ground vegetation* (GV) comprises three classes (low, medium and high vegetation), while *climbing vegetation* (CV) consists of 2 classes (short and tall climbers). *Terrestrial surfaces* (TS) are constituted by two classes (impervious and pervious) and six sub-classes; while *aquatic surfaces* (AS) include two classes (vegetated and non-vegetated) [Figure 4.7].

Roof structures (RS) are constituted by three classes (intensive, semi-intensive and extensive) and six sub-classes; while *vertical structure* (VS) includes two classes (living walls and green facades) and four sub-classes. In addition, to represent areas totally lacking in green assets, a section of *no vegetation* has been included at the bottom of the matrix [Figure 4.7].

Besides the differentiation of vegetation layers, four types of spatial arrangements have been proposed according to Lehmann et al. (2014) and Mathey et al. (2011). These can be found in the lower-right corner of the table and correspond to *aligned*, *scattered*, *clustered*, and *dense*.

Given the simple and flexible nature of the conceptual matrix, this enables the addition, subtraction and recombination of typologies according to specific purposes and site conditions. Hence, the nomenclature is governed by names rather than codes; those that obey a set of conventions described below.

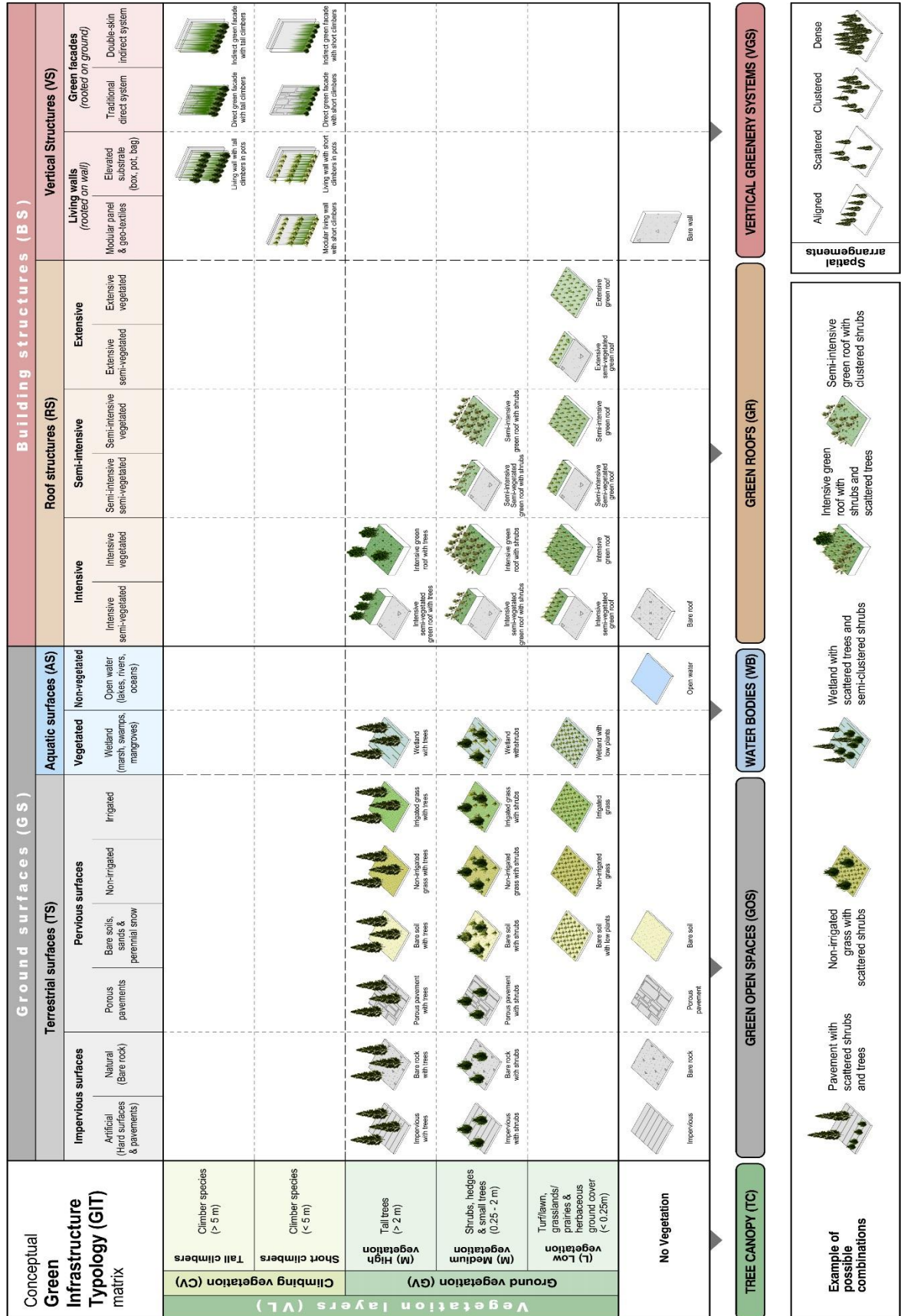


Figure 4.7 Proposed conceptual green infrastructure typology (GIT) as a double-entry matrix. (Modified after Bartesaghi Koc et al., 2016).

1. The nomenclature starts with the *ground surface* or *building structure* sub-/class chosen from the x-axis (*i.e.* impervious) followed by a *vegetation layer* class (if applicable) from the y-axis (*i.e.* shrubs) preceded by the word ‘*with*’. For example, this is the case of the ‘*Impervious with trees*’ typology.
2. If applicable, vegetation layers classes may be also preceded by a *spatial arrangement* descriptor (*i.e.* ‘*irrigated grasses with aligned trees*’).
3. A combination of sub-classes is also allowed, in which case the word ‘*and*’ must be added. For instance, a possible typology can be ‘*Non-irrigated grasses with shrubs and scattered trees*’.
4. Fine-grain typologies may be required to represent smoother transitions from one landscape condition to another. In case the typology comprises a combination of ground surfaces; the word ‘*Mostly*’ should be used before the most dominant one. For example, ‘*Mostly impervious with grasses and scattered trees*’. If a dominant surface cannot be clearly identified the term ‘*Mixed*’ might be used instead (*i.e.* *Mixed surfaces* or *Mixed grasses*). This sort of typologies is presented in the streamlined and practical version of this matrix; which is described in the next section.

4.11 Streamlined green infrastructure typology for remotely sensed applications

Mapping and classifying GITs with distinctive *functional behaviour* requires defining a spatial unit characterised by *morphological* and *configurational* descriptors as well as determining specific threshold values given the large variability of surface fractions and possible permutations that each typology can contain. To respond to this need, a streamlined GIT for remote sensing applications is introduced in this section [Figure 4.8]. This GIT particularly focuses on the green open spaces, tree canopy and water bodies categories; and is tested and validated in Chapters 6 and 7.

This simplified version comprises 34 GITs representing the *grey-green-blue spectrum* that are organised in four subgroups of GITs: (a) impervious, (b) mixed, (c) pervious, and (d) aquatic [Figure 4.8]. The GITs are individually named, ordered and coded based on surface properties and height of vegetated features for an easy identification and standardised comparison.

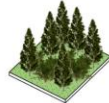

























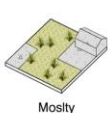

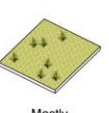

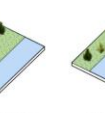
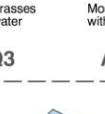

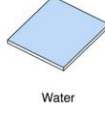
Streamlined GIT for remotely sensed applications		Ground surfaces (from spectral imagery)								
		Impervious	Mixed		Pervious		Aquatic			
Height of vegetated features (from LiDAR)	High Vegetation (trees)	Dense			 Dense trees with shrubs and grasses PV11					
		Clustered	 Mostly impervious with clustered trees IM6	 Mixed surfaces with clustered trees MX9	 Mixed grasses with clustered trees MX10	 Mostly non-irrigated grasses with clustered trees PV9	 Mostly irrigated grasses with clustered trees PV10	 Water with clustered trees AQ7		
		Scattered	 Mostly impervious with scattered trees IM5	 Mixed surfaces with scattered trees MX7	 Mixed grasses with scattered trees MX8	 Mostly non-irrigated grasses with scattered trees PV7	 Mostly irrigated grasses with scattered trees PV8	 Water with scattered trees AQ6		
		Aligned	 Mostly impervious with aligned trees IM4	 Mixed surfaces with aligned trees MX5	 Mixed grasses with aligned trees MX6	 Mostly non-irrigated grasses with aligned trees PV5	 Mostly irrigated grasses with aligned trees PV6	 Water with aligned trees AQ5		
		Medium Vegetation (shrubs)	 Mostly impervious with shrubs IM3	 Mixed surfaces without trees MX3	 Mixed grasses and bare soils MX4	 Mixed grasses with shrubs and trees PV3	 Mostly shrubs PV4	 Mixed surfaces with water AQ4		
			Low Vegetation (grasses)	 Mostly impervious with grasses IM2	 Mostly non-irrigated grasses with impervious MX1	 Mostly irrigated grasses with impervious MX2	 Mostly non-irrigated grasses PV1	 Mostly irrigated grasses PV2	 Mostly grasses with water AQ3	 Mostly water with grasses AQ2
				No vegetation	 Highly impervious IM1					 Water AQ1

Figure 4.8 Streamlined green infrastructure typology (GIT) for remotely sensed applications.

The *impervious* subset consists of 6 GITs (IM1 – IM6) characterised by a large proportion of impermeable surfaces (*i.e.* roads, pavements, ballast, bitumen) and buildings of various characteristics with scarce vegetated features and permeable surfaces.

The *mixed* subset comprises 10 GITs (MX1-MX10) characterised by a large variety of land covers and structures. Within this subset, odd numbered GITs (*i.e.* MX1, MX3) encompass a mixture of natural and man-made surfaces; while even numbered GITs (*i.e.* MX2, MX4) are only comprised of natural components.

The *pervious* subset encompasses 11 GITs (PV1-PV11) where odd numbered GITs (*i.e.* PV1, PV5), excepting PV11, are constituted by non-irrigated surfaces; while even numbered GITs (*i.e.* PV6, PV8) are constituted by irrigated surfaces.

The *aquatic* subset consists of 7 GITs (AQ1-AQ7) which are either open water (AQ1) or include different proportions of greenery and pavements (AQ3 to AQ7). The latter are meant to characterise transitional conditions between terrestrial and aquatic surfaces (*i.e.* coastlines, shorelines, and riversides).

The differentiation between ground surfaces (impervious, non-irrigated pervious, irrigated pervious, water) and vegetation layers (shrubs and trees) is essential as each element has specific bio-physical and thermal properties that contribute in different ways to the energy budget of a place and to the modification of airflows, amount of shading and evapotranspiration (Erell et al., 2011; Oke, 1988b; Oke et al., 1989).

Thus, the streamlined GIT applies a morphological-based approach combining different remotely sensed data such as spectral imagery (multi-/hyper-spectral) and LiDAR. It emphasises the distinction between irrigated and non-irrigated pervious surfaces as water content significantly influences the photosynthetic activity and evapotranspirative capacity of plants, and consequently their thermal and radiative effects on near-surface air (Erell et al., 2011; Oke et al., 1989; Oke, 1992). In the present research, irrigated pervious surfaces correspond to all types of well-irrigated low plants (grasses, turf, lawn) no higher than 0.5 m; while non-irrigated pervious surfaces refer to permeable bare-soil and drought tolerant low plants (<0.5m) without artificial irrigation.

However, the estimation of the proportion of different land cover types is not sufficient for a comprehensive thermal analysis since the local climate may also be affected by the height of vegetation layers and the patterns of tree coverage (Bowler et al., 2010b; Lehmann et al., 2014).

For example, a continuous and compact row of trees can provide more substantial shading and function as a windbreak compared with a discontinuous line of small trees that tends to be more permeable (Erell et al., 2011; Heisler & Dewalle, 1988; Stathopoulos et al., 1994). A comparable situation occurs between clustered and dispersed trees even though

they account for the same proportion of a greenspace, since the former tend to trap more heat underneath the canopy at night than the latter (Bowler et al., 2010b; Lehmann et al., 2014; Stewart & Oke, 2009).

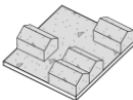
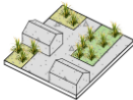

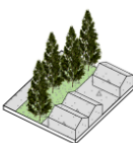
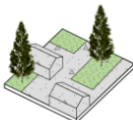

Configurational parameters can be estimated using LiDAR data and landscape metrics. FRAGSTATS metrics are typically utilised to assess landscape composition and configuration of greenspaces that can affect ecological processes (McGarigal, 2015). Accordingly, the GIT differentiates between low ($<0.5\text{m}$), medium ($0.5\text{--}2.0\text{m}$) and high ($>2\text{m}$) vegetation and combines two FRAGSTATS indices to distinguish between scattered, aligned, clustered, and dense trees: the *related circumscribing circle* (area-weighted mean) or CIRCLE_AM, and the *normalised landscape shape index* (nLSI) (McGarigal et al., 2002).

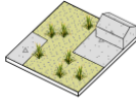
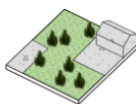





On the one hand, CIRCLE_AM provides a measure of the overall elongation and narrowness of a patch in relation to the whole landscape (or grid in our case), so it is used to distinguish aligned trees from other arrangements. The index ranges between zero and one ($0 \leq \text{CIRCLE_AM} < 1$), where a rounded patch corresponds to a value approaching to zero while a narrow and linear patch has a high index value (McGarigal, 2015).

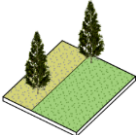
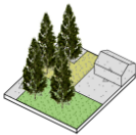
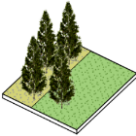
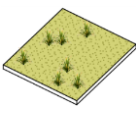
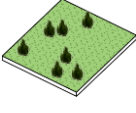
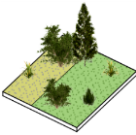
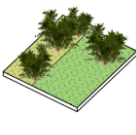
On the other hand, nLSI is a metric measuring the level of aggregation or clumpiness of features, hence, it is used to distinguish between scattered and clustered trees. Values also range from zero to one ($0 \leq \text{nLSI} < 1$) where zero corresponds to a single and maximally compacted patch and the index value increases as the patch becomes increasingly disaggregated and randomly dispersed (McGarigal, 2015). Both indices are unitless and not affected by the grain size or spatial resolution of imagery, resulting in standardised metrics that can be applied across multiple spatial scales and grid sizes.

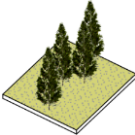
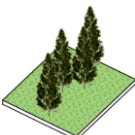
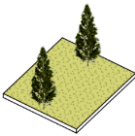
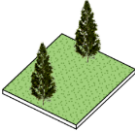
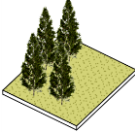
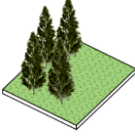
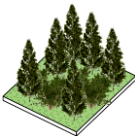
Qualitative descriptions (definitions) and quantitative classification parameters and cut-off values for all GITs are presented in [Table 4.14](#). A complete overview of all GITs is presented in Appendix E. Whereas values of surface cover descriptors are based on modified values defined by Bartesaghi Koc, Osmond, Peters et al. (2018), Irger (2014) and Stewart and Oke (2012); values for landscape metrics were determined after multiple tests using Jenks optimization method (Jenks, 1967) and decimal values adjusted according to the local context.

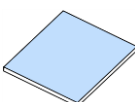
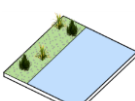
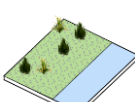

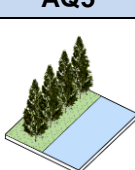
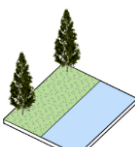
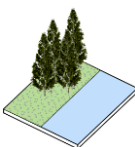
Table 4.14 Overview of quantitative and qualitative descriptors for all the 34 green infrastructure typologies (GITs) proposed.

GIT	Definition	Surface fractions [%]						Configuration	
		Total impervious [Fr_Tot_Imp]	Non-irrigated grasses [Fr_Low_NIR]	Irrigated grasses [Fr_Low_IRR]	Shrubs [Fr_Med_Veg]	Trees [Fr_High_Veg]	Total water [Fr_Tot_Wat]	CIRCLE_AM	nLSI
IMPERVIOUS GITs									
IM1	Highly impervious								
	Extensive built-up land with little or no grasses and shrubs; few or no trees. Abundance of buildings of different heights and arrangements (open and close), paved areas, roads and bare rocks.	>75	≤ 25	≤ 25	≤ 25	≤ 25	≤ 25	-	-
IM2	Mostly impervious with grasses								
	Treeless built-up land with abundant pavements and/or buildings with different heights and arrangements. Few and sporadic herbaceous plants and mix of irrigated and non-irrigated grasses.	>50 ≤75	< 50	< 50	≤ 25	≤ 5	≤ 25	-	-
IM3	Mostly impervious with shrubs								
	Built-up land with abundant pavements and/or buildings with different heights and arrangements. Few and sporadic bare soil, grasses, and small trees. Extensive shrubbery and hedges.	>25 ≤75	< 40	< 40	>25 ≤50	≤25	≤ 25	-	-
IM4	Mostly impervious with aligned trees								
	Built-up land with abundant pavements and/or open arrangement of buildings with different heights. Few bare soils, and grasses with poorly- to well-structured trees in rows.	>50 ≤75	< 40	< 40	≤ 25	>5 ≤40	≤ 25	≥ 0.61	< 0.25
IM5	Mostly impervious with scattered trees								
	Built-up land with abundant pavements and buildings with different heights and arrangements. Individual or few dispersed trees with sporadic bare soils, grasses, and shrubbery.	>50 ≤75	< 40	< 40	≤ 25	>5 ≤25	≤ 25	< 0.61	> 0.065
IM6	Mostly impervious with clustered trees								
	Built-up land with extensive pavements and open arrangement of buildings with different heights. Small clusters of small, medium or large trees; bare soils, grasses and shrubbery.	>50 ≤75	< 40	< 40	≤ 25	>5 ≤40	≤ 25	< 0.61	≤ 0.065

GIT	Definition	Surface fractions [%]						Configuration	
		Total impervious [Fr_Tot_Imp]	Non-irrigated grasses [Fr_Low_NIR]	Irrigated grasses [Fr_Low_IRR]	Shrubs [Fr_Med_Veg]	Trees [Fr_High_Veg]	Total water [Fr_Tot_Wat]	CIRCLE_AM	nLSI
MIXED GITs									
MX1	Mostly non-irrigated grasses with impervious								
	Treeless landscape with sparsely distributed pavements and small or medium-sized buildings. Abundance of non-irrigated plants, dry grasses, bare soils and sporadic paving.	>25 ≤50	> 50	≤ 25	≤ 25	≤ 5	≤ 25	-	-
MX2	Mostly irrigated grasses with impervious								
	Treeless landscape with sparsely distributed pavements and small or medium-sized buildings. Abundance of well-irrigated and healthy grasses, with sporadic shrubbery and paving.	>25 ≤50	≤ 25	> 50	≤ 25	≤ 5	≤ 25	-	-
MX3	Mixed surfaces without trees								
	Treeless landscape with sparsely distributed pavements and small or medium-sized buildings interspersed with non-irrigated and irrigated plants, bare soils and shrubbery.	>25 ≤50	≤ 50	≤ 50	≤ 25	≤ 5	≤ 25	-	-
MX4	Mixed grasses and bare soils								
	Treeless greenspace of extensive natural covers including non-irrigated and irrigated grasses, bare soils, and shrubbery is spots.	≤ 25	≤ 75	≤ 75	≤ 25	≤ 5	≤ 25	-	-
MX5	Mixed surfaces with aligned trees								
	Lightly to moderately wooded landscape with aligned trees surrounded by sparsely distributed pavements, small or medium-sized buildings, non-irrigated and irrigated grasses, bare soils and shrubbery.	>25 ≤50	≤ 50	≤ 50	≤ 25	>5 ≤50	≤ 25	≥ 0.61	< 0.25
MX6	Mixed grasses with aligned trees								
	Lightly to moderately wooded greenspace with well-structured aligned trees surrounded by non-irrigated and irrigated grasses, bare soils and sporadic shrubbery.	≤ 25	≤ 50	≤ 50	≤ 25	>5 ≤75	≤ 25	≥ 0.61	< 0.25
MX7	Mixed surfaces with scattered trees								
	Lightly wooded landscape with individual or few trees interspersed by pavements and small or medium-sized buildings, non-irrigated and irrigated grasses, bare soils, and sporadic shrubs.	>25 ≤50	≤ 50	≤ 50	≤ 25	>5 ≤50	≤ 25	< 0.61	> 0.065

GIT	Definition	Surface fractions [%]						Configuration	
		Total impervious [Fr_Tot_Imp]	Non-irrigated grasses [Fr_Low_NIR]	Irrigated grasses [Fr_Low_IRR]	Shrubs [Fr_Med_Veg]	Trees [Fr_High_Veg]	Total water [Fr_Tot_Wat]	CIRCLE_AM	nLSI
MX8	Mixed grasses with scattered trees								
	Lightly wooded greenspace with individual or few dispersed trees surrounded by extensive non-irrigated and irrigated grasses, and sporadic bare soils, and shrubbery.	≤ 25	≤ 50	≤ 50	≤ 25	>5 ≤ 75	≤ 25	< 0.61	> 0.065
MX9	Mixed surfaces with clustered trees								
	Moderately wooded landscape with small and medium trees arranged in medium-sized clusters surrounded by sparsely distributed pavements, small-sized buildings, non-irrigated and irrigated grasses, bare soils, and shrubbery.	>25 ≤ 50	≤ 50	≤ 50	≤ 25	>5 ≤ 75	≤ 25	< 0.61	≤ 0.065
MX10	Mixed grasses with clustered trees								
	Moderately wooded greenspace with mature and tall trees arranged in medium and large-sized clusters surrounded by non-irrigated and irrigated grasses, bare soils, and shrubbery in spots.	≤ 25	≤ 50	≤ 50	≤ 25	>5 ≤ 75	≤ 25	< 0.61	≤ 0.065
PERVIOUS GITs									
PV1	Mostly non-irrigated grasses								
	Featureless greenspace of extensive non-irrigated plants, dry grasses, sands, bare soils and sporadic shrubbery.	≤ 25	> 75	≤ 25	≤ 25	≤ 5	≤ 25	-	-
PV2	Mostly irrigated grasses								
	Featureless greenspace of extensive well-irrigated grasses, and sporadic shrubbery.	≤ 25	≤ 25	> 75	≤ 25	≤ 5	≤ 25	-	-
PV3	Mixed grasses with shrubs and trees								
	Greenspace with individual or small group of trees, sporadic shrubbery and abundance of non-irrigated and irrigated grasses, bare soils and sands.	≤ 25	< 60	< 60	>25 ≤ 50	≤ 50	≤ 25	-	-
PV4	Mostly shrubs								
	Greenspace with close arrangement of bushes, shrubs and small trees interspersed with grasses and bare soils. Few or no trees.	≤ 25	< 50	< 50	> 50	≤ 25	≤ 25	-	-

GIT	Definition	Surface fractions [%]						Configuration	
		Total impervious [Fr_Tot_Imp]	Non-irrigated grasses [Fr_Low_NIR]	Irrigated grasses [Fr_Low_IRR]	Shrubs [Fr_Med_Veg]	Trees [Fr_High_Veg]	Total water [Fr_Tot_Wat]	CIRCLE_AM	nLSI
PV5	Mostly non-irrigated grasses with aligned trees								
	Lightly to moderately wooded greenspace with well-structured aligned trees surrounded by non-irrigated grasses, dry plants, bare soils, sands and sporadic shrubbery.	≤ 25	> 50	< 40	≤ 25	>5 ≤50	≤ 25	≥ 0.61	< 0.25
PV6	Mostly irrigated grasses with aligned trees								
	Lightly to moderately wooded greenspace with well-structured aligned trees surrounded by well-irrigated grasses, and sporadic shrubbery.	≤ 25	< 40	> 50	≤ 25	>5 ≤50	≤ 25	≥ 0.61	< 0.25
PV7	Mostly non-irrigated grasses with scattered trees								
	Lightly wooded greenspace with individual or few dispersed trees surrounded by extensive non-irrigated grasses, and sporadic bare soils, sands and shrubbery.	≤ 25	> 50	< 40	≤ 25	>5 ≤50	≤ 25	< 0.61	> 0.065
PV8	Mostly irrigated grasses with scattered trees								
	Lightly wooded greenspace with individual or few dispersed trees surrounded by extensive well-irrigated grasses, and sporadic shrubbery.	≤ 25	< 40	> 50	≤ 25	>5 ≤50	≤ 25	< 0.61	> 0.065
PV9	Mostly non-irrigated grasses with clustered trees								
	Moderately wooded greenspace with mature and tall trees arranged in large clusters surrounded by non-irrigated grasses, bare soils, and sporadic shrubbery.	≤ 25	> 50	< 40	≤ 25	>5 ≤50	≤ 25	< 0.61	≤ 0.065
PV10	Mostly irrigated grasses with clustered trees								
	Moderately wooded greenspace with mature and tall trees arranged in large clusters surrounded by well-irrigated grasses, healthy plants and sporadic shrubbery.	≤ 25	< 40	> 50	≤ 25	>5 ≤50	≤ 25	< 0.61	≤ 0.065
PV11	Dense trees with shrubs and grasses								
	Heavily wooded greenspace with mature, tall and dense trees, extensive shrubbery, and variety of grasses and bare soils.	≤ 25	≤ 25	≤ 25	≤ 75	> 75	≤ 25	-	-

GIT	Definition	Surface fractions [%]						Configuration	
		Total impervious [Fr_Tot_Imp]	Non-irrigated grasses [Fr_Low_NIR]	Irrigated grasses [Fr_Low_IRR]	Shrubs [Fr_Med_Veg]	Trees [Fr_High_Veg]	Total water [Fr_Tot_Wat]	CIRCLE_AM	nLSI
AQUATIC GITs									
AQ1	Water								
	Large open water bodies with few or no presence of vegetation.	≤ 25	≤ 25	≤ 25	≤ 25	≤ 25	> 75	-	-
AQ2	Mostly water with grasses								
	Treeless waterfront landscape with minimal presence of herbaceous plants, grasses, reed-beds and shrubbery.	≤ 25	< 40	< 40	≤ 25	≤ 5	>50 ≤75	-	-
AQ3	Mostly grasses with water								
	Treeless waterfront landscape with moderate presence of tall herbaceous plants, grasses, reed-beds and mature shrubbery.	≤ 25	< 60	< 60	≤ 25	≤ 5	>25 ≤50	-	-
AQ4	Mixed surfaces with water								
	Waterfront landscape with moderate presence of pavements and small buildings, herbaceous plants, grasses, and sporadic shrubbery and small trees.	>25 ≤50	≤ 50	≤ 50	≤ 25	≤ 25	>25 ≤75	-	-
AQ5	Water with aligned trees								
	Lightly to moderately wooded waterfront landscape with poorly to well-structured trees in rows, and presence of herbaceous plants, grasses, and sporadic shrubbery.	≤ 25	< 40	< 40	≤ 25	>5 ≤75	>25 ≤75	≥ 0.61	-
AQ6	Water with scattered trees								
	Lightly wooded waterfront landscape with individual or few dispersed trees and moderate presence of herbaceous plants, grasses, and sporadic shrubbery.	≤ 25	< 40	< 40	≤ 25	>5 ≤40	>25 ≤75	< 0.61	-
AQ7	Water with clustered trees								
	Moderately wooded waterfront landscape with medium and large clusters of mature and tall trees and presence of herbaceous plants, grasses, and sporadic shrubbery.	≤ 25	< 40	< 40	≤ 25	> 40	>25 ≤75	< 0.61	-

4.12 Summary

The comparison of the thermal benefits provided by different typologies of green infrastructure across varied urban contexts is of great importance in climate research. However, there is a lack of classification frameworks and commonly agreed protocols to describe and compare the vegetation characteristics under study.

Several approaches for assessing the microclimatic conditions of urban greenery have been discussed in theory and practice, particularly the LULC (Anderson et al., 1976), LCZ (Stewart, 2011b; Stewart & Oke, 2012), HERCULES (Cadenasso et al., 2007) and UVST (Lehmann et al., 2014; Mathey et al., 2011). In this chapter, approaches, parameters and criteria of the above-mentioned schemes are combined to propose a new classification framework for identifying and cataloguing green infrastructure assets from a climatological perspective.

This new scheme requires the logical division of green infrastructure into three main groups: *vegetation layers*, *ground surfaces* and *building structures*, which are subdivided into classes and sub-classes. These are combined in a double-entry matrix to generate a conceptual green infrastructure typology (GIT). This GIT is capable to represent the continuity and heterogeneity of urban landscapes at different locations and spatial scales.

A set of conventions are introduced for the nomenclature of typologies to ease the inter-site and inter-typology comparison and reporting. Furthermore, the GIT has been conceptually conceived to work in line with the LCZ scheme if necessary. Although this scheme is essentially intended for climate-related studies, it is sufficiently flexible to be applied for other performance-based analyses.

No classification scheme can represent precisely and accurately the complex characteristics of urban landscapes. Thus, a streamlined GIT is specifically developed for remotely-sensed applications. This includes surface parameters, landscape metrics, and their corresponding threshold values. Although classification parameters and thresholds respond to a specific method and context, the scheme is flexible and can be equally applied to other locations with modifications where necessary.

Methods for the computation of variables and the automated classification based on remotely-sensed data are presented in Chapter 5; and validated in Chapters 6, using Sydney as case study. The streamlined GIT is aimed at supporting the analysis of thermal conditions of green infrastructure and for LST predictions; the results of these analyses are presented in Chapter 7 and discussed in Chapter 8.

Chapter 5

Research methodology¹⁰

This chapter outlines the methodological framework that is implemented in this research, which is aimed at answering the research questions and achieving the aims and objectives outlined in the introductory chapter. This is also intended to tackle important knowledge gaps identified in the literature. The present methodology draws on the theoretical background discussed in Chapter 4 and the approaches, methods and parameters reviewed in Chapters 3 and 4.

5.1 The methodological framework

The methodological framework presented here, requires identifying pertinent dependent and independent variables and corresponding data sources, defining adequate data acquisition protocols and designing a logical workflow for its implementation based on the reviewed literature. These aspects are summarised and described in the following sections.

5.1.1 Dependent and independent variables

Based on the theoretical assumptions discussed in Chapters 1 and 2 and the review of common variables of investigation conducted in Chapters 3 and 4, the following dependent and independent variables have been identified for this research. This selection was guided by the research aims and considered available resources (equipment and funding), data sources, and technical expertise for data processing and analysis. [Table 5.1](#) presents a

¹⁰ Versions of Chapter 5 have been published or have been submitted for publication:

- Bartesaghi Koc, C., Osmond, P., Peters, A. (2019), Mapping and classifying green infrastructure typologies for climate-related studies based on remote sensing data. *Urban Forestry and Urban Greening*.
- Bartesaghi Koc, Osmond, Peters et al. (2018), Understanding land surface temperature differences of Local Climate Zones based on airborne remote, *Journal of Selected Topics in Applied Earth Observations and Remote Sensing (JSTARS)*.
- Bartesaghi Koc, Osmond, Peters, and Irger (2017a) A methodological framework to assess the thermal performance of green infrastructure through airborne remote sensing, *Procedia Engineering*, 180, p. 1306-1315.
- Bartesaghi Koc, Osmond, Peters, and Irger (2017b) Mapping Local Climate Zones for urban morphology classification based on airborne remote sensing data. In *2017 Joint Urban Remote Sensing Event (JURSE)* (p. 1–4). IEEE Xplore.

detailed list of variables and their corresponding units, abbreviations and symbols. Detailed descriptions of the methods and procedures for the computation of these variables are provided in Chapter 6, as these depended on the type of data collected and the conditions for each case study.

Table 5.1 List of dependent and independent variables selected for the present research

Variables	Type	Indicator	Abbreviation / symbol	Unit ^a
Dependent	Climatological	Diurnal surface temperature	<i>DAY_T_s</i>	°C
		Nocturnal surface temperature	<i>NIG_T_s</i>	°C
Independent	Functional	Normalised difference vegetation index	<i>NDVI</i>	
	Morphological	Fraction of total impervious (buildings and ground)	<i>Fr_Tot_Imp</i>	%
		Fraction of impervious building	<i>Fr_Imp_Bld</i>	%
		Fraction of impervious ground	<i>Fr_Imp_Grnd</i>	%
		Fraction of non-irrigated low vegetation (grasses)	<i>Fr_Low_NIR</i>	%
		Fraction of irrigated low vegetation (grasses)	<i>Fr_Low_IRR</i>	%
		Fraction of medium vegetation (shrubs)	<i>Fr_Med_Veg</i>	%
		Fraction of high vegetation (trees)	<i>Fr_High_Veg</i>	%
		Fraction of total water	<i>Fr_Tot_Wat</i>	%
		Altitude	<i>Alt</i>	m
	Configurational (<i>FRAGSTATS</i>)	Related circumscribing circle (area-weighted mean)	<i>CIRCLE_AM</i>	
		Normalised landscape shape index	<i>nLSI</i>	

^a. Unitless indicators are blank

5.1.2 Data sources

As defined in previous chapters and in line with the aims of this dissertation, airborne remote sensing has been selected as an ideal tool for investigating the relationships between diurnal and nocturnal surface temperatures (dependent variables) and independent variables corresponding to functional, morphological and configurational attributes of green infrastructure at the local scale (Bartesaghi Koc, Osmond, Peters, & Irger, 2017a). This is because airborne-based analysis (1) enables capturing the thermal and physical conditions of a diversity of urban landscapes simultaneously in a single mission, and in very high resolutions (0.5-2m); (2) allows the identification of individual landscape elements and surfaces that are essential for an accurate, precise and detailed analysis of

highly heterogeneous conditions at the local scale; and (3) provides the necessary flexibility in prescribing the flight times and flight paths according to the requirements of this research. The advantages and limitations of this methodology are further discussed in Chapter 8.

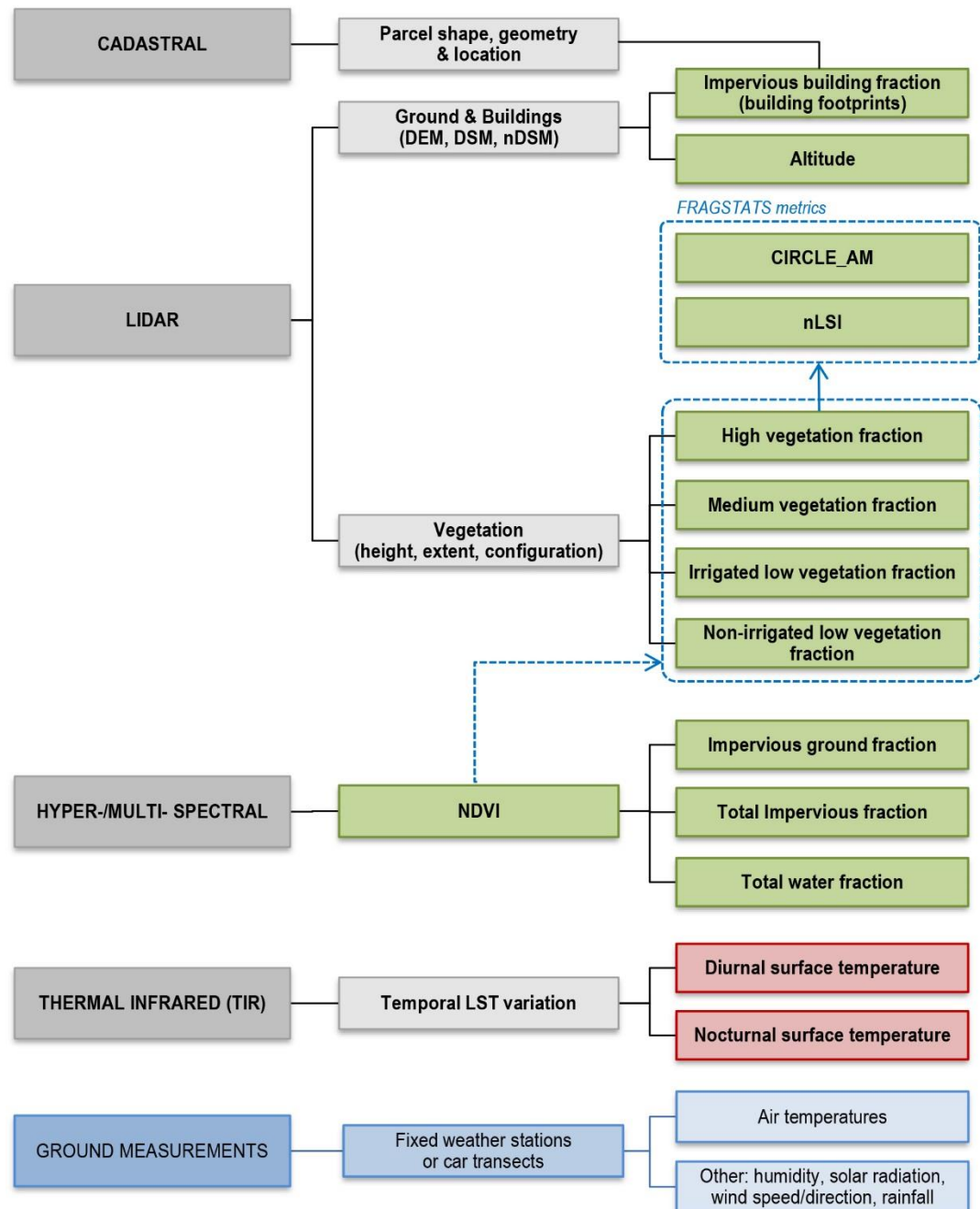


Figure 5.1 Schematic overview of dependent (red) and independent (green) variables derived from their corresponding data sources (dark grey). Complementary ground-based data (blue) may be incorporated if available or necessary.

Figure 5.1 presents a schematic overview of the most essential dependent, independent and intervening variables [as per Table 5.1] and how these can be derived from airborne-based

data sources. A detailed review of the data sources relevant to this research (listed below) is presented in Section 3.8.2. Procedures for the collection, and pre-/post-processing of datasets to compute each variable are described in Chapter 6. Besides airborne-based data, cadastral data provide auxiliary information about the shape, geometry and location of private and public parcels (or lots) that is required for the generation of building footprints.

Additionally, complementary air temperature measurements may be used for cross-validation to ensure accurate LST estimations from remotely-sensed thermal imagery. This should be taken on the ground at the time that flights are deployed. For this research, ground-based measurements obtained from car transects were only available for winter and did not cover the total extent of the study area. Given the focus of this thesis on LST, and the lack of sufficient data for summer, air temperature measurements were obviated; however, they are recommended for studies documenting surface-air temperature correlations.

5.1.3 Airborne-based data acquisition protocols

Following a review of studies (Coutts et al., 2016; Harris & Coutts, 2011; Irger, 2014), a set of specifications is proposed for data acquisition that can be applied irrespective of geographic locations; even so, flight protocols depend on several temporal, meteorological and sensor requirements (Harris & Coutts, 2011; Irger, 2014). A summary of abovementioned requirements and specifications are presented in [Table 5.2](#).

Temporal considerations

Most severe UHIs are likely to happen during summer after several days of continuous heatwave; however, such warming conditions may be more desirable in winter as this reduces energy demand used for heating (Irger, 2014).

The best time to study the thermal profiles of vegetation, collect spectral imagery and study SUHIs is during the day, especially around noon given the high angle and intensity of the sun which enables capturing the maximum surface temperatures with minimal shading effects (Harris & Coutts, 2011; Roth, 2012).

Contrastingly, UHIs within the urban canopy layer are usually more pronounced at night-time, especially in the early morning (pre-dawn) when surfaces have lost the maximum amount of radiative energy and the urban-rural thermal differences are greatest (Coutts et al., 2016; Harris & Coutts, 2011; Irger, 2014). Nocturnal flights may also be beneficial since surface to air temperature correlations are stronger at night due to higher atmospheric

stability, and the lack of building shade and traffic flows contributing to the anthropogenic heat (Harris & Coutts, 2011).

Furthermore, flight paths and times should focus on areas suffering excessive urban warming and should ideally be undertaken during periods of two to three consecutive hot days. Missions should be brief (<60 minutes) to avoid large temperature differences between locations (Coutts et al., 2016; Harris & Coutts, 2011).

Nevertheless, some degree of flexibility when allocating the flight times and duration is needed to reduce the risk of missing suitable opportunities. The acquisition of LiDAR data can be carried out either simultaneously or separately from the TIR and spectral imagery; however, this must correspond to the same period/season to prevent changes caused by the vegetation phenology.

Table 5.2 Summary of protocols for the acquisition of airborne remotely sensed and ground-based data. Modified after Coutts et al. (2016) and Harris and Coutts (2011).

<i>Flight time</i>	<ul style="list-style-type: none"> • Seasons: Summer and winter. • Day-time flights: At the time of maximum solar exposure (around noon), between 12:00h – 15:00h. • Night-time flights: Ideally pre-dawn between 03:00h – 05:00h. Flights around midnight, between 23:00h – 2:00h are also useful and more practical in certain conditions.
<i>Flight duration</i>	<ul style="list-style-type: none"> • Ideally <60 minutes. Possibly between 60 – 120 min.
<i>Flight altitude</i>	<ul style="list-style-type: none"> • Constant altitude during the whole flight, between 1000 and 3000 metres.
<i>Sensors and resolution</i>	<ul style="list-style-type: none"> • Best resolution between 0.5 – 5.0 metres. Thermal camera, LiDAR scanner and hyper-spectral camera (preferable); multi-spectral camera is also useful.
<i>Meteorological conditions</i>	<ul style="list-style-type: none"> • Preferable 2 – 3 consecutive hot days. • Clear skies. • Low or no wind speeds (< 5ms-1). • No precipitation 3 – 5 days prior observations.
<i>Ground validation (conditional)</i>	<ul style="list-style-type: none"> • Canopy layer observations concurrently with flights. • Mobile transects (with a GPS tracker) and/or fixed meteorological stations across the whole study area. • All instruments must be installed between 1 – 2 metres above the ground.

Meteorological conditions

Successful data collection requires suitable meteorological conditions. Clear skies are essential since cloud cover may obstruct the aircraft's sensors. Cloudy skies hinder capturing accurate thermal imagery by irregularly shading the ground at daytime and preventing long-wave radiative cooling at night-time (Harris & Coutts, 2011).

Similarly, low or no wind speeds are preferable as high velocities increase surface cooling effects, reduce atmospheric stability, and cause air turbulence (Harris & Coutts, 2011; Irger, 2014; Oke, 1992). Increasing wind speeds may also affect the accuracy of thermal data and prevent optimal correlations between air and surface temperatures due to microscale advection conditions. Another crucial factor is that study areas must not have experienced any precipitation three to five days prior to the flights as this can alter estimations and distort surface temperatures.

Sensor requirements

The type of sensors and altitude of flights are important to determine the spatial resolution of imagery and corrections required, that also depend on the type of analysis. It is recommended to use very high-resolution imagery (<2m) for the identification of individual elements and surfaces and for a more precise and accurate thermal analysis of green infrastructure at local and micro scales.

Additionally, airborne-based measurements can be complemented by concurrent ground-based monitoring (Coutts et al., 2016; Harris & Coutts, 2011). Mobile transects can be used to obtain a good spatial coverage of canopy layer conditions and should include a GPS tracker, meanwhile fixed meteorological stations can be used if higher temporal resolutions are required. In both cases, devices must be placed between one to two metres above the ground.

5.1.4 Workflow and implementation

This section presents the overall workflow for the implementation of the proposed methodological framework [Figure 5.2], which draws on a method developed by Irger (2014), modified and tested by (Bartesaghi Koc, Osmond, Peters et al., 2018; Bartesaghi Koc, Osmond, Peters, and Irger (2017b) and Bartesaghi Koc, Osmond, Peters, and Irger (2017a).

In the first place, the airborne-based data collection campaign must be arranged as per the protocols outlined in the previous section [Table 5.2]. In particular, this requires the control of intervening climatological variables [see Table 3.3] as these have a considerable influence on the thermal performance of green infrastructure and the variability of UHIs. Accordingly, measurements must be conducted in calm, clear and dry conditions to reduce the confounding effects of wind (especially sea breezes), cloud cover and rainfall. A detailed description of the flights, the extent of the case study and the data collected are provided in Chapter 6.

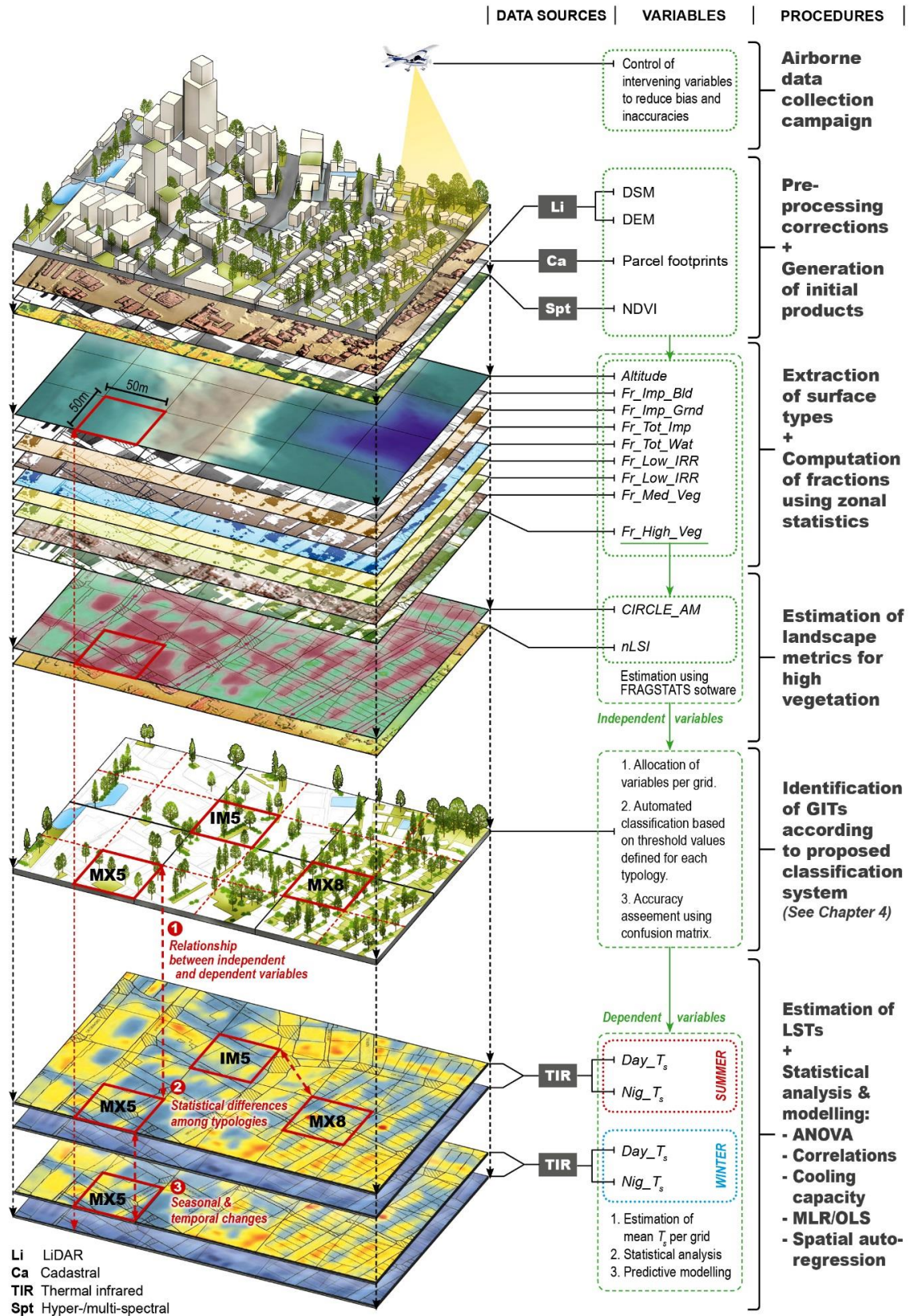


Figure 5.2 Schematic representation of the implementation of the methodological framework and list of relevant data sources and variables.

Based on Bartesaghi Koc, Osmond, Peters, and Irger (2017a).

Secondly, a DEM is calculated from LiDAR data to determine the altitude of ground surfaces; while a DSM is applied in conjunction with cadastral data to identify and extract building footprints. After performing the necessary orthorectification, atmospheric and radiometric corrections, a NDVI image is derived from spectral data to extract different surface types (impervious, pervious, water) using a simple threshold NDVI classification analysis and implementing the Jenks optimization method (Jenks, 1967) for defining thresholds according to the literature. To improve and validate spectral-based extractions and discriminate between grasses, shrubs and trees, LiDAR data is utilised to extract medium and high vegetation. Pre- and post-processing of collected data for the calculation of initial airborne-based products is presented in Chapter 6.

Once land covers (as raster images) have been extracted from LiDAR and spectral data, all surface fractions are computed using zonal statistics in ArcGIS® (ESRI, 2012); and values assigned to grids of 50x50m. The size of grids has been defined after applying a sensitivity analysis which is presented in Chapter 7. The high vegetation raster is used in FRAGSTATS 4.2 software (McGarigal et al., 2002) to calculate CIRCLE_AM and nLSI values for all grids. After estimating independent variables, grids are automatically classified into GITs according to the threshold values defined in [Table 4.14](#) (Chapter 4). The workflow and steps for the computation of all variables and automated classification of grids are summarised in Chapter 6.

For the purpose of this research, only a portion of the total extent of the case study is selected for accuracy assessment due to time and resource constraints. To assess the accuracy of classification results, independent validation data for ground-truthing are selected using very high resolution (0.5m) aerial images. Four quality indices are employed to evaluate the accuracy of predictions. The producer accuracy (PA), the user accuracy (UA), the overall accuracy (OA) and, the kappa coefficient. Then, a percentage of the total number of classified grids per typology are chosen for accuracy assessment through a confusion matrix using a stratified random sampling method. To reduce flaws in the assessment, the percentage of grids for validation was increased for typologies with an insufficient number of samples. In addition, the classification learner app available in Matlab® software (MathWorks, 2017b) is applied to assess the predictability of the classification scheme using various supervised machine learning classifiers (*i.e.* decision trees, discriminant analysis, support vector machines). Further details on the implementation of each method and the results of accuracy evaluations are presented in Section 7.2.3.

The next step in the methodology involves the computation of absolute LSTs using a normalised emissivity method (NEM) [Eq. 3.1] (Gillespie, 2015; Realmuto, 1990) assuming a constant emissivity value of 0.96 for each channel (see Section 3.8.2.1). This approach enables reliable and rapid estimations that can be easily implemented by researchers with varied skill levels. As with spectral data, TIR imagery has to be orthorectified, and corrected for atmospheric and radiometric errors. Further information on the computation of LSTs is provided in Chapter 6.

As per LCZ-related analyses, the statistical analysis in this research is based on the initial assumption that GITs should exhibit mean LST distinct from each other (Bartesaghi Koc, Osmond, Peters et al., 2018; Geletič et al., 2016). Hence, average diurnal and nocturnal LST (in both summer and winter periods) are estimated for each GIT using zonal statistics in ArcGIS® (ESRI, 2012). The statistical significance of variances is evaluated with the Welch's one-way ANOVA test; while post hoc tests are used for pairwise comparisons of means to identify statistically significant differences between GITs.

Before applying ANOVA, normality tests using the Kolmogorov-Smirnov tests, Q-Q plots, histogram comparisons and test of homogeneity of variances (Levene's test) are carried out for the assessment of assumptions. These tests are also utilised to analyse the statistical distribution and spatio-temporal patterns and seasonal differences of mean LSTs.

Additionally, the cooling capacity of each GIT is estimated (1) to identify the coolest and warmest typologies, and (2) to analyse the temporal (diurnal versus nocturnal) and seasonal (summer versus winter) differences of mean LST. Correlational analysis is complementary applied to examine the strength of the relationship between different vegetation-related variables (*i.e.* NDVI, imperviousness) and the cooling capacities of typologies.

In the last stage, preceding analyses lead to the development of a statistical model for the prediction of average surface temperature using the independent variables computed for GITs as predictors. To find the best predictive model(s), various statistical methods are tested and compared, such as the classic multiple linear regression (MLR) using an ordinary least squares (OLS) model; the spatial autoregressive models such as *spatial error model* (SEM) and *spatial lag model* (LAG) (Anselin, 1995, 2005); the artificial neural network (ANN) method; and the adaptive neuro-fuzzy inference system (ANFIS). The results of all statistical tests are provided in Chapter 7.

5.2 Summary

This chapter outlines the overall methodological framework that is applied in the thesis and draws on the theoretical background presented in Chapter 2, the systematic review of methods and indicators described in Chapter 3 and incorporates the classification system proposed in Chapter 4.

Airborne remote sensing and numerical modelling have been identified as ideal tools for mapping, quantifying and examining the cooling effects of green infrastructure at the local scale in a precise, accurate, reliable, and time-effective manner. Information on the data collection and specific data processing methods required for the implementation of this framework are presented in Chapter 6; while results of its application in a case study located in Sydney, Australia are provided in Chapter 7. Although this methodology has been developed for a specific context and goals, it can be equally replicated for similar researches in other urban settings.

Chapter 6

Data collection and data processing¹¹

Initially, this chapter describes the location, extent, physical characteristics and climate of the study area. Next, it documents the equipment and procedures utilised for the collection of datasets through airborne remote sensing, as well as the meteorological conditions experienced during the flight campaign. Finally, it presents the pre- and post-processing methods applied for the calculation of variables required for subsequent analysis.

6.1 Case study area

The methodological framework defined in Chapter 5 has been implemented in two related case studies of the Sydney metropolitan area [Figure 6.1], corresponding to summer and winter seasons. The morphological characteristics, vegetation abundance, climate, UHI conditions and sporadic extreme weather events (*i.e.* heatwaves, droughts) of Sydney are advantageous for the data acquisition and study of the cooling capacities of green infrastructure in different seasons and times of the day.

Due to prohibitive costs, time constraints, logistic problems (*i.e.* adequate weather and air traffic conditions) and limited resources for the acquisition of airborne-based imagery of desirable areas, the selection of case studies mainly responds to data availability. Although both case studies differ in terms of data acquisition times, extent, and climatic conditions, the selected study area represents a cross section of distinct green infrastructure typologies, typical urban morphologies and varied microclimate conditions of the Sydney metropolitan area.

¹¹ Versions of Chapter 6 have been published or have been submitted for publication:

- Bartesaghi Koc, C., Osmond, P., Peters, A. (2019), Mapping and classifying green infrastructure typologies for climate-related studies based on remote sensing data, *Urban Forestry and Urban Greening*.
- Bartesaghi Koc, Osmond, Peters et al. (2018), Understanding land surface temperature differences of Local Climate Zones based on airborne remote, *Journal of Selected Topics in Applied Earth Observations and Remote Sensing (JSTARS)*.
- Bartesaghi Koc, Osmond, Peters, and Irger (2017b), Mapping Local Climate Zones for urban morphology classification based on airborne remote sensing data. In *2017 Joint Urban Remote Sensing Event (JURSE)* (p. 1–4). IEEE Xplore.

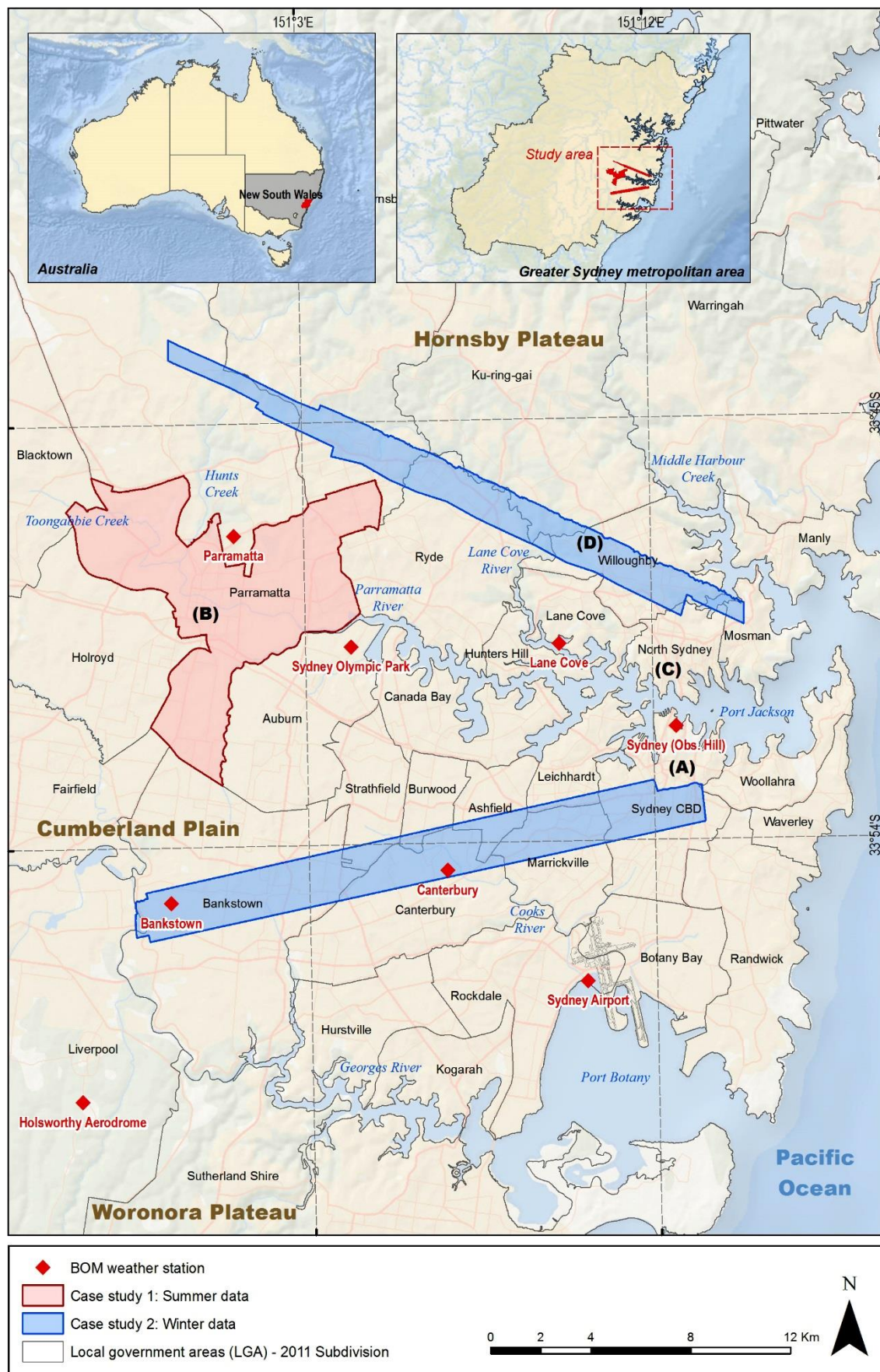


Figure 6.1 Map of main geographical features, location of case studies and spatial coverage of the datasets within the Sydney metropolitan area.

6.1.1 Geographic location and climate

The study area is located within the greater metropolitan area of Sydney which is the capital of the state of New South Wales (NSW) and the largest and most densely populated city in Australia, with a population of 4.8 million distributed across 12,368 km² (ABS, 2017). Sydney is located on the south-eastern coast of the country (33°45'S latitude) and is made up to 43 local councils (2011 subdivision) that have been amalgamated into 30 since this research was conducted; hence, the content of this thesis refers to pre-amalgamation conditions.

The geography of Sydney is characterised by coastal conditions, and it is located in a basin bordered by the *Pacific Ocean* to the east, the *Blue Mountains* to the west, the *Woronora Plateau* to the south and the *Hawkesbury River* to the north. Sydney sprawls over two major geographical regions: the hilly *Hornsby Plateau* towards the North which elevates up to 200 metres and is dissected by steep valleys; and the relatively flat *Cumberland Plain* which extends towards the South and West of Sydney Harbour (Department of the Environment and Energy, 2018) [Figure 6.1].

The *Nepean River* originates in the southern side of the *Woronora Plateau* and wraps around the western fringe of the city. The south and southwest areas of Sydney are drained by the *Georges River*, which rises near Appin, flows north towards Liverpool and finally turns east towards Botany Bay. Another major tributary of Botany Bay is the *Cooks River* which runs throughout the inner-south western suburbs from Strathfield South to Woll Creek (near Sydney International Airport). *Parramatta River* is another important water course –which main tributaries are the *Toongabbie Creek* and *Hunts Creek*– that flows into *Port Jackson*, commonly known as *Sydney Harbour*. *Lane Cove River* and *Middle Harbour Creek* are other major tributaries that flow into the same harbour (WaterNSW, 2018) [Figure 6.1].

In general, Sydney exhibits mixed urban form dominated by low and medium density (to a lesser degree) areas interspersed with greenspaces, brownfield, industrial land and transport facilities (such as railway corridors). Compact, dense and high-rise structures are mainly located in the central business district (CBD) (A) in the eastern side, City of Parramatta (B) in the western side, and North Sydney (C) and Chatswood (D) in the northern side [Figure 6.1]. The largest forested areas and greenspaces typically concentrate along the rivers and creeks mentioned above that are usually low-lying.

According to the Köppen-Geiger climate classification, Sydney has a humid subtropical (*Cfa*) climate with cool winters and warm summers (Bureau of Meteorology, 2017; Kottek

et al., 2006). The annual monthly average temperature registered by Observatory Hill weather station in Sydney's CBD ranges from 16.4°C to 26.0°C according to the average data estimated between 1859 to 2018 (BOM, 2018).

The mean daily maximum and minimum air temperatures vary between 25.9°C during the summer (January) and 8.1°C during the winter (July). January is typically the warmest month with an average daily air temperature fluctuating between 18.7 °C and 25.9°C and the highest recorded maximum of 45.8°C. Contrastingly, July is commonly the coldest month with temperatures usually staying above 5°C with the lowest recorded minimum temperature of 2.1°C (BOM, 2018).

However, inland Western suburbs exhibit daily average maximum and minimum temperatures that are considerably higher than those of Sydney CBD (2°-5°C), with an average of 45.5 days per year with temperatures falling above 30°C (BOM, 2018). These conditions are significantly influenced by wind speed and direction, and coastal proximity as the effect of sea breeze decreases towards inland western suburbs (Santamouris et al., 2017). The cooling effect of wind is normally less pronounced on calm days as well as in locations further than two kilometres from the coastal border (Irger, 2014). In average wind speeds range from 11.5 to 14 km/h at a height of 10 m, but these values largely vary across the region (Spagnolo & Dear, 2003a).

Average rainfall patterns follow a similar east-west gradient, with higher mean annual rainfall towards the coast (above 1500 mm/annum) and the north shore around Turrumurra (above 1400 mm/annum) (BOM, 2018).

6.1.2 Vegetation conditions

Multiple biomes including rainforests, wet/dry sclerophyll forests, grassy woodlands, heathlands, and freshwater, forested and saline wetlands can be found across the Sydney metropolitan region (Office of Environment and Heritage, 2018).

The plant communities in the Sydney metropolitan area (Cumberland Plain) are predominantly dry and wet *Sclerophyll forests*. These plants are characterised by perennial hard leaves, short internodes (distance between leaves and stem) and leaf oriented parallel or oblique to sunlight. Common wet sclerophyll plant species within the study area include the forest red gums, blue gums, boxes, iron barks, peppermints, karrabina, mahoganies, eucalyptus and green-leaved ashes (OEH, 2018). The most dominant native plant species in Sydney are the eucalyptus trees, which possess narrow, relatively tall, and dense canopies (10-30 metres height) and are usually found in open woodlands with dry shrubs

and sparse grasses in the understory. Estuaries and riparian zones are characterised by swamp oaks, common reeds and mangroves (OEH, 2018).

6.1.3 Case study 1: Summer

The first case study, corresponding to the summer season, comprises the inland Western suburbs within the Parramatta City Council (PCC)¹² local government area (LGA) covering a total area of 61.33km². Parramatta is situated 19 km from Sydney's CBD and is 26km from the coast. It is a prominent and major business and commercial centre, that was settled by the British in 1788, and it is popularly regarded as the second CBD of the Sydney metropolitan area (Domain, 2016).

Over the last 40 years, the Western Sydney suburbs have experienced exacerbated urban warming and a significant rise in the number of extreme temperature events such as heatwaves. These are particularly stronger in Parramatta, as well as in Blacktown, Camden, Liverpool, Penrith and Richmond LGAs. For instance, the number of days over 35°C has considerably increased since 1965 (Beshara, 2018). These patterns are also consistent with the considerable increase in population and new urban development that Parramatta has been experiencing in recent decades.

Compared to the coastal suburbs, Parramatta exhibits a hotter climate as it is not influenced by the cooling easterly sea breezes, especially during the afternoon when air temperatures reach their maximum values (Osmond & Sharifi, 2017). Moreover, this hotter climate may be also exacerbated by occasional western hot winds coming from the desert. For example, a maximum temperature difference of up to 9°C between PCC and Sydney's CBD was recorded on a hot summer day (around 1pm) in January 2017 (BOM, 2018; Hannam, 2017).

The morphological composition of Parramatta also plays a key role in defining particular microclimate conditions across the LGA. Parramatta's suburbs predominantly lie on the Cumberland Plain; hence, they exhibit a relatively flat topography with a number of ridges towards the north-eastern portion of the area [Figure 6.2]. Accordingly, since it is situated in a rain shadow due to the hills to the northeast, it tends to be drier than coastal areas and less green than the hilly Northern suburbs. Typically, summer rainfall is lower than in autumn and higher than winter and spring, with a monthly average rainfall in summer ranging between 73 to 121 mm (Osmond & Sharifi, 2017).

¹² Currently named as City of Parramatta Council.

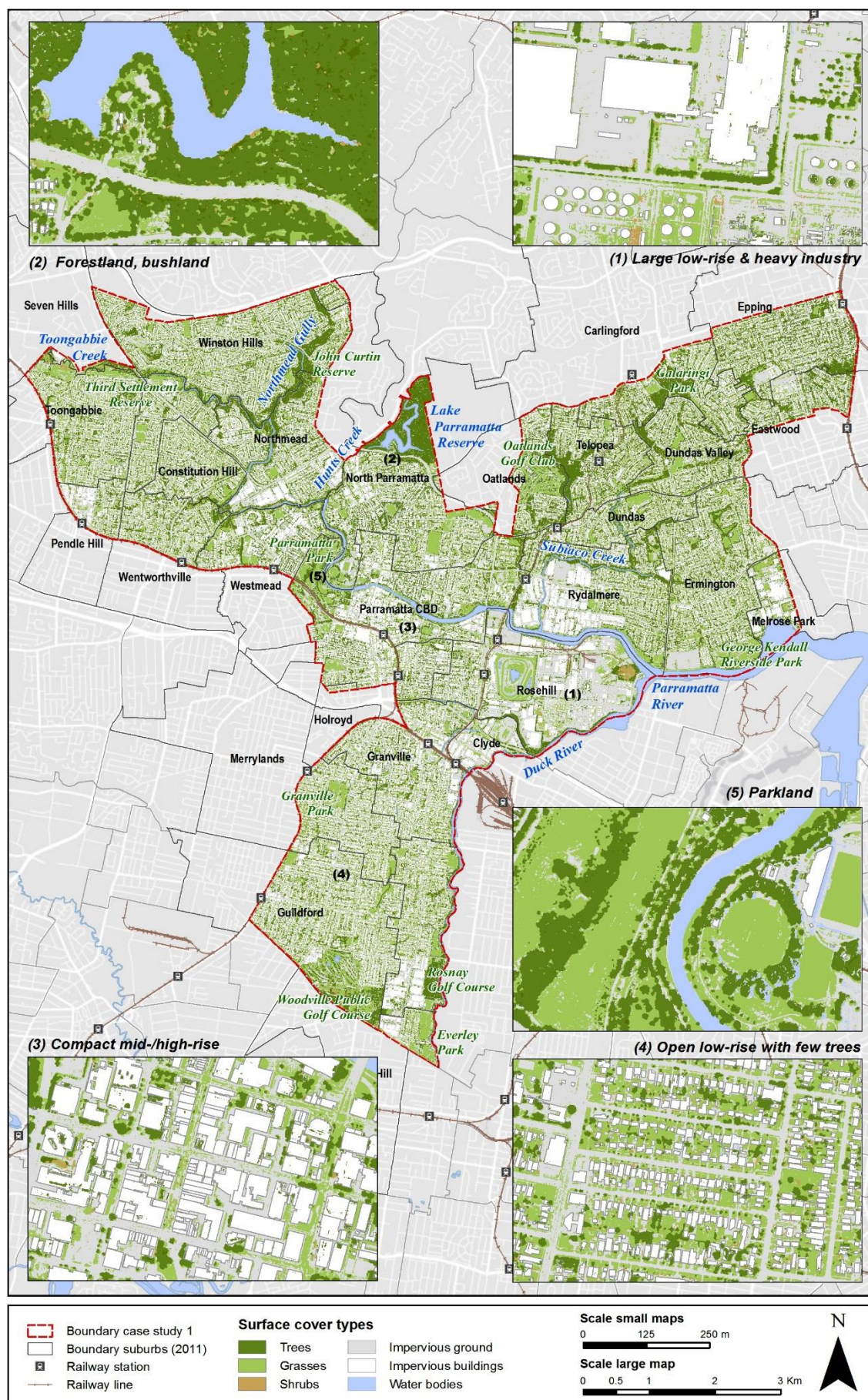


Figure 6.2 Location, extent, and main morphological characteristics of case study 1.

Like the vast majority of Sydney, Parramatta is dominated by low and medium density residential suburbs characterised by semi-detached and detached dwellings on medium sized lots featuring gardens and sporadic trees. Streets are generally wide and dominated by asphalt, and paved driveways with sparse trees and grasses [Figure 6.2].

However, over the last few decades average plots sizes have shrunk, size of houses increased, and minimum setbacks reduced as part of state government policies to increase density and affordability (City of Parramatta, 2018; Irger, 2014). Furthermore, the Parramatta CBD is currently undergoing a significant transformation due to unprecedented levels of private and public investment, triggered by state and federal government and property developers (City of Parramatta, 2018).

On the other hand, the areas located in the central core and along the Parramatta river (Clyde, Northmead, Parramatta CBD, Rosehill, Rydalmere, and Westmead) mainly comprise compact and highly dense commercial zones, largely paved low-rise precincts, brownfield land, heavy industry (*i.e.* refinery, waste facilities, factories, warehouses) and railway facilities with scarce or no vegetation [Figure 6.2].

Most parkland and greenspaces are located towards the north and northeast of the LGA along the main tributaries of Parramatta River; the *Toongabbie Creek* and *Hunts Creek*. Lake Parramatta, located in the northern edge, is an important recreational area and nature reserve surrounded by extensive bushland and forest. Parramatta Park is another major greenspace which is adjacent to the River and the Parramatta Stadium and close to the CBD. There are also a number of golf courses to the North (Oatlands) and South (Woodville, Rosnay), and medium and small parks sparsely distributed across the whole LGA, and along the Parramatta River and creeks [Figure 6.2].

Based on previous facts, Parramatta possesses many physical characteristics and climate conditions that make it an ideal case study to assess the thermal performance of green infrastructure, especially in summer and during extreme temperature conditions. The sampling intensity of the summer case study is defined by the number of GITs or grid cells classified using the frameworks proposed in Chapters 4 and 5 (see Sections 6.3 and 7.2 for further information).

6.1.4 Case study 2: Winter

Since airborne-based imagery corresponding to the winter season were not available for Parramatta LGA, a second case study within the Sydney metropolitan region was chosen from the data collected for a similar research (see Irger, 2014).

This comprises two longitudinal strips: one over the Sydney's *northern suburbs* with a swath length of 25.7km and varying width (0.8-1.5km), covering an area of 44.6km²; and a second strip over the *southern suburbs* with an average swath width of 1.9km and a length of 23.4km, covering an area of 31.93km² [Figure 6.3]. The shape, extent and path of both strips respond to the flight transects defined by Irger, 2014; progressing from the coast inland.

On the one hand, the southern strip comprises multiple LGAs and extends from Sydney's CBD towards the southwest middle ring suburbs of the Sydney metropolitan area. Like Parramatta, the topography of this area is relatively flat, low-lying and contains relatively compact residential areas interspersed by pockets of green. Major greenspaces concentrate along the Cooks River and near Centennial Park [Figure 6.3].

Contrastingly, the northern strip presents a steep and rough topography with extensive and dense tree canopy (forest, reserves) and higher vegetation content in residential areas (mature trees, larger gardens and parks) than its southern counterpart. Greenspaces are also mostly concentrated along rivers and creeks [Figure 6.3].

In summary, the morphological characteristics of the second case study are varied and include: (1) extensive parkland, bushland, or forestland; (2) open low-/mid-rise zones of detached houses with large gardens and matures trees; (3) compact mid-/high-rise areas with few vegetation (mostly street trees, roadside verges and small parks) typical of city centres; (4) large mid-/low-rise and industrial areas (*i.e.* factories, warehouses, shopping malls); (5) compact low-rise zones of terraced and semi-detached houses; and (6) highly paved transport facilities (*i.e.* Bankstown airport, central station) [Figure 6.3].

In addition, both strips cover a sufficient number and variety of vegetation types and abundance, topography, distances to the coast and local climate conditions to investigate the cooling effects of green infrastructure in winter and across different urban contexts. The sampling intensity of the winter case study is defined by the number of GITs or grid cells classified using the frameworks proposed in Chapters 4 and 5 (see Sections 6.3 and 7.2 for further information).

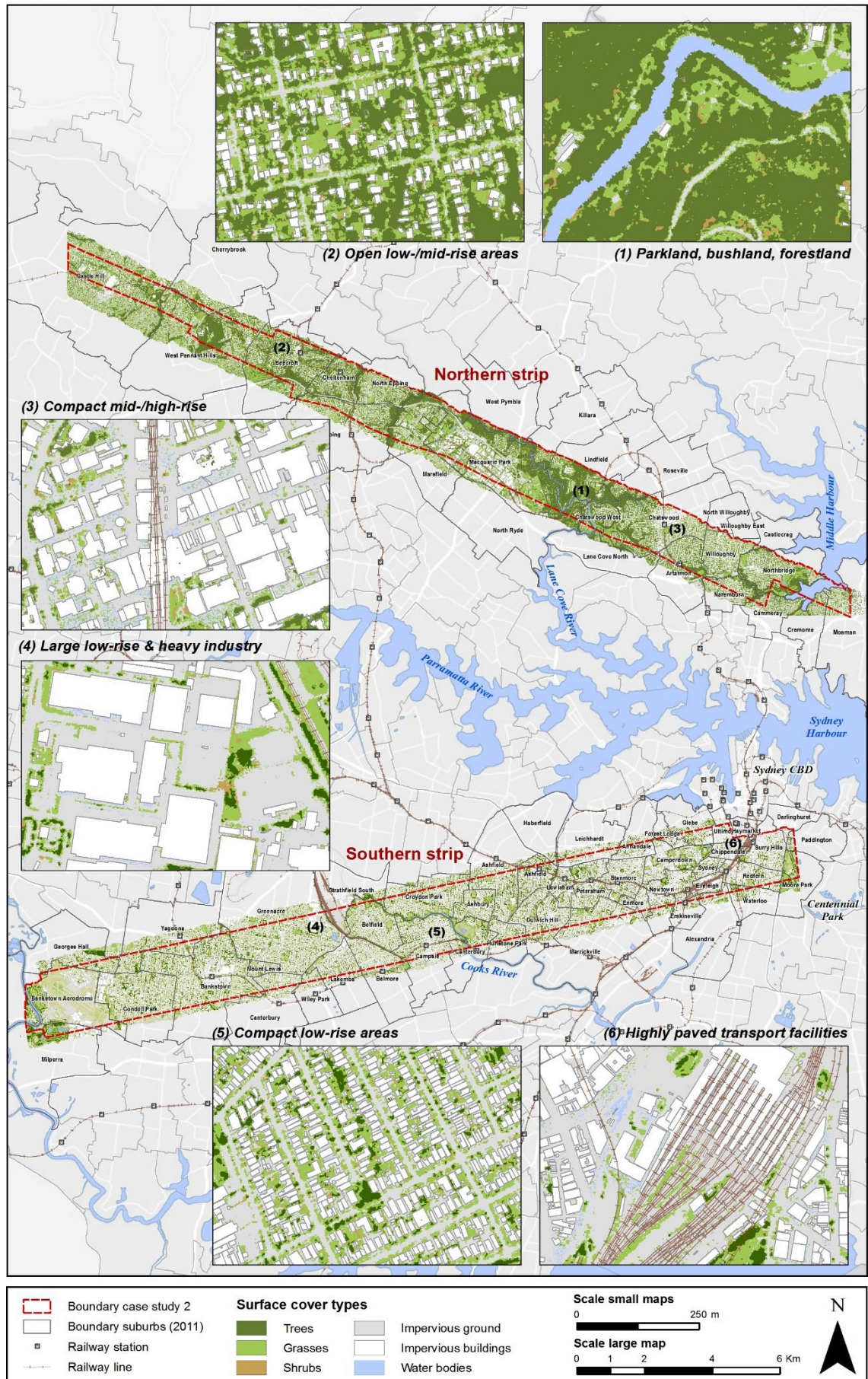


Figure 6.3 Location, extent, and main morphological characteristics of case study 2.

6.2 Airborne data collection and pre-processing

For this research, four main datasets were employed separately for each case study (summer and winter), namely TIR imagery, hyper-/multi-spectral data (including aerial images), LiDAR data, and cadastral data as listed in Chapter 5 (Section 5.1.2). The spatial coverage of datasets for each case study are shown in [Figure 6.1](#).

6.2.1 Summer data collection

On January 2013, *Spatial Scientific Inc.* undertook a thermal and multispectral imaging survey commissioned by the PCC in the context of an UHI-related project. Due to technical problems, the data collection was repeated and completed on February 2013 in similar meteorological and temporal conditions as those outlined in Chapter 5. The airborne campaign was carried out with a Piper Comanche 250 single-engine aircraft that flew at average ground speeds of 120 to 140kn.

Initially, it was planned to acquire thermal and multispectral imagery on 17 and 18 January 2013 as weather conditions were favourable with maximum air temperatures of 31.2°C and 45.5°C respectively (BOM, 2018). On the afternoon of 17 January multispectral imagery was captured between 2:48 and 3:26pm EDT¹³ at a flight height of 10000 ft (3048m) above ground level. The aircraft departed from Bankstown aerodrome at 2:20pm and landed at 3:41pm EDT. The acquisition took place under clear skies and with light northerly winds. Maximum air temperatures of 32.5°C and 26°C were recorded the days preceding the flight without rainfall, except for 14 January that recorded 12mm of rain (BOM, 2018).

On the evening of 17 January thermal imagery was captured at an altitude of 6000ft (1829m) between 11:18pm and 1:10am EDT on 18 January. The data was also captured under adequate weather conditions. However, on the 18 January the acquisition of day-time thermal imagery was suspended due to extreme temperatures (45.7°C) that damaged the traffic control radar and prevented the aircraft from entering controlled airspace. To complete the data acquisition and ensure the best quality in terms of temporal requirements, both day-time and night-time thermal imagery were acquired on 8 February 2013, which was the hottest day of the month with 34°C. The day was cloudless and calm, with light northerly winds and no precipitation 72 hours prior to the flight. Maximum air temperatures recorded the days preceding the flight ranged between 26°C and 30°C (BOM, 2018).

¹³ Eastern Daylight Time (EDT)

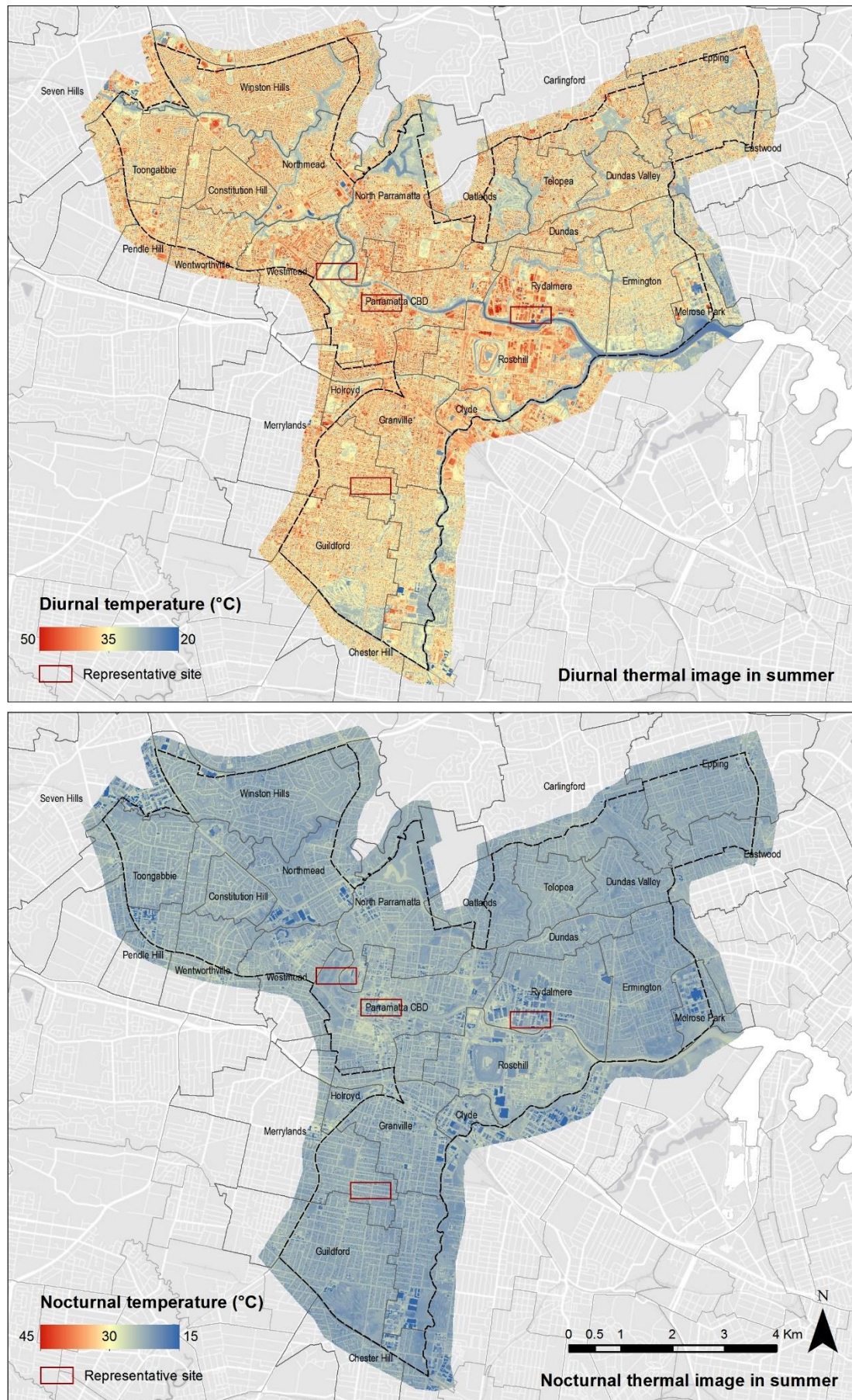


Figure 6.4 Extent of the airborne diurnal and nocturnal thermal images acquired in summer.



Figure 6.5 Diurnal thermal imagery of representative sites in summer captured around 1pm on 8 February 2013.

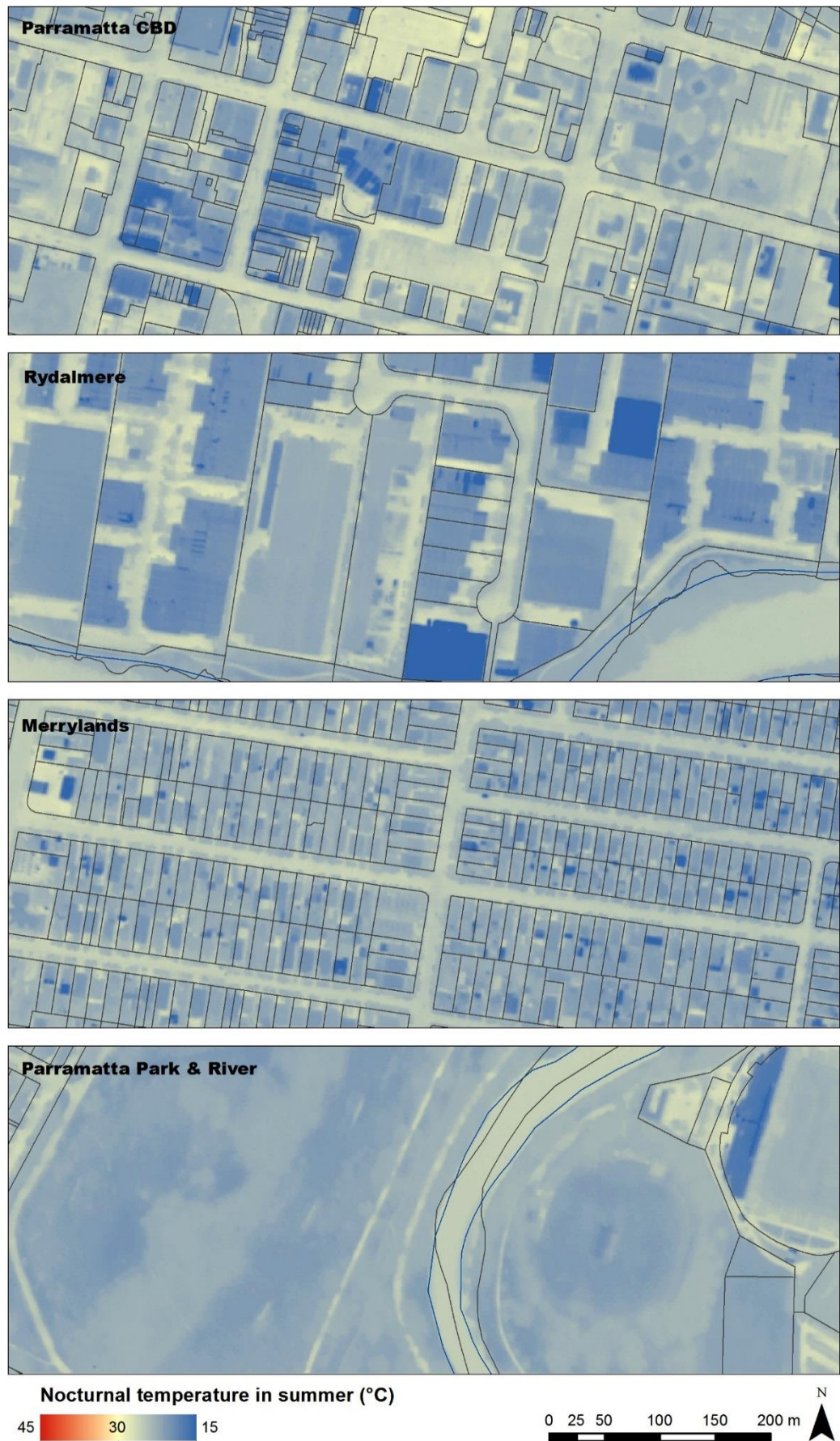


Figure 6.6 Nocturnal thermal imagery of representative sites in summer captured around 1am on 9 February 2013.

The *day-time* image was captured at an altitude of 10000ft (3048m) between 1:36 and 2:20pm EDT. The aircraft departed Bankstown aerodrome at 1:06pm and landed at 2:35pm EDT. The *night-time* image was acquired at a flight height of 6000ft (1829m) between 11:24pm and 12:58am EDT. The aircraft departed Bankstown aerodrome at 11:13pm and landed on 9 February at 1:11am EDT.

Several overpasses were carried out across the LGA to secure the best quality of images and the adequate number of swaths to avoid missing information. Adjacent flight swaths were scanned consecutively rather than in a continuous loop to minimise temperature differences among distinct locations that may be caused by the time lag of scans. All multi-spectral and thermal swaths were mosaicked and cropped using the LGA as boundary.

Thermal imagery

Diurnal and nocturnal thermal data were collected using a FLIR A615 thermal camera that measured surface brightness temperature with a thermal accuracy of $\pm 2^{\circ}\text{C}$ or $\pm 2\%$ of reading, and a broad field of view (FOV) of $80^{\circ} \times 64.4^{\circ}$ (92.8° diagonal). At a flight height of 3048m the *day-time* thermal recording produced an image with a spatial (pixel) resolution of 2.11m; while at an altitude of 1829m the *night-time* thermal recording produced an image with a spatial resolution of 1.20m. The spatial coverage of both TIR images is shown in [Figure 6.4](#).

The pre-processing of recorded images was performed by the remote sensing contractor which included the following procedures: (1) the ortho-rectification and geo-referencing using aerial photography; (2) the calculation of LSTs using constant emissivity value; (3) resampling images to 1m pixel resolution (16 bits per pixel); (4) the continuous mosaicking and cropping of images using the LGA as boundary; (5) aligning and projecting rasters to *GDA 1994 MGA Zone 56* projected coordinate system; and (6) the creation of look-up tables with temperatures in Kelvin and Celsius degrees.

To estimate absolute LSTs the contractor applied a NEM model (Gillespie, 2015; Realmuto, 1990) assuming a constant emissivity value of 0.96 for all channels based on measured radiances. The maximum of those temperatures (T_{NEM}) is considered as the absolute LST for a given pixel as per [Eq. 3.1](#) described in Section 3.8.2.1.

Detailed samples of diurnal and nocturnal thermal images are presented in [Figures 6.5](#) and [6.6](#). These will also serve as representative sites for the reminder of the airborne-based products and data processing steps conducted in this research. It is worth mentioning that since thermal images only provide a bird's eye view of the study area, surfaces beneath the

tree canopy and building facades are not considered in the analysis of results presented in Chapter 7.

Multi-spectral imagery

Airborne multi-spectral data were acquired on 17 August 2013 as per the flight plan detailed in Section 6.2.1 using a SpecTerra's HiRAM sensor (Serial 0502). The sensor recorded short-wave radiation in four bands (16-bit integers): blue (450nm), green (550nm), red (670nm) and NIR (780nm); with a spatial resolution of 0.8m.

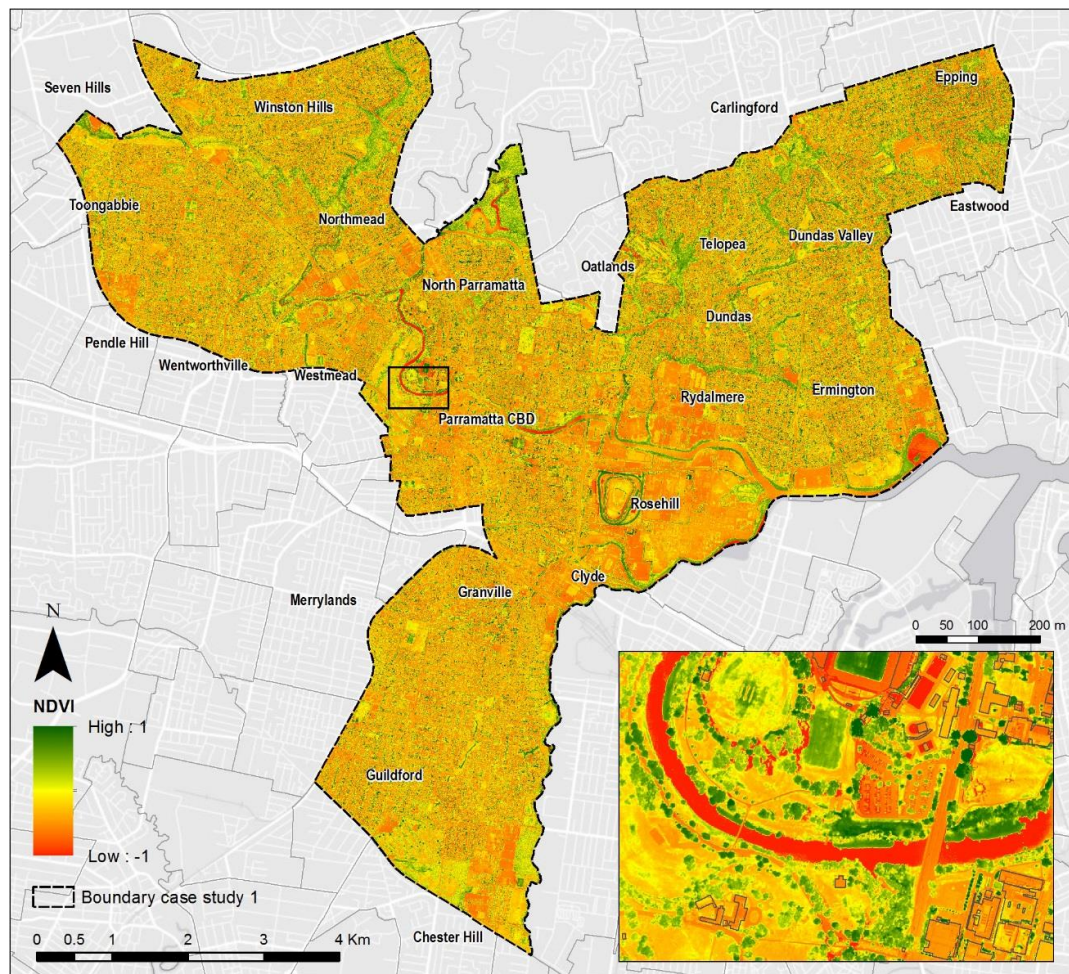


Figure 6.7 Extent of the airborne-based multispectral imagery acquired in summer 2013 presented as a NDVI image.

The data were pre-processed by the contractor using SpecTerra's proprietary image processing software and included the following procedures: (1) the geometric corrections of spectral swaths, (2) the radiometric corrections to reduce errors in the digital numbers and remove illumination effects, (3) mosaicking swaths into a single continuous image covering the extent of the LGA; (4) resampling images to 1m pixel resolution, and (5) projecting rasters to *GDA 1994 MGA Zone 56* projected coordinate system.

The data were delivered by the contractor as a continuous multi-spectral true colour (RGB) image and a separate multi-spectral false colour infrared (CIR) image (NIR, Green, Red bands), instead of a single image with four bands and bandwidths. Figure 6.7 shows the spatial coverage of the multispectral data presented as a NDVI raster created using the NIR and Red bands from both images (see Section 6.3 for details).

LiDAR data

LiDAR data were not collected in the flight campaign organised by the PCC. Hence, LiDAR point clouds, known as LAS datasets, were acquired from the *ELVIS – Elevation Foundation Spatial Data* portal managed by Geoscience Australia (2018).

The acquisition of LiDAR data over the Sydney metropolitan area was undertaken by the ‘spatial services’ division of the New South Wales Land and Property Information (LPI) service¹⁴. The mission was conducted between 10 and 24 April 2013 at an average flying height of 1530m from east to west. It employed a Leica ALS50-II (S/N: 101m) sensor scanner that generated LAS tiles of 2 x 2km with an average point density of 1.57/m² and nadir point density of 1.03/m². The LAS data have a spatial horizontal accuracy of 0.8m and spatial vertical accuracy of 0.3m at 95% confidence. A metadata statement for these LiDAR datasets is provided in Appendix C.

Table 6.1 Standard point classification of LiDAR data based on LPI protocols. (Modified after Land Property Information, 2015)

No.	Point class	Description	No.	Point class	Description
0	Unclassified	Created, never classified	7	Low high points	Spurious high/low point returns (not useable)
1	Default	Unclassified	8	Model key points	Reserved for ‘Model Key Points’
2	Ground	Bare ground	9	Water	Any point in water
3	Low vegetation	0 – 0.3m vegetation	10	Bridge	Any bridge or overpass
4	Medium vegetation	0.3 – 2m vegetation	11	Not used	Reserved for future definition
5	High vegetation	>2m vegetation	12	Overlap points	Flight line overlap points
6	Building	Houses, shed, etc.	13-31	Not used	Reserved for future definition

The LAS datasets were pre-processed and points clouds classified as per the LPI’s Category 3 (C3) classification level which included manual ground correction of misclassified points (LPI, 2015). LiDAR point clouds were classified by LPI’s operators according to the American Society of Photogrammetry and Remote Sensing (ASPRS) guidelines, which are

¹⁴ Currently named as New South Wales Land Registry Services as a division of NSW Finance, Service and Innovation.

presented in Table 6.1. Model key points (MKP) and intensity images of 0.5m of spatial resolution for all point returns were also supplied along with the LAS datasets. All datasets were projected to *GDA 1994 MGA Zone 56* projected coordinate system.

During the classification process, several anomalies or issues were identified by LPI which include: (1) interpolation lines can be observed across water courses when a DEM/DSM is generated using a triangulation process; (2) dropout from the sensor due to close proximity between the ground and the scanner (not present within the study area); (3) edges of buildings (particularly pitched roofs) misclassified as vegetation; (4) linear surfaces in tree canopy were misclassified as buildings; and (5) presence of spurious points over water caused by excessive solar glare and intense reflection.

A DSM of 1m spatial resolution was generated from the LAS datasets and is presented in Figure 6.8 to illustrate the spatial coverage of the LiDAR data retrieved for the case study 1. Figure 6.9 presents three-dimensional representations of classified point cloud data of several representative sites visualised with LP360 software (QCoherent, 2012).

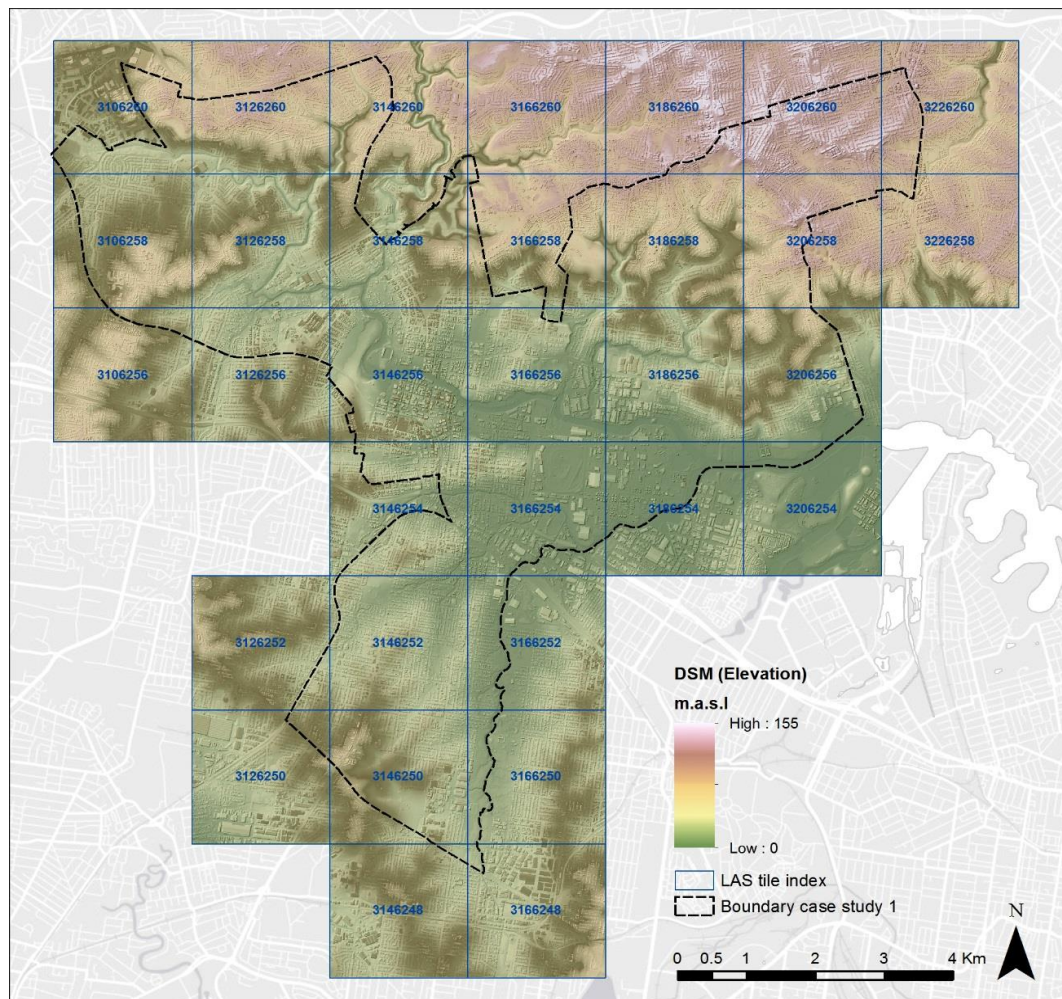


Figure 6.8 Digital surface model (DSM) depicting the spatial extent of LiDAR data acquired for the case study 1.

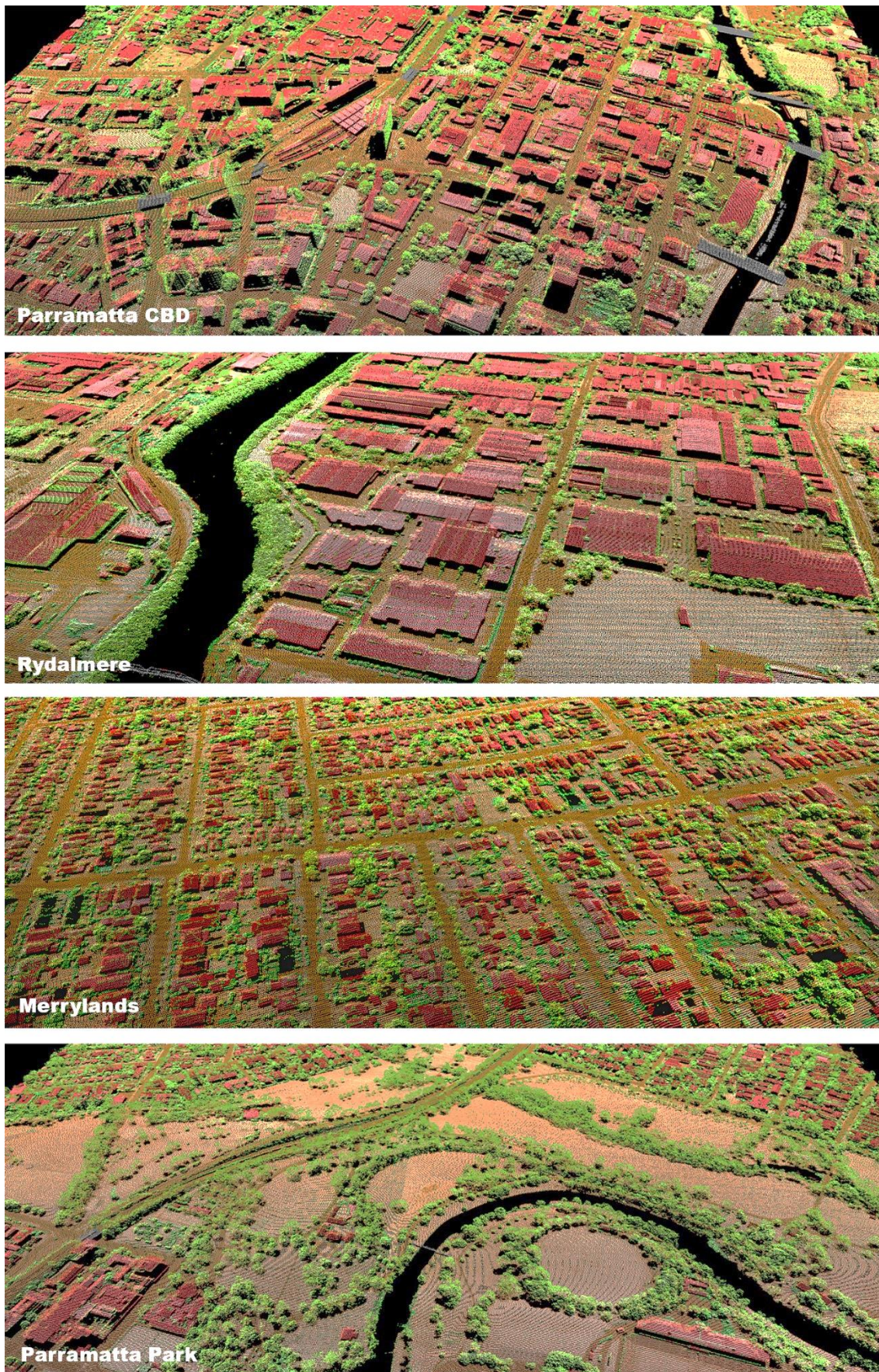


Figure 6.9 Examples of three-dimensional representations of LiDAR point cloud data of representative sites.

Cadastral data

Cadastral data, specifically information of diverse types of administrative boundaries (suburbs, statistical areas, LGA, etc.), land tenures (parcels), land uses, and geographical features (greenspaces, water bodies) were obtained from multiple sources including the Australian Statistical Geography Standard (ASGS) (Australian Bureau of Statistics, 2018); the Australian Urban Research Infrastructure Network portal (AURIN, 2018); public datasets from the Australian Government accessible through the *data.gov.au* portal (Australian Government, 2018) and by courtesy of the PCC and Irger (2014).

6.2.2 Winter data collection

Digital Mapping Australia (DIMAP), a contractor to the Commonwealth Scientific and Industrial Research Organisation (CSIRO), carried out the collection of hyper-spectral, thermal and LiDAR data using a twin-engine fixed wing aircraft in the context of a doctoral research conducted by Irger (2014).

Initially, airborne-based data were supposed to be captured for both summer and winter periods; however, unusual wet and cold weather during the summers of 2011 and 2012 – due to a strong La Niña event– prevented the acquisition of data (Irger, 2014). Instead a winter campaign was carried out in early August 2012 that met the meteorological and temporal requirements established in Chapter 5. These winter datasets are employed in the present research.

The day-time flight was undertaken on 6 August 2012 between 12:00pm and 2:00pm EDT at an altitude of 10000ft (3048m) while the night-time flight was deployed on 4 August 2012 between 11:30pm and 1:30am EDT (on 5 August). Both flights were carried out under cloud free, windless and dry conditions with no precipitation 72 hours prior to the flight. Also, according to the BOM (2018), the weeks preceding the winter mission were the warmest and driest recorded in recent years.

The area covered by flights [Figure 6.1]–corresponding to two longitudinal strips (northern and southern)– is a result of the swath width, which in turn, depends on the type of sensor and flying height. Despite the efforts of maintaining a constant altitude of 1500m on the afternoon of 6 August, the flying height was increased to 3000m due to heavy air traffic. This produced a temporal failure in the thermal recording that created gaps in the data and caused a lower spatial resolution in the hyperspectral data (from 90cm to 2m). Accordingly, the width, length and shape of diurnal and nocturnal swaths differ from each other [Figure 6.10].

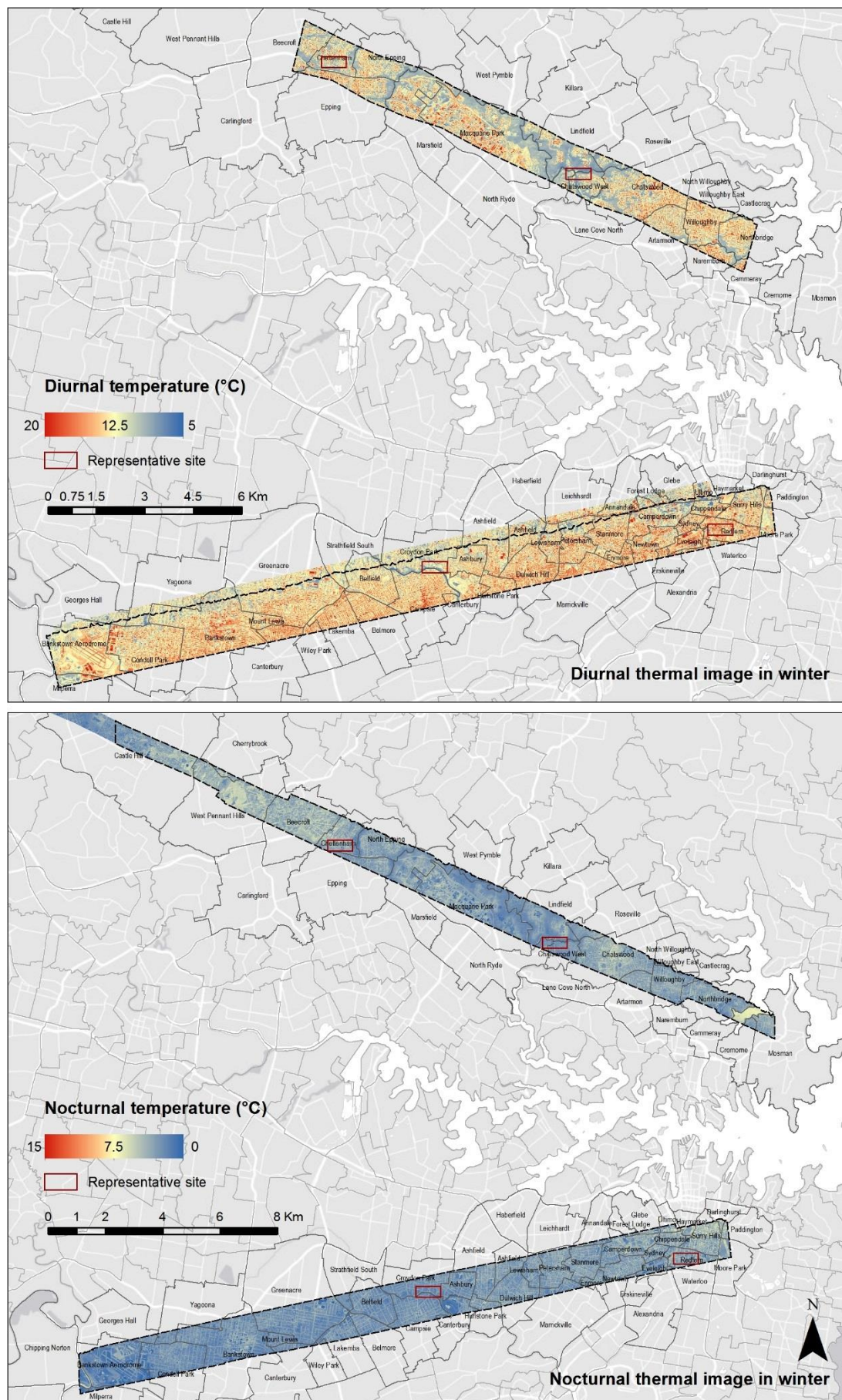


Figure 6.10 Extent of the airborne diurnal and nocturnal thermal images acquired in winter.

Thermal imagery

Diurnal and nocturnal thermal data were collected on 6 and 4 August 2012 respectively using a FLIR SC series camera (formerly Cedip Infrared Systems) that measured surface brightness temperature at a spatial resolution of 0.5m and thermal resolution of 0.018K. The spatial coverage of both TIR images (32-bit integers) is shown in [Figure 6.10](#).

The pre-processing of recorded images was performed by the remote sensing contractor which included the following procedures: (1) correcting radiometric and atmospheric noise using Altair software and IDL script, (2) ortho-rectification and geo-referencing of images representing radiances using ISAT software for triangulation and LPS software for ortho-photo corrections; (3) calculating absolute LSTs using a NEM approach (Gillespie, 1985; Realmuto, 1990) assuming a constant emissivity value of 0.96 as per [Eq. 3.1](#) presented in Section 3.8.2.1 and equally applied in case study 1 presented in Section 6.2.1; and (4) aligning and projecting rasters to *GDA 1994 MGA Zone 56* projected coordinate system.

Pre-processing results produced thermal images with a spatial accuracy of 0.5m and nominated thermal accuracy of $\pm 1\text{K}$. Detailed samples of diurnal and nocturnal thermal images of exemplary sites are presented in [Figures 6.11](#) and [6.12](#). As with the summer TIR images, several consecutive overpasses were carried out across the study area as per the flight path defined by Irger (2014) to minimise thermal differences and avoid missing information. In this way the average time lag between two adjacent swaths was limited to a maximum of six minutes.

Hyper-spectral imagery

Airborne hyper-spectral data were acquired during the *day-time* flight on 6 August 2012 (see flight details in Section 6.2.2) using a Norsk Elektro Optikk (NEO) VNIR1600 HySpex Hyperspectral Camera. The sensor collected short-wave radiation in 160 spectral bands (400 – 1000nm) at 2m spatial resolution and 2.5nm spectral resolution. [Figure 6.13](#) presents the spatial coverage of the hyperspectral data presented as NDVI rasters corresponding to the northern and southern swaths.

Atmospheric corrections were performed for all datasets by the data supplier using ATCOR 4 software, while orthorectification and geometric corrections were applied using PARGE software. The pre-processing also includes the correction for aircraft movements such as roll, pitch, and changes in altitude due to variations in the flight path caused by heavy air traffic at the time of the mission. A boresight calibration was performed to correct possible angular misalignments of the sensor. This was conducted by the data supplier using ground control points from a DEM that were compared against an RGB aerial image.

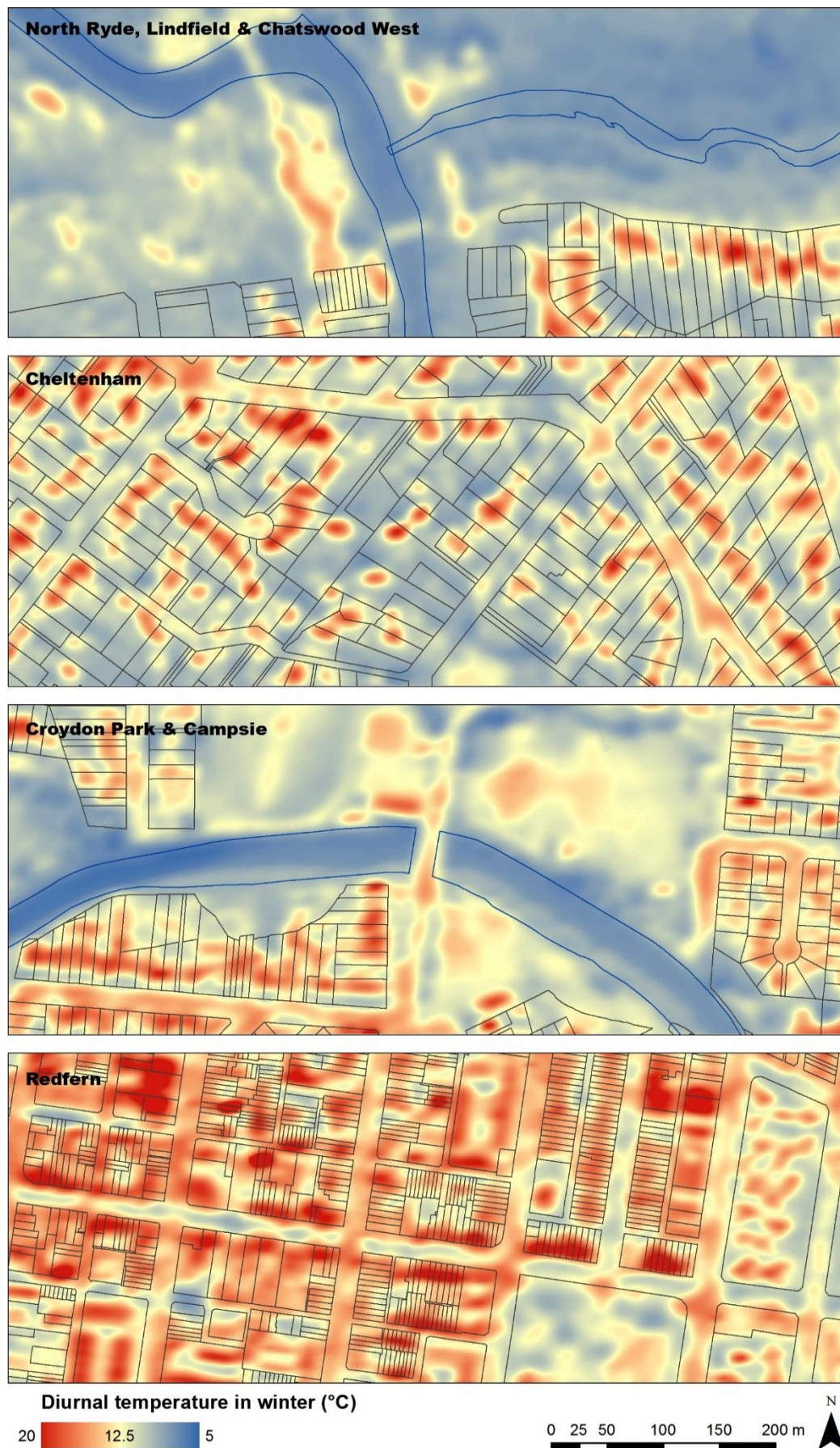


Figure 6.11 Diurnal thermal imagery of representative sites in winter captured around 12pm on 6 August 2012.

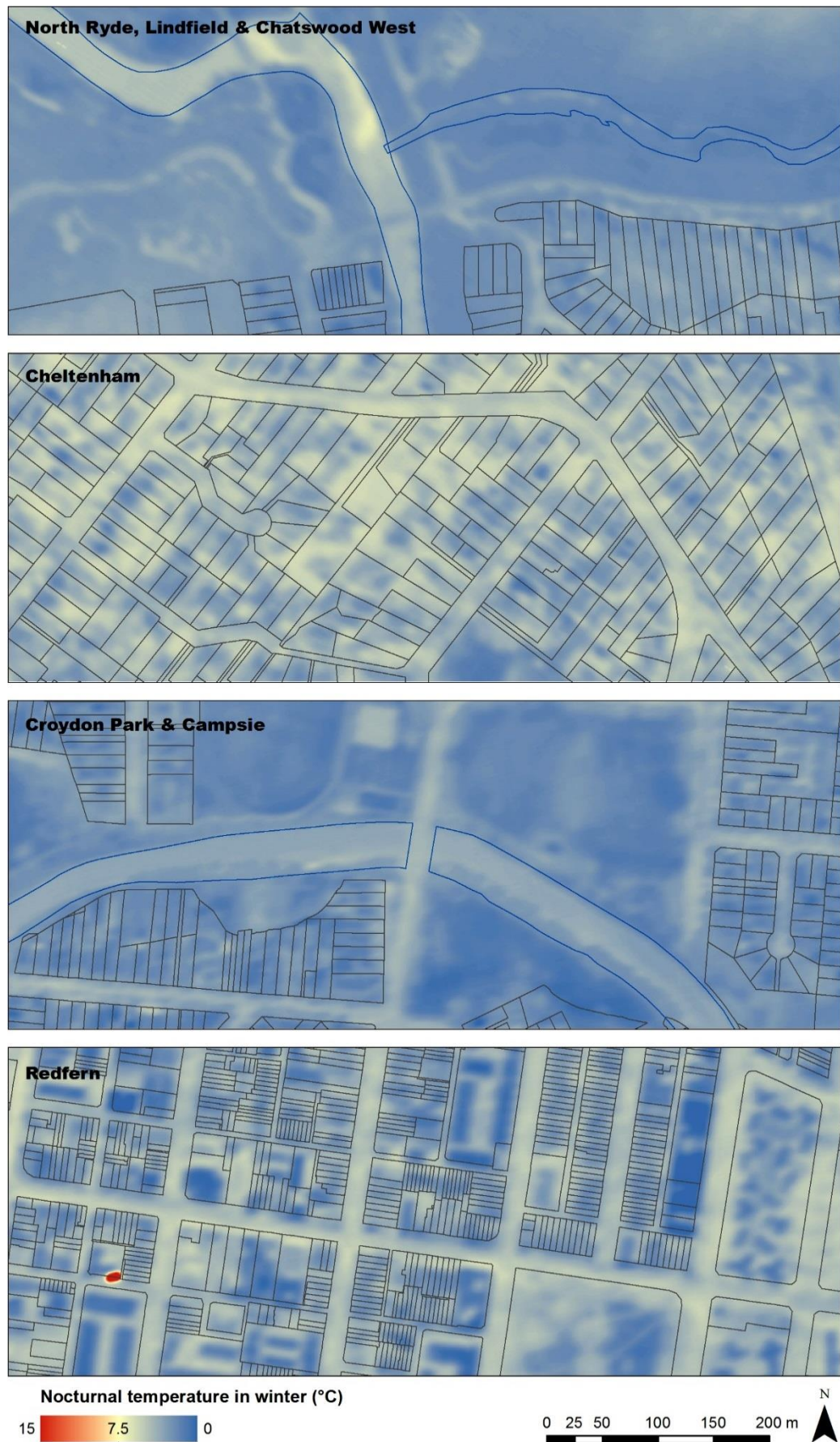


Figure 6.12 Nocturnal thermal imagery of representative sites in winter captured around 12am on 4 August 2012.

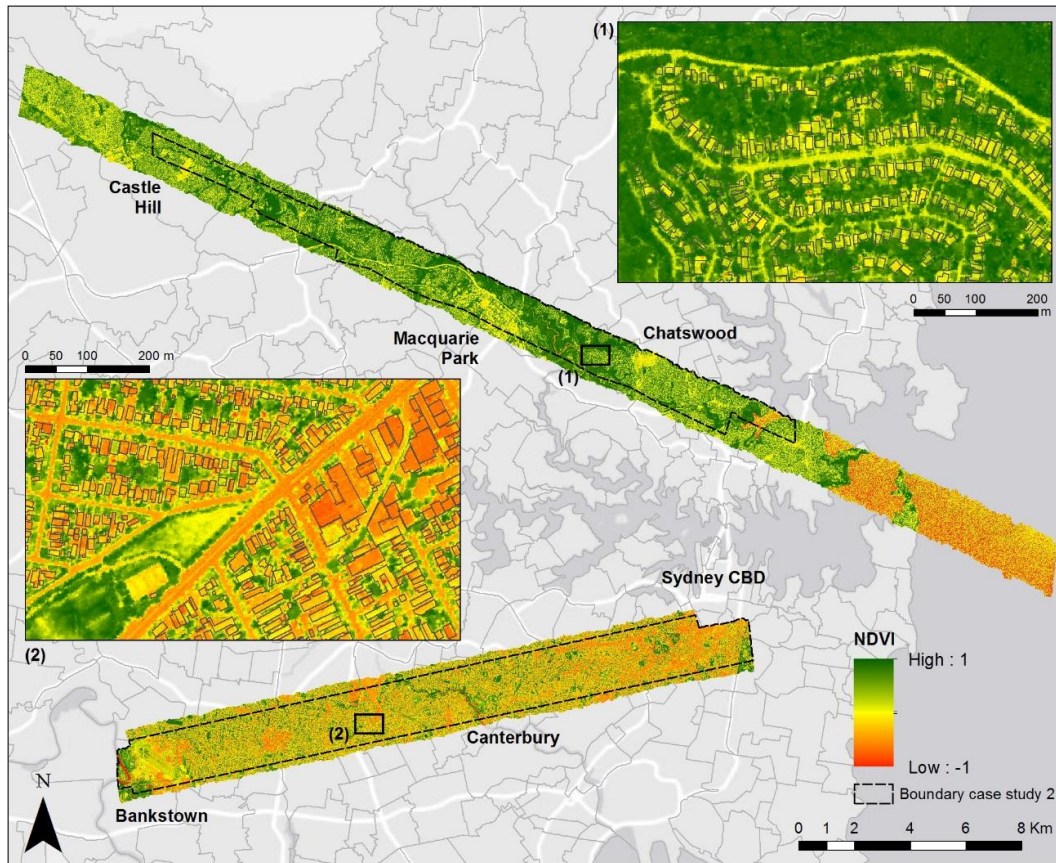


Figure 6.13 Extent of the airborne-based hyperspectral imagery acquired in winter 2012 presented as a NDVI image.

LiDAR data

LiDAR data were collected during the night-time flight commissioned by CSIRO on 4 August 2012. LiDAR point clouds with average point density of $0.8/\text{m}^2$ were supplied to Irger (2014) for the purpose of his research. However, the relatively low point cloud density of datasets was inadequate to extract accurate and precise three-dimensional information, specifically building footprints and tree crowns.

Alternatively, LiDAR data for the extent of the winter case study were acquired from the *ELVIS – Elevation Foundation Spatial Data* portal (Geoscience Australia, 2018); which have the same data collection period/sensor, specifications, quality (point density) and point cloud pre-classification that the data used for case study 1 (see Section 6.2.1 and Appendix C). Since LiDAR and spectral data for this case study were collected in two different periods (early autumn and late winter respectively), additional corrections were applied for excluding deciduous tree canopy as this enables solar penetration to the ground in winter. These corrections are explained in detail in the Section 6.3.

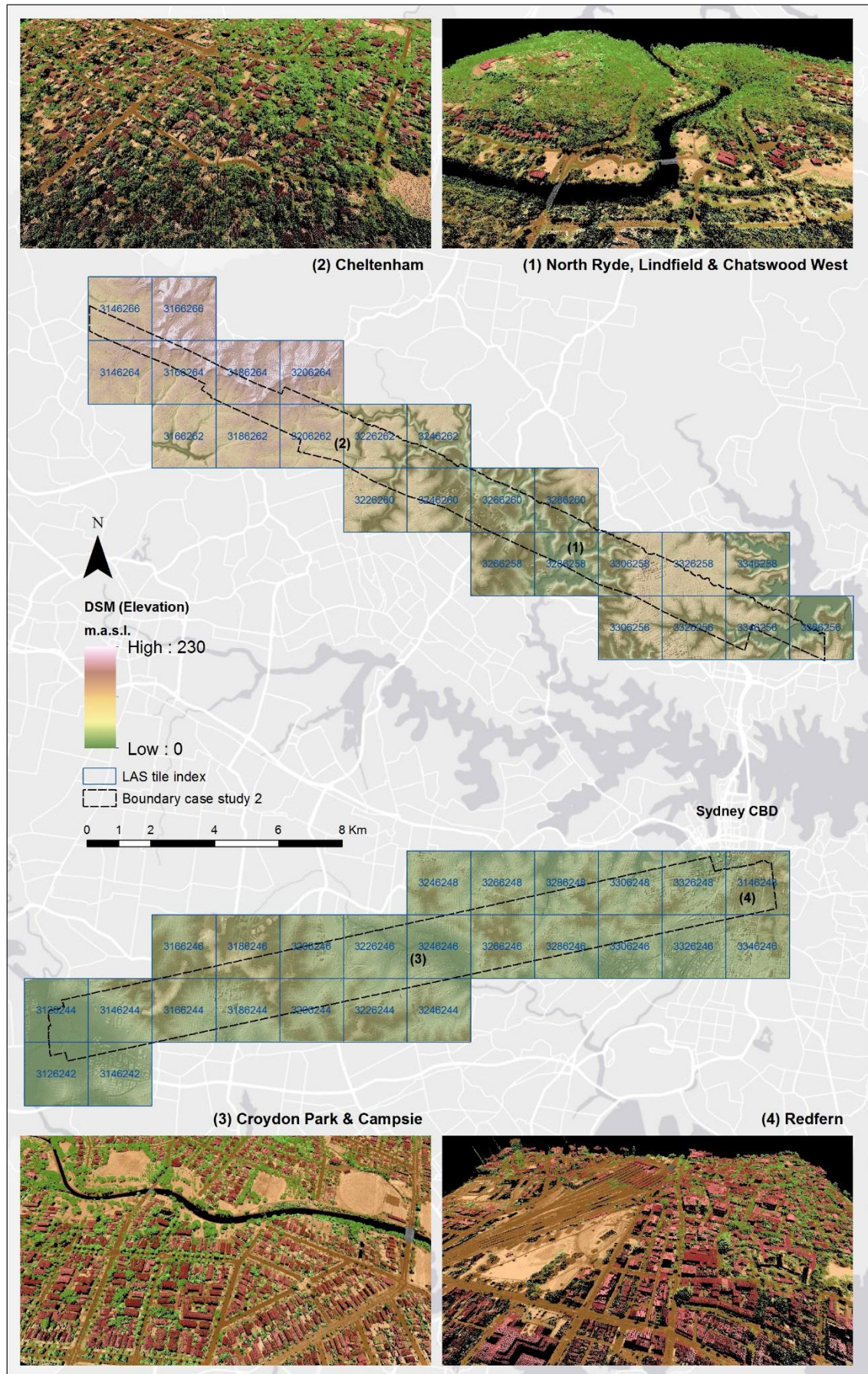


Figure 6.14 Digital surface model (DSM) depicting the spatial extent of LiDAR data acquired for the case study 2 and three-dimensional representations of LiDAR point cloud data of exemplary sites.

Two DSMs of 1m spatial resolution corresponding to the northern and southern suburbs were generated to show the spatial coverage of the LiDAR data retrieved for case study 2 [Figure 6.14]. Figure 6.14 also presents three-dimensional representations of classified point cloud data of some representative sites visualised with LP360 software (QCoherent, 2012).

Cadastral data

Cadastral data employed for case study 2 corresponds to the same data utilised in case study 1, which includes diverse types of administrative boundaries (suburbs, statistical areas, LGA, etc.), land tenures (parcels), land uses, and geographical features (greenspaces, water bodies).

6.3 Computation of variables

This section presents the workflow and procedures conducted to derive the independent and dependent variables from the airborne remote sensing data, and the computation of all variables for each spatial unit for the automated classification of GITs and subsequent statistical analysis (Chapter 7). These procedures were applied to both case studies with minor variations.

The workflow for the data processing and automated classification of GITs implemented by this research draws on a method introduced by Irger (2014) for the classification of LCZs, which was subsequently modified by Bartesaghi Koc, Osmond, Peters, and Irger (2017b) and applied by Bartesaghi Koc, Osmond, Peters et al. (2018) [Figure 6.15]. Descriptions of all critical steps and specifications of the data processing are detailed in Appendix D.

6.3.1 Surface covers

6.3.1.1 Initial identification of surface covers from NDVI

To identify different surface covers (vegetated, impervious, water), NDVI images for summer and winter case studies were calculated based on the available multi-spectral and hyper-spectral data respectively. Since the type of spectral data differ for both cases, two different methods were employed.

For case study 1 (summer), an NDVI image was generated as per Eq. 3.2 below using the *Raster calculator* tool in ArcGIS 10.3 software (ESRI, 2012):

$$(NDVI) = \frac{Float (NIR-VIS)}{Float (NIR+VIS)} \quad [\text{Eq 6.1}]$$

where *Float* indicates the pixel type, in this case a floating point; the near-infrared (NIR) band corresponds to the *Band 1* from the CIR image and the visible (VIS) band is the *Band 1 (Red band)* of the aerial imagery. The resulting raster (in *.Tiff* format) was projected to GDA 1994 MGA Zone 56 and resampled from 0.8 to 0.5m spatial resolution [Figure 6.7].

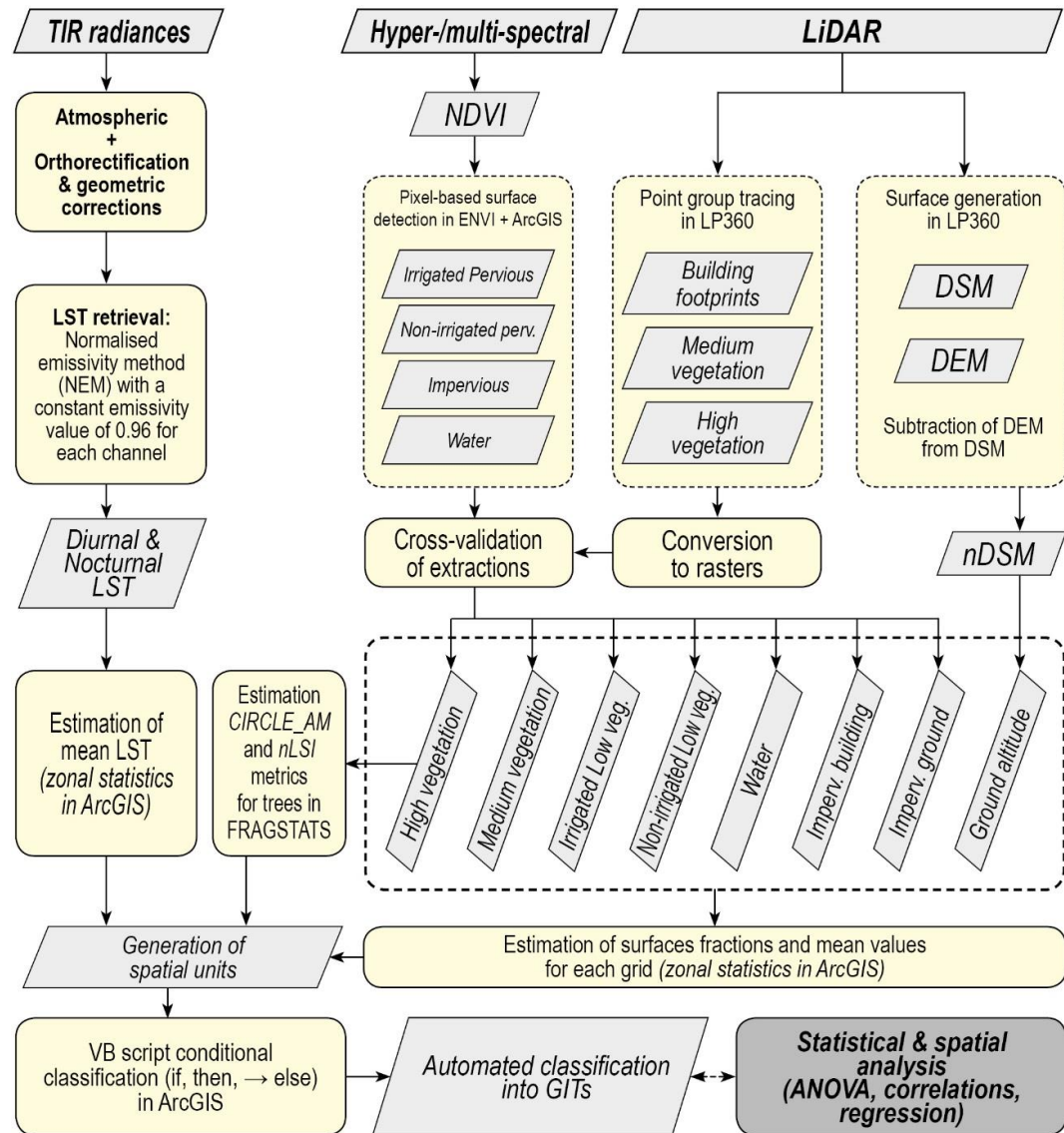


Figure 6.15 Workflow for the computation of variables, automated classification of GITs, and statistical and spatial analysis based on airborne-based data.

For case study 2 (winter), two NDVI images corresponding to the north and south swaths were derived from hyperspectral data using the *Spectral indices - NDVI* tool in ENVI 5.3.1 software (Exelis, 2015). Both rasters were mosaicked together, exported as *.Tiff* files,

projected to GDA 1994 MGA Zone 56, and resampled from 2 to 1m spatial resolution [Figure 6.13].

Calculated NDVI values range from -1 to +1, and particular thresholds can be typically used to distinguish different types of surfaces. For instance, values from 0.2 to 0.9 correspond to various vegetated surfaces, values close to zero represent impervious surfaces, rock, bare soils and sand, and very negative values indicate the presence of water (Badamasi et al., 2010; Black & Stephen, 2014; Cheng et al., 2008; Gaitani et al., 2016; Gandhi et al., 2015; Irger, 2014; Weier & Herring, 2000). However, these thresholds are sensitive to factors such as season, vegetation phenology, irrigation levels, and the climatic conditions prior and during the data collection (Cheng et al., 2008); thus, in this research classification thresholds differ between case studies.

Accordingly, a simple threshold NDVI classification analysis was applied individually for each case study to identify total impervious (ground and buildings), non-irrigated and irrigated pervious, and water surfaces. Thresholds were defined using the Jenks optimization method (Jenks, 1967) and readjusted by human operator according to ranges found in the literature (Badamasi et al., 2010; Black & Stephen, 2014; Cheng et al., 2008; Gaitani et al., 2016; Gandhi et al., 2015; Irger, 2014). Even though this approach is highly replicable, the threshold values summarised in Table 6.2 may differ for other locations and seasons.

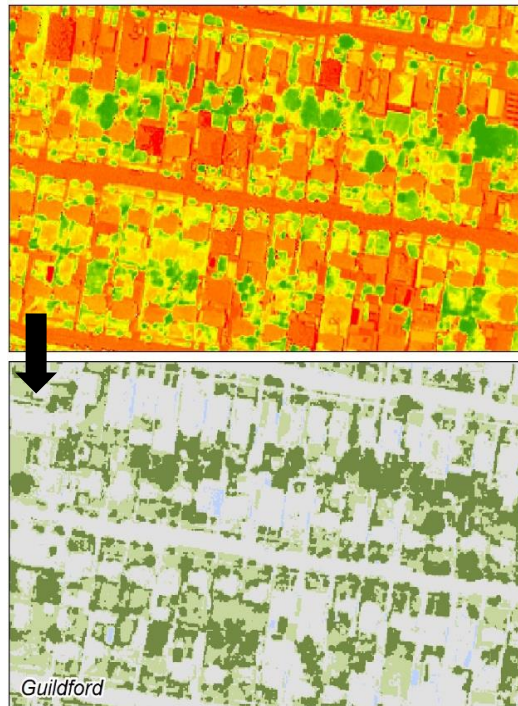
Table 6.2 NDVI thresholds defined for the identification of surface covers in summer and winter.

Surface cover	NDVI threshold values	
	Summer	Winter
Water	≤ -0.50	≤ -0.20
Total impervious (including barren land, rock, sand, ground and buildings)	-0.50 to -0.15	-0.20 to 0.25
Non-irrigated pervious (including bare soil and dry low plants)	-0.15 to 0.08	0.25 to 0.60
Irrigated pervious (including low plants, shrubs, sparse and dense trees)	≥ 0.08	≥ 0.60

NDVI images were reclassified, using the *Reclassify* tool in ArcGIS, to create separate rasters for each surface cover with a spatial resolution of 0.5m. Figure 6.16 shows some examples of surface covers identified from the NDVI for summer and winter. This initial identification of surfaces is refined in subsequent steps to discriminate between impervious ground and impervious building, and between low (grasses), medium (shrubs), and high (trees) vegetation layers. Since seasonal variation is expected due to the presence of

deciduous trees, additional corrections were applied for the estimation of true tree coverage in winter.

Case study 1 - Summer



Case study 2 - Winter

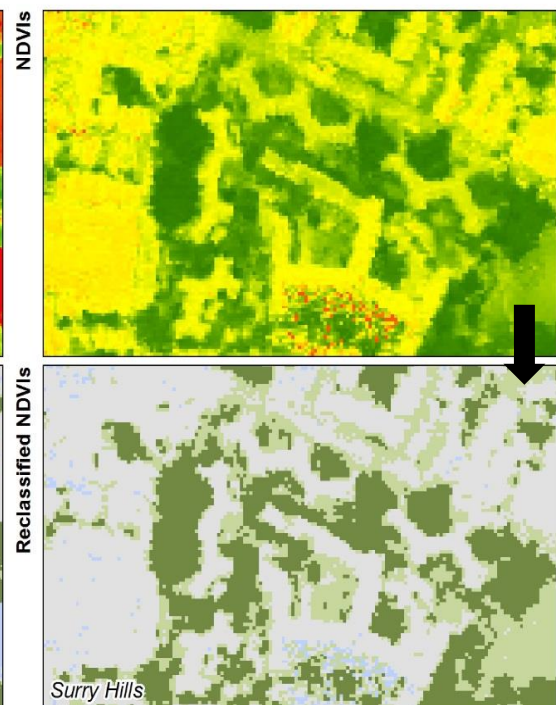
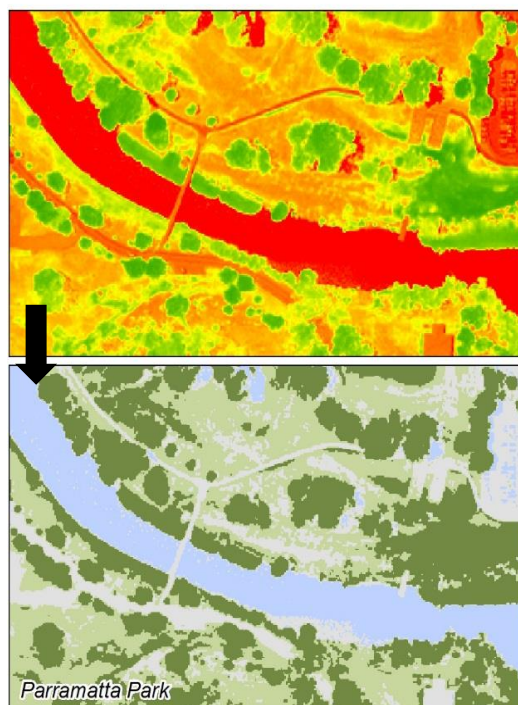
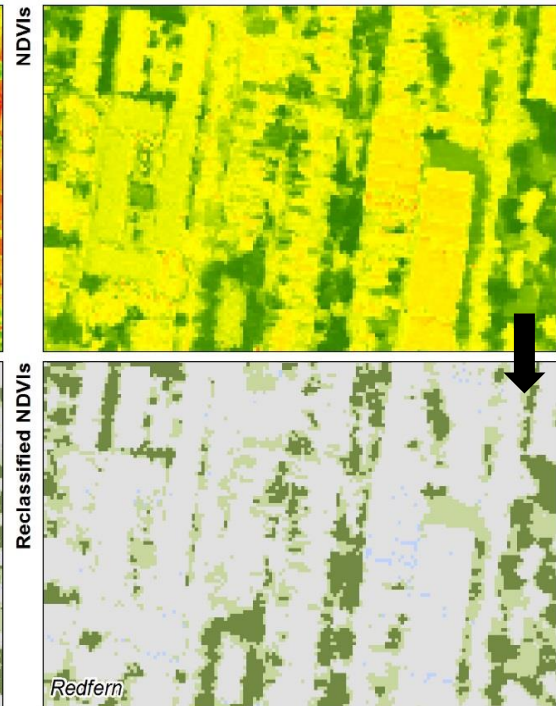


Figure 6.16 Identification of surface covers from reclassified NDVI images.

6.3.1.2 Estimation of building footprints and impervious ground surfaces

Building footprints were extracted from LiDAR data in LP360 software (QCoherent, 2012) using a *Point group tracing* operation (object-based approach) applied to only points pre-classified as buildings.

This algorithm consists of creating vector polygons from similar points that are clustered based on user-specified proximity parameters (Graham, 2013; Irger, 2014). The *Grow window* parameter controls the point clustering by defining which points of the same class will be grouped within a specified distance, so larger values generate coarser clusters. On the other hand, the *Trace Window* parameter determines the minimum distance between vertices of the polygon created around the clusters; in other words, it controls the smoothness of the traced outlines of the polygon so smaller values create more detailed edges (Graham, 2013).

Different settings were tested, and optimum results were achieved when the group tracing occurred within a distance of 2m (grow window) and a trace window of 3m. Buildings smaller than 10m² were filtered out from the extracted output. These parameters returned extremely irregular polygons with innumerable line segments and relatively good amount of detail along outlines. Additionally, adjacent buildings with narrow distances between them were combined into a single polygon, while some buildings and smaller gardens or courtyards were not identified [Figure 6.17].

Since the complexity and number of vector polygons are inadequate and impractical for further analysis, additional corrections were performed to improve the accuracy and simplify the geometry of extracted building footprints. Firstly, extracted features were converted from polygons ZM to normal polygons by disabling the M and Z values in ArcGIS¹⁵. Secondly, geometries were repaired, duplicates deleted, multipart polygons were separated and resulting polygons split along parcel (property) lines obtained from cadastral data. Thirdly, polygons smaller than 15m² were deleted and remaining features squared using the *Square-Up algorithm* available in Feature-Analyst software (Overwatch, 2015). In this process, a smoothing tolerance of one metre and squaring tolerance of 5.5-6m (depending on the area) were utilised. Furthermore, adjoining features were considered when computing all likely feature orientations.

The squaring process significantly improved the geometry and quality of extractions [Figure 6.17]. However, the process returned round shapes as hexagonal polygons, so these

¹⁵ A Polygon ZM typically results from LiDAR extractions. This represents a 3D polygon feature class with z- and m- values that have to be disabled in order to perform certain operations.

were manually redrawn in all datasets. Missing or wrongly extracted features due to low point cloud density in some areas were also added manually. Squared polygons less than 12m² were discarded to remove small fragments from the process.

After generating building footprints, height information was calculated from a nDSM which contains the absolute height for each polygon. LiDAR data were processed in LP360 software to generate a DEM representing the elevation of bare earth (employing only points reclassified as *ground*) and a DSM combining *ground* and *building* points. A nDSM with a spatial resolution of 0.5m was produced in ArcGIS by subtracting the DEM from the DSM.

The average height of each building footprint was computed with the *Zonal statistics* tool in ArcGIS using the nDSM as input value raster and the vector building footprints as feature zone data. Figure 6.18 shows the building footprints extracted from LiDAR represented according to the average building height.

To obtain the *impervious building surfaces*, vector footprints were converted into a raster image with a spatial resolution of 0.5m using the *Polygon to raster* tool in ArcGIS and the average building height as value field. The *impervious surfaces* derived from the NDVI image presented some errors; for instance, some buildings were misclassified as pervious surfaces and water surfaces as impervious ground cover. To solve this issue, the *impervious building surface image* generated from LiDAR was added to and the *water surface image* subtracted from the *impervious surfaces* derived from NDVI to obtain the true *total impervious surface cover*. After that, *building surfaces* were subtracted from the *total impervious surfaces* to distinguish between *impervious ground* and *impervious building surfaces* [Figure 6.18].

Appendix D provides a detailed summary of procedures, tools and values implemented for the estimation of impervious ground and impervious building surfaces from LiDAR and spectral data.

6.3.1.3 Estimation of vegetation layers and water surfaces

LiDAR data was processed in LP360 software (QCoherent, 2012) to extract medium (0.3–2m) and high (>2m) vegetation features using a *Point group tracing* operation. Different settings were tested, and optimum results were achieved when the point tracing (known as *grow window*) occurred within a distance of 2m in areas with medium and small green patches and 1.75m in areas with large patches. The limit for aggregating point groups to patches (known as *trace window*) was limited to a maximum of 3m for medium and small

patches and 2.75m for large patch sizes. Features smaller than 5m² were excluded while overlapping polygons larger than 850m² were disaggregated into smaller shapes.

Case study 1 - Summer



Extracted footprints



After splitting and squaring

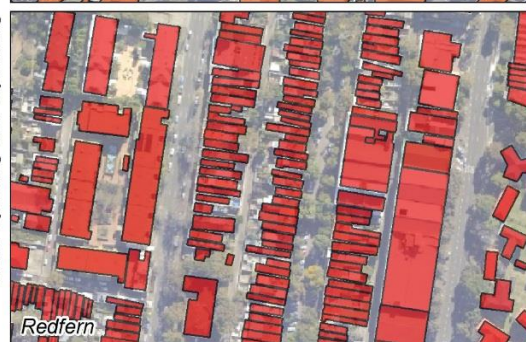
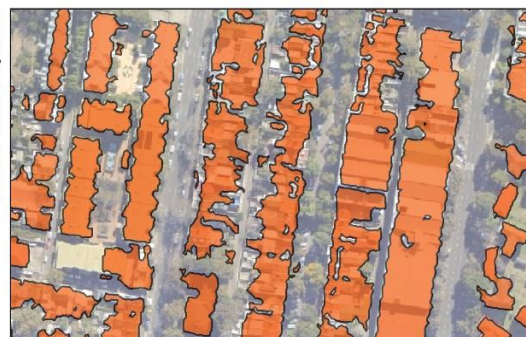


Extracted footprints



After splitting and squaring

Case study 2 - Winter



0 25 50 100 150 m

Figure 6.17 Comparison of building footprints extracted from LiDAR data using LP360 software and the results after the splitting and squaring process.

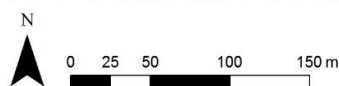
Case study 1 - Summer**Case study 2 - Winter**

Figure 6.18 Differentiation between impervious ground and impervious building coloured according to the average building height.

In areas with extensive and dense tree canopies, extractions showed several errors including vegetated areas considered as empty spaces and buildings, man-made structures, and treeless spaces extracted as vegetation. These errors may be attributed to wrong pre-classification of point clouds by the data provider due to similar waveform of LiDAR laser

returns reflected by leaves, branches and building edges (see Section 6.2.1). To correct these issues, erroneous features were deleted and replaced with vector polygons reextracted from a smaller spatial extent. Overlapping polygons were then combined using the *Merge* tool from the editor mode in ArcGIS. Multipart polygons were disaggregated, duplicated polygons deleted, and geometries repaired for all features. Vector files containing medium and high vegetation footprints were converted to raster images with a spatial resolution of 0.5m using the *Polygon to raster* tool in ArcGIS.

To improve the spatial accuracy of all LiDAR-derived extractions and discard areas without real vegetation content, high and medium vegetation raster images were overlaid on NDVI-derived total pervious surfaces, so nonintersecting pixels were eliminated.

Discrepancies between LiDAR and spectral extractions occurred in the case study 2 (winter) because datasets were collected in different periods (early autumn and late winter respectively). Hence, a complete tree canopy (evergreen and deciduous) was only retrieved by LiDAR data, since winter's NDVI values for leafless deciduous trees corresponded to ground surfaces (identified as non-irrigated pervious or impervious ground) underneath the canopy. To solve these discrepancies and discard deciduous trees in winter, LiDAR-derived high vegetation surfaces were assessed against *irrigated* pervious surfaces derived from the NDVI, so non-intersecting pixels were filtered out.

Since total irrigated pervious surfaces included low plants, shrubs, and trees; corrected high and medium vegetation were subtracted to obtain true irrigated low plants. The same process was repeated to obtain non-irrigated low vegetation cover. Medium vegetation as well as irrigated and non-irrigated low vegetation pixels overlapping buildings and water surfaces were discarded.

Water surface extracted from NDVI images also presented errors as some pixels were misclassified as impervious or pervious surfaces. To solve this problem, water features (in vector format) from cadastral data were converted to raster with a pixel size of 0.5m and added to the NDVI-derived image. The resulting image was then refined by removing pixels that intersect with high vegetation and building footprints.

When visually assessing the resulting rasters against aerial images, a small number of errors were identified. These include impervious surfaces misclassified as bare soils or non-irrigated grasses, missing tree canopy, non-irrigated grasses wrongly classified as irrigated plants, some elongated buildings (*i.e.* chimneys) misidentified as high vegetation, and industrial machinery, trucks, cars and containers erroneously classified as shrubs or trees.

These inherent errors can be mostly attributed to the cut-off values used in the classification of NDVI images and problems in the LiDAR datasets.

Figure 6.19 presents the results of the estimation of different vegetation layers and water surfaces for both case studies. Appendix D provides a detailed summary of steps, tools and specific values for the estimation of vegetation layers and water bodies from LiDAR and spectral data.

6.3.2 Landscape metrics

The high vegetation raster (with 0.5m spatial resolution) was used in FRAGSTATS 4.3 software (McGarigal et al., 2002) to quantify the spatial configuration of trees by computing the CIRCLE_AM (shape metric) and nLSI (aggregation metric) indices at a *class level*. Uniform tiles (also referred as grids or spatial units) of 50 x 50m of side length and an *8 cell neighbourhood rule* were applied over the entire extent of both case studies.

Since FRAGSTATS was unable to process large rasters due to lack of virtual memory, tiles were grouped in sections that were merged into single polygons used to clip the raster images in smaller sections. For each section, calculations returned a GeoTIFF image (.tif) with tiles' IDs, and a table with FRAGSTATS indices associated to each ID. GeoTIFFs were converted into vector polygons and values from tables assigned to each tile using IDs as universal identifiers. These spatial units correspond to GITs that will be used for statistical analyses.

In some cases, nLSI values were reported as *N/A* in the output files whenever the maximum class edge equalled the minimum class edge. This occurred when trees (the focal class) covered the totality of the grid. To correct this issue, *N/A* values were replaced with 0 as these tiles contain a single or maximally compacted patch. Examples of landscape metrics computed for grid cells are shown in Figure 6.20.

6.3.3 Altitude

In a similar research, Irger (2014) found that the average altitude of a given location has a warming effect on mean LSTs, especially at night-time; thus, it was decided to include this variable in the present thesis. The average ground surface height (or altitude above sea level) was estimated from the DEM generated in LP360 from LiDAR data by computing the *mean* of all pixel values within each grid with the *Zonal statistics* tool in ArcGIS.

Case study 1 - Summer



Case study 2 - Winter

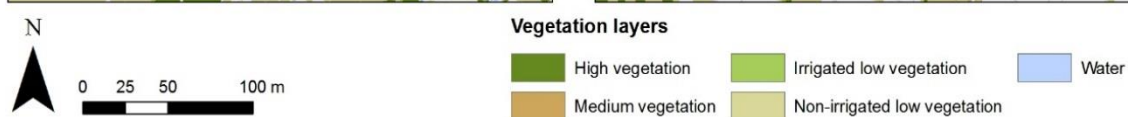
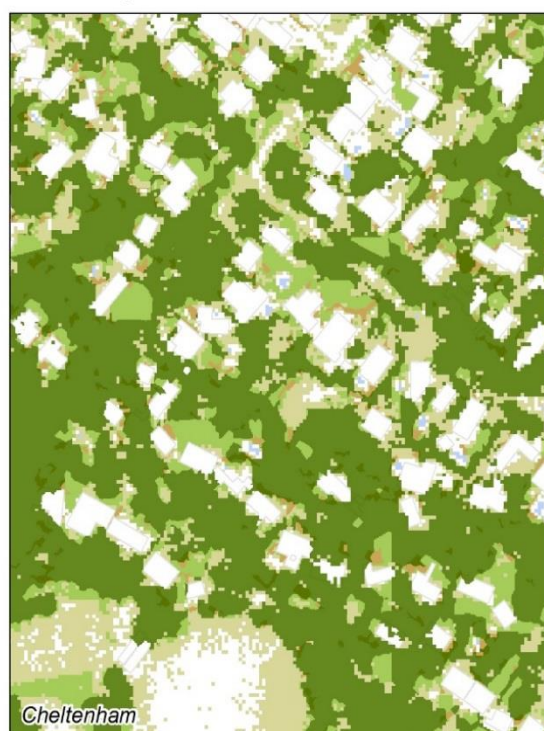
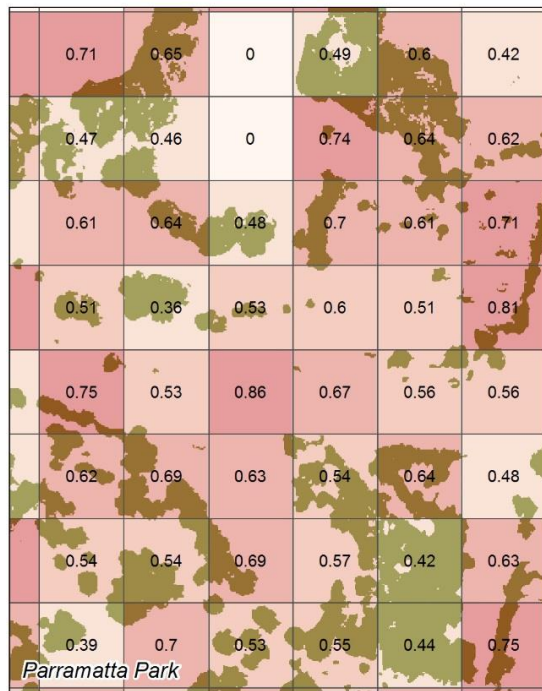


Figure 6.19 Identification of vegetation layers (based on height and irrigation regimes) and water surfaces using a refinement method combining spectral-derived imagery and LiDAR data.

Case study 1 - Summer



Case study 2 - Winter

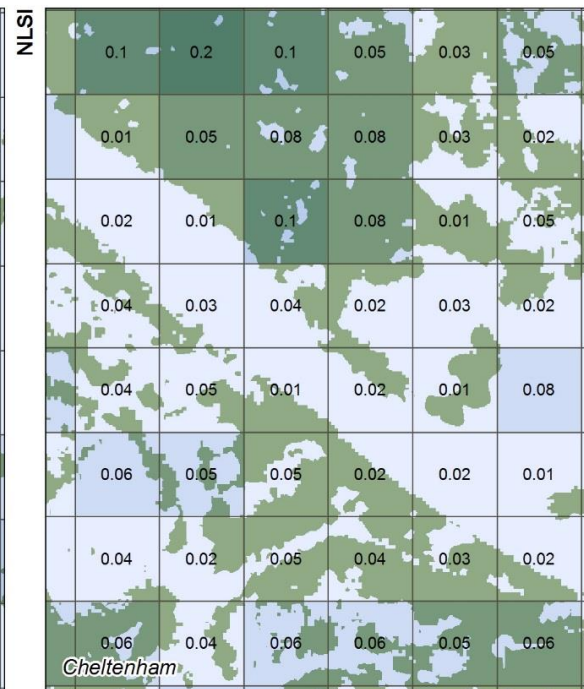
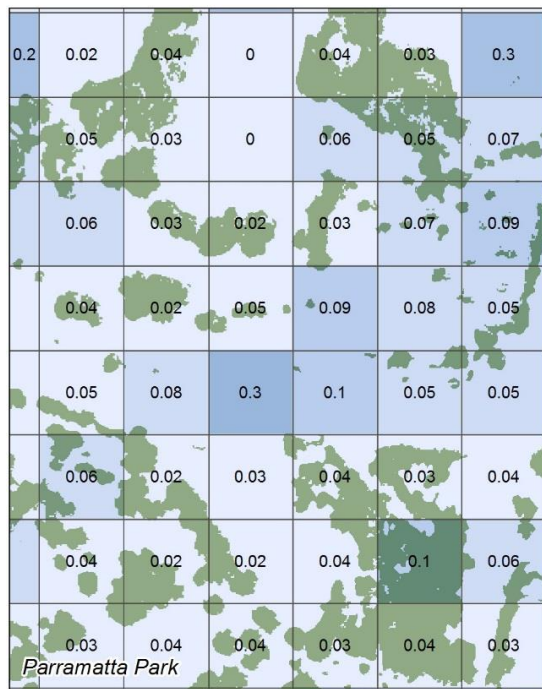
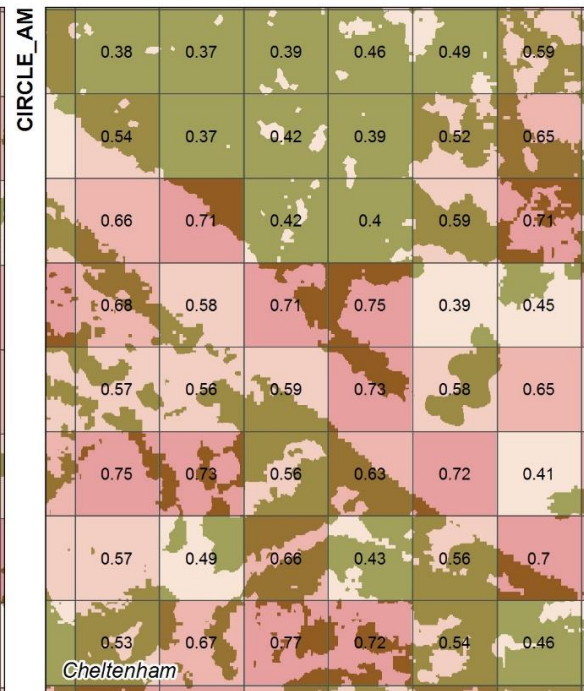


Figure 6.20 Examples of landscape metrics (CIRCLE_AM and NLSI) calculated for each grid cell to determine the compactness and linearity of tree arrangements.

6.3.4 Computation of variables per each spatial unit

6.3.4.1 Generation of spatial units

Regular spatial units of 25 x 25m, 50 x 50m and 100 x 100m were chosen to conduct statistical and comparative analyses at the local scale instead of using conventional *precinct* or *neighbourhood* delineations as the latter respond to non-standardised –and somehow subjective or ambiguous– administrative or jurisdictional boundaries that largely vary among cities and contexts. Furthermore, the above grid sizes are those suggested for the study of climatic phenomena at the local scale (Bechtel et al., 2015; Erell et al., 2011; Oke et al., 1989; Oke, 2006; Stewart & Oke, 2012) (see Section 2.4.1)

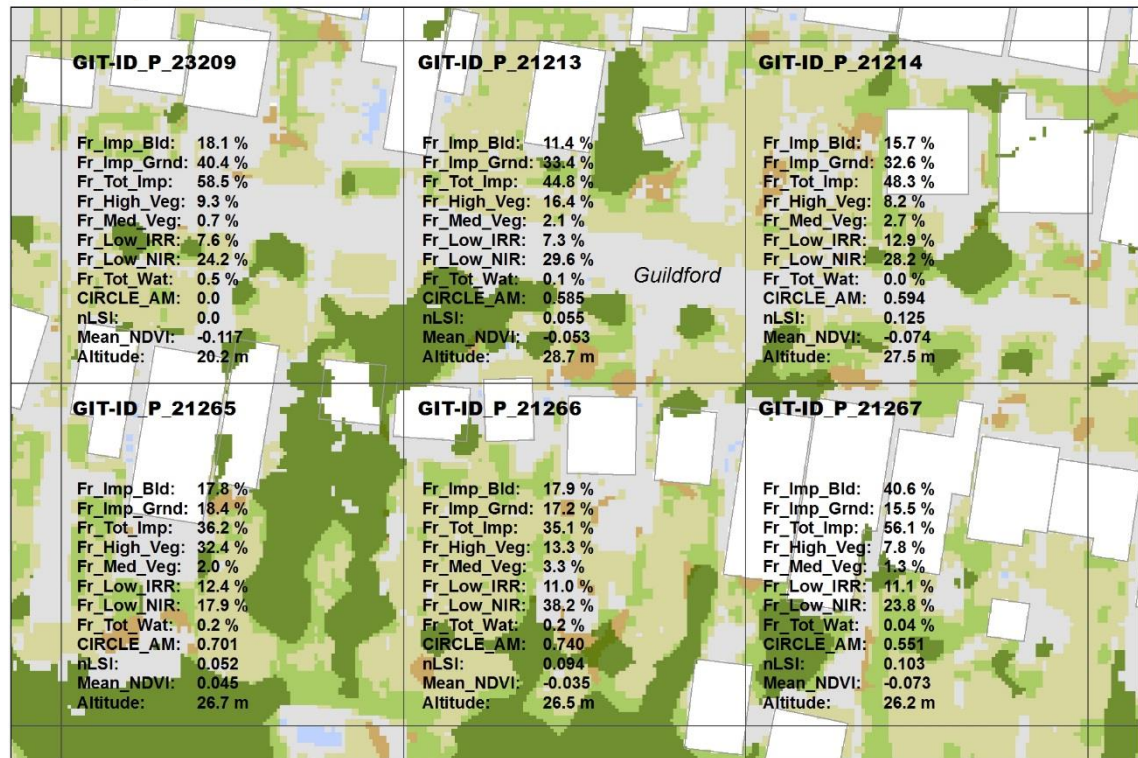
Among the three sizes, a 50 x 50m was selected as an adequate spatial unit for this research as finer grids were too small to identify different spatial arrangements of trees, so large greenspaces and buildings are extremely fragmented, and cells tend to be occupied by a single surface cover. Conversely, coarser grids were more heterogeneous as features are highly disaggregated (except for very large and homogenous areas). Results and justifications for this selection are presented in Chapters 7 and 8 respectively.

Accordingly, grids of 50 x 50m were created with the *Grid index feature* available in ArcGIS to identically duplicate (same extent and location) those tiles generated as a sub-product of FRAGSTATS calculations (see Section 6.3.2). Grids that were not completely within the study area were discarded. Unique IDs were created to differentiate grids from both cases studies. A total number of 23774 grids were generated for case study 1 (summer) and 29009 grids for case study 2 (winter) of 2500m² each.

6.3.4.2 Computation of surface fractions and other variables

Surface fractions per grid were estimated using *Zonal statistics* and *Field calculator* tools in ArcGIS by dividing the total number of pixels (*SUM*) of each surface cover by the total number of pixels (*COUNT*) per grid (10000 pixels of 0.5 x 0.5m each). Results were multiplied by 100 to be expressed in percentage and tables were joined to the attribute tables of the vector grids generated in Section 6.3.4.1. Landscape metrics and altitude values previously estimated in Sections 6.3.2 and 6.3.2 were directly assigned to each vector grid. [Figure 6.21](#) presents examples of calculated surface fractions and other independent variables for each spatial unit.

Case study 1 - Summer



Case study 2 - Winter

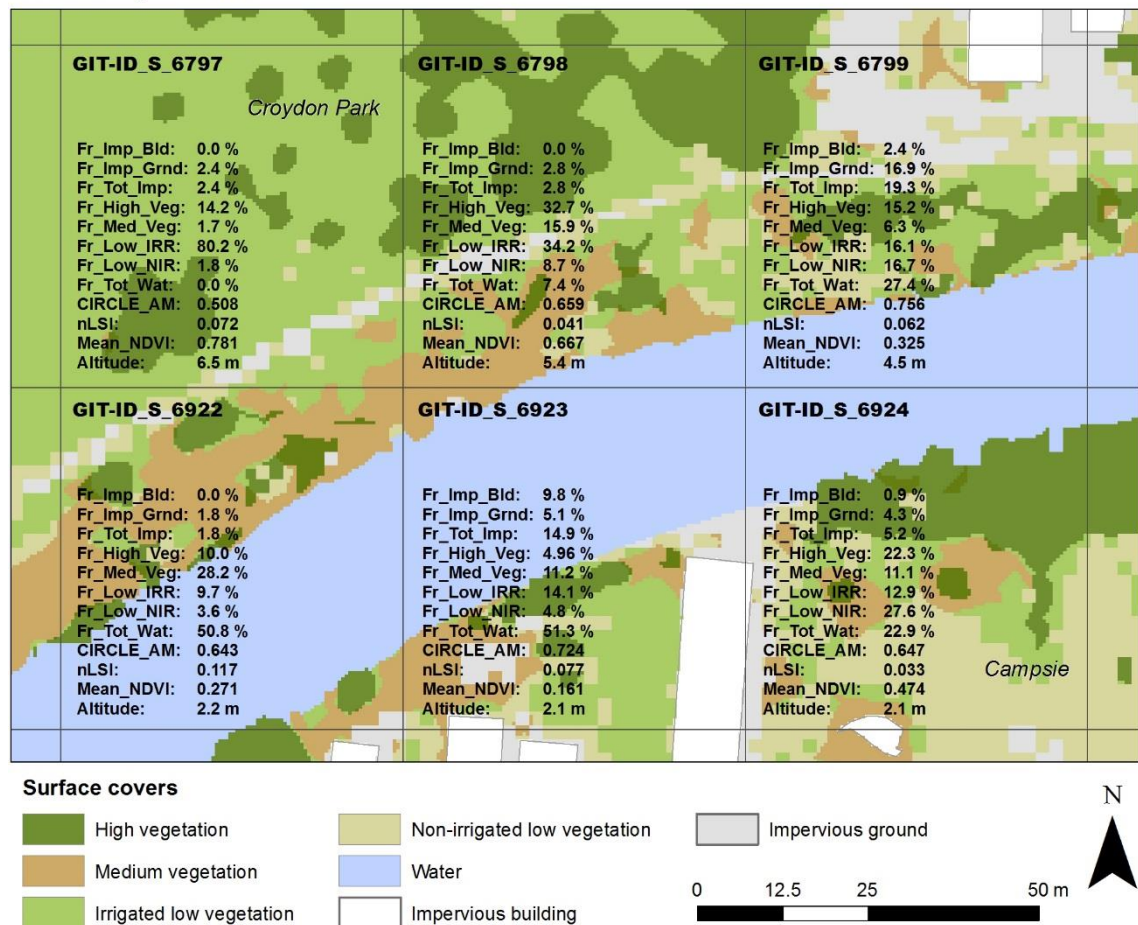
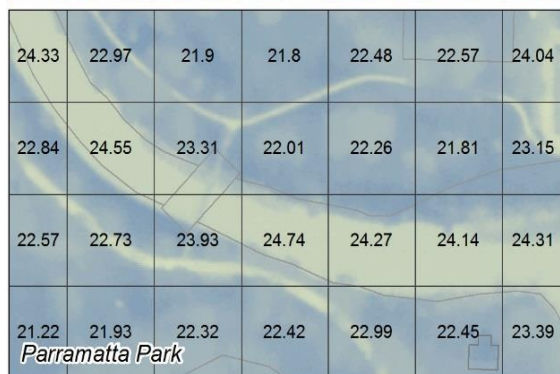
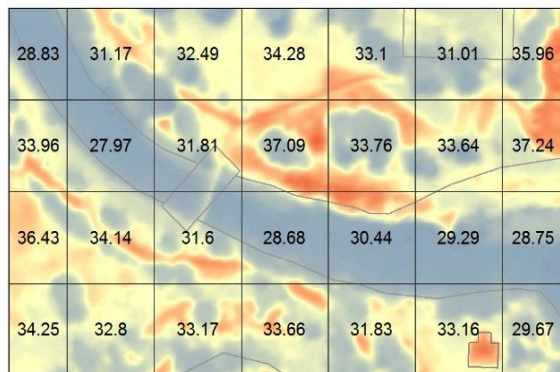
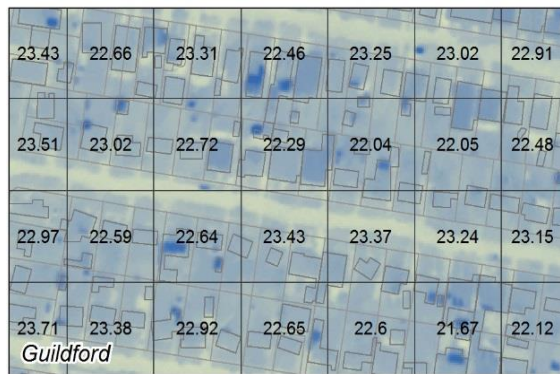
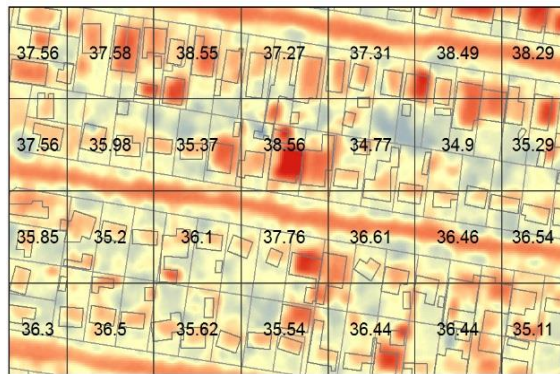


Figure 6.21 Examples of computed surface fractions and other independent variables per spatial unit using *Zonal statistics* in ArcMap.

Case study 1 - Summer



Case study 2 - Winter

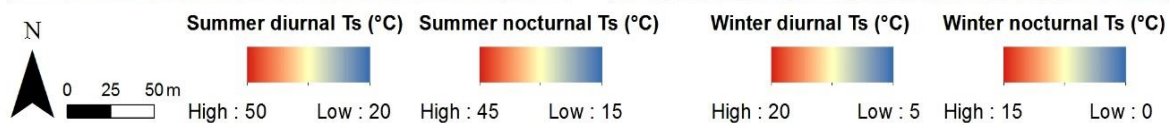
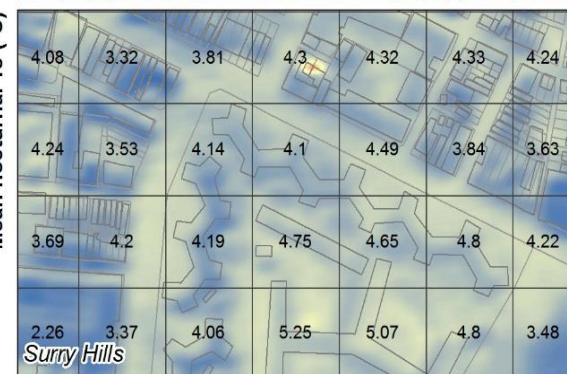
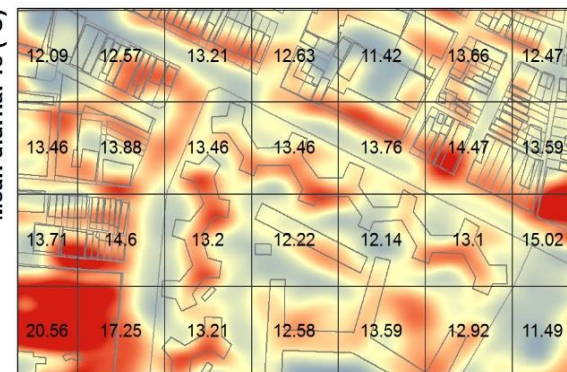
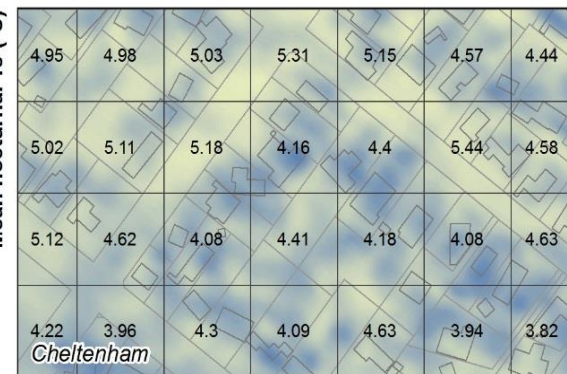
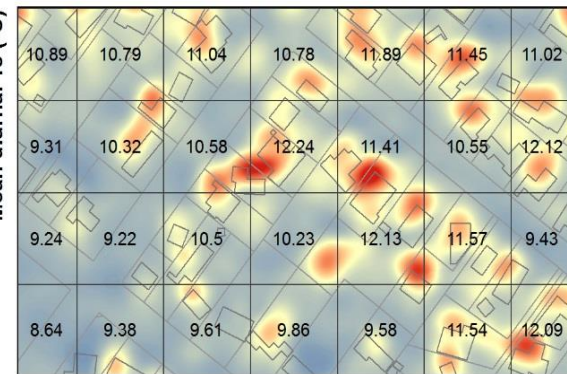


Figure 6.22 Examples of mean diurnal and nocturnal temperature calculated per spatial unit using *Zonal statistics* in ArcMap.

6.3.4.3 Estimation of mean NDVI and mean surface temperatures

Average NDVI, diurnal and nocturnal surface temperatures per grid were calculated with *Zonal statistics* tool in ArcGIS by computing the mean of all pixels (*MEAN*) within each spatial unit using the NDVI and TIR images as input value rasters and the vector grids as feature zone data.

As described in Section 6.2.2 the diurnal and nocturnal thermal images collected for the case study 2 (winter) are dissimilar and covered a smaller spatial extent than the hyperspectral and LiDAR data. Consequently, in winter, temperature data were only retrieved for 25238 grids at daytime, and for 23752 grids at night-time. Figure 6.22 shows some examples of mean diurnal and nocturnal temperature calculated per each spatial unit.

6.4 Classification of green infrastructure typologies (GITs)

As previously outlined in Chapters 4 and 5, a main component of this research is the mapping and classification of green infrastructure typologies (GITs) using an automated GIS-based workflow for an accurate and precise thermal analysis of green infrastructure at the local scale.

To achieve this, a new classification scheme for green infrastructure was developed (described in Chapter 4 – Part II) to categorise each spatial unit (or grid) into a GIT class according to the surface descriptors and configurational parameters computed in previous sections. This classification was conducted by using the quantitative descriptors defined for all the 34 green infrastructure typologies (GITs) [see Table 4.14] as threshold (or cut-off) values in a conditional algorithm implemented in ArcGIS ®.

The classification process required writing *VB scripts (if-then-logic)* for each GIT using the *Field calculator* available in the attribute table of grid features. Accordingly, a specific GIT code was automatically assigned to each grid after running the generic statement on the next page.

This algorithm classifies grids in a hierarchical way as it tests if conditions based on defining parameters are met for a specific GIT. The complete statement of the algorithm in *VB script* format is presented in Appendix D. Table 6.3 summarises the number of *classifiable* and *non-classifiable* (unknown) grids identified for each case study. A complete analysis of results is presented in Chapter 7.


```

IF  "Fraction of total impervious [Fr_Tot_Imp] <a1 and >a2 AND
    "Fraction of non-irrigated low vegetation [Fr_Low_NIR] <b1 and
>b2 AND
    "Fraction of irrigated low vegetation" [Fr_Low_IRR] <h1 and
>h2 AND
    "Fraction of medium vegetation" [Fr_Med_Veg] <i1 and >i2 AND
    "Fraction of high vegetation" [Fr_High_Veg] <w1 and >w2 AND
    "Fraction of total water" [Fr_Tot_Wat] <x1 and >x2 AND
    "Related circumscribing circle" [CIRCLE_AM] <y1 and >y2 AND
    "Normalised landscape shape index" [nLSI] <z1 and >z2 AND
THEN  "Green infrastructure typology" [GIT_type] = "N1"

ELSEIF  "Fraction of total impervious [Fr_Tot_Imp] <a1 and >a2 AND
    "Fraction of non-irrigated low vegetation [Fr_Low_NIR] <b1 and
>b2 AND
    "Fraction of irrigated low vegetation" [Fr_Low_IRR] <h1 and
>h2 AND
    "Fraction of medium vegetation" [Fr_Med_Veg] <i1 and >i2 AND
    "Fraction of high vegetation" [Fr_High_Veg] <w1 and >w2 AND
    "Fraction of total water" [Fr_Tot_Wat] <x1 and >x2 AND
    "Related circumscribing circle" [CIRCLE_AM] <y1 and >y2 AND
    "Normalised landscape shape index" [nLSI] <z1 and >z2 AND
THEN  "Green infrastructure typology" [GIT_] = "Nn"

ELSE    [GIT_type] = "Unknown"

END IF

```

Table 6.3 Distribution of ‘classifiable’ and ‘unknown’ number of grids per case study.

Case study	# Classifiable grids (%)	# Non-classifiable grids (%)	Totals
1. Summer	23460 (98.68)	314 (1.32)	23774
2. Winter	28830 (99.38)	179 (0.62)	29009
Totals	52290 (99.07)	493 (0.93)	52783

Figures 6.23 and 6.24 present datasheets containing the grid ID, independent variables, classification parameters, and mean diurnal/nocturnal surface temperature calculated for selected GITs. A complete summary of datasheets for all GITs is provided in Appendix E.

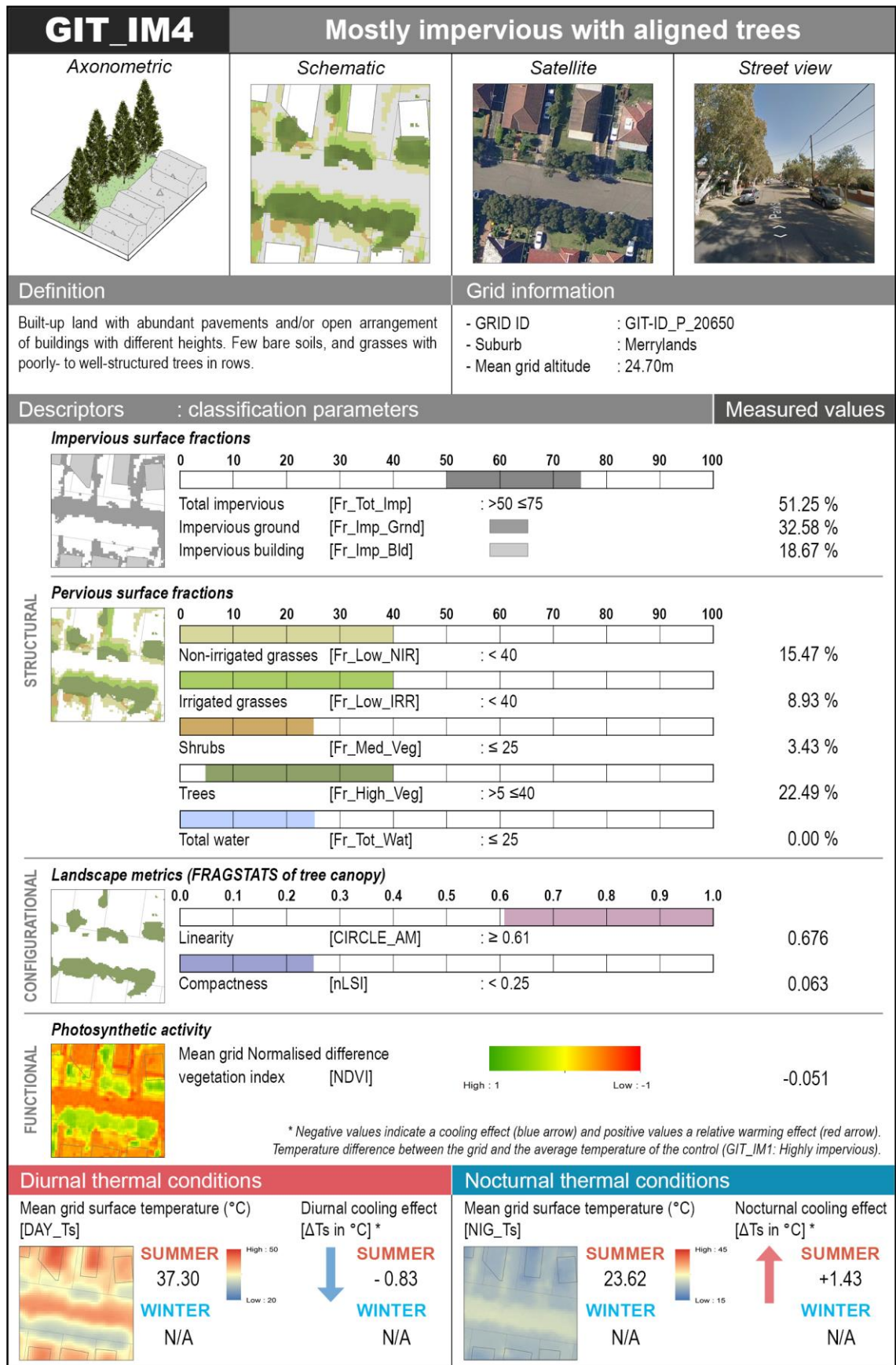


Figure 6.23 Datasheet containing all variables and classification parameters calculated in summer for the green infrastructure typology IM4: Mostly impervious with aligned trees.

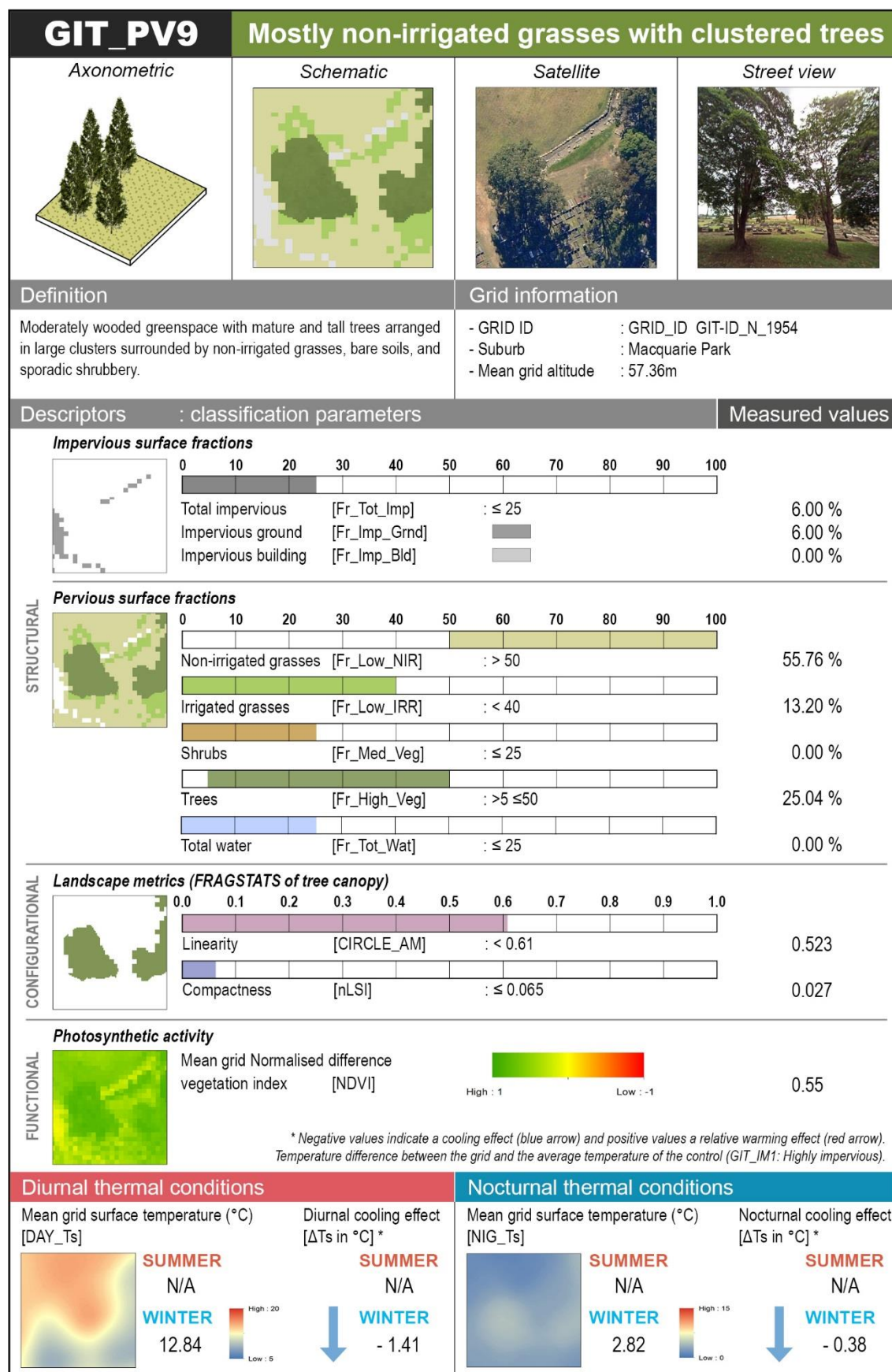


Figure 6.24 Datasheet containing all variables and classification parameters calculated in winter for the green infrastructure typology PV9: Mostly non-irrigated grasses with clustered trees.

6.5 Summary

This chapter presents the location, extent, and morphological characteristics of two related case studies of the Sydney metropolitan area. It also describes the extent, protocols, equipment and procedures employed for the collection of airborne-based data that was conducted in two different seasons: summer and winter. Furthermore, this chapter presents the GIS-based pre- and post-processing workflow, methods and tools applied for the computation of variables required for the automated classification of GITs that will be used for subsequent statistical analyses.

This chapter demonstrates the capacity and quality of airborne remote sensing for acquiring high-resolution information of the built environment in a time-efficient way through the combination of multiple remote sensing products. It also demonstrates the applicability and effectivity of the classification scheme developed in Chapter 4 and the methodological approach presented in Chapter 5 for an accurate and precise mapping and classification of green infrastructure for climate-related studies.

The following chapter describes the results and assesses the quality of the above classifications. It also presents several statistical and spatial analyses conducted for a better understanding of the spatio-temporal variability of thermal conditions of different types of green infrastructure. This includes the formulation of a statistical model based on the variables computed for all GITs for the prediction of LSTs in summer and winter.

Data analysis and results¹⁶

7.1 Introduction

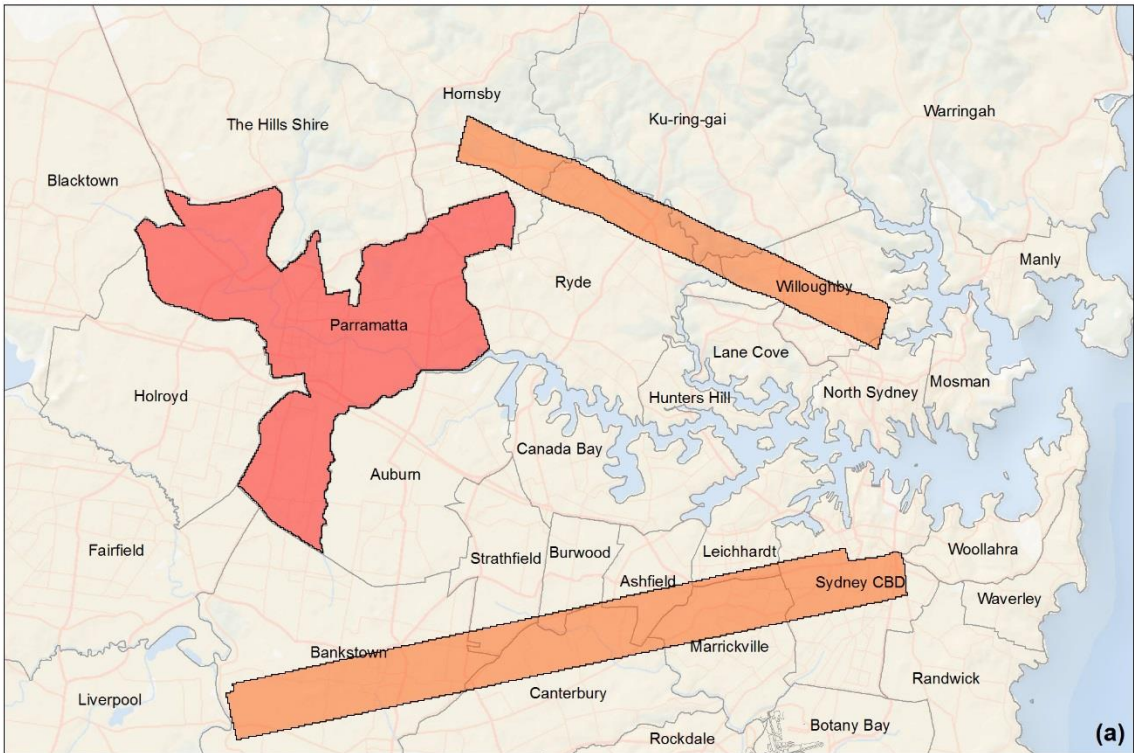
As described in the previous chapter, two related case studies of the Sydney metropolitan area –corresponding to summer and winter seasons– were selected according to the available data. Airborne-based data were processed for both case studies to assess the cooling effects of green infrastructure across different urban morphologies, seasons and times of the day. Accordingly, the key aim of this chapter is to present and analyse the processed data and results from both case studies to address the research questions and objectives outlined in Chapter 1.

This Chapter is organised as follows: Section 7.2 presents and evaluates the results of the automated classification of GITs introduced in Chapter 4; this section addresses objective 2 of this thesis. Section 7.3 validates the research framework presented in Chapter 5 by analysing the spatio-temporal variability of LSTs and the cooling capacity of identified GITs; this section addresses objectives 1 and 2 of this research. Finally, Section 7.4 presents the results of several statistical models for an accurate and precise prediction of LSTs of GITs at the local scale. This section also includes the estimation of regression coefficients and the analysis of the contributions of each variable to the modification of diurnal and nocturnal temperatures in both seasons, which are necessary to develop the cooling scenarios and heat mitigation strategies discussed in Chapter 8; this last section addresses objectives 3 and 4 of this dissertation.

The extent of the data analysis and results differs between case studies and times of the day as it is governed by the spatial coverage of the remotely-sensed spectral, TIR and LiDAR data. The area of the spatial units corresponding to the ‘Case study 1: Summer’ (same for *diurnal* and *nocturnal* data analyses) totals 59.44km² [Figure 7.1a-b]. In the ‘Case study 2: Winter’, the area of the spatial units considered for the *diurnal* data analysis totals 63.10km² [Figure 7.1a]; while the area of the spatial units considered for the *nocturnal* data analysis totals 59.38km² [Figure 7.1b].

¹⁶ A portion of Chapter 7 has been submitted for publication: Bartesaghi Koc, C., Osmond, P., Peters, A. (2019), Mapping and classifying green infrastructure typologies for climate-related studies based on remote sensing data. *Urban Forestry and Urban Greening*.

Extent of the 'diurnal' data analysis



Extent of the 'nocturnal' data analysis

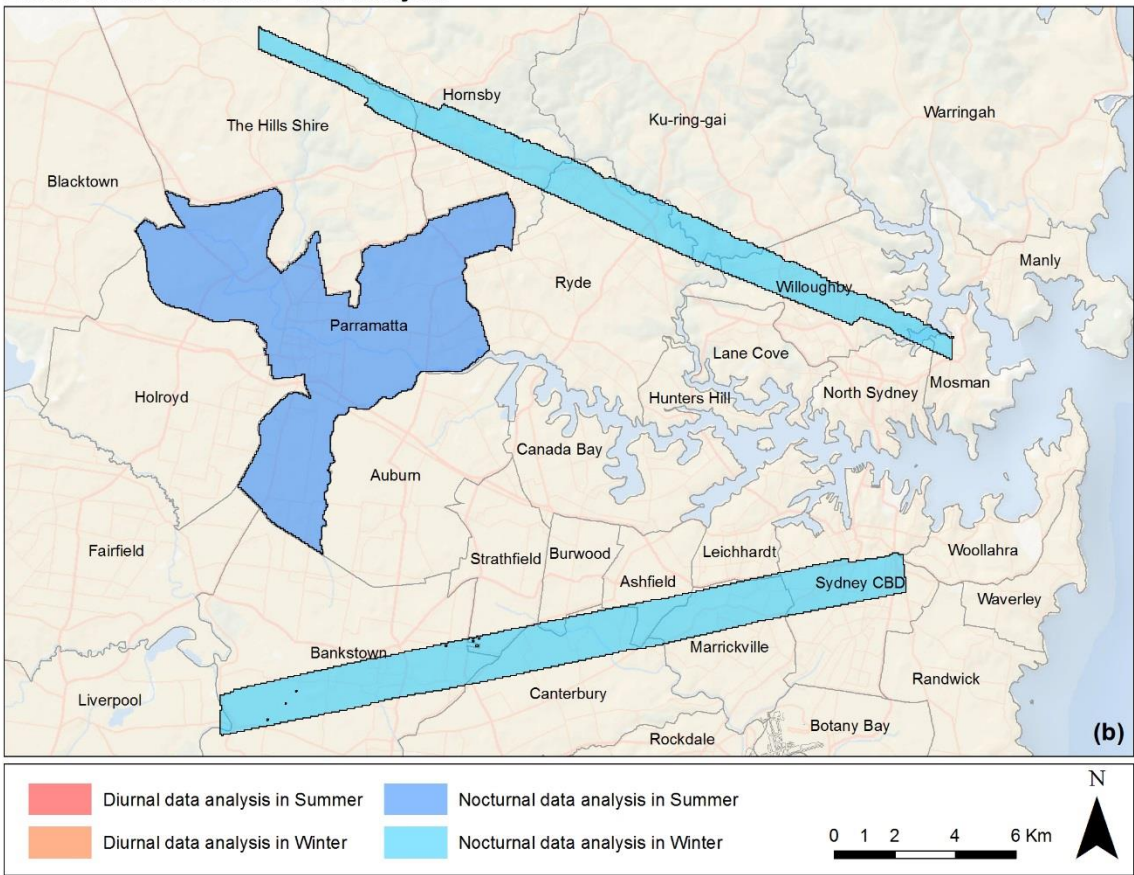


Figure 7.1 Extent of the (a) diurnal and (b) nocturnal data analyses conducted for the summer and winter case studies.

7.2 Green infrastructure typologies classifications

7.2.1 Classification results at different spatial scales

The classification framework for green infrastructure proposed in Chapter 4 – Part II and described in detail in Section 4.11 was successfully applied to both case studies. The classifications were automatically performed using a conditional algorithm implemented in ArcMap® (see Section 6.4 and Appendix D for details) based on the quantitative descriptors and threshold values defined in Table 4.14.

Since the notion of local scale [see Table 2.2] refers to horizontal dimensions between hundreds of meters and several kilometres, this allows a certain range of appropriate scales in which valid GITs can be identified (contingent on image pixel resolution); and that sometimes may lie between micro- (less than 100m) and meso-scales (more than 5km) (Bechtel et al., 2015; Erell et al., 2011). In this sense, before conducting the automated classification of GITs for the totality of the study area, it was necessary to determine the most adequate spatial unit (or grid size) for the comparative analysis of mean diurnal and nocturnal LSTs at the local scale.

Due to the considerable extent of the study area and potential processing time of remote sensing data, a small portion of 15.50km²—hereinafter referred as *pilot study*—representing a cross-section of Sydney's urban conditions was selected to test the classification framework using spatial units lying between the micro and local scales (25m, 50m and 100m). The extent of the pilot study and the results of classifications at three spatial scales is presented in Figure 7.2.

The pilot study was successfully classified into 23812 grids of 25 x 25m, 5953 grids of 50 x 50m and 1445 grids of 100 x 100m [Figure 7.2]. The classification approach and thresholds were effective in identifying GITs at different spatial scales, and results were satisfactory with less than 0.25% of unclassified grids for all cases. GITs at 50m grid resolution exhibit the lowest percentage (0.10%) of unknown spatial units in comparison to 25m (0.243%) and 100m (0.21%) grid resolutions.

Consequently, and as mentioned in Section 6.3.4, a 50 x 50m grid was identified as an *optimal spatial unit* for this research as it was found to be the smallest possible grid size in which structural characteristics and spatial patterns of surfaces and features can be distinctively recognised. In fact, 100 x 100m grids were highly heterogeneous and showed an increased aggregation of features. Contrastingly, 25 x 25m grids resulted in a much larger fragmentation of the landscape, providing a limited amount of contextual information to the grids as these were mostly occupied by single surface covers [Figure 7.3]. Further discussion on defining this optimal grid size is presented in Chapter 8.



Figure 7.2 Extent of the pilot study and results of classifications using spatial units of 25 x 25m, 50 x 50m and 100 x 100m. Note: See comparison of detailed portion in [Figure 7.3](#).

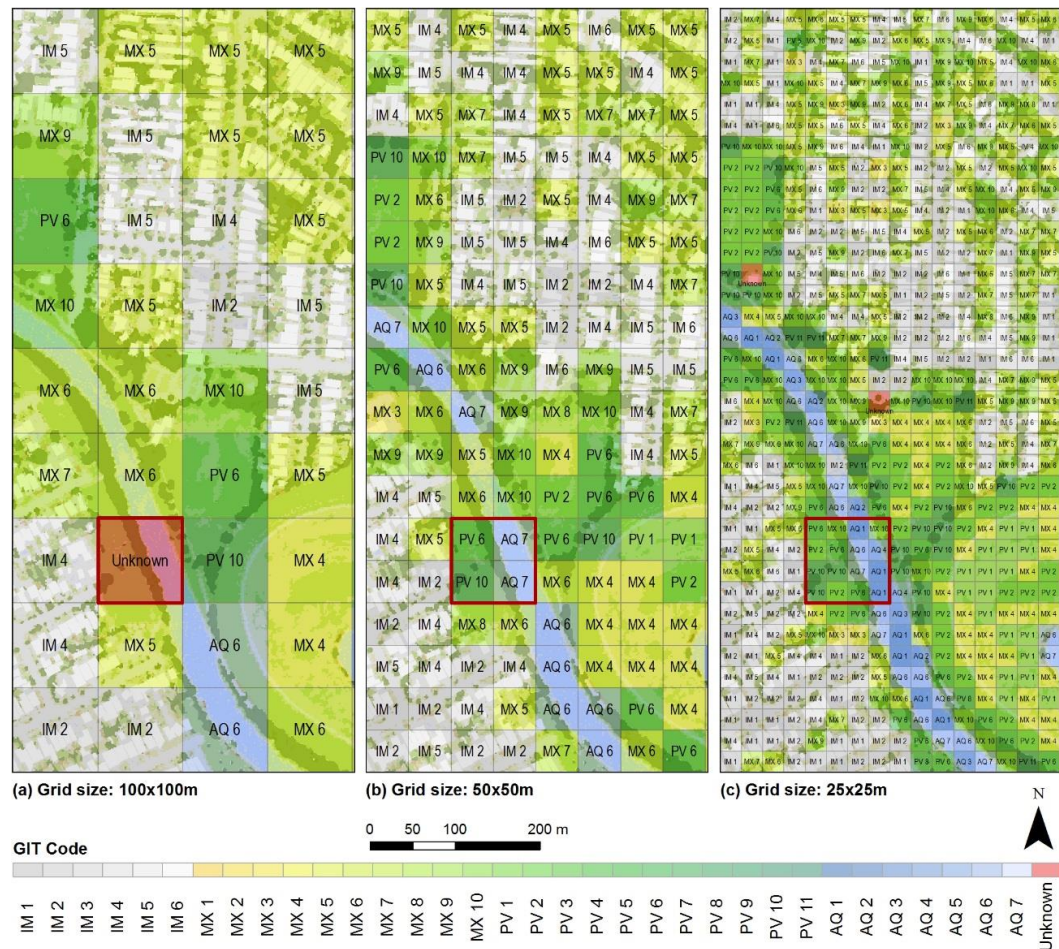


Figure 7.3 Comparison of classification results of a small portion of the pilot study area into 25x25m, 50x50m and 100x100m grid resolutions.

7.2.2 Classification results at the local scale (50m grid)

7.2.2.1 Case study 1: Summer

The automated classification of GITs at the local scale for the whole extent of the case study 1 using a grid size of 50 x 50m is presented in [Figure 7.4](#). A total of 23774 grid cells, for which either daytime or night-time LSTs were available, were generated for the case study 1. Due to an erroneous extraction of surface covers from spectral and LiDAR data, 340 grids (1.43%) were excluded from further analyses (see [Section 8.3.3](#) for further details). From the remaining total (23434 grids), 23120 grids (98.65%) were successfully classified into 33 typologies as per [Table 4.14](#); leaving 314 grids (1.34%) as non-classifiable.

[Figure 7.5](#) presents a comparison of the total number of grids, percentage of total area, distribution of surface fractions, and mean values of independent and dependent variables (listed in [Table 5.1](#)) estimated for each GIT identified for the case study 1.

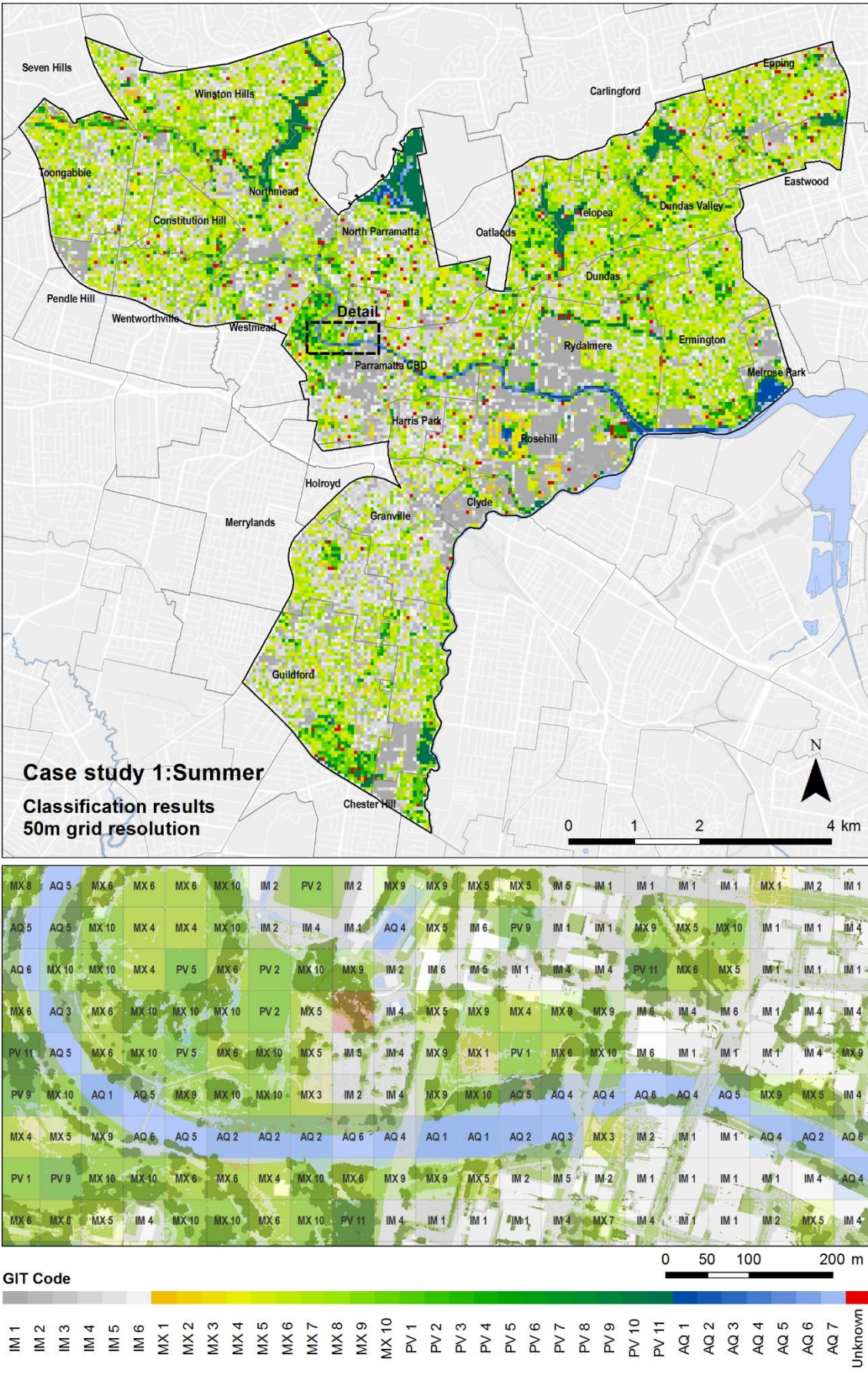
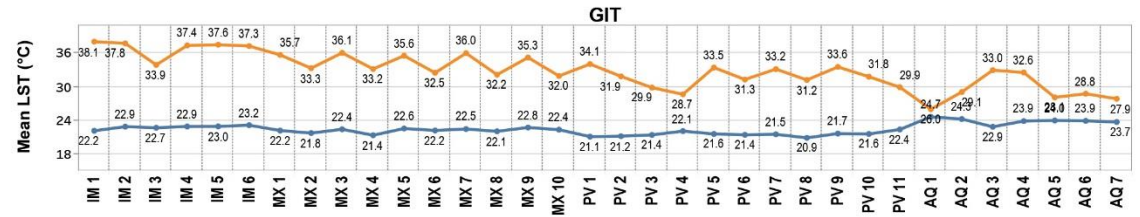


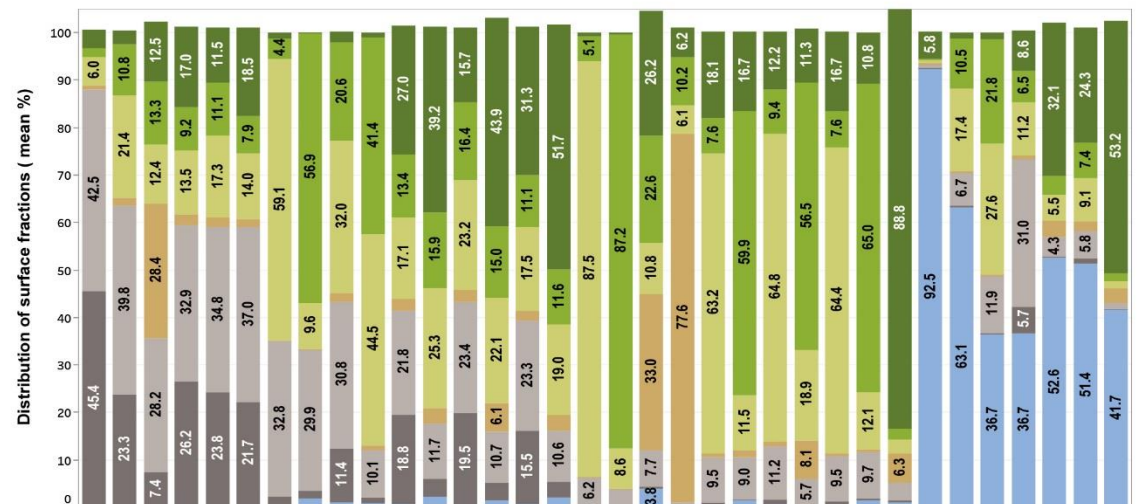
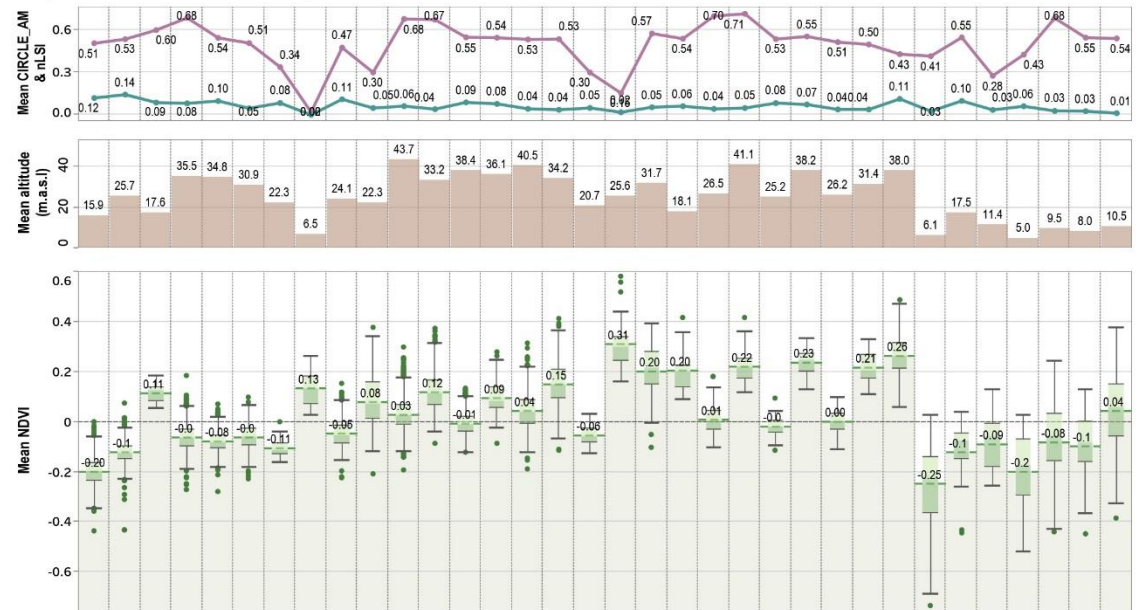
Figure 7.4 Automated GIT classification for the Case study 1: Summer (above) and a detailed fraction (below) using spatial units of 50 x 50m.

Case study 1: Summer

Dependent variables measured per GIT



Independent variables measured per GIT



Distribution of classified GITs

	IM 1	IM 2	IM 3	IM 4	IM 5	IM 6	MX 1	MX 2	MX 3	MX 4	MX 5	MX 6	MX 7	MX 8	MX 9	MX 10	PV 1	PV 2	PV 3	PV 4	PV 5	PV 6	PV 7	PV 8	PV 9	PV 10	PV 11	AQ 1	AQ 2	AQ 3	AQ 4	AQ 5	AQ 6	AQ 7
% of total	10.00%	4.59%	0.03%	16.19%	9.04%	5.31%	0.39%	0.08%	0.92%	0.97%	19.36%	3.55%	5.43%	0.25%	10.64%	4.64%	0.83%	0.19%	0.12%	0.06%	0.96%	0.16%	0.15%	0.02%	0.72%	0.08%	3.59%	0.67%	0.07%	0.06%	0.10%	0.44%	0.14%	0.24%
# of grids	2,313	1,062	7	3,742	2,090	1,228	91	19	212	225	4,475	820	1,255	58	2,461	1,073	192	44	27	14	223	36	35	5	167	18	829	156	16	15	24	101	32	55



Figure 7.5 Comparison of the total number of grids, percentage of total area, distribution of surface fractions, and mean values of independent and dependent variables estimated for each GIT identified for the case study 1.

By analysing the four high-level subgroups of GITs [see Figure 4.8], it can be observed that the case study 1 is mostly dominated by *mixed* ($n=10689$, 46.23%) and *impervious* ($n=10442$, 45.16%) GITs, with a small proportion of *pervious* ($n=1590$, 6.88%) and *aquatic* ($n=399$, 1.72%) GITs. The most abundant GITs are MX5 *Mixed surfaces with aligned trees* ($n=4475$, 19.36%) and IM4 *Mostly impervious with aligned trees* ($n=3742$, 16.19%), followed by MX9 *Mixed surfaces with clustered trees* ($n=2461$, 10.64%), IM1 *Highly impervious* ($n=2313$, 10.0%), and IM5 *Mostly impervious with scattered trees* ($n=2090$, 9.04%). Other popular GITs identified are MX7 *Mixed surfaces with scattered trees* ($n=1255$, 5.43%), IM6 *Mostly impervious with clustered trees* ($n=1228$, 5.31%), MX10 *Mixed grasses with clustered trees* ($n=1073$, 4.64%), IM2 *Mostly impervious with grasses* ($n=1062$, 4.59%), PV11 *Dense trees with shrubs and grasses* ($n=829$, 3.59%), and MX6 *Mixed grasses with aligned trees* ($n=820$, 3.55%).

The least common GITs ($n<20$) correspond to PV8 *Mostly irrigated grasses with scattered trees* ($n=5$, 0.02%), IM3 *Mostly impervious with shrubs* ($n=7$, 0.03%), PV4 *Mostly shrubs* ($n=14$, 0.06%), AQ3 *Mostly grasses with water* ($n=15$, 0.06%), AQ2 *Mostly water with grasses* ($n=16$, 0.07%), PV10 *Mostly irrigated grasses with clustered trees* ($n=18$, 0.08%), and MX2 *Mostly irrigated grasses with impervious* ($n=19$, 0.08%). Unidentified grids named as *unknown* ($n=314$, 1.34%) correspond to areas that were not properly classified as these possess characteristics of multiple GITs and/or a large variability of parameters.

In Figure 7.6, it can be observed the correspondence between the urban patterns described in Section 6.1.3 and the degree of imperviousness and proportion of tree canopy estimated for GITs. Most *highly impervious* GITs (IM1), were identified in areas comprising office, retail, residential and industrial buildings, that were situated in the central core of the LGA, namely Parramatta CBD and adjacent suburbs (Rosehill, Harris Park, Rydalmere, Westmead, Clyde, and North Parramatta). Other *impervious* GITs (IM4-6) were commonly found in the suburbs of Granville, Guildford, Chester Hill and Melrose Park which are typical suburban neighbourhoods of low and very low density where street trees and bushes are generally absent as these are replaced by a large proportion of impermeable surfaces and dry lawns. In these areas, mature and large clusters of trees were mostly confined to large parks, golf courses and nature reserves.

Most of the wooded *mixed* GITs (MX5-10) are located in the Northwest (Dundas, Oatlands, Telopea, Dundas Valley, Ermington, Carlingford, Eastwood, Epping) and Northeast (Winston Hills, Toongabbie, Constitution Hill) suburbs of the LGA, where neighbourhoods exhibit a higher proportion of trees and grasses. Although *pervious* and *aquatic* GITs were scarcer, the automated classifications were successful in identifying small, medium and large green spaces with various amounts of tree canopy and different types of water bodies (lakes, rivers, swamps) across the LGA, and particularly concentrated to the north and northeast.

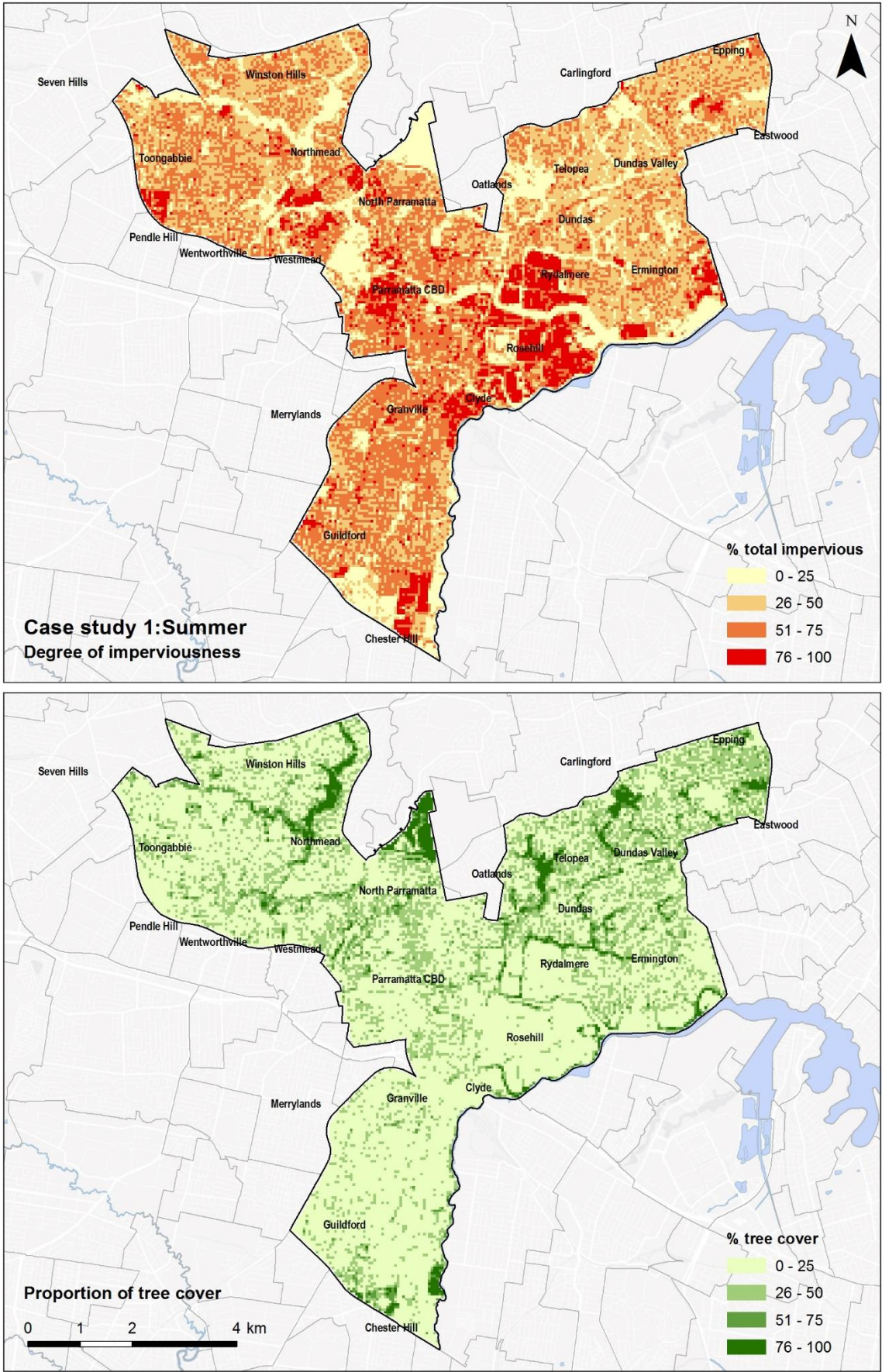


Figure 7.6 Degree of imperviousness and proportion of tree canopy measured for GITs identified for the case study 1.

The most abundant surface covers across all GITs and the case study 1 were *impervious ground* (26.15% of the case study area) and *impervious buildings* (19.78%). On the other hand, the most common pervious surfaces were *trees* (22.37%) and *non-irrigated grasses* (17.25%), followed by *irrigated grasses* (10.52%). Bushes (2.24%) and water (1.69%) were the least common among all surfaces.

The differences between identified GITs in terms of the proportion of surface fractions is presented in [Figure 7.5](#). A close similarity can be seen in the distribution of surface fractions between sets of typologies, such in the case of IM4-5-6, MX5-7-9, MX6-8-10, PV5-7-9, PV6-8-10 and AQ5-6 GITs. However, these differ from each other in terms of tree arrangement quantified by landscape metrics (CIRCLE_AM and nLSI).

Regarding the relationships between *low*, *medium* and *high* vegetation surface fractions, it is evident that *mixed* GITs have the highest proportion of wooded areas among GITs excepting for PV11 *Dense trees with shrubs and grasses* that possess the largest proportion of trees among all typologies (88.8%). Conversely, *pervious* GITs have a very high proportion of grasses (irrigated and non-irrigated), shrubs and bare soil compared to other typologies.

Regarding the *aquatic* GITs, AQ1 *Water* contains a minimal amount of vegetation features (5.8%) that correspond to transitional zones with terrestrial surfaces. Conversely, AQ 7 *Water with clustered trees* exhibits the largest proportion of trees (53.2%) followed by AQ5 *Water with aligned trees* (32.1%) and AQ6 *Water with scattered trees* (24.3%). AQ3 *Mostly grasses with water* and AQ4 *Mixed surfaces with water* present the same amount of water (36.7%); however, the former has more mixed grasses while the latter has more impervious surfaces.

In few cases, *aquatic* GITs with grasses (*i.e.* AQ2, AQ3) were identified in the middle of open water; this can be attributed to the presence of superficial vegetation or to errors at the sensor due to excessive water reflections. All abovementioned surface and spatial distributions match with the typical characteristics defined for GITs as per [Table 4.14](#).

While GITs are classified in terms of morphological and configurational parameters, these enable the estimation of indicators for performance-based analyses across different ESS such as climate regulation. For this research, mean NDVI, mean altitude, and mean diurnal and nocturnal LSTs were additionally calculated per typology based on average values of grids. All the variables presented in [Figure 7.5](#) are employed in the statistical analyses presented in Sections 7.3 and 7.4.

Figure 7.5 presents a statistical summary of mean NDVI values for individual GITs. Overall, mean NDVI is significantly low for all GITs due to the severe water stress, dryness of the land, and extreme weather conditions experienced during the data collection campaign. Boxplots indicate considerable differences among GITs in terms of mean NDVI values. GITs combining larger proportions of irrigated grasses and forested areas were among the highest, specifically PV2 *Mostly irrigated grasses* (0.31), PV11 *Dense trees with shrubs and grasses* (0.26), PV8 *Mostly irrigated grasses with scattered trees* (0.23), PV6 *Mostly irrigated grasses with aligned trees* (0.22), PV10 *Mostly irrigated grasses with clustered trees* (0.21), PV4 *Mostly shrubs* (0.20) and PV3 *Mixed grasses with shrubs and trees* (0.20).

Mean NDVI of *pervious* GITs with irrigated grasses were generally higher than *mixed* GITs as the latter are constrained by the presence of pavements, buildings, poorly irrigated grasses and bare soils. A similar situation occurs with *pervious* GITs with considerable amount of non-irrigated grasses that have very low or even negative mean NDVI values. Generally, *impervious* GITs exhibit negative mean NDVI values (-0.20 to -0.05), except for IM3 *Mostly impervious with shrubs* that presents a positive and higher mean value (0.11) due to the presence of hedges, shrubbery and small trees. *Aquatic* GITs and IM1 *Highly impervious* display the lowest and very negative mean NDVI (-0.25 to -0.08) corresponding to the presence of extensive water and impermeable surfaces. However, the disproportion in the number of grids among GITs may also have influenced in the average NDVI value of each typology.

Furthermore, the variation of mean NDVI is higher (long boxplots) on *aquatic* GITs and typologies with a substantial variation of green cover and levels of irrigation. In contrast, a lower variation of mean NDVI (short boxplots) is observed for GITs with a dominant surface (*i.e.* MX1, PV1, PV7). It is observed repetitive spikes on mean NDVI and mean diurnal LSTs between GITs, specifically MX2-3, MX3-4, PV5-6, PV6-7 [Figure 7.5]. This can be explained by differences in the proportion of irrigated and non-irrigated low plants that have a significant impact on mean NDVI and LSTs.

In terms of mean altitude, the majority of GITs exhibit varied values ranging between 15 and 47 metres above sea level (MASL), except for the *aquatic* GITs which are mostly low-lying with mean altitudes between 0 and 17.5MASL. A comprehensive analysis of summer diurnal and nocturnal LST differences in summer and among GITs is presented in Section 7.3.

7.2.2.2 Case study 2: Winter

The automated classification of GITs at the local scale for the whole extent of the case study 2 using a grid size of 50 x 50m is presented in Figure 7.7. A total of 29009 grid cells, for which either daytime or night-time LSTs were available, were generated for the case study 2. Due to an erroneous extraction of surface covers from spectral and LiDAR data, 173 grids (0.60%) were excluded from further analyses (see Section 8.3.3 for further details). From the remaining total (28836 grids), 28657 grids (99.38%) were successfully classified into 34 typologies as per Table 4.14; leaving 179 grids (0.62%) as non-classifiable. PV4 *Mostly shrubs* were not identified for this case study. From the total amount of classifiable grids, diurnal LSTs were only available for 24981 grids, while nocturnal LSTs were available for 23501 grids.

Figure 7.8 presents a comparison of the total number of grids, percentage of total area, distribution of surface fractions, and mean values of independent and dependent variables estimated for each GIT identified for the case study 2. It also shows the number of grids for which either diurnal or nocturnal LSTs were available.

Similar to the previous case study, the case study 2 is mostly dominated by *impervious* ($n=13292$, 46.3%) and *mixed* ($n=12007$, 41.83%) GITs, with a smaller proportion of *pervious* ($n=3033$, 10.57%) and few *aquatic* ($n=375$, 1.31%) typologies. The most abundant GITs are MX5 *Mixed surfaces with aligned trees* ($n=4935$, 17.19%), IM4 *Mostly impervious with aligned trees* ($n=3976$, 13.85%), and IM1 *Highly impervious* ($n=3876$, 13.5%). Other prevalent GITs identified are IM2 *Mostly impervious with grasses* ($n=2325$, 8.10%), PV11 *Dense trees with shrubs and grasses* ($n=1943$, 6.77%), IM5 *Mostly impervious with scattered trees* ($n=1836$, 6.40%), MX9 *Mixed surfaces with clustered trees* ($n=1755$, 6.11%), MX6 *Mixed grasses with aligned trees* ($n=1656$, 5.77%), MX10 *Mixed grasses with clustered trees* ($n=1633$, 5.69%), IM6 *Mostly impervious with clustered trees* ($n=1277$, 4.45%), and MX7 *Mixed surfaces with scattered trees* ($n=961$, 3.35%).

The least common GITs ($n<20$) correspond to IM3 *Mostly impervious with shrubs* ($n=2$, 0.01%), AQ3 *Mostly grasses with water* ($n=5$, 0.02%), AQ4 *Mixed surfaces with water* ($n=9$, 0.03%), AQ2 *Mostly water with grasses* ($n=10$, 0.03%), MX2 *Mostly irrigated grasses with impervious* ($n=10$, 0.03%) and PV7 *Mostly non-irrigated grasses with scattered trees* ($n=14$, 0.05%). 179 *unknown* grids (0.62%) correspond to areas with large surface fraction variability that were difficult to classify.

Figure 7.9 illustrates different levels of imperviousness and tree cover estimated for GITs which correspond to distinct urban patterns described in Section 6.1.4. The winter case

study can be differentiated into two longitudinal areas –northern and southern– defined by the spatial extent of the airborne remote sensing data. These areas exhibit distinct morphological and vegetation characteristics that are described below.

The northern swath is mostly dominated by *pervious* and *mixed* GITs characterised by sparsely distributed buildings, large proportion of irrigated grasses, bushes and mature trees (Castle Hill, West Pennant Hills, Beecroft, Cheltenham, Epping, North Epping, Marsfield and Northbridge). Large clusters of trees and dense forested areas situate along the Lane Cove River (Chatswood West, Lindfield, Macquarie Park and West Pymble), near Middle Harbour (Northbridge), and in the suburbs of North Epping, Cheltenham, Beecroft and West Pennant Hills. Most of the *impervious* GITs, featuring scant vegetation mostly in the form of scarce street trees, concentrate within or adjacent to major city centres or industrial parks, namely Chatswood, Macquarie Park and Castle Hill. An increased level of imperviousness is also observed to the east of Chatswood. Most *aquatic* GITs (AQ1-7) were identified in Middle Harbour and Lane Cove River.

In contrast, a higher degree of imperviousness and significantly smaller proportion of trees is observed in the southern swath. Most *impervious* GITs with no or few trees are largely dominant and principally identified within or adjacent to major city centres of medium and high urban density (Sydney CBD, Haymarket, Surry Hills, Chippendale, Redfern, Ultimo, Newtown, Enmore, Stanmore, Petersham, Lewisham, Ashfield), industrial sites, and transport facilities/corridors (Redfern, Strathfield South, Lakemba, Campsie, Bankstown Aerodrome). For instance, the Bankstown airport was mainly classified into treeless *impervious* and *mixed* GITs comprising a combination of non-irrigated low plants, large low-/mid-rise buildings and extensive paved areas.

Impervious and *mixed* GITs with trees arranged in rows or small groups were commonly found in middle ring suburbs characterised by a distinct decline in vegetation cover, open arrangements of low-rise buildings, and large paved areas (*i.e.* roads, parking and driveways). *Pervious* GITs were scarcer and mostly situated along the Cooks River (Croydon Park, Canterbury, Campsie), within and nearby Moore Park and the University of Sydney (Camperdown), and towards the inner ring suburbs to the west of Bankstown airport (Milperra, Chipping Norton). A limited number of *aquatic* GITs were found along the Cook and Georges rivers as water features were commonly smaller than the size of spatial units.

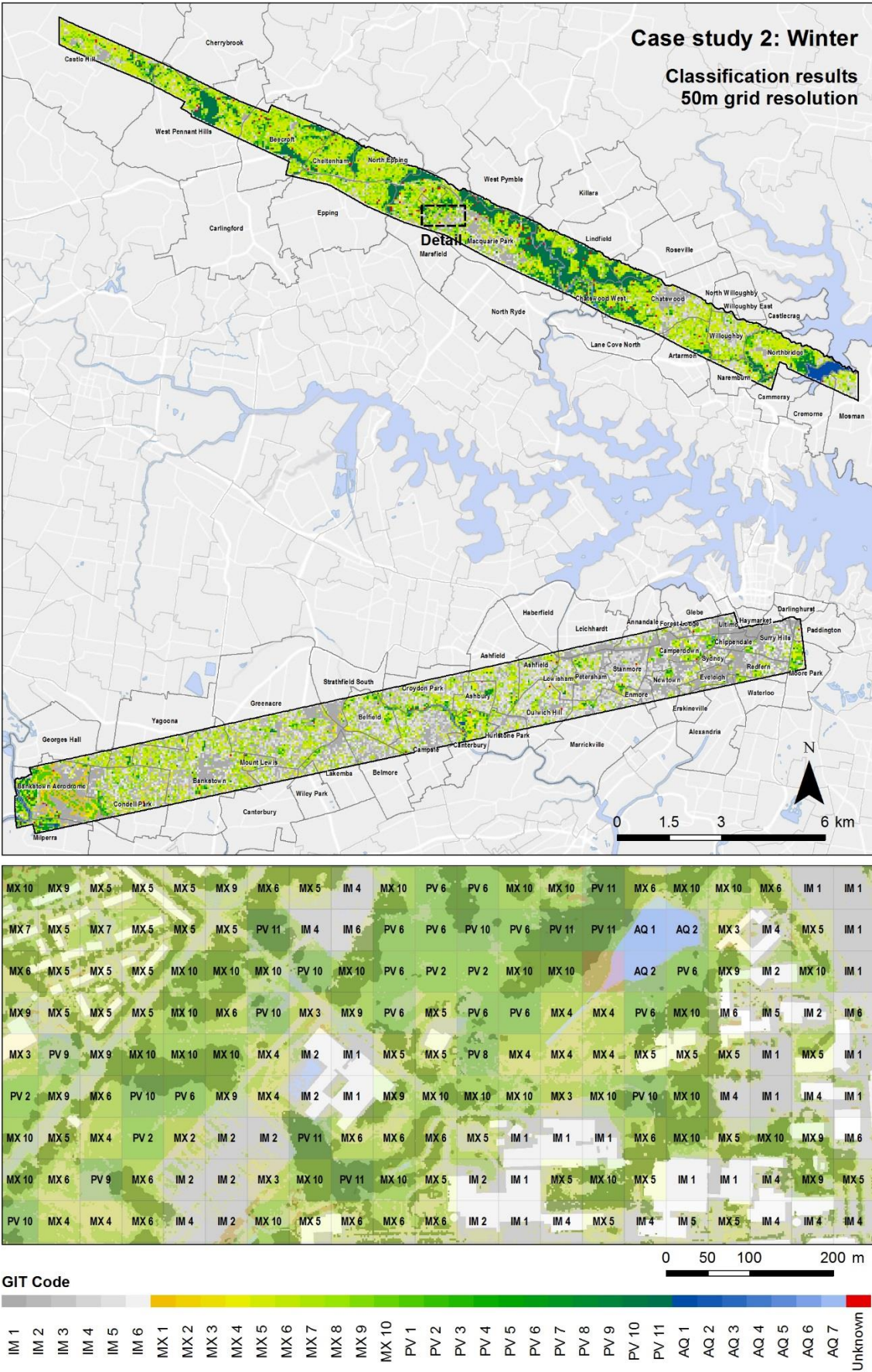
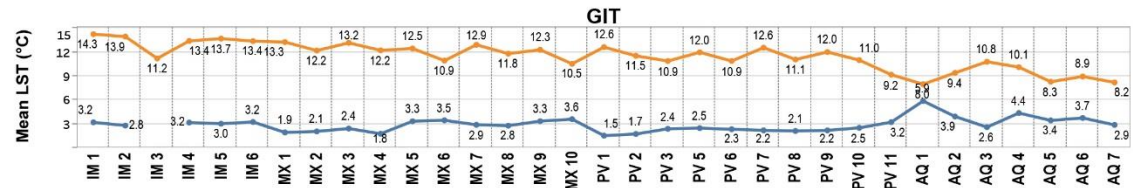


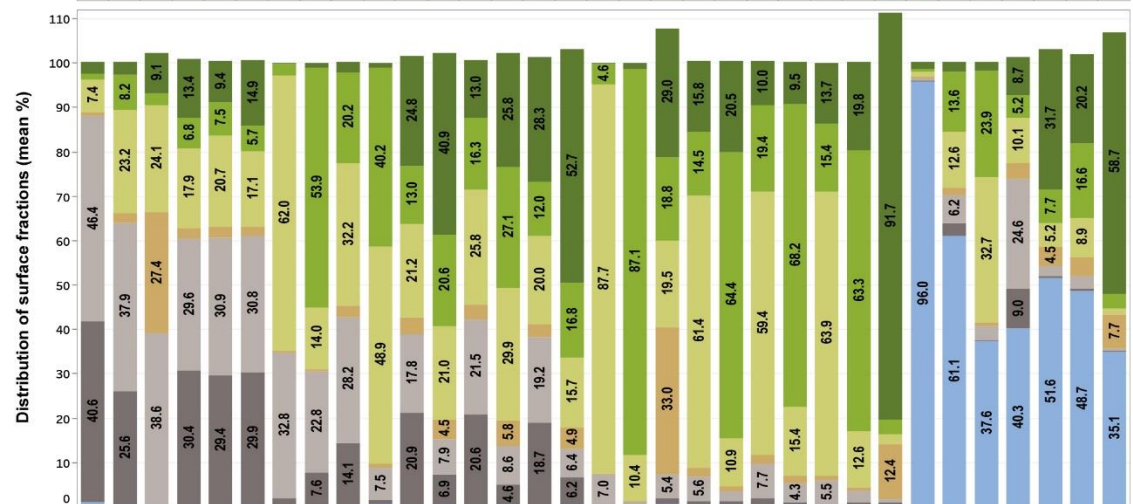
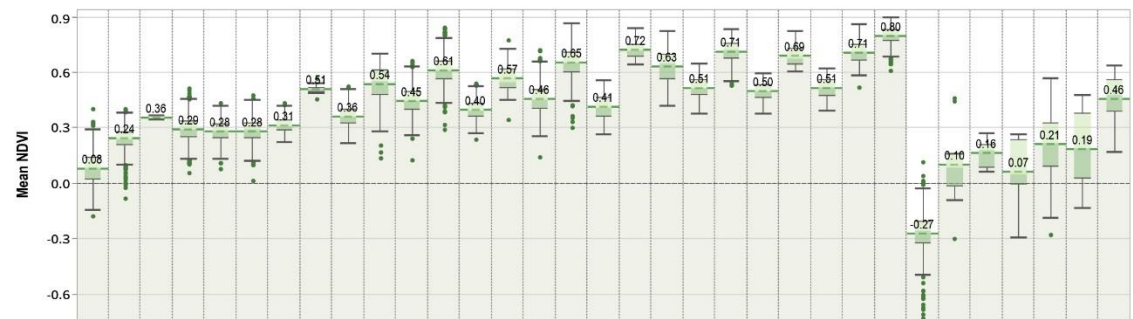
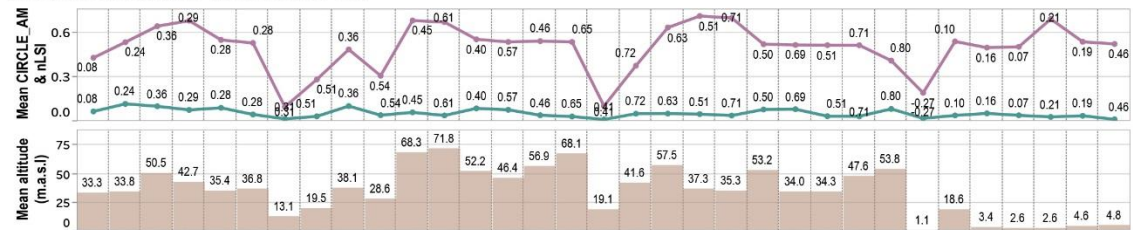
Figure 7.7 Automated GIT classification for the Case study 2: Winter (above) and a detailed fraction (below) using spatial units of 50 x 50m.

Case study 2: Winter

Dependent variables measured per GIT



Independent variables measured per GIT



Distribution of classified GITs

	IM 1	IM 2	IM 3	IM 4	IM 5	IM 6	MX 1	MX 2	MX 3	MX 4	MX 5	MX 6	MX 7	MX 8	MX 9	MX 10	PV 1	PV 2	PV 3	PV 5	PV 6	PV 7	PV 8	PV 9	PV 10	PV 11	AQ 1	AQ 2	AQ 3	AQ 4	AQ 5	AQ 6	AQ 7
# of grids (diurnal)	3,769	2,264	2	3,693	1,770	1,235	221	10	361	363	3,925	1,185	852	55	1,547	1,215	327	82	28	90	181	7	28	55	138	1,403	15	6	5	3	103	14	23
# of grids (nocturnal)	3,124	1,827	0	3,175	1,435	1,013	197	10	303	326	4,094	1,452	754	46	1,384	1,387	278	88	30	81	170	14	26	56	141	1,749	162	9	2	8	115	26	22
Total # of grids	3,976	2,325	2	3,976	1,836	1,277	222	10	386	388	4,935	1,656	961	61	1,755	1,633	328	103	36	104	232	14	33	64	176	1,943	168	10	5	9	133	26	24
% of total	13.50%	8.10%	0.01%	13.85%	6.40%	4.45%	0.77%	0.03%	1.34%	1.35%	17.19%	5.77%	3.35%	0.21%	6.11%	5.69%	1.14%	0.36%	0.13%	0.36%	0.81%	0.05%	0.11%	0.22%	0.61%	6.77%	0.59%	0.03%	0.02%	0.03%	0.46%	0.09%	0.08%



Figure 7.8 Comparison of the total number of grids, percentage of total area, distribution of surface fractions, and mean values of independent and dependent variables estimated for each GIT identified for the case study 2.

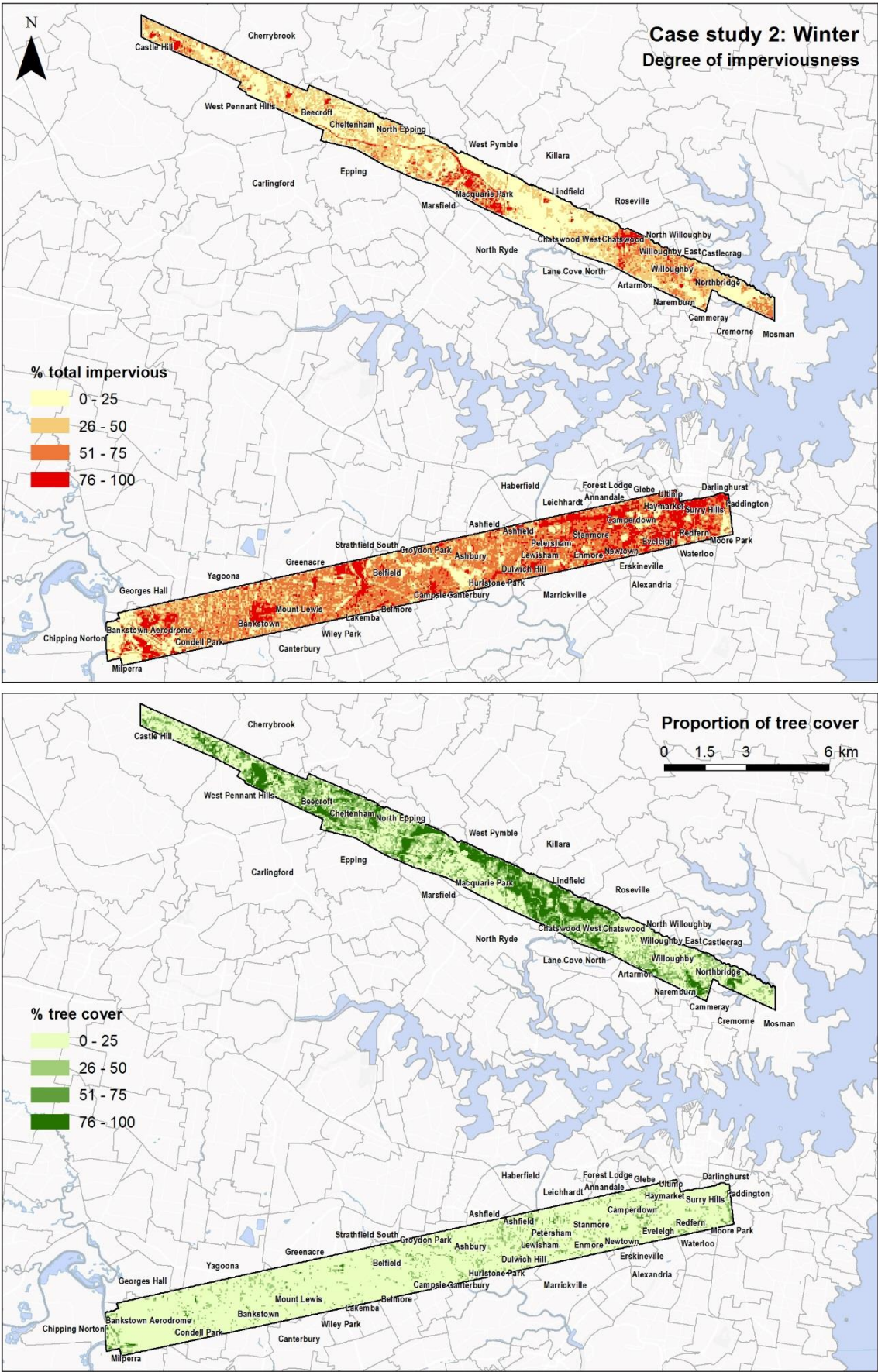


Figure 7.9 Degree of imperviousness and proportion of tree canopy measured for GITs identified for the case study 2.

The most abundant surface covers across all GITs and the case study 2 were *impervious ground* (23.17% of the case study area) and *impervious buildings* (21.16%). On the other hand, the most common pervious surfaces were *trees* (22.08%) and *non-irrigated grasses* (18.42%), followed by *irrigated grasses* (10.65%). Bushes (3.26%) and water (1.27%) were the least common surfaces. These values are similar to those estimated for the case study 1, with slight differences in the proportion of buildings (19.78% versus 21.16%) and bushes (2.24% versus 3.26%) respectively.

Despite differences in extent and season, the distribution of surface fractions across all GITs in winter are very similar to those estimated for summer [Figure 7.8] (see Section 7.2.2.1). In all cases, this match with the typical properties defined for GITs [Table 4.14].

Among the *mixed* GIT subgroup, MX8 *Mixed grasses with scattered trees* presents a significant difference in the proportion of trees when comparing winter (25.8%) and summer (43.9%) results. This may be explained by the considerable presence of deciduous trees and the variation in the proportion of irrigated and non-irrigated grasses between both case study areas.

Figure 7.8 presents a statistical summary of mean NDVI vales for all GITs identified in the case study 2. Overall, boxplots show similar patterns in the variability and differences of mean NDVI among GITs as those observed for the case study 1 (see Section 7.2.2.1 and Figure 7.5). Nonetheless, mean NDVI values for winter are significantly higher than summer, especially for terrestrial GITs. For instance, GITs with the largest proportion of irrigated grasses and forested areas, namely PV11, PV2, PV6, PV10 and PV8, display very high mean NDVI values (0.69 to 0.80) compared to summer that vary between 0.20 and 0.31.

Due to the presence of healthier vegetation in winter, mean NDVI of *impervious* GITs show low positive values (0.08 to 0.36) while *mixed* GITs are considerably higher (0.31 to 0.65). Overall, mean NDVI variability (length of boxplots) for all GITs is relatively lower in winter than summer. *Aquatic* GITs commonly present the lowest NDVIs values and the highest variation of means (longer boxplots) compared to other typologies; however, AQ1 *Water* was the only GIT with a very negative mean NDVI value of -0.20.

In terms of mean altitude, the majority of GITs display varied values ranging between 13 and 72 MASL. Particularly, the altitudes of GITs identified for the northern portion are among the highest as these situate in the hilly Hornsby Plateau of Sydney (see Section 6.1.4). *Aquatic* GITs are usually low-lying with most of mean altitudes between 0 and 5

MASL. A comprehensive analysis of diurnal and nocturnal LST differences in winter and among GITs is presented in Section 7.3.

7.2.3 Accuracy and quality evaluation

The quality evaluation of the proposed classification scheme for green infrastructure was conducted using two distinct methods. The first method consists of comparing the accuracy of classified GIT maps against validation data from ground-truthing using a confusion matrix. The second method consists of assessing the accuracy or performance of several supervised machine learning algorithms (or classifiers) based on the parameters and threshold values defined for each GIT class. The results of both assessment methods are presented in the following sections.

7.2.3.1 Accuracy analysis of classifications using ground-truthing and confusion matrix

In this research, the extent of the *pilot study* (see Section 7.2.1) was selected for accuracy assessment of classification results since conducting an evaluation for the whole extent of both case studies was resource intensive and time consuming.

Accordingly, 5.4% ($n=322$) of the total number of classified grids per typology were chosen for accuracy assessment through a confusion matrix. The total number of grids of each GIT class employed for validation were determined proportionally to its fraction of the total area using a stratified random sampling method. The resulting classified GIT maps were compared against very high resolution (0.5m) aerial imagery provided by Nearmap (2017) at each validation point by applying a careful visual interpretation based on expert knowledge. To reduce flaws in the assessment, the proportion of validation points was increased for GITs with an insufficient number of samples.

The accuracy of predictions was estimated using a confusion matrix where true classes (y-axis) were plotted against predicted classes (x-axis). The diagonal cells show the number of observations where true and predicted classes matched well, while other cells show the number of misclassifications. In addition, four quality indices were calculated based on the confusion matrix. First, the producer accuracy (PA) estimates the fraction of correctly classified grids of a certain typology regarding the total number of grids of that ground truth typology. Second, the user accuracy (UA) represents the reliability of classifications by measuring the proportion of correctly classified grids of a certain typology divided by the total number of predicted grids of that typology. Third, the overall accuracy (OA) corresponds to the total number of correctly classified grids divided by the total number of

grids. Fourth, the kappa coefficient measures the agreement between predicted and ground truth grids where a value of 1 represents a perfect agreement, while a value of 0 represents no agreement at all.

Table 7.1 Confusion matrix of the GIT classification results for the pilot study at 50m grid resolution showing user accuracy (UA), producer accuracy (PA), overall accuracy (OA) and Kappa index.

GIT	IM 1	IM 2	IM 3	IM 4	IM 5	IM 6	MX 1	MX 2	MX 3	MX 4	MX 5	MX 6	MX 7	MX 8	MX 9	MX 10	PV 1	PV 2	PV 3	PV 4	PV 5	PV 6	PV 7	PV 8	PV 9	PV 10	PV 11	AQ 2	AQ 3	AQ 4	AQ 5	AQ 7	# Predict	UA	
IM 1	32	0	0	1	0	0	0	0	0	0	0	0	0	0	0	0	0	0	0	0	0	0	0	0	0	0	0	0	0	0	0	0	33	97.0%	
IM 2	0	34	0	2	8	0	0	0	3	0	0	0	0	0	0	0	0	0	0	0	0	0	0	0	0	0	0	0	0	0	0	0	47	72.3%	
IM 3	0	0	0	0	1	0	0	0	0	0	0	0	0	0	0	0	0	0	0	0	0	0	0	0	0	0	0	0	0	0	0	0	1	0.0%	
IM 4	0	1	0	34	8	5	0	0	1	0	0	0	2	0	2	0	0	0	0	0	0	0	0	0	0	0	0	0	0	0	0	0	53	64.2%	
IM 5	0	0	0	3	27	4	0	0	0	0	1	0	0	0	0	0	0	0	0	0	0	0	0	0	0	0	0	0	0	0	0	0	35	77.1%	
IM 6	0	0	0	0	4	10	0	0	0	0	0	0	0	0	0	0	0	0	0	0	0	0	0	0	0	0	0	0	0	0	0	0	14	71.4%	
MX 1	0	0	0	0	0	0	2	0	0	0	0	0	0	0	0	0	0	0	0	0	0	0	0	0	0	0	0	0	0	0	0	0	2	100.0%	
MX 2	0	0	0	0	0	0	0	2	0	0	0	0	0	7	0	0	0	0	0	0	0	0	0	0	0	0	0	0	0	0	0	0	2	100.0%	
MX 3	0	0	0	0	1	0	0	0	4	0	0	0	1	0	0	0	0	0	0	0	0	0	0	0	0	0	0	0	0	0	0	0	6	66.7%	
MX 4	0	0	0	0	0	0	0	0	0	7	0	0	0	0	0	0	0	0	0	0	0	0	0	0	0	0	0	0	0	0	0	0	7	100.0%	
MX 5	0	0	0	0	0	0	0	0	0	0	30	1	5	0	5	0	0	0	0	0	0	0	0	0	0	0	0	0	0	0	0	0	41	73.2%	
MX 6	0	0	0	0	0	0	0	0	0	0	0	7	1	0	0	2	0	0	0	0	0	0	0	0	0	0	0	0	0	0	0	0	10	70.0%	
MX 7	0	0	0	0	0	0	0	0	1	0	1	0	13	0	0	0	0	0	0	0	0	0	0	0	0	0	0	0	0	0	0	0	15	86.7%	
MX 8	0	0	0	0	0	0	0	0	0	0	0	0	0	2	0	0	0	0	0	0	0	0	0	0	0	0	0	0	0	0	0	0	2	100.0%	
MX 9	0	0	0	0	0	0	0	0	0	0	6	1	0	1	11	0	0	0	0	0	0	0	0	0	0	0	0	0	0	0	0	0	19	57.9%	
MX 10	0	0	0	0	0	0	0	0	0	0	0	1	0	0	0	6	0	0	0	0	0	0	0	0	0	0	0	0	0	0	0	0	7	85.7%	
PV 1	0	0	0	0	0	0	0	0	0	0	0	0	0	0	0	0	2	0	0	0	0	0	0	0	0	0	0	0	0	0	0	0	2	100.0%	
PV 2	0	0	0	0	0	0	0	0	0	0	0	0	0	0	0	0	0	2	0	0	0	0	0	0	0	0	0	0	0	0	0	0	2	100.0%	
PV 3	0	0	0	0	0	0	0	0	0	0	0	0	0	0	0	0	0	0	1	0	0	0	0	0	0	0	0	0	0	0	0	0	1	100.0%	
PV 4	0	0	0	0	0	0	0	0	0	0	0	0	0	0	0	0	0	0	0	1	0	0	0	0	0	0	0	0	0	0	0	0	1	100.0%	
PV 5	0	0	0	0	0	0	0	0	0	0	0	0	0	0	0	0	0	0	0	0	2	0	0	0	0	0	0	0	0	0	0	0	2	100.0%	
PV 6	0	0	0	0	0	0	0	0	0	0	0	0	0	0	0	0	0	0	0	0	0	2	0	1	0	0	0	0	0	0	0	0	3	66.7%	
PV 7	0	0	0	0	0	0	0	0	0	0	0	0	0	0	0	0	0	0	0	0	0	0	1	0	0	0	0	0	0	0	0	0	1	100.0%	
PV 8	0	0	0	0	0	0	0	0	0	0	0	0	0	0	0	0	0	0	0	0	0	0	0	2	0	0	0	0	0	0	0	0	2	100.0%	
PV 9	0	0	0	0	0	0	0	0	0	0	0	0	0	0	0	0	0	0	0	0	0	0	0	0	2	0	0	0	0	0	0	0	2	100.0%	
PV 10	0	0	0	0	0	0	0	0	0	0	0	0	0	0	0	0	0	0	0	0	0	0	0	0	0	2	0	0	0	0	0	0	2	100.0%	
PV 11	0	0	0	0	0	0	0	0	0	0	0	0	0	0	0	0	0	0	0	0	0	0	0	0	0	0	2	0	0	0	0	0	2	100.0%	
AQ 2	0	0	0	0	0	0	0	0	0	0	0	0	0	0	0	0	0	0	0	0	0	0	0	0	0	0	0	2	0	0	0	0	2	100.0%	
AQ 3	0	0	0	0	0	0	0	0	0	0	0	0	0	0	0	0	0	0	0	0	0	0	0	0	0	0	0	0	1	0	0	0	1	100.0%	
AQ 4	0	0	0	0	0	0	0	0	0	0	0	0	0	0	0	0	0	0	0	0	0	0	0	0	0	0	0	0	1	0	0	0	1	0.0%	
AQ 5	0	0	0	0	0	0	0	0	0	0	0	0	0	0	0	0	0	0	0	0	0	0	0	0	0	0	0	0	0	0	2	0	2	100.0%	
AQ 7	0	0	0	0	0	0	0	0	0	0	0	0	0	0	0	0	0	0	0	0	0	0	0	0	0	0	0	0	0	0	1	1	2	50.0%	
# Truth	32	35	0	40	49	19	2	2	9	7	38	10	22	3	18	8	2	2	1	1	2	2	1	3	2	2	2	2	2	0	3	1	322		
PA	100.0%	97.1%	0.0%	85.0%	55.1%	52.6%	100.0%	100.0%	44.4%	100.0%	78.9%	70.0%	59.1%	66.7%	61.1%	75.0%	100.0%	100.0%	100.0%	100.0%	100.0%	100.0%	100.0%	66.7%	100.0%	100.0%	100.0%	100.0%	50.0%	0.0%	66.7%	100.0%			
OA	0.764																																		
Kappa	0.741																																		

Table 7.1 shows the error matrix and quality indices for the classification accuracy assessment of the pilot study at 50m grid resolution. The *overall accuracy* of the GIT

classification is 76.4%, while the kappa coefficient value is 0.741, which represents overall satisfactory classification results.

When observing the *user accuracy*, it can be found that *pervious* GITs obtained the highest accuracy among GITs (>85%), while *impervious* and *mixed* GITs had a relatively lower accuracy than other GITs (58-77%). A similar situation occurs when observing the *producer accuracy*; however, *mixed* and *aquatic* GITs achieved much lower values compared to other typologies. Particular attention causes the variability of accuracies exhibited by *aquatic* GITs as the number of validation points was too small.

The results also show that there is considerable confusion between IM4, IM5 and IM6; between IM2, IM5 and MX3, and between MX5, MX7 and MX9 given the large variability of surface fractions and the difficulty of distinguishing different arrangement of trees. This has resulted in relatively low user accuracies for MX9 (0.58), IM4 (0.64), MX3 (0.67), MX6 (0.70), IM6 (0.71) and IM2 (0.72). The lowest user accuracies (0.00) were calculated for IM3 and AQ4 due to the very small number of validation points and grids identified for these classes.

7.2.3.2 Quality assessment of the classification scheme using deep learning

After performing the accuracy evaluation of GIT classifications, it was conducted an evaluation of the predictability or performance of the classification scheme (implemented using the conditional algorithm in ArcGIS presented in Section 6.4) which is based on parameters and threshold values defined for each GIT.

Due to the extensive coverage of the study area and the large number of classified grids (51827 samples), *deep learning* was selected to perform the quality assessment for the totality of the extent of each case study. Deep learning is defined as a type of *machine learning* in which several classifiers or models learn to perform classifications tasks from a large amount of training data provided by the user. Deep learning is usually implemented using a neural network architecture (which typically contains multiple nonlinear processing layers), so it is suitable for non-parametric data (MathWorks, 2017a). In fact, it is an excellent classification technique that in recent years has concentrated the attention of remote sensing researchers as it proved effective in implementing and evaluating supervised object-based classification frameworks like the GIT scheme proposed in this thesis (Ma et al., 2017).

The *classification learner* app available in Matlab® software (MathWorks, 2017b) was applied to assess the accuracy of categorical predictions (or responses) and the overall

quality of the classification parameters (or predictors) by training several supervised machine learning classifiers (also referred as models or algorithms). Model comparisons were performed to determine their sensitivity or specificity by plotting true positive rates versus false positive rates (MathWorks, 2018b).

Table 7.2 Summary of selected and excluded predictors and responses for the supervised machine learning models performed for each case study.

Predictors	Responses	Summer dataset		Winter dataset	
		# samples	Included	# samples	Included
Included	IM 1	2313	Yes	3876	Yes
	- Fraction of total impervious	IM 2	1062	Yes	2325
	- Fraction of trees	IM 3	7	No	2
	- Fraction of shrubs	IM 4	3742	Yes	3976
	- Fraction of non-irrigated grasses	IM 5	2090	Yes	1836
	- Fraction of irrigated grasses	IM 6	1228	Yes	1277
	- Fraction of total water	MX 1	91	Yes	222
	- CIRCLE_AM	MX 2	19	No	10
	- nLSI	MX 3	212	Yes	386
		MX 4	225	Yes	388
		MX 5	4475	Yes	4935
Excluded	- Fraction of impervious building	MX 6	820	Yes	1656
	- Fraction of impervious ground	MX 7	1255	Yes	961
	- Mean altitude	MX 8	58	Yes	61
	- Mean NDVI	MX 9	2461	Yes	1755
		MX 10	1073	Yes	1633
		PV 1	192	Yes	328
		PV 2	44	Yes	103
		PV 3	27	Yes	36
		PV 4	14	No	0
		PV 5	223	Yes	104
		PV 6	36	Yes	232
		PV 7	35	Yes	14
		PV 8	5	No	33
		PV 9	167	Yes	64
		PV 10	18	No	176
		PV 11	829	Yes	1943
		AQ 1	156	Yes	168
		AQ 2	16	No	10
		AQ 3	15	No	5
		AQ 4	24	Yes	9
		AQ 5	101	Yes	133
		AQ 6	32	Yes	26
		AQ 7	55	Yes	24
TOTALS		23120	23026	28707	28657






Initially, information of classified GIT grids corresponding to each case study were pre-processed to extract meaningful parameters or *features* to help improve the machine learning algorithms by focusing on the data that will produce more accurate predictions. This step is crucial to eliminate redundancy and facilitate the generalisation during the

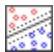








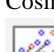


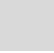




learning phase to avoid model overfitting (MathWorks, 2018a). Accordingly, GITs with less than 20 samples were excluded as well as several redundant variables. Table 7.2 provides a summary of selected and excluded predictors and responses for each case study.

Before training classifiers, datasets were divided into training and validation sets to reduce the possibility of model overfitting. The validation set is usually employed to measure the accuracy of the model developed from the training data (MathWorks, 2018a). Due to the large number of samples [Table 7.2], a holdout validation was performed with 25% of the data.

A total of 22 machine learning algorithms were trained and included: (1) decision trees (fine, medium, coarse), (2) discriminant (linear, quadratic), (3) support vector machine (SVM) (linear, quadratic, cubic, Gaussian), (4) k -nearest neighbour (KNN) (fine, medium, coarse, cosine, cubic, weighted), and (5) ensemble classifiers (boosted trees, bagged trees, subspace discriminant, subspace K -nearest neighbour and RUSBoosted trees). Classifiers were tested for each case study individually to assess the reliability of the scheme using two different datasets. Table 7.3 presents a summary of accuracy scores achieved by each classifier.

Table 7.3 Summary of model's accuracy achieved for each dataset accompanied by a description of classifiers. Models with highest accuracies (in bold) were selected for further assessment. Descriptions based on MathWorks (2018b).

Classifiers	Model accuracy		Description	Interpreta- bility
	Summer	Winter		
Decision trees (Tree)			It is fast for fitting and prediction but tends to have low predictive accuracy and is prone to overfitting	
Fine tree 	99.8 %	100.00 %	Many leaves (splits) to make many fine distinctions	Easy interpretation
Medium tree 	95.8 %	96.8 %	Medium number of splits for finer distinctions	Easy interpretation
Coarse tree 	65.5 %	59.5 %	Few splits to make coarse distinctions between classes	Easy interpretation
Discriminant			It estimates a Gaussian distribution for each class. Good for large datasets, fast and accurate predictions.	
Linear 	71.4 %	71.7 %	Create linear boundaries between classes	Easy interpretation
Quadratic 	80.4 %	81.8 %	Creates non-linear boundaries between classes	Easy interpretation
Support vector machines (SVM)			Classifies data by finding the best hyperplane (largest margin) that separates points between classes. Good for medium to large datasets.	

Linear SVM 	96.6 %	97.2 %	Makes a linear separation between classes. Good for small problems	Easy interpretation
Quadratic SVM 	96.8 %	97.1 %	Makes a quadratic separation between classes. Good for large datasets	Hard interpretation
Cubic SVM 	95.5 %	96.0 %	Makes a cubic separation between classes. Good for large datasets	Hard interpretation
Fine Gaussian SVM 	80.4 %	84.3 %	Makes finely detailed distinctions between classes using a kernel scale set to $\sqrt{P}/4$.	Hard interpretation
Medium Gaussian SVM 	94.0 %	94.9 %	Makes medium distinctions between classes using a kernel scale set to \sqrt{P} .	Hard interpretation
Coarse Gaussian SVM 	91.2 %	92.3 %	Makes medium distinctions between classes using a kernel scale set to $\sqrt{P} \cdot 4$.	Hard interpretation
K-nearest neighbour (KNN)			Identifies classes based on the distance to a n number of neighbours. It has good predictive accuracy in low dimensions	
Fine KNN 	80.8 %	82.7 %	Finely detailed distinctions between classes. # neighbours=1	Hard interpretation
Medium KNN 	84.8 %	86.1 %	Medium distinctions between classes. # neighbours=10	Hard interpretation
Coarse KNN 	81.1 %	83.8 %	Coarse distinctions between classes. # neighbours=100	Hard interpretation
Cosine KNN 	76.8 %	76.4 %	Medium distinctions between classes using a cosine distance metric. # neighbours=10	Hard interpretation
Cubic KNN 	82.7 %	84.7 %	Medium distinctions between classes using a cubic distance metric. # neighbours=10	Hard interpretation
Weighted KNN 	85.5 %	86.7 %	Medium distinctions between classes using a distance weight. # neighbours=10	Hard interpretation
Ensemble			It melds results from many weak learners into one high-quality ensemble model. High accuracy and good performance for small to medium datasets	
Boosted trees 	98.0 %	98.6 %	It merges AdaBoost with Decision Tree learners	Hard interpretation
Bagged trees 	99.8 %	99.9 %	It merges Breiman's 'random forest' algorithm with Decision Tree learners. It tends to achieve high accuracies	Hard interpretation
Subspace discriminant 	65.2 %	68.9 %	It merges Subspace with Discriminant learners. Good for many predictors.	Hard interpretation
Subspace KNN 	66.3 %	74.2 %	It merges Subspace with Nearest neighbour learners. Good for many predictors	Hard interpretation
RUSBoosted trees 	92.5 %	93.1 %	It merges RUSBoost with Decision Tree learners. Good for skewed data	Hard interpretation

P = Number of predictors

Results in Table 7.3 shows a high accuracy (>80%) of predictions for most models, and especially for classifiers including fine decision trees learners such as *Ensemble-Bagged trees* (99.8% summer – 99.9% winter) and *Fine Tree* (99.8% summer – 100.0% winter), linear and quadratic discriminations such as *Linear SVM* (97.2% winter), *Quadratic SVM* (96.8% summer), and *Quadratic discriminant* (80.4% summer – 81.8% winter), and weighted distance learners such as *Weighted KNN* (85.5% summer – 86.7% winter). Only very few models achieved low scores ($\approx 65\%$), corresponding to classifiers implementing coarse and subspace learners. Very close similarities on the accuracy scores were identified between summer and winter datasets; however, the latter obtained slightly higher values.

Models with the highest accuracy scores (highlighted in bold in Table 7.3) were selected for further evaluation. Figures F1 to F10 in Appendix F show the performance assessment of selected models using confusion matrices and the results of *receiver operating characteristic* (ROC) curves¹⁷ calculated for each GIT class. Confusion matrices were calculated using the predictions on the held-out observations to identify areas where the model performed poorly. The diagonal cells in green show where the classifier performed well and classified observations of the true GIT class correctly.

Values of the *false positive rate* (FPR), *true positive rate* (TPR) and *area under curve* (AUC) are provided along confusion matrices to compare the predictability of each class. For instance, FPR of 0.1 means that the selected model assigned 10% of observations incorrectly to the actual class, while TPR of 0.8 indicates that the selected classifier assigned 80% of the observations to the positive class. The AUC measures the overall quality of the model per class, so larger AUC values indicates better classification performance (MathWorks, 2018b).

Results at class level show that FPRs were significantly low and AUCs considerable high for all selected models, while TPRs were relatively varied. This means that all classifiers tend to assign most observations correctly to actual GIT classes. *Fine tree* algorithms outperformed among classifiers by exhibiting a very high classification performance for all classes (average AUC of 99%); except for PV3 *Mixed grasses with shrubs and trees*, AQ6 *Water with scattered trees*, and PV7 *Mostly non-irrigated grasses with scattered trees* with 29%, 22%, and 12% of misclassifications respectively [Figure F1]. Similar high classification scores (AUCs $\approx 100\%$) for all GIT classes were obtained by the *Ensemble–*

¹⁷ In machine learning, a ROC curve is typically used to select a threshold for a classifier which maximises the true positives, while minimising the false positives. Values of the ROC curve (*i.e.* FPR, TPR and AUC) can also be interpreted as estimates of the performance of the classifier over its entire operating range.

bagged trees classifier –as it also implements a decision tree learner–, except for PV3 with only 44% of the observations correctly assigned to the actual class [Figure F10].

Linear and Quadratic SVM classifiers also achieved a considerably high classification performance for all classes (AUCs $\approx 100\%$) [Figures F3 and F8]; however, low classification rates (TPRs as percentages) can be seen for PV7 *Mostly non-irrigated grasses with scattered trees* (38%), PV8 *Mostly irrigated grasses with scattered trees* (50%), AQ6 *Water with scattered trees* (56%), AQ7 *Water with clustered trees* (67%), and MX8 *Mixed grasses with scattered trees* (60-71%). The rate of misclassifications for the remaining classes ranges from 1% to 25%.

The classification performance of the *Weighted KNN* classifier for the majority of classes was slightly lower than previously mentioned algorithms (average AUCs of 98%). The lowest rates of correctly classified classes corresponded to MX8 *Mixed grasses with scattered trees* (21%), MX3 *Mixed surface without trees* (32%), AQ6 *Water with scattered trees* (33%), and PV7 *Mostly non-irrigated grasses with scattered trees* (38%). Additionally, medium classification rates were obtained by IM2 *Mostly impervious with grasses* (56%), MX1 *Mostly non-irrigated grasses with impervious* (64%), and MX4 *Mixed grasses and bare soils* (66%), and AQ5 *Water with aligned trees* (68%) [Figure F4].

Quadratic discriminant classifier displayed the lowest classification performance among models and for most classes with a minimum AUC of 76% and average AUC of 93%. The lowest percentage of correctly classified GITs corresponded to PV8 (25%) *Mostly irrigated grasses with scattered trees*, PV5 (46%) *Mostly irrigated grasses with aligned trees* and AQ7 *Water with clustered trees* (50%), while misclassification rates of remaining GITs ranges from 6% to 37% [Figure F7].

7.3 Land surface temperature differences and cooling capacity of green infrastructure typologies

After classifying the study area into identifiable GITs, a comprehensive thermal evaluation was conducted involving the estimation of mean diurnal and nocturnal LST for each individual grid in summer and winter, and the subsequent analysis of the spatial and temporal LST variability and the cooling capacity of identified GITs.

7.3.1 Thermal differentiation of GITs

In summer, daytime and night-time thermal imagery were simultaneously available for a total of 23022 GITs; while in winter, thermal data were only available for 24948 GITs at

daytime and 23458 GITs at night-time. Figures 7.10 to 7.13 show the number of grids per GIT class for which mean LSTs were calculated for each season and time of the day. Typologies with less than 20 observations were excluded.

A general comparison between GITs in terms of their mean LSTs shows a clear differentiation among typologies; thus, further statistical analysis was carried out to examine their variability and the occurrence of outliers. Boxplots summarising the maximum, minimum, median, average and interquartile values of mean diurnal and nocturnal LSTs for each GIT and case study are presented in Figures 7.10 to 7.13. Detailed summary statistics of mean LSTs for each GIT are presented in Appendix G.

When analysing the inter-typology differences of boxplots, in a rank order –from one (warmest) to 14 (coldest)– and within particular subgroups (impervious, mixed, pervious and aquatic GITs), the following observations were made [Figures 7.10 and 7.13]:

A. Summer case study:

- Mean daytime LSTs varied significantly across the summer case study area with a maximum difference of 12.12°C between the warmest (IM1) and coldest (AQ1) GITs. However, this variance was less pronounced at night-time, with only 3.54°C between the highest (AQ1) and the lowest (PV1) recorded mean LSTs.
- The highest diurnal mean LSTs were achieved by *impervious* GITs, namely IM1 (38.13°C), IM2 (37.79°C), IM5 (37.55°C), IM4 (37.41°C) and IM6 (37.31°C). A second tier of warm GITs is comprised by a subset of *mixed* GITs with a considerable presence of impermeable surfaces (25-50% of the grid) corresponding to MX3 (36.09°C), MX7 (36.03°C), MX1 (35.72°C), MX5 (35.58°C) and MX9 (35.26°C). The average LST of previous subset was up to 2.23°C warmer than the average temperature of *pervious* GITs with more than 50% of non-irrigated surfaces (PV1//5/7/9) and 4.69°C warmer than *pervious* GITs with a substantial presence of irrigated grasses and trees (PV2/6/11).
- The lowest diurnal mean LSTs corresponded to open water AQ1 (26.01°C), while lower temperatures also occurred in classes with a high proportion of water and dense trees, such as AQ7 (27.88°C), AQ5 (28.14°C), AQ6 (28.78°C), and PV11 (29.95°C).
- At night, the highest mean LSTs were achieved by *aquatic* GITs such as AQ1 (24.66°C), AQ5 (24.00°C), AQ6 (23.94°C), AQ4 (23.90°C) and AQ7 (23.73°C). The second warmest group, with mean LSTs ranging from 22.19 to 23.16°C, corresponded to GITs comprising

a variety of impervious, non-irrigated grasses and trees. The lowest nocturnal temperatures occurred in treeless GITs with a large proportion of grasses such as PV1 (21.12°C), PV2 (21.20°C) and MX4 (21.37°C); followed by *pervious* GITs with aligned and dispersed trees (PV3/5/6/7/9) showing temperatures between 21.43 and 21.67°C.

- A repetitive pattern of ups and downs (spikes) on mean diurnal LSTs occurred between pairs of *mixed* and *pervious* GITs. Accordingly, GITs finishing with odd numbers (MX1/3/5/7/9; PV1/5/7/9/11) exhibited higher temperatures (from 1.87°C to 3.84°C) than typologies with even numbers (MX4/6/8/10; PV2/6) as the latter display a larger proportion of irrigated grasses and the presence of paved areas is negligible. These peaks were not so obvious for nocturnal LSTs, with differences between 0.08°C and 1.20°C.
- Distinct temperature variances were observed among forested GITs sharing the same configuration of trees (*i.e.* IM5, MX7/8, PV7/8) due to the disproportion in *pervious* and *impervious* surface fractions. For instance, typologies with dense and clustered trees (PV11, MX10) displayed lower mean diurnal LSTs (up to 5.35°C) than those with clusters of trees enclosed by impermeable surfaces (IM6, MX9). Similarly, GITs with scattered and aligned trees that were surrounded by irrigated grasses (*i.e.* PV6, MX8) were up to 6.09°C cooler than typologies encircled by abundant pavements and/or buildings (*i.e.* IM4, MX7). Although a similar situation occurred at night (except for *aquatic* GITs), the temperature differences were substantially lower with a maximum of 1.49°C.
- Conversely, a close similarity of mean LSTs was observed when forested GITs were compared within the same subgroup (*i.e.* *pervious*, *mixed*, etc.) regardless of tree configuration. At daytime, it was identified a maximum difference of 0.24°C among IM4/5/6; 0.39°C among PV5/7/9; 0.57°C among MX6/8/10; 0.77°C among MX5/7/9; and 0.9°C among AQ5/6/7. Whereas a similar situation occurred at night, the temperature variance is considerable smaller for all subsets, ranging from 0.14 to 0.29°C.
- Intra-typology variability of diurnal LSTs (length of boxplots) is relatively homogenous for most classes (except for IM1), with generally symmetrical boxes and whiskers. This indicates a not significant departure from normality. Outliers mostly occurred in *impervious* GITs and PV11, with special attention to IM1 that also exhibited the larger temperature variation among classes. Outliers rarely occurred in the rest of the typologies. Nocturnal LSTs show a similar pattern with relatively symmetrical boxes and whiskers; nonetheless, a larger disparity on LST variation was observed among typologies. A larger occurrence of outliers was identified in *impervious* and *mixed* GITs compared to daytime.

Case study 1: Summer daytime

Boxplots with mean LSTs

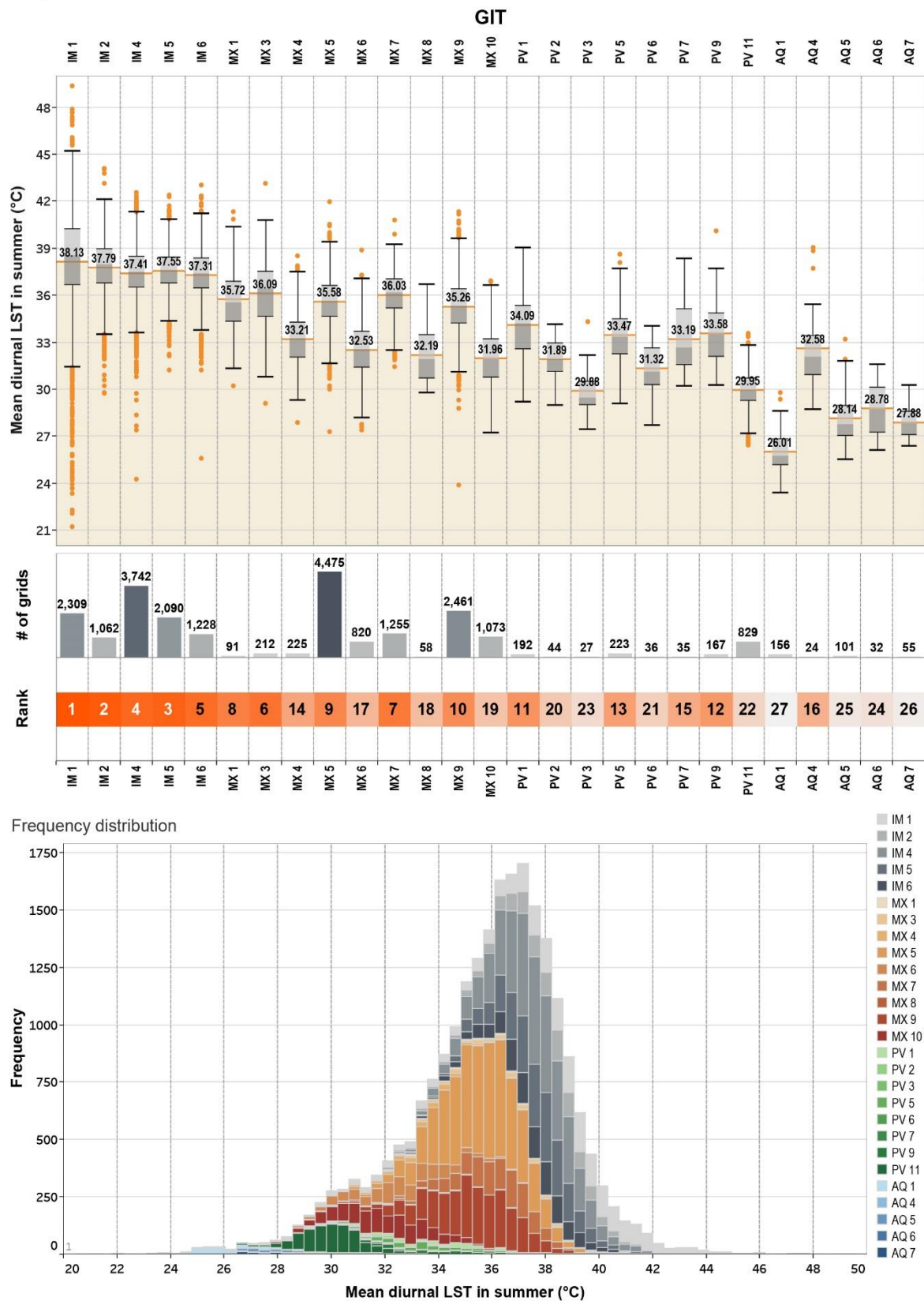


Figure 7.10 Box-plots, number of samples and frequency distribution of mean diurnal LSTs recorded in summer. Average mean LSTs estimated per each GIT are presented in bold.

Case study 1: Summer night-time

Boxplots with mean LSTs

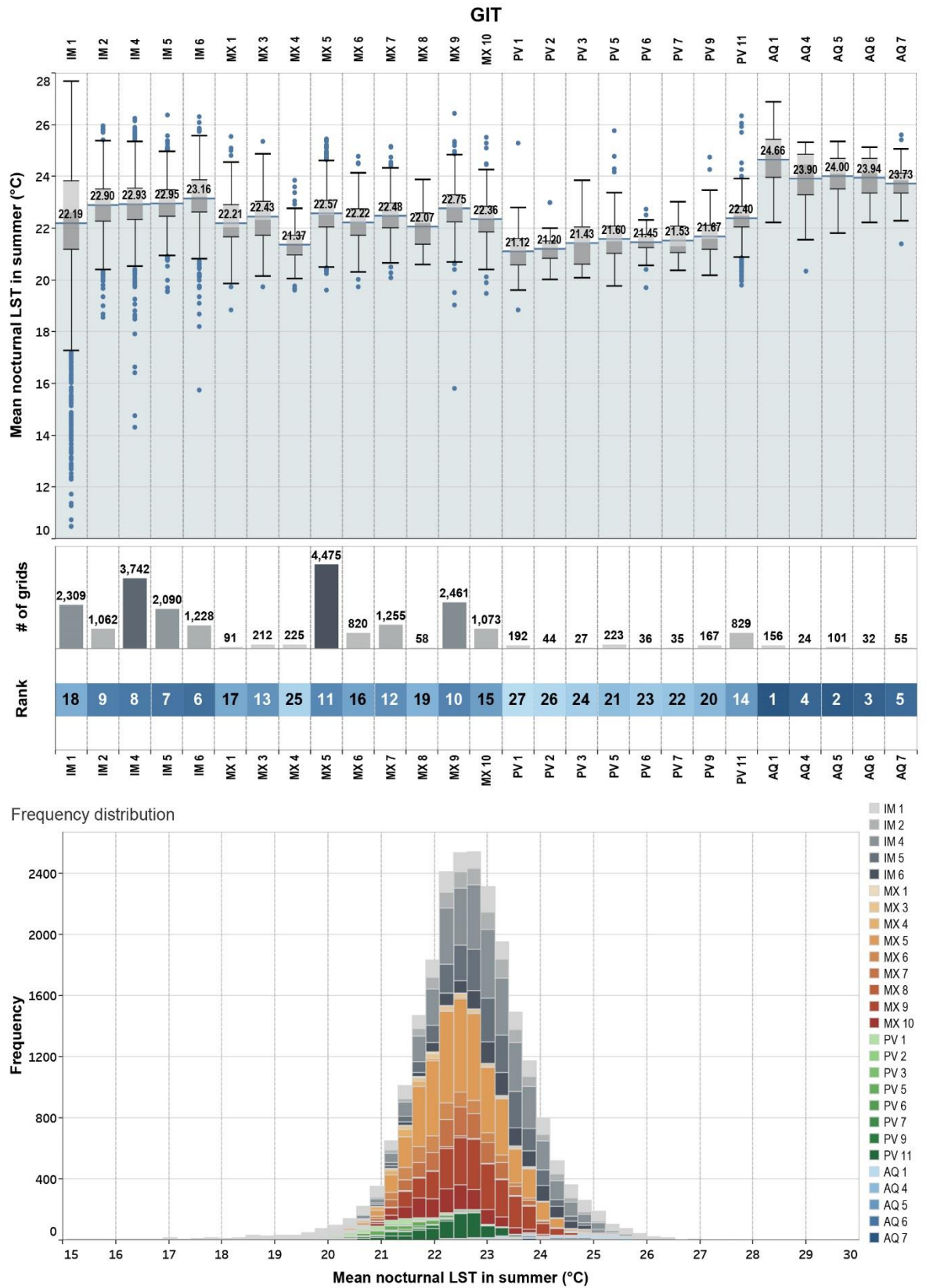


Figure 7.11 Box-plots, number of samples and frequency distribution of mean nocturnal LSTs recorded in summer. Average mean LSTs estimated per each GIT are presented in bold.

B. Winter case study:

- The winter case study shows similar LST patterns, differences and variability than results in summer. Nonetheless, the maximum LST differences between the warmest and coldest GITs were less pronounced with only 6.27°C during the day and 4.34°C at night, but still considerable.
- At daytime, treeless *impervious* GITs (IM1/2/3) displayed the highest mean LSTs (13.95°-14.25°C); while *aquatic* GITs and *Dense trees* (PV11) showed the lowest (7.98°-9.18°C). Within the *mixed* and *pervious* subgroups, GITs with a considerable presence of paved and non-irrigated surfaces (11.53°-13.27°C) were warmer than those with a large proportion of irrigated surfaces (10.53°-11.08°C).
- During night-time, open water AQ1 (5.87°C) was significantly warmer than other typologies; while temperature differences among remaining GITs were not as pronounced as daytime, ranging from 2.12°C to 3.75°C. Likewise summer, lower nocturnal temperatures occurred in treeless GITs with a large proportion of grasses, namely PV1, PV2, MX4 and MX1 (1.53°-1.93°C).
- Repetitive peaks on mean diurnal LSTs also occurred between pairs of *mixed* and *pervious* GITs; however, temperature variances between typologies with and without irrigated surfaces were smaller in winter (0.24 to 1.99°C) than summer (from 1.87°C to 3.84°C). In contrast, nocturnal spikes of LST are relatively more evident in winter than summer, with differences of up to 1.57°C.
- Temperature differences among GITs sharing the same tree configuration (*i.e.* IM6, MX9, MX10, PV9, PV10) were evident and followed a similar pattern than summer, although variances were less marked with a maximum of 2.85°C during day and 1.49°C during night. When comparing forested GITs within subgroups and irrespective of the spatial configuration of trees, a maximum difference of 0.63°C was detected for IM4/5/6, MX5/7/9, PV6/8/10 and AQ5/6/7. However, this is not the case of MX6/8/10, with a maximum variance of 1.28°C among classes. Similar temperature differences within each subgroup were also observed at night-time.
- Intra-typology variability of diurnal LSTs is relatively homogeneous and symmetrical for most GITs –except for *aquatic* GITs. This indicates a no significant departure from normality for most typologies. Outliers mostly occurred in *impervious* GITs and PV11 with

special attention to IM1 which shows the larger temperature variability among classes. Overall, outliers were less frequent in winter than summer. At night, there is an increased variation and asymmetry of boxplots which indicate a departure from normality, especially for *aquatic* GITs. Also, occurrences of outliers were more common in *impervious* GITs.

Aggregated histograms representing the frequency distributions of mean LSTs for all GITs in summer and winter are presented in [Figures 7.10 to 7.13](#). GIT subgroups are displayed with four distinct sequential colours for an easier identification of typologies. In summer, the most frequent diurnal temperatures are between 35.0°C and 38.0°C and display a bimodal distribution with two LSTs peaks, a smaller at 30°-32°C and a larger at 36°C. Compared to other subgroups the mean diurnal LSTs of *pervious* and *aquatic* GITs have larger frequencies (wide temperature range) with most bars shifted to the left [[Figure 7.10](#)]. In contrast, mean nocturnal LSTs for all GITs displayed a unimodal distribution with most temperatures ranging between 22°C and 23°C [[Figure 7.11](#)].

Winter histograms display a similar pattern with the most frequent diurnal temperatures ranging between 12.0 °C and 14.0°C; however, the bimodal distribution is more pronounced than summer with two distinct peaks, a smaller at 9°-10°C and a larger at 12.5°-14°C. Compared to other subgroups the mean diurnal LSTs of *impervious* GITs are relatively higher with most frequency bars shifted to the right [[Figure 7.12](#)]. Although mean nocturnal LSTs for all GITs displayed a unimodal distribution with most temperatures ranging between 2.5 and 3.5°C, *pervious* GITs have no specific range with large frequencies and most frequency bars shifted to the left [[Figure 7.13](#)].

Normality tests for each GIT were carried out as it is an important assumption to consider for the subsequent analysis of variance and due to the large variability of the number of samples among typologies. The analysis of normality of LST distribution for each GIT has also served to corroborate the relevance of previous observations and for an exploratory data analysis before the formulation of the predictive models presented in Section 7.4.

[Table 7.4](#) summarises the frequency distribution of mean diurnal LSTs in summer for each GIT with a fitted Gaussian curve representing a normal distribution. A summary of histograms for both case studies and times of the day are provided in Appendix G. The *Kolmogorov-Smirnov* test is a nonparametric test that has been applied in similar climate studies to determine if two samples (or datasets) have significantly different distributions (Geletič et al., 2016; Geletič et al., 2017; Zheng et al., 2017). Results of the *Kolmogorov-Smirnov* test are presented alongside graphs in Appendix G with significant departures from normality corresponding to *p*-values less than 0.05.

Case study 2: Winter daytime
Boxplots with mean LSTs

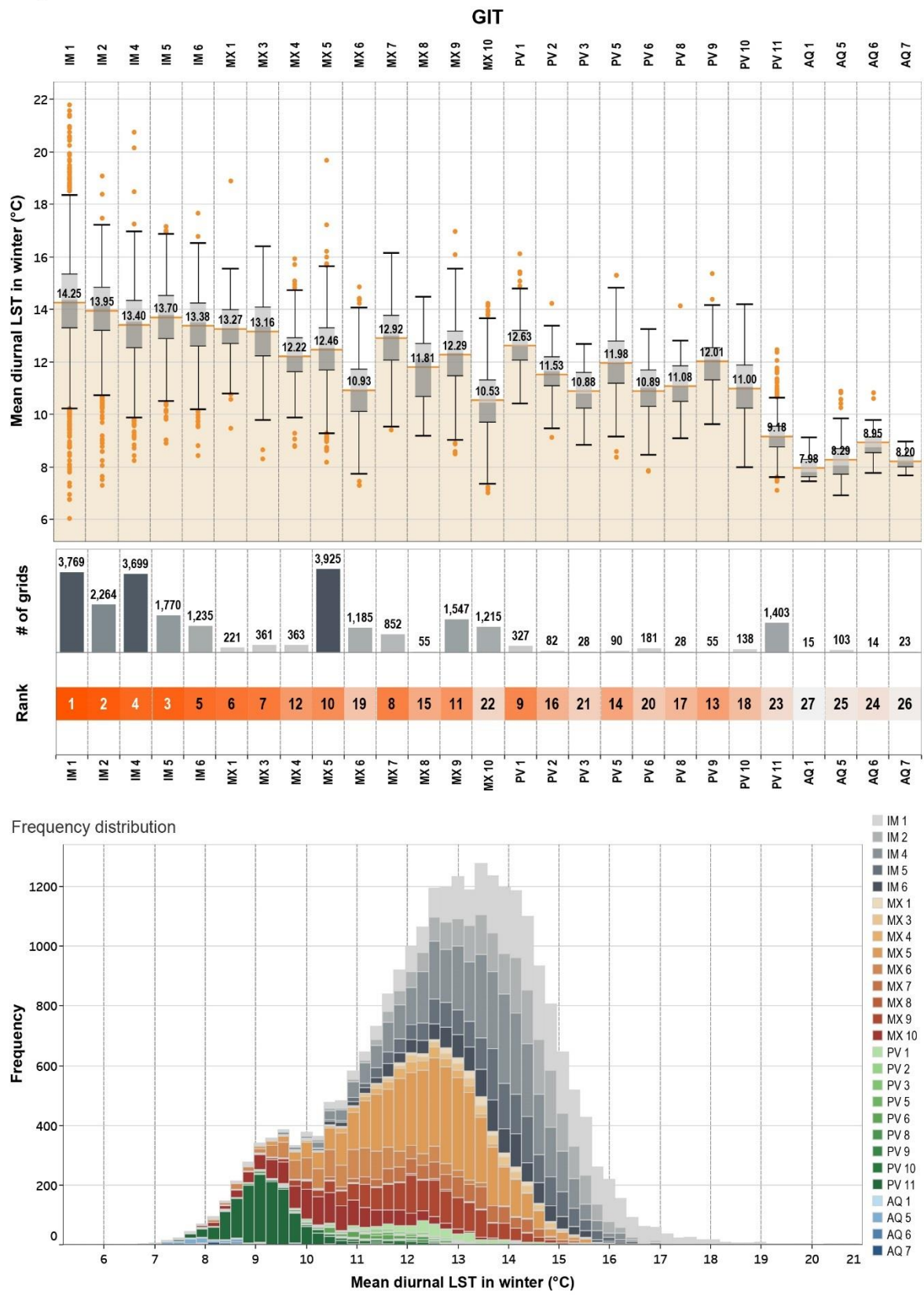


Figure 7.12 Box-plots, number of samples and frequency distribution of mean diurnal LSTs recorded in winter. Average mean LSTs estimated per each GIT are presented in bold.

Case study 2: Winter night-time

Boxplots with mean LSTs

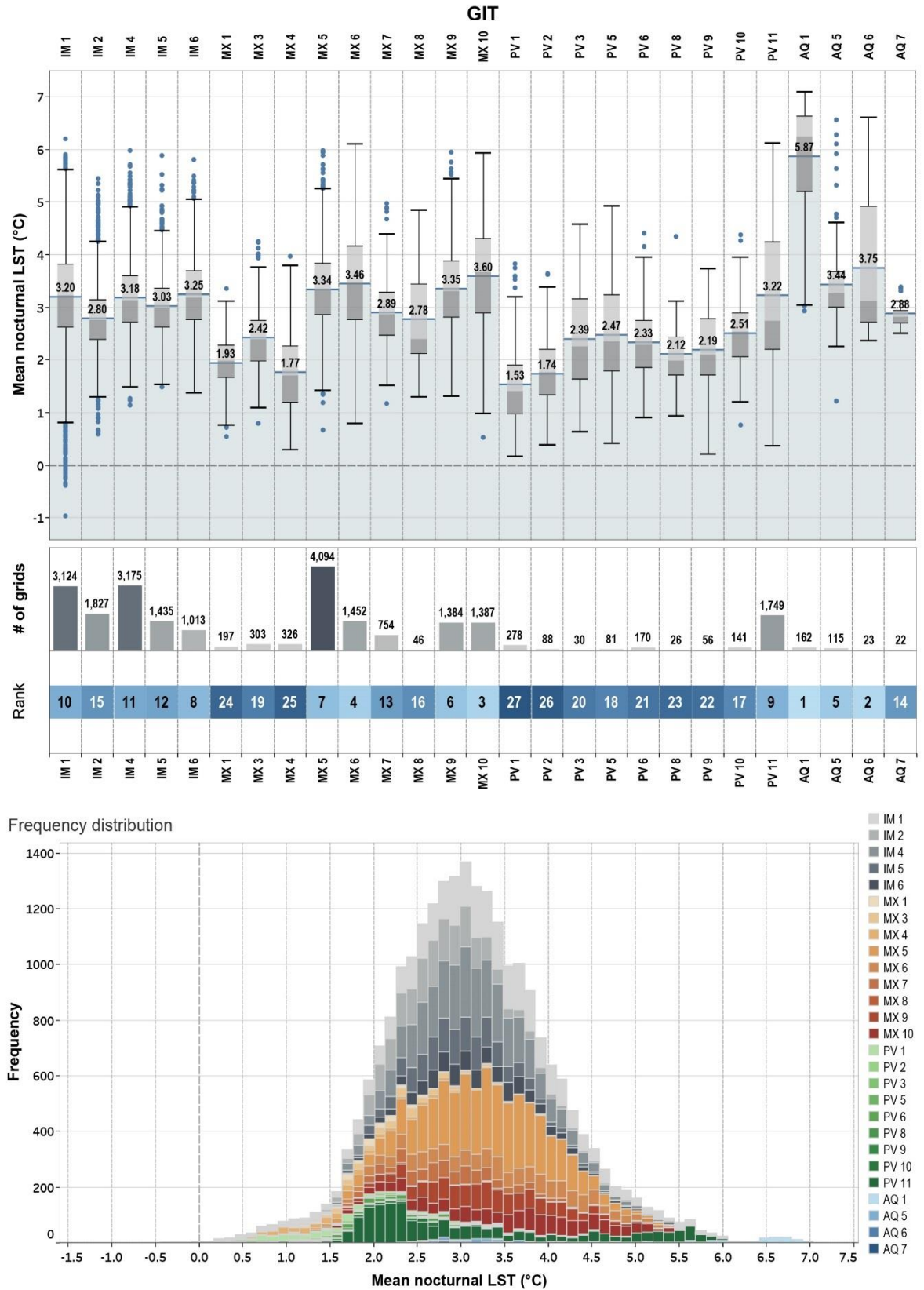


Figure 7.13 Box-plots, number of samples and frequency distribution of mean nocturnal LSTs recorded in winter. Average mean LSTs estimated per each GIT are presented in bold.

Results show that in summer departures from normality were more common at day (48.1% of GITs) than at night (37.0%) and mostly occurred for *impervious* and *aquatic* GITs [Tables G2 and G3]. Overall, departures from normality were more common in winter than summer. These were more common at night (63.0% of GITs), especially for *impervious*, *aquatic* and *mixed* GITs. In contrast, departures from normality at daytime (51.9%) mostly occurred for *impervious* and *mixed* GITs [Tables G5 and G6].

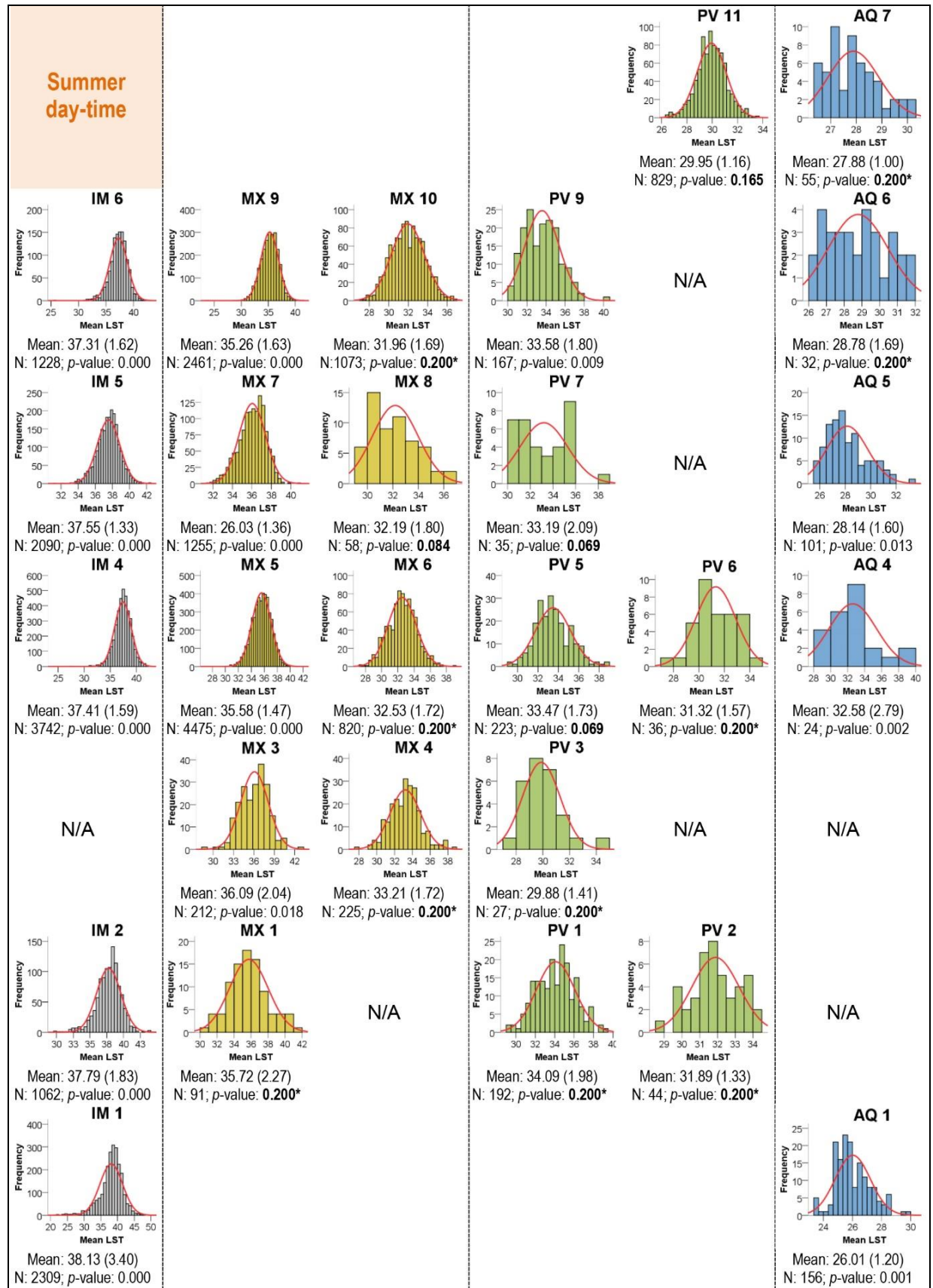
Results of normality tests and comparison of LST variances indicate that *analysis of variance* (ANOVA) can be employed to determine whether the differences in mean LSTs among GITs described before are statistically significant or not. Since the assumption of homogeneity of variances was violated for both case studies as assessed by *Levene's* test for equality of variances ($p=0.000$), *one-way Welch-ANOVA* and *Games-Howell post hoc test* were chosen for multiple comparisons.

In summer, results show statistically significant differences among mean diurnal LSTs (Welch's $F(26, 838.410, p=0.000)$) and nocturnal LSTs (Welch's $F(26, 839.110, p=0.000)$) for all GITs. In winter, results also reveal statistically significant differences among mean diurnal LSTs (Welch's $F(26, 660.848, p=0.000)$) and nocturnal LSTs (Welch's $F(26, 868.509, p=0.000)$) for all GITs.

Subsequently, results of the *Games-Howell post hoc* tests for pairwise comparisons were interpreted in the form of binary matrices (diurnal versus nocturnal results) for each case study [Figures 7.14 and 7.16]. Points in table's cells indicate *no statistically significant difference* in mean LSTs between two specific GITs ($p\text{-value} > 0.05$); so, these represent a *poor* differentiation between a pair of GITs in terms of their mean LSTs. Conversely, empty cells indicate a *statistically significant difference* between two typologies ($p\text{-value} < 0.05$); hence, a *good* thermal differentiation between two typologies.

Considering that well-delineated GITs should exhibit distinct LST variability (Bartesaghi Koc, Osmond, Peters et al., 2018; Geletič et al., 2016; Geletič & Lehnert, 2016); Figures 7.15 and 7.17 present estimations of the total number of multiple comparison tests in which statistically significant differences ($p < 0.05$) among GITs were identified. The scores –expressed in percentage– allow the identification of typologies with unique thermal profiles (those with higher scores). By analysing the results of multiple comparisons presented in Figures 7.14 to 7.17, the following observations and patterns were identified:

Table 7.4 Frequency distribution of mean diurnal LSTs in summer for each GIT with a fitted normal distribution and results of the Kolmogorov-Smirnov test (N=sample size; standard deviations are in parenthesis, p -values <0.05 indicates a non-normal distribution, * This is a lower bound of the true significance).



- Overall, it is observed that significant LST differences prevail for most GITs at daytime (86.9% in summer and 85.5% in winter) and night-time (80.9% in summer and 73.8% in winter); however, temperature differences are more distinguishable in summer and during the day.

A. *Summer case study:*

- Mean LSTs of all *impervious* GITs were well differentiated at daytime especially IM1, IM2 (100.0%) followed by IM5, IM6 (>96%), and IM4 (92.3%). Although most *impervious* GITs were also well delineated at night, their temperatures were not significantly different to AQ4 as it also comprises impermeable surfaces. In addition, IM1 was relatively distinguishable at night (73.1%) and exhibited similar temperatures to some *mixed* and *pervious* GITs.
- Most *mixed* GITs were well differentiated at daytime, especially MX9 (96.2%) and MX5, MX7 (92.3%). At night-time, MX9 was also well distinguished (100.0%); nonetheless, treeless GITs such as MX1 and MX3 registered similar LSTs than GITs with few or aligned trees (MX5 to MX8). Also, the thermal profiles of MX4 and MX8 were not significantly different from *pervious* GITs with no or few trees (PV1 to PV7).
- At daytime, *pervious* GITs were relatively well differentiated from other typologies (average 81.3%), particularly PV11 was the most distinguishable within this subgroup (92.3%). Compared to previous subgroups, the effect of tree configuration on diurnal temperature differences was not significant. In fact, PV7 (65.4%) was the least distinguishable as mean diurnal LSTs were similar to *mixed* and *pervious* GITs dominated by non-irrigated grasses. Despite disparities in tree arrangement and proportion/type of low plants, there were no significant temperature differences among *pervious* GITs at night-time, except for PV11 that has a considerable amount of tree canopy and bushes.
- A comparable situation occurs with *aquatic* GITs that are better differentiated at daytime than night-time. Accordingly, AQ1 (100.0%) was the most distinguishable during the day, while AQ4 was the least distinguishable at both daytime (61.5%) and night-time (69.2%).

B. Winter case study:

- Most *impervious* GITs were well differentiated at daytime, especially IM1, IM2, IM5 that achieved the highest scores among all typologies (100.0%). Conversely, at night-time the thermal profiles of GITs within this subgroup were comparable to those of MX8 and forested *aquatic* GITs (AQ5 to AQ7).
- At daytime, mean LSTs of *mixed* GITs were significantly different within the same subgroup, yet relatively distinguishable compared to average temperatures from some *pervious* GITs (*i.e.* PV3, PV5, PV8, PV9). MX7 and MX10 were the most distinguishable during the day (96.2 and 92.3% respectively); in contrast, MX8 was poorly distinguished at both day (69.2%) and night (38.5%). Also, thermal conditions from forested *mixed* GITs (MX5 to MX10) were not significantly different from those of forested *aquatic* GITs (AQ5 to AQ7).
- Treeless *pervious* GITs (PV1, PV2) were well differentiated at both times of the day (>76%). On the contrary, forested *pervious* GITs were relatively distinguishable at daytime (average 77.5%), but poorly differentiated at night (average 63.5%). This ambivalence typical from forested typologies was also observed in PV11 that was better differentiated at daytime (96.2%) than night-time (69.2%). Only in this subgroup, the influence of tree configuration on LSTs was negligible, as there were no statistically significant differences among *pervious* GITs with scattered, aligned and clustered trees.
- A similar pattern is observed in *aquatic* GITs that became less distinguishable as the proportion of trees and paved areas increase; especially at night-time. Except for AQ1 that was well differentiated at both times of the day (>88.5%), mean LSTs of *aquatic* GITs were very similar to several *mixed* and *impervious* GITs as explained before.

Detailed explanations and discussion on the reasons behind the abovementioned results are provided in Section 8.4.

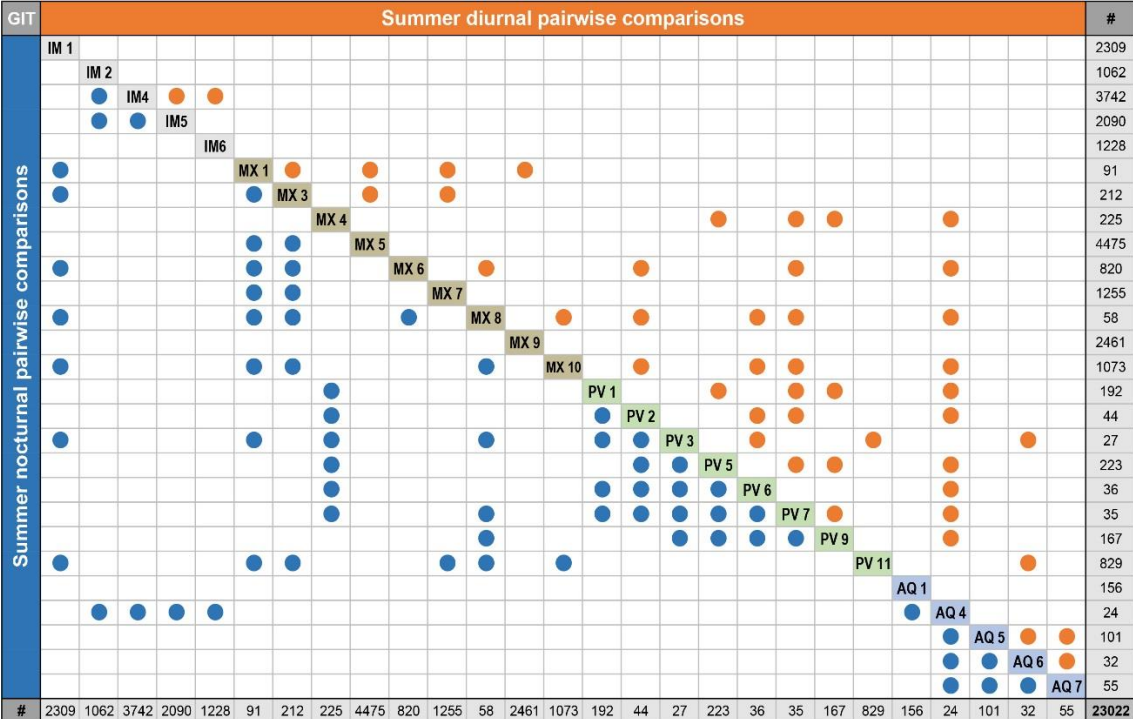


Figure 7.14 Binary matrix showing the results of the Games-Howell post hoc tests for all pairwise comparisons of mean diurnal and nocturnal LSTs in summer. Points in cells indicate pairs of GITs for which mean LSTs were not significantly different ($p > 0.05$).

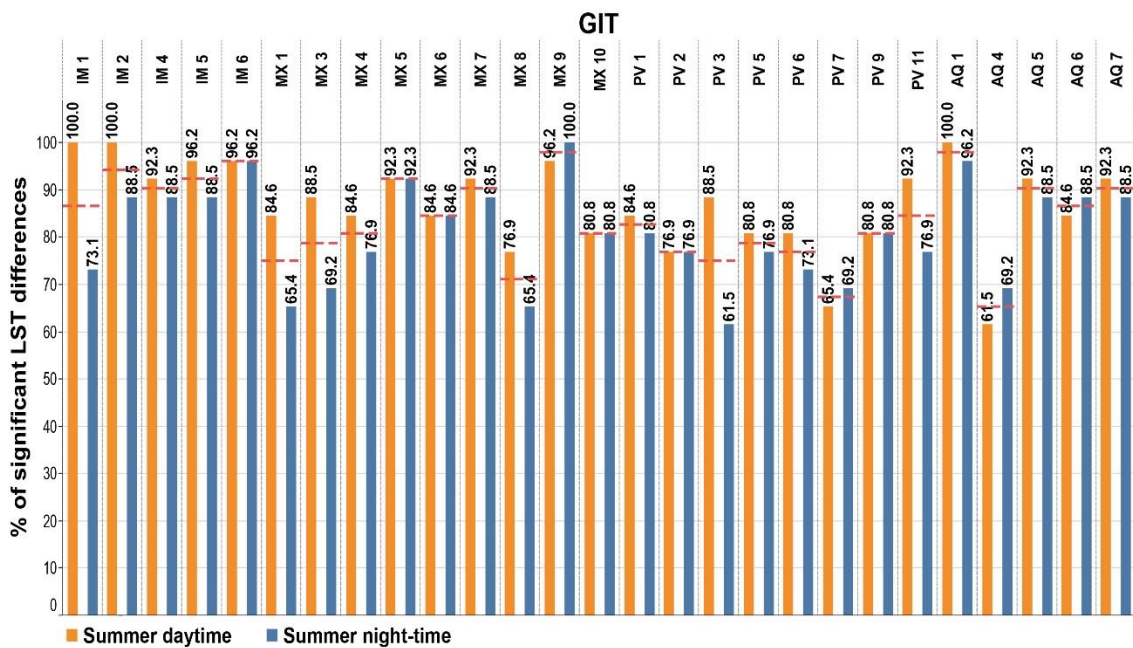


Figure 7.15 Percentage of significant diurnal and nocturnal LST differences in summer ($p < 0.05$) achieved by each GIT as a result of multiple comparison tests. Dotted lines represent average values for both times of the day.

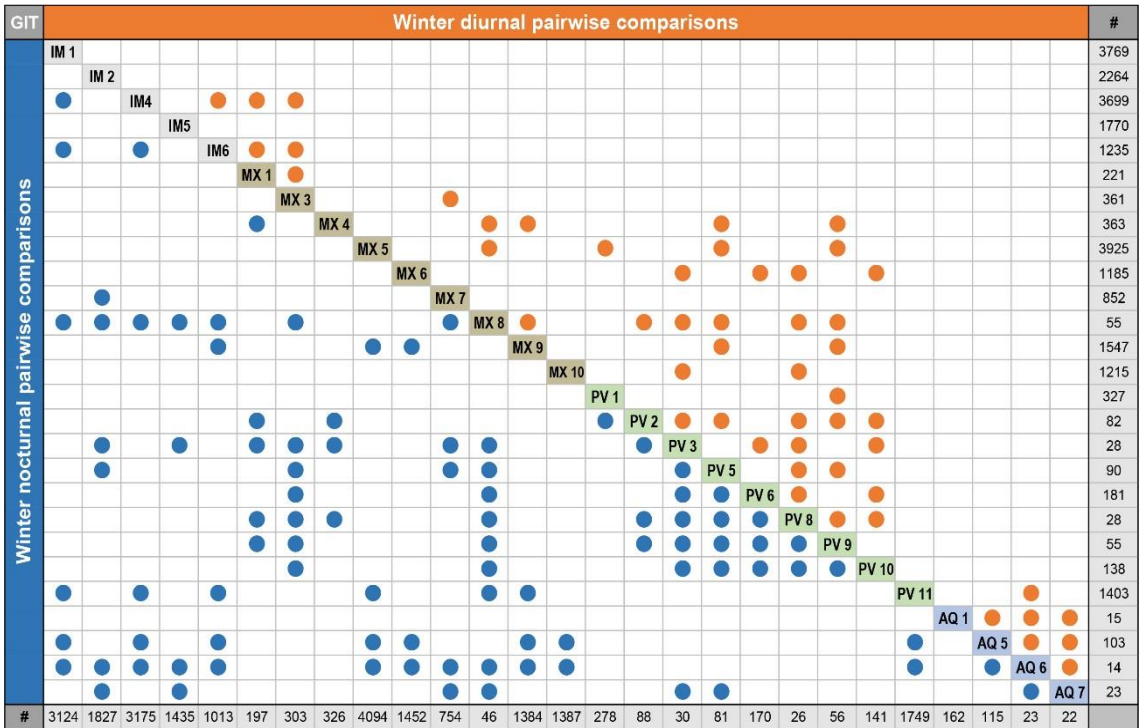


Figure 7.16 Binary matrix showing the results of the Games-Howell post hoc tests for all pairwise comparisons of mean diurnal and nocturnal LSTs in winter. Points in cells indicate pairs of GITs for which mean LSTs were not significantly different ($p > 0.05$).

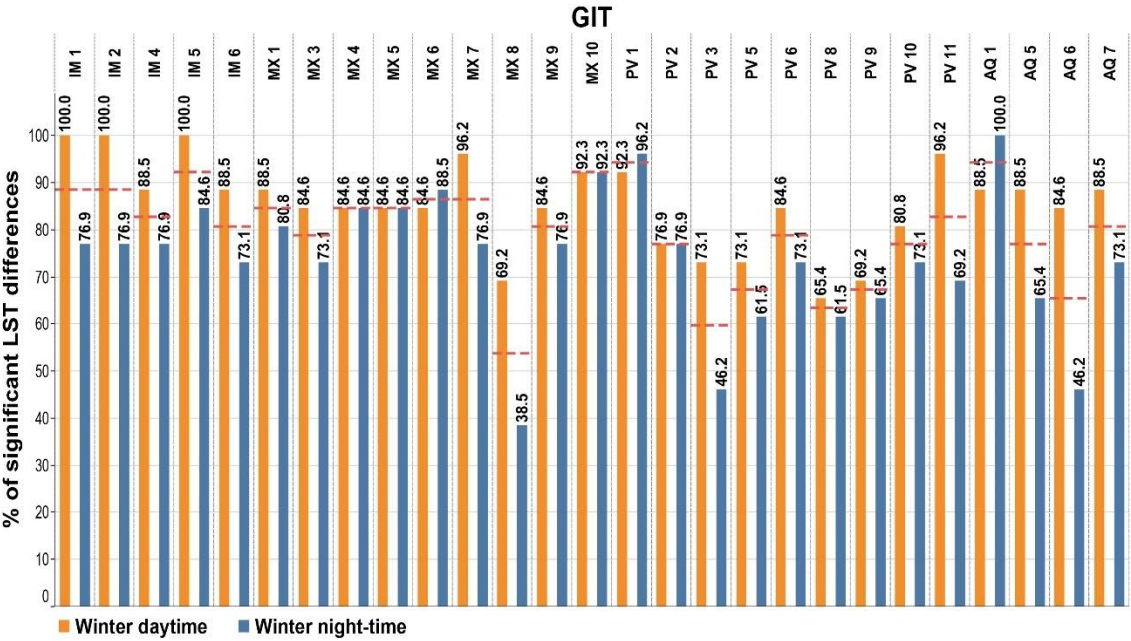


Figure 7.17 Percentage of significant diurnal and nocturnal LST differences in winter ($p < 0.05$) achieved by each GIT as a result of multiple comparison tests. Dotted lines represent average values for both times of the day.

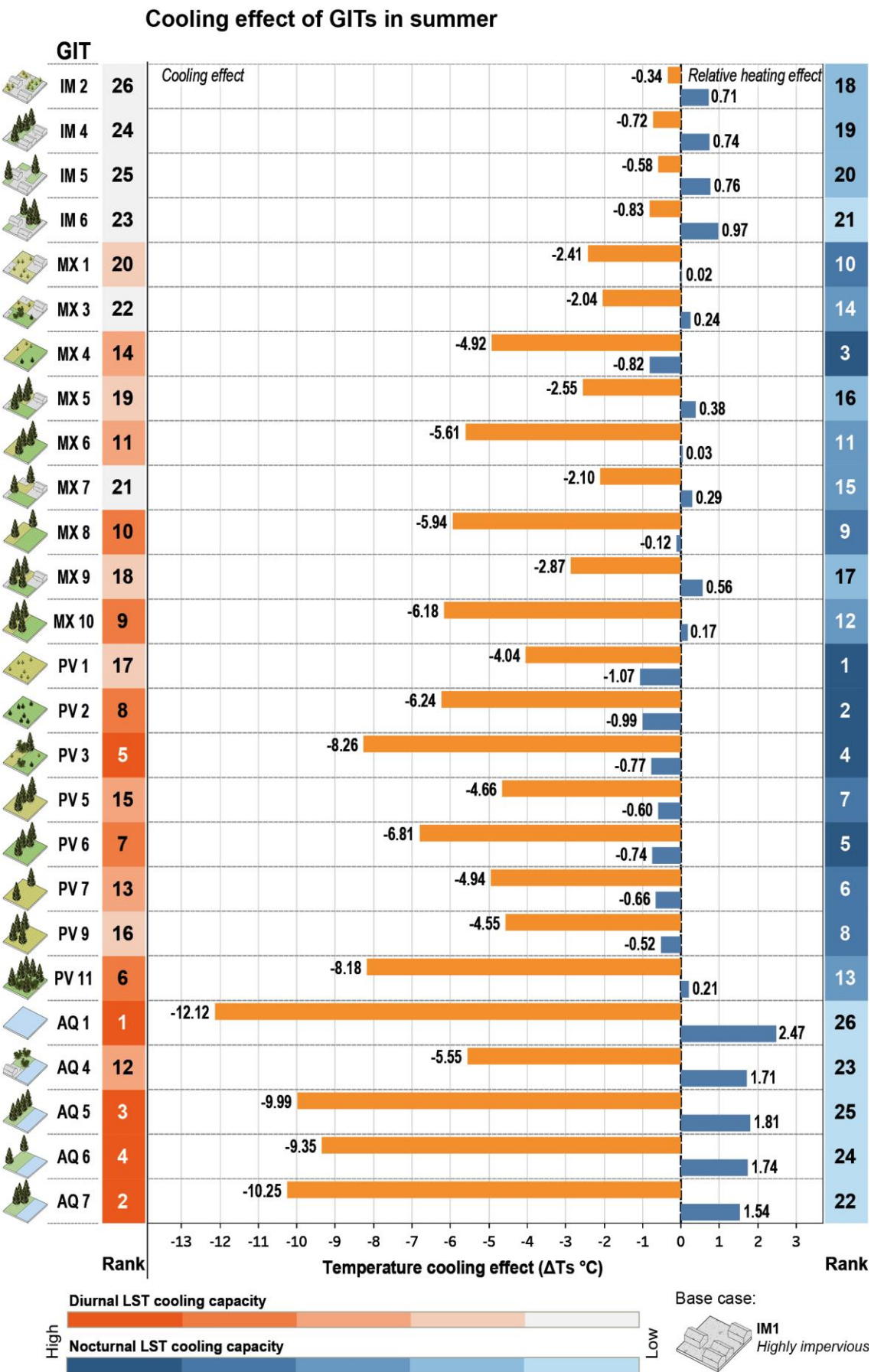


Figure 7.18 Cooling effect of GITs in summer relative to the base case (IM1 *Highly impervious*).

Cooling effect of GITs in winter

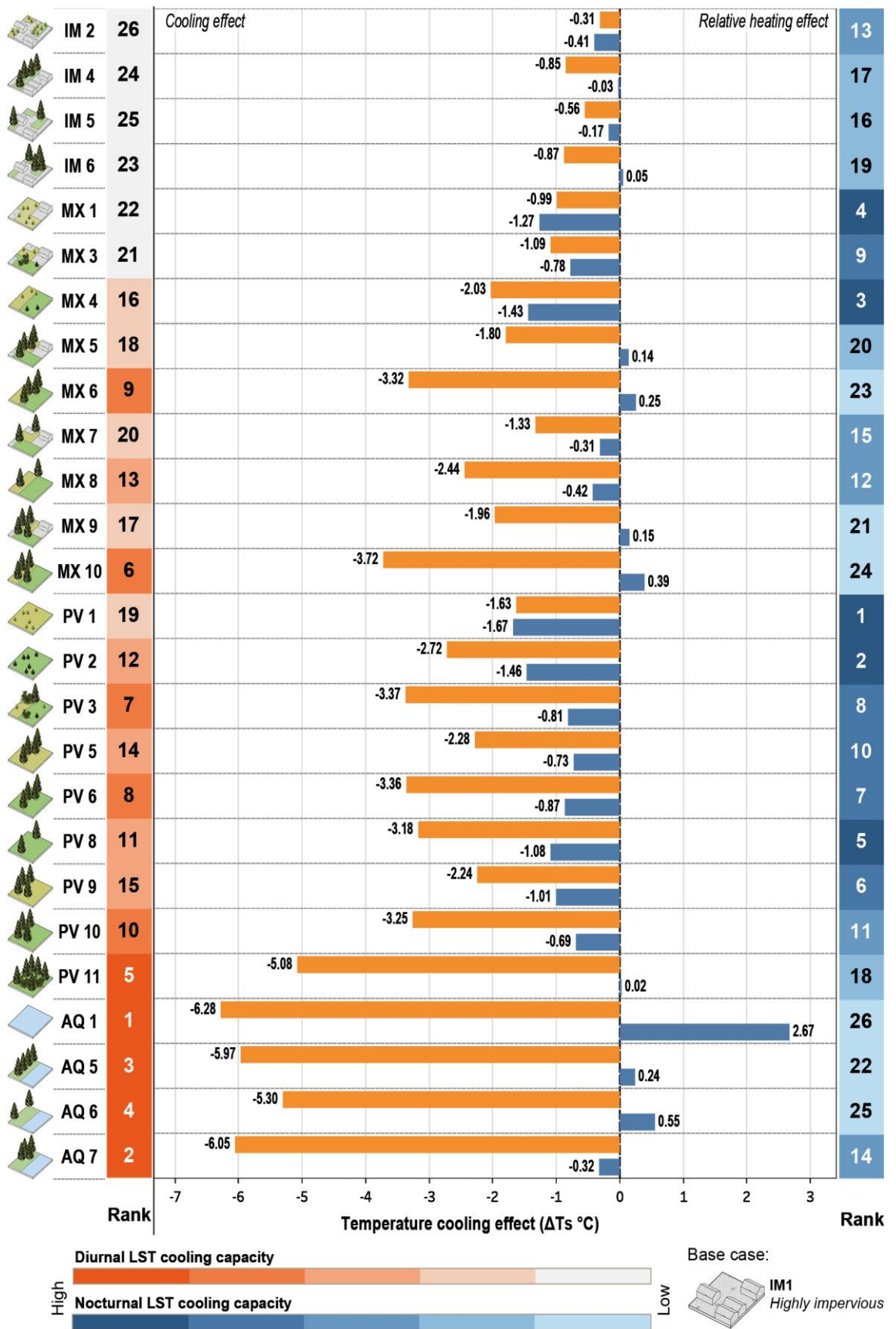


Figure 7.19 Cooling effect of GITs in winter relative to the base case (IM1 Highly impervious).

7.3.2 Assessing the cooling effects of GITs

The overall cooling effect (ΔT_s , °C) of different types of green infrastructure is expressed here as the reduction in mean LST produced by a given typology (as a combination of different surface covers and tree arrangements), relative to that measured in a reference case corresponding to highly impervious contexts with no vegetation or the IM1 *Highly impervious* typology. Figures 7.18 and 7.19 illustrate the diurnal and nocturnal cooling effects of different GITs in summer and winter respectively. Negative values indicate cooling while positive values indicate relative heating effects compared to the base case.

In summertime, the maximum LSTs reductions were obtained in the daytime hours by the *aquatic* and *pervious* GIT subgroups. The largest temperature departures from the base case (between 9.99°C and 12.12°C) were achieved by *aquatic* GITs combining water and vegetated surfaces (AQ1, AQ5-7); except for AQ4 that comprised up to 35% of paved areas and reduced temperatures by only 5.55°C.

The effect of tree configuration on cooling capacity was negligible when GITs from the same subgroup shared the same proportion of surface covers (*i.e.* PV5/7/9 or MX6/8/10), while considerably large temperature reductions (between 5.61°C and 8.26°C) were achieved by irrigated grasses and shrubs when combined with dense, clustered and aligned trees (PV3/6/11, MX6/8/10). In contrast, trees (with different spatial configurations) were only capable to reduce LSTs by 2.10°C when surrounded by mixed surfaces (MX5/7/9) and by 4.94°C when combined with non-irrigated grasses (PV5/7/9).

In the absence of trees, irrigated grasses (PV2) exceeded the cooling capacity of non-irrigated low plants (PV1) by 2.2°C. Lower cooling capacities (between 2.04°C and 4.92°C) were observed for treeless GITs when grasses with different irrigation regimes were combined with paved areas (MX1/3/4). The lowest cooling capacity (between 0.34°C and 0.83°C) was registered by *impervious* GITs (IM2/4/5/6) with a limited amount of vegetation [Figure 7.18].

During the night, the cooling effects of vegetation shows a reverse pattern for most typologies. Compared to highly impervious areas (IM1), *aquatic* and *impervious* GITs provided a relative heating effect of up to 2.47°C and 0.97°C respectively. *Mixed* GITs and dense trees (PV11) were warmer than the base case by 0.03°-0.56°C; however, the presence of irrigated grasses reduced this relative heating effect (between 0.21°C and 1.38°C) as occurred with MX4 and MX8. In contrast, *pervious* GIT was the only subgroup that contributed to reduce LSTs in a relatively same proportion (between 0.52°C and 1.07°C), yet this was not as significant as during the day.

In wintertime, the largest cooling capacity (between 5.08°C and 6.28°C) was observed for *aquatic* GITs (AQ1, AQ5/6/7) and dense trees (PV11). Trees (in different arrangements) surrounded by non-irrigated grasses and mixed surfaces (PV9/5, MX5/7/8/9) were not as effective in reducing LSTs (between 1.33°C and 2.28°C) as when surrounded by irrigated grasses (MX6/10, PV3/6/8/10) (between 3.18°C and 3.72°C).

In the absence of trees, irrigated grasses (PV2) surpassed the cooling effect of non-irrigated low plants (PV1) by 1.09°C and had a similar cooling capacity as typologies with scattered trees. Low plants with diverse irrigation regimes (MX4) reduced temperatures by 2.03°C, and by 1.09°C when combined with impervious surfaces (MX1, MX3). The lowest cooling capacity (between 0.31°C and 0.87°C) was observed for *impervious* GITs (IM2/4/5/6) [Figure 7.19].

During night-time, the cooling capacity of most GITs was considerably greater than summer as mostly *aquatic* GITs provided a considerable heating effect. The largest cooling capacity (1.27°-1.67°C) was achieved by treeless GITs (PV1/2, MX1/4) with considerable amount of grasses. GITs combining scattered trees and irrigated grasses (PV3/8/6) caused temperature reductions between 0.81°C and 1.08°C; while a comparable cooling capacity (0.69° to 1.08°C) was also observed when trees (in different arrangements) were encircled by a large proportion of grasses (irrigated and non-irrigated). Lower LST reductions (0.03°-0.42°C) occurred when aligned or scattered trees were added to paved areas (MX7/8, IM4-5). In contrast, open water (AQ1) provide the largest heating effect of 2.67°C and increased nocturnal LTSs between 0.24°C and 0.55°C when combined with aligned and scattered trees respectively. Conversely, water surfaces combined with clustered trees (AQ7) caused a temperature reduction of 0.32°C. Dense, clustered and aligned trees also provided a relative heating effect of up to 0.39°C when combined with mixed grasses and/or impervious surfaces (IM6, MX5/6/9/10, PV11).

7.3.2.1 Correlation between vegetation abundance and cooling capacity of GITs

As mentioned in Section 3.8, the effect of vegetation on SUHI mitigation has been extensively studied by examining the relationship between LSTs and vegetation abundance –usually described by vegetation indices such as NDVI or fractional vegetation covers (Weng, 2009).

In this section, three directions were chosen to analyse the correlation between the cooling effects of GITs and the amount of vegetation. First, the TVX (thermal-vegetation index) approach (Carlson et al., 1994; Quattrochi & Ridd, 1994) was implemented by combining

LSTs and NDVI values from all observations (or samples) in a scatterplot to analyse their associations and the effect of wetness (*i.e.* irrigation, evapotranspiration, etc.) in thermal cooling (Carlson, 2007). Second, it was conducted a statistical analysis between the cooling capacity (calculated in previous section) and mean NDVI and fractional vegetation cover averaged for each GIT class. Third, a hierarchical cluster analysis was conducted to partition terrestrial GITs into subsets of similar cooling capacity; represented here by the nearest mean LST reduction of typologies at daytime and night-time, and for both seasons.

TVX analysis of NDVI-LST relationship

Figure 7.20 presents a TVX matrix of scatterplots of NDVI values plotted against mean diurnal and nocturnal LSTs for summer and winter seasons. Given that water bodies show a different thermal behaviour and higher heat capacity than terrestrial surfaces (Oke, 1992; Zhao, 2018), *aquatic* GITs were excluded and new results compared to scatterplots including all GITs. Except for nocturnal LSTs in winter, TVX scatterplots including all GITs resulted in a typical triangular pattern with distinct *warm* and *cold edges* that also correspond to driest and wettest grids respectively (Carlson, 2007). These shapes are better defined for diurnal temperatures and summer; in contrast, triangular shapes are not well preserved when *aquatic* GITs are excluded.

Scatterplots with well-defined triangular patterns (S-d1, W-d1) exhibit a sharp *warm edge* defined by the right side of the data envelope that corresponds to dry surfaces (Carlson et al., 1994; Carlson, 2007). Accordingly, it is observed a decrease in LSTs with increasing NDVI and evapotranspiration which are typical of *pervious* GITs with irrigated grasses and dense tree canopy (dark green dots). Conversely, higher LSTs are correlated with lower NDVI and drier surfaces corresponding to *impervious* GITs (grey dots) and treeless GITs with non-irrigated grasses and paved areas (light brown/green dots). The bottom vertices of triangles show a smaller variation in LSTs due to the presence of dense vegetation; in contrast, the top vertices exhibit a larger variation in LSTs linked to *impervious* GITs, especially IM1 *Highly impervious*.

A clear *cold edge* of the data envelope is also well defined in diurnal scatterplots (S-d1, W-d1), exhibiting a small tail toward low NDVI values [Figure 7.20]. This edge comprises the lowest LSTs that are associated to fully wetted surfaces with high vegetation (high NDVI) and water (low NDVI) content. Hence, *aquatic* GITs (blue dots) and *pervious* GITs with trees over irrigated grasses (dark green dots) can be recognised on this side of the triangle. Scatterplots with poorly defined triangular patterns correspond to LSTs (S-n1, W-n1) in which a *cold edge* cannot be identified as water bodies exhibit high nocturnal LSTs.

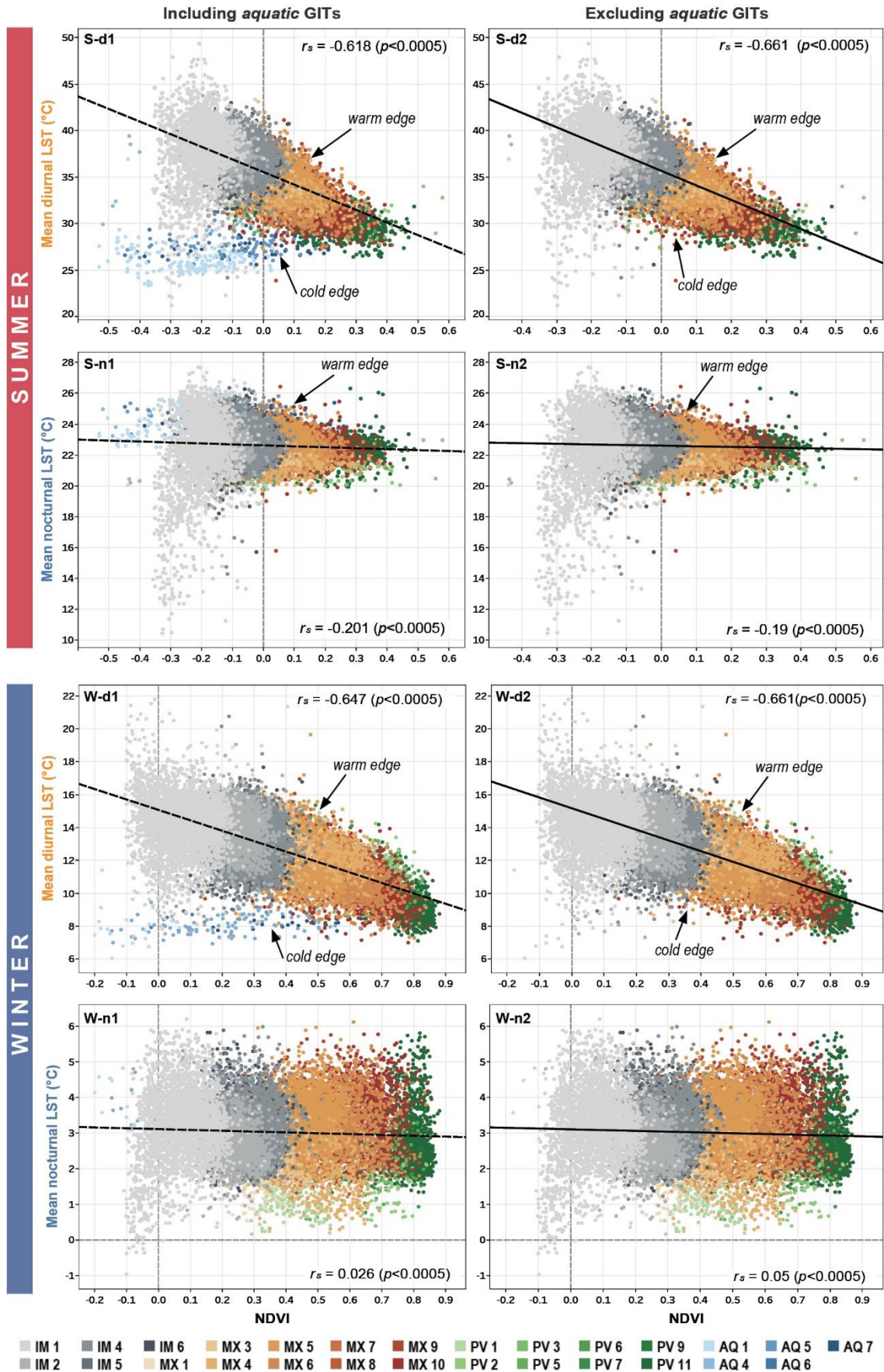


Figure 7.20 TVX matrix with scatterplots of mean NDVI versus mean diurnal and nocturnal LSTs for summer and winter times. Sequential colours represent each GIT subgroup.

Most scatterplots in Figure 7.20 exhibit a typical slope (also referred as TVX slope) toward the left, that indicate a negative correlation between NDVI and LSTs (decreasing LSTs with increasing vegetation fraction); however, these relationships varied during the day and between seasons. Results of the Spearman's correlations¹⁸ for all samples (including *aquatic* GITs) shows a moderate negative correlation between diurnal LSTs and NDVI values in summer ($r_s=-0.618$, $p<0.0005$) and winter ($r_s=-0.647$, $p<0.0005$) respectively. Conversely, weak and no relationships were identified between nocturnal LSTs and NDVI values in summertime ($r_s=-0.201$, $p<0.0005$) and wintertime ($r_s=0.026$, $p<0.0005$) respectively [Figure 7.20].

Nonetheless, TVX scatterplots include a large number of observations reflecting a full range of water and ground surfaces with different fractional vegetation cover and wetness. As suggested by Carlson (2007), observations corresponding to standing water were excluded to favour monotonic relationships and reduce their outlying effect. After discarding *aquatic* GITs, slight improvements were achieved in diurnal LST-NDVI relationships for both summertime ($r_s=-0.661$, $p<0.0005$) and wintertime ($r_s=-0.661$, $p<0.0005$) (S-d2, W-d2). This moderate correlation can be attributed to the large disparity of temperatures observed for the *impervious* and *mixed* subgroups. On the other hand, the results of nocturnal LSTs remained unchanged for both seasons (S-n2, W-n2). Further analysis on these findings is provided in Section 8.4.

Statistical analysis

Correlation analysis and simple linear regression were used to understand the statistical relationship between the LST reductions achieved by each GIT (summarised in Figures 7.18 and 7.19), and different indicators of vegetation abundance. As previously suggested, *aquatic* GITs were excluded from this analysis to favour linear relationships and minimise their outlying effect as the thermal behaviour and cooling mechanisms of aquatic surfaces differ from those of terrestrial surfaces.

Values of mean NDVI, pervious fraction (aggregated high, medium and low fractional surface covers), and tree cover fraction were averaged per typology and used as indicators of vegetation abundance. Statistics (means and standard deviations) per GIT class are presented in Appendix G [Table G7].

The bivariate Pearson's correlation coefficients (r) between vegetation abundance descriptors and the cooling capacity of GITs are shown in Table 7.5. Figure 7.21 presents

¹⁸ Spearman's rank-order correlation test was selected since the assumption of normality was violated by all variables as assessed by the Kolmogorov-Smirnov test ($p=0.000$).

the results of simple linear regressions between vegetation-related indicators and LST reductions achieved by typologies.

Table 7.5 Bivariate correlations between mean NDVI and vegetation abundance indicators.

Season	Time of day	LST reduction / Mean NDVI	LST reduction / Mean pervious fraction	LST reduction / Mean tree cover fraction	
Summer	Daytime	-0.879**	-0.899**	-0.529*	
	Night-time	-0.428*	-0.738**	0.215	
Winter	Daytime	-0.952**	-0.841**	-0.737**	
	Night-time	-0.189	-0.469*	0.557**	
Correlation strengths	0.01-0.19 Negligible	0.2-0.39 Weak	0.4-0.59 Moderate	0.6-0.79 Strong	0.8-1.0 Very strong

** Correlation is significant at the 0.01 level (2-tailed)

* Correlation is significant at the 0.05 level (2-tailed)

Based on bivariate correlations [Table 7.5], the impact of vegetation abundance on diurnal and nocturnal cooling capacity (LST reduction) of terrestrial GITs is better explained in summer by the proportion of pervious surfaces rather than by the mean NDVI or amount of tree cover. In contrast, in winter the cooling effects of typologies are better explained by the photosynthetic activity (represented by NDVI) during the daytime, while by the percent of trees at night-time.

By inspecting the results of simple linear regressions [Figure 7.21], mean NDVI and mean pervious fraction have very-/strong negative relationships with LST reductions at daytime for both summer ($R^2=0.74$, $R^2=0.82$, $p<0.0001$) and winter ($R^2=0.91$, $R^2=0.67$, $p<0.0001$). In comparison, at night-time percent of perviousness ($R^2=0.75$ $p<0.0001$) has a strong effect on cooling capacities compared to mean NDVI that showed weak ($R^2=0.21$ $p<0.05$) or inexistent associations ($R^2=0.01$ $p=0.61$) with LST reductions.

On the other hand, tree coverage has a moderate negative influence on diurnal LST reductions in winter ($R^2=0.541$ $p<0.0001$) while a weak and statistically not significant influence in summer ($R^2=0.26$, $p<0.189$). Although the coefficient of determination between nocturnal cooling effects and the proportion of trees was relatively low in winter ($R^2=0.37$, $p<0.005$), this was negligible and statistically not significant in summer ($R^2=0.05$, $p=0.334$).

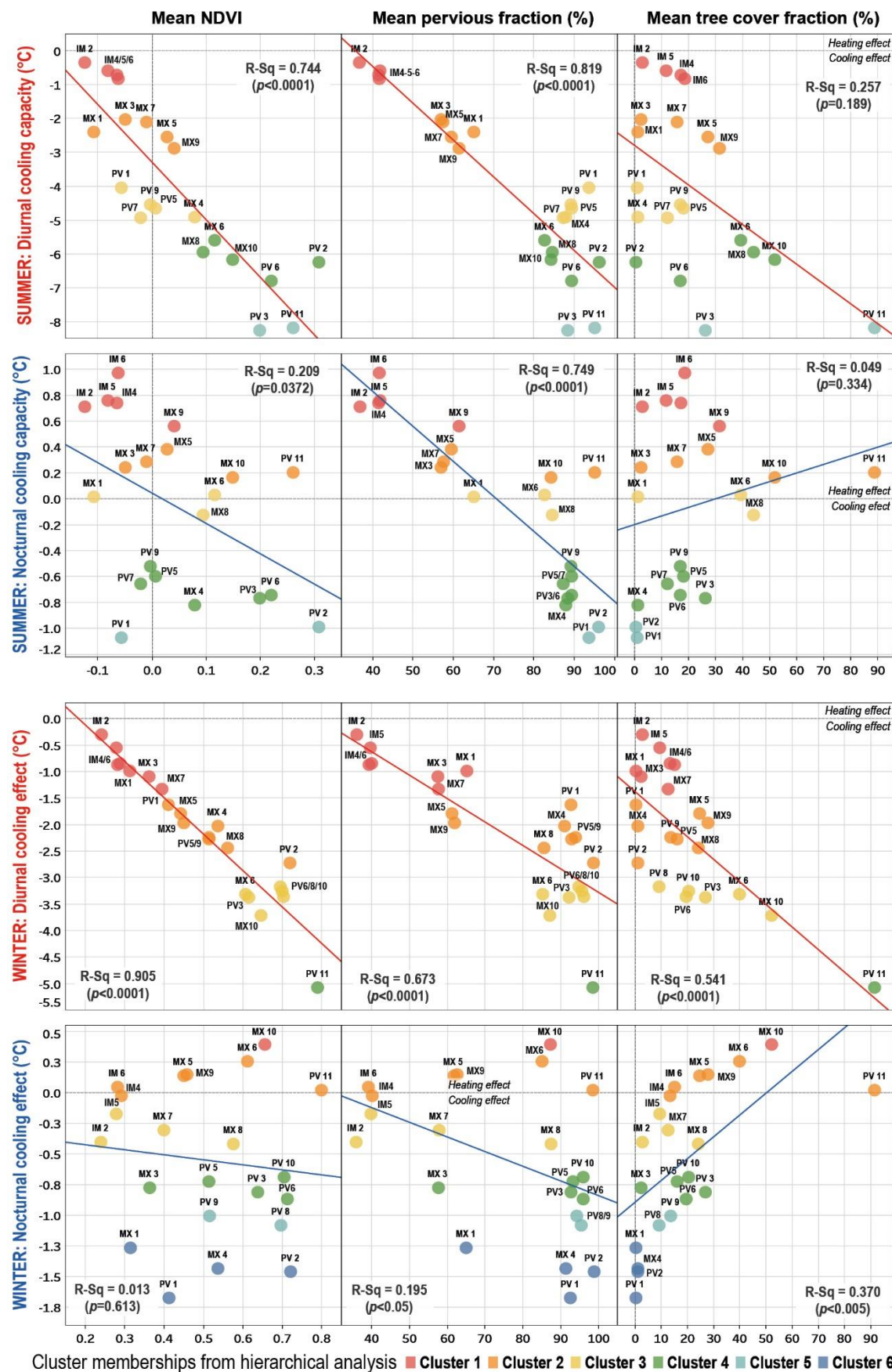


Figure 7.21 Results of simple linear regressions between vegetation abundance descriptors and diurnal and nocturnal LST reductions of terrestrial GITs in summer and winter. Clusters identified through hierarchical analysis are represented by distinct colours.

Cluster analysis

A hierarchical cluster analysis was conducted in SPSS (IBM, 2016) to partition terrestrial GITs into subsets based on the average LST reduction (or cooling capacity) of each typology at daytime and night-time, and for both seasons. A *between-groups linkage* method with *Squared Euclidean distance* was implemented as cluster method. Statistical results (dendrograms) are provided in Appendix G [Table G8].

Generally, terrestrial GITs can be grouped into four to six clusters –depending on the season and time of the day– each exhibiting distinct thermal cooling capacities. Cluster memberships are listed in Table G8 and represented in Figure 7.21 by different colours. Detailed lists and discussion on the cooling capacity and significance of detected GIT clusters is provided in Section 8.4.2. These clusters are consistent with GIT subgroups presented in Figure 4.8 and confirm the thermal differentiations described in Section 7.3.1.

In Figure 7.21 it can be observed that the proximity of cluster members vary considerably between scatterplots from different seasons and time of the day since their relative location within the data space also depends on the vegetation-related descriptor used in the regression. For instance, *Mixed surfaces with aligned* (MX5) and *Clustered trees* (MX9) are separated from other cluster members when using the percent of perviousness instead of mean NDVI to predict their diurnal cooling effect in winter. Similarly, whereas PV11 *Dense trees* registered similar LST reductions than *impervious* GITs (IM4/5/6), this has a considerably higher proportion of tree cover, so it is visually segregated from the rest of the group (see winter night-time scatterplot).

7.4 Prediction of land surface temperatures

In regard to the third objective of this thesis (see Section 1.3), this section describes the methodology and the results of the statistical models developed for a more accurate and precise prediction of LSTs based on GIT classifications. The following statistical analysis is intended to:

1. propose a set of equations to predict diurnal and nocturnal LSTs at local-scale for each season using a combination of functional, morphological and configurational variables listed in Table 5.1.
2. understand the relationships between LSTs and different functional, structural and configurational attributes of green infrastructure.

3. calculate the extent and magnitude of the contributions of green infrastructure in the urban microclimate to determine the amount of vegetation cover and type of changes in built surfaces necessary to reduce LSTs more effectively.

7.4.1 Multiple linear regressions

On a first stage, multiple linear regression (MLR) was used to produce predictive models using all the independent variables listed in Table 5.1 as predictors in SPSS software (IBM, 2016). Since the abundance of certain roofing materials associated with building fractions proved to be an important factor contributing on LSTs differences within a same GIT class (see Section 8.4.2); fraction of total impervious surfaces (*Fr_Tot_Imp*) is excluded and replaced instead by the fraction of impervious building (*Fr_Imp_Bld*) and ground (*Fr_Imp_Grnd*) surfaces.

In climate research, MLR has been widely applied for the analysis of spatial data and to predict a continuous dependent variable (*i.e.* air and surface temperatures) based on multiple independent variables (Adams & Smith, 2014; Cao et al., 2010; Heusinkveld et al., 2014; Kong et al., 2016; Li et al., 2012; Onishi et al., 2010; Sun & Chen, 2012; Zhou et al., 2011). MLR also enables to determine the overall fit (variance explained) of the model and the relative contribution of each temperature predictor to the total variance explained (Laerd Statistics, 2015).

The classic Ordinary Least Square (OLS) method was implemented to produce MLR models for each time of the day (daytime and night-time) and season (summer and winter). The OLS estimator aims to minimise the sum of squared vertical distances between the observed dependent variable and those predicted by the linear function for a number of observations (n) of a given dataset; and can be expressed by the following equation:

$$y_i = \beta_0 + \sum_{j=1..p} \beta_j x_{ij} + \varepsilon_i \quad [\text{Eq. 7.1}]$$

where y_i is the *dependent variable* (in this case LST), β_0 is the *constant* (or intercept) of the model, β_j are the *regression coefficients* for j independent variables, x_{ij} are the *independent variables* and ε_i is the *error term* for spatial units indexed by i . Before running a multiple regression, major assumptions or conditions have to be fulfilled to generate a valid OLS model and these are:

Assumption #1, non-autocorrelation: there should be an independence of observations and their residuals. This means that errors from adjacent observations are not correlated,

including temporal and spatial dependencies between measurements. This condition was initially checked using *Durbin-Watson statistic* (Durbin & Watson, 1951) as part of the MLR procedure in SPSS. As MLRs tested positively for spatial autocorrelation, this condition was further investigated (see Section 7.4.2.1) using the *Moran's I* test, *Lagrange Multiplier (LM)* test and *Local Indicators of Spatial Association (LISA)* (Anselin, 1995) using GeoDA (Anselin et al., 2006). This analysis helped in identifying appropriate spatial regression models presented in Section 7.4.2.2;

Assumption #2, exogeneity: this means that errors (also known as residuals) from regression are not correlated with the regressors, so they have a mean of zero.

Assumption #3, linearity: a linear relationship should exist between the dependent variable and each of the independent variables separately and collectively. This was assessed by inspecting the scatterplots of the *studentised residuals* against the *unstandardized predicted values*;

Assumption #4, homoskedasticity: this means that residuals have a constant variance, in other words, the errors are equally distributed along the line of best fit for all values of the predicted dependent variable. To check for homoskedasticity, the *Breusch-Pagan* (Breusch & Pagan, 1979) and *Koenker-Bassett* (Koenker & Bassett, 1982) tests were used along with the scatterplots generated for the previous assumption;

Assumption #5, no multicollinearity: this means that two or more independent variables must not be highly correlated with each other as this leads to problems with understanding the individual contribution of each independent variable to the variance of the dependent variable. The violation of this condition was determined by inspecting *Pearson's correlation coefficients* between variables and the *Variance Inflation Factor (VIF)* values generated as part of the MLR procedure in SPSS;

Assumption #6, no significant outliers: this means that the data should not contain significant outliers, high leverage points or highly influential points. This condition was assessed by checking the *leverage points*, *influential points*, and *Cook's Distance* (Cook, 1977) values generated for *n* observations of each dataset as part of the multiple regressions; and

Assumption #7, normality of residuals: this condition establishes that residuals (errors) should be approximately normally distributed. The *Jarque-Bera test* (Jarque & Bera, 1987), *P-P plots* and *histograms* with superimposed normal curves were used to check for this assumption.

Table 7.6 Summary statistics of Ordinary Least Square (OLS) regression models for the prediction of diurnal and nocturnal LSTs in summer and winter using all independent variables.

Season	SUMMER		WINTER	
Time of day	Day-time	Night-time	Day-time	Night-time
Model (dependent variable)	1A (DAY_T _s)	2A (NIG_T _s)	3A (DAY_T _s)	4A (NIG_T _s)
Regression	OLS	OLS	OLS	OLS
N cases	23022	23022	24948	23458
R	0.802	0.626	0.777	0.737
R ²	0.643	0.391	0.603	0.543
Adjusted R²	0.643	0.391	0.603	0.543
Standard Error (S.E)	1.763	0.937	1.196	0.626
F-statistic	3767.942	1345.201	3446.427	2537.152
df1	11	11	11	11
df2	23010	23010	24936	23446
Sig. F (p-value)	0.000	0.000	0.000	0.000
Log-Likelihood	-45720.3	-31171.7	-39856.2	-22298.8
Akaike information criterion (AIC)	91464.5	62367.4	79736.3	44621.7
Schwarz criterion (SC)	91561.1	62463.9	79833.8	44718.4
Durbin-Watson	1.065	0.943	1.015	1.074
Multicollin. cond. number	218.001	218.001	199.910	185.675
Jarque-Bera (Sig.) DF	107148.5507 (0.000) 2	140438.0544 (0.000) 2	2452.7424 (0.000) 2	1964.0973 (0.000) 2
Breusch-Pagan (Sig.) DF	23670.8246 (0.000) 11	34768.8775 (0.000) 11	2438.8289 (0.000) 11	4684.8502 (0.000) 11
Koenker-Bassett (Sig.) DF	3934.6607 (0.000) 11	5033.0809 (0.000) 11	1461.0536 (0.000) 11	2774.7879 (0.000) 11
Predictors	(Constant), Fr_Imp_Bld, Fr_Imp_Grnd, Fr_Low_NIR, Fr_Low_IRR, Fr_Med_Veg, Fr_High_Veg, Fr_Tot_Wat, Mean_NDVI, CIRCLE_AM, nLSI, Altitude			

Initially, four OLS models (1A, 2A, 3A, 4A) were produced in SPSS for the prediction of diurnal and nocturnal LSTs in summer and winter using all independent variables listed in [Table 5.1](#) (excepting *Fr_Tot_Imp* as explained before) that were calculated for each grid cell (or spatial unit) as explained in Section 6.3.4. The total number of cases (or observations) used in each model correspond to the total number of valid grid cells correctly classified for each case study as described in Section 7.2.2. The resulting statistics for the four models are summarised in [Table 7.6](#).

The *coefficient of determination* –also referred as R^2 – provides a measure of how well performs a predictive model, in other words, it represents the proportion of variance in the dependent variable that is explained by the independent variables (Laerd Statistics, 2015). As R^2 is based on the sample, this is positively-biased by the number of cases. The *adjusted R^2* corrects for this bias as it only increases if additional variables improve the model performance more than would be expected by chance; hence, it is a better indicator of the *goodness-of-fit* of models (Theil, 1961).

The results of OLS regressions indicate that the 11 independent variables statistically significantly predicted diurnal LSTs in summer, $F(11, 23010) = 3767.942, p < 0.001, adj.R^2 = 0.643$; and winter $F(11, 24936) = 3446.427, p < 0.001, adj.R^2 = 0.603$, indicating a *moderate* performance for these models. The same number of variables also predicted the nocturnal LSTs in summer, $F(11, 23010) = 1345.201, p < 0.001, adj.R^2 = 0.391$; and winter $F(11, 23446) = 2537.152, p < 0.001, adj.R^2 = 0.543$, showing a *weak* and *moderate* performance respectively.

By checking the regression assumptions, there were no leverage values greater than 0.2, and values for Cook's distance above one. Nevertheless, the models violated several statistical assumptions which suggests stability problems and compromise the reliability of the regression models. First, the assumption of normality of residuals was violated, as assessed by *P-P plots* and the *Jarque-Bera test* ($p < 0.001$). Second, the *Durbin-Watson statistic*¹⁹ generated relatively low values of 1.065, 0.943, 1.015 and 1.074 for models 1A, 2A, 3A and 4A respectively [Table 7.6]; which shows a significant positive correlation between residuals.

Third, the results of the *Breusch-Pagan* and *Koenker-Bassett* tests shows there is evidence of serious heteroskedasticity (no constant variance of errors) as *p-values* for both tests²⁰ were less than 0.05 [Table 7.6], so the null-hypothesis of homoskedasticity was rejected (Breusch & Pagan, 1979; Koenker & Bassett, 1982).

Fourth, the explanatory variables are significantly correlated with each other and provide insufficient separate information as demonstrated by the very high multicollinearity condition numbers (218.01 for model 1A and 2A, 199.91 for model 3A, and 185.675 for model 4A) that suggest considerable problems for values over 30 [Table 7.6] (Anselin,

¹⁹ The *Durbin-Watson statistic* ranges from 0 to 4, with an approximate value of 2 indicating no correlation between residuals; < 2 indicating a positive and > 2 a negative correlation respectively (Durbin and Watson, 1951).

²⁰ Interpretation of results from both tests is similar, except that the residuals in the *Koenker-Bassett* test are studentised; therefore, they are more robust to outliers or non-normality (Anselin, 2005).

2005). The *Variance Inflation Factor* (VIF) also provides information regarding the magnitude of the multicollinearity between variables. If a tolerance value is less than 0.1 – which corresponds to a VIF greater than ten²¹ – typically signals the presence of problems, so it may be required to exclude certain variable(s) from regressions (Laerd Statistics, 2015). As observed in [Table H1](#) (Appendix H), the VIF values are considerably high for a number of variables which confirm the presence of multi-collinearity that may cause parameter instability, reduce the predictability power of models, and increase the presence of standard errors.

The *t-statistic* provides a measure of the precision with which the regression coefficient of variables is measured; therefore, it can help determining which variable could be included or omitted in models. Accordingly, the larger the *t*-value, the smaller the *p*-value (or *Sig.*), and the greater the evidence against the null-hypothesis; in other words, *p*-values < 0.05 (95% of confidence) indicates a greater significance of the variable in the model. [Table H1](#) in Appendix H shows the results of the *t-statistic* for the OLS models. The null-hypothesis was rejected at a significance level of 0.01 for all variables except *Fr_Tot_Wat* (*p*=0.804) in model 1A; *nLSI* (*p*=0.396) and *Fr_Med_Veg* (*p*=0.012) in model 2A; *Fr_Low_NIR* (*p*=0.635) in model 3A; and *Fr_Low_NIR* (*p*=0.046) in model 4A.

The results of the *t-statistic* confirm that further analysis is required to determine which variable(s) should be omitted to reduce multicollinearity. To respond to this need, the *Pearson's product-moment correlation coefficient* (or *Pearson's r statistic*) demonstrates the magnitude, direction and significance of the linear relationships between variables. Thus, *Pearson's r* values close to -1 (perfect negative correlation) and +1 (perfect positive correlation) can be interpreted as problematic, while values close to zero as favourable.

Results of *Pearson's* correlations for all models are presented in [Tables H3 to H6](#) (Appendix H) and indicate a moderate to strong correlation between mean NDVI and most surface covers as the latter were directly derived from this index. These relationships are particularly stronger in winter due to the good quality of the hyperspectral image retrieved for this season. As a strong relationship between NDVI and vegetation fractional vegetation cover (as well as impervious surfaces) has been confirmed in this research (see Section 7.3.2.1) and extensively reported in the literature (Weng, 2009), this variable should be omitted from all models to minimise multicollinearity. Indeed, it has been demonstrated in previous sections the little or no contribution of NDVI to explain the thermal conditions of a place at night-time.

²¹ Recommended cut-off values of three and five are also found in the literature (Ott and Longnecker, 2004).

On the other hand, weak to moderate negative relationships were identified between impervious surfaces (*Fr_Imp_Bld* and *Fr_Imp_Grnd*) and pervious covers (low plants, shrubs and trees) as the increment in the proportion of one naturally results in the decreasing of the other. Among pervious surfaces, fraction of water (*Fr_Tot_Wat*) and irrigated low plants (*Fr_Low_IRR*) showed to be uncorrelated with the majority of land covers.

Similarly, *CIRCLE_AM* and *nLSI* are mostly uncorrelated with other independent variables, yet weakly correlated with each other, as both reflect the spatial configuration of tree cover. Altitude is a variable that shows no relationship with other independent variables in summer. An exception to this can be found in winter, where a weak relationship between altitude and impervious ground and tree cover responds to varied topographic conditions displayed in this case study.

Furthermore, for each spatial unit (50x50m) it is assumed that $Fr_Imp_Bld + Fr_Imp_Grnd + Fr_Low_IRR + Fr_Low_NIR + Fr_Med_Veg + Fr_High_Veg + Fr_Tot_Wat \geq 100\%$, indicating that the seven variables are collinear. Therefore, in an attempt to reduce collinearity, fraction of non-irrigated grasses (*Fr_Low_NIR*) was omitted in subsequent regressions and became the reference variable. Several OLS models were tested with different combinations of the remaining variables guided by the results of the *t-statistic*, *Durbin-Watson statistic*, the VIF values of selected predictors, the multicollinearity condition number, and overall model performance. A summary of resulting statistics for the best regressions for each time of the day and season are presented in [Table 7.7](#).

Although the regression performances of models have not improved (except for model 3B that slightly decreased), multicollinearity between independent variables improved considerably as it can be observed in the multicollinearity condition numbers presented in [Table 7.7](#) with values at an acceptable level less than 30. Similarly, [Table H2](#) in Appendix H shows that VIF values of all independent variables reduced significantly up to an acceptable level of less than 3.5.

Despite previous improvements, heteroskedasticity is still a present issue as demonstrated by the high and significant values of *Breusch-Pagan* and *Koenker-Bassett statistics* ($p < 0.05$). Non-normality of residuals is also a recurrent problem as assessed by *P-P plots* and the *Jarque-Bera test* ($p < 0.001$). As shown by *Durbin-Watson statistics* (between 0.9 and 1.1), there is strong evidence of autocorrelation of residuals that may be caused by spatial dependencies. As this is a serious issue affecting the overall predictive performance of models, this is properly investigated and addressed in the following section.

Table 7.7 Summary statistics of revised OLS regression models for the prediction of diurnal and nocturnal LSTs in summer and winter using a selection of independent variables.

Season	SUMMER		WINTER	
Time of day	Day	Night	Day	Night
Model (dependent variable)	1B (DAY_ T_s)	2B (NIG_ T_s)	3B (DAY_ T_s)	4B (NIG_ T_s)
Regression	OLS	OLS	OLS	OLS
<i>N</i> cases	23022	23022	24948	23458
R	0.800	0.595	0.776	0.734
R ²	0.640	0.354	0.603	0.539
Adjusted R²	0.640	0.353	0.602	0.539
Standard Error (S.E)	1.771	0.965	1.197	0.629
<i>F</i> -statistic	4538.556	1403.516	4200.067	3048.077
df1	9	9	9	9
df2	23012	23012	24938	23448
Sig. F (p-value)	0.000	0.000	0.000	0.000
Log-Likelihood	-45828.6	-31851	-39878.6	-22408.6
AIC	91677.3	63722.1	79777.3	44837.2
SC	91757.7	63802.5	79858.5	44917.8
Durbin-Watson	1.052	0.907	1.018	1.062
Multicollin. cond. number	20.485	20.485	18.521	18.887
Jarque-Bera (Sig.) DF	112182.5236 (0.000) 2	150644.4182 (0.000) 2	2571.2485 (0.000) 2	2019.8261 (0.000) 2
Breusch-Pagan (Sig.) DF	22177.1111 (0.000) 9	36322.8178 (0.000) 9	2445.5106 (0.000) 9	5013.832 (0.000) 9
Koenker-Bassett (Sig.) DF	4149.5824 (0.000) 9	5113.7158 (0.000) 9	1454.5364 (0.000) 9	2934.3725 (0.000) 9
Predictors	(Constant), <i>Fr_Imp_Bld</i> , <i>Fr_Imp_gr</i> , <i>Fr_LowIRR</i> , <i>Fr_Med_Veg</i> , <i>Fr_High_Veg</i> , <i>Fr_Tot_wat</i> , <i>CIRCLE_AM</i> , <i>nLSI</i> , <i>Altitude</i> ,			

7.4.2 Spatial regression models

7.4.2.1 Spatial autocorrelation analysis

The independent variables used for the OLS models are discrete and represent the composition and spatial distribution of urban landscape. As a consequence, the physical boundaries between spatial units (or observations) and different surface covers are abrupt as they were derived from spectral and LiDAR data. Nonetheless, LST is a continuous phenomenon that gradually varies across those delineations in space and time (Stewart, 2011b); thus, LST observations made at different locations might not be totally

independent. This spatial dependency and interaction between variables and the residuals is commonly referred as *spatial autocorrelation* (Anselin, 1995; Getis, 2010); which is also explained by Tobler’s first law of geography: “*Everything is related to everything else, but near things are more related than distant things*” (Tobler, 1970).

If spatial association exists, the performance of OLS regressions is affected as this causes spatial structural instability or spatial drift leading to an inefficient estimation of predicted values and serious mistakes in the interpretation of regressions (Anselin, 1995; Getis & Ord K. J., 2010; Ward & Gleditsch, 2008). Assuming that spatial autocorrelation is observed, the next step is to determine the proper regression models to incorporate the effect of spatial dependencies. Figure 7.22 illustrates the two most common types of spatial autocorrelation from which two common spatial autoregressive models have been developed; as explained below (Baller et al., 2001; Ward & Gleditsch, 2008):

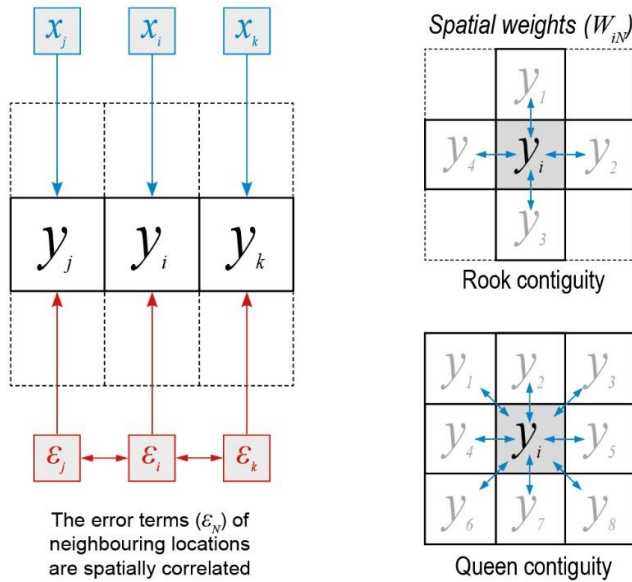
- A. *Spatial dependence among residuals.* This occurs when the error terms across neighbouring locations are correlated. The *Spatial Error Model* (SEM) deals with this issue by evaluating the extent to which the clustering of the dependent variable –not explained by the measured independent variables– can be accounted for the clustering of error terms. In other words, the SEM captures the effect of unknown predictor variables by introducing a *spatial error term* or *Lambda* (λ) at the end of the regression equation which is calculated with the use of a spatial connectivity matrix or spatial weight matrix (Baller et al., 2001) (left-hand diagram in Figure 7.22).
- B. *Spatial dependence among variables.* This occurs when the values of a dependent variable y in a specific location i are directly influenced by the values of y in neighbouring locations (for example j and k) as well as by the spatial influence of unmeasured independent variables (Baller et al., 2001). To deal with this type of spatial dependence, the *Spatial Lag Model* (LAG) –also called *spatially lagged y model* (Ward & Gleditsch, 2008)– incorporates a *spatially lagged* dependent variable at the end of the regression equation which is also estimated through contiguity-based spatial weights (right-hand diagram in Figure 7.22).

In this research, spatial autocorrelation analysis was performed using two well-known tests and visualisations available in GeoDa software (Anselin et al., 2006), namely, the global spatial autocorrelation index Moran’s I^{22} –a test to determine if ‘clustering’ exists– (Moran, 1950); and its local version known as *local indicators of spatial association* (LISA) or

²² Measured between -1, indicating negative spatial autocorrelation or dispersion of like-values, and +1, signalling positive spatial autocorrelation or clustering of like-values; while a value of zero signifies spatial randomness.

Local Moran's I —a test for identifying the location of ‘clusters’ based on the contribution of each individual observation (Anselin, 1995). Along with the diagnostics for spatial dependence, five *Lagrange multiplier (LM)* test statistics are provided, which can be used as criteria to identify the spatial regression model that best fits the current datasets.

A. Spatial error model (SEM)

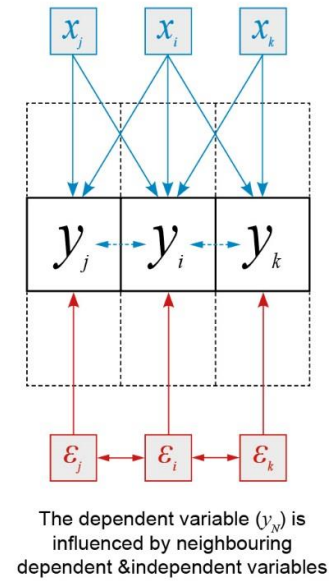


$$y_i = x_i\beta + \lambda W_i \cdot \xi_i + \varepsilon_i$$

where β regression coefficients
 ξ uncorrelated error term

ρ spatial autocorrelation parameter
 ε spatially correlated error term

B. Spatial lag model (LAG)



$$y_i = x_i\beta + \rho W_i \cdot y_i + \varepsilon_i$$

λ autoregressive coefficient
 W row-sum standardise spatial weight matrix

Figure 7.22 Main types of spatial dependence applied to spatial regression models.
(graphs adapted from Baller et al., 2001 and equations from Song et al., 2014)

Before running above tests, a *spatial weight matrix (SWM)* using the *queen criterion of contiguity*²³ was constructed for each case study (or dataset) to identify neighbouring observations with at least one point of common boundary in a regular grid (middle diagram in Figure 7.22). Table 7.8 present the results of the diagnostics for spatial dependence for revised OLS models produced in previous section (Models 1B, 2B, 3B, and 4B) which include the statistics of Moran's I test of residuals and *Lagrange multipliers*.

Global Moran's I statistics are significant ($p=0.000$) for all the revised OLS models showing a considerable positive spatial autocorrelation of residuals with reported values of more than 0.55 and z -values of more than 160.0. This indicates that it exists homogeneity of residuals and hence a clustering of like-values.

²³ With a first-order queen contiguity as recommended by Song et al. (2014).

Table 7.8 Diagnostics for spatial dependence for revised OLS models 1B, 2B, 3B, and 4B.

Season		SUMMER		WINTER	
Time of day		Day	Night	Day	Night
Model (dependent variable)		1B (DAY_T _s)	2B (NIG_T _s)	3B (DAY_T _s)	4B (NIG_T _s)
Regression		OLS	OLS	OLS	OLS
N cases		23022	23022	24948	23458
Global Moran's I (errors)	MI	0.5678	0.6584	0.6064	0.6262
	z-value (Sig.)	167.4366 (0.000)	194.1534 (0.000)	187.0957 (0.000)	186.1231 (0.000)
Lagrange multiplier (lag)	DF	1	1	1	1
	z-value (Sig.)	11433.5357 (0.000)	21692.7033 (0.000)	17678.6676 (0.000)	27619.9025 (0.000)
Robust LM (lag)	DF	1	1	1	1
	z-value (Sig.)	0.4823 (0.487)	16.9387 (0.00004)	0.1411 (0.70721)	486.8075 (0.000)
Lagrange multiplier (error)	DF	1	1	1	1
	z-value (Sig.)	27969.6203 (0.000)	37611.7092 (0.000)	34927.3914 (0.000)	34556.0368 (0.000)
Robust LM (error)	DF	1	1	1	1
	z-value (Sig.)	16536.5669 (0.000)	15935.9446 (0.000)	17248.8649 (0.000)	7422.9418 (0.000)
Lagrange multiplier (SARMA)	DF	2	2	2	2
	z-value (Sig.)	16536.5669 (0.000)	37628.6478 (0.000)	34927.5325 (0.000)	35042.84429 (0.000)
Predictors		(Constant), Fr_Imp_Bld, Fr_Imp_gr, Fr_LowIRR, Fr_Med_Veg, Fr_High_Veg, Fr_Tot_wat, CIRCLE_AM, nLSI, Altitude,			

Furthermore, the *LM-Lag* and *LM-Error* statistics are highly significant ($p=0.000$) for all revised OLS models. However, as the rejection of the null-hypothesis for both statistics is commonly found in practice, Anselin (2005) recommends to consider the robust forms and select the appropriate test with the most significant p -value, or otherwise, with the largest z -value.

In general, results favour SEM over LAG as the *Robust LM-Error* has a significantly higher z -value than the *Robust LM-Lag*. In addition, *Robust LM-Lag* was not significant for models 1B and 3B suggesting there is no spatial dependence among variables from neighbouring locations (or grid cells). Indeed, this coincides with Irger (2014) who suggested that it is improbable that LSTs in a given location are directly influenced by those of neighbouring areas or their independent variables since surface temperatures result from the thermal properties of the immediate context.

On the contrary, *Robust LM-Error* tests suggest that it is more likely that the spatial clustering of LST could be caused by geographic patterning (*i.e.* typical urban morphology) of measured independent variables and unmeasured factors that were obviated in the models. Thereupon, LISA or Local Moran's I test (Anselin, 1995) was used to identify

local spatial clusters (hot- and cold-spots) of like-values that may explain the observed spatial dependence of LSTs.

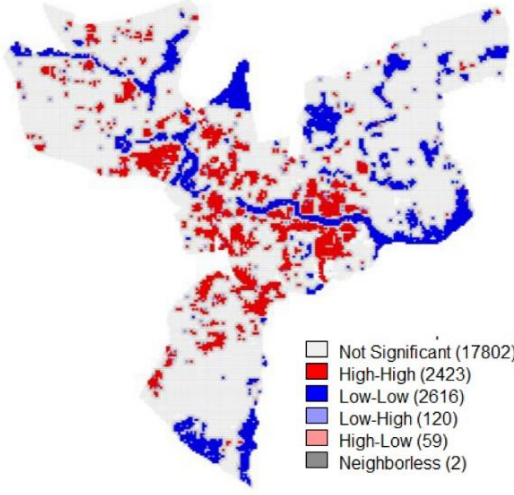
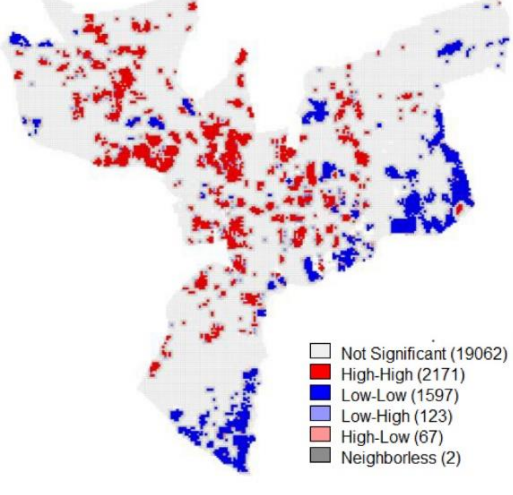
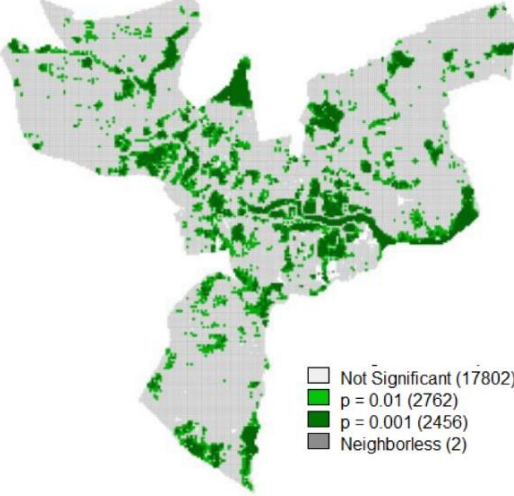
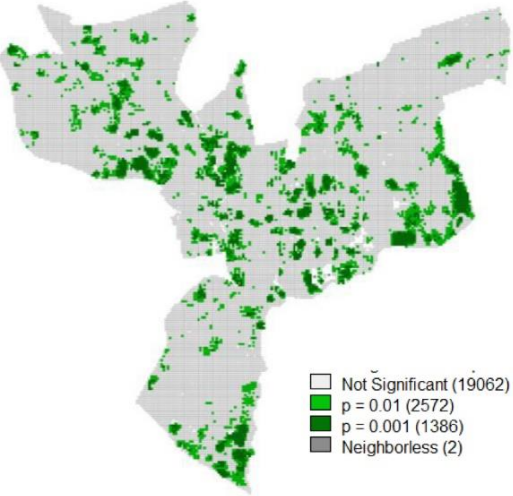
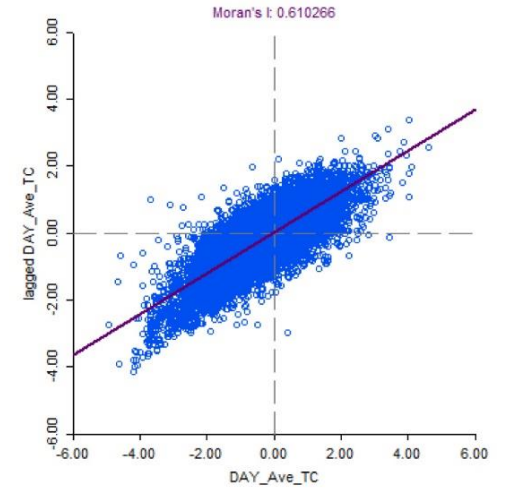
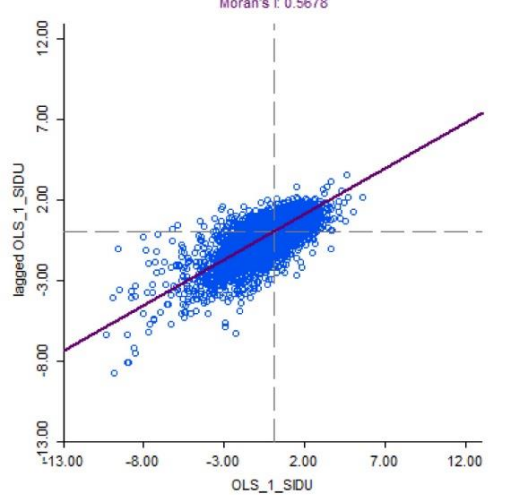
Firstly, the typical pair of cluster and significance maps were generated using the dependent variable (LST) of each model with default permutations ($n=99$) and significance level ($p=0.05$). As suggested by Anselin (2005), the number of permutations was increased to 9999 to obtain more robust results followed by a sensitivity analysis to determine the presence of spatial clusters and spatial outliers with different significance cut-off values. Secondly, the same univariate Local Moran's I was computed for residuals and results compare to those of the dependent variable. LISA values –at a significance level of 0.01–, maps and Moran scatterplot for model 1B are presented in Table 7.9 and for all models in Tables H7 to H10 in Appendix H.

The high-high (HH) and low-low (LL) locations are considered as the *spatial clusters* of high and low LSTs respectively, corresponding to areas with positive local spatial autocorrelation. On the other hand, high-low (HL) and low-high (LH) are typically referred as the *spatial outliers* and represent areas with a negative spatial autocorrelation (dispersion).

A significant positive local spatial autocorrelation (spatial concentration) of the dependent variable and residuals were identified for all models, with no significant evidence of spatial outliers in either case. As expected, the overall pattern of clusters coincides with typical urban forms of Sydney described in Sections 6.1.3 and 6.1.4 and particular distributions and clustering of GITs explained in Section 7.2.2; therefore, this is likely the main cause of the spatial dependence between residuals.

Accordingly, at daytime, HH clusters (hotspots) of LSTs typically occurred in compact, dense, and highly impervious areas, while LL clusters correspond to places with high vegetation intensity and water surfaces. On the contrary, at night-time, HH clusters comprise water surfaces, compact mid- and low-rise buildings with extensive paved areas and highly forested zones; while LL clusters (cold-spots) occurred in places with extensive grasses and large low-rise buildings with light-coloured/high-albedo roofing materials. Interestingly, in model 4B (night-time LSTs in winter) HH clusters mostly situated in high-lying areas (and vice versa) as in the case of the hilly suburbs in Sydney's north; this suggests a considerable influence of topography on nocturnal LSTs (which is demonstrated in next section). In comparison with the clusters of LSTs, the spatial clusters from residuals occurred in similar locations, but were smaller in extent as areas with dense tree canopy and water surfaces were omitted.

Table 7.9 LISA results (Moran scatterplot, cluster and significance maps) for the dependent variable and residuals of Model 1B showing the presence of spatial clusters (hot-/coldspots) and spatial outliers.

Sum	Model 1B					
	Local Moran's / of LSTs			Local Moran's / of residuals		
	MI: 0.610	p-value: 0.01	z-value: 181.1566	MI: 0.567	p-value: 0.01	z-value: 167.3701
Cluster map						
						
Moran scatterplot						

7.4.2.2 Spatial error models (SEM)

In light of evidence of spatial autocorrelation and in accordance with the results of *Robust Lagrange Multiplier* statistics, the SEM was chosen as an appropriate spatial regression method for predicting LSTs using the same combination of independent variables selected for the revised OLS models 1B to 4B. As shown in Figure 7.22, the SEM is implemented for the standard ordinary least squares regression with spatial dependency supported by a Maximum Likelihood (ML) estimator (Anselin et al., 2006) as expressed in the following equation:

$$y_i = \beta_0 + \sum_p \beta_p x_{ip} + \lambda w_i \xi_i + \varepsilon_i \quad [\text{Eq. 7.2}]$$

where y_i is the *dependent variable* (in this case the mean LST of spatial units) indexed by i , β_0 is the *constant* (or intercept) of the model, β_p are the *regression coefficients* for p independent variables, x_{ip} are the predictors or *independent variables*, λ is the *autoregressive coefficient* signalling the extent of the spatial correlation, w_i is the *vector of connectivities* indicating the proximity of spatial units, ξ_i is the *spatial component of errors*, and ε_i is the *spatially uncorrelated error* of the regression (Song et al., 2014; Ward & Gleditsch, 2008).

Four separate SEM were estimated in GeoDa and results compared against the predictive performance of typical OLS MLR models produced in previous section (Table 7.10).

As shown in Table 7.10, the estimates and measures of fit have a considerable improvement with very high coefficients of determination (R^2) of 0.844 for Model 1C, 0.798 for Model 2C, 0.837 for Model 3C, and 0.866 for Model 4C. However, this traditional measure is not appropriate in a spatial regression model as the spatial lag does not generate a real R^2 , but a so-called *pseudo- R^2* that cannot be compared with classic OLS results (Anselin, 2005). Instead, Anselin (2005) recommends to use *Log-Likelihood*, *Akaike information criterion* (AIC), and *Schwarz criterion* (SC) as proper metrics of fit to determine if the introduction of an error term coefficient improves the regression performance of OLS.

By analysing the three statistical tests presented in Table 7.10, it is noticed a considerable increase in the *Log-Likelihood* of Models 1C, 2C, 3C and 4C compared with the classic OLS Models 1B, 2B, 3B, and 4B. Compensating the improved fit for the added spatially autocorrelated variable, the AIC and SC also decrease relative to OLS; consequently, estimates in Table 7.10 also confirm a significant improvement of regressions for the spatial error specification.

Table 7.10 Summary of the Maximum Likelihood Estimation of SEMs for the prediction of diurnal and nocturnal LSTs in summer and winter, in comparison with the performance of revised OLS models.

Season	SUMMER				WINTER			
Model (dependent var.)	1B (DAY_T _s)	1C (DAY_T _s)	2B (NIG_T _s)	2C (NIG_T _s)	3B (DAY_T _s)	3C (DAY_T _s)	4B (NIG_T _s)	4C (NIG_T _s)
Regression	OLS	SEM	OLS	SEM	OLS	SEM	OLS	SEM
N cases	23022	23022	23022	23022	24948	24948	23458	23458
Adj. R ² / R ²	0.640	0.844	0.353	0.798	0.602	0.837	0.539	0.866
S.E.	1.771	1.165	0.965	0.540	1.197	0.767	0.629	0.339
df1	9	9	9	9	9	9	9	9
df2	23012	23012	23012	23012	24938	24938	23448	23448
Lag coefficient (Sig.)	-	0.829 (0.000)	-	0.886 (0.000)	-	0.829 (0.000)	-	0.908 (0.000)
Log-Likelihood	-45828.6	-37792.87	-31851	-20459.63	-39878.6	-30496.31	-22408.6	-10125.3
AIC	91677.3	75605.7	63722.1	40939.3	79777.3	61012.6	44837.2	20270.6
SC	91757.7	75686.2	63802.5	41019.7	79858.5	61093.9	44917.8	20351.2
Breusch-Pagan (Sig.)	22177.1 1 (0.000)	19069.77 (0.000)	36322.8 2 (0.000)	33816.04 (0.000)	2445.51 (0.000)	4467.24 (0.000)	5013.83 (0.000)	5807.74 (0.000)
DF	9	9	9	9	9	9	9	9
Likelihood R. (Sig.)	-	16071.52 (0.000)	-	22782.82 (0.000)	-	18764.65 (0.000)	-	24566.59 (0.000)
DF		1		1		1		1
Predictors	(Constant), (Lambda) ^a , Fr_Imp_Bld, Fr_Imp_gr, Fr_LowIRR, Fr_Med_Veg, Fr_High_Veg, Fr_Tot_wat, CIRCLE_AM, nLSI, Altitude							

a. Only for SEMs. Results of revised OLS models are greyed-out.

The *Likelihood Ratio* (LR) test is a classic specification test that enables comparison between the null-model (or classic regression) and the alternative SEM. The very high values and low probability ($p < 0.000$) for Models 1C, 2C, 3C and 4C confirm a strong significance of the spatial autoregressive coefficient; and hence, a superior performance of SEM compared to OLS.

The results confirm a strong and highly significant ($p < 0.000$) spatial autoregressive (*lambda*) coefficient for all models²⁴, estimated as 0.829 for Model 1C, 0.886 for Model 2C, 0.829 for Model 3C, and 0.908 for Model 4C. There are some slight differences in the magnitude of most regression coefficients between SEM and revised OLS [Table 7.11]; however, the coefficients of *CIRCLE_AM* and *nLSI* varied significantly. This illustrates the misleading effect that spatial error autocorrelation has on OLS estimates and justifies the use of spatial regression models.

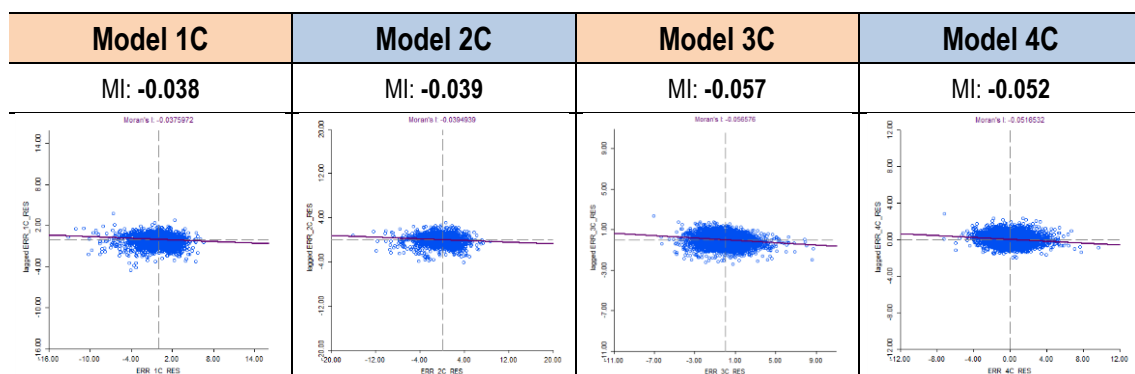
²⁴ According to Anselin (2005) this is typical for large datasets (>1000 cases) and partially caused by the asymptotic characteristic of the analytical expressions used for the variance.

Table 7.11 Comparison of regression coefficients (β) for all variables included in SEM versus revised OLS.

Season	SUMMER				WINTER			
Model	1B	1C	2B	2C	3B	3C	4B	4C
Regression	OLS	SEM	OLS	SEM	OLS	SEM	OLS	SEM
β_{CONSTANT} (z-value)	33.8028 ** (398.696)	34.4474 ** (338.949)	20.7854 ** (449.909)	21.444 ** (364.966)	12.8710 ** (256.3317)	12.2598 ** (182.731)	1.2598 ** (45.2001)	1.8262 ** (42.899)
$\beta_{\text{FR_IMP_BLD}}$ (z-value)	0.0579 ** (61.4008)	0.0526 ** (59.4232)	-0.0097 ** (-18.7882)	-0.0166 ** (-39.9763)	0.0259 ** (41.1557)	0.0337 ** (57.699)	0.0057 ** (16.3694)	-0.0084 ** (-30.7744)
$\beta_{\text{FR_IMP_GRND}}$ (z-value)	0.0525 ** (48.8229)	0.0566 ** (58.3693)	0.0399 ** (68.0378)	0.0399 ** (87.7915)	0.0115 ** (16.9678)	0.0222 ** (35.9959)	0.0224 ** (58.8993)	0.0164 ** (56.2468)
$\beta_{\text{FR_LOW_IRR}}$ (z-value)	-0.0270 ** (-15.7777)	-0.0310 ** (-21.5122)	0.0034 ** (3.6608)	0.0026 ** (3.9479)	-0.0212 ** (-23.3988)	-0.0132 ** (-17.1847)	-0.0037 ** (-7.5728)	-0.0064 ** (-18.164)
$\beta_{\text{FR_MED_VEG}}$ (z-value)	-0.0176 ** (-4.2781)	-0.0210 ** (-6.4883)	-0.0077 ** (-3.4089)	-0.0018 (-1.1878)	-0.0069 ** (-3.4525)	-0.0065 ** (-4.1090)	-0.0313 ** (-32.0240)	-0.0082 ** (-12.2608)
$\beta_{\text{FR_HIGH_VEG}}$ (z-value)	-0.0497 ** (-50.8823)	-0.0497 ** (-56.6522)	0.0136 ** (25.6184)	0.0147 ** (35.7224)	-0.0415 ** (-68.6225)	-0.0329 ** (-54.5499)	0.0176 ** (55.5057)	0.0152 ** (55.9317)
$\beta_{\text{FR_TOT_WAT}}$ (z-value)	-0.0933 ** (-63.4058)	-0.0873 ** (-56.9353)	0.0343 ** (42.7583)	0.0334 ** (46.0094)	-0.0731 ** (-41.5504)	-0.0614 ** (-43.1389)	0.0423 ** (81.5689)	0.0278 ** (50.6653)
$\beta_{\text{CIRCLE_AM}}$ (z-value)	1.7380 ** (22.7574)	0.3427 ** (6.1181)	1.1233 ** (26.9931)	0.1405 ** (5.4167)	-0.1046 * (-2.3231)	-0.3597 ** (-9.94251)	0.6735 ** (27.9144)	0.1789 ** (10.7363)
β_{NLSI} (z-value)	-1.6885 ** (-8.3614)	-0.6950 ** (-4.7634)	-0.1389 (-1.2626)	0.0444 (0.6576)	0.9062 ** (5.2358)	0.5508 ** (4.56278)	-1.4003 ** (-15.1849)	-0.3589 ** (-6.6706)
β_{ALTITUDE} (z-value)	0.0049 ** (10.8379)	0.0090 ** (5.71575)	-0.0012 ** (-4.8143)	-0.0004 (-0.3609)	0.0036 ** (11.9375)	0.00520 ** (5.34192)	0.0128 ** (114.6258)	0.0146 ** (27.3852)
β_{LAMBDA} (z-value)	n/a	0.8292 ** (171.189)	n/a	0.8863 ** (233.76)	n/a	0.8285 ** (176.802)	n/a	0.9075 ** (276.071)

* Significant at the 0.05 level (two-tailed); ** Significant at the 0.01 level (two-tailed). Results of OLS regressions are greyed-out.

Global Moran's I scatterplots were constructed for the residuals of each SEM and results indicate that the introduction of the error term eliminated all spatial autocorrelation as statistics are essentially zero ($MI < 0.06$) [Table 7.12].

Table 7.12 Global Moran's I of residuals for SEM 1C, 2C, 3C and 4C.

Despite the abovementioned favourable results, the highly significant values of *Breusch-Pagan* test indicate that heteroskedasticity is still a serious problem as shown in the residual plots of Table H12 in Appendix H; therefore, further refinements of SEM are necessary.

7.4.2.3 Improved spatial error models (SEM)

Although the introduction of the spatial autoregressive error term improved the performance of classic OLS regressions significantly, it did not entirely reduce heteroskedasticity; hence, further improvements are required. Accordingly, residual plots in Table H12 show increasing funnel shapes for Models 1C and 3C; and a decreasing funnel shape for Model 2C which are typical of non-homoskedastic data.

By taking a close look at the tails of funnel shapes it is noticed that the majority of farthest residuals with respect to the line of good fit correspond to observations classified as IM1 *Highly impervious* and *aquatic* GIT classes, contributing both substantially to heteroskedasticity. This is because LSTs from highly impervious contexts (IM1) cannot be predicted accurately from the combination of independent variables defined in this study as their thermal condition is influenced by unmeasured factors related to the built form and material-specific properties (*i.e.* building volume, H/W ratio, SVF, albedo, emissivity, etc.) of horizontal and vertical impervious surfaces. On the other hand, the distinct thermal capacity of water bodies relative to terrestrial surfaces also partially contributed to heteroskedasticity.

Consequently, it is demonstrated that a single spatial regression equation is not suitable for all locations using the totality of observations. To correct for this issue and minimise heteroskedasticity to the maximum extent possible, datasets were partitioned into *aquatic observations*, and *terrestrial observations*²⁵. Cases classified as IM1 were also excluded from the *terrestrial* subset and subsequent statistical models as per previous assumptions and because the presence of vegetation covers, and water surfaces is negligible.

Spatial regressions were calculated in GeoDa to produce Models 1D, 2D, 3D, and 4D that are applicable to *aquatic* locations; and Models 1E, 2E, 3E, and 4E that are applicable to *terrestrial* locations using the combination of independent variables defined for the revised OLS models 1B, 2B, 3B, and 4B. A statistical summary for revised SEMs is presented in Table 7.13.

Tables H11 and H12 provide a summary of statistical estimations and residual plots for all SEM and OLS models produced in this thesis respectively. Except for Model 3D, all revised SEMs exhibit a superior *goodness-of-fit* as demonstrated by the substantial improvement of *Log-Likelihood*, *AIC*, and *SC* values. Whereas heteroskedasticity was not

²⁵ This coincides with the findings of TVX analysis which demonstrated that *aquatic* cases (GITs) possess a distinct diurnal and nocturnal thermal behaviour than terrestrial surfaces that causes an outlying effect on regressions.

completely eliminated, it was significantly reduced as demonstrated by the smaller values of *Breusch-Pagan* tests and the randomly dispersed data points in residual plots [Table H12].

Table 7.13 Summary of the Maximum Likelihood Estimation of revised SEMs for the prediction of diurnal and nocturnal LSTs in summer and winter that are applicable separately to aquatic and terrestrial locations.

Locations	Aquatic				Terrestrial ^a			
Season	SUMMER		WINTER		SUMMER		WINTER	
Model (dependent var.)	1D (DAY_T _s)	2D (NIG_T _s)	3D (DAY_T _s)	4D (NIG_T _s)	1E (DAY_T _s)	2E (NIG_T _s)	3E (DAY_T _s)	4E (NIG_T _s)
Regression	SEM	SEM	SEM	SEM	SEM	SEM	SEM	SEM
N cases	368	368	155	322	20345	20345	21024	20012
R ²	0.861	0.909	0.565	0.907	0.860	0.799	0.846	0.876
S.E.	0.841	0.311	0.529	0.472	0.958	0.408	0.695	0.310
df1	9	9	9	9	9	9	9	9
df2	358	358	145	312	20335	20335	21014	20002
Lag coefficient (Sig.)	0.551 (0.000)	0.915 (0.000)	0.383 (0.000)	0.801 (0.000)	0.782 (0.000)	0.862 (0.000)	0.810 (0.000)	0.887 (0.000)
Log-Likelihood	-478.455	-181.203	-126.736	-262.824	-29335.9	-12429.57	-23747.31	-6946.26
AIC	976.911	382.407	273.472	545.649	58691.8	24879.2	47514.6	13912.5
SC	1015.99	421.487	303.906	583.394	58771.0	24958.4	47594.2	13991.6
Breusch-Pagan (Sig.)	247.4531 (0.000)	382.9133 (0.000)	63.8665 (0.000)	56.6246 (0.000)	3313.721 (0.000)	6898.934 (0.000)	980.105 (0.000)	568.682 (0.000)
DF	9	9	9	9	9	9	9	9
Likelihood R. (Sig.)	96.9575 (0.000)	558.6579 (0.000)	18.4510 (0.000)	162.4745 (0.000)	12027.35 (0.000)	18961.35 (0.000)	16138.4 (0.000)	19855.3 (0.000)
DF	1	1	1	1	1	1	1	1
Predictors	(Constant), (Lambda), Fr_Imp_Bld, Fr_Imp_gr, Fr_LowIRR, Fr_Med_Veg, Fr_High_Veg, Fr_Tot_wat, CIRCLE_AM, nLSI, Altitude							

^a Observations classified as IM1 Highly impervious are excluded.

Table 7.14 presents the regression coefficients (β_n), standard errors and significance values for all the independent variables included in SEMs 1D-4D and 1E-4E. As a result of data partitions, some independent variables became statistically insignificant for the aquatic context. As a consequence, confidence levels can be used to determine which variables should be omitted in the final equations presented in Section 8.5.

Table 7.14 Summary of regression coefficients (β) for all variables included in the revised SEM applicable for aquatic and terrestrial contexts.

Context	Aquatic				Terrestrial ^a			
Season	SUMMER		WINTER		SUMMER		WINTER	
Model	1D (DAY_T _s)	2D (NIG_T _s)	3D (DAY_T _s)	4D (NIG_T _s)	1E (DAY_T _s)	2E (NIG_T _s)	3E (DAY_T _s)	4E (NIG_T _s)
Regression	SEM	SEM	SEM	SEM	SEM	SEM	SEM	SEM
β_{CONSTANT}	39.2647	20.0435	9.59973	3.88436	34.292	21.5092	12.2815	1.78813
S.E.	0.932064	0.345076	1.00808	0.840143	0.0810004	0.0422614	0.0626628	0.0363625
z-value	42.1266	58.0842	9.52281	4.62345	423.355	508.955	195.993	49.1751
(Sig.)	(0.000)	(0.000)	(0.000)	(0.000)	(0.000)	(0.000)	(0.000)	(0.000)
$\beta_{\text{FR_IMP_BLD}}$	0.0650234	0.00342534	0.181019	0.0765922	0.0616927	-0.0105317	0.0316284	-0.00642942
S.E.	0.0168159	0.00602178	0.105876	0.0319444	0.00085338	0.00036799	0.00064248	0.000299391
z-value	3.86678	0.568825	1.70973	2.39767	72.2921	-28.6198	49.2289	-21.475
(Sig.)	(0.000)	(0.56947)	(0.08732)	(0.0165)	(0.000)	(0.000)	(0.000)	(0.000)
$\beta_{\text{FR_IMP_GRND}}$	-0.0243743	0.0373822	-0.00464001	-0.0346662	0.0634627	0.0421121	0.0228746	0.0184353
S.E.	0.0133013	0.00472993	0.0288914	0.0198017	0.00086048	0.000370488	0.00065143	0.000305167
z-value	-1.83248	7.90334	-0.160602	-1.75067	73.7525	113.667	35.1145	60.4105
(Sig.)	(0.0669)	(0.000)	(0.87241)	(0.08)	(0.000)	(0.000)	(0.000)	(0.000)
$\beta_{\text{FR_LOW_IRR}}$	-0.0922489	-0.00350875	0.0177194	-0.0102109	-0.029133	0.0023836	-0.0129012	-0.00597982
S.E.	0.0198972	0.00732081	0.0132043	0.0113426	0.00120683	0.000519446	0.00071966	0.000330868
z-value	-4.63628	-0.479285	1.34194	-0.900223	-24.1402	4.58874	-17.9269	-18.0732
(Sig.)	(0.000)	(0.63174)	(0.17962)	(0.368)	(0.000)	(0.000)	(0.000)	(0.000)
$\beta_{\text{FR_MED_VEG}}$	0.00316143	-0.00430663	-0.0072801	0.00827245	-0.026064	-0.0039772	-0.00651486	-0.00887949
S.E.	0.0162053	0.00585805	0.01033	0.00809914	0.00272564	0.00116578	0.001454	0.000616157
z-value	0.195086	-0.735165	-0.704752	1.0214	-9.56252	-3.41163	-4.48063	-14.4111
(Sig.)	(0.84533)	(0.46224)	(0.48096)	(0.30707)	(0.000)	(0.00065)	(0.000)	(0.000)
$\beta_{\text{FR_HIGH_VEG}}$	-0.105179	0.0198475	-0.0124776	-0.0108237	-0.0465437	0.0154435	-0.0329822	0.0159509
S.E.	0.00951147	0.00337171	0.0100146	0.00849349	0.000742196	0.000321481	0.0005664	0.000256383
z-value	-11.0582	5.88649	-1.24594	-1.27436	-62.7108	48.0384	-58.2318	62.2151
(Sig.)	(0.000)	(0.000)	(0.21278)	(0.20254)	(0.000)	(0.000)	(0.000)	(0.000)
$\beta_{\text{FR_TOT_WAT}}$	-0.136812	0.0390074	-0.0254368	0.0150019	-0.0864254	0.0259394	-0.116303	0.0288495
S.E.	0.00922572	0.00325552	0.00990869	0.00836143	0.00361254	0.00153975	0.00412332	0.00172743
z-value	-14.8295	11.9819	-2.56712	1.79418	-23.9237	16.8465	-28.2061	16.7008
(Sig.)	(0.000)	(0.000)	(0.01025)	(0.07278)	(0.000)	(0.000)	(0.000)	(0.000)
$\beta_{\text{CIRCLE_AM}}$	0.134762	-0.138563	0.394851	-0.567041	0.188179	-0.0992245	-0.34953	0.191559
S.E.	0.204617	0.0731579	0.352269	0.141528	0.057477	0.0244222	0.0423606	0.0198415
z-value	0.658605	-1.89402	1.12088	-4.00656	3.274	-4.06289	-8.2513	9.65448
(Sig.)	(0.51015)	(0.05822)	(0.26234)	(0.000)	(0.001)	(0.000)	(0.000)	(0.000)
β_{NLSI}	1.18417	0.321217	0.950073	-1.19175	-0.230356	0.139828	0.806862	-0.440389
S.E.	1.01493	0.321217	2.18236	0.809946	0.168859	0.0719525	0.128347	0.0567956
z-value	1.16676	0.94825	0.435342	-1.47139	-1.36419	1.94334	6.28656	-7.75393
(Sig.)	(0.24331)	(0.34300)	(0.66331)	(0.14119)	(0.17251)	(0.05198)	(0.000)	(0.000)
β_{ALTITUDE}	-0.0112455	0.0283315	-0.00764065	-0.00077340	0.00556751	-0.00190106	0.00535216	0.0138517
S.E.	0.00877362	0.00627242	0.0107472	0.00920217	0.00109105	0.000696389	0.00084278	0.000423005
z-value	-1.28174	4.51683	-0.710941	-0.0840453	5.10287	-2.72988	6.35062	32.746
(Sig.)	(0.19993)	(0.000)	(0.47712)	(0.93302)	(0.000)	(0.00634)	(0.000)	(0.000)
β_{LAMBDA}	0.55133	0.915327	0.382638	0.800643	0.782332	0.862121	0.809815	0.887256
S.E.	0.0435905	0.0111999	0.0691887	0.0251691	0.00554605	0.00414646	0.00492091	0.0035974
z-value	12.6479	81.7262	5.53036	31.8106	141.061	207.918	164.566	246.638
(Sig.)	(0.000)	(0.000)	(0.000)	(0.000)	(0.000)	(0.000)	(0.000)	(0.000)

^a Observations classified as IM1 *Highly impervious* are excluded.

Non-significant independent variables are greyed-out.

Overall, by analysing the signs and magnitude (z -values) of relevant regression coefficients [Table 7.14], the following interpretations can be inferred:

In aquatic locations:

1. Among all variables, water surfaces contribute most to the modification of LSTs, followed by impervious ground surfaces and trees. In summer, irrigated grasses, tree cover and water surfaces contribute to the reduction of diurnal LSTs, while the presence of buildings contribute to increase diurnal LSTs. At night-time, LSTs increase with increasing proportion of buildings, impervious ground surfaces, trees and water as well as with altitude.
2. In winter, proportion of water is the only significant predictor of diurnal LSTs. The sign of the coefficient indicates that diurnal LSTs decrease with increasing water surfaces. At night-time, the amount of buildings and water contribute to an increase of LSTs while increasing elongation of tree patches (*high CIRCLE_AM*) decreases LSTs.

In terrestrial locations:

3. In both seasons, the proportion of buildings and impervious ground surfaces contribute to the increase in diurnal LSTs significantly, while increasing amount of irrigated grasses, shrubs, trees and water contribute to the drop in diurnal LSTs. Furthermore, diurnal LSTs generally increase with increasing altitude. In contrast, nocturnal LSTs decrease with increasing proportion of buildings and shrubs, while an increase in the amount of impervious ground, water and forested areas leads to an increase in nocturnal LSTs.
4. The proportion of irrigated grasses has a positive influence on nocturnal LSTs in summer, while a negative influence in winter. This means that in summer an increase in the proportion of water results in an increasing nocturnal thermal capacity of natural surfaces.
5. *Altitude* shows a similar pattern at night-time, thus, nocturnal LSTs are decreasing with increasing altitude in summer and with decreasing altitude in winter (see Section 8.5 for interpretation of results).
6. *CIRCLE_AM* shows an inverse pattern between seasons and times of the day. As a consequence, an increasing elongation of tree patches causes a reduction of LSTs during the night in summer, while during the day in winter. Conversely, increasing elongation of tree patches results in increasing LSTs during the day in summer, and during the night in winter.
7. Dispersion of trees (*nLSI*) was a significant predictor at night-time in summer and both times of the day in winter. In summer scattered trees can be associated with higher LSTs at

night-time; conversely, in winter increasing dispersion of trees contribute to higher diurnal LSTs and lower nocturnal LSTs.

8. Among all independent variables, impervious surfaces (buildings and ground) contribute the most to mean LSTs, followed by trees, water, and low-irrigated grasses.
9. In all cases, the composition or abundance of a particular land cover is more influential in LSTs than the spatial configuration of trees.

Further interpretations of regression coefficients in the context of the study area are presented in Section 8.5. The application of previous statistical analysis for the formulation of SUHI mitigation scenarios at local scale is presented in Section 8.6.

7.5 Summary

This chapter demonstrates the applicability of the proposed assessment framework and standardised classification scheme for the study of the thermal performance of green infrastructure in response to the first, second and third objectives (and their associated research questions) of this thesis (Section 1.3). It also presents the quality assessment classifications, the analysis of thermal differentiations and the statistical models for the prediction of LST using surface composition and spatial configuration predictors.

The proposed classification framework for green infrastructure was successfully tested with three different grid sizes or spatial scales. Classification results were satisfactory for all scales with less than 0.25% of unclassified grids. Among the three scales, 50 x 50m was identified as an optimal spatial unit for LST analysis of typologies at local scale as it provides appropriate spatial information.

The quality of the proposed classification scheme was assessed through two methods. Firstly, a pilot study representing a cross-section of Sydney's urban conditions was selected due to resource and time constraints; where the accuracy of classified spatial units was compared versus validation data from ground-truthing using a confusion matrix. Results were satisfactory with an overall accuracy of 76.4% and Kappa coefficient value of 0.741. Secondly, the evaluation of the predictability and quality of the classification parameters and threshold values defined for each GIT class was conducted using 22 supervised machine learning algorithms and the totality of observations (or grid cells). Results show a high accuracy (>80%) of predictions for all models, and especially for classifiers implementing fine decision trees learners.

Inter-typology comparisons of mean LSTs show clear thermal differentiations among GITs. The warmest typologies during the day are the *impervious* GIT subgroup followed by *mixed* GITs with a considerable presence of impermeable surfaces; while the coldest typologies correspond to *aquatic* and highly forested GITs. At night the pattern is reversed, so the warmest typologies are those characterised by a larger proportion of water bodies and dense canopy, while the lowest LSTs occurred in treeless GITs with a large proportion of irrigated grasses, followed by *pervious* GITs with aligned and dispersed trees. These patterns are similar in summer and winter; however, intra- and inter- typology thermal differences are less pronounced in winter.

Further statistical tests including the *Kolmogorov-Smirnov* statistic and *one-way Welch-ANOVA* with *Games-Howell post hoc test* were implemented for multiple comparisons. Results show that statistically significant differences among LSTs prevail for most GITs at daytime and night-time and for both seasons (73-87% of differentiation); nonetheless, temperature differences are more distinguishable in summer and daytime.

The overall cooling effect of each typology was calculated relative to a reference case corresponding to the IM1 *Highly impervious* typology. In both seasons, maximum diurnal cooling capacities were obtained by the *aquatic* and *pervious* typologies (especially dense and clustered trees) while the lowest cooling capacity was registered by *impervious* GITs due to the limited presence of vegetation and significant amount of buildings and pavements.

It was also found that the influence of tree configuration in thermal cooling depends on land cover composition of the immediate environment and the proportion of forested areas. Accordingly, larger tree canopy is more effective in reducing diurnal LSTs if this is surrounded by irrigated grasses and shrubs. Furthermore, irrigated grasses exceeded by far the cooling capacity of non-irrigated low plants. At night, a reversed pattern is observed, so *aquatic*, *impervious* and heavily forested GITs provided a relative heating effect; however, an increased surface wetness can reduce this situation. Despite the similarity of results between both seasons, it was observed a relatively greater cooling capacity of most vegetated GITs in winter. Previous evidence is corroborated by the results of the TVX, correlational and hierarchical cluster analyses.

TVX analysis and simple linear regression between vegetation abundance descriptors and the cooling capacity of GITs demonstrate that *aquatic* GITs (particularly water bodies) exhibit a distinct diurnal and nocturnal thermal behaviour. Since this subgroup has an outlying effect, it is recommended to perform statistical analysis separately from terrestrial

GITs. Based on bivariate correlations, the impact of vegetation abundance on diurnal and nocturnal LST reductions of terrestrial GITs is generally better explained by the proportion of pervious surfaces. Since photosynthetic activity is negligible at night, NDVI can only explain the cooling effects of typologies in the day. Tree coverage, however, cannot completely explain the cooling effects of GITs as single predictor.

A total of four OLS models (1A, 2A, 3A, 4A) were developed, one each for a time of the day and season, for the prediction of LSTs at the local scale using the GIT classifications as observations. The statistical analysis process determined that several assumptions were violated, particularly multicollinearity, homoskedasticity, and non-autocorrelation. In an attempt to address these issues, several combinations of omitted variables were tested to produce four revised OLS models. Although multicollinearity between independent variables improved considerably, heteroskedasticity was still a serious issue, as well as there was strong evidence of autocorrelation of residuals caused by spatial dependencies.

Accordingly, global and local spatial autocorrelation analysis recognised the presence of considerable positive spatial associations among residuals and suggested the *Spatial Error Model* (SEM) as the most appropriate spatial regression method to produce robust predictive equations for all four models. Whereas the introduction of the spatial autoregressive error term (*Lambda*) improved the performance of the four classic OLS regressions significantly, it did not entirely reduced heteroskedasticity; so further corrections were implemented.

By analysing the residual plots of all models and according to the evidence of TVX analysis, it can be concluded that a single spatial regression equation is not suitable for all locations using the totality of observations. In this sense, datasets from each model were partitioned into *aquatic* and *terrestrial* observations, and cases belonging to IM1 class excluded. A total of eight revised SEMs were developed than can be applied either in *aquatic* (Models 1D, 2D, 3D, and 4D) or *terrestrial* (Models 1E, 2E, 3E, and 4E) contexts for the prediction of diurnal and nocturnal LSTs in summer and winter. Summary of the Maximum Likelihood Estimations of the eight revised SEMs display a superior performance in comparison to all previous attempts. Whereas heteroskedasticity was not completely eliminated, this was significantly reduced as shown by the new residual plots.

The interpretation of results of the final eight SEMs (1D, 2D, 3D, 4D, 1E, 2E, 3E, and 4E) including the analysis of the individual contributions (from regressions coefficients) of each independent variable for the formulation of SUHI mitigation strategies are presented and discussed in the next chapter.

Chapter 8

Discussion²⁶

8.1 Introduction

This chapter summarises and discusses the research findings in relation to the four objectives of this thesis outlined in Section 1.3. First, Section 8.2 evaluates the application of the research methodology presented in Chapter 5 which was applied in two related case studies of the Sydney metropolitan region. This section also focuses on the advantages and disadvantages of the research framework and selected data processing methods, in particular, the potential of high-resolution airborne remote sensing to map spatio-temporal thermal patterns and analyse the cooling effects of green infrastructure with higher accuracy and precision. This section also includes a discussion on the quality of remote sensing datasets and derived products for the computation of variables.

Second, the suitability of the application of the green infrastructure typology –introduced in Chapter 4– as a framework for characterising urban green infrastructure and assessing thermal conditions is demonstrated in Sections 8.3 and 8.4. Section 8.3 examines the quality of the automated classifications of GITs at different spatial scales, evaluates the accuracy of these classifications, and explores other potential applications and improvements for similar research in the future. Section 8.4 provides an expanded summary of research findings and presents a comparative analysis of the spatial and seasonal variability of the diurnal and nocturnal LST characteristics of GITs identified for the study area. It analyses the factors influencing on the cooling effects of different GITs and provides a ranking of typologies according to the provision of their cooling benefits.

Third, Section 8.5 presents the outcomes of different statistical models developed for the prediction of LSTs in different urban contexts, and times of the day and year. This includes

²⁶ A portion of Chapter 8 has been submitted for publication: Bartesaghi Koc, C., Osmond, P., Peters, A. (2019), Mapping and classifying green infrastructure typologies for climate-related studies based on remote sensing data. *Urban Forestry and Urban Greening*.

the quantification of the relationships between day and night LSTs and the physical and configurational descriptors estimated for the spatial units. Additionally, it provides a comparison and evaluation of the most adequate statistical methods for the prediction of LSTs.

This chapter concludes with a discussion of the most significant practical implications of the research outcomes and model prediction for urban design, planning and policy making (Section 8.6). This chapter concludes with the application of the statistical analysis for the assessment of SUHI and scenario modelling of heat mitigation strategies.

8.2 Airborne remote sensing for mapping green infrastructure and thermal conditions

In this thesis, it has been demonstrated that hyperspectral, multispectral, and thermal imagery, supported by LiDAR and cadastral data, can be employed to obtain very highly detailed two- and three-dimensional information of extensive urban areas; which is essential to understand and quantify the impact of green infrastructure on the microclimate of a specific site.

In this research, an array of airborne remote sensors enabled the acquisition of very high-resolution imagery of 0.5 - 2m per pixel that facilitated the identification of surface materials and thermal profiles of large areas more accurately. No significant differences in surface cover recognition were found between products derived from images with 0.5, 1 and 2m pixel resolutions. However, more reliable NDVI values were retrieved from hyperspectral imagery, as they covered a wider short-wave spectrum compared to multispectral images.

Although the application of an NDVI threshold method produced good results, these are sensitive to season, vegetation phenology, irrigation levels, and climatic conditions prior and during the data collection; factors that hampered the definition of consistent threshold values for identifying distinct land cover types. Multiple endmember spectral mixture analysis (MESMA) and deep learning (*i.e.* Convolutional Neural Networks-CNN) are relatively recent powerful state-of-the-art techniques that have shown superior results for image processing and thematic classification of land covers. Despite their demonstrated quality and accuracy; it was not possible to implement them in the present research due to skill and resource limitations.

As spectral and TIR imagery provide a bird's eye view of horizontal surfaces, the incorporation of LiDAR data provided a detailed three-dimensional information (specifically height) of structural elements such as buildings, plants and topographic characteristics. The combination of an NDVI threshold method with LiDAR extractions improved land cover recognition considerably as structures obscured by tree crowns were identified. Despite this advantage, initial building extractions required several refinements to obtain more accurate and reliable products; and these included: splitting building footprints along cadastral property lines, squaring polygons and completing missing structures manually. This process was very tedious and time consuming, and it could have been obviated if LiDAR data with a higher point cloud density were available.

Airborne mapping typically provides information of thermal and spectral reflectance of horizontal surfaces, rather than urban canopy layer conditions, such as air temperature, which are more relevant to HTC. In this sense, evidence presented in this thesis is not representative of the overall thermal conditions of GITs as LSTs of vertical surfaces (building facades) are obviated.

As recommended by Geletič et al. (2016), an important condition for an appropriate comparison of LSTs between different classes of a typology requires mutual independence between thermal and classification data. Whereas the present research fulfils this requirement; classifications were assessed using thermal imagery from specific times (day and night, summer and winter) from which quantitative information for temperature ranges and dynamics for each GIT cannot be retrieved.

Furthermore, airborne remote sensing provides limited information of the temporal evolution of LSTs within each GIT class, unless time-series of imagery are collected. However, multi-temporal analysis remains unaffordable and laborious for many users due to prohibitive costs and complicated logistics required for conducting periodic flight campaigns. For instance, in this thesis, the acquired data was subject to satisfactory meteorological conditions, availability of sensors (and imagery), air traffic restrictions imposed by local authorities and limited research budget. As a consequence, all data were obtained from a third party or contractor, which restricted the quality control of final remote sensing products. The advent of unmanned aerial vehicles (UAVs) and smaller spectral imagers can help overcome these issues, as very high resolution images can be retrieved by drones in a flexible, easy, and less costly way (Gaitani et al., 2016; Gaitani et al., 2017); and this is subject to future research.

In this thesis, TIR imagery was collected, processed and provided by a contractor who opted to use a NEM method initially described by Gillespie (1985) and implemented by Realmuto (1990) as it can produce reliable LST estimations for a variety of surface materials in an easily replicable and rapid way; thus, it can be implemented by users with different skill levels (Gillespie, 2015). Similar satisfactory results were obtained when the NEM approach was tested using high-resolution radiance spectra from hyper- and multi-spectral imagers by other studies (Gillespie, 2015; Mushkin et al., 2005; Sobrino et al., 2008; Tang & Li, 2014).

As suggested by N. Chrysoulakis (personal communication, 2017), a constant emissivity value can be employed if LST is only required for identifying hotspots and representative temperature differences among GIT classes in a specific moment, such as in the case of the present dissertation. However, this method should be avoided if analyses are conducted at pixel-/sub-pixel levels as it may cause certain inaccuracies in the estimation of absolute LSTs. If hyperspectral data is available, the application of spectral unmixing techniques (*i.e.* MESMA) is recommended as it assigns emissivity values to specific land cover types using spectral libraries and estimating the total emissivity of the pixel as a weighting average.

Due to abovementioned limitations of airborne remote sensing, satellite products (*i.e.* Landsat, Sentinel) could alternatively be tested within the same framework as they are routinely captured and easily accessible, offer good spatial coverage, and require corrections that are well documented. In fact, Coutts et al. (2016) suggest non-specialised users (*i.e.* municipalities) employ satellite-based imagery for the identification of hotspots at neighbourhood and city levels.

Further discussion on the advantages and disadvantages of the proposed GIS-based methodology and the influence of remote sensing data on the quality of classifications, and potential latent errors, is provided in Section 8.3.3.

8.3 Classification of green infrastructure for climate-related studies

Several approaches for assessing the microclimatic conditions of urban greenery have been discussed in detail in Chapters 3 and 4, particularly the LULC (Anderson et al., 1976), LCZ (Stewart & Oke, 2012), HERCULES (Cadenasso et al., 2007) and UVST (Lehmann et al., 2014). The classification framework developed for this research –in response to the first

and second objectives (Section 1.3)– combines aspects of the above-mentioned approaches; however, it is not intended to supersede them, rather to complement them.

A streamlined GIT and its corresponding GIS-based automated classification framework (workflow) were developed to classify green infrastructure (as a combination of biotic and man-made features) in a universally applicable convention to support climate research at multiple spatial scales. These were successfully tested at the local scale and applied in two related case studies of the Sydney metropolitan area. This represents a major outcome of this research and a significant contribution to knowledge.

The capacity of quantifying green infrastructure descriptors based on high-resolution airborne remote sensing data enabled an accurate, realistic, rapid and automated representation and classification of extensive areas and varied urban conditions. Although the process, parameters and threshold values respond to a specific method and context, the scheme can be similarly replicated in any given location if comparable data are available (*i.e.* spaceborne imagery). It is also highly flexible as it allows refinements where necessary. For instance, *aquatic* GITs can be expanded for locations with widespread water systems. Furthermore, additional parameters can be explored, and cut-off values updated for a specific type of analysis and setting.

8.3.1 Identifying an optimal grid size for classifications

The classification scheme and workflow were successfully tested at different spatial scales with satisfactory results. However, the application of GITs entails certain constraints regarding the most optimal grid size for thermal analyses. When mapping urban contexts, finer grids tend to be more aggregated and homogenous as single elements (*i.e.* large trees, warehouses, extensive parking lots) occupy most part of the grid; while coarser grids are more heterogeneous since features are highly disaggregated and discontinuous (except for very large and homogenous areas, for example, extensive forestland or large lakes). Accordingly, the most optimal sampling distance depends on the context of analysis, so it should be sufficiently small to reduce granularity and avoid fragmentation and large enough to include representative land cover types and arrangements of vegetation structures.

Unfortunately, defining the ‘best’ grid size for all purposes is impractical as this may depend on the morphological characteristics of the built environment, the type of research, and the type of climatic phenomena targeted, which will likely differ between locations. However, an approximate range of sizes can be specified. In this investigation, three spatial units of 25m, 50m and 100m side were tested and compared. As a result, 25 x 25m grid

resolution was too small to effectively identify different spatial arrangements of trees, as cells were mostly dominated by one or two surfaces [Figure 7.3c]. Conversely, 100 x 100m grid resolution was too coarse and exhibited a large variation of surface and configurational descriptors, so conditions tend to be generalised for the whole grid [Figure 7.3a].

After conducting visual inspections and a comparative analysis, grids of 50 x 50m demonstrated to be a more appropriate sampling size for local scale analyses (neighbourhood, precinct, street) as results preserved representative morphological and configurational information necessary for urban microclimate studies [Figure 7.3b]. Hence, the remainder of analyses were conducted at this spatial scale. Future research could focus on quantifying and comparing the thermal differences of GITs across multiple spatial scales.

8.3.2 Defining relevant classification descriptors and cut-off values

This research has demonstrated that the classification scheme for green infrastructure presented in Chapter 4 can be successfully applied to catalogue urban landscapes into 34 specific GITs with distinct characteristics. When analysing the classification results, a high similarity was found between the spatial pattern of GITs and the existing morphological conditions of two case studies of the Sydney metropolitan area.

A major challenge related to the identification of distinct GITs was selecting appropriate classification parameters and threshold values. Initially, cut-off values for surface fractions were based on those defined by Stewart and Oke (2012) for the LCZ scheme. As these provided relatively limited information about the bio-physical characteristics of natural features, a second step required modifying the values suggested by Irger (2014) and readjusted by Bartesaghi Koc, Osmond, Peters et al. (2018) for the application of LCZs to the context of Sydney. To reduce the number of unclassified grids, classification values were refined and tested several times until obtaining optimum results. Although significant modifications to the original LCZ values were introduced in most cases, this process was essential to adapt the parameters to typical landscape conditions in accordance with the purpose of this research.

As mentioned earlier, a close similarity is observed in the land cover composition between certain set of typologies, such as IM4-5-6, MX5-7-9, MX6-10, PV5-7-9, PV6-8-10 and AQ6-8 GITs. As these subsets are part of the same GIT subgroup (*i.e.* impervious, mixed, pervious, aquatic), they are mainly differentiated by the type of tree arrangement –namely *aligned*, *scattered*, and *clustered*; hence, the importance of considering the spatial

fragmentation of the tree canopy in classifications. Due to time constraints, this research only considered the spatial configuration of trees as these can considerably alter wind speeds/direction, intercept solar radiation and provide significant transpiration. Future research could potentially consider incorporating the spatial distribution of other surface covers into the proposed scheme.

Several FRAGSTATS indices defined by McGarigal and Marks (1995) and McGarigal (2015) were evaluated to identify the most optimal combination of metrics and threshold values for an effective tree canopy pattern recognition. Tests were conducted at a *class level* using the grid size as the total *landscape* and tree patches as the target *class*.

Contiguity index (CONTIG) and *fractal dimension index* (FRAC) are perimeter-to-area ratio indices that were assessed on their capacity to quantify spatial connectedness and complexity of shapes (McGarigal, 2015; McGarigal & Marks, 1995). However, their main limitation is the relative insensitivity to differences in patch morphology, so it is difficult to discriminate between aligned and clustered patterns, and isolated and small groups of trees when patches have similar areas and perimeters. Alternatively, *related circumscribing circle* (CIRCLE) performed better in identifying patch elongation as the index is based on the ratio of patch area to the area of the smallest circumscribing circle and is not influenced by patch size (McGarigal, 2015).

Similarly, *contagion index* (CONTAG), *aggregation index* (AI), *landscape shape index* (LSI), *percentage of like adjacencies* (PLADJ), *clumpiness index* (CLUMPY) and *patch cohesion index* (COHESION) were tested to identify the level of dispersion, interspersion, and adjacency of trees. However, indices based on like-adjacencies (*i.e.* CONTAG, AI, PLADJ and CLUMPY) are strongly affected by image resolution and grid sizes, so results differed for the same area at different spatial scales. Furthermore, COHESION is based on perimeter-area calculations, therefore it is subject to the same limitations described above. LSI provides a standardised measure without upper bounds, thus consistent thresholds are not possible to be defined; however, better results were obtained when its normalised version was applied (nLSI) (McGarigal, 2015; McGarigal & Marks, 1995).

After multiple trials, the combination of *CIRCLE_AM* and *nLSI* proved to be effective in distinguishing dispersed, clustered and aligned tree canopies across multiple spatial scales as they are normalised metrics (between 0 and 1) that are easier to interpret and robust to changes in the grain (grid sizes). Cut-off values for both metrics were determined –after several tests– using the Jenks optimization method (Jenks, 1967). Slight variations in cut-offs were identified when the method was applied to each case study separately due to

differences in minimum and maximum values of each dataset. Thus, decimal values were repeatedly readjusted until obtaining optimal results that can satisfy both case studies.

Despite the satisfactory classification results, the range of values proposed for all the classification descriptors of GITs, and especially the FRAGSTATS metrics, should be treated as guidelines as they are contingent on further adjustments to better reflect the urban characteristics of other locations.

In [Figures 7.5](#) and [7.8](#) it can be seen that the proportion of high vegetation varies among classes sharing the same type of spatial arrangement of trees. For instance, MX10 *Clustered trees with mixed low plants* has a higher proportion of tree cover (>50%) than IM6 *Mostly impervious with clustered trees* and PV10 *Mostly irrigated low plants with clustered trees* (<20%). Likewise, the proportion of aligned trees is larger in MX6 *Aligned trees with mixed low plants* (>35%) and MX5 *Mixed surfaces with aligned trees* (>20%) than in IM4 *Mostly impervious with aligned trees*, and PV5 *Mostly non-irrigated low plants with aligned trees* (<20%). This disparity occurs because of the presence of a dominant surface (described by the adverb ‘*mostly*’) that tends to occupy the totality of the grid. Therefore, trees are surrounded by a high proportion of sealed surfaces and buildings in *impervious* GITs, and by extensive grassy areas in *pervious* GITs. In contrast, in *mixed* GITs the amount of tree canopy is higher as the proportion of vegetated and non-vegetated ground surfaces is more variable.

These discrepancies are less pronounced among typologies with scattered tree arrangements with a difference of 4-9%; except for MX8 *Scattered trees with mixed low plants* that has a disproportionate amount of wooded land compared to other GITs with the same spatial distribution (10-20% extra). Consequently, the categorisation into a specific spatial arrangement is not indicative of the abundance of tree cover, so this should be taken into account when interpreting the LST differences among typologies.

Significant differences of mean NDVI values were found among GITs, and especially between summer and winter case studies. The significantly elevated NDVI in winter can be mainly attributed to an increment in vegetation healthiness due to better irrigation regimes and reduced heat stress on plants due to mild weather conditions. The deciduous nature of some trees throughout the whole study area may also have contributed to differences in the percentages of tree canopy and mean NDVI values.

Despite these facts, the percentage distributions of pervious surfaces for all GITs were closely similar for both seasons (with minor exceptions). This demonstrates the robustness and applicability of the proposed classification scheme to different contexts, extents and

seasons. The findings also suggest that the proposed method for the identification and extraction of surface covers from spectral-based imagery and LiDAR data can be successfully applied, provided that NDVI thresholds are adjusted according to contextual and phenological changes.

The Jenks optimisation method is a classic data clustering method that arranges values by maximising the homogeneity of a group; hence, it proved useful in defining meaningful cut-off values for NDVI and FRAGSTATS metrics. Nonetheless, this method was dependent on the minimum and maximum values of each dataset, so additional refinements may be necessary if applied in future studies. In addition, the differentiation between deciduous and evergreen vegetation could potentially be explored in future research, although this should be evaluated with care as it may add a number of variations that might be redundant or useless in some cases.

8.3.3 Evaluating the accuracy of classifications

The accuracy of GIT classifications was assessed through a confusion matrix by comparing actual observations from high resolution aerial imagery against class predictions. In this research, the extent of the pilot study was selected for accuracy assessment of classifications due to time constraints.

An accuracy rate of 85% has been generally accepted as an optimum target for an accurate classification of remote sensing imagery into specific classes (Anderson et al., 1976; Wang et al., 2018). Although the overall accuracy of GIT classifications of the pilot study (76.4%) has not reached this target, this can be considered as ‘acceptable’ since these were not intended for the thematic mapping of major LULC types at a pixel level, but for a newly developed scheme considering a combination of morphological and spatial descriptors. The achieved rate can be used as an indicative value of the overall quality of classifications for both case studies (summer and winter); however, this should be considered with caution as it only covers a small portion of the whole study area.

In-depth analysis was performed to classifications and higher accuracies were obtained by treeless typologies and/or with a highly-differentiated proportion of land covers. It was identified that common misclassifications, and consequently low *user accuracies*, occurred due to the following reasons:

1. The considerable disproportion in the number of validation points among typologies (*i.e.* 53 samples for *IMI* versus 3 samples for *PV6*). Thus, the present scheme is contingent on additional accuracy assessment with a larger number of ground truthing samples.

2. Tree canopy was not properly identified and extracted from LiDAR data for some areas (errors of commission and omission). This was mainly caused by errors in the pre-classified LiDAR points cloud data in which parts of buildings (commonly pitched roofs) were recognised as high vegetation [Figure 8.1a]. Small, hollowed or elongated structures (*i.e.* containers, cars/trucks, trains, reservoirs, antennas) were also misidentified as vegetation structures [Figure 8.1b]. These errors are potentially produced by similar waveform of laser return signals from leaves, branches, and built structures that shared common morphological characteristics. To correct erroneous feature extraction from LiDAR data and improve the quality and accuracy of vegetation surfaces recognitions, results were cross-validated against land covers identified from NDVI imagery.

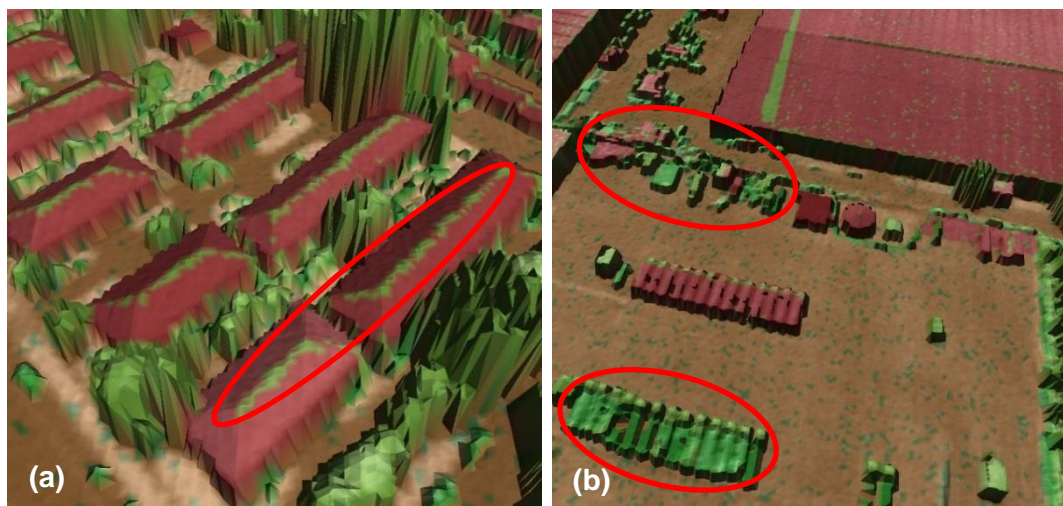


Figure 8.1 Examples of common errors identified in the pre-classified LiDAR points cloud data.

3. Spectral similarities between some surfaces generated several identification errors which include: (a) impervious surfaces (*i.e.* roads, ballast, paved parking) were mistaken for bare soils, (b) non-irrigated grasses confused with compacted soils or pavements, and (c) shadows considered as water or non-irrigated grasses [Figure 8.2]. Falsely classified pixels are due to distorting errors caused by overshadowed areas, drought, and latent errors in the NDVI generation process. These issues could be minimised by performing additional shadow corrections, implementing multitemporal analysis to replace erroneous pixels based on images captured at other times, and by tuning NDVI classification thresholds; which are subject to future research.
4. The proportion of spectral-based errors was higher in summer datasets as NDVI values were derived using the red bands of two separate images (CIR and RGB) rather than from a single multi-spectral image (see Section 6.3.1.1). On the other hand, the pixel resolution of the hyperspectral image (2m) used for the winter case study –which was twice the pixel

size of the multi-spectral image (1m)– was insufficient to identify small vegetation patches such as hedgerows [Figure 8.2]. A potential area of research can be the quantification of the effect of spatial and spectral resolutions (*i.e.* number of bands, pixel sizes) on thematic mapping using NDVI images.

Errors related to spectral issues



Figure 8.2 Examples of errors and inaccuracies on the surface cover extractions related to spectral issues and spatial resolution of images.

5. Surface covers underneath the vegetation canopy were not retrieved by spectral imagery in summer so these were considered as vegetated areas even though they corresponded to other surfaces (*i.e.* roofs or pavements). Conversely, full tree canopy was not detected in

winter, so partially leaved deciduous trees were classified as the land cover below (usually non-irrigated grasses) [Figure 8.2]. These errors were reduced for most cases by cross-validating spectral and LiDAR derived products one against each other.

6. There was a large variation of pervious and impervious surface fractions within some spatial units. Moreover, grids with surface fraction values close to upper or lower bounds were incorrectly assigned to the subsequent class.
7. FRAGSTATS indices were limited in distinguishing different tree patterns when these had similar areas and perimeters. Accordingly, common misclassifications include: (a) small clusters, discontinuous, convoluted or partial rows of trees were considered as isolated or dispersed trees respectively [Figure 8.3a]; (b) typologies with scattered trees were classified as aligned [Figure 8.3b]; (c) large mature trees were mistaken for clustered arrangements [Figure 8.3c]; (d) wide linear forested areas were considered as clusters [Figure 8.3d]. Further research could focus on improving current cut-off values and exploring additional combinations of *shape* and *aggregation* indices to resolve these shortcomings.

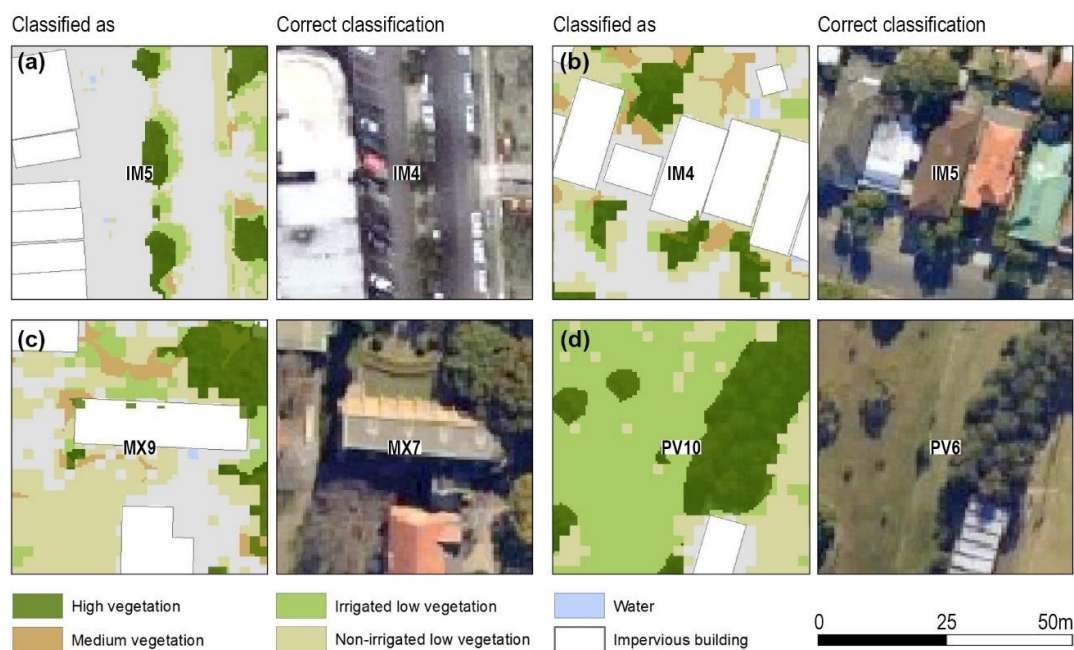


Figure 8.3 Example of misclassifications related to the limitations of FRAGSTATS metrics.

Despite that several corrections were conducted to improve the accuracy and quality of LiDAR and spectral derived extractions, a limited number of grids (1.43% of the total number of grids in summer and 0.60% in winter) were incorrectly classified. These were excluded from statistical analyses to minimise errors and improve the results of models.

8.3.4 Assessing the predictability of the classification scheme

As shown before, the overall accuracy of classified GIT maps was subject to the quality of surface cover recognition and adequate discrimination of tree configurations; in contrast, the overall quality of the classification scheme mainly depended on defining relevant parameters and threshold values for each typology; hence the differences in the results and interpretations between both accuracy evaluation methods (described in Section 7.2.3).

In this sense, the assessment of the performance of the classification scheme was conducted by comparing the overall accuracy of GIT predictions from several machine learning classifiers. Predictive models used the totality of grids (referred as dataset) from each case study that were randomly divided into training and validation data. On one hand, 75% of the dataset was employed to train models, so algorithms understood the classification parameters or predictors and associated them with a corresponding GIT class. On the other hand, 25% of the dataset was held out to validate predictions and avoid overfitting.

No single machine learning classifier is suitable for every problem as identifying the right model is usually a process of trial and error (MathWorks, 2018a); thus, several algorithms available in the *classification learner app* in Matlab were tested. Moreover, the best overall accuracy scores do not necessarily indicate the best model for a particular goal as classifiers with a slightly lower accuracy might be more suitable for a certain size of dataset, type of phenomenon (non-/linear), and type and number of predictors.

Findings presented in Section 7.2.3.2 show *high to very high* predictability for most models (>80%) and demonstrate the robustness of classification descriptors and threshold values proposed in Chapter 4 [see Table 4.14]. No substantial differences between accuracy scores of summer and winter datasets were identified. This proves the applicability and reliability of the classification scheme despite differences in location and season. As the winter dataset contained a larger number of samples than the summer dataset, this presumably might have influenced in their slightly higher accuracy scores.

Classifiers implementing *decision trees* learners (*Fine decision tree* and *Ensemble-Bagged trees*) achieved the highest scores ($\approx 100\%$) as they are good generalists and subdivided the data using a binary format [Figure 8.4a]; however, they are prone to overfitting if no or small number of validations are selected. The very high overall accuracy of these learners [Table 7.3] can be explained by several factors. First, the class subdivision in decision trees is similar to the logical division implemented in Section 4.9 for the standard classification of green infrastructure [Figure 4.5] and the cut-off values defined in Table 4.14.

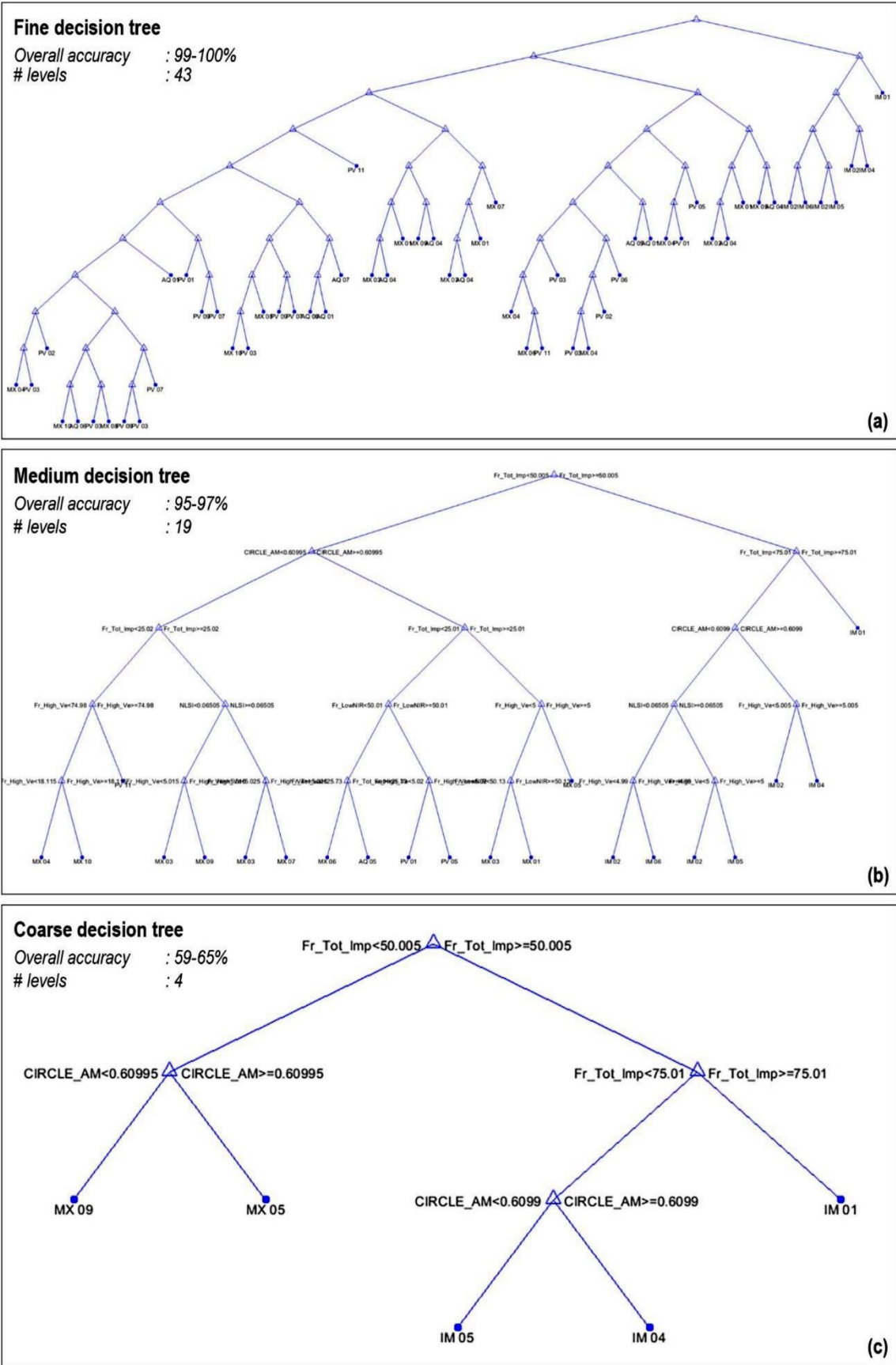


Figure 8.4 Comparison of the number of levels (binary splits) and overall accuracies calculated by the fine, medium, and coarse decision trees classifiers.

Second, the use of many branches or deeper splits (43 levels) provided *fine* distinctions and better results than medium and coarse learners (19 and 4 levels respectively) [Figures 8.4b – 8.4c]. Therefore, a *fine tree* is usually highly accurate and particularly suitable for many predictors and large number of classes. Third, *Ensemble* models are typically characterised by a high accuracy and good performance for medium-sized datasets as they combine two algorithms to power their predictability.

SVM classifiers also performed well (80-97% of accuracy), especially the algorithms implementing *linear* and *quadratic* separation hyperplanes ($\approx 96\%$). The hyperplane is defined as the best margin that segregates data points from two classes [Figure 8.5]. Based on the results presented in Table 7.3, it can be assumed that the classification of GITs exhibits clear separation boundaries that are characteristic of less complex problems. Additionally, *SVM* classifiers offer confident accuracy rates as they are effective in high dimensional spaces (large number of classes and features).

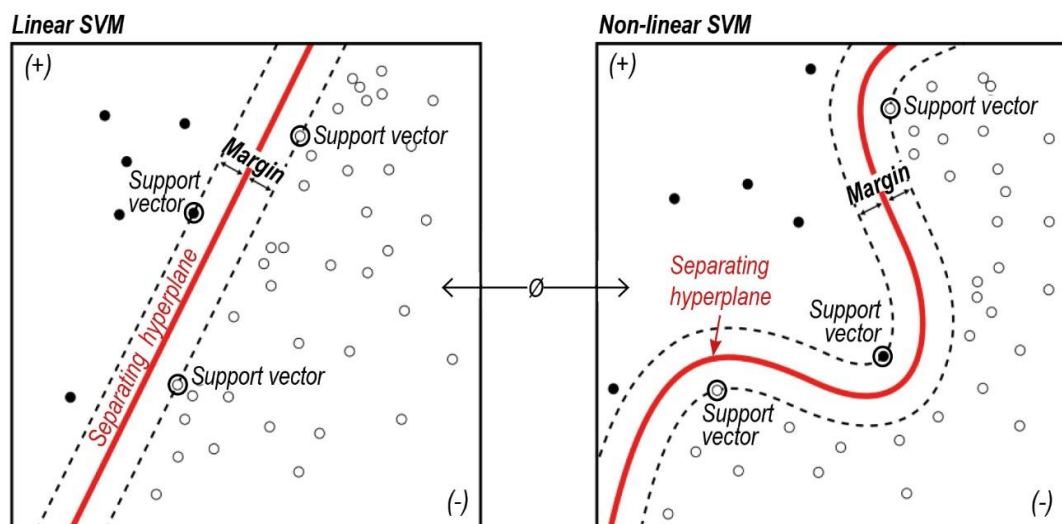


Figure 8.5 Example of class discrimination applied by linear and non-linear support vector machines classifiers (SVM) classifiers.

Despite being the most popular, fast and easy to interpret classifiers, *linear* and *quadratic discriminant* models did not perform as well as *SVM* algorithms, achieving between 71% and 81% of accuracy. This is because discriminant analysis tends to reduce the dimension of data to decrease the computational time; so, such reductions caused a loss of information that led to lower classification accuracies. Also, to train the classifier, the algorithm calculates the parameters of a Gaussian distribution for each class, which may not be appropriate for current datasets (MathWorks, 2018b).

KNN classifiers performed slightly better than *discriminant* models (76-87% of accuracy); however, these are typically more suitable and have better predictive accuracy in low dimensions rather than high dimensions. Since none of the trained classifiers were tuned to improve the accuracy of predictions, advanced *KNN* options may be potentially explored such as testing various distance metrics and weights.

Despite optimum results, accuracy assessment of selected classifiers indicates that further calibrations on certain GIT classes may be required to improve the quality of predictions. This is the case for AQ6 *Water with scattered trees*, AQ7 *Water with clustered trees*, MX8 *Mixed grasses with scattered trees*, PV7 *Mostly non-irrigated grasses with scattered trees*, and PV8 *Mostly irrigated grasses with scattered trees* that repeatedly showed the lowest predictability rates in most models.

GITs with scattered trees were the most difficult to distinguish from other tree configurations as shown in Figures F1 to F10 (in Appendix F). They also indicate that in the absence of a considerable number of trees some confusion occurs between *mixed* and *pervious* GITs (*i.e.* PV3 predicted as MX4). These issues could potentially be amended in future by: (1) improving the cut-off values of FRAGSTATS metrics, (2) introducing more accurate spatial configuration descriptors, or (3) simplifying the categorisation of tree arrangements (*i.e.* scattered and clustered trees only).

8.4 Thermal performance of green infrastructure typologies at local-scale

8.4.1 Understanding the thermal profiles and cooling effects of GITs

In response to the first and second objectives of this thesis (see Section 1.3), the empirical results presented in Section 7.3 demonstrate the applicability of the GIT classification system as an assessment framework for the study of the intra- and inter-variability of LSTs and cooling effects of different compositions, amounts and spatial arrangements of green infrastructure. The cooling effects (or cooling capacity) is expressed here as the difference in mean LST between a typology with vegetated and/or water features compared to a base case or reference which corresponds to a highly impervious context with no vegetation (IM1 *Highly impervious*). In accordance with this notion, GITs can be considered as cooling strategies that can be used to prescribe a potential LST reduction resulting from the combination of functional (irrigation, evapotranspiration), structural (fractional cover), and configurational characteristics of green infrastructure.

During calm and clear conditions, statistically significant thermal contrasts among GITs varied as function of the composition, abundance and distribution of surface covers. This is the case of IM1 *Highly impervious* and AQ1 *Water* which difference in LSTs in summer exceeded 12°C during the day and 2.4°C during the night. However, thermal differences among typologies are complex in nature as they are also disrupted by surface wetness/roughness, concentration/distribution of tree canopy, proportion of buildings and impervious ground, as well as the diurnal, seasonal and topographic conditions of surfaces (Mathey et al., 2011; Stewart, 2011b).

Either in summer or winter, the highest diurnal LSTs and consequently the lowest cooling capacity correspond principally to typologies with a large proportion of impermeable surfaces, reduced surface moisture, and no or few vegetation (IM2-6). Lower cooling effects were also registered for open and sparsely built areas with mixed surface covers (MX1/3/5/7/9); and by green open spaces with poor irrigation conditions (PV1/5/7/9). On the other hand, as the proportion of water features, trees, shrubs, and surface moisture increases, the diurnal LST cooling capacity of typologies also increases (*i.e.* AQ1/5/6/7, PV3/6/8/10/11, MX6/8/10).

In contrast, at night-time a relative heating effect was registered by areas comprising considerable amount of water and impervious surfaces (AQ1-7, IM2-6), followed by those with aligned, clustered or dense tree canopy surrounded by mixed surfaces (MX3/5/7/9/10). Conversely, treeless greenspaces with shrubs and no or few trees were the most effective in reducing nocturnal LSTs (PV1/2/3, MX4) in accordance with the literature (Hong & Lin, 2015; Lehmann et al., 2014).

Previous evidence confirms the significant role of surface wetness and irrigation in reducing LST and mitigating the SUHI by improving the cooling performance of typologies through increased evapotranspiration, as described by other studies (Coutts et al., 2007; Coutts et al., 2013; Halper et al., 2012; Spronken-Smith & Oke, 1998).

Evidence also indicates an inverse thermal behaviour of *aquatic* and *pervious* GITs between day and night [see Figure 7.24]. Accordingly, the higher the proportion of superficial water, the lower the diurnal LSTs while the higher the nocturnal LSTs. This proves the typical thermal ambivalence displayed by water bodies as described in the literature (Oke, 1988b, 1992). Accordingly, a considerable volume of water (AQ1 *Water*) exhibits low LSTs during the day by absorbing most of the incoming solar radiation while it becomes a major heat source at night because of the considerable amount of energy stored (Oke, 1988b; Oke et al., 2017).

However, thermal patterns of large water bodies differ from smaller systems as the latter are affected by the presence of organic components, turbidity and the depth of water due to a notable amount of runoff from adjacent urban land (Oke, 1992). This is demonstrated by the significant difference of thermal profiles between open water (AQ1) and the remainder of *aquatic* GITs (AQ4/5/6/7). This contrast is more evident during the night and in wintertime because of the enhanced warming effect caused by vegetation and impervious surfaces. This illustrates the typical edge-effect caused by shallow waters in shorelines as short-wave radiation can penetrate to the floor, warming up the lower part of the aquatic system (Oke, 1992).

Similarly, the higher the proportion and concentration of tree canopy, the lower the LST at daytime. This confirms the cooling effect of vegetation through shading –by limiting solar penetration and reducing the energy absorbed by surfaces during the day–, and through evapotranspiration which is essential to cool down surfaces (Erell et al., 2011; Hunter et al., 2012; Lehmann et al., 2014; Norton et al., 2015; Oke, 1988a; Oke et al., 1989; Spronken-Smith et al., 2000).

On the contrary, denser trees and shrubs contribute to a relative heating effect at night as medium to high vegetation tend to trap heat by decreasing the SVF which in turn reduces advection (air velocity) preventing the rapid dissipation of heat to the open atmosphere (Oke et al., 1989) [Figures 7.24 and 7.27]. While this can be arguably desirable during winter nights, the nocturnal warming effect of trees during summer was remarkably higher than expected, while considerably outweighed by the diurnal cooling effects. An opposite situation occurs with featureless *mixed* and *pervious* GITs (*i.e.* PV1/2, MX3/4) as low plants open to the sky vault release heat more rapidly than dense forests. Moreover, daily temperature fluctuations of typologies were more evident in summer than winter as solar radiation is more intense, and more energy is absorbed by materials due to higher solar angles. Furthermore, at night the cooling processes in the lower section of the UCL are mostly controlled by the thermal properties of surfaces and the radiative geometry of sites (Erell et al., 2011). This condition can be clearly evidenced in *impervious* GITs (IM4/5/6) and *mixed* GITs (MX3/5/7/9) in which the cooling effects of grasses and trees, regardless of their spatial configuration, are masked by the influence of surrounding materials. This occurs because vegetation traps the radiant heat emitted by pavements and building surfaces and reduce cold air infiltration, resulting in higher air temperatures that may significantly affect human thermal comfort in both indoor and outdoor spaces. This situation is particularly exacerbated in summer due to the low wind speeds and heatwave-related conditions reported during the data collection.

Analysing the inter- and intra-typology variability of LSTs

Overall, the thermal differentiation of GITs is more pronounced during the day and summer conditions as surfaces are exposed to solar radiation which enables a clearer distinction of thermal profiles. However, discernibility of thermal profiles is more limited at night-time as these are governed by the combinatory radiative responses (*i.e.* thermal inertia) of various surfaces.

Among typologies, thermal profiles of *impervious* GITs (IM1/2/4/5/6) are the most distinguishable at daytime and night-time and for both seasons. Nonetheless, this subgroup is characterised by a high intra-variability of LSTs represented by a non-normal distribution of frequencies and a large number of outliers [see Tables G2, G3, G5 and G6]. This is particularly more evident for IM1 *Highly impervious* that displays a diurnal variation between the minimum and maximum mean LSTs of 28.14°C in summer and 15.74°C in winter; and a nocturnal variation of 17.21°C in summer and 7.17°C in winter. This may be attributed to the following reasons:

1. The proportion of roof area and impervious ground vary greatly across the *impervious* subgroup. Therefore, as the amount of buildings increases, its influence on mean LSTs is more pronounced since this is highly dependent on the different thermal and spectral properties (*i.e.* surface emissivity, albedo, admittance) of the roofing materials (Akbari & Levinson, 2008; Geletič et al., 2016; Irger, 2014). This is particularly obvious in IM1 *Highly impervious*, where large, low-rise warehouses covered by corrugated light-coloured metal roofs registered significantly lower average LSTs at daytime and night-time than spatial units covered by roofing materials with high thermal inertia such as concrete, ceramic tiles, gravel, and dark-coloured surfaces (*i.e.* asphalt) that are typically found in extensive car parks and roads.
2. The cooling effect of pervious surfaces and trees around buildings might be limited when positioned within predominately impervious surfaces; and may be affected by the height and compactness of buildings (Erell et al., 2011; Meier & Scherer, 2012; Oke, 1981, 1988a; Oke et al., 2017). As such, tall and compact structures generally decrease SVF and provide significant amount of shade, so ground surfaces and trees are protected from solar radiation during the day while trapping more radiative heat at night, yet this varies depending on the season, latitude and background climate and weather of each city. Conversely, open and low-rise building arrangements usually expose more area to incoming solar radiation during the day, facilitating thermal cooling at night. This can be corroborated by the apparent nocturnal heating effect of trees in areas with a substantial presence and compactness of impervious surfaces (IM4/5/6, MX5//7/9) [Figures 7.24 and 7.27]. This

warming effect is more pronounced in summer than winter as it could be attributed to constant warming conditions due to higher solar angles enabling more radiative energy to penetrate urban canyons.

3. The contribution of building facades to thermal cooling is also important as LSTs may be biased by the high proportion of vertical surfaces that cause uneven solar exposure of surfaces, increased radiative energy balance due to multiple reflections, and thermal anisotropy effects (Bechtel et al., 2016; Geletič et al., 2016; Krayenhoff & Voogt, 2016). The latter occurs when directional brightness temperatures (or radiances) recorded by a radiometer result from the sensor viewing angle, so they are the product of the urban form combined with surface temperature variation, instead of being the actual temperature of horizontal surfaces (Krayenhoff & Voogt, 2016).

Considering the nadir (or very close to nadir) position of sensors, the effect of vertical surfaces on apparent LSTs should be negligible (Geletič et al., 2016). Nevertheless, evidence in this research coincides with Krayenhoff and Voogt (2016) which suggest a higher anisotropy in compact high-rise contexts at midday, and in open high-rise areas in the morning and afternoon, that simultaneously cause larger temperature variation between day and night. However, the occurrence of high and closely-spaced buildings in the study area is minimal; so, it could be assumed a limited negative effect of thermal anisotropy. The use of multitemporal data (if available) might be effective to ease the effects of anisotropy as suggested by Bechtel et al. (2016). Although the present research only focused on horizontal surfaces due to data acquisition limitations, the integration of vertical surfaces in the proposed framework could be a potential area for future development.

4. The high concentration of cars (in car parks or streets) as well as air conditioning units, heat exchangers (usually located on top of commercial and retail buildings), or isolated hotspots such as chimneys may have also contributed to above average LSTs in a limited number of cases, which had a localised effect mostly at daytime.

The thermal profiles of *mixed* GITs were well distinguished among typologies, and better differentiated at daytime rather than night-time, despite their high heterogeneity of surface covers. Generally, treed typologies (MX5-10, excluding MX8) were among the most distinguishable during the day and night, while typologies lacking trees (MX1/3/4, including MX8) were not well differentiated, especially at night-time. This confirms the important role of trees in defining particular thermal profiles due to different levels of shade provided.

At daytime, *pervious* and *aquatic* GITs were relatively well differentiated from other typologies. Conversely, at night-time these cooling effects were relatively similar among typologies within each subgroup. As previously mentioned, this confirms the ambivalent thermal behaviour of trees and water features as well as their significant temperature-moderating effect during night-time hours.

Analysing the effect of spatial configuration

As described by Millward et al. (2014), this research has shown that changes in tree cover configuration (scattered, aligned and clustered) does not necessarily result in additional cooling benefits when (1) typologies have a similar proportion of tree cover or (2) when holding the land cover composition constant (*i.e.* IM4/5/6, MX6/8/10 or PV5/7/9) [Table 8.1]. For instance, when situated over non-irrigated grasses, clustered trees (PV9) were 0.39°C and 0.28°C cooler than scattered (PV7) and aligned trees (PV5) respectively [Figures 8.6a].

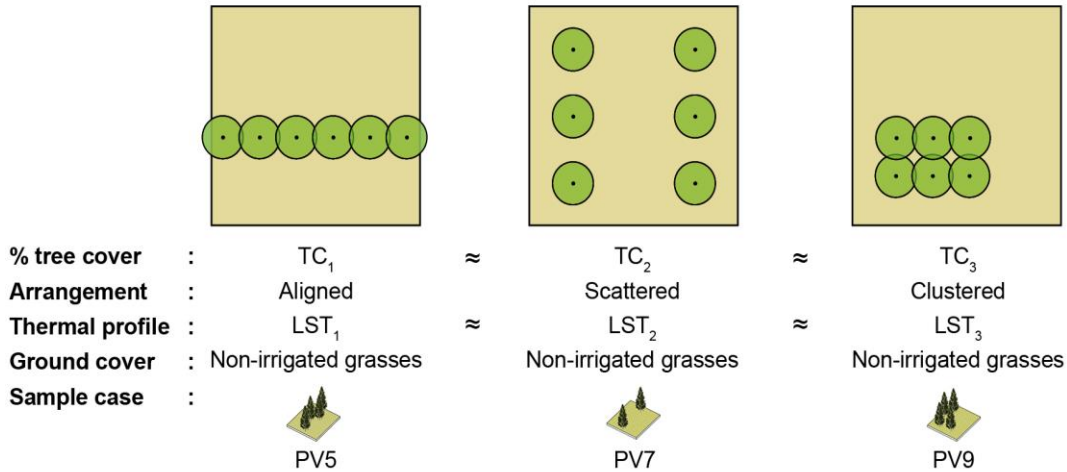
The previous situation occurs because LSTs were averaged per typology, so the thermal conditions are generalised for the totality of the spatial unit regardless of the specific location and distribution of trees. This is expected to be different for air temperature observations as the concentration of trees may influence advection and thermal induced circulations. Furthermore, unlike remote sensing, ground-based measurements are affected by the location of instruments; for example, lower air temperatures may be registered near trees or grassy surfaces than over paved areas.

Likewise, similar studies on the effects of trees on air temperatures found that tree clusters can mitigate high temperatures to a greater extent than individual trees since a higher concentration of medium and high vegetation (depending on tree-planting) can substantially contribute to a larger shaded area and evapotranspiration and hence to improve HTC conditions (Abreu-Harbach et al., 2015; Konarska, Uddling et al., 2015). Tree-specific characteristics such as shape, height, distance between crowns, and type of foliage were not considered in this research, however, they can also influence on LSTs due to variations on shading and transpiration through defoliated trees (Konarska et al., 2014). These aspects could be incorporated by future studies since they are important for planting design of streets, especially in high latitude cities with limited solar access in winter (Kong, Yin, Wang et al., 2014).

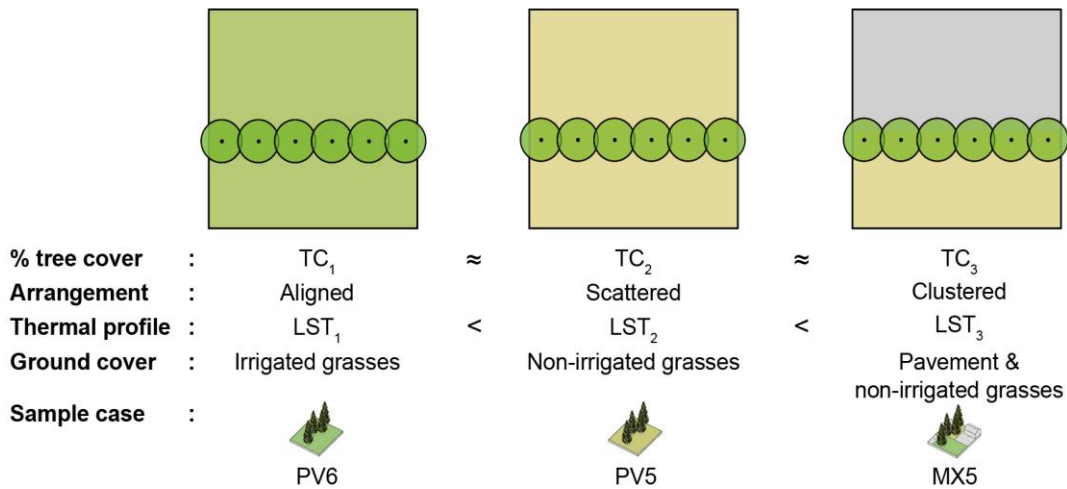
In several cases, GITs categorised as *aligned* display similar proportions of trees as *scattered* and *clustered* arrangements [Figures 7.5 and 7.8] as a consequence of the threshold values defined for each subgroup as per Table 4.14. Thus, potential improvements of the present framework could include: (1) the simplification of tree

arrangements by only considering aligned and clustered arrangements and/or (2) establishing a better distinction in the proportion of trees among the existing configurations (see also discussion in Section 8.3.3).

a. Similar tree coverage and ground cover, but different tree arrangement



b. Similar tree coverage and tree arrangement but different ground cover



c. Similar tree coverage but different tree arrangement and ground cover

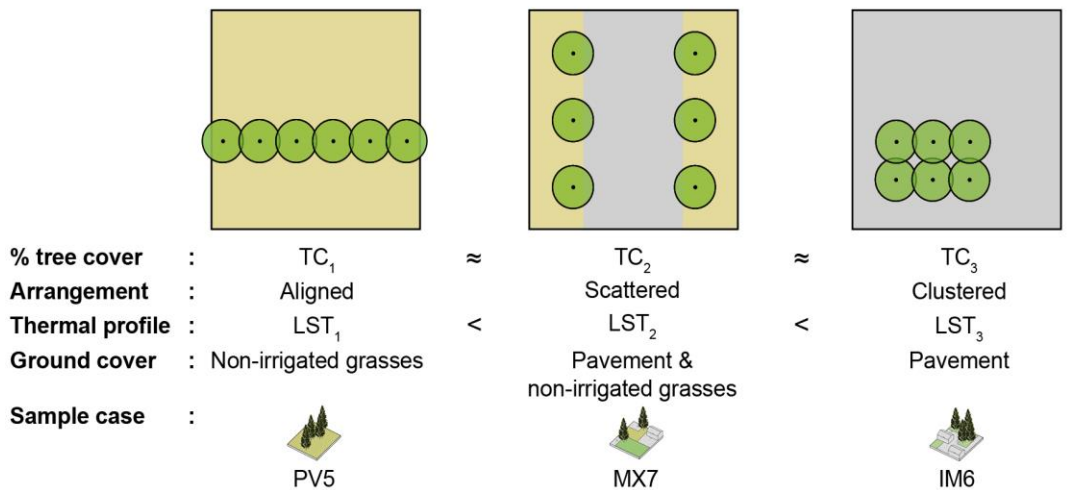


Figure 8.6 Examples of the combinatory effect of ground surface covers and spatial configuration of trees on diurnal LSTs.

Given that land cover composition plays an important role in the thermal performance of typologies, it was found that the impact of tree clustering in LST reduction is stronger as the proportion of impervious surfaces decreases, and surface moisture increases (*i.e.* MX10, PV10) [Figure 8.6b]. For example, in a summer morning, a linear formation of trees positioned over well-watered grasses (*i.e.* PV6) can be up to 4.26°C cooler than when surrounded by paved areas (*i.e.* MX5) and up to 2.15°C cooler than when placed near non-irrigated plants (*i.e.* PV5). In addition, the cooling effects of the same proportion of trees (irrespective of their configuration) can be severely undermined as perviousness and surface wetness decreases (*i.e.* IM6, MX7) [Figure 8.6c].

In summary, composition of pervious surfaces (*i.e.* proportion of different types of vegetation) and their irrigation regimes are more influential in defining the cooling capacity of a spatil unit than the spatial configuration of the tree canopy, as confirmed by several studies (Cao et al., 2010; Kong, Yin, Wang et al., 2014; Meier & Scherer, 2012; Milošević et al., 2017; Zhou et al., 2011). This is also statistically demonstrated in Sections 7.3.2.1, 8.4.2 and 8.5.

8.4.2 Understanding the factors that influence the thermal performance of GITs at local-scale

The TVX approach, correlation analysis and simple linear regression were carried out to understand the statistical relationships between vegetation abundance descriptors (NDVI, percent of pervious area, and percent of tree cover) and the cooling capacity of typologies. Additionally, hierarchical cluster analysis was performed to (1) group GITs into subsets with similar thermal behaviour that can be used to prescribe different urban cooling strategies, and (2) to test whether subgroups of GITs can be distinguished by automated cluster algorithms.

Considering the raw scatterplots composed by LSTs versus NDVI values from all observations [Figure 7.26], it can be observed that in both seasons diurnal NDVI-LST relationships display a typical triangular shape as described in the literature (Carlson et al., 1994; Carlson, 2007; Higuruchi et al., 2007; Weng, 2009). However, these shapes are not identified for nocturnal LSTs as NDVI depends on photosynthetic activity which is negligible at night; hence, the weak or no relationship between both variables.

Figure 8.7 depicts several salient aspects of the triangle that explain the interactions between surface dryness, water surfaces and vegetation abundance, and their relationships with mean diurnal LSTs. The so-called ‘warm edge’ corresponds to terrestrial GITs which slope is defined by the increment of sunlit vegetation. Thus, the larger the percentage,

healthiness and wetness of vegetation cover, the higher the NDVI values and correspondingly, the lower the mean diurnal LSTs. Accordingly, *pervious* GITs comprising well irrigated grasses and dense trees are found in lower right vertex of the triangle.

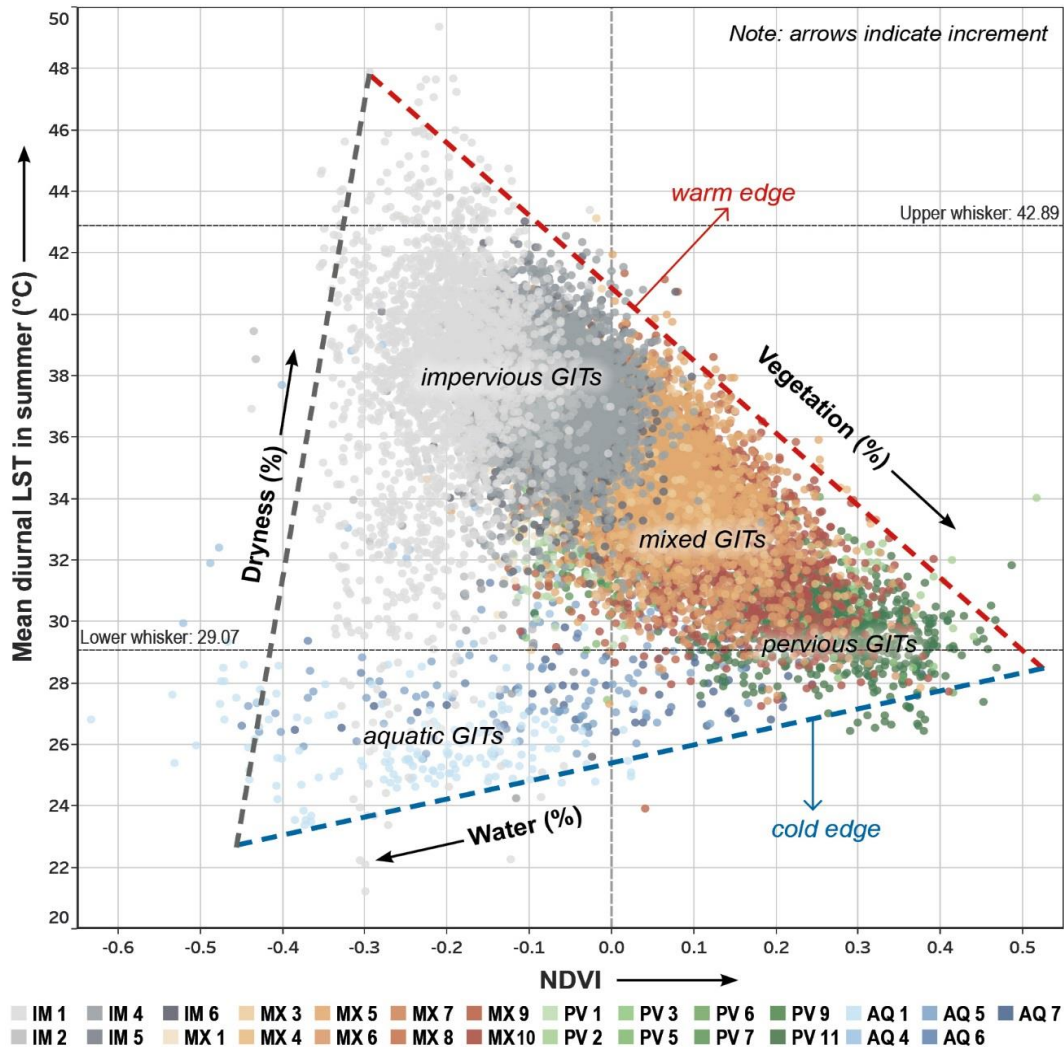


Figure 8.7 Interpretation of the TVX scatterplot of mean NDVI versus mean diurnal LSTs for summer.

In contrast, the higher the imperviousness and dryness of an area, the lower the NDVI values and hence, the higher the LSTs. These relationships are commonly found in *impervious* GITs which situate in the upper vertex of the triangle, while *mixed* GITs and *pervious* GITs with non-irrigated grasses locate half way between both vertices of the warm edge. It should be noted the gradual spread of observations towards the upper vertex as the percent of imperviousness increases. This can be attributed to the differences in the proportion of roof area and impervious ground (as explained in previous section) that create a larger intra-typology variation of LSTs within subgroups; those that are more obvious for highly impervious areas. Conversely, the lower left vertex shows a smaller LST variability that is explained by the high vegetation intensity.

The co-called ‘cold edge’ is associated with *aquatic* and well-irrigated *pervious* GITs and reflects the transition between open water and fully wet terrestrial areas (transition from low to high NDVI). In this sense, the higher the amount of water surfaces, the lower the NDVI and mean LSTs; while the higher the surface moisture and vegetation content, the higher the NDVI and relatively warmer temperatures (compared to water). Whereas the lower right vertex is populated by the AQ1 *Water*, the rest of typologies of this subgroup (AQ3-7) locate in intermediate positions depending on their vegetation content. Due to the high thermal capacity of water, the lower left vertex virtually disappears at night-time (see scatterplots in [Figure 7.26](#)).

Well-defined edges of the data envelope denote a good representation of the full range of soil wetness (or dryness) and fractional vegetation cover, reflecting real physical limits between surfaces (Carlson, 2007). Although diurnal scatterplots from both seasons show these typical characteristics; the triangular shape and edges are sharper in summer since a prolonged exposure of surfaces to solar radiation enhanced the already existing dryness conditions.

Despite the demonstrated effectiveness of the triangle method with high resolution imagery, the subjectivity in the determination and interpretation of the warm and cold edges is one of its major limitations (Carlson, 2007). In this research, this was significantly reduced by using a larger number of samples. Another issue that draws attention is the significant spread of observations exhibited by highly impervious observations. The identification of mean centres for each GIT class has proved effective to correct this problem by favouring the statistical relationships between vegetation abundance descriptors and estimated cooling capacity of typologies as shown later.

Among GIT subgroups, *aquatic* typologies (mostly standing water) have a different thermal behaviour than terrestrial GITs, causing an outlying effect that hinders linear relationships between NDVI and LSTs (Carlson, 2007). This can be corroborated in [Figure 8.7](#) where most *aquatic* observations locate below the dotted line representing the limit of the lower interquartile range (or the lower whisker) of a boxplot of mean diurnal LSTs. Thus, this subgroup was omitted from linear regressions (presented later) to exclusively focus on the cooling capacities of terrestrial typologies.

Correlation analysis and simple linear regression were carried out to analyse the influence of vegetation abundance descriptors (NDVI, pervious surface fraction and tree cover

fraction) on diurnal and nocturnal cooling capacity²⁷ of each typology. As mentioned before, mean values of variables were estimated per typology to facilitate this analysis [Figure 7.27].

In general, pervious surface fraction shows a higher stability and stronger negative correlations on diurnal LSTs in summer than the other two parameters, as this can be considered the opposite of imperviousness (Weng, 2009). This may happen because NDVI cannot provide areal estimates of the amount of vegetation, or because NDVI-LST relationships still required further calibration (Weng, 2009). However, results also show that diurnal cooling effects of typologies cannot solely be explained in terms of vegetation fraction, but also by wetness and healthiness of plants (both associated with high NDVI values) as evapotranspirative cooling is dependent upon them. For instance, even though PV1 *Mostly non-irrigated grasses* and PV2 *Mostly irrigated grasses* display the same proportion of pervious land (85-100%), their mean NDVI values are significantly distant (>0.3 units); hence, their considerable difference in diurnal cooling capacity (2.2°C in summer and 1.09°C in winter).

As previously explained, nocturnal thermal conditions are mostly dominated by the radiative properties of impervious surfaces (buildings and ground), so the relationships between vegetation abundance and temperature reductions tend to be weaker, more complex and varied between seasons. Whereas there is a strong negative influence of fractional pervious cover on nocturnal cooling effects in summer, the amount of wooded areas can explain slightly better the relative nocturnal warming effect (positive influence on LSTs) of typologies in winter. Nonetheless, the predictive power of tree coverage is relatively low, especially for heavily forested areas (PV11) as they combine the effects of medium to high vegetation. Additionally, NDVI has shown no relationship with nocturnal thermal cooling as this is calculated from sunlit vegetation (representing photosynthetic activity) which is absent at night. Hence, typologies with irrigated (PV1) and non-irrigated (PV2) grasses display a similar cooling capacity at night ($<0.3^{\circ}\text{C}$) despite their differences in NDVI.

Results presented in Section 8.4.1 highlight the importance of maintaining well-watered and healthy vegetation to mitigate SUHI more effectively. However, irrigation levels are linked to water demand and water availability that largely varies among cities and seasons as it is tied to precipitation and weather conditions (Oke et al., 2017). Since airborne-based

²⁷ Expressed as the difference in mean LST between each typology and a reference case representing a totally impervious area with no vegetation (IM1).

data were collected within a period of no rainfall to reduce LST distortions, non-irrigated surfaces are more abundant across the whole study area. Consequently, the available soil moisture is considerably lower (especially in summer) as it mainly resulted from artificial (piped) watering, and the proportion of irrigated grasses and surface wetness might not be representative for the entire season.

8.4.3 Defining SUHI mitigation strategies based on GITs

Hierarchical cluster analysis was carried out to group GITs with similar cooling effects. Between four and six clusters (or subsets) of terrestrial typologies were identified and results varied between each time of the day and season [Table G8]. These subsets correspond with the subgroups defined in the streamlined GIT matrix in Section 4.11 [Figure 4.8] and coincide with the thermal differentiations discussed before. When analysing the variability of cluster memberships between seasons, a larger disparity was observed at night-time as vegetation exhibited a relatively increased cooling capacity in winter than in summer.

As demonstrated in this research, the GIT scheme can support a large-scale SUHI assessment by providing a representation of thermal performances of green infrastructure. Thus, the thermal capacities of typologies were partitioned according to the subsets defined by the hierarchical cluster analysis, which range from *very significant decrease* to *significant increase* of LSTs. Considering that the thermal behaviour of GITs changes during the course of the day, ranges were calculated separately for diurnal and nocturnal conditions [Figure 8.8].

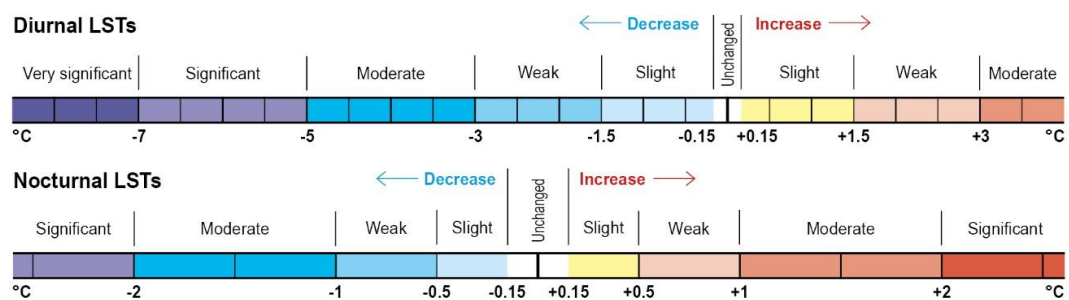


Figure 8.8 Diurnal and nocturnal thermal performance of GITs defined by the results of cluster analysis.

Since members of each cluster display similar cooling capacity, this demonstrates that the same climatic outcome can be achieved by different GITs, so they can be used interchangeably to prescribe a specific SUHI mitigation strategy at local-scale (or unit area of 50 x 50m). Tables 8.1 to 8.4 summarise these strategies along with the average fractional surface covers and spatial configuration (from the empirical data) required to attain a given thermal effect.

Table 8.1 Summary of diurnal SUHI mitigation strategies for summer using GITs. Typologies are ordered and organised in groups according to similar thermal performance.


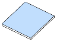
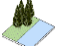
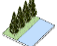
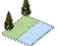




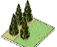
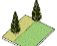
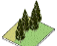








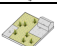

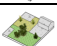

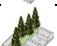
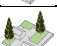

Diurnal SUHI mitigation strategies for summer								
 Diurnal thermal performance in summer	GIT: Cooling strategy	Total impervious [Fr_Tot_Imp]	Non-irrigated grasses [Fr_Low_NIR]	Irrigated grasses [Fr_Low_IRR]	Shrubs [Fr_Med_Veg]	Trees [Fr_High_Veg]	Total water [Fr_Tot_Wat]	Diurnal LST reduction (°C)
Very significant decrease (> 7°C)	 AQ1 Water	0.6	0.6	0.4	0.4	5.8	92.5	-12.12
	 AQ7 Water with clustered trees	1.5	1.4	1.7	3.1	53.2	41.7	-10.25
	 AQ5 Water with aligned trees	4.5	5.5	4.0	3.4	32.1	52.6	-9.99
	 AQ6 Water with scattered trees	6.7	9.1	7.4	2.2	24.3	51.4	-9.35
	 PV3 Mixed grasses with shrubs and trees	8.1	10.8	22.6	33.0	26.2	3.8	-8.26
	 PV11 Dense trees with shrubs and grasses	4.0	2.8	2.3	6.3	88.8	1.1	-8.18
Significant decrease (-7° to -5°C)	 PV6 Mostly irrigated grasses with aligned trees	9.2	11.5	59.9	1.3	16.7	1.4	-6.81
	 PV2 Mostly irrigated grasses	3.6	8.6	87.2	0.1	0.3	0.3	-6.24
	 MX10 Mixed grasses with clustered trees	14.1	19.0	11.6	3.5	51.7	2.0	-6.18
	 MX8 Mixed grasses with scattered trees	14.6	22.1	15.0	6.1	43.9	1.4	-5.94
	 MX6 Mixed grasses with aligned trees	15.3	25.3	15.9	3.3	39.2	2.4	-5.61
	 AQ4 Mixed surfaces with water	36.6	11.2	6.5	0.9	8.6	36.7	-5.55
Moderate decrease (-5° to -3°C)	 PV7 Mostly non-irrigated grasses with scattered trees	12.5	64.8	9.4	1.0	12.2	0.4	-4.94
	 MX4 Mixed grasses and bare soils	11.2	44.5	41.4	1.0	17.0	0.9	-4.92
	 PV5 Mostly non-irrigated grasses with aligned trees	10.5	63.2	7.6	0.7	18.1	0.2	-4.66
	 PV9 Mostly non-irrigated grasses with clustered trees	10.6	64.4	7.6	0.6	16.7	0.2	-4.55
	 PV1 Mostly non-irrigated grasses	6.3	87.5	5.1	0.2	0.9	0.0	-4.04
Weak decrease (-3° to -1.5°C)	 MX9 Mixed surfaces with clustered trees	38.7	17.5	11.1	2.1	31.3	0.6	-2.87
	 MX5 Mixed surfaces with aligned trees	40.6	17.1	13.4	2.6	27.0	0.7	-2.55
	 MX1 Mostly non-irrigated grasses with impervious	34.8	59.1	4.4	0.4	1.2	0.1	-2.41
	 MX7 Mixed surfaces with scattered trees	42.9	23.2	16.4	2.5	15.7	0.4	-2.10
	 MX3 Mixed surfaces without trees	42.2	32.0	20.6	2.0	2.4	1.0	-2.04
Slight decrease (-1.5° to -0.15°C)	 IM6 Mostly impervious with clustered trees	58.7	14.0	7.9	1.5	18.5	0.4	-0.83
	 IM4 Mostly impervious with aligned trees	59.1	13.5	9.2	2.2	17.0	0.4	-0.72
	 IM5 Mostly impervious with scattered trees	58.6	17.3	11.1	2.1	11.5	0.4	-0.58
	 IM2 Mostly impervious with grasses	63.1	21.4	10.8	1.8	2.8	0.5	-0.34

Table 8.2 Summary of diurnal SUHI mitigation strategies for winter using GITs. Typologies are ordered and organised in groups according to similar thermal performance.


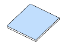
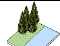





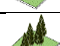


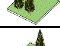


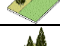

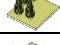
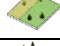

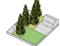
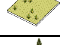
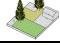




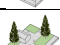
Diurnal SUHI mitigation strategies for winter									
 Diurnal thermal performance in winter	GIT: Cooling strategy		Total impervious [Fr_Tot_Imp]	Non-irrigated grasses [Fr_Low_NIR]	Irrigated grasses [Fr_Low_IRR]	Shrubs [Fr_Med_Veg]	Trees [Fr_High_Veg]	Total water [Fr_Tot_Wat]	Diurnal LST reduction (°C)
Significant decrease (-7° to -5°C)		AQ1 Water	1.9	5.7	5.6	0.8	3.9	82.8	-6.28
		AQ7 Water with clustered trees	0.5	1.5	3.5	7.5	58.2	35.5	-6.05
		AQ5 Water with aligned trees	1.9	5.4	8.6	3.9	31.3	51.7	-5.97
		AQ6 Water with scattered trees	3.3	9.6	24.7	1.3	17.6	44.0	-5.30
		PV11 Dense trees with shrubs and grasses	1.3	2.4	3.3	13.2	91.6	0.3	-5.08
Moderate decrease (-5° to -3°C)		MX10 Mixed grasses with clustered trees	12.8	16.2	16.8	4.6	52.1	0.5	-3.72
		PV3 Mixed grasses with shrubs and trees	7.7	21.6	18.2	32.8	27.0	0.0	-3.37
		PV6 Mostly irrigated grasses with aligned trees	3.4	11.9	64.0	0.9	19.6	0.5	-3.36
		MX6 Mixed grasses with aligned trees	14.6	21.9	21.1	4.3	39.8	0.4	-3.32
		PV10 Mostly irrigated grasses with clustered trees	4.1	12.8	62.0	0.6	20.4	0.3	-3.25
		PV8 Mostly irrigated grasses with scattered trees	4.7	15.2	69.5	0.9	9.3	0.4	-3.18
Weak decrease (-3° to -1.5°C)		PV2 Mostly irrigated grasses	1.3	10.6	86.9	0.1	1.1	0.0	-2.72
		MX8 Mixed grasses with scattered trees	14.0	30.1	27.7	5.9	24.1	0.5	-2.44
		PV5 Mostly non-irrigated grasses with aligned trees	7.0	61.2	14.2	1.7	16.1	0.2	-2.28
		PV9 Mostly non-irrigated grasses with clustered trees	6.1	64.3	15.3	0.8	13.7	0.0	-2.24
		MX4 Mixed grasses and bare soils	8.4	49.2	40.1	0.7	1.1	0.6	-2.03
		MX9 Mixed surfaces with clustered trees	38.3	20.1	12.0	2.9	27.8	0.3	-1.96
		MX5 Mixed surfaces with aligned trees	39.1	21.4	12.7	3.4	24.6	0.5	-1.80
		PV1 Mostly non-irrigated grasses	7.3	87.7	4.6	0.2	0.2	0.0	-1.63
Slight decrease (-1.5° to -0.15°C)		MX7 Mixed surfaces with scattered trees	42.4	25.8	16.3	3.2	12.7	0.2	-1.33
		MX3 Mixed surfaces without trees	42.3	32.5	20.2	2.5	2.4	0.3	-1.09
		MX1 Mostly non-irrigated grasses with impervious	34.8	62.0	2.5	0.4	0.2	0.0	-0.99
		IM6 Mostly impervious with clustered trees	60.8	17.1	5.6	1.9	15.0	0.4	-0.87
		IM4 Mostly impervious with aligned trees	60.3	18.0	6.6	2.4	13.4	0.3	-0.85
		IM5 Mostly impervious with scattered trees	60.4	20.7	7.5	2.3	9.4	0.2	-0.56
		IM2 Mostly impervious with grasses	63.6	23.3	8.1	2.1	2.7	0.4	-0.31

Table 8.3 Summary of nocturnal SUHI mitigation strategies for summer using GITs. Typologies are ordered and organised in groups according to similar thermal performance.




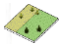
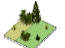






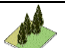
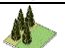











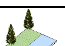
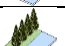
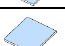

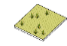
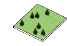
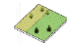
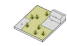
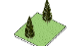
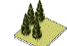
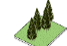
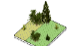



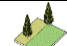


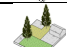











Nocturnal SUHI mitigation strategies for summer									
 Nocturnal thermal performance in summer	GIT: Cooling strategy		Total impervious [Fr_Tot_Imp]	Non-irrigated grasses [Fr_Low_NIR]	Irrigated grasses [Fr_Low_IRR]	Shrubs [Fr_Med_Veg]	Trees [Fr_High_Veg]	Total water [Fr_Tot_Wat]	Nocturnal LST reduction (°C)
Moderate decrease (-2° to -1°C)		PV1 Mostly non-irrigated grasses	6.3	87.5	5.1	0.2	0.9	0.0	-1.07
		PV2 Mostly irrigated grasses	3.6	8.6	87.2	0.1	0.3	0.3	-0.99
Weak decrease (-1° to -0.5°C)		MX4 Mixed grasses and bare soils	11.2	44.5	41.4	1.0	17.0	0.9	-0.82
		PV3 Mixed grasses with shrubs and trees	8.1	10.8	22.6	33.0	26.2	3.8	-0.77
		PV6 Mostly irrigated grasses with aligned trees	9.2	11.5	59.9	1.3	16.7	1.4	-0.74
		PV7 Mostly non-irrigated grasses with scattered trees	12.5	64.8	9.4	1.0	12.2	0.4	-0.66
		PV5 Mostly non-irrigated grasses with aligned trees	10.5	63.2	7.6	0.7	18.1	0.2	-0.60
		PV9 Mostly non-irrigated grasses with clustered trees	10.6	64.4	7.6	0.6	16.7	0.2	-0.52
Almost unchanged (-0.15° to +0.15°C)		MX8 Mixed grasses with scattered trees	14.6	22.1	15.0	6.1	43.9	1.4	-0.12
		MX1 Mostly non-irrigated grasses with impervious	34.8	59.1	4.4	0.4	1.2	0.1	+0.02
		MX6 Mixed grasses with aligned trees	15.3	25.3	15.9	3.3	39.2	2.4	+0.03
Slight increase (+0.15° to +0.5°C)		MX10 Mixed grasses with clustered trees	14.1	19.0	11.6	3.5	51.7	2.0	+0.17
		PV11 Dense trees with shrubs and grasses	4.0	2.8	2.3	6.3	88.8	1.1	+0.21
		MX3 Mixed surfaces without trees	42.2	32.0	20.6	2.0	2.4	1.0	+0.24
		MX7 Mixed surfaces with scattered trees	42.9	23.2	16.4	2.5	15.7	0.4	+0.29
		MX5 Mixed surfaces with aligned trees	40.6	17.1	13.4	2.6	27.0	0.7	+0.38
Weak increase (+0.5° to +1°C)		MX9 Mixed surfaces with clustered trees	38.7	17.5	11.1	2.1	31.3	0.6	+0.56
		IM2 Mostly impervious with grasses	63.1	21.4	10.8	1.8	2.8	0.5	+0.71
		IM4 Mostly impervious with aligned trees	59.1	13.5	9.2	2.2	17.0	0.4	+0.74
		IM5 Mostly impervious with scattered trees	58.6	17.3	11.1	2.1	11.5	0.4	+0.76
		IM6 Mostly impervious with clustered trees	58.7	14.0	7.9	1.5	18.5	0.4	+0.96
Moderate increase (+1° to +2°C)		AQ7 Water with clustered trees	1.5	1.4	1.7	3.1	53.2	41.7	+1.54
		AQ4 Mixed surfaces with water	36.6	11.2	6.5	0.9	8.6	36.7	+1.71
		AQ6 Water with scattered trees	6.7	9.1	7.4	2.2	24.3	51.4	+1.74
		AQ5 Water with aligned trees	4.5	5.5	4.0	3.4	32.1	52.6	+1.81
Significant increase (>2°)		AQ1 Water	0.6	0.6	0.4	0.4	5.8	92.5	+2.47

Table 8.4 Summary of nocturnal SUHI mitigation strategies for winter using GITs. Typologies are ordered and organised in groups according to similar thermal performance.

Nocturnal SUHI mitigation strategies for winter									
<div> Nocturnal thermal performance in winter</div>	GIT: Cooling strategy		Total impervious [Fr_Tot_Imp]	Non-irrigated grasses [Fr_Low_NIR]	Irrigated grasses [Fr_Low_IRR]	Shrubs [Fr_Med_Veg]	Trees [Fr_High_Veg]	Total water [Fr_Tot_Wat]	Nocturnal LST reduction (°C)
Moderate decrease (-2° to -1°C)		PV1 Mostly non-irrigated grasses	7.4	87.6	4.6	0.2	0.2	0.0	-1.67
		PV2 Mostly irrigated grasses	1.0	10.2	87.3	0.1	1.3	0.0	-1.46
		MX4 Mixed grasses and bare soils	7.9	49.9	39.7	0.7	1.1	0.7	-1.43
		MX1 Mostly non-irrigated grasses with impervious	34.9	62.0	2.4	0.5	0.3	0.0	-1.27
		PV8 Mostly irrigated grasses with scattered trees	4.1	15.5	68.8	1.9	9.4	0.5	-1.08
		PV9 Mostly non-irrigated grasses with clustered trees	5.8	63.9	15.4	1.3	13.8	0.0	-1.01
Weak decrease (-1° to -0.5°C)		PV6 Mostly irrigated grasses with aligned trees	3.7	11.2	63.8	1.1	20.4	0.3	-0.87
		PV3 Mixed grasses with shrubs and trees	6.6	19.4	19.0	32.8	29.3	0.7	-0.81
		MX3 Mixed surfaces without trees	42.1	32.2	20.5	2.7	2.3	0.3	-0.78
		PV5 Mostly non-irrigated grasses with aligned trees	6.5	61.2	15.1	2.1	15.2	0.4	-0.73
		PV10 Mostly irrigated grasses with clustered trees	3.8	13.0	63.5	0.7	19.0	0.3	-0.69
Slight decrease (-0.5° to -0.15°C)		MX8 Mixed grasses with scattered trees	12.6	31.5	26.3	5.6	26.3	0.0	-0.42
		IM2 Mostly impervious with grasses	63.8	23.3	7.9	2.2	2.7	0.4	-0.41
		AQ7 Water with clustered trees	0.4	1.4	3.0	8.1	59.6	34.6	-0.32
		MX7 Mixed surfaces with scattered trees	42.2	25.5	16.3	3.4	13.1	0.2	-0.31
		IM5 Mostly impervious with scattered trees	60.3	20.6	7.6	2.4	9.5	0.2	-0.17
Almost unchanged (-0.15° to +0.15°C)		PV11 Dense trees with shrubs and grasses	1.3	2.1	3.3	12.8	91.8	0.3	+0.02
		IM4 Mostly impervious with aligned trees	60.1	18.7	6.9	2.5	13.4	0.3	+0.03
		IM6 Mostly impervious with clustered trees	60.9	17.0	5.7	2.0	15.0	0.4	+0.05
		MX5 Mixed surfaces with aligned trees	38.7	21.1	13.3	3.6	24.7	0.2	+0.14
		MX9 Mixed surfaces with clustered trees	37.8	19.9	12.2	3.0	28.4	0.3	+0.15
Slight increase (+0.15° to +0.5°C)		AQ5 Water with aligned trees	2.7	4.8	7.4	4.5	32.0	52.0	+0.24
		MX6 Mixed grasses with aligned trees	14.9	20.9	20.5	4.6	40.9	0.5	+0.25
		MX10 Mixed grasses with clustered trees	12.8	15.4	17.0	4.8	52.7	0.5	+0.39
Weak increase		AQ6 Water with scattered trees	3.5	8.2	16.4	4.2	19.9	49.9	+0.55
Significant Increase (>2°)		AQ1 Water	0.5	0.8	0.5	0.5	1.6	96.4	+2.67

Although tables present an overview of which GITs are more and less effective in reducing LSTs, these may differ for air temperature observations, other cities and times of the year. Therefore, it is important to differentiate which type of climatic effect is desirable for a particular aim, location, season and time.

8.4.4 Caveats

Despite the demonstrated applicability of the GIT framework to study the spatio-temporal variability of LST of extensive urban areas, there are certain limitations that respond to the inherently reductionist nature of any classification system. These were also identified for similar schemes such as the LCZ (Stewart, 2011b; Stewart & Oke, 2012), HERCULES (Cadenasso et al., 2007), the UVST (Lehmann et al., 2014; Mathey et al., 2011), and the LULC (Anderson et al., 1976).

First, the GIT framework cannot capture the singularities of every single location as it tries to categorise a general composition of surface covers in varying amounts and arrangements into 34 distinct typologies. This simplified and relatively uniform vision of urban landscapes is unlikely to be found in the real world (except for some man-made or intensively planned interventions) and it is scale-dependent.

Second, although GITs comprise a combination of different surface and spatial descriptors, these are discrete, and hence, the physical boundaries or transitions between materials and elements are quite abrupt. Conversely, LSTs across those delineations are continuous and gradually change in space and time, so particular or localised thermal conditions caused by individual buildings, vegetation features or materials might differ from the average, or integrated, LSTs estimated for any spatial unit. Nonetheless, it is the recurrence of these individual features what provides the characteristic physical and thermal uniformity of each typology. The thermal profile of each GIT is therefore defined by the average of all observations available for that particular class; however, this entails a sort of over-simplification, so inter-typology thermal differentiations should be interpreted according to the scale and context.

Third, in this research the thermal behaviour exhibited by each GIT exclusively refers to LST and SUHI conditions; hence, their heating and cooling responses may differ from the results of studies focusing on the urban boundary and canopy layers employing air temperature observations. Since the thermal climate of a given place is continuously variable, findings are only representative for the period of time that data was collected. In

fact, a small variation of recorded LSTs is expected for the entire scene that is caused by the time lag between the first and last scans over the course of the flight mission.

Fourth, a GIT class is not strictly permanent for a location and might vary over time due to changes in the composition and distribution of elements defined by vegetation phenology, irrigation levels, and available built structures. In this sense, classification results may be limited for multi-temporal or time-series analyses since the data collected in a specific moment might not account for significant urban morphology changes over a long period of time. This issue was not identified in this research because seasonal analysis was conducted from data retrieved in two different times for two different spatial extents within the same study area [see Figure 6.1]. Furthermore, daytime and night-time thermal imagery for each season were captured within a short period (1-2 days) and were simultaneously available for the same location in the majority of classified grids.

8.5 Prediction of land surface temperatures

The thermal differentiation of GITs provided an indication of which land cover compositions, vegetation abundance and spatial configurations are the most and least efficient in reducing surface temperatures at local scale²⁸; however, previous evidence cannot be used to accurately predict the LSTs of a specific place²⁹. To do so, it is necessary to quantify the exact contribution (or influence) of each independent variable (or predictor) on diurnal and nocturnal LSTs in each season. This section provides the interpretation of the statistical analysis and predictive models developed in Section 7.4 and translate them into design and planning guidelines for the mitigation of SUHI through scenario modelling.

In accordance with other studies and previous analysis, evidence presented in Section 7.4 shows that land cover composition has a statistically significant effect on LSTs, and this is more influential than spatial configuration (Song et al., 2014; Zhou et al., 2011). After several attempts of producing reliable OLS MLR models, it was identified a strong spatial autocorrelation among residuals for all models that was quantified by global and local Moran's *I* indices. These results confirm the need for incorporating the effect of spatial dependency into traditional MLR models, otherwise autocorrelation leads to model instability and misleading interpretation of estimates.

In this regard, the use of spatial regression models was advantageous as it increased the overall *goodness-of-fit* of models substantially by capturing the effect of unmeasured

²⁸ In relation to the research questions established for the second objective of this dissertation (see Section 1.3)

²⁹ As defined in the third objective of this thesis (see Section 1.3)

predictors and incorporating the spatial autocorrelation as an explanatory variable. Furthermore, as independence between observations is not required for spatial regression models, parameter estimates are more reliable.

However, Song et al. (2014) suggest that higher model performances do not necessarily imply a better understanding of the relationships between independent and dependent variables as the explanatory power of the spatial error term can be attributed to a myriad of factors. For example, they proved that finer scales contribute to an increased spatial autocorrelation as LSTs are likely to be affected by neighbouring locations, thus, higher model fitness may result from the powerful explanatory capacity of the spatial error term. Owing to limited time and the particular scope of this thesis, the effect of spatial scales and resolution on model performance was not fully examined, and it could be potentially incorporated in future studies.

Choosing the appropriate spatial regression model and spatial weight matrix is also crucial. In this research, a *first-order queen* contiguity matrix was selected for all models because of the regularity of grids (or cases) and as suggested in the literature (Anselin, 2005; Song et al., 2014). As demonstrated by Song et al. (2014), it was found that the spatial association of LSTs at local level induced the spatial autocorrelation among residuals in OLS models; hence, results of LM tests indicated that either SEM or LAG were suitable to deal with such spatial dependencies. As this situation is typically found in practice, Anselin (2005) suggests the use of robust LM tests instead; results that finally favoured SEM over LAG [see Table 7.8].

To confirm the appropriateness of SEM as spatial regression method, LAG models were also produced with the same combination of independent variables and number of cases. Statistics from LAG models (presented in Table H11 – Appendix H) are relatively similar to those from SEM; however, they show lower *goodness-of-fit* as assessed by the *pseudo- R^2* and values of the *Likelihood Ratio* test. This contradicts the results of Song et al. (2014) who preferred LAG over SEM for the study of LSTs at coarser scales. This may be explained by discrepancies between both studies in terms of predictors, spatial resolutions and method for retrieving LSTs, opening new avenues for research.

Based on the equation of SEM as a multiple linear regression with spatial dependency [Eq. 7.2] and the results of the statistical analysis presented in Section 7.4.2, the relationship between diurnal and nocturnal LSTs and the relevant predictors listed in Table 7.13 at local scale can be explained through the following general equation:

$$T_s = \beta_0 + \beta_1 Fr_{Imp_{Bld}} + \beta_2 Fr_{Imp_{Grnd}} + \beta_3 Fr_{Low_{IRR}} + \beta_3 Fr_{Med_{veg}} + \beta_4 Fr_{High_{veg}} + \beta_5 Fr_{Tot_{Wat}} + \beta_6 CIRCLE_{AM} + \beta_7 nLSI + \beta_8 Alt + \lambda + \varepsilon_i \quad [Eq. 8.1]$$

where T_s corresponds to the diurnal or nocturnal LST in a given location and season (dependent variable), β_0 is the model constant, β_n represents the regression coefficients of each independent variable, λ is the autoregressive coefficient or spatial error term, and ε_i refers to the spatially uncorrelated error term of the regression. Values in Eq 8.1 were replaced by the statistically significant regression coefficients of SEMs listed in Tables 7.13 and 7.14³⁰ to derive eight equations for the estimation of diurnal and nocturnal LSTs for aquatic and terrestrial locations in Sydney metropolitan area during summertime and wintertime [Table 8.5].

The coefficient β_n of a variable n in equations from Table 8.5 indicates that if the variable increases by one unit, while other variables are held constant, the predicted LST will also increase³¹ in β_n units. Since the fraction of non-irrigated grasses (Fr_{Low_NIR}) was excluded to avoid perfect collinearity (see Section 7.4.1), this variable functions as reference to which other included variables are compared. Accordingly, the increase of a surface cover fraction by a given amount will result in the decrease in Fr_{Low_NIR} by the same amount and vice versa.

Taking this into consideration, Tables 8.6 and 8.7 provide an estimation of the relative effect that the change in each individual independent variable has on mean LST of a spatial unit in Kelvin (K) for a specific context and time of the day, in summer and winter respectively, when all other variables are held constant.

Overall, estimation of the individual contribution of each independent variable in mean LST of a spatial unit confirms the theory related to the surface energy balance of urban, vegetated and water surfaces (outlined in Section 2.4) and advances the evidence on the thermal differentiation of GITs discussed in previous sections. As indicated by the magnitude and sign of regression coefficients of the variables, the influence of surface and spatial predictors on LSTs varies depending on the context (aquatic versus terrestrial locations), season (summer and winter) and time of the day (daytime and night-time) as follows.

³⁰ p - and z -values of regression coefficients were used to determine which variables should be omitted from each equation.

³¹ Or decrease depending on the sign of the coefficient.

Table 8.5 Summary of equations for the prediction of diurnal and nocturnal LSTs for aquatic and terrestrial locations in Sydney metropolitan area derived from revised SEMs.

SUMMER		Predictability
Model 1D	Estimation of diurnal LSTs for aquatic locations in summer	Very high
$DAY_T_s = 39.2647 + 0.0650234 Fr_{ImpBld} - 0.0922489 Fr_{LowIRR} - 0.105179 Fr_{HighVeg} - 0.136812 Fr_{TotWat} + 0.55133 + 0.841077$		
Model 2D	Estimation of nocturnal LSTs for aquatic locations in summer	Very high
$NIG_T_s = 20.0435 + 0.0373822 Fr_{ImpGrnd} + 0.0198475 Fr_{HighVeg} + 0.0390074 Fr_{TotWat} + 0.0283315 Alt + 0.915327 + 0.31049$		
Model 1E	Estimation of diurnal LSTs for terrestrial location in summer	Very high
$DAY_T_s = 34.292 + 0.0616927 Fr_{ImpBld} + 0.0634627 Fr_{ImpGrnd} - 0.029133 Fr_{LowIRR} - 0.026064 Fr_{MedVeg} - 0.0465437 Fr_{HighVeg} - 0.0864254 Fr_{TotWat} + 0.188179 CIRCLE_{AM} + 0.00556751 Alt + 0.782332 + 0.958335$		
Model 2E	Estimation of nocturnal LSTs for terrestrial locations in summer	High
$NIG_T_s = 21.5092 - 0.0105317 Fr_{ImpBld} + 0.0421121 Fr_{ImpGrnd} + 0.0023836 Fr_{LowIRR} - 0.0039772 Fr_{MedVeg} + 0.0154435 Fr_{HighVeg} + 0.0259394 Fr_{TotWat} - 0.0992245 CIRCLE_{AM} + 0.139828 nLSI - 0.00190106 Alt + 0.862121 + 0.408394$		
WINTER		Predictability
Model 3D	Estimation of diurnal LSTs for aquatic locations in winter	Moderate
$DAY_T_s = 9.59973 - 0.0254368 Fr_{TotWat} + 0.382638 + 0.52887$		
Model 4D	Estimation of nocturnal LSTs for aquatic locations in winter	Very high
$NIG_T_s = 3.88436 + 0.0765922 Fr_{ImpBld} + 0.0150019 Fr_{TotWat} - 0.567041 CIRCLE_{AM} + 0.800643 + 0.472184$		
Model 3E	Estimation of diurnal LSTs for terrestrial location in winter	Very high
$DAY_T_s = 12.2815 + 0.0316284 Fr_{ImpBld} + 0.0228746 Fr_{ImpGrnd} - 0.0129012 Fr_{LowIRR} - 0.00651486 Fr_{MedVeg} - 0.0329822 Fr_{HighVeg} - 0.116303 Fr_{TotWat} - 0.34953 CIRCLE_{AM} + 0.806862 nLSI + 0.00535216 Alt + 0.809815 + 0.695283$		
Model 4E	Estimation of nocturnal LSTs for terrestrial locations in winter	Very high
$NIG_T_s = 1.78813 - 0.00642942 Fr_{ImpBld} + 0.0184353 Fr_{ImpGrnd} - 0.00597982 Fr_{LowIRR} - 0.00887949 Fr_{MedVeg} + 0.0159509 Fr_{HighVeg} + 0.0288495 Fr_{TotWat} + 0.191559 CIRCLE_{AM} - 0.440389 nLSI + 0.0138517 Alt + 0.887256 + 0.309781$		

Table 8.6 Relative effect of each individual independent variable on mean LSTs at local scale in summer.

Variable	Change	Effect on mean LSTs in summer			
		Aquatic locations		Terrestrial locations	
		Day	Night	Day	Night
Area of buildings (<i>Fr_Imp_Bld</i>)	+ 10%	↑ + 0.65K	<i>insignificant</i>	↑ + 0.62K	↓ – 0.11K
Area of impervious ground (<i>Fr_Imp_Grd</i>)	+ 10%	<i>insignificant</i>	↑ + 0.37K	↑ + 0.63K	↑ + 0.42K
Area of irrigated grasses (<i>Fr_Low_IRR</i>)	+ 10%	↓ – 0.92K	<i>insignificant</i>	↓ – 0.29K	↑ + 0.02K
Area of shrubbery (<i>Fr_Med_Veg</i>)	+ 10%	<i>insignificant</i>	<i>insignificant</i>	↓ – 0.26K	↓ – 0.04K
Area of tree cover (<i>Fr_High_Veg</i>)	+ 10%	↓ – 1.05K	↑ + 0.19K	↓ – 0.47K	↑ + 0.15K
Area of water surfaces (<i>Fr_Imp_Bld</i>)	+ 10%	↓ – 1.37K	↑ + 0.39K	↓ – 0.86K	↑ + 0.26K
Elongation of tree cover (<i>CIRCLE_AM</i>)	+ 0.1	<i>insignificant</i>	<i>insignificant</i>	↑ + 0.02K	↔ – 0.01K
Dispersion of tree cover (<i>nLSI</i>)	+ 0.1	<i>insignificant</i>	<i>insignificant</i>	<i>insignificant</i>	↔ – 0.01K
Altitude (<i>Alt</i>)	+ 10m	<i>insignificant</i>	↑ + 0.28K	↑ + 0.06K	↓ – 0.02K

Table 8.7 Relative effect of each individual independent variable on mean LSTs at local scale in winter.

Variable	Change	Effect on mean LSTs in winter			
		Aquatic locations		Terrestrial locations	
		Day	Night	Day	Night
Area of buildings (<i>Fr_Imp_Bld</i>)	+ 10%	<i>insignificant</i>	↑ + 0.76K	↑ + 0.32K	↓ – 0.06K
Area of impervious ground (<i>Fr_Imp_Grd</i>)	+ 10%	<i>insignificant</i>	<i>insignificant</i>	↑ + 0.23K	↑ + 0.18K
Area of irrigated grasses (<i>Fr_Low_IRR</i>)	+ 10%	<i>insignificant</i>	<i>insignificant</i>	↓ – 0.13K	↓ – 0.06K
Area of shrubbery (<i>Fr_Med_Veg</i>)	+ 10%	<i>insignificant</i>	<i>insignificant</i>	↓ – 0.07K	↓ – 0.09K
Area of tree cover (<i>Fr_High_Veg</i>)	+ 10%	<i>insignificant</i>	<i>insignificant</i>	↓ – 0.33K	↑ + 0.16K
Area of water surfaces (<i>Fr_Imp_Bld</i>)	+ 10%	↓ – 0.25K	↑ + 0.15K	↓ – 1.16K	↑ + 0.29K
Elongation of tree cover (<i>CIRCLE_AM</i>)	+ 0.1	<i>insignificant</i>	↓ – 0.06K	↓ – 0.04K	↑ + 0.02K
Dispersion of tree cover (<i>nLSI</i>)	+ 0.1	<i>insignificant</i>	<i>insignificant</i>	↑ + 0.08K	↓ – 0.04K
Altitude (<i>Alt</i>)	+ 10m	<i>insignificant</i>	<i>insignificant</i>	↑ + 0.06K	↑ + 0.14K

In terrestrial locations, impervious surfaces contributed the most to increase mean diurnal LSTs of a spatial unit in both seasons. As a consequence, an increase of 10% of the area of buildings increased mean diurnal LSTs by 0.62K in summer and by 0.32K in winter, while an increment in impervious ground surfaces by the same amount resulted in an increase of 0.63K in summer and 0.23K in winter. During night-time hours, an increase of 10% of impervious ground surfaces caused an increase of 0.42K in mean nocturnal LSTs in summer and 0.18K in winter. In contrast, during the night, many buildings' roofs exhibited

below average LSTs, resulting in a reduction of mean LSTs of 0.11K in summer and 0.06K in winter per 10% area fraction.

The fact that buildings contributed to a general reduction of nocturnal LSTs reflects the effect of material-specific properties such as emissivity, albedo, thermal capacity/inertia. Indeed, this thermal variation can also be explained by the over-proportional abundance of light-coloured, high albedo, or low thermal inertia roofing materials (*i.e.* corrugated metal roofs) which released heat more rapidly than typical ground surfaces materials (*i.e.* tiles, asphalt, bricks) that possess higher heat storage capacity and contributed to an enhanced surface warming during the night.

Moreover, distortion or recorded LSTs and the significant warming conditions in certain areas may be caused by (a) the large number of moving and stationary vehicles, –which surfaces tend to be significantly hotter than other materials–, and (b) the large proportion of asphalt and concrete, (*i.e.* highways, car parks, driveways and footpaths). This effect seems to be amplified in summer due to prevalent heatwave conditions experienced over the course of the data collection. This occurs because heatwaves exacerbate the magnitude and intensity of SUHIs by enhancing the thermal storage capacity of materials due to reduced evaporation and wind speeds (Li & Bou-Zeid, 2013; Oke et al., 2017). On the other hand, the accuracy of LSTs might be compromised by the application of a bulk emissivity value. In either case, the accuracy of predicted LSTs could be improved by identifying the individual thermal contribution of certain materials (*i.e.* bricks, metal, concrete, asphalt, etc.) and the estimation of corresponding material-specific emissivity values as implemented by Coutts et al. (2016), which is subject to future research.

Within the same context, water surfaces and tree cover contributed the most to reduce mean LSTs during the day, where for a 10% increase in each of these land covers, there was a reduction in LSTs of 0.86K and 0.47K in summer, and 1.16K and 0.33K in winter, respectively. Surprisingly, at night-time the magnitude of the warming effect of water and trees appeared to be the same in both seasons, so a 10% increase in water and forested areas caused a similar increase in mean nocturnal LSTs of 0.26 and 0.29K, and 0.15 and 0.16K respectively. Given the similar nocturnal temperature moderating effect of water and vegetated surfaces, it is confirmed the significant role that the abundance of impervious surface materials plays in defining the thermal profile of a given area.

The effect of shrubs and hedges on average LSTs is relatively the same throughout the day in wintertime, with a cooling effect of 0.07K during the day and an almost identical cooling effect of 0.09K at night per 10% area fraction. The cooling effects of medium vegetation

in summer, however, are more pronounced during the day (0.26K/10% area fraction) than during the night (0.04K/10% area fraction).

The cooling effect of irrigated grasses is quite distinctive at different times of the day and year. In summer, a 10% increase in area fraction resulted in a cooling effect of 0.29K during the day, but a warming effect of 0.02K during the night. Contrastingly, in wintertime an increment of the same proportion of irrigated grasses decreased diurnal LSTs by 0.13K and nocturnal LSTs by 0.06K. This behaviour is in accordance with the literature, so at daytime increasing surface wetness reduces LST as the evaporation of this water converts sensible into latent heat which is interpreted as a cooling effect (Erell et al., 2011; Oke et al., 1989; Oke, 1992). However, in constant warming conditions such as in summer, an increasing soil moisture resulted in an enhanced thermal capacity and higher thermal admittance, so watered surfaces may not cool as rapidly as dry plants and bare soils at night (Coutts et al., 2012; Spronken-Smith & Oke, 1998; Spronken-Smith et al., 2000).

The thermal effect of the spatial configuration of trees in LSTs was measured by two landscape metrics, the dispersion of trees represented by *nLSI* and the elongation of tree patches represented by *CIRCLE_AM* (see Section 4.11 for further details). As discussed in Sections 8.4.1 and 8.4.3, spatial predictors contributed the least to explain the thermal conditions of a given area as LSTs depend on areal estimates and thermal conditions are averaged for the totality of the spatial unit; hence, it is highly dependent on land cover composition rather than spatial configuration. This assumption, however, might be different for air temperature observations, particularly if air movement is considered.

As expected, increasing tree dispersion by 0.1 units resulted in an increment in diurnal LSTs of 0.08K and a decrease in nocturnal LSTs of 0.04K, although no significant changes were registered in summer. This coincides with other studies that suggest that concentrated tree canopy reduces solar penetration during the day (Erell et al., 2011; Norton et al., 2015; Oke et al., 1989). However, this should be interpreted with caution as TIR imagery typically represents top-of-canopy LSTs instead that those of the underlying ground surfaces. Furthermore, it is also proved that at night-time compact arrangements tend to trap more heat and reduce advection, which slows the liberation of the energy stored in surfaces to the open atmosphere.

Counter-intuitively, an increase of elongated arrangement of trees by 0.1 units provided a slight warming effect of 0.02K during the day in summer and during the night in winter. Conversely, the same change resulted in a diurnal LST reduction of 0.04K in winter and a nocturnal LST reduction of 0.01K in summer. This can be attributed to the nature of the

FRAGSTAT index. Since *CIRCLE_AM* estimates the narrowness of a patch irrespective of its size or area, this is not representative of the abundance of vegetation, and consequently the amount of shade provided by trees; thus, it can hardly explain the LST conditions of a specific area.

In both seasons, increasing the average altitude of a given area by 10m had an identical warming effect of 0.06K in LSTs during the day. However, at night-time the same change in altitude caused a decrease of 0.02K in summer, while an increase of 0.14K in winter. Accordingly, higher diurnal LSTs correspond to elevated locations as these are exposed to higher solar irradiance and experience less overshadowing, while at night surfaces at higher locations cool faster due to a higher longwave radiation loss (Oke et al., 2017). In winter, however, lower nocturnal LSTs are associated to low-lying locations (especially in hilly conditions) as solar penetration was limited during the day due to lower solar angles.

In aquatic locations the contributions of independent variables are considerably different as many predictors are irrelevant (or statistically insignificant) for this context. In summer, a 10% increase of building area resulted in an increase of 0.65K in diurnal LSTs, while the same increase in impervious ground surfaces, water and tree cover caused a warming effect of 0.37K, 0.39K, and 0.19K at night-time, respectively.

Conversely, a significant cooling effect of 1.37K, 1.05K and 0.92K during the day was reached by increasing by 10% the proportion of water, trees and irrigated grasses respectively. Furthermore, increasing elevation of water surfaces by 10m raised mean LSTs by 0.28K at night-time, although the effect of altitude was insignificant at daytime.

In wintertime, for a 10% increase in water surfaces, there was a reduction in LSTs of 0.25K during the day and an increase in LSTs of 0.15K at night. The same increment in the area of buildings contributed to an increase in nocturnal LSTs of 0.76K; while increased elongated tree patches caused a temperature reduction of 0.06K during the night.

However, the reduction in the number of predictors in models for aquatic locations is accompanied by an increase in the coefficient, magnitude (z -value) and significance of the spatial error term (λ), which indicates that LSTs are in fact better explained by unknown factors instead of measured variables. For example, this is the case of the equations derived from Models 2D and 4D that have considerable high β_{λ} (0.915 and 0.80 respectively) and z -values (81.73 and 31.81 respectively) compared to the equations derived from Models 1C and 3D [Tables 7.14 and 8.5]. Consequently, the interpretation of coefficient estimates for aquatic locations should be considered with caution.

8.6 Implications of the evidence in planning and design

As defined in the fourth objective of this dissertation (Section 1.3), a key reason to study the thermal performance of different green infrastructure typologies is to apply the knowledge acquired to incorporate climate-sensitive considerations when planning, designing and retrofitting settlements, so cities can address and mitigate urban warming more effectively.

Since the microclimatic conditions of a specific place can be managed through purposeful design, governments and practitioners are currently exploring how to best implement green infrastructure to respond to elevated urban temperatures across the world (Oke et al., 2017). Unfortunately, in many cases scientific evidence is not properly communicated to the public so there is still little practical guidance and readily accessible, affordable and rapidly available tools that can help inform policy and support planners and designers in their decision-making processes (Bowler et al., 2010b; Coutts et al., 2016; Irger, 2014; Norton et al., 2015).

To respond to this need, the evidence presented in Chapters 7 and 8 can be utilised to propose general principles, strategies (or mitigation scenarios) and guidance on how to implement green infrastructure to improve urban microclimates and mitigate the urban heat effectively. Given the scope of this thesis and the range of microclimatic aspects that can be considered when planning, designing and implementing a project, the recommendations and guidance provided in this section are restricted to the local-scale (see Section 2.4.1) and mitigation of SUHIs.

8.6.1 Guiding principles of climate-sensitive green infrastructure interventions

Before applying any particular heat mitigation strategy, it is worth to define some basic guiding principles for the implementation of green infrastructure as a countermeasure to SUHI; which are based on similar studies (Hansen et al., 2017; Klemm et al., 2017; Mathey et al., 2011; Oke et al., 2017).

The overarching principles of green infrastructure matter

Green infrastructure, as an urban living system, is spatially heterogeneous and temporally dynamic, combining natural, semi-natural and man-made structures (Cadenasso et al., 2013; Hansen et al., 2017; Pickett et al., 2017). Consequently, the climate effects provided by green infrastructure strategies are inherently ephemeral as they vary over the course of the day and year. Furthermore, they depend on functional, structural and configurational

properties that also change over time and space. In this sense, offsets between different possible climatic outcomes for a particular strategy should be considered; and will depend on specific climate objectives.

To support and enhance the multi-functionality and constant provision of ESS, particularly climate regulation, the ‘functional and structural connectivity’ of green infrastructure must be secured and prioritised (Hansen et al., 2017; Mazza et al., 2011; Naumann et al., 2011). Therefore, urban greening interventions should not be conceived and provided in isolation, but instead as part of greater interconnected ecological networks.

The location and background climate define the cooling strategies

Cooling strategies should be carefully implemented as they should respond to particular climate drivers, which in turn depend on geographic locations (*i.e.* topographic situations, latitude, hydrological conditions, existing urban form), background climate, and regional weather. This means that to a considerable degree, the selection of green infrastructure typologies should be customised to fit the needs of each city or site. In fact, interventions are subject to existing urban form parameters such as parcel size, type and size of buildings, street canyon characteristics (widths, heights, network), size of open spaces, etc.

Moreover, cooling scenarios should be chosen according to the background climate comprising the integrated effects of temperature, humidity, wind, solar radiation, etc. Accordingly, a location and time period with an acceptable range of climate conditions will require less intervention than situations exhibiting extreme circumstances (*i.e.* excessive warming or cooling); and this may vary throughout the year. This illustrates the need to conduct a pre-assessment of the climate and site to guide green infrastructure planning and design.

Cooling strategies vary across spatial scales

Green infrastructure typologies (GITs) –considered here as cooling strategies providing singular climatic outcomes– can be applied across several spatial scales (as demonstrated in Sections 7.2.1 and 8.3.1). However, the magnitude of thermal impacts are scale-dependent as they are related to the type of surface modification and typical characteristics of a given spatial extent (Oke et al., 2017; Song et al., 2014) (see Section 2.4.1).

In this research, the LST estimates of GITs are more relevant for interventions at street, neighbourhood (or precinct), and urban block levels (50-500m), which according to [Table 2.2](#) correspond to typical horizontal lengths lying between the micro and local scales. Although the proposed LST reductions may be of limited value for other scales or climate

objectives (*i.e.* improvement of HTC), the proposed assessment framework is replicable at coarser or finer levels, and applicable to comparable climatic data (*i.e.* air temperature observations) if this is available. However, its meaningfulness at other scales is subject to further investigation.

No single best strategy can satisfy all microclimate objectives

As a consequence of the inherent variability of green infrastructure (over space and time, and across scales), there is no single strategy that can respond to all possible climatic demands. Thus, green infrastructure interventions should attempt to address the majority, and sometimes conflicting needs, so disadvantages have to be outweighed or sometimes offset by the benefits.

For example, *aquatic* GITs are among the most effective strategies for reducing diurnal LSTs by absorbing most of the short-wave radiation from the sun, which is tremendously beneficial on hot summer days. On the other hand, a considerable amount of water act as a heat sink, promoting night-time heating which is more desirable during winter nights. Accordingly, trade-offs between diurnal cooling and nocturnal heating must be considered to define the adequate proportion of water bodies for a specific place.

A comparable situation occurs when defining the amount of tree canopy of a street, so in summer it should provide sufficient shelter from the sun during the day while allowing the dispersion of heat during night-time hours. An opposite effect is, perhaps, required in the same street for winter, so tree canopy should facilitate solar penetration (*i.e.* by planting more deciduous trees) while mid-storey vegetation would be needed to control wind speeds and retain some of the heat emitted from surfaces after sunset.

The same climatic outcome can be achieved by different strategies

As it can be observed in [Tables 8.1 to 8.4](#), a desirable thermal condition can be achieved in a number of different ways and might result from the combination of different surfaces (*i.e.* plan area fractions of grasses, trees, impervious ground and buildings, etc.). For instance, during winter nights a desirable heating effect in locations where water is scarce, can be comparably achieved by increasing the concentration of trees and proportion of bare ground, or by modifying certain urban form parameters (*i.e.* reducing SVF or increasing H/W ratios). Although different strategies (GITs) can be adopted to achieve a similar LST reduction, they may entail unforeseen climatic outcomes.

8.6.2 SUHI mitigation: strategies and design guidelines at the local scale

The GIT proposed in this dissertation was implemented to characterise and classify urban landscapes based on a typical range of surface cover fractions and the spatial configuration of trees. These values can be used as guidance on which amount, composition and arrangement of green infrastructure are required to achieve a particular climatic outcome (or average LST) at the local scale (spatial units of 50 x 50m). Table 4.14 presents the typical ranges of quantitative descriptors for all typologies, while Tables 8.1 to 8.4 provide a summary of corresponding SUHI mitigation strategies.

Interpretations of the relative thermal effects of each independent variable presented in Tables 8.6 and 8.7 can be used to prescribe different measures for the reduction of average LSTs within the study area (at local scale) by modifying its surface and spatial parameters. Figures 8.9 to 8.12 provide examples of individual and combinatory effects of a number of SUHI mitigation strategies for representative GIT classes. These illustrate the potential of GITs and predictive modelling (SEM) to test different possible climatic scenarios to support policy, planning and design decisions.







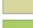




GIT_IM2		Mostly impervious with grasses			
Measured parameters				Summertime	
 % Impervious ground	21.98	 % Trees	1.16	Aerial	Diurnal TIR
 % Impervious building	39.45	 % Total water	0.04		
 % Non-irrigated grasses	27.86	CIRCLE_AM	0.726		Nocturnal TIR
 % Irrigated grasses	6.05	nLSI	0.067		
 % Shrubs	4.38	Altitude (m)	17.33		
SUHI mitigation measure				Effect	DAY_T _s
0 None: existing conditions				–	40.47 °C
1 Increase the proportion of trees by 25% by replacing almost all non-irrigated grasses				↓ – 1.18 °C	39.29 °C
2 Provide adequate irrigation to all current non-irrigated vegetated surfaces and bare soils				↓ – 0.81 °C	39.66 °C
3 Replace all shrubs and irrigated grasses with water and provide proper irrigation to remaining vegetated surfaces				↓ – 1.42 °C	39.05 °C
4 Replace 100% of roof area with green roofs (equivalent to well irrigated grasses)				↓ – 3.59 °C	36.88 °C
Option 1 + 4				↓ – 4.77 °C	35.70 °C
Option 2 + 4				↓ – 4.40 °C	35.70 °C
Option 3 + 4				↓ – 5.01 °C	35.46 °C
				↑ + 0.38 °C	22.44 °C
				↑ + 0.06 °C	22.12 °C
				↑ + 0.28 °C	22.34 °C
				↑ + 0.51 °C	22.57 °C
				↑ + 0.89 °C	22.95 °C
				↑ + 0.57 °C	22.63 °C
				↑ + 0.79 °C	22.85 °C

Figure 8.9 Example of potential SUHI mitigation measures and their individual and cumulative effect on average diurnal and nocturnal LSTs in a *Mostly impervious with grasses* (IM2) typology during summer.


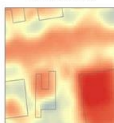

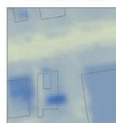
GIT_IM5		Mostly impervious with scattered trees				
Measured parameters		Summertime				
<div><div></div><div></div><div></div><div></div><div></div></div>	<div><div>% Impervious ground</div><div>44.61</div></div> <div><div>% Impervious building</div><div>28.40</div></div> <div><div>% Non-irrigated grasses</div><div>8.50</div></div> <div><div>% Irrigated grasses</div><div>6.61</div></div> <div><div>% Shrubs</div><div>0.68</div></div>	<div><div>% Trees</div><div>11.53</div></div> <div><div>% Total water</div><div>0.63</div></div> <div><div>CIRCLE_AM</div><div>0.559</div></div> <div><div>nLSI</div><div>0.135</div></div> <div><div>Altitude (m)</div><div>13.38</div></div>	<div>Aerial</div> <div></div>	<div>Diurnal TIR</div> <div></div>	<div>Schematic</div> <div></div>	<div>Nocturnal TIR</div> <div></div>
SUHI mitigation measure		Effect	DAY T_s	Effect	NIG T_s	
0	None: existing conditions	–	39.23 °C	–	22.45 °C	
1	Increase the proportion of trees by 20% by reducing the area of impervious ground by nearly 50%	↓ – 2.20 °C	37.03 °C	↓ – 0.54 °C	21.91 °C	
2	Increase the proportion of water features by 10% by decreasing the same proportion of impervious ground	↓ – 1.49 °C	37.74 °C	↓ – 0.16 °C	22.29 °C	
3	Replace 50% of roof area with the same proportion of green roofs (equivalent to well irrigated grasses)	↓ – 1.28 °C	37.95 °C	↑ + 0.18 °C	22.63 °C	
	Option 1 + 3	↓ – 3.48 °C	35.75 °C	↓ – 0.70 °C	21.75 °C	
	Option 2 + 3	↓ – 2.77 °C	36.46 °C	+ 0.02 °C	22.47 °C	
	Option 1 + 2 + 3	↓ – 4.97 °C	34.26 °C	↓ – 0.52 °C	21.93 °C	

Figure 8.10 Example of potential SUHI mitigation measures and their individual and cumulative effect on average diurnal and nocturnal LSTs in a *Mostly impervious with scattered trees* (IM5) typology during summer.








GIT_IM4				Mostly impervious with aligned trees			
Measured parameters				Wintertime			
				Axonometric	Diurnal TIR	Schematic	Nocturnal TIR
	% Impervious ground	27.11		% Trees	9.48		
	% Impervious building	35.93		% Total water	0.00		
	% Non-irrigated grasses	23.69		CIRCLE_AM	0.693		
	% Irrigated grasses	1.95		nLSI	0.095		
	% Shrubs	3.37		Altitude (m)	17.41		
SUHI mitigation measure				Effect	DAY_T _s	Effect	NIG_T _s
0	None: existing conditions			–	15.24 °C	–	2.77 °C
1	Increase the proportion of trees by 25% by reducing the area of impervious ground by 75%			↓ – 1.40 °C	13.84 °C	↓ – 0.05 °C	2.72 °C
2	Replace 100% of irrigated grasses and shrubs with water features			↓ – 0.57 °C	14.67 °C	↑ + 0.20 °C	2.97 °C
3	Provide adequate irrigation to all current non-irrigated vegetated surfaces and bare soils			↓ – 0.31 °C	14.93 °C	↓ – 0.14 °C	2.63 °C
Option 1 + 2				↓ – 1.97 °C	13.27 °C	↑ + 0.15 °C	2.92 °C
Option 1 + 3				↓ – 1.71 °C	13.53 °C	↓ – 0.19 °C	2.58 °C
Option 1 + 2 + 3				↓ – 2.28 °C	12.96 °C	– 0.01 °C	2.76 °C

Figure 8.11 Example of potential SUHI mitigation measures and their individual and cumulative effect on average diurnal and nocturnal LSTs in a *Mostly impervious with aligned trees* (IM4) typology during winter.

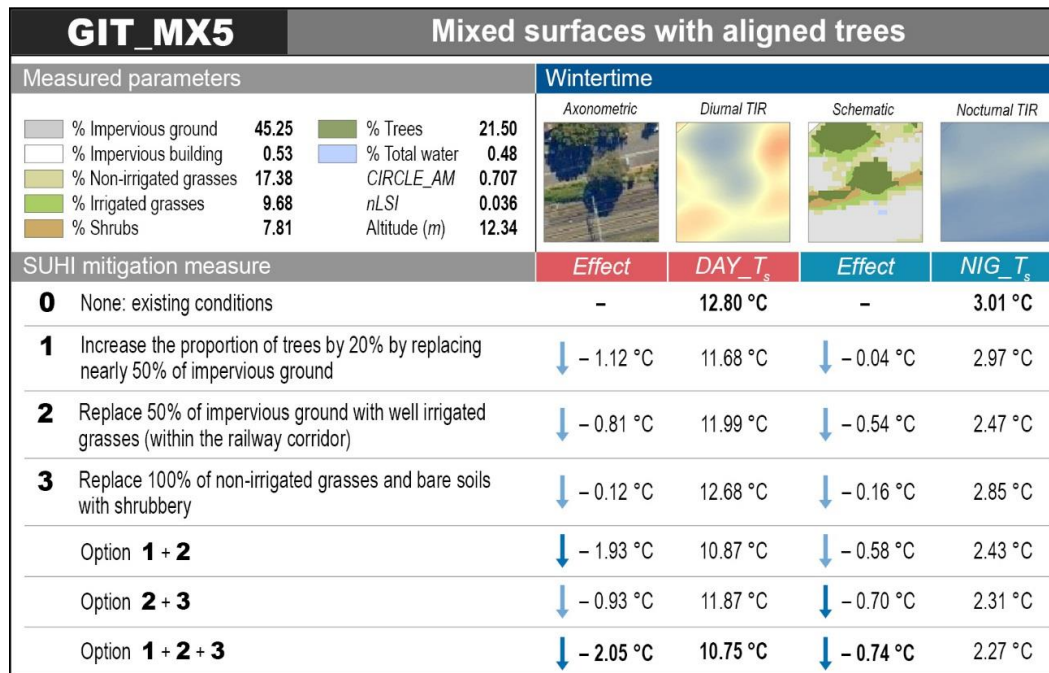


Figure 8.12 Example of potential SUHI mitigation measures and their individual and cumulative effect on average diurnal and nocturnal LSTs in a *Mixed surfaces with aligned trees* (MX5) typology during winter.

In accordance with the evidence, statistical analysis and cooling scenarios previously discussed in this chapter, the following nine general green infrastructure guidelines can be implemented for a more effective mitigation of SUHIs at the local scale:

- G.1** Water features (*i.e.* fountains, lakes, rivers, ponds, ocean, marshes, wetlands, etc.) are the most efficient in reducing diurnal LSTs (especially large water bodies); nonetheless, they provide a relative heating effect during the night that should also be considered by any intervention. The effect of water bodies on built-up areas will depend on how adjacent they are, so intermediate greenery can be used to regulate these impacts if necessary. For example, nocturnal warming effect can be controlled by increasing the proportion of grasses, shrubs and tree cover in the immediate surroundings. Additionally, the thermal profiles of water features can be controlled by modifying the depth and extent of water surfaces or changing the type of materials of the underlying floor (in case of shallow water).
- G.2** Well-irrigated vegetation can provide a more effective thermal cooling (or LST reduction) at all times of the day than dry plants and bare soils. This is because, dryness restricts evaporation, so an increasing amount of sensible heat flux is transferred to the atmosphere. Ideally, adequate water supply (natural and/or artificial) should be ensured or preserved for all greenery interventions to enhanced evapotranspiration and reduce surface radiative temperatures, especially during summer. Water regimes should be carefully defined

especially with regard to expected climate-related water shortages or periods of droughts which are site-related. For instance, passive irrigation systems –by harvesting stormwater runoffs– can be applied as it involves less-constructed in-ground works and piping. In cases that rainfall is scarce, or locations do not allow for passive irrigation, other technologies or solutions should be considered to increase soil moisture and maintain healthy vegetation (*i.e.* planting drought-resistant species).

- G.3** Generally, increasing tree canopy reduces average LSTs more effectively than other types of vegetation covers. Despite this fact, low and medium vegetation open to the sky vault can achieve a moderate decrease of LSTs either at daytime or night-time provided that surfaces are adequately watered so water infiltration, soil moisture and consequently evaporation are ensured. In larger contexts, treeless vegetated typologies can help create flexible, multi-functional and diverse microclimates to facilitate individual thermal adaptation of users. For example, gradients or borders between open and forested vegetated areas can be created where sun and sufficient shade or shelter are available in close vicinity.
- G.4** Dense tree canopies can provide significant LST reductions during the day, however, they have a considerable warming effect at night-time; therefore, they should be implemented with care. Instead, aligned, clustered or closely spaced trees over irrigated grasses as well as mixed grasses with shrubs and trees can provide a constant decrease of LSTs irrespective of the time and season. This is because they can provide consistent solar protection and evapotranspiration in the morning, and spaces for wind circulation to ease heat dissipation at night.
- G.5** In large open spaces, scattered trees should be preferably placed over or near vegetated surfaces with adequate irrigation. Alternatively, large tree crown species are preferred if these are located in highly paved areas (*i.e.* open plazas, public squares) and should be preferably accompanied by shrubbery.
- G.6** In narrow street canyons or areas with highly compacted arrangement of buildings³², it is a priority to minimise the contribution of impervious surfaces (especially vertical surfaces or building facades) to overall thermal warming. Accordingly, vertical greenery systems should be prioritised over other types of green infrastructure as they occupy less space, can help reduce solar exposure of building facades, facilitate solar penetration in specific places and enhance natural ventilation (if necessary) by reducing wind obstruction. They could also be accompanied by permeable pavements, shrubs and hedges (for shelter near the

³² Typically found in compact high-, mid-, and low-rise areas (*i.e.* LCZ1, LCZ2, and LCZ3).

ground), as well as vegetated pergolas in strategic locations. Alternatively, a careful selection of deciduous and evergreen trees of elongated crown shapes could be implemented with abovementioned strategies to regulate solar access for selected areas at certain times of the day and year.

G.7 In wide street canyons or typical suburban neighbourhoods³³, it is recommended consistent rows of tall trees with large crowns, or alternatively multiple-lined or staggered layouts for increasing shaded areas. Trees should be preferably accompanied by permeable and high albedo pavements, and green elements at various heights including irrigated grassy areas, shrubbery, and hedges in public and private spaces. Additionally, biofiltration systems (*i.e.* raingardens, bioswales) could be placed in the middle or at either side of the street to collect rainwater run-off and facilitate water infiltration (passive irrigation). To reduce solar exposure of asphalt and pavements, in some cases, median tree planting should be additionally added along with roadside trees. As in previous cases, the proportion and location of deciduous and evergreen trees will depend on the amount of solar penetration and aerodynamic characteristics required for adjacent areas.

G.8 Areas with a large proportion of roofs³⁴, for instance, in the case of large warehouses or shopping malls could be either replaced by cool roofs covered with light-coloured materials or extensive green roofs covered by mixed grasses, shrubs and small trees. In the latter case, proper irrigation should be also provided to secure evaporative cooling.

G.9 In areas with a large proportion of impervious ground (*i.e.* carparks, transport facilities/corridors)³⁵, surfaces should be partially or totally replaced by low plantings and/or permeable and high albedo materials (*i.e.* cool interlocking paving units) with extensive canopy crowns strategically distributed to increase shaded areas. Furthermore, tree planting in the middle or at both sides of transport corridors should be implemented (*i.e.* in light-rail transport systems, railway corridors).

A summary of main findings from this and previous chapters in response to the objectives and research questions of this dissertation are presented in the next and final chapter.

³³ Commonly found in open high-, mid-, and low-rise and sparsely built areas (*i.e.* LCZ4, LCZ5, LCZ6, LCZ9).

³⁴ Typically found in large low-rise and heavy industry areas (*i.e.* LCZ8 and LCZ10).

³⁵ Commonly found in LCZE and LCZF.

Chapter 9

Conclusive summary

The motivation for this research is the apparent gap in knowledge regarding the complex interplay and cumulative effects of different types of green infrastructure on urban microclimate. Hence, the central aim of this thesis is to close this gap with a special emphasis on the amounts, compositions and distributions of greenery that are required for a more effective reduction of LSTs at the local scale. In the opening chapter of this dissertation, four research objectives were defined in response to the following key gaps identified during the review of the literature (see Sections 1.2 and 1.3):

1. There is a perceived lack of quantitative assessment methodologies to support the analysis and accurate prediction of LSTs based on bio-physical and configurational parameters of green infrastructure. To respond to this methodological challenge, the first objective of this thesis focused on proposing a more comprehensive assessment framework for the automated classification of green infrastructure and subsequent statistical analysis using very high-resolution airborne remote sensing data.

To define a practical methodological framework, the strengths and weaknesses of existing methods, indicators and data sources were analysed by systematically reviewing representative climatic studies. Then, the proposed framework was successfully tested and validated in the Australian context in two distinct seasons and times of the day.

Furthermore, as defined in the third objective, several statistical models were produced to better understand, quantify and predict the extent and magnitude of the effects of functional, structural and configurational attributes of green infrastructure on average LSTs at the local scale.

2. From a methodological point of view, improvements in collecting and reporting surface temperatures associated with different green infrastructure typologies and at various spatial scales and sites are urgently needed. To analyse and compare the cooling effects of different

types of green infrastructure, the second objective of this research concentrated on constructing a standardised classification scheme for green infrastructure based on the synthesis and analysis of current terminology, and classification principles, approaches and systems.

The new classification system provided the opportunity to propose an automated GIS-based workflow that can be easily replicated by a broad spectrum of users, from novices to experts, if comparable data is available. In this thesis, the scheme was satisfactorily applied to assist in the evaluation, comparability and reporting of the spatio-temporal variability of diurnal and nocturnal LSTs of a variety of typical urban settings. The scheme was also rigorously validated using a combination of quality assessment techniques; therefore, it can be confidently implemented in future climate research or for similar performance-based analyses across other ESS categories.

3. In terms of the practical use of the existing scientific evidence, it was found that there is still little technical guidance on how to plan and design climate-sensitive neighbourhoods and urban precincts by incorporating green infrastructure for more effective climate adaptation and mitigation of urban warming. In accordance with the fourth objective, the comparative thermal analysis of LSTs associated with the different typologies and estimates of predictive models was employed to (1) explore the implications of findings in planning and design, (2) propose key guiding principles and recommendations, and (3) for scenario modelling of different SUHI mitigation strategies.

Within this context, the next section presents a summary of findings that are based on the results of two systematic literature reviews and the successful implementation of the methodological framework and classification scheme in two related case studies of the Sydney metropolitan area.

9.1 Summary of findings

The analysis and evaluation of the cooling effects of green infrastructure on LSTs required the formulation of a methodological framework and classification system for green infrastructure that overcome the deficiencies identified in the literature (presented below). Accordingly, 250 scientific publications were systematically analysed for their key concepts, approaches, methodological aspects, and current evidence which resulted in the following general findings (see Chapters 3 and 4):

- There is limited information about the cooling benefits of green infrastructure in developing countries, and locations with tropical, semi-arid and desert climates. Moreover, little research has been conducted in Australian cities which are currently experiencing a significant population growth, densification process, and increasingly frequent climate change-related events such as heatwaves, droughts, bushfires and flooding.
- As defining clear boundaries between the natural and the built world is difficult, the mapping and characterisation of green infrastructure should contemplate the combining effects of biotic and abiotic elements using holistic (integrative) and three-dimensional approaches.
- The classification, evaluation, and delivery of green infrastructure should embrace the overarching principles of multi-functionality, connectivity, and dynamic spatial and temporal heterogeneity, and consider the ecological functioning, physical properties, and spatial interrelationships of both natural and artificial features.
- A universal set of typologies cannot be proposed for all locations and research purposes; however, green infrastructure can be grouped into five high-level categories of (1) tree canopy; (2) green open spaces; (3) water bodies, (4) green roofs; and (5) vertical greenery systems. These categories can be broken down into a flexible number of typologies resulting from the combination of different types of surface covers and vegetated features of varying heights and distributions.
- Vegetation abundance, plant structure and shade from trees are the most common aspects assessed by studies; nonetheless, less attention is given to the climatic effects of water bodies, irrigation and evapotranspirative cooling.
- Little is known about the most optimal type, abundance and distribution of green infrastructure necessary to maximise the mitigation of the urban heat at neighbourhood and street canyon levels. Hence, there is a need to translate the existing evidence into an effective set of practical rules and design guidelines for policy makers, governments, planners and designers.

This thesis has demonstrated that the combination of multiple airborne remote sensing technologies can be successfully employed to map, categorise and assess the physical and spatial characteristics of extensive urban areas and provide very highly detailed two- and three-dimensional information for conducting urban microclimate analyses. Although

airborne remote sensing can be implemented in a flexible and time-efficient way, its application among most users is constrained by its relatively high costs, sensor availability, complex logistics, and technical knowledge necessary for the acquisition, processing and interpretation of some data.

The methodological framework for the automated mapping and classification of green infrastructure into 34 distinct typologies (or GITs) was satisfactorily tested at the local scale in two related case studies within Sydney, and fully validated using a confusion matrix and deep learning. In this study, classification parameters and threshold values for GITs were defined based on the approaches and parameters proposed by similar schemes, particularly, HERCULES, LCZ, LULC and UVST. Variables were derived from remote sensing data and results of classifications offered the following insights (see Section 8.3):

- It was demonstrated the applicability of the approach and methodology at various spatial scales with less than 0.25% of unclassified areas for all cases. It was observed that the accuracy of predictions is scale-dependent and influenced by grid resolution. However, the identification of an optimal grid size is impractical as this will depend on the type of research, the level of fragmentation of the landscape, and the size of mapped structures, therefore it is context-related. For the purpose of this research, a spatial unit of 50 x 50m was the most adequate to conduct microclimatic analyses at the local scale (*i.e.* neighbourhood, precinct, street) as grids preserved representative structural and configurational information.
- The quality assessment of classification maps of a portion of the study area shows satisfactory results with an overall accuracy of 76.4% and kappa index of 0.741. The main flaws and inaccuracies occurred due to erroneous land cover recognition from remote sensing products (spectral imagery and LiDAR), large variation of the proportion of land cover types, and the difficulty of distinguishing different arrangement of trees (problems with FRAGSTATS metrics), so additional improvements are required (Sections 8.2 and 9.3 provide some recommendations).
- The overall predictability or performance of the entire classification scheme was assessed using several machine learning algorithms. Results show *high to very high* predictability for most classifiers (>80%) and demonstrate the robustness of classification descriptors and typical ranges proposed in this research. This proves the applicability and reliability of the classification scheme despite differences in location, season and dataset.

The empirical results presented in Sections 7 and 8 demonstrate the applicability of the GIT scheme as a framework for the study of the intra- and inter-variability of LSTs and the estimation of the cooling capacity of different typologies resulting from the variation of the composition, abundance and distribution of surface covers. In that sense, the comparative analysis of diurnal and nocturnal average LSTs of GITs in summer and winter provided the following specific findings (see Section 8.4):

- 34 typologies were identified across the study area, each of them exhibiting a unique average thermal profile and intra-typology variability of LSTs.
- Temperature differences among GIT classes are statistically significant for both seasons and at different times of the day, and these vary as a function of the amount of buildings, the proportion of ground surface covers, trees arrangement, and surface wetness.
- Significant thermal contrasts among GITs are more pronounced at daytime and summer conditions. In contrast, thermal profiles are less discernible at night, while diurnal temperature fluctuations are smaller in winter.
- The thermal difference ($\Delta T_{IM1-GIT}$) between each typology and a reference or control class—in this case, IM1 *Highly impervious*—provides a reliable measure of the cooling capacity (or effect) of each typology and it can be used as an indicator of SUHI magnitude.
- In both summer and winter, the highest diurnal LSTs and consequently the lowest cooling effects are registered by typologies with a high degree of imperviousness, dryness and lack of vegetation (especially tree canopy). Lower cooling capacity also correspond to open and sparsely built areas with mixed surface covers, and green spaces with poor irrigation conditions.
- An inverse thermal behaviour is observed for *aquatic* and *pervious* GITs between day and night. Accordingly, water bodies, well irrigated grasses and aligned and clustered trees provide substantial cooling benefits during the day; meanwhile at night a relative heating effect is provided in areas with large water bodies, very dense tree canopy and extensive shrubbery surrounded by mixed surfaces (especially impervious surfaces). In contrast, treeless areas with well irrigated grasses are the most efficient in reducing the SUHI intensity during the night.
- Surface wetness and irrigation play a significant role in reducing LSTs and mitigating the SUHI by improving the overall cooling performance of typologies through increased evapotranspiration.

- Average LSTs also depend on the thermal properties of surfaces (*i.e.* thermal inertia, albedo, emissivity), with particular attention to roof materials that have an important effect on the thermal profile of a given area (*i.e.* contrasting temperatures between light-coloured metal roofs and dark-coloured roof tiles).
- The positive cooling effects of grasses, shrubs and trees are significantly diminished when positioned within predominately impervious materials. These are also confounded by the height and compactness of buildings due to lower SVF and higher proportion of shade from tall buildings.
- Changes in tree arrangement (scattered, aligned and clustered) does not necessarily result in additional LST reductions for a spatial unit if (1) the proportion of tree cover remains unchanged or (2) when holding the land cover composition constant.
- As the composition and abundance of surface covers is more influential in defining the thermal profile of GITs than the spatial distribution of vegetated structures; the cooling effects of the same proportion of trees are severely undermined as imperviousness and surface dryness increases. Indeed, the positive impact of tree clustering in LSTs is stronger as the abundance of well irrigated grasses increases in the immediate surroundings.

The thermal characterisation of GITs is particularly valuable as it can be utilised to identify which urban areas will be more vulnerable or likely to experience higher urban temperatures. To understand which factors can be manipulated to prevent that happening, the relationship between the cooling capacity of typologies and vegetation abundance descriptors (NDVI, proportion of pervious area, and amount of tree cover) were statistically analysed using a TVX approach, correlation analysis and simple linear regression. This analysis provided the following insights (see Sections 7.3.2 and 8.4.2):

- Average diurnal LSTs decrease with increasing percentage, health and wetness of vegetation covers, which correspond to higher NDVI values.
- Among GIT subgroups, the thermal behaviour of *aquatic* typologies is considerably dissimilar from those exhibited by terrestrial GITs; hence, they cause an outlying effect which hampers linear relationships between LSTs and NDVI. This should be considered when conducting statistical analyses.

- Average diurnal LSTs of typologies are well explained by either pervious surface fraction or NDVI, as the latter is an indicator of evapotranspirative cooling resulting from the wetness and health of plants. Conversely, average nocturnal LSTs are better explained by the fraction of pervious surfaces than by NDVI, as the latter is calculated from sunlit vegetation (representing photosynthetic activity) which is absent at night.
- The predictive power of tree coverage is normally low, especially for heavily forested areas as they combine the effects of medium to high vegetation.
- Results reconfirm the importance of maintaining well-watered and healthy vegetation to mitigate SUHI more effectively.

Since GITs exhibit a combination of different surface covers and FRAGSTATS metrics, it cannot clearly be defined to what extent each parameter contributes to the temperature reduction capacity of each type. Thus, previous evidence cannot be confidently used to predict the average LST of a place in an accurate and precise way. The assessment methodology proposed in this research, however, enables quantifying the relationships between green infrastructure descriptors and mean diurnal and nocturnal LSTs in summer and winter (see list of dependent and independent variables in Section 5.1.1). The interpretation of the statistical analysis and predictive models developed in Section 7.4 provided the following additional findings:

- The spatial association of LSTs at local level induced the spatial autocorrelation among residuals in OLS models. This confirms the need of incorporating the effect of spatial dependency into classic OLS MLR models for a reliable and accurate prediction of LSTs.
- Spatial regression models (in particular SEM) are found to be more appropriate than OLS models as they increased significantly the overall *goodness-of-fit* of all predictive equations.
- SEM and OLS models show significant heteroskedasticity that is mainly caused by: (1) the large temperature variability of the control class (IM1) –as thermal conditions in highly impervious areas are influenced by unmeasured factors related to the built form and material-specific properties–, and (2) the distinct thermal behaviour of water bodies relative to terrestrial surfaces. This issue was solved by partitioning the data and excluding observations corresponding to the control case.

- In terrestrial locations, imperviousness contributed the most to increase mean diurnal LSTs in both seasons. Accordingly, an increase of 10% of building areas results in an increase of 0.62K in summer and 0.32K in winter; while an increment in impervious ground surfaces by the same amount results in an increase of 0.63K in summer and 0.23K in winter.
- During the night, the same increment in impervious grounds surfaces causes an increase of 0.42K in mean nocturnal LSTs in summer and 0.18K in winter. Conversely, an increment of building areas in the same proportion results in a reduction of mean LSTs of 0.11K in summer and 0.06K in winter.
- The presence of water surfaces and trees contributed the most to reduce mean LSTs during the day, causing a decrease in LSTs at a rate of 0.86K and 0.47K in summer, and 1.16K and 0.33K in winter, per 10% increase in area coverage respectively.
- At night the magnitude of the warming effect of water and trees is relatively the same in both seasons, causing an increase in LSTs at a rate of 0.26K and 0.29K, and 0.15K and 0.16K per 10% increase in area coverage respectively.
- The cooling effect of irrigated grasses is quite distinctive at different times of the day and year. An increase of 10% in area fraction results in a cooling effect of 0.29K during the day, and a warming effect of 0.02K at night. In winter, an increment of the same proportion decreases diurnal LSTs by 0.13K and nocturnal LSTs by 0.06K. This demonstrates that increasing soil wetness results in an enhanced thermal capacity as watered surfaces release heat more slowly than dry plants and bare soils during the night.
- In terms of spatial configuration, an increase in the concentration of trees results in a decrease of diurnal LSTs and an increase of nocturnal LSTs as compacted arrangements provide more shade during the day yet reduce heat dissipation at night. Counter-intuitively, elongated arrangements cause a slight warming effect during the day in summer and during the night in winter. This suggests that CIRCLE_AM does not necessarily account for the real effect of patch elongation on LSTs. This occurs because the metric is not representative of the amount of tree cover, and hence of the amount of shade and evapotranspirative cooling.
- Higher diurnal LSTs correspond to elevated locations as there is less overshadowing, while at night surfaces at higher locations cool faster due to a higher longwave radiation loss. In contrast, in winter lower nocturnal LSTs correspond to low-lying locations as solar penetration was limited during the day due to lower solar angles. Accordingly, the effect

of altitude should be interpreted in terms of topographic undulation rather than absolute elevation.

- In aquatic locations the contributions of independent variables are considerably different as diurnal and nocturnal LSTs mostly depend on the proportion of water and trees.
- The reduction in the number of predictors in models for aquatic locations is accompanied by an increase in the magnitude and significance of the spatial error term which indicates that LSTs are, in fact, better explained by unknown factors instead of measured variables.

Understanding the thermal performance of green infrastructure is crucial to plan, design and implement more sustainable, liveable, climate-adapted and low-carbon communities, especially in the context of climate change and global warming. With the hope of informing policy and assisting governments and practitioners to achieve abovementioned goals, previous evidence was translated into practical design guidelines and heat mitigation strategies.

Thus, the GIT framework can be implemented to support a large-scale SUHI assessment by facilitating the representation of the magnitude and intensity of SUHI conditions in urban and rural settings. On the other hand, the characteristic physical and thermal uniformity of each typology can be employed to prescribe specific SUHI mitigation strategies, while estimates of predictive equations facilitate simulative scenario modelling of desirable climatic outcomes for a given location.

9.2 Significance of research

This research advances the study of the thermal performance of green infrastructure on urban microclimate and addresses the weaknesses identified in the literature through the following innovative contributions to knowledge:

A more comprehensive and holistic methodological framework to describe the bio-physical and configurational characteristics of green infrastructure are proposed to analyse the interplay and cumulative cooling effects provided by both biotic and abiotic features.

Based on this framework, a novel and comprehensive classification system for green infrastructure is developed to support climate-related studies by embracing the key green infrastructure principles of dynamic spatial and temporal heterogeneity, connectivity, and

multi-functionality. This new taxonomy includes guidelines, protocols, and procedures for the automated classification of urban and rural landscapes based on remote sensing data. Although the scheme is originally intended for climatic research, it is sufficiently flexible to be applied in related fields such as nature conservation, water and resource management, forestry and agriculture, human health, remote sensing, and more. It is also compatible with other similar well-established approaches such as LULC, LCZ, and UVST and can be easily replicated and broadly managed by users from novices to experts.

An illustrative set of datasheets³⁶ to standardise the characterisation and categorisation of green infrastructure into typologies based on functional, structural and spatial parameters with specific cut-off values is presented. These datasheets can facilitate the inventory, comparison and performance assessment of GITs across several ESS categories and improve the communication of evidence among scientists, governments and practitioners from diverse backgrounds.

The outcomes of the statistical analyses provide a significant contribution to better understand which characteristics and parameters of green infrastructure and urban form are more influential on LSTs at the local scale. Furthermore, the proposed statistical models enable the prediction of LSTs and subsequent assessment of potential cooling interventions by changing the composition, abundance and distribution of land covers.

Theoretical and empirical evidence discussed on this thesis are examined and synthesised to propose a set of guiding principles, recommendations and strategies³⁷ on how neighbourhoods and urban precincts should be planned and designed to incorporate green infrastructure for a more effective SUHI amelioration. These are intended to inform and support various audiences including climate investigators, policy makers, local governments, landscape architects, and urban planners and designers.

9.3 Limitations and potential directions for further research

This thesis was mainly limited by the type, amount and quality of airborne remote sensing data, which were not readily accessible as originally expected. As a result, summer and winter datasets were obtained from two different sources so they differ in terms of extent, spatial and spectral resolutions and type of products/technologies (*i.e.* hyper- versus multi-spectral imaging), sensors and methods employed for the acquisition and processing of

³⁶ Presented in Appendix E.

³⁷ Provided in Sections 8.4.3, 8.6.1 and 8.6.2

data. Furthermore, as data were acquired from a third party or contractor, it was difficult to perform a thorough quality control of the final remote sensing products.

An improved thematic mapping of surface materials at pixel-based level would have been possible with the application of state-of-the-art techniques such as Multiple Endmember Spectral Mixture Analysis (MESMA) and deep learning (*i.e.* Convolutional Neural Networks-CNN). However, this was out of the scope of this study and it was not technically feasible due to time, skill and resource constraints. As information of the materiality of a particular place can provide important insights about its thermal conditions, future studies could incorporate MESMA and CNN methods into the proposed framework to improve the accuracy and precision of surface cover recognitions.

Thermal imagery was collected, processed and provided by a contractor who opted to use a generic value for emissivity corrections. Although this produced reliable LST values that served the purpose of this thesis, it is recommended to assign specific emissivity values to each land cover type or material for the calculation of surface radiances and absolute LSTs.

The data collection was limited to thermal and spectral reflectance of horizontal surfaces; rather than urban canopy layer conditions, such as air temperature, which are more relevant to HTC. Thus, further research could focus on (1) incorporating the effect of vertical surfaces, (2) quantifying the relationships between air temperatures and green infrastructure parameters defined for each GIT, and (3) analysing the thermal profiles of GITs in the context of HTC. Under a three-dimensional and holistic approach, the cooling effects of green roofs and vertical greenery systems –as part of a network of green infrastructure– could be also mapped and incorporated to the current approach.

In addition, owing to the large spatial extent of the study area and nature of the present research, information regarding the amount, timing and frequency of active irrigation (from artificial sources) was not collected; thus, future research can focus on the influence of antecedent soil moisture and rainfall on LST reductions.

A potential development of the present methodological framework is the inclusion of multi-temporal analysis (time-series) to (1) minimise erroneous pixels and discard shadows from surface cover extractions, (2) study the effect of temporal changes of vegetation and surface wetness (*i.e.* foliage type, phenology, maturity, precipitation, etc.), and (3) analyse the temporal dynamics of air and surface temperatures of each GIT class. As this could be unaffordable and laborious for many users due to high costs and complicated logistics, UAVs or drone-based technology could be useful as periodic flights can be deployed in an easy, flexible, and less costly way.

In terms of the application of the proposed framework, the following aspects or improvements could be also explored by future studies:

- Quantifying and comparing the thermal differences of GITs across multiple spatial scales.
- Examining the effect of spatial resolution and grid size on classifications and the performance of statistical models.
- Quantifying the influence of different types of species and deciduous and evergreen vegetation on air and surface temperatures due to variations on shading, transpiration and air velocity.
- Estimating evapotranspiration rates in heterogeneous urban contexts and analysing their role on CLUHI and SUHI mitigation.
- Determining minimum irrigation and humidity requirements to provide adequate thermal benefits, as not all vegetated surfaces and plant species are capable of tolerating severe temperatures or providing the same amount of evaporative cooling.
- Improving the classification results by modifying the proposed NDVI classification ranges, calibrating cut-off values of parameters, exploring additional combinations of landscape metrics, and simplifying the categorisation of tree arrangements.
- Extending the present research by conducting similar quantitative and qualitative analyses across a diverse selection of ecosystem services (*i.e.* carbon sequestration, air quality, biodiversity, aesthetic impact, etc.).

Although the present thesis entails several limitations and is contingent on further developments, it is expected that the findings and recommendations can contribute theoretically to the existing body of knowledge. Also, it is hoped that this research can offer a few more tools to help scientists, city managers and designers to avoid certain methodological pitfalls when examining the thermal behaviour of green infrastructure and assist them in the delivery of more sustainable and climate-oriented solutions.

References

- Abreu-Harbach, L. V. de, Labaki, L. C., & Matzarakis, A. (2015). Effect of tree planting design and tree species on human thermal comfort in the tropics. *Landscape and Urban Planning*, 138, 99–109. doi:10.1016/j.landurbplan.2015.02.008
- Abunnasr, Y. F. (2013). *Climate Change Adaptation: A Green Infrastructure Planning Framework for Resilient Urban Regions* (PhD). University of Massachusetts Amherst.
- Adams, M. P., & Smith, P. L. (2014). A systematic approach to model the influence of the type and density of vegetation cover on urban heat using remote sensing. *Landscape and Urban Planning*, 132, 47–54. doi:10.1016/j.landurbplan.2014.08.008
- Ahern, J. (1995). Greenways as a planning strategy. *Landscape and Urban Planning*, 33(1-3), 131–155. doi:10.1016/0169-2046(95)02039-V
- Ahern, J. (2007). Green infrastructure for cities: the spatial dimension. In V. Novotny & P. Brown (Eds.), *Cities of the Future: Towards Integrated Sustainable Water and Landscape Management*. London: IWA Publishing.
- Akbari, H. (2002). Shade trees reduce building energy use and CO₂ emissions from power plants. *Environmental Pollution*, 116(Supplement 1), S119-S26.
- Akbari, H. (2009). *Cooling our Communities: A Guidebook on Tree Planting and Light-Colored Surfacing*.
- Akbari, H., & Levinson, R. (2008). Evolution of Cool-Roof Standards in the US. *Advances in Building Energy Research*, 2(1), 1–32. doi:10.3763/aber.2008.0201
- Akbari, H., & Taha, H. (1992). The impact of trees and white surfaces on residential heating and cooling energy use in four Canadian cities. *Energy*, 17(2), 141–149. doi:10.1016/0360-5442(92)90063-6
- Alavipanah, S., Wegmann, M., Qureshi, S., Weng, Q., & Koellner, T. (2015). The Role of Vegetation in Mitigating Urban Land Surface Temperatures: A Case Study of Munich, Germany during the Warm Season. *Sustainability*, 7(4), 4689–4706. doi:10.3390/su7044689
- Aldous, D. E. (2014). Australia's national classification system for green open space. *Australasian Parks and Leisure*, 16(2), 30–33.
- Alexander, P., & Mills, G. (2014). Local Climate Classification and Dublin's Urban Heat Island. *Atmosphere*, 5(4), 755–774. doi:10.3390/atmos5040755
- Alexander, P. J., Mills, G., & Fealy, R. (2015). Using LCZ data to run an urban energy balance model. *Urban Climate*, 13, 14–37. doi:10.1016/j.uclim.2015.05.001
- Alexandri, E., & Jones, P. (2008). Temperature decreases in an urban canyon due to green walls and green roofs in diverse climates. *Building and Environment*, 43(4), 480–493. doi:10.1016/j.buildenv.2006.10.055
- Al-Gretawee, H., Rayburg, S., & Neave, M. (2016). The cooling effect of a medium sized park on an urban environment. *International Journal of GEOMATE*, 11(26), 2541–2546.
- Allen, R. G., Pereira, L. S., Raes, D., & Smith, M. (1998). *Crop evapotranspiration - Guidelines for computing crop water requirements - FAO Irrigation and drainage paper 56*. Rome.
- Amiri, R., Weng, Q., Alimohammadi, A., & Alavipanah, S. K. (2009). Spatial-temporal dynamics of land surface temperature in relation to fractional vegetation cover and land use/cover in the Tabriz urban area, Iran. *Remote Sensing of Environment*, 113(12), 2606–2617. doi:10.1016/j.rse.2009.07.021
- Anderson, J. R., Hardy, E. E., Roach, J. T., & Witmer, R. E. (1976). A Land Use and Land Cover Classification System for Use with Remote Sensor Data: Geological survey professional paper 964.

- Anselin, L. (1995). Local Indicators of Spatial Association - LISA. *Geographical Analysis*, 27(2), 93–115.
- Anselin, L. (2005). *Exploring Spatial Data with GeoDa: A Workbook*. Urbana-Champaign: Center for Spatially Integrated Social Science. Tuesday, January 30, 2018.
- Anselin, L., Ibnu, S., & Youngihn, K. (2006). *GeoDa: An Introduction to Spatial Data Analysis* (Vol. 38).
- Arlt, G., Hennersdorf, J., Lehmann, I., & Thinh, N. X. (Eds.). (2005). *IÖR-Schriften. Auswirkungen städtischer Nutzungsstrukturen auf Grünflächen und Grünvolumen*. Impact of City's Structures of Land Use on Green Spaces and Green Volume (47th ed.). Dresden.
- Armson, D., Stringer, P., & Ennos, A. R. (2012). The effect of tree shade and grass on surface and globe temperatures in an urban area. *Urban Forestry & Urban Greening*, 11(3), 245–255. doi:10.1016/j.ufug.2012.05.002
- Arnfield, A. J. (2003). Two decades of urban climate research: A review of turbulence, exchanges of energy and water, and the urban heat island. *International Journal of Climatology*, 23(1), 1–26. doi:10.1002/joc.859
- ASHRAE. (2017). *Standard 55.: Thermal Environmental Conditions for Human Occupancy*.
- AURIN. (2018). *AURIN portal*. Retrieved from <https://portal.aurin.org.au/>. Accessed Wednesday, March 07, 2018.
- Australian Bureau of Statistics (ABS). (2017). *3222.0 - Population Projections, Australia, 2006 to 2101*. Retrieved from http://www.censusdata.abs.gov.au/census_services/getproduct/census/2016/quickstat/1GSYD?opendocument. Accessed Thursday, January 12, 2017.
- Australian Bureau of Statistics (ABS). (2018). *Australian Statistical Geography Standard (ASGS)*. Retrieved from [http://www.abs.gov.au/websitedbs/D3310114.nsf/home/Australian+Statistical+Geography+Standard+\(ASGS\)](http://www.abs.gov.au/websitedbs/D3310114.nsf/home/Australian+Statistical+Geography+Standard+(ASGS)). Accessed Wednesday, March 07, 2018.
- Australian Government (AG). (2018). *Welcome - data.gov.au*. Retrieved from <https://data.gov.au/>. Accessed Wednesday, March 07, 2018.
- Baccini, M., & Schindler, C. (2008). Heat effects on mortality in 15 European cities. *Epidemiology*, 19, 711–719.
- Badamasi, M. M., Yelwa, S. A., AbdulRahim, M. A., & Noma, S. S. (2010). NDVI threshold classification and change detection of vegetation cover at the Falgore Game Reserve in Kano State, Nigeria. *Sokoto Journal of the Social Sciences*, 2(2), 174–194.
- Baller, R. D., Anselin, L., Messner, S. F., Deane, G., & Hawkins, D. F. (2001). Structural covariates of U.S. county homicide rates: Incorporating spatial effects. *Criminology*, 39(3), 561–588. doi:10.1111/j.1745-9125.2001.tb00933.x
- Bartesaghi Koc, C., Osmond, P., & Peters, A. (2016). A Green Infrastructure Typology Matrix to Support Urban Microclimate Studies. *Procedia Engineering*, 169, 183–190. doi:10.1016/j.proeng.2016.10.022
- Bartesaghi Koc, C., Osmond, P., & Peters, A. (2017). Towards a comprehensive green infrastructure typology: A systematic review of approaches, methods and typologies. *Urban Ecosystems*, 20, 15–35. doi:10.1007/s11252-016-0578-5
- Bartesaghi Koc, C., Osmond, P., & Peters, A. (2018). Evaluating the cooling effects of green infrastructure: A systematic review of methods, indicators and data sources. *Solar Energy*, 166, 486–508. doi:10.1016/j.solener.2018.03.008
- Bartesaghi Koc, C., Osmond, P., Peters, A., & Irger, M. (2017a). A methodological framework to assess the thermal performance of green infrastructure through airborne remote sensing. *Procedia Engineering*, 180, 1306–1315. doi:10.1016/j.proeng.2017.04.293
- Bartesaghi Koc, C., Osmond, P., Peters, A., & Irger, M. (2017b). Mapping Local Climate Zones for urban morphology classification based on airborne remote sensing data. In *2017 Joint Urban Remote Sensing Event (JURSE)* (pp. 1–4). IEEE. Thursday, June 01, 2017.
- Bartesaghi Koc, C., Osmond, P., Peters, A., & Irger, M. (2018). Understanding land surface temperature differences of Local Climate Zones based on airborne remote sensing data. *Journal of Selected Topics in Applied Earth Observations and Remote Sensing (JSTARS)*, 10(11). doi:10.1109/JSTARS.2018.2815004

- Bartesaghi-Koc, C., Osmond, P., & Peters, A. (2019). Mapping and classifying green infrastructure typologies for climate-related studies based on remote sensing data. *Urban Forestry & Urban Greening*. doi:10.1016/j.ufug.2018.11.008
- Beauchamp, P., & Adamowski, J. (2013). An Integrated Framework for the Development of Green Infrastructure: A Literature Review. *European Journal of Sustainable Development*, 2(3), 1–24. doi:10.14207/ejsd.2013.v2n3p1
- Bechtel, B., Alexander, P., Böhner, J., Ching, J., Conrad, O., Feddema, J., . . . Stewart, I. (2015). Mapping Local Climate Zones for a Worldwide Database of the Form and Function of Cities. *ISPRS International Journal of Geo-Information*, 4(1), 199–219. doi:10.3390/ijgi4010199
- Bechtel, B., & Daneke, C. (2012). Classification of Local Climate Zones Based on Multiple Earth Observation Data. *IEEE Journal of Selected Topics in Applied Earth Observations and Remote Sensing*, 5(4), 1191–1202. doi:10.1109/JSTARS.2012.2189873
- Bechtel, B., See, L., Mills, G., & Foley, M. (2016). Classification of Local Climate Zones Using SAR and Multispectral Data in an Arid Environment. *IEEE Journal of Selected Topics in Applied Earth Observations and Remote Sensing*, 1–9. doi:10.1109/JSTARS.2016.2531420
- Bell, S., Montarzino, A., & Travlou, P. (2007). Mapping research priorities for green and public urban space in the UK. *Urban Forestry & Urban Greening*, 6(2), 103–115. doi:10.1016/j.ufug.2007.03.005
- Bencheikh, H., & Rchid, A. (2012). The Effects of Green Spaces (Palme Trees) on the Microclimate in Arides Zones, Case Study: Ghardaia, Algeria. *Energy Procedia*, 18, 10–20. doi:10.1016/j.egypro.2012.05.013
- Benedict, M. A., & McMahon, E. T. (2002). *Green Infrastructure: Smart Conservation for the 21st Century*.
- Benedict, M. A., & McMahon, E. T. (2006). *Green Infrastructure: Linking Landscapes and Communities*: Island Press.
- Beshara, T. (2018). *The Urban Heat Island Effect and Western Sydney*. Retrieved from <https://www.parliament.nsw.gov.au/committees/DBAssets/InquirySubmission/Summary/39702/08%20-%20Greening%20Australia.pdf>. Accessed Saturday, February 24, 2018.
- Bevilacqua, P., Coma, J., Pérez, G., Chocarro, C., Juárez, A., Solé, C., . . . Cabeza, L. F. (2015). Plant cover and floristic composition effect on thermal behaviour of extensive green roofs. *Building and Environment*, 92, 305–316. doi:10.1016/j.buildenv.2015.04.026
- Bilgili, B. C., Şahin, Ş., Yilmaz, O., Gürbüz, F., & Arici, Y. K. (2013). Temperature distribution and the cooling effects on three urban parks in Ankara, Turkey. *International Journal of Global Warming*, 5(3), 296. doi:10.1504/IJGW.2013.055364
- Black, A., & Stephen, H. (2014). Relating temperature trends to the normalized difference vegetation index in Las Vegas. *GIScience & Remote Sensing*, 51(4), 468–482. doi:10.1080/15481603.2014.940695
- Bokwa, A., Hajto, M. J., Walawender, J. P., & Szymanowski, M. (2015). Influence of diversified relief on the urban heat island in the city of Kraków, Poland. *Theoretical and Applied Climatology*, 122(1–2), 365–382. doi:10.1007/s00704-015-1577-9
- Bowler, D. E., Buyung-Ali, L., Knight, T. M., & Pullin, A. S. (2010a). *How effective is 'greening' of urban areas in reducing human exposure to ground level ozone concentrations, UV exposure and the 'urban heat island effect'? : CEE review 08-004 (SR41)*. *Environmental Evidence*. Retrieved from School of the Environment and Natural Resources - Bangor University website: www.environmentalevidence.org/SR41.html
- Bowler, D. E., Buyung-Ali, L., Knight, T. M., & Pullin, A. S. (2010b). Urban greening to cool towns and cities: A systematic review of the empirical evidence. *Landscape and Urban Planning*, 97(3), 147–155.
- Brady, R. F., Tobias, T., Eagles, P. F.J., Ohrner, R., Micak, J., Veale, B., & Dorney, R. S. (1979). A typology for the urban ecosystem and its relationship to larger biogeographical landscape units. *Urban Ecology*, 4(1), 11–28. doi:10.1016/0304-4009(79)90020-2
- Breusch, T. S., & Pagan, A. R. (1979). A Simple Test for Heteroscedasticity and Random Coefficient Variation. *Econometrica*, 47(5), 1287. doi:10.2307/1911963
- Brown, C., & Harder, C. (2016). *The ArcGIS Imagery Book: New View, New vision* (1st ed.): Esri Press. Monday, January 29, 2018.

- Bruse, M. (2011). *ENVI-met model homepage*. Retrieved from <http://www.envi-met.com>. Accessed.
- Buchholz, N. (2013). *Low-impact development & green infrastructure implementation. Creating a Replicable GIS Suitability Model for Stormwater Management & the Urban Heat Island Effect in Dallas, Texas* (Master thesis), Columbia University. Thursday, June 18, 2015.
- Bureau of Meteorology (BOM). (2013). *Special Climate Statement 43 – Extreme heat in January 2013*. Retrieved from www.bom.gov.au/climate/current/statements/scs43e.pdf. Accessed Thursday, January 12, 2017.
- Bureau of Meteorology (BOM). (2016). *Australian Climate Change*. Retrieved from [http://www.abs.gov.au/ausstats/abs@.nsf/Lookup/3222.0main+features32012%20\(base\)%20to%202101](http://www.abs.gov.au/ausstats/abs@.nsf/Lookup/3222.0main+features32012%20(base)%20to%202101). Accessed Thursday, January 12, 2017.
- Bureau of Meteorology (BOM). (2017). *Climate classification maps*. Thursday, June 08, 2017.
- Bureau of Meteorology (BOM). (2018). *Climate statistics for Australian locations*. Retrieved from http://www.bom.gov.au/climate/averages/tables/cw_066062.shtml. Accessed Thursday, February 22, 2018.
- Bureau of Meteorology (BOM), & Commonwealth Scientific and Industrial Research Organisation (CSIRO). (2016). *State of The Climate 2016*. Australia.
- Buyantuyev, A., & Wu, J. (2010). Urban heat islands and landscape heterogeneity:: Linking spatiotemporal variations in surface temperatures to land-cover and socioeconomic patterns. *Landscape Ecology*, 25, 17–33.
- Byrne, J., & Sipe, N. (2010). *Green and open space planning for urban consolidation - A review of the literature and best practice* (No. 11). Brisbane.
- Caborn, J. M. (1965). *Shelterbelts and windbreaks*.: Faber & Faber Ltd.
- Cadenasso, M. L., Pickett, S. T. A., McGrath, B., & Marshall, V. (2013). Ecological Heterogeneity in Urban Ecosystems: Reconceptualized Land Cover Models as a Bridge to Urban Design. In S.T.A. Pickett, M. L. Cadenasso, & B. McGrath (Eds.), *Resilience in Ecology and Urban Design. Linking Theory and Practice for Sustainable Cities*. New York: Springer.
- Cadenasso, M. L., Pickett, S.T.A., & Schwarz, K. (2007). Spatial heterogeneity in urban ecosystems: reconceptualizing land cover and a framework for classification. *Front. Ecol. Environ.*, 5(2), 80–88.
- Cai, M., Ren, C., & Xu, Y. (2017). Investigating the relationship between Local Climate Zone and land surface temperature. In *2017 Joint Urban Remote Sensing Event (JURSE)* (pp. 1–4). IEEE.
- Cameron, R. W.F., Taylor, J. E., & Emmett, M. R. (2014). What's 'cool' in the world of green façades?: How plant choice influences the cooling properties of green walls. *Building and Environment*, 73, 198–207. doi:10.1016/j.buildenv.2013.12.005
- Cao, X., Onishi, A., Chen, J., & Imura, H. (2010). Quantifying the cool island intensity of urban parks using ASTER and IKONOS data. *Landscape and Urban Planning*, 96(4), 224–231. doi:10.1016/j.landurbplan.2010.03.008
- Carlson, T. (2007). An Overview of the "Triangle Method" for Estimating Surface Evapotranspiration and Soil Moisture from Satellite Imagery. *Sensors*, 7(8), 1612–1629. doi:10.3390/s7081612
- Carlson, T. N., Gillies, R. R., & Perry, E. M. (1994). A method to make use of thermal infrared temperature and NDVI measurements to infer surface soil water content and fractional vegetation cover. *Remote Sensing Reviews*, 9(1-2), 161–173. doi:10.1080/02757259409532220
- Chang, C.-R., & Li, M.-H. (2014). Effects of urban parks on the local urban thermal environment. *Urban Forestry & Urban Greening*, 13(4), 672–681. doi:10.1016/j.ufug.2014.08.001
- Chang, C.-R., Li, M.-H., & Chang, S.-D. (2007). A preliminary study on the local cool-island intensity of Taipei city parks. *Landscape and Urban Planning*, 80(4), 386–395. doi:10.1016/j.landurbplan.2006.09.005
- Charoenkit, S., & Yiemwattana, S. (2016). Living walls and their contribution to improved thermal comfort and carbon emission reduction: A review. *Building and Environment*, 105, 82–94. doi:10.1016/j.buildenv.2016.05.031
- Cheltenham Borough Council (CBC). (2008). *Green Space Audit-Final Report*. Worcestershire, UK.
- Chen, A., Yao, X. A., Sun, R., & Chen, L. (2014). Effect of urban green patterns on surface urban cool islands and its seasonal variations. *Urban Forestry & Urban Greening*, 13(4), 646–654. doi:10.1016/j.ufug.2014.07.006

- Chen, L., & Ng, E. (2013). Simulation of the effect of downtown greenery on thermal comfort in subtropical climate using PET index: A case study in Hong Kong. *Architectural Science Review*, 56(4), 297–305. doi:10.1080/00038628.2012.684871
- Chen, Q., Li, B., & Liu, X. (2013). An experimental evaluation of the living wall system in hot and humid climate. *Energy and Buildings*, 61, 298–307. doi:10.1016/j.enbuild.2013.02.030
- Chen, X., Su, Y., Li, D., Huang, G., Chen, W., & Chen, S. (2012). Study on the cooling effects of urban parks on surrounding environments using Landsat TM data: A case study in Guangzhou, southern China. *International Journal of Remote Sensing*, 33(18), 5889–5914. doi:10.1080/01431161.2012.676743
- Chen, Y., & Wong N. H. (2006). Thermal benefits of city parks. *Energy and Buildings*, 38(2), 105–120. doi:10.1016/j.enbuild.2005.04.003
- Cheng, C. Y., Cheung, K. K.S., & Chu, L. M. (2010). Thermal performance of a vegetated cladding system on facade walls. *Building and Environment*, 45(8), 1779–1787. doi:10.1016/j.buildenv.2010.02.005
- Cheng, W.-C., Chang, J.-C., Chang, C.-P., Su, Y., & Tu, T.-M. (2008). A Fixed-Threshold Approach to Generate High-Resolution Vegetation Maps for IKONOS Imagery. *Sensors*, 8(7), 4308–4317. doi:10.3390/s8074308
- Cheng, X., Wei, B., Chen, G., Li, J., & Song, C. (2014). Influence of Park Size and Its Surrounding Urban Landscape Patterns on the Park Cooling Effect. *Journal of Urban Planning and Development*. doi:10.1061/(ASCE)UP.1943-5444.0000256
- Choi, H.-A., Lee, W.-K., & Byun, W.-H. (2012). Determining the Effect of Green Spaces on Urban Heat Distribution Using Satellite Imagery. *Asian Journal of Atmospheric Environment*, 6(2), 127–135. doi:10.5572/ajae.2012.6.2.127
- Christchurch City Council (CCC). (2010). *Public Open Space Strategy 2010-2040*. New Zealand.
- City of Parramatta. (2018). *Property developments | City of Parramatta*. Retrieved from <https://www.cityofparramatta.nsw.gov.au/business-development/invest-in-parramatta/property-developments>. Accessed Monday, February 26, 2018.
- Cohen, P., Potchter, O., & Matzarakis, A. (2012). Daily and seasonal climatic conditions of green urban open spaces in the Mediterranean climate and their impact on human comfort. *Building and Environment*, 51, 285–295. doi:10.1016/j.buildenv.2011.11.020
- Colunga, M. L., Cambrón-Sandoval, V. H., Suzán-Azpíri, H., Guevara-Escobar, A., & Luna-Soria, H. (2015). The role of urban vegetation in temperature and heat island effects in Querétaro city, Mexico. *Atmósfera*, 28(3), 205–218. doi:10.20937/ATM.2015.28.03.05
- Connors, J. P., Galletti, C. S., & Chow, W. T. L. (2013). Landscape configuration and urban heat island effects: Assessing the relationship between landscape characteristics and land surface temperature in Phoenix, Arizona. *Landscape Ecology*, 28(2), 271–283. doi:10.1007/s10980-012-9833-1
- Cook, R. D. (1977). Detection of Influential Observation in Linear Regression. *Technometrics*, 19(1), 15. doi:10.2307/1268249
- Cooper, L. M. (2010). Network analysis in CEA, ecosystem services assessment and green space planning. *Impact Assessment and Project Appraisal*, 28(4), 269–278. doi:10.3152/146155110X12838715793048
- Correa, E., Ruiz, M. A., Canton, A., & Lesino, G. (2012). Thermal comfort in forested urban canyons of low building density. An assessment for the city of Mendoza, Argentina. *Building and Environment*, 58, 219–230. doi:10.1016/j.buildenv.2012.06.007
- Coutts, A., Beringer, J., & Tapper, N. (2010). Changing Urban Climate and CO₂ Emissions: Implications for the Development of Policies for Sustainable Cities. *Urban Policy and Research*, 28(1), 27–47. doi:10.1080/08111140903437716
- Coutts, A. M., Beringer, J., & Tapper, N. J. (2007). Impact of Increasing Urban Density on Local Climate: Spatial and Temporal Variations in the Surface Energy Balance in Melbourne, Australia. *Journal of Applied Meteorology and Climatology*, 46(4), 477–493. doi:10.1175/JAM2462.1
- Coutts, A. M., Daly, E., Beringer, J., & Tapper, N. J. (2013). Assessing practical measures to reduce urban heat: Green and cool roofs. *Building and Environment*, 70, 266–276. doi:10.1016/j.buildenv.2013.08.021
- Coutts, A. M., & Harris, R. J. (2012). *A multi-scale assessment of urban heating in Melbourne during an extreme heat event: policy approaches for adaptation*. Melbourne, Australia.

- Coutts, A. M., Harris, R. J., Phan, T., Livesley, S. J., Williams, N., & Tapper, N. J. (2016). Thermal infrared remote sensing of urban heat: Hotspots, vegetation, and an assessment of techniques for use in urban planning. *Remote Sensing of Environment*, 186, 637–651.
- Coutts, A. M., Tapper, N. J., Beringer, J., Loughnan, M., & Demuzere, M. (2012). Watering our cities: The capacity for Water Sensitive Urban Design to support urban cooling and improve human thermal comfort in the Australian context. *Progress in Physical Geography*, 37(1), 2–28. doi:10.1177/0309133312461032
- Coutts, A. M., White, E. C., Tapper, N. J., Beringer, J., & Livesley, S. J. (2015). Temperature and human thermal comfort effects of street trees across three contrasting street canyon environments. *Theoretical and Applied Climatology*. doi:10.1007/s00704-015-1409-y
- CSIRO, & BOM. (2015). *Climate Change in Australia Information for Australia's Natural Resource Management Regions*.
- Davies, C., MacFarlane, R., McGloin, C., & Roe, M. (2006). *Green Infrastructure Planning Guide. North-East Community Forests, Durham, Marea Britanie*. Retrieved from <https://www.scribd.com/doc/55042694/Green-Infrastructure-Guide-Project-Davies-Et-Al-2006>. Accessed Monday, March 30, 2015.
- Davis, M. (2010). *Green Infrastructure In-Depth Case Analysis.: Theme 7: Mapping For Planning. Task 4.1: In-depth Case Analysis – Green Infrastructure Implementation and Efficiency – ENV.B.2./SER/2010/0059*.
- Davis, M. M., & Hirmer, S. (2015). The potential for vertical gardens as evaporative coolers: An adaptation of the 'Penman Monteith Equation'. *Building and Environment*, 92, 135–141. doi:10.1016/j.buildenv.2015.03.033
- Davis, M.J.M., Ramírez, F., & Vallejo, A. L. (2015). Vertical Gardens as Swamp Coolers. *Procedia Engineering*, 118, 145–159. doi:10.1016/j.proeng.2015.08.413
- Declet-Barreto, J., Brazel, A. J., Martin, C. A., Chow, W. T. L., & Harlan, S. L. (2013). Creating the park cool island in an inner-city neighborhood: Heat mitigation strategy for Phoenix, AZ. *Urban Ecosystems*, 16(3), 617–635. doi:10.1007/s11252-012-0278-8
- DEFRA. (2008). *Case Study to Develop Tools and Methodologies to deliver an Ecosystem-based Approach - Thames Gateway Green Grids*. Research Project Final Report. UK.
- Department for Transport, Local Government and the Regions (DTLR). (2002). *Green Spaces, Better Places: Final Report of the Urban Green Spaces Taskforce*. London.
- Department of the Environment and Energy (DEE). (2018). *Australia's bioregions (IBRA)*. Retrieved from <http://www.environment.gov.au/land/nrs/science/ibra>. Accessed Thursday, February 22, 2018.
- Di Giuseppe, E., & D'Orazio, M. (2014). Assessment of the effectiveness of cool and green roofs for the mitigation of the Heat Island effect and for the improvement of thermal comfort in Nearly Zero Energy Building. *Architectural Science Review*, 58(2), 134–143. doi:10.1080/00038628.2014.966050
- Di Gregorio, A., & Jansen, L. J. M. (Eds.). (1998). *Land Cover Classification System (LCCS): Classification concepts and user manual*. Food and Agriculture Organization (FAO). Rome, Italy.
- Djedjig, R., Bozonnet, E., & Belarbi, R. (2015). Analysis of thermal effects of vegetated envelopes: Integration of a validated model in a building energy simulation program. *Energy and Buildings*, 86, 93–103. doi:10.1016/j.enbuild.2014.09.057
- Dobbs, C., Escobedo, F. J., Zipperer, W. C., &. (2011). A framework for developing urban forest ecosystem services and goods indicators. *Landscape and Urban Planning*, 99(3-4), 196–206. doi:10.1016/j.landurbplan.2010.11.004
- Dobrovolný, P. (2013). The surface urban heat island in the city of Brno (Czech Republic) derived from land surface temperatures and selected reasons for its spatial variability. *Theoretical and Applied Climatology*, 112(1-2), 89–98. doi:10.1007/s00704-012-0717-8
- Domain. (2016). *What's next for Sydney's second CBD?* Retrieved from <https://www.domain.com.au/news/whats-next-for-sydneys-second-cbd-20160822-ggyrxt/>. Accessed Saturday, February 24, 2018.
- Duarte, D. H.S., Shinzato, P., Gusson, C. d. S., & Alves, C. A. (2015). The impact of vegetation on urban microclimate to counterbalance built density in a subtropical changing climate. *Urban Climate*, 14, 224–239. doi:10.1016/j.uclim.2015.09.006

- Dunnett, N., & Kingsbury, N. (2004). *Planting Green Roofs and Living Walls*. Portland, Oregon: Timber Press.
- Dunnett, N., Swanwick, C., & Woolley, H. (2002). *Improving Urban Parks, Play Areas, and Open Space: Urban research report*. London.
- Durbin, J., & Watson, G. S. (1951). *Testing for serial correlation in least squares regression. I. Reprint series / University of Cambridge. Department of Applied Economics* no. 36. [Cambridge]: University of Cambridge, Department of Applied Economics.
- East Midlands Development Agency (EMDA). (2010). *A guide and toolkit. Green Infrastructure: Playind an important role in achieving sustainable economic growth*. Nottingham.
- East Midlands Green Infrastructure Network (EMGIN). (2006). *Green Infrastructure Guide for the East Midlands*.
- Ely, M., & Pitman, S. (2014). *Green Infrastructure: Life support for human habitats. The compelling evidence for incorporating nature into urban environments: Green Infrastructure Evidence Base 2014*. Green Infrastructure Project, Botanic Gardens of South Australia. South Australia.
- Emmanuel, R., & Krüger, E. (2012). Urban heat island and its impact on climate change resilience in a shrinking city: The case of Glasgow, UK. *Building and Environment*, 53, 137–149. doi:10.1016/j.buildenv.2012.01.020
- Emmanuel, R., & Loconsole, A. (2015). Green infrastructure as an adaptation approach to tackling urban overheating in the Glasgow Clyde Valley Region, UK. *Landscape and Urban Planning*, 138, 71–86. doi:10.1016/j.landurbplan.2015.02.012
- English Nature. (2003). *Providing Accessible Natural Greenspaces in Towns and Cities: A practical guide to Assessing the Resources and Implementing Local Standards for Provision*. UK.
- Erell, E., Pearlmutter, D., & Williamson, T. (2011). *Urban Microclimate: Designing the Spaces Between Buildings*. London, Washington, DC.: Earthscan. Saturday, November 28, 2015.
- ESRI. (2012). ArcGIS 10.3. Redlands, CA, USA.
- European Commission (EC). (2012). *The Multifunctionality of Green Infrastructure: Science for Environment Policy, In-depth Report*. Thursday, June 18, 2015.
- European Environment Agency (EEA). (2011). *Green infrastructure and territorial cohesion: The concept of green infrastructure and its integration into policies using monitoring systems*. EEA Technical report No. 18/2011.
- European Environment Agency (EEA). (2013). *Building a green infrastructure for Europe*. Luxembourg: Publications Office. Thursday, June 18, 2015.
- Exelis. (2015). ENVI 5.3.1.
- Faehnle, M. (2014). *Collaborative planning of urban green infrastructure – need, quality, evaluation, and design*. University of Helsinki, Helsinki. Tuesday, June 09, 2015.
- Fan, C., Myint, S. W., & Zheng, B. (2015). Measuring the spatial arrangement of urban vegetation and its impacts on seasonal surface temperatures. *Progress in Physical Geography*, 39(2), 199–219. doi:10.1177/0309133314567583
- Fanger, P. O. (1972). *Thermal comfort*. New York: McGraw-Hill.
- Feyisa, G. L., Dons, K., & Meilby, H. (2014). Efficiency of parks in mitigating urban heat island effect: An example from Addis Ababa. *Landscape and Urban Planning*, 123, 87–95. doi:10.1016/j.landurbplan.2013.12.008
- Fintikakis, N., Gaitani, N., Santamouris, M., Assimakopoulos, M., Assimakopoulos, D. N., Fintikaki, M., . . . Doumas, P. (2011). Bioclimatic design of open public spaces in the historic centre of Tirana, Albania. *Sustainable Cities and Society*, 1(1), 54–62. doi:10.1016/j.scs.2010.12.001
- Forest Research. (2010a). *Benefits of green infrastructure*. Report to Defra and CLG.
- Forest Research. (2010b). *Green infrastructure and the urban heat island*. Retrieved from [http://www.forestry.gov.uk/pdf/urpg_evidence_note_004_Heat_amelioration.pdf/\\$FILE/urpg_evidence_note_004_Heat_amelioration.pdf](http://www.forestry.gov.uk/pdf/urpg_evidence_note_004_Heat_amelioration.pdf/$FILE/urpg_evidence_note_004_Heat_amelioration.pdf). Accessed Thursday, June 18, 2015.
- Foster, J., Lowe, A., & Winkelmann, S. (2011). *The Value of Green Infrastructure for Urban Climate Adaptation*.
- Francis, R. A., & Lorimer, J. (2011). Urban reconciliation ecology: the potential of living roofs and walls. *Journal of environmental management*, 92(6), 1429–1437. doi:10.1016/j.jenvman.2011.01.012

- Gaitani, N., Burud, I., Thiis, T., & Santamouris, M. (Eds.) 2016. *Aerial survey and in-situ measurements of materials and vegetation in the urban fabric*. : International High-Performance Built Environment Conference – A Sustainable Built Environment Conference 2016 Series (SBE16), iHBE 2016.
- Gaitani, N., Burud, I., Thiis, T., & Santamouris, M. (2017). High-resolution spectral mapping of urban thermal properties with Unmanned Aerial Vehicles. *Building and Environment*, 121, 215–224. doi:10.1016/j.buildenv.2017.05.027
- Gaitani, N., Spanou, A., Saliari, M., Synnefa, A., Vassilakopoulou, K., Papadopoulou, K., . . . Lagoudaki, A. (2011). Improving the microclimate in urban areas: A case study in the centre of Athens. *Building Services Engineering Research and Technology*, 32(1), 53–71. doi:10.1177/0143624410394518
- Gandhi, G. M., Parthiban, S., Thummalu, N., & Christy, A. (2015). Ndvi: Vegetation Change Detection Using Remote Sensing and Gis – A Case Study of Vellore District. *Procedia Computer Science*, 57, 1199–1210. doi:10.1016/j.procs.2015.07.415
- Gartland, L. (2008). *Heat Islands: Understanding and Mitigating Heat in Urban Areas*: Earthscan. Friday, January 27, 2017.
- Geletiĉ, J., Dobrovolný, P., & Lehnert, M. (Eds.) 2017. *Statistical analyses of Land Surface Temperature in Local Climate Zones: Case study of Brno and Prague (Czech Republic): 6 - 8 March 2017, Dubai, United Arab Emirates*. Piscataway, NJ: IEEE.
- Geletiĉ, J., & Lehnert, M. (2016). GIS-based delineation of local climate zones: The case of medium-sized Central European cities. *Moravian Geographical Reports*, 24(3), 1062. doi:10.1515/mgr-2016-0012
- Geletiĉ, J., Lehnert, M., & Dobrovolný, P. (2016). Land Surface Temperature Differences within Local Climate Zones, Based on Two Central European Cities. *Remote Sensing*, 8(10), 788. doi:10.3390/rs8100788
- Gémes, O., Tobak, Z., & van Leeuwen, B. (2016). Satellite Based Analysis of Surface Urban Heat Island Intensity. *Journal of Environmental Geography*, 9(1-2), 23–30. doi:10.1515/jengeo-2016-0004
- Georgescu, M., Moustauoui, M., Mahalov, A., & Dudhia, J. (2011). An alternative explanation of the semiarid urban area “oasis effect”. *Journal of Geophysical Research: Atmospheres*, 116(D24), n/a-n/a. doi:10.1029/2011JD016720
- Geoscience Australia. (2018). *Elevation - Foundation Spatial Data*. Retrieved from <http://elevation.fsdf.org.au/>. Accessed Tuesday, March 06, 2018.
- Getis, A. (2010). Spatial Interaction and Spatial Autocorrelation: A Cross-Product Approach. In L. Anselin & S. J. Rey (Eds.), *Advances in spatial science. Perspectives on spatial data analysis* (pp. 23–33). Heidelberg, New York: Springer.
- Getis, A., & Ord K. J. (2010). The Analysis of Spatial Association by Use of Distance Statistics. In L. Anselin & S. J. Rey (Eds.), *Advances in spatial science. Perspectives on spatial data analysis*. Heidelberg, New York: Springer.
- Gill, S., Handley, J., Ennos, A., & Pauleit, S. (2007). Adapting Cities for Climate Change: The Role of the Green Infrastructure. *Built Environment*, 33(1), 115–133.
- Gill, S. E. (2006). *Climate Change and Urban Greenspace* (PhD thesis). Faculty of Humanities - University of Manchester. Thursday, June 18, 2015.
- Gillespie, A. (2015). Land Surface Emissivity. In E. Njoku (Ed.), *The encyclopedia of earth sciences series. Encyclopedia of remote sensing* (pp. 303–311). New York [New York], Boston, Massachusetts: Springer Reference; Credo Reference.
- Gillespie, A. R. (Ed.) 1985. *Lithologic mapping of silicate rocks using TIMS. Jet Propulsion Laboratory Publication 86-36: The TIMS Data Users' Workshop*. Pasadena, CA.
- Gillner, S., Vogt, J., Tharang, A., Dettmann, S., & Roloff, A. (2015). Role of street trees in mitigating effects of heat and drought at highly sealed urban sites. *Landscape and Urban Planning*, 143, 33–42. doi:10.1016/j.landurbplan.2015.06.005
- Gómez-Baggethun, E., & Barton, D. N. (2013). Classifying and valuing ecosystem services for urban planning. *Ecological Economics*, 86, 235–245. doi:10.1016/j.ecolecon.2012.08.019
- Graham, L. (2013). *Point Group Tracing and Squaring in LP360 A Heuristic Discussion of Parameter Settings*. Tuesday, March 13, 2018.

- Grell, G. A., Dudhia, J., & Stauffer, D. (1994). *A Description of the Fifth-Generation Penn State/NCAR Mesoscale Model (MM5)*. NCAR Technical Note TN- 398+STR. Boulder, CO.
- Grigg, D. (1965). The logic of Regional systems. *Ann. Assoc. Amer. Geogr.*, 55, 465–491.
- Grimmond, C. S. B. (2006). Progress in measuring and observing the urban atmosphere. *Theoretical and Applied Climatology*, 84(1-3), 3–22. doi:10.1007/s00704-005-0140-5
- Gromke, C., Blocken, B., Janssen, W., Merema, B., van Hooff, T., & Timmermans, H. (2015). CFD analysis of transpirational cooling by vegetation: Case study for specific meteorological conditions during a heat wave in Arnhem, Netherlands. *Building and Environment*, 83, 11–26. doi:10.1016/j.buildenv.2014.04.022
- Groot, R. S. de, Alkemade, R., Braat, L., Hein, L., & Willemen, L. (2010). Challenges in integrating the concept of ecosystem services and values in landscape planning, management and decision making. *Ecological Complexity*, 7(3), 260–272. doi:10.1016/j.ecocom.2009.10.006
- Groot, R. S. de, Wilson, M. A., & Boumans, R. M. J. (2002). A typology for the classification, description and valuation of ecosystem functions, goods and services. *Ecological Economics*, 41(3), 393–408. doi:10.1016/S0921-8009(02)00089-7
- Gunawardena, K. R., Wells, M. J., & Kershaw, T. (2017). Utilising green and bluespace to mitigate urban heat island intensity. *The Science of the total environment*, 584-585, 1040–1055. doi:10.1016/j.scitotenv.2017.01.158
- Halper, E. B., Scott, C. A., & Yool, S. R. (2012). Correlating Vegetation, Water Use, and Surface Temperature in a Semiarid City: A Multiscale Analysis of the Impacts of Irrigation by Single-Family Residences. *Geographical Analysis*, 44(3), 235–257. doi:10.1111/j.1538-4632.2012.00846.x
- Hamada, S., & Ohta, T. (2010). Seasonal variations in the cooling effect of urban green areas on surrounding urban areas. *Urban Forestry & Urban Greening*, 9(1), 15–24. doi:10.1016/j.ufug.2009.10.002
- Hamada, S., Tanaka, T., & Ohta, T. (2013). Impacts of land use and topography on the cooling effect of green areas on surrounding urban areas. *Urban Forestry & Urban Greening*, 12(4), 426–434. doi:10.1016/j.ufug.2013.06.008
- Hannam, P. (2017). *Sydney weather: 'Exceptional' heat shows little sign of easing its grip*. Retrieved from <http://www.smh.com.au/environment/weather/sydney-weather-exceptional-heat-shows-little-sign-of-easing-its-grip-20170130-gu17eg.html>. Accessed Saturday, February 24, 2018.
- Hansen, R., Rall, E., Chapman, E., Rolf, W., & Pauleit, S. (2017). *Urban green infrastructure planning: A guide for practitioners*. Munich, Germany. Friday, July 06, 2018.
- Harris, R. J., & Coutts, A. M. (2011). *Airborne Thermal Remote Sensing for Analysis of the Urban Heat Island*. Melbourne, Australia.
- Hathway, E. A., & Sharples, S. (2012). The interaction of rivers and urban form in mitigating the Urban Heat Island effect: A UK case study. *Building and Environment*, 58, 14–22. doi:10.1016/j.buildenv.2012.06.013
- Hawken, S., Metternicht, G., Chang, C., Liew, S., & Gupta, A. (Eds.) 2014. *Remote sensing of urban ecological infrastructure in Desakota environments: A review of current approaches*. : 35th Asian Conference on Remote Sensing (ACRS 2014).
- Hedquist, B. C., & Brazel, A. J. (2014). Seasonal variability of temperatures and outdoor human comfort in Phoenix, Arizona, U.S.A. *Building and Environment*, 72, 377–388. doi:10.1016/j.buildenv.2013.11.018
- Heisler, G. (1986). Energy savings with trees. *Journal of Arboriculture*, 12(5), 113–125.
- Heisler, G. M., & Dewalle, D. R. (1988). Effects of windbreak structure on wind flow. *Agriculture, Ecosystems & Environment*, 22-23, 41–69. doi:10.1016/0167-8809(88)90007-2
- Heldens, W. (2010). *Use of airborne hyperspectral data and height information to support urban micro climate characterisation* (PhD thesis). Bayerischen Julius-Maximilians-Universität Würzburg. Wednesday, October 18, 2017.
- Heusinkveld, B. G., Steeneveld, G. J., van Hove, L. W. A., Jacobs, C. M. J., & Holtslag, A. A. M. (2014). Spatial variability of the Rotterdam urban heat island as influenced by urban land use. *Journal of Geophysical Research: Atmospheres*, 119(2), 677–692. doi:10.1002/2012JD019399
- Hiemstra, J. A., Saaroni, H., & Amorim J. H. (2017). The Urban Heat Island: Thermal Comfort and the Role of Urban Greening. In Pearlmutter, David, et al. (Ed.), *The Urban Forest. Cultivating Green Infrastructure for People and the Environment* (Vol. 7, pp. 7–19). Springer. Monday, July 31, 2017.

- Higuchi, A., Hiyama, T., Fukuta, Y., Suzuki, R., & Fukushima, Y. (2007). The behaviour of a surface temperature/vegetation index (TVX) matrix derived from 10-day composite AVHRR images over monsoon Asia. *Hydrological Processes*, 21(9), 1157–1166. doi:10.1002/hyp.6676
- Hoelscher, M.-T., Nehls, T., Jänicke, B., & Wessolek, G. (2016). Quantifying cooling effects of facade greening: Shading, transpiration and insulation. *Energy and Buildings*, 114, 283–290. doi:10.1016/j.enbuild.2015.06.047
- Höfle, B., & Hollaus, M. (2010). Urban Vegetation Detection using high Density Full-waveform Airborne Lidar Data -: Combination of Object-based image and point Cloud Analysis, XXXVIII, Part 7B, 281–286.
- Hong, B., & Lin, B. (2015). Numerical studies of the outdoor wind environment and thermal comfort at pedestrian level in housing blocks with different building layout patterns and trees arrangement. *Renewable Energy*, 73, 18–27. doi:10.1016/j.renene.2014.05.060
- Hou, P., Chen, Y., Qiao, W., Cao, G., Jiang, W., & Li, J. (2013). Near-surface air temperature retrieval from satellite images and influence by wetlands in urban region. *Theoretical and Applied Climatology*, 111(1-2), 109–118. doi:10.1007/s00704-012-0629-7
- Hough, M. (2002). *Cities and natural process*. New York: Routledge. Taylor & Francis. Saturday, February 03, 2018.
- Howard, L. (1818). *The Climate of London*. London: W. Phillips. Monday, January 16, 2017.
- Hsieh, C.-M., Jan, F.-C., & Zhang, L. (2016). A simplified assessment of how tree allocation, wind environment, and shading affect human comfort. *Urban Forestry & Urban Greening*, 18, 126–137. doi:10.1016/j.ufug.2016.05.006
- Huang, H.-Y., Margulis, S. A., Chu, C. R., & Tsai, H.-C. (2011). Investigation of the impacts of vegetation distribution and evaporative cooling on synthetic urban daytime climate using a coupled LES-LSM model. *Hydrological Processes*, 25(10), 1574–1586. doi:10.1002/hyp.7919
- Huang, L., Shen, H., Wu, P., Zhang, L., & Zeng, C. (Eds.) 2015. *Relationships analysis of land surface temperature with vegetation indicators and impervious surface fraction by fusing multi-temporal and multi-sensor remotely sensed data*. : Joint Urban Remote Sensing Event (JURSE), 2015.
- Huang, Y. J., Akbari, H., & Taha, H. (1990). *The wind-shielding and shading effects of trees on residential heating and cooling requirements*: University of California.
- Hunter, A., Livesley, S. J., & Williams, N. S. G. (2012). *Literature Review. Responding to the Urban Heat Island: A Review of the Potential of Green Infrastructure*. Report funded by the Victorian Centre for Climate Change Adaptation (VCCCAR). Melbourne, Australia.
- Hunter, A. M., Williams, N. S.G., Rayner, J. P., Aye, L., Hes, D., & Livesley, S. J. (2014). Quantifying the thermal performance of green façades: A critical review. *Ecological Engineering*, 63, 102–113. doi:10.1016/j.ecoleng.2013.12.021
- IBM. (2016). IBM SPSS Statistics for Windows. NY.
- Institute of Anthropological and Spatial Studies (IASS). (2018). *Relief Visualization Toolbox (RVT)*. Retrieved from <https://iaps.zrc-sazu.si/en/rvt#v>. Accessed.
- IPCC. (2013). *Climate Change 2013: The Physical Science Basis. Contribution of Working Group I to the Fifth Assessment Report of the Intergovernmental Panel on Climate Change*.
- Irger, M. (2014). *The Effect of Urban Form on Urban Microclimate* (PhD Thesis). Faculty of Built Environment, UNSW, Sydney. Wednesday, August 26, 2015.
- Jacobs, B., Mikhailovich, N., & Delaney, C. (2014). *Benchmarking Australia's Urban Tree Canopy: An i-Tree Assessment.: Final Report*. Prepared for Horticulture Australia Limited. Sydney.
- Jamei, E., Rajagopalan, P., Seyedmahmoudian, M., & Jamei, Y. (2016). Review on the impact of urban geometry and pedestrian level greening on outdoor thermal comfort. *Renewable and Sustainable Energy Reviews*, 54, 1002–1017. doi:10.1016/j.rser.2015.10.104
- Jansson, C., Jansson, P.-E., & Gustafsson, D. (2007). Near surface climate in an urban vegetated park and its surroundings. *Theoretical and Applied Climatology*, 89(3-4), 185–193. doi:10.1007/s00704-006-0259-z
- Jarque, C. M., & Bera, A. K. (1987). A Test for Normality of Observations and Regression Residuals. *International Statistical Review / Revue Internationale de Statistique*, 55(2), 163. doi:10.2307/1403192
- Jenerette, G. D., Harlan, S. L., Buyantuev, A., Stefanov, W. L., Delet-Barreto, J., Ruddell, B. L., . . . Li, X. (2016). Micro-scale urban surface temperatures are related to land-cover features and

- residential heat related health impacts in Phoenix, AZ USA. *Landscape Ecology*. doi:10.1007/s10980-015-0284-3
- Jenks, G. F. (1967). The data model concept in statistical mapping. *International yearbook of cartography*, 7(1), 186–190.
- Jim, C. Y. (1989). Tree-Canopy Characteristics and Urban Development in Hong Kong. *Geographical Review*, 79(2), 210–225.
- Jim, C. Y. (2012). Effect of vegetation biomass structure on thermal performance of tropical green roof. *Landscape and Ecological Engineering*, 8(2), 173–187. doi:10.1007/s11355-011-0161-4
- Jim, C. Y. (2015a). Assessing climate-adaptation effect of extensive tropical green roofs in cities. *Landscape and Urban Planning*, 138, 54–70. doi:10.1016/j.landurbplan.2015.02.014
- Jim, C. Y. (2015b). Greenwall classification and critical design-management assessments. *Ecological Engineering*, 77, 348–362. doi:10.1016/j.ecoleng.2015.01.021
- Jim, C. Y. (2015c). Thermal performance of climber greenwalls: Effects of solar irradiance and orientation. *Applied Energy*, 154, 631–643. doi:10.1016/j.apenergy.2015.05.077
- Jim, C.Y., & Chen, S. S. (2003). Comprehensive greenspace planning based on landscape ecology principles in compact Nanjing city, China. *Landscape and Urban Planning*, 65(3), 95–116. doi:10.1016/S0169-2046(02)00244-X
- Kaloustian, N., & Bechtel, B. (Eds.) 2016. *Local Climatic Zoning and Urban Heat Island in Beirut*. : 4th International Conference on Countermeasures to Urban Heat Island. Singapore: NUS.
- Keeley, M. (2011). The Green Area Ratio: An urban site sustainability metric. *Journal of Environmental Planning and Management*, 54(7), 937–958. doi:10.1080/09640568.2010.547681
- Khan, K. S., Kunz, R., Kleijnen, J., & Antes, G. (2003). Five steps to conducting a systematic review. *Journal of the Royal Society of Medicine*, 96, 118–121.
- Kjelgren, R., & Montague, T. (1998). Kjelgren, R., Montague, T., 1998. Urban tree transpiration over turf and asphalt surfaces. *Atmos. Environ.* 32, 35–41. *Atmos. Environ.*, 32, 35–41.
- Klemm, W., Heusinkveld, B. G., Lenzholzer, S., Jacobs, M. H., & van Hove, B. (2015). Psychological and physical impact of urban green spaces on outdoor thermal comfort during summertime in The Netherlands. *Building and Environment*, 83, 120–128. doi:10.1016/j.buildenv.2014.05.013
- Klemm, W., Heusinkveld, B. G., Lenzholzer, S., & van Hove, B. (2015). Street greenery and its physical and psychological impact on thermal comfort. *Landscape and Urban Planning*, 138, 87–98. doi:10.1016/j.landurbplan.2015.02.009
- Klemm, W., Lenzholzer, S., & van den Brink, A. (2017). Developing green infrastructure design guidelines for urban climate adaptation. *Journal of Landscape Architecture*, 12(3), 60–71. doi:10.1080/18626033.2017.1425320
- Koenker, R., & Bassett, G. (1982). Robust Tests for Heteroscedasticity Based on Regression Quantiles. *Econometrica*, 50(1), 43. doi:10.2307/1912528
- Kokalj, Ž., Hesse, R., Cukut, J., Laharnar, B., Goldman, L., Lockett, B., . . . Wilson, M. (2017). *Airborne laser scanning raster data visualization: A guide to good practice* (1st ed., 1st print). *Prostor, kraj, čas / ZRC SAZU Vol. 14*. Ljubljana: Založba ZRC.
- Kokalj, Ž., Zakšek, K., & Oštir, K. (2011). Application of sky-view factor for the visualisation of historic landscape features in lidar-derived relief models. *Antiquity*, 85(327), 263–273. doi:10.1017/S0003598X00067594
- Kolokotsa, D., Santamouris, M., & Zerefos, S. C. (2013). Green and cool roofs' urban heat island mitigation potential in European climates for office buildings under free floating conditions. *Solar Energy*, 95, 118–130. doi:10.1016/j.solener.2013.06.001
- Konarska, J., Holmer, B., Lindberg, F., & Thorsson, S. (2015). Influence of vegetation and building geometry on the spatial variations of air temperature and cooling rates in a high-latitude city. *International Journal of Climatology*, n/a-n/a. doi:10.1002/joc.4502
- Konarska, J., Lindberg, F., Larsson, A., Thorsson, S., & Holmer, B. (2014). Transmissivity of solar radiation through crowns of single urban trees—application for outdoor thermal comfort modelling. *Theoretical and Applied Climatology*, 117(3-4), 363–376. doi:10.1007/s00704-013-1000-3
- Konarska, J., Uddling, J., Holmer, B., Lutz, M., Lindberg, F., Pleijel, H., & Thorsson, S. (2015). Transpiration of urban trees and its cooling effect in a high latitude city. *International journal of biometeorology*. doi:10.1007/s00484-015-1014-x

- Kong, F., Yan, W., Zheng, G., Yin, H., Cavan, G., Zhan, W., . . . Cheng, L. (2016). Retrieval of three-dimensional tree canopy and shade using terrestrial laser scanning (TLS) data to analyze the cooling effect of vegetation. *Agricultural and Forest Meteorology*, 217, 22–34. doi:10.1016/j.agrformet.2015.11.005
- Kong, F., Yin, H., James, P., Hutyrá, L. R., & He, H. S. (2014). Effects of spatial pattern of greenspace on urban cooling in a large metropolitan area of eastern China. *Landscape and Urban Planning*, 128, 35–47. doi:10.1016/j.landurbplan.2014.04.018
- Kong, F., Yin, H., Wang, C., Cavan, G., & James, P. (2014). A satellite image-based analysis of factors contributing to the green-space cool island intensity on a city scale. *Urban Forestry & Urban Greening*, 13(4), 846–853. doi:10.1016/j.ufug.2014.09.009
- Kong, F. H., Yin, H. W., Liu J.Y., Yan, W. J., & Sun C.F. (2013). A Review of Research on the Urban Green Space Cooling Effect. *Journal of Natural Resources*, 28(1), 171–181.
- Kong, L., Lau, K. K.-L., Yuan, C., Chen, Y., Xu, Y., Ren, C., & Ng, E. (2017). Regulation of outdoor thermal comfort by trees in Hong Kong. *Sustainable Cities and Society*, 31, 12–25. doi:10.1016/j.scs.2017.01.018
- Kontoleon, K. J., & Eumorfopoulou, E. A. (2010). The effect of the orientation and proportion of a plant-covered wall layer on the thermal performance of a building zone. *Building and Environment*, 45(5), 1287–1303. doi:10.1016/j.buildenv.2009.11.013
- Kotharkar, R., & Bagade, A. (Eds.) 2016. *Local Climate Zone Classification for Indian Cities: A Case study of Nagpur*. : 4th International Conference on Countermeasure to Urban Heat Islands. Singapore: NUS.
- Kottek, M., Grieser, J., Beck, C., Rudolf, B., & Rubel, F. (2006). World Map of the Köppen-Geiger climate classification updated. *Meteorologische Zeitschrift*, 15(3), 259–263. doi:10.1127/0941-2948/2006/0130
- Kotthaus, S., Smith, T. E.L., Wooster, M. J., & Grimmond, C.S.B. (2014). Derivation of an urban materials spectral library through emittance and reflectance spectroscopy. *ISPRS Journal of Photogrammetry and Remote Sensing*, 94, 194–212. doi:10.1016/j.isprsjprs.2014.05.005
- Koyama, T., Yoshinaga, M., Hayashi, H., Maeda, K.-i., & Yamauchi, A. (2013). Identification of key plant traits contributing to the cooling effects of green façades using freestanding walls. *Building and Environment*, 66, 96–103. doi:10.1016/j.buildenv.2013.04.020
- Koyama, T., Yoshinaga, M., Maeda, K.-i., & Yamauchi, A. (2015). Transpiration cooling effect of climber greenwall with an air gap on indoor thermal environment. *Ecological Engineering*, 83, 343–353. doi:10.1016/j.ecoleng.2015.06.015
- Krayenhoff, E., & Voogt, J. (2016). Daytime Thermal Anisotropy of Urban Neighbourhoods: Morphological Causation. *Remote Sensing*, 8(2), 108–130. doi:10.3390/rs8020108
- Krayenhoff, E. S., Christen, A., Martilli, A., & Oke, T. R. (2014). A Multi-layer Radiation Model for Urban Neighbourhoods with Trees. *Boundary-Layer Meteorology*, 151(1), 139–178. doi:10.1007/s10546-013-9883-1
- Kropf, K. S. (1993). *An enquiry into the definition of built form in urban morphology* (PhD thesis). Geography, University of Birmingham, Birmingham. Friday, January 12, 2018.
- Kvalevåg, M. M., Myhre, G., Bonan, G., & Levis, S. (2010). Anthropogenic land cover changes in a GCM with surface albedo changes based on MODIS data. *International Journal of Climatology*, 30(13), 2105–2117. doi:10.1002/joc.2012
- La Rosa, D., & Privitera, R. (2013). Characterization of non-urbanized areas for land-use planning of agricultural and green infrastructure in urban contexts. *Landscape and Urban Planning*, 109(1), 94–106. doi:10.1016/j.landurbplan.2012.05.012
- Laerd Statistics. (2015). *Multiple regression using SPSS Statistics*. Retrieved from <https://statistics.laerd.com/>. Accessed Monday, June 11, 2018.
- Lam, C. K. C., Loughnan, M., & Tapper, N. (2016). Visitors' perception of thermal comfort during extreme heat events at the Royal Botanic Garden Melbourne. *International journal of biometeorology*. doi:10.1007/s00484-015-1125-4
- Land Property Information (LPI). (2015). *Elevation data products specification and description: Airborne Light Detecting and Ranging (LiDAR)*. Sydney, Australia.
- Landscape Institute. (2009). *Green Infrastructure connected and multifunctional landscapes.: Position Statement*.

- Lawrence, P. J., & Chase, T. N. (2010). Investigating the climate impacts of global land cover change in the community climate system model. *International Journal of Climatology*, 30(13), 2066–2087. doi:10.1002/joc.2061
- Leconte, F., Bouyer, J., Claverie, R., & Pétrissans, M. (2015). Using Local Climate Zone scheme for UHI assessment: Evaluation of the method using mobile measurements. *Building and Environment*, 83, 39–49. doi:10.1016/j.buildenv.2014.05.005
- Lehmann, I., Mathey, J., Rößler, S., Bräuer, A., & Goldberg, V. (2014). Urban vegetation structure types as a methodological approach for identifying ecosystem services – Application to the analysis of micro-climatic effects. *Ecological Indicators*, 42, 58–72. doi:10.1016/j.ecolind.2014.02.036
- Lehmann, S. (2014). Low carbon districts: Mitigating the urban heat island with green roof infrastructure. *City, Culture and Society*, 5, 1–8. doi:10.1016/j.ccs.2014.02.002
- Lehnert, M., Geletič, J., Husák, J., & Vysoudil, M. (2015). Urban field classification by “local climate zones” in a medium-sized Central European city: The case of Olomouc (Czech Republic). *Theoretical and Applied Climatology*, 122(3-4), 531–541. doi:10.1007/s00704-014-1309-6
- Lelovics, E., Unger, J., Gál, T., & Gál, C. V. (2014). Design of an urban monitoring network based on Local Climate Zone mapping and temperature pattern modelling. *Climate Research*, 60(1), 51–62. doi:10.3354/cr01220
- Leuzinger, S., Vogt, R., & Körner, C. (2010). Tree surface temperature in an urban environment. *Agricultural and Forest Meteorology*, 150(1), 56–62. doi:10.1016/j.agrformet.2009.08.006
- Li, D., & Bou-Zeid, E. (2013). Synergistic Interactions between Urban Heat Islands and Heat Waves: The Impact in Cities Is Larger than the Sum of Its Parts. *Journal of Applied Meteorology and Climatology*, 52(9), 2051–2064. doi:10.1175/JAMC-D-13-02.1
- Li, F., Wang, R., Paulussen, J., & Liu, X. (2005). Comprehensive concept planning of urban greening based on ecological principles: a case study in Beijing, China. *Landscape and Urban Planning*, 72(4), 325–336. doi:10.1016/j.landurbplan.2004.04.002
- Li, J., Song, C., Cao, L., Zhu, F., Meng, X., & Wu, J. (2011). Impacts of landscape structure on surface urban heat islands: A case study of Shanghai, China. *Remote Sensing of Environment*, 115(12), 3249–3263. doi:10.1016/j.rse.2011.07.008
- Li, X., Zhou, W., & Ouyang, Z. (2013). Relationship between land surface temperature and spatial pattern of greenspace: What are the effects of spatial resolution? *Landscape and Urban Planning*, 114, 1–8. doi:10.1016/j.landurbplan.2013.02.005
- Li, X., Zhou, W., Ouyang, Z., Xu, W., & Zheng, H. (2012). Spatial pattern of greenspace affects land surface temperature: Evidence from the heavily urbanized Beijing metropolitan area, China. *Landscape Ecology*, 27(6), 887–898. doi:10.1007/s10980-012-9731-6
- Li, X.-X., & Norford, L. K. (2016). Evaluation of cool roof and vegetations in mitigating urban heat island in a tropical city, Singapore. *Urban Climate*, 16, 59–74. doi:10.1016/j.uclim.2015.12.002
- Libelle, T., Morau, D., Clain, A., & Garde, F. (Eds.) 2011. *Energetic performance of a green roof in the tropical environment of La Reunion Island (Indian Ocean)*. : Solar World Congress 2011.
- Lin, B., Meyers, J., Beaty, R., & Barnett, G. (2016). Urban Green Infrastructure Impacts on Climate Regulation Services in Sydney, Australia. *Sustainability*, 8(8), 788. doi:10.3390/su8080788
- Lin, B.-S., & Lin, Y.-J. (2010). Cooling Effect of Shade Trees with Different Characteristics in a Subtropical Urban Park. *Hort Science*, 45(1), 83–86.
- Lin, B.-S., Yu, C.-C., Su, A.-T., & Lin, Y.-J. (2013). Impact of climatic conditions on the thermal effectiveness of an extensive green roof. *Building and Environment*, 67, 26–33. doi:10.1016/j.buildenv.2013.04.026
- Lin, W., Yu, T., Chang, X., Wu, W., & Zhang, Y. (2015). Calculating cooling extents of green parks using remote sensing: Method and test. *Landscape and Urban Planning*, 134, 66–75. doi:10.1016/j.landurbplan.2014.10.012
- Lindén, J. (2011). Nocturnal Cool Island in the Sahelian city of Ouagadougou, Burkina Faso. *International Journal of Climatology*, 31(4), 605–620. doi:10.1002/joc.2069
- Liu, K., Gao, W., Gu, X., & Gao, Z. (Eds.) 2013. *The relation between the urban heat island effect and the underlying surface LUCC of meteorological stations*. : Proceedings of SPIE - The International Society for Optical Engineering 8869 - 88690R.

- Liu, K., Su, H., Zhang, L., Yang, H., Zhang, R., & Li, X. (2015). Analysis of the Urban Heat Island Effect in Shijiazhuang, China Using Satellite and Airborne Data. *Remote Sensing*, 7(4), 4804–4833. doi:10.3390/rs70404804
- Liu, T., & Yang, X. (2013). Mapping vegetation in an urban area with stratified classification and multiple endmember spectral mixture analysis. *Remote Sensing of Environment*, 133, 251–264. doi:10.1016/j.rse.2013.02.020
- Llewellyn-Davies. (2000). *Urban Design Compendium 1*. London: English Partnerships & The Housing Corporation.
- Llewellyn-Davies Planning (Ed.). (1992). *Open Space Planning in London*. London (UK): The Committee.
- Luo, X., & Li, W. (2014). Scale effect analysis of the relationships between urban heat island and impact factors: case study in Chongqing. *Journal of Applied Remote Sensing*, 8(1), 84995.
- Ma, L., Li, M., Ma, X., Cheng, L., Du, P., & Liu, Y. (2017). A review of supervised object-based land-cover image classification. *ISPRS Journal of Photogrammetry and Remote Sensing*, 130, 277–293. doi:10.1016/j.isprsjprs.2017.06.001
- Mackey, C. W., Lee, X., & Smith, R. B. (2012). Remotely sensing the cooling effects of city scale efforts to reduce urban heat island. *Building and Environment*, 49, 348–358. doi:10.1016/j.buildenv.2011.08.004
- Maimaitiyiming, M., Ghulam, A., Tiyp, T., Pla, F., Latorre-Carmona, P., Halik, Ü., . . . Caetano, M. (2014). Effects of green space spatial pattern on land surface temperature: Implications for sustainable urban planning and climate change adaptation. *ISPRS Journal of Photogrammetry and Remote Sensing*, 89, 59–66. doi:10.1016/j.isprsjprs.2013.12.010
- Manteghi, G., Limit, H. B., & Remaz, D. (2015). Water Bodies an Urban Microclimate: A Review. *Modern Applied Science*, 9(6). doi:10.5539/mas.v9n6p1
- Mathey, J., Röbber, S., Lehmann, I., & Bräuer, A. (2010). Urban Green Spaces: Potentials and Constraints for Urban Adaptation to Climate Change. *Resilient Cities, Local Sustainability Volume 1, 2011*, pp 479-485, Volume 1, 479.
- Mathey, J., Röbber, S., Lehmann, I., Bräuer, A., Goldberg, V., Kurbjuhn, C., & Westbeld, A. (Eds.). (2011). *Naturschutz und Biologische Vielfalt Vol. 111. Noch wärmer, noch trockener? Stadtnatur und Freiraumstrukturen im Klimawandel.: Even warmer, even drier? Urban nature and green spacedevelopment under climate change*. Bonn-Bad Godesberg: Bundesamt für Naturschutz (Bfn. Ed.).
- MathWorks. (2017a). *Introducing Deep Learning with MATLAB*. Tuesday, May 01, 2018.
- MathWorks. (2017b). *MATLAB and Statistics Toolbox*. Natick, Massachusetts, United States.
- MathWorks. (2018a). *Mastering Machine Learning: A Step-by-Step Guide with MATLAB*. Wednesday, May 02, 2018.
- MathWorks. (2018b). *Statistics and Machine Learning Toolbox™: User's guide*. Wednesday, May 02, 2018.
- Matzarakis, A., & Mayer H. (1996). *Another Kind of Environmental Stress: Thermal Stress (NEWSLETTER)*.
- Mayer, H., & Höppe, P. (1987). Thermal comfort of man in different urban environments. *Theoretical and Applied Climatology*, (38), 43–49.
- Mazza, L., Bennett, G., Nocker, L. de, Gantioler, S., Losarcos, L., Margerison, C., . . . van Diggelen, R. (2011). *Green Infrastructure Implementation and Efficiency: Final report for the European Commission, DG Environment on Contract ENV.B.2/SER/2010/0059*. Institute for European Environmental Policy, Brussels and London.
- Mazzali, U., Peron, F., Romagnoni, P., Pulselli, R. M., & Bastianoni, S. (2013). Experimental investigation on the energy performance of Living Walls in a temperate climate. *Building and Environment*, 64, 57–66. doi:10.1016/j.buildenv.2013.03.005
- McGarigal, K. (2015). *Fragstats Help Manual 4.2*. USA: University of Massachusetts, Amherst. Saturday, October 01, 2016.
- McGarigal, K., Cushman, S. A., Neel, M. C., & Ene, E. (2002). FRAGSTATS: University of Massachusetts, Amherst (www.umass.edu/landeco/research/fragstats/fragstats.html). Retrieved from www.umass.edu/landeco/research/fragstats/fragstats.html. Accessed.

- McGarigal, K., & Marks, B. J. (1995). *FRAGSTATS: spatial pattern analysis program for quantifying landscape structure*. Portland, OR: U.S. Department of Agriculture, Forest Service, Pacific Northwest Research Station. Sunday, September 18, 2016.
- McPherson, E. G., Simpson, J. R., Xiao, Q., & Wu, C. (2011). Million trees Los Angeles canopy cover and benefit assessment. *Landscape and Urban Planning*, 99(1), 40–50. doi:10.1016/j.landurbplan.2010.08.011
- Meier, F., & Scherer, D. (2012). Spatial and temporal variability of urban tree canopy temperature during summer 2010 in Berlin, Germany. *Theoretical and Applied Climatology*, 110(3), 373–384. doi:10.1007/s00704-012-0631-0
- Mell, I. C. (2008). Green Infrastructure: concepts and planning. *FORUM Ejournal - Newcastle University*, (8), 69–80.
- Mell, I. C. (2010). *Green infrastructure: concepts, perceptions and its use in spatial planning* (PhD). Newcastle University, UK.
- Mell, I. C. (2013). Can you tell a green field from a cold steel rail? Examining the “green” of Green Infrastructure development. *Local Environment*, 18(2), 152–166. doi:10.1080/13549839.2012.719019
- Mell, I. C. (2014). Aligning fragmented planning structures through a green infrastructure approach to urban development in the UK and USA. *Urban Forestry & Urban Greening*, 13(4), 612–620. doi:10.1016/j.ufug.2014.07.007
- Millennium Ecosystem Assessment (MEA). (2005). *Ecosystems and Human Well-being: Synthesis*. Washington, DC.: Island Press. Friday, June 12, 2015.
- Miller, R. W., Hauer, R. J., & Werner L. P. (2015). *Urban Forestry: Planning and Managing Urban Greenspaces Third Edition* (3rd): Waveland Press inc.
- Millward, A. A., Torchia, M., Laursen, A. E., & Rothman, L. D. (2014). Vegetation placement for summer built surface temperature moderation in an urban microclimate. *Environmental management*, 53(6), 1043–1057. doi:10.1007/s00267-014-0260-8
- Milošević, D. D., Bajšanski, I. V., & Savić, S. M. (2017). Influence of changing trees locations on thermal comfort on street parking lot and footways. *Urban Forestry & Urban Greening*, 23, 113–124. doi:10.1016/j.ufug.2017.03.011
- Mitraka, Z., Del Frate, F., Chrysoulakis, N., & Gastellu-Etchegorry, J.-P. (Eds.) 2015. *Exploiting Earth Observation data products for mapping Local Climate Zones*. : Joint Urban Remote Sensing Event (JURSE), 2015 Joint.
- Morakinyo, T. E., Adegun, O. B., & Balogun, A. A. (2016). The effect of vegetation on indoor and outdoor thermal comfort conditions: Evidence from a microscale study of two similar urban buildings in Akure, Nigeria. *Indoor and Built Environment*, 25(4), 603–617. doi:10.1177/1420326X14562455
- Morakinyo, T. E., Kong, L., Lau, K. K.-L., Yuan, C., & Ng, E. (2017). A study on the impact of shadow-cast and tree species on in-canyon and neighborhood's thermal comfort. *Building and Environment*, 115, 1–17. doi:10.1016/j.buildenv.2017.01.005
- Morakinyo, T. E., & Lam, Y. F. (2016). Simulation study on the impact of tree-configuration, planting pattern and wind condition on street-canyon's micro-climate and thermal comfort. *Building and Environment*, 103, 262–275. doi:10.1016/j.buildenv.2016.04.025
- Moran, P. A. P. (1950). Notes on Continuous Stochastic Phenomena. *Biometrika*, 37(1/2), 17. doi:10.2307/2332142
- Motazedian, A., & Leardini, P. (Eds.) 2012. *Impact of green infrastructures on urban microclimates. A critical review*. : 46th Annual Conference of the Architectural Science Association (ANZAScA). Australia.
- Müller, N., Kuttler, W., & Barlag, A.-B. (2014). Counteracting urban climate change: Adaptation measures and their effect on thermal comfort. *Theoretical and Applied Climatology*, 115(1-2), 243–257. doi:10.1007/s00704-013-0890-4
- Mushkin, A., Balick, L. K., & Gillespie, A. R. (2005). Extending surface temperature and emissivity retrieval to the mid-infrared (3–5 μm) using the Multispectral Thermal Imager (MTI). *Remote Sensing of Environment*, 98(2-3), 141–151. doi:10.1016/j.rse.2005.06.003
- Natural Economy Northwest (NEN). (2010). *Building natural value for sustainable economic development: The green infrastructure valuation toolkit user guide*. Retrieved from

- <http://bit.ly/givaluationtoolkit>
http://www.greeninfrastructurenw.co.uk/resources/Green_Infrastructure_Valuation_Toolkit_User_Guide.pdf. Accessed Thursday, June 18, 2015.
- Naumann, S., Davis, M., Kaphengst, T., Pieterse, M., & Rayment, M. (2011). *Design, implementation and cost elements of Green Infrastructure projects.: Final report to the European Commission, DG Environment*. Contract no. 070307/2010/577182/ETU/F.1.
- Nearmap. (2017). *High resolution imagery*. Retrieved from <http://www.nearmap.com.au/>. Accessed Tuesday, August 08, 2017.
- Neuman, M. (2005). The Compact City Fallacy. *Journal of Planning Education and Research*, 25(1), 11–26. doi:10.1177/0739456X04270466
- Newton, P., Marchant, D., Mitchell, J., Plume, J., Seo S., & Roggema R. (2013). *Performance Assessment Urban Precinct Design: A scoping study*. Sydney.
- Ng, E., Chen, L., Wang, Y., & Yuan, C. (2012). A study on the cooling effects of greening in a high-density city: An experience from Hong Kong. *Building and Environment*, 47, 256–271. doi:10.1016/j.buildenv.2011.07.014
- Ng., Y. X. Y. (2015). A Study of Urban Heat Island using “Local Climate Zones”: The Case of Singapore. *British Journal of Environment & Climate Change*, 5(2), 116–133.
- Norton, B., Coutts, A., Livesley, S., & Williams, N. (2013). *Technical Report. Decision principles for the selection and placement of Green Infrastructure: Technical report*.
- Norton, B. A., Coutts, A. M., Livesley, S. J., Harris, R. J., Hunter, A. M., & Williams, N. S.G. (2015). Planning for cooler cities: A framework to prioritise green infrastructure to mitigate high temperatures in urban landscapes. *Landscape and Urban Planning*, 134, 127–138. doi:10.1016/j.landurbplan.2014.10.018
- Nouri, H., Anderson, S., Beecham, S., & Bruce, D. (Eds.) 2013. *Estimation of Urban Evapotranspiration through Vegetation Indices Using WorldView2 Satellite Remote Sensing Images*. : EFITA-WCCA-CIGR Conference Sustainable Agriculture through ICT Innovation.
- Nouri, H., Beecham, S., Anderson, S., Hassanli, A. M., & Kazemi, F. (2015). Remote sensing techniques for predicting evapotranspiration from mixed vegetated surfaces. *Urban Water Journal*, 12(5), 380–393. doi:10.1080/1573062X.2014.900092
- Nouri, H., Beecham, S., Kazemi, F., & Hassanli, A. M. (2013). A review of ET measurement techniques for estimating the water requirements of urban landscape vegetation. *Urban Water Journal*, 10(4), 247–259. doi:10.1080/1573062X.2012.726360
- Nouri, H., Glenn, E., Beecham, S., Chavoshi Boroujeni, S., Sutton, P., Alaghmand, S., . . . Nagler, P. (2016). Comparing Three Approaches of Evapotranspiration Estimation in Mixed Urban Vegetation: Field-Based, Remote Sensing-Based and Observational-Based Methods. *Remote Sensing*, 8(6), 492. doi:10.3390/rs8060492
- Nunez, M., & Oke, T. R. (1977). The energy balance of an urban canyon. *Journal of Applied Meteorology*,
- Oberndorfer, E., Lundholm, J., Bass, B., Coffman R. R., Doshi, H., Dunnett, N., . . . Rowe, B. (2007). Green Roofs as Urban Ecosystems: Ecological Structures, Functions, and Services. *Bioscience*, 57(10).
- Ochoa, J. M. (1999). *La vegetacion como instrumento para el control microclimatico* (PhD). Universitat Politecnica de Catalunya, Barcelona, Spain.
- Office of Environment and Heritage (OEH). (2015). *Urban Green Cover. Technical Guidelines*.
- Office of Environment and Heritage (OEH). (2018). *Dry sclerophyll forests (shrub/grass sub-formation) / NSW Environment & Heritage*. Retrieved from [http://www.environment.nsw.gov.au/threatenedSpeciesApp/VegFormation.aspx?formationName=Dry+sclerophyll+forests+\(shrub%2Fgrass+sub-formation\)](http://www.environment.nsw.gov.au/threatenedSpeciesApp/VegFormation.aspx?formationName=Dry+sclerophyll+forests+(shrub%2Fgrass+sub-formation)). Accessed Thursday, February 22, 2018.
- Office of the Deputy Prime Minister (ODPM). (2002a). *Assessing needs and opportunities a companion guide to PPG17*.
- Office of the Deputy Prime Minister (ODPM). (2002b). *Planning Policy Guidance 17: Planning for open space, sport and recreation*.
- Oke, T. R. (1976). The distinction between canopy and boundary-layer heat islands. *Atmosphere*, 14(268–277).

- Oke, T. R. (1979). *Review of urban climatology 1973-1976* (No. 539). Geneva: Secretariat of the World Meteorological Organization.
- Oke, T. R. (1981). Canyon geometry and the nocturnal urban heat island: Comparison of scale model and field observations. *Journal of Climatology*, 1, 237–254.
- Oke, T. R. (1982). The energetic basis of the urban heat island. *Quarterly Journal of the Royal Meteorological Society*, 108(455), 1–24.
- Oke, T. R. (1988a). Street design and urban canopy layer climate. *Energy and Buildings*, 11(1-3), 103–113. doi:10.1016/0378-7788(88)90026-6
- Oke, T. R. (1988b). The urban energy balance. *Progress in Physical Geography*, 12(4), 471–508.
- Oke, T. R. (1992). *Boundary Layer Climates*. London [England], New York: Routledge.
- Oke, T. R. (1997). Urban environments. In W. G. Bailey, T. R. Oke, & W. R. Rouse (Eds.), *The Surface Climates of Canada* (pp. 303–327). Montreal: McGill-Queens University Press.
- Oke, T. R. (2006). Towards better scientific communication in urban climate. *Theoretical and Applied Climatology*, 84(1-3), 179–190. doi:10.1007/s00704-005-0153-0
- Oke, T. R. (Ed.) 2009. *The Need to Establish Protocols in Urban Heat Island Work*. : 8th Symposium on Urban Environments.
- Oke, T. R., Crowther, J. M., McNaughton, K. G., Monteith, J. L., & Gardiner, B. (1989). The Micrometeorology of the Urban Forest. *Phil. Trans. R. Soc. Lond. B*, 324, 335–349.
- Oke, T. R., Mills, G., Christen, A., & Voogt, J. A. (2017). *Urban Climates*: Cambridge University Press. Wednesday, May 30, 2018.
- Olivieri, F., Di Perna, C., D’Orazio, M., Olivieri, L., & Neila, J. (2013). Experimental measurements and numerical model for the summer performance assessment of extensive green roofs in a Mediterranean coastal climate. *Energy and Buildings*, 63, 1–14. doi:10.1016/j.enbuild.2013.03.054
- Olivieri, F., Olivieri, L., & Neila, J. (2014). Experimental study of the thermal-energy performance of an insulated vegetal façade under summer conditions in a continental mediterranean climate. *Building and Environment*, 77, 61–76. doi:10.1016/j.buildenv.2014.03.019
- Onishi, A., Cao, X., Ito, T., Shi, F., & Imura, H. (2010). Evaluating the potential for urban heat-island mitigation by greening parking lots. *Urban Forestry & Urban Greening*, 9(4), 323–332. doi:10.1016/j.ufug.2010.06.002
- Osmond, P. (2008). *An enquiry into new methodologies for evaluating sustainable urban form* (PhD dissertation). University of New South Wales (UNSW), Sydney. Friday, January 12, 2018.
- Osmond, P., & Sharifi, E. (2017). *Guide to Urban Cooling Strategies*. Sydney.
- Osmond, P., & Sharifi E. (2017). *Guide to Urban Cooling Strategies*. Sydney.
- Osmond, P., & Zakiur Rahman, K. M. (Eds.) 2016. *Developing a leaf area index database to inform green infrastructure and urban microclimate research*. : 4th International Conference on Countermeasures to Urban Heat Island: National Univeristy of Singapore.
- Ott, R. L., & Longnecker, M. T. (2004). *A first course in statistical methods*. Belmont, Calif.: Thomson.
- Ottelé, M., Perini, K., Fraaij, A.L.A., Haas, E. M., & Raiteri, R. (2011). Comparative life cycle analysis for green façades and living wall systems. *Energy and Buildings*, 43(12), 3419–3429. doi:10.1016/j.enbuild.2011.09.010
- Ouldboukhitine, S.-E., Belarbi, R., Jaffal, I., & Trabelsi, A. (2011). Assessment of green roof thermal behavior: A coupled heat and mass transfer model. *Building and Environment*, 46(12), 2624–2631. doi:10.1016/j.buildenv.2011.06.021
- Overwatch. (2015). Feature Analyst for ArcGIS. v5.2.0.
- Pakzad, P. (2017). *CITIES WITHIN GARDENS. An indicator-based model for assessing sustainability performance of urban green infrastructure* (PhD). The University of New South Wales, Sydney. Wednesday, January 03, 2018.
- Pakzad, P., & Osmond, P. (2016). Corrigendum to Developing a Sustainability Indicator Set for Measuring Green Infrastructure Performance. *Procedia - Social and Behavioral Sciences*, 216, 1006. doi:10.1016/j.sbspro.2016.02.001
- Panduro, T. E., & Veie, K. L. (2013). Classification and valuation of urban green spaces—A hedonic house price valuation. *Landscape and Urban Planning*, 120, 119–128. doi:10.1016/j.landurbplan.2013.08.009

- Parizotto, S., & Lamberts, R. (2011). Investigation of green roof thermal performance in temperate climate: A case study of an experimental building in Florianópolis city, Southern Brazil. *Energy and Buildings*, 43(7), 1712–1722. doi:10.1016/j.enbuild.2011.03.014
- Pauleit, S., & Duhme, F. (1998). Assessing the Metabolism of Urban Systems for Urban Planning. In J. Breuste, H. Feldmann, & O. Uhlmann (Eds.), *Urban Ecology* (pp. 65–69). Berlin, Heidelberg: Springer Berlin Heidelberg.
- Pauleit, S., & Duhme, F. (2000). Assessing the environmental performance of land cover types for urban planning. *Landscape and Urban Planning*, 52(1), 1–20. doi:10.1016/S0169-2046(00)00109-2
- Pauleit, S., Liu, L., Ahern, J., & Kazmierczak, A. (2014). Multifunctional Green Infrastructure Planning to Promote Ecological Services in the City. In J. Niemelä, J. Breuste, E. Thomas, G. Glenn, J. Philip, & M. N. E (Eds.), *Oxford biology. Urban ecology. Patterns, processes, and applications* (pp. 272–285). Oxford, ©2011.: University Press.
- Pauleit, S., Slinn, P., Handley, J., & Lindley, S. (2003). Promoting the Natural Greenstructure of Towns and Cities: English Nature's *Accessible Natural Greenspace Standards Model*. *Built Environment*, 29(2), 157–170.
- Pearlmutter, D., Jiao, D., & Garb, Y. (2014). The relationship between bioclimatic thermal stress and subjective thermal sensation in pedestrian spaces. *International journal of biometeorology*, 58(10), 2111–2127. doi:10.1007/s00484-014-0812-x
- Pearlmutter, D., Krüger, E. L., & Berliner, P. (2009). The role of evaporation in the energy balance of an open-air scaled urban surface. *International Journal of Climatology*, 29(6), 911–920. doi:10.1002/joc.1752
- Peng, S.-S., Piao, S., Zeng, Z., Ciais, P., Zhou, L., Li, L. Z. X., . . . Zeng, H. (2014). Afforestation in China cools local land surface temperature. *Proceedings of the National Academy of Sciences*, 111(8), 2915–2919. doi:10.1073/pnas.1315126111
- Pérez, G., Coma, J., Martorell, I., & Cabeza, L. F. (2014). Vertical Greenery Systems (VGS) for energy saving in buildings: A review. *Renewable and Sustainable Energy Reviews*, 39, 139–165. doi:10.1016/j.rser.2014.07.055
- Pérez, G., Rincón, L., Vila, A., González, J. M., & Cabeza, L. F. (2011a). Behaviour of green facades in Mediterranean Continental climate. *Energy Conversion and Management*, 52(4), 1861–1867. doi:10.1016/j.enconman.2010.11.008
- Pérez, G., Rincón, L., Vila, A., González, J. M., & Cabeza, L. F. (2011b). Green vertical systems for buildings as passive systems for energy savings. *Applied Energy*, 88(12), 4854–4859. doi:10.1016/j.apenergy.2011.06.032
- Perini, K., & Magliocco, A. (2014). Effects of vegetation, urban density, building height, and atmospheric conditions on local temperatures and thermal comfort. *Urban Forestry & Urban Greening*, 13(3), 495–506. doi:10.1016/j.ufug.2014.03.003
- Perini, K., Ottelé, M., Fraaij, A.L.A., Haas, E. M., & Raiteri, R. (2011). Vertical greening systems and the effect on air flow and temperature on the building envelope. *Building and Environment*, 46(11), 2287–2294. doi:10.1016/j.buildenv.2011.05.009
- Peters, E. B., Hiller, R. V., & McFadden, J. P. (2011). Seasonal contributions of vegetation types to suburban evapotranspiration. *Journal of Geophysical Research*, 116(G1). doi:10.1029/2010JG001463
- Peters, E. B., & McFadden, J. P. (2010). Influence of seasonality and vegetation type on suburban microclimates. *Urban Ecosystems*, 13(4), 443–460. doi:10.1007/s11252-010-0128-5
- Pickering, C., & Byrne, J. (2013). The benefits of publishing systematic quantitative literature reviews for PhD candidates and other early-career researchers. *Higher Education Research & Development*, 33(3), 534–548. doi:10.1080/07294360.2013.841651
- Pickett, S. T. A., Cadenasso, M. L., Rosi-Marshall, E. J., Belt, K. T., Groffman, P. M., Grove, J. M., . . . Warren, P. S. (2017). Dynamic heterogeneity: A framework to promote ecological integration and hypothesis generation in urban systems. *Urban Ecosystems*, 20(1), 1–14. doi:10.1007/s11252-016-0574-9
- Pitman, S. D., Daniels, C. B., & Ely, M. E. (2015). Green infrastructure as life support: Urban nature and climate change. *Transactions of the Royal Society of South Australia*, 139(1), 97–112. doi:10.1080/03721426.2015.1035219

- Potchter, O., Cohen, P., & Bitan, A. (2006). Climatic behavior of various urban parks during hot and humid summer in the mediterranean city of Tel Aviv, Israel. *International Journal of Climatology*, 26(12), 1695–1711. doi:10.1002/joc.1330
- Pullin, A. S., & Stewart, G. B. (2006). Guidelines for systematic review in conservation and environmental management. *Conservation biology : the journal of the Society for Conservation Biology*, 20(6), 1647–1656. doi:10.1111/j.1523-1739.2006.00485.x
- QCoherent. (2012). LP360. v.2012.1.22.0.
- Qiao, Z., Tian, G., & Xiao, L. (2013). Diurnal and seasonal impacts of urbanization on the urban thermal environment: A case study of Beijing using MODIS data. *ISPRS Journal of Photogrammetry and Remote Sensing*, 85, 93–101. doi:10.1016/j.isprsjprs.2013.08.010
- Quattrochi, D. A., & Ridd, M. K. (1994). Measurement and analysis of thermal energy responses from discrete urban surfaces using remote sensing data. *International Journal of Remote Sensing*, 15(10), 1991–2022. doi:10.1080/01431169408954224
- Rahman, M. A., Moser, A., Rötzer, T., & Pauleit, S. (2017). Within canopy temperature differences and cooling ability of *Tilia cordata* trees grown in urban conditions. *Building and Environment*, 114, 118–128. doi:10.1016/j.buildenv.2016.12.013
- Rashid, Z. A., Al Junid, S. A. M., & Thani, S. K. S. O. (2014). Trees' cooling effect on surrounding air temperature monitoring system: Implementation and observation. *International Journal of Simulation*, 15(2), 70–77.
- Rasul, A., Balzter, H., & Smith, C. (2015). Spatial variation of the daytime Surface Urban Cool Island during the dry season in Erbil, Iraqi Kurdistan, from Landsat 8. *Urban Climate*, 14, 176–186. doi:10.1016/j.uclim.2015.09.001
- Razzaghamanesh, M., Beecham, S., & Salemi, T. (2016). The role of green roofs in mitigating Urban Heat Island effects in the metropolitan area of Adelaide, South Australia. *Urban Forestry & Urban Greening*, 15, 89–102. doi:10.1016/j.ufug.2015.11.013
- Realmuto, V. J. (Ed.) 1990. *Separating the effects of temperature and emissivity: Emissivity spectrum normalization*. : 2nd TIMS Workshop. Pasadena, CA: pp. 31–36.
- Rotem-Mindali, O., Michael, Y., Helman, D., & Lensky, I. M. (2015). The role of local land-use on the urban heat island effect of Tel Aviv as assessed from satellite remote sensing. *Applied Geography*, 56, 145–153. doi:10.1016/j.apgeog.2014.11.023
- Roth, M. (2012). Urban Heat Islands. In *Handbook of Environmental Fluid Dynamics, Volume Two* (pp. 143–160). CRC Press.
- Roy, S., Byrne, J., & Pickering, C. (2012). A systematic quantitative review of urban tree benefits, costs, and assessment methods across cities in different climatic zones. *Urban Forestry & Urban Greening*, 11(4), 351–363. doi:10.1016/j.ufug.2012.06.006
- Rupprecht, C. D.D., Byrne, J. A., Garden, J. G., & Hero, J.-M. (2015). Informal urban green space: A trilingual systematic review of its role for biodiversity and trends in the literature. *Urban Forestry & Urban Greening*, 14(4), 883–908. doi:10.1016/j.ufug.2015.08.009
- Ryu, Y.-H., Bou-Zeid, E., Wang, Z.-H., & Smith, J. A. (2015). Realistic Representation of Trees in an Urban Canopy Model. *Boundary-Layer Meteorology*. doi:10.1007/s10546-015-0120-y
- Salata, F., Golasi, I., Petitti, D., Lieto Vollaro, E. de, Coppi, M., & Lieto Vollaro, A. de. (2017). Relating microclimate, human thermal comfort and health during heat waves: An analysis of heat island mitigation strategies through a case study in an urban outdoor environment. *Sustainable Cities and Society*, 30, 79–96. doi:10.1016/j.scs.2017.01.006
- Santamouris, M. (2014). Cooling the cities – A review of reflective and green roof mitigation technologies to fight heat island and improve comfort in urban environments. *Solar Energy*, 103, 682–703. doi:10.1016/j.solener.2012.07.003
- Santamouris, M. (2015). Regulating the damaged thermostat of the cities—Status, impacts and mitigation challenges. *Energy and Buildings*, 91, 43–56. doi:10.1016/j.enbuild.2015.01.027
- Santamouris, M., Haddad, S., Fiorito, F., Osmond, P., Ding, L., Prasad, D., . . . Wang, R. (2017). Urban Heat Island and Overheating Characteristics in Sydney, Australia. An Analysis of Multiyear Measurements. *Sustainability*, 9(5), 712. doi:10.3390/su9050712
- Scheitlin, K. N., & Dixon, P. G. (2010). Diurnal Temperature Range Variability due to Land Cover and Air mass Types in the Southeast. *Journal of Applied Meteorology and Climatology*, 49(5), 879–888. doi:10.1175/2009JAMC2322.1

- Schilling, J., & Logan, J. (2008). Greening the Rust Belt: A Green Infrastructure Model for Right Sizing America's Shrinking Cities. *Journal of the American Planning Association*, 74(4), 451–466.
- Schwarz, N., Schlink, U., Franck, U., & Großmann, K. (2012). Relationship of land surface and air temperatures and its implications for quantifying urban heat island indicators—An application for the city of Leipzig (Germany). *Ecological Indicators*, 18, 693–704. doi:10.1016/j.ecolind.2012.01.001
- Schweitzer, O., & Erell, E. (2014). Evaluation of the energy performance and irrigation requirements of extensive green roofs in a water-scarce Mediterranean climate. *Energy and Buildings*, 68, 25–32. doi:10.1016/j.enbuild.2013.09.012
- Shahidan, M. F., Jones, P. J., Gwilliam, J., & Salleh, E. (2012). An evaluation of outdoor and building environment cooling achieved through combination modification of trees with ground materials. *Building and Environment*, 58, 245–257. doi:10.1016/j.buildenv.2012.07.012
- Shahidan, M. F., Shariff, M. K.M., Jones, P., Salleh, E., & Abdullah, A. M. (2010). A comparison of *Mesua ferrea* L. and *Hura crepitans* L. for shade creation and radiation modification in improving thermal comfort. *Landscape and Urban Planning*, 97(3), 168–181. doi:10.1016/j.landurbplan.2010.05.008
- Shashua-Bar, L., & Hoffman, M. E. (2000). Vegetation as a climatic component in the design of an urban street. An empirical model for predicting the cooling effect of urban green areas with trees. *Energy and Buildings*, 31, 221–235.
- Shashua-Bar, L., Pearlmutter, D., & Erell, E. (2011). The influence of trees and grass on outdoor thermal comfort in a hot-arid environment. *International Journal of Climatology*, 31(10), 1498–1506. doi:10.1002/joc.2177
- Shashua-Bar, L., Potchter, O., Bitan, A., Boltansky, D., & Yaakov, Y. (2010). Microclimate modelling of street tree species effects within the varied urban morphology in the Mediterranean city of Tel Aviv, Israel. *International Journal of Climatology*, n/a-n/a. doi:10.1002/joc.1869
- Shashua-Bar, L., Tsiros, I. X., & Hoffman, M. (2012). Passive cooling design options to ameliorate thermal comfort in urban streets of a Mediterranean climate (Athens) under hot summer conditions. *Building and Environment*, 57, 110–119. doi:10.1016/j.buildenv.2012.04.019
- Shashua-Bar, L., Tsiros, I. X., & Hoffman, M. E. (2010). A modeling study for evaluating passive cooling scenarios in urban streets with trees. Case study: Athens, Greece. *Building and Environment*, 45(12), 2798–2807. doi:10.1016/j.buildenv.2010.06.008
- Sheate, W., Eales, R., Day, E., Baker, J., Murdoch, A., Hill, C., . . . Karpouzoglou, T. (2012). Spatial representation and specification of Ecosystem Services: A Methodology using land use/land cover data and stakeholder Engagement. *Journal of Environmental Assessment Policy and Management*, 14(01), 1250001. doi:10.1142/S1464333212500019
- Shen, M., Piao, S., Jeong, S.-J., Zhou, L., Zeng, Z., Ciais, P., . . . Yao, T. (2015). Evaporative cooling over the Tibetan Plateau induced by vegetation growth. *Proceedings of the National Academy of Sciences*, 112(30), 9299–9304. doi:10.1073/pnas.1504418112
- Shen, X., Liu, B., Li, G., Yu, P., & Zhou, D. (2015). Impacts of grassland types and vegetation cover changes on surface air temperature in the regions of temperate grassland of China. *Theoretical and Applied Climatology*. doi:10.1007/s00704-015-1567-y
- Skarbit, N., Gál, T., & Unger, J. (Eds.) 2015. *Airborne surface temperature differences of the different Local Climate Zones in the urban area of a medium sized city*. : Joint Urban Remote Sensing Event (JURSE), 2015.
- Skelhorn, C., Lindley, S., & Levermore, G. (2014). The impact of vegetation types on air and surface temperatures in a temperate city: A fine scale assessment in Manchester, UK. *Landscape and Urban Planning*, 121, 129–140. doi:10.1016/j.landurbplan.2013.09.012
- Skoulika, F., Santamouris, M., Kolokotsa, D., & Boemi, N. (2014). On the thermal characteristics and the mitigation potential of a medium size urban park in Athens, Greece. *Landscape and Urban Planning*, 123, 73–86. doi:10.1016/j.landurbplan.2013.11.002
- Smith, K. R., & Roebber, P. J. (2011). Green Roof Mitigation Potential for a Proxy Future Climate Scenario in Chicago, Illinois. *Journal of Applied Meteorology and Climatology*, 50(3), 507–522. doi:10.1175/2010JAMC2337.1
- Snir, K., Pearlmutter, D., & Erell, E. (2016). The moderating effect of water-efficient ground cover vegetation on pedestrian thermal stress. *Landscape and Urban Planning*, 152, 1–12. doi:10.1016/j.landurbplan.2016.04.008

- Sobrino, J. A., Jimenez-Muoz, J. C., Soria, G., Romaguera, M., Guanter, L., Moreno, J., . . . Martinez, P. (2008). Land Surface Emissivity Retrieval From Different VNIR and TIR Sensors. *IEEE Transactions on Geoscience and Remote Sensing*, 46(2), 316–327. doi:10.1109/TGRS.2007.904834
- Song, J., Du, S., Feng, X., & Guo, L. (2014). The relationships between landscape compositions and land surface temperature: Quantifying their resolution sensitivity with spatial regression models. *Landscape and Urban Planning*, 123, 145–157. doi:10.1016/j.landurbplan.2013.11.014
- Song, J., & Wang, Z.-H. (2015). Impacts of mesic and xeric urban vegetation on outdoor thermal comfort and microclimate in Phoenix, AZ. *Building and Environment*, 94, 558–568. doi:10.1016/j.buildenv.2015.10.016
- Spagnolo, J., & Dear, R. d. (2003a). A field study of thermal comfort in outdoor and semi-outdoor environments in subtropical Sydney Australia. *Building and Environment*, 38(5), 721–738. doi:10.1016/S0360-1323(02)00209-3
- Spagnolo, J., & Dear, R. d. (2003b). A human thermal climatology of subtropical Sydney. *International Journal of Climatology*, 23(11), 1383–1395. doi:10.1002/joc.939
- Spronken-Smith, R. A., & Oke, T. R. (1998). The thermal regime of urban parks in two cities with different summer climates. *International Journal of Remote Sensing*, 19(11), 2085–2104. doi:10.1080/014311698214884
- Spronken-Smith, R. A., Oke, T. R., & Lowry, W. P. (2000). Advection and the surface energy balance across an irrigated urban park. *International Journal of Climatology*, 20. doi:10.1002/1097-0088(200007)20:9<1033::AID-JOC508>3.0.CO;2-U
- Srivanit, M., & Hokao, K. (2013). Evaluating the cooling effects of greening for improving the outdoor thermal environment at an institutional campus in the summer. *Building and Environment*, 66, 158–172. doi:10.1016/j.buildenv.2013.04.012
- Stathopoulos, T., Chiovitti, D., & Dodaro, L. (1994). Wind shielding effects of trees on low buildings. *Building and Environment*, 29(2), 141–150. doi:10.1016/0360-1323(94)90065-5
- Steeneveld, G. J., Koopmans, S., Heusinkveld, B. G., van Hove, L. W. A., & Holtslag, A. A. M. (2011). Quantifying urban heat island effects and human comfort for cities of variable size and urban morphology in the Netherlands. *Journal of Geophysical Research*, 116(D20). doi:10.1029/2011JD015988
- Steffen, W., Persson, Å., Deutsch, L., Zalasiewicz, J., Williams, M., Richardson, K., . . . Svedin, U. (2011). The Anthropocene: From Global Change to Planetary Stewardship. *AMBIO*, 40(7), 739–761. doi:10.1007/s13280-011-0185-x
- Sternberg, T., Viles, H., & Cathersides, A. (2011). Evaluating the role of ivy (*Hedera helix*) in moderating wall surface microclimates and contributing to the bioprotection of historic buildings. *Building and Environment*, 46(2), 293–297. doi:10.1016/j.buildenv.2010.07.017
- Stewart, I. D. (2011a). A systematic review and scientific critique of methodology in modern urban heat island literature. *International Journal of Climatology*, 31(2), 200–217. doi:10.1002/joc.2141
- Stewart, I. D. (2011b). *Redefining the Urban Heat Island* (Doctor of Philosophy - PhD). University of British Columbia, Canada. Saturday, October 31, 2015.
- Stewart, I. D., & Oke, T. R. (Eds.) 2009. *Newly developed “thermal climate zones” for defining and measuring urban heat island “magnitude” in the canopy layer.* : T.R. Oke Symposium & 8th Symposium on Urban Environment. USA.
- Stewart, I. D., & Oke, T. R. (Eds.) 2010. *Thermal differentiation of local climate zones using temperature observations from urban and rural field sites.* : 9th Symposium, on Urban Environment. Keystone, CO.
- Stewart, I. D., & Oke, T. R. (2012). Local Climate Zones for Urban Temperature Studies. *Bulletin of the American Meteorological Society*, 93(12), 1879–1900. doi:10.1175/BAMS-D-11-00019.1
- Stewart, I. D., Oke, T. R., & Krayenhoff, E. S. (2014). Evaluation of the ‘local climate zone’ scheme using temperature observations and model simulations. *International Journal of Climatology*, 34(4), 1062–1080. doi:10.1002/joc.3746
- Stocco, S., Cantón, M. A., & Correa, E. N. (2015). Design of urban green square in dry areas: Thermal performance and comfort. *Urban Forestry & Urban Greening*, 14(2), 323–335. doi:10.1016/j.ufug.2015.03.001

- Su, W., Zhang, Y., Yang, Y., & Ye, G. (2014). Examining the Impact of Greenspace Patterns on Land Surface Temperature by Coupling LiDAR Data with a CFD Model. *Sustainability*, 6(10), 6799–6814. doi:10.3390/su6106799
- Sun, H., Chen, Y., & Zhan, W. (2015). Comparing surface- and canopy-layer urban heat islands over Beijing using MODIS data. *International Journal of Remote Sensing*, 36(21), 5448–5465.
- Sun, R., Chen, A., Chen, L., & Lü, Y. (2012). Cooling effects of wetlands in an urban region: The case of Beijing. *Ecological Indicators*, 20, 57–64. doi:10.1016/j.ecolind.2012.02.006
- Sun, R., & Chen, L. (2012). How can urban water bodies be designed for climate adaptation? *Landscape and Urban Planning*, 105(1-2), 27–33. doi:10.1016/j.landurbplan.2011.11.018
- Sun, S., Xu, X., Lao, Z., Liu, W., Li, Z., Higuera García, E., . . . Zhu, J. (2017). Evaluating the impact of urban green space and landscape design parameters on thermal comfort in hot summer by numerical simulation. *Building and Environment*, 123, 277–288. doi:10.1016/j.buildenv.2017.07.010
- Sung, C. Y. (2013). Mitigating surface urban heat island by a tree protection policy: A case study of The Woodland, Texas, USA. *Urban Forestry & Urban Greening*, 12(4), 474–480. doi:10.1016/j.ufug.2013.05.009
- Susca, T., Gaffin, S. R., & Dell'osso, G. R. (2011). Positive effects of vegetation: urban heat island and green roofs. *Environmental pollution (Barking, Essex : 1987)*, 159(8-9), 2119–2126. doi:10.1016/j.envpol.2011.03.007
- Susorova, I. (2015). Green facades and living walls: vertical vegetation as a construction material to reduce building cooling loads. In F. Pacheco-Torgal, J. A. Labrincha, L. F. Cabeza, & C.-G. Granqvist (Eds.), *Eco-efficient materials for mitigating building cooling needs: Design, properties and applications* (pp. 127–153). Woodhead Publishing. Thursday, March 31, 2016.
- Susorova, I., Angulo, M., Bahrami, P., & Brent Stephens. (2013). A model of vegetated exterior facades for evaluation of wall thermal performance. *Building and Environment*, 67, 1–13. doi:10.1016/j.buildenv.2013.04.027
- Susorova, I., Azimi, P., & Stephens, B. (2014). The effects of climbing vegetation on the local microclimate, thermal performance, and air infiltration of four building facade orientations. *Building and Environment*, 76, 113–124. doi:10.1016/j.buildenv.2014.03.011
- Szulczewska, B. (2012). *Spatial planning measures for green infrastructure protection and development: Urban biodiversity and green infrastructure*. Lecture notes. Brussels.
- Taha, H. (1997). Urban climates and heat islands: Albedo, evapotranspiration, and anthropogenic heat. *Energy and Buildings*, 25, 99–103.
- Taha, H., Akbari, H., & Rosenfeld, A. (1991). Heat island and oasis effects of vegetative canopies: Micro-meteorological field-measurements. *Theoretical and Applied Climatology*, 44, 123–138.
- Taleghani, M. (2017). Outdoor thermal comfort by different heat mitigation strategies- A review. *Renewable and Sustainable Energy Reviews*. doi:10.1016/j.rser.2017.06.010
- Taleghani, M., Sailor, D., & Ban-Weiss, G. A. (2016). Micrometeorological simulations to predict the impacts of heat mitigation strategies on pedestrian thermal comfort in a Los Angeles neighborhood. *Environmental Research Letters*, 11(2), 24003. doi:10.1088/1748-9326/11/2/024003
- Taleghani, M., Sailor, D. J., Tenpierik, M., & van den Dobbelsteen, A. (2014). Thermal assessment of heat mitigation strategies: The case of Portland State University, Oregon, USA. *Building and Environment*, 73, 138–150. doi:10.1016/j.buildenv.2013.12.006
- Tan, C. L., Wong, N. H., & Jusuf, S. K. (2014). Effects of vertical greenery on mean radiant temperature in the tropical urban environment. *Landscape and Urban Planning*, 127, 52–64. doi:10.1016/j.landurbplan.2014.04.005
- Tan, C. L., Wong, N. H., Tan, P. Y., Jusuf, S. K., & Chiam, Z. Q. (2015). Impact of plant evapotranspiration rate and shrub albedo on temperature reduction in the tropical outdoor environment. *Building and Environment*, 94, 206–217. doi:10.1016/j.buildenv.2015.08.001
- Tan, M., & Li, X. (2013). Integrated assessment of the cool island intensity of green spaces in the mega city of Beijing. *International Journal of Remote Sensing*, 34(8), 3028–3043. doi:10.1080/01431161.2012.757377
- Tan, Z., Lau, K. K.-L., & Ng, E. (2015). Urban tree design approaches for mitigating daytime urban heat island effects in a high-density urban environment. *Energy and Buildings*. doi:10.1016/j.enbuild.2015.06.031

- Tan, Z., Lau, K. K.-L., & Ng, E. (2017). Planning strategies for roadside tree planting and outdoor comfort enhancement in subtropical high-density urban areas. *Building and Environment*, 120, 93–109. doi:10.1016/j.buildenv.2017.05.017
- Tang, H., & Li, Z. (2014). *Quantitative Remote Sensing in Thermal Infrared: Theory and Applications*. Berlin: Springer. Monday, January 08, 2018.
- Tayyebi, A., & Darrel, J. G. (2016). Increases in the climate change adaption effectiveness and availability of vegetation across a coastal to desert climate gradient in metropolitan Los Angeles, CA, USA. *The Science of the total environment*, 548-549, 60–71. doi:10.1016/j.scitotenv.2016.01.049
- TEP. (2005). *East Midlands Green Infrastructure Scoping Study. Final report: Prepared for East Midlands Regional Assembly and partners*.
- The Mersey Forest (TMF). (2010). *Liverpool Green Infrastructure Strategy: Technical Document. Version 1.0*. Liverpool, UK.
- The Mersey Forest (TMF). (2011). *The Value of Mapping Green Infrastructure*. London.
- The Scottish Government (TSG). (2008). *Planning Advice Note: PAN 65 Planning and Open Space*. UK.
- Theil, H. (1961). *Economic Forecasts and Policy - Second Revised Edition*: Amsterdam, The Netherlands, North-Holland Publishing Company.
- Tobler, W. R. (1970). A Computer Movie Simulating Urban Growth in the Detroit Region. *Economic Geography*, 46, 234. doi:10.2307/143141
- Tooke, T. R., Coops, N. C., Goodwin, N. R., & Voogt, J. A. (2009). Extracting urban vegetation characteristics using spectral mixture analysis and decision tree classifications. *Remote Sensing of Environment*, 113(2), 398–407. doi:10.1016/j.rse.2008.10.005
- Tsiros, I. X. (2010). Assessment and energy implications of street air temperature cooling by shade trees in Athens (Greece) under extremely hot weather conditions. *Renewable Energy*, 35(8), 1866–1869. doi:10.1016/j.renene.2009.12.021
- Tsiros, I. X., & Hoffman, M. E. (2014). Thermal and comfort conditions in a semi-closed rear wooded garden and its adjacent semi-open spaces in a Mediterranean climate (Athens) during summer. *Architectural Science Review*, 57(1), 63–82. doi:10.1080/00038628.2013.829021
- Tzoulas, K., Korpela, K., Venn, S., Yli-Pelkonen, V., Kaźmierczak, A., Niemela, J., & James, P. (2007). Promoting ecosystem and human health in urban areas using Green Infrastructure: A literature review. *Landscape and Urban Planning*, 81(3), 167–178. doi:10.1016/j.landurbplan.2007.02.001
- United Nations (UN). (2012). *World Urbanization Prospects The 2011 Revision*. New York,.
- United States Environmental Protection Agency (EPA). (2011). *Evaluation of Urban Soils: Suitability for Green Infrastructure or Urban Agriculture*. Retrieved from <http://water.epa.gov/infrastructure/greeninfrastructure/upload/Evaluation-of-Urban-Soils.pdf>. Accessed Thursday, June 18, 2015.
- United States Geological Survey (USGS). (1992). *Multi-resolution land characteristics*. Retrieved from <http://www.mrlc.gov/>. Accessed Sunday, December 20, 2015.
- United States Geological Survey (USGS). (2003). *National land cover classification*. Retrieved from <http://landcover.usgs.gov/usgslandcover.php>. Accessed Sunday, December 20, 2015.
- Upmanis, H., Eliasson, I., & Linqvist, S. (1998). The influence of green areas on nocturnal temperatures in a high latitude city (Göteborg, Sweden). *International Journal of Climatology*, 18, 681–700.
- van Hove, L.W.A., Jacobs, C.M.J., Heusinkveld, B. G., Elbers, J. A., van Driel, B. L., & Holtslag, A.A.M. (2015). Temporal and spatial variability of urban heat island and thermal comfort within the Rotterdam agglomeration. *Building and Environment*, 83, 91–103. doi:10.1016/j.buildenv.2014.08.029
- Vaz Monteiro, M., Doick, K. J., Handley, P., & Peace, A. (2016). The impact of greenspace size on the extent of local nocturnal air temperature cooling in London. *Urban Forestry & Urban Greening*, 16, 160–169. doi:10.1016/j.ufug.2016.02.008
- Victorial Environmental Assessment Council (VEAC). (2011). *Metropolitan Melbourne investigation final report*. East Melbourne, Vic.
- Vidrih, B., & Medved, S. (2013). Multiparametric model of urban park cooling island. *Urban Forestry & Urban Greening*, 12(2), 220–229. doi:10.1016/j.ufug.2013.01.002

- Völker, S., Baumeister, H., Claßen, T., Hornberg, C., & Kistemann, T. (2013). Evidence for the temperature-mitigating capacity of urban blue space – a health geographic perspective. *Erdkunde*, 67(04), 355–371. doi:10.3112/erdkunde.2013.04.05
- Voogt, J. A. (2002). Urban Heat Island. In T. Munn I., M. C. Douglas, MacCracken H. A., P. Mooney, M. K. Timmerman, & J. G. Tolba (Eds.), *Encyclopedia of Global Environmental Change* (pp. 660–666). Chichester, UK: Wiley.
- Voogt, J. A., & Oke, T. R. (1997). Complete Urban Surface Temperatures. *Journal of Applied Meteorology*, 36(9), 1117–1132. doi:10.1175/1520-0450(1997)036<1117:CUST>2.0.CO;2
- Voogt, J.A., & Oke, T.R. (2003). Thermal remote sensing of urban climates. *Remote Sensing of Environment*, 86(3), 370–384. doi:10.1016/S0034-4257(03)00079-8
- Wang, C., Middel, A., Myint, S. W., Kaplan, S., Brazel, A. J., & Lukasczyk, J. (2018). Assessing local climate zones in arid cities: The case of Phoenix, Arizona and Las Vegas, Nevada. *ISPRS Journal of Photogrammetry and Remote Sensing*, 141, 59–71. doi:10.1016/j.isprsjprs.2018.04.009
- Wang, M., Xiong, Z., & Yan, X. (2015). Modeling the climatic effects of the land use/cover change in eastern China. *Physics and Chemistry of the Earth, Parts A/B/C*, 87-88, 97–107. doi:10.1016/j.pce.2015.07.009
- Wang, X.-J. (2001). Type, quantity and layout of urban peripheral green space. *Journal of Forestry Research*, 12(1), 67–70.
- Wang, Y., Bakker, F., Groot, R. de, Wörtche, H., & Leemans, R. (2015). Effects of urban green infrastructure (UGI) on local outdoor microclimate during the growing season. *Environmental monitoring and assessment*, 187(12). doi:10.1007/s10661-015-4943-2
- Wang, Z., Xing, W., Huang, Y., & Xie, T. (2016). Studying the Urban Heat Island Using a Local Climate Zone Scheme. *Polish Journal of Environmental Studies*, 25(6), 2609–2616. doi:10.15244/pjoes/63672
- Wang, Z.-H., Zhao, X., Yang, J., & Song, J. (2016). Cooling and energy saving potentials of shade trees and urban lawns in a desert city. *Applied Energy*, 161, 437–444. doi:10.1016/j.apenergy.2015.10.047
- Ward, M., & Gleditsch, K. (2008). *Spatial Regression Models*. 2455 Teller Road, Thousand Oaks California 91320 United States of America: SAGE Publications, Inc.
- WaterNSW. (2018). *Sydney's Water supply*. Retrieved from <http://www.waternsw.com.au/home>. Accessed.
- Weber, T. C., & Allen, W. L. (2010). Beyond on-site mitigation: An integrated, multi-scale approach to environmental mitigation and stewardship for transportation projects. *Landscape and Urban Planning*, 96(4), 240–256. doi:10.1016/j.landurbplan.2010.04.003
- Weier, J. & Herring, D. (2000). *Measuring Vegetation (NDVI & EVI) : Feature Articles*. Retrieved from <https://earthobservatory.nasa.gov/Features/MeasuringVegetation/>. Accessed Monday, March 12, 2018.
- Weng, Q. (2009). Thermal infrared remote sensing for urban climate and environmental studies: Methods, applications, and trends. *ISPRS Journal of Photogrammetry and Remote Sensing*, 64(4), 335–344. doi:10.1016/j.isprsjprs.2009.03.007
- Weng, Q. (2012). Remote sensing of impervious surfaces in the urban areas: Requirements, methods, and trends. *Remote Sensing of Environment*, 117, 34–49. doi:10.1016/j.rse.2011.02.030
- Weng, Q., Lu, D., & Schubring, J. (2004). Estimation of land surface temperature–vegetation abundance relationship for urban heat island studies. *Remote Sensing of Environment*, 89(4), 467–483. doi:10.1016/j.rse.2003.11.005
- Wicki, A., & Parlow, E. (2017). Attribution of local climate zones using a multitemporal land use/land cover classification scheme. *Journal of Applied Remote Sensing*, 11(2), 026001-16. doi:10.1117/1.JRS.11.026001
- Wickop, E. (1998). Environmental Quality Targets for Urban Structural Units in Leipzig with a View to Sustainable Urban Development. In J. Breuste, H. Feldmann, & O. Uhlmann (Eds.), *Urban Ecology* (pp. 49–54). Berlin, Heidelberg: Springer Berlin Heidelberg.
- Willemsen, P., & Pardyjak, E. R. (2012). *Impact of Green Infrastructure on Urban Microclimate & Air Quality: Lecture Notes*.

- Williams, N.S.G., Rayner, J. P., & Raynor, K. J. (2010). Green roofs for a wide brown land: Opportunities and barriers for rooftop greening in Australia. *Urban Forestry & Urban Greening*, 9(3), 245–251. doi:10.1016/j.ufug.2010.01.005
- Williamson, K. S. (2003). *Growing with Green Infrastructure*.
- Wilmers, F. (1988). Green for melioration of urban climate. *Energy and Buildings*, 11(1-3), 289–299. doi:10.1016/0378-7788(88)90045-X
- Wong, K. K. (2011). Urban Open Space System in Northern Kowloon Peninsula: An emerging Green Infrastructure network in Hong Kong. *Asian Geographer*, 27(1-2), 13–28. doi:10.1080/10225706.2010.9684150
- Wong, N. H., & Jusuf, S. K. (2010). Study on the microclimate condition along a green pedestrian canyon in Singapore. *Architectural Science Review*, 53(2), 196–212. doi:10.3763/asre.2009.0029
- Wong, N.-H., & Chen, Y. (2010). The Role of Urban Greenery. In E. Ng (Ed.), *High-Density Cities. The Role of Urban Greenery* (pp. 227–262).
- Wong, N.-H., Kwang Tan, A. Y., Chen, Y., Sekar, K., Tan, P. Y., . . . Wong, N. C. (2010). Thermal evaluation of vertical greenery systems for building walls. *Building and Environment*, 45(3), 663–672. doi:10.1016/j.buildenv.2009.08.005
- Woolley, H. (2006). *Urban Open Spaces*. London & New York: Spon Press & Taylor and Francis Group.
- Xiao, J. (2014). Satellite evidence for significant biophysical consequences of the “Grain for Green” Program on the Loess Plateau in China. *Journal of Geophysical Research: Biogeosciences*, 119(12), 2261–2275. doi:10.1002/2014JG002820
- Xu, J., Wei, Q., Huang, X., Zhu, X., & Li, G. (2010). Evaluation of human thermal comfort near urban waterbody during summer. *Building and Environment*, 45(4), 1072–1080. doi:10.1016/j.buildenv.2009.10.025
- Yahia, M. W., & Johansson, E. (2014). Landscape interventions in improving thermal comfort in the hot dry city of Damascus, Syria—The example of residential spaces with detached buildings. *Landscape and Urban Planning*, 125, 1–16. doi:10.1016/j.landurbplan.2014.01.014
- Yang, F., Lau, S. S.Y., & Qian, F. (2011). Thermal comfort effects of urban design strategies in high-rise urban environments in a sub-tropical climate. *Architectural Science Review*, 54(4), 285–304. doi:10.1080/00038628.2011.613646
- Yang, W., Wong, N. H., & Li, C.-Q. (2016). Effect of Street Design on Outdoor Thermal Comfort in an Urban Street in Singapore. *Journal of Urban Planning and Development*, 142(1), 5015003. doi:10.1061/(ASCE)UP.1943-5444.0000285
- Yang, X., Li, Y., Luo, Z., & Chan, P. W. (2017). The urban cool island phenomenon in a high-rise high-density city and its mechanisms. *International Journal of Climatology*, 37(2), 890–904. doi:10.1002/joc.4747
- Young, R., Zanders, J., Lieberknecht, K., & Fassman-Beck, E. (2014). A comprehensive typology for mainstreaming urban green infrastructure. *Journal of Hydrology*, 519, 2571–2583. doi:10.1016/j.jhydrol.2014.05.048
- Youngquist, T. D. (2009). *What is green infrastructure? An evaluation of green infrastructure plans from across the United States* (Master thesis). Iowa State University. Thursday, June 18, 2015.
- Zakšek, K., Oštir, K., & Kokalj, Ž. (2011). Sky-View Factor as a Relief Visualization Technique. *Remote Sensing*, 3(12), 398–415. doi:10.3390/rs3020398
- Zhang, Z., Lv, Y., & Pan, H. (2013). Cooling and humidifying effect of plant communities in subtropical urban parks. *Urban Forestry & Urban Greening*, 12(3), 323–329. doi:10.1016/j.ufug.2013.03.010
- Zhao, C. (2018). Linking the Local Climate Zones and land surface temperature to investigate the surface urban heat island, a case study of San Antonio Texas, U.S. *ISPRS Annals of Photogrammetry, Remote Sensing and Spatial Information Sciences*, IV-3, 277–283. doi:10.5194/isprs-annals-IV-3-277-2018
- Zhao, T. F., & Fong, K. F. (2017). Characterization of different heat mitigation strategies in landscape to fight against heat island and improve thermal comfort in hot–humid climate (Part I): Measurement and modelling. *Sustainable Cities and Society*, 32, 523–531. doi:10.1016/j.scs.2017.03.025
- Zhao-wu, Y. U., Qing-hai, G. U. O., & Ran-hao, S. U. N. (2015). Impacts of urban cooling effect based on landscape scale: A review. (基于景观尺度的城市冷岛效应研究综述). *Chinese Journal of Applied Ecology*, 26(2), 636–642.

- Zheng, B., Myint, S. W., & Fan, C. (2014). Spatial configuration of anthropogenic land cover impacts on urban warming. *Landscape and Urban Planning*, 130, 104–111. doi:10.1016/j.landurbplan.2014.07.001
- Zheng, S., Zhao, L., & Li, Q. (2016). Numerical simulation of the impact of different vegetation species on the outdoor thermal environment. *Urban Forestry & Urban Greening*, 18, 138–150. doi:10.1016/j.ufug.2016.05.008
- Zheng, Y., Ren, C., Wang, R., Ho, J., Lau, K., & Ng, E. (Eds.) 2016. *GIS-based Mapping of Local Climate Zone in the High-density City of Hong Kong*. : 4th International Conference on Countermeasures to Urban Heat Island. Singapore.
- Zheng, Y., Ren, C., Xu, Y., Wang, R., Ho, J., Lau, K., & Ng, E. (2017). GIS-based mapping of Local Climate Zone in the high-density city of Hong Kong. *Urban Climate*. doi:10.1016/j.uclim.2017.05.008
- Zhongli, L., & Hanqiu, X. (2016). A study of Urban heat island intensity based on “local climate zones”: A case study in Fuzhou, China. In Q. Weng (Ed.), *Proceedings of EORSA 2016. The Fourth International Workshop on Earth Observation and Remote Sensing Applications (EORSA 2016)* (pp. 250–254). [Piscataway, New Jersey]: IEEE.
- Zhou, J., Chen, Y., Zhang, X., & Zhan, W. (2013). Modelling the diurnal variations of urban heat islands with multi-source satellite data. *International Journal of Remote Sensing*, 34(21), 7568–7588. doi:10.1080/01431161.2013.821576
- Zhou, W., Cadenasso, M., Schwarz, K., & Pickett, S. (2014). Quantifying Spatial Heterogeneity in Urban Landscapes: Integrating Visual Interpretation and Object-Based Classification. *Remote Sensing*, 6(4), 3369–3386. doi:10.3390/rs6043369
- Zhou, W., Huang, G., & Cadenasso, M. L. (2011). Does spatial configuration matter?: Understanding the effects of land cover pattern on land surface temperature in urban landscapes. *Landscape and Urban Planning*, 102(1), 54–63. doi:10.1016/j.landurbplan.2011.03.009
- Zhou, W., Qian, Y., Li, X., Li, W., & Han, L. (2014). Relationships between land cover and the surface urban heat island: Seasonal variability and effects of spatial and thematic resolution of land cover data on predicting land surface temperatures. *Landscape Ecology*, 29(1), 153–167. doi:10.1007/s10980-013-9950-5
- Zhou, W., & Troy, A. (2009). Development of an object-based framework for classifying and inventorying human-dominated forest ecosystems. *International Journal of Remote Sensing*, 30(23), 6343–6360. doi:10.1080/01431160902849503
- Zhou, Y., & Shepherd, J. M. (2010). Atlanta’s urban heat island under extreme heat conditions and potential mitigation strategies. *Natural Hazards*, 52(3), 639–668. doi:10.1007/s11069-009-9406-z
- Zinzi, M., & Agnoli, S. (2012). Cool and green roofs. An energy and comfort comparison between passive cooling and mitigation urban heat island techniques for residential buildings in the Mediterranean region. *Energy and Buildings*, 55, 66–76. doi:10.1016/j.enbuild.2011.09.024
- Zupancic, T., Westmacott, C., & Buyung-Ali, L. (2015). *The impact of green space on heat and air pollution in urban communities: A meta-narrative systematic review*. Vancouver, Canada.
- Žuvela-Aloise, M., Koch, R., Buchholz, S., & Früh, B. (2016). Modelling the potential of green and blue infrastructure to reduce urban heat load in the city of Vienna. *Climatic Change*, 135(3–4), 425–438. doi:10.1007/s10584-016-1596-2

Appendices

Appendix A – List of questions used for the systematic review of studies analysing the cooling effects of green infrastructure

1. Which countries are more actively researching on the topic and what is the geographic distribution of publications (affiliations)?
2. What locations and climates zones were investigated most and why?
3. What are the seasons and times of the day on which studies concentrated most?
4. Which type of equipment and instruments were employed for collecting relevant data?
5. What are the typical times, frequency and duration of measurements?
6. Which datasets were commonly employed by studies and what are the typical data sources and resolutions (spatial and temporal)?
7. What are the main research focus or interest of studies?
8. Which green infrastructure types receive most attention and why?
9. What are the available methods, approaches and indicators of investigation and what are the advantages and disadvantages of one over another?
10. What are the climatological scales that are studied most?
11. What is the relationship between climatological scales and green infrastructure types investigated?

Appendix B –

Key extracted information from reviewed studies assessing the cooling effects of green infrastructure (ordered by author and year)

<i>Geographic patterns</i>				<i>Investigation period</i>			<i>Methodological aspects</i>						
#	Author (year)	Country	Study area	Climate ¹	Season ²	Duration (year)	Time of day ³	Study Design ⁴	Scale ⁵	Topic (sub-topic) ⁶	Methods ⁷	GI Type ⁸	GI features / comparator
001	Abreu-Harbich et al. (2015)	Brazil	Campinas	Cfa	Su, Wi	Several months (2007, 2010)	DT, NT	LN	Mi	AIRT (HTC)	OS-Fx, NMS	TC	12 tree species
002	Adams and Smith (2014)	Australia	Sydney	Cfb	Su	Dec 2000 - Feb 2001	-	LN	Me	SUT	RS, NMS	TC-GOS	Several GOS / non-grass
003	Alavipanah et al. (2015)	Germany	Munich	Cfb	Su	11 years (2002-12)	DT, NT	LN	Me	SUT	RS, NMS	TC-GOS	Several LULC / built-up
004	Al-Gretawee et al. (2016)	Australia	Melbourne	Cfb	Au	April-May (2015)	DT, NT	LN	Lo, Mi	AIRT/SUT (PCI)	OS-Fx, OS-Mb	GOS	1 medium park / within & nearby
005	Armson et al. (2012)	UK	Manchester	Cfb	Su	June-July (2009 & 2010)	DT	LN	Mi	AIRT/SUT	OS-Fx, EX, NMS	TC	Trees and grasses /non-green site
006	Bencheikh and Rchid (2012)	Algeria	Ghardaia	BWh	Su	7 consecutive days	DT, NT	LN	Mi	AIRT (PCI)	OS-Fx	TC	4 street with trees / beneath & nearby
007	Bevilacqua et al. (2015)	Spain	Lleida	BSk	Su, Wi	2 years (2010-12)	DT, NT	LN	Mi	AIRT	OS-Fx	GR	1 extensive GR
008	Bilgili et al. (2013)	Turkey	Ankara	Dsa	Su	Several days (2006 & 2008)	DT, NT	CS	Lo	AIRT	OS-Fx, OS-Mb, RS, NMS	GOS	3 parks / surroundings
009	Black and Stephen (2014)	USA	Las Vegas	BWh	Su, Au, Wi, Sp	10 years (2000-10)	DT, NT	LN	Me	AIRT	OS-Fx, RS, NMS	GOS	Several GOS / built-up areas
010	Cameron et al. (2014)	UK	Reading	Cfb	Su, Au	Several months (2009-10)	DT, NT	LN	Mi	AIRT/SUT	OS-Fx, EX, NMS	VGS	Several VGS / near & surroundings
011	Cao et al. (2010)	Japan	Nagoya	Cfa	Su, Au, Sp	3 non-consecutive days (2000, 2003, 2004)	DT	LN	Me	SUT (PCI, SC)	RS, NMS	GOS	18 parks / surroundings
012	Chang and Li (2014)	Taiwan	Taipei	Cfa	Su, Wi	Several months (2003 and 2004)	DT, NT	LN	Lo	AIRT (PCI)	OS-Mb, NMS	GOS	60 parks / nearby & built-up
013	Chen et al. (2014)	China	Beijing	Dwa	Su, Au, Wi, Sp	1 day per season (2002)	DT	CS	Me	SUT (UCI, SC)	RS, NMS	GOS	6 types of GOS
014	Chen et al. (2013)	China	Wuhan	Cfa	Su	Several non-consecutive days (2012)	DT, NT	CS	Mi	SUT	OS-Fx, EX	VGS	2 living walls / bare wall
015	Chen et al. (2012)	China	Guangzhou	Cwa	Su, Au	2 non-consecutive days	DT	CS	Me	SUT	RS	GOS	10 parks / surroundings

<i>Geographic patterns</i>				<i>Investigation period</i>				<i>Methodological aspects</i>					
#	Author (year)	Country	Study area	Climate ¹	Season ²	Duration (year)	Time of day ³	Study Design ⁴	Scale ⁵	Topic (sub-topic) ⁶	Methods ⁷	GI Type ⁸	GI features / comparator
016	Chen and Ng (2013)	HK	Hong Kong	Cwa	Su	1 day in June (2008)	DT	CS	Mi	AIRT (HTC)	OS-Fx, NMS	TC	1 site with trees / non-green
017	Cheng et al. (2014)	China	Shanghai	Cfa	Su	1 day (2001)	DT	CS	Lo	SUT (SC)	RS, NMS	GOS	37 parks / surroundings
018	Cheng et al. (2010)	HK	Hong Kong	Cwa	Su	40 consecutive days	DT, NT	LN	Mi	AIRT	OS-Fx, EX, NMS	VGS	2 green walls / bare wall
019	Choi et al. (2012)	S. Korea	Seoul	Dwa	Su, Au, Wi, Sp	Several days (2002)	-	CS	Me	SUT	RS	GOS	Several GOS / built-up area
020	Cohen et al. (2012)	Israel	Tel Aviv	Csa	Su, Wi	Several days (2007-11)	DT	CS	Mi	AIRT (HTC)	OS-Fx	TC-GOS	3 parks, 2 squares, 3 streets with trees / control case
021	Colunga et al. (2015)	Mexico	Queretaro	BSh	Su, Au, Wi, Sp	1 year (2012-13)	DT, NT	LN	Lo	AIRT	OS-Fx, NMS	TC-GOS	GOS in 4 LCZ
022	Connors et al. (2013)	USA	Phoenix	BWh	Su	2 non-consecutive days (2008 & 2009)	NT	CS	Me	SUT (SC)	RS, NMS	GOS	Several LULC
023	Correa et al. (2012)	Argentina	Mendoza	BWk	Su	Several months (2009)	DT, NT	LN	Mi	AIRT (HTC)	OS-Fx, NMS	TC	9 street with trees
024	Coutts et al. (2016)	Australia	Melbourne	Cfb	Su	Several non-consecutive days (2011 & 2012)	DT, NT	CS	Me, Lo	AIRT/SUT	OS-Fx, OS-Mb, RS, NMS	TC-GOS	Several LULC / built-up area
025	Coutts et al. (2015)	Australia	Melbourne	Cfb	Su	May 2011 – June 2013	DT	LN	Mi	AIRT (HTC)	OS-Fx	TC	3 street with trees / beneath and nearby
026	Coutts et al. (2013)	Australia	Melbourne	Cfb	Su, Au	3 consecutive days (2012)	DT, NT	LN	Mi	AIRT/SUT (ET)	OS-Fx, EX	GR	4 rooftops / control
027	Davis and Hirmer (2015)	Ecuador	Quito	Cfb	-	-	-	LN	Mi	AIRT (ET)	OS-Fx	VGS	1 green wall / control
028	Davis et al. (2015)	Ecuador	Quito	Cfb	-	-	-	LN	Mi	AIRT (ET)	OS-Fx	VGS	1 green wall / control
029	Declet-Barreto et al. (2013)	USA	Phoenix	BWh	Su	1 day (2006)	DT, NT	CS	Lo	AIRT/SUT (PCI)	OS-Fx, NMS	GOS	2 modeled scenarios
030	Di Giuseppe and D'Orazio (2014)	Italy	Ancona	Cfa	Su	Several days (2011)	DT, NT	LN	Mi	AIRT	OS-Fx, EX	GR	4 types of GR / non-green
031	Djedjig et al. (2015)	France, Greece	La Rochelle, Athens	Cfb, Csa	Su	1 day (2012)	DT, NT	CS	Mi	AIRT	OS-Fx, EX, NMS	GR, VGS	3 GR and 1 green wall / control
032	Dobrovolný (2013)	Czech R.	Brno	Cfb	Su	2 non-consecutive days (2001 & 2006)	DT	CS	Me	SUT	RS, NMS	GOS	Several LULC
033	Duarte et al. (2015)	Brazil	Sao Paulo	Cfb	Au	Several days, March – April (2013)	DT, NT	CS	Lo	AIRT/SUT (HTC)	OS-Fx, NMS	TC-GOS	4 scenarios

<i>Geographic patterns</i>				<i>Investigation period</i>			<i>Methodological aspects</i>						
#	Author (year)	Country	Study area	Climate ¹	Season ²	Duration (year)	Time of day ³	Study Design ⁴	Scale ⁵	Topic (sub-topic) ⁶	Methods ⁷	GI Type ⁸	GI features / comparator
034	Emmanuel and Loconsole (2015)	UK	Glasgow	Cfb	Sp	1 day	DT, NT	CS	Lo	AIRT/SUT	RS, NMS	TC-GOS	Several LCZ
035	Fan et al. (2015)	USA	Phoenix	BWh	Su, Sp	Several non-consecutive days (2005 & 2007)	DT, NT	CS	Me	SUT (SC)	RS, NMS	TC-GOS	Several LULC
036	Feyisa et al. (2014)	Ethiopia	Addis Ababa	Cwb	Au	15 consecutive days (2010)	DT	LN	Mi	AIRT/SUT (PCI)	OS-Fx, RS, NMS	GOS	21 parks / surroundings
037	Fintikakis et al. (2011)	Albania	Tirana	Cfa	Su	Several consecutive days (2008)	DT	LN	Lo	AIRT/SUT (HTC)	OS-Mb, NMS	TC-GOS	Several GOS
038	Gaitani et al. (2011)	Greece	Athens	Csa	Sp	Several non-consecutive days (2009)	DT	CS	Mi	AIRT/SUT	OS-Mb, NMS	TC-GOS	1 square
039	Georgescu et al. (2011)	USA	Phoenix	BWh	Su	1 month (1999)	DT	LN	Me	SUT	OS-Fx, NMS	GOS	Several LULC built-up area
040	Gillner et al. (2015)	Germany	Dresden	Cfb	Su	Several consecutive months (2013)	DT, NT	LN	Mi	AIRT/SUT (ET)	OS-Fx, NMS	TC	6 tree species / beneath & control
041	Gromke et al. (2015)	The Netherlands	Arnhem	Cfb	Su	1 day (2003)	DT	CS	Mi	AIRT (ET)	OS-Fx, NMS	TC, GR, VGS	1 street with TC, GR & VGS / non-green site
042	Halper et al. (2012)	USA	Tuson	BSh	Sp	Several non-consecutive days (1984 – 2008)	DT	CS	Me	SUT	RS, NMS	GOS	6 types LULC
043	Hamada et al. (2013)	Japan	Nagoya	Cfa	Su	1 day per year (2000, 2004, 2006, 2008, 2010-2011)	DT	CS	Lo	SUT	RS	TC-GOS	1 park / surroundings
044	Hamada and Ohta (2010)	Japan	Nagoya	Cfa	Su, Au, Wi, Sp	1 year (August 2006 - July 2007)	DT, NT	LN	Lo	AIRT	OS-Fx, NMS	GOS	1 park / surroundings
045	Hathway and Sharples (2012)	UK	Sheffield	Cfb	Su	Several consecutive days (2010)	DT	LN	Me	AIRT	OS-Fx, NMS	WB	1 urban river / urban site
046	Hedquist and Brazel (2014)	USA	Phoenix	BWh	Su, Au, Wi, Sp	Several days in different months (2007, 2008)	DT, NT	CS	Lo	AIRT (HTC)	OS-Fx, NMS	TC	4 scenarios with trees
047	Heusinkveld et al. (2014)	The Netherlands	Rotterdam	Cfb	Su	1 day (2009)	DT, NT	CS	Lo	AIRT	OS-Fx, OS-Mb, RS, NMS	WB	Several GOS with WB / built-up areas
048	Hong and Lin (2015)	China	Beijing	Dwa	Su	1 day in July	DT	CS	Mi	AIRT (HTC)	NMS	TC	6 tree configurations
049	Hoelscher et al. (2016)	Germany	Berlin	Cfb	Su	Several consecutive days (2013 & 2014)	DT, NT	LN	Mi	AIRT/SUT (ET)	OS-Fx, EX	VGS	3 green facades / bare wall
050	Hou et al. (2013)	China	Beijing	Dwa	Sp	1 day (2007)	DT	CS	Me	AIRT	RS	WB	7 lakes and wetlands / residential area
051	Hsieh et al. (2016)	Taiwan	Tainan	Aw	Su	1 day	DT	CS	Lo	AIRT (HTC)	OS-Fx, OS-Mb, NMS	GOS	1 GOS

<i>Geographic patterns</i>				<i>Investigation period</i>			<i>Methodological aspects</i>						
#	Author (year)	Country	Study area	Climate ¹	Season ²	Duration (year)	Time of day ³	Study Design ⁴	Scale ⁵	Topic (sub-topic) ⁶	Methods ⁷	GI Type ⁸	GI features / comparator
052	Huang et al. (2011)	Taiwan	Taipei	Cfa	Su	1 day (2008)	DT	CS	Mi	AIRT	OS-Fx, NMS	GOS	6 types LULC / non-green
053	Jenerette et al. (2016)	USA	Phoenix	BWh	Su	5 days (2011)	DT, NT	CS	Lo	SUT	RS, NMS	GOS	6 types LULC / built-up area
054	Jim (2015a)	HK	Hong Kong	Cwa	Su	1 year (2011-2012)	DT, NT	LN	Mi	AIRT/SUT (SST)	OS-Fx, EX	GR	2 GR / control
055	Jim (2015c)	HK	Hong Kong	Cwa	Su	Several days (2012)	DT, NT	CS	Mi	AIRT/SUT	OS-Fx, EX	VGS	1 cylindrical green wall / control wall and air
056	Jim (2012)	HK	Hong Kong	Cwa	Su, Au, Wi, Sp	1 year (2009)	DT, NT	LN	Mi	AIRT/SUT (SST)	OS-Fx, EX	GR	3 extensive GR / control
057	Klemm, Heusinkveld, Lenzholzer, and van Hove (2015)	The Netherlands	Utrecht	Cfb	Su	5 non-consecutive days (2012)	DT	CS	Mi	AIRT (HTC)	OS-Mb, NMS	TC-GOS	9 street with trees / non-green
058	Klemm, Heusinkveld, Lenzholzer, Jacobs et al. (2015)	The Netherlands	Utrecht	Cfb	Su	2 non-consecutive days (2012)	DT	CS	Mi	AIRT (HTC)	OS-Mb, NMS	TC-GOS	13 parks / built-up
059	Kolokotsa et al. (2013)	Greece	Chania	Csa	Su	Several months	DT, NT	LN	Mi	SUT	NMS	GR	1 GR & 1 cool roof / control
060	Konarska, Uddling et al. (2015)	Sweden	Gothenburg	Cfb	Su	Several days (2012 & 2013)	DT	CS	Mi	AIRT (ET)	OS-Mb	TC	47 trees (7 species) / beneath
061	Konarska, Holmer et al. (2015)	Sweden	Gothenburg	Cfb	Su, Au, Wi, Sp	2 years (2012 - 2013)	DT, NT	LN	Lo	AIRT (PCI)	OS-Fx, RS, NMS	TC-GOS	6 parks, 3 street with trees, 1 open site / built-up areas
062	Kong et al. (2017)	HK	Hong Kong	Cwa	Su	1 day	DT, NT	CS	Mi	AIRT (HTC)	NMS	TC	12 tree species
063	Kong et al. (2016)	China	Nanjing	Cfa	Su	6 consecutive days (2013)	DT, NT	LN	Mi	AIRT	OS-Fx, NMS	TC	4 woodlands / control (no canopy)
064	Kong, Yin, James et al. (2014)	China	Nanjing	Cfa	Su	2 days (2009)	DT	CS	Me	SUT (UCI, SC)	RS, NMS	TC-GOS	6 types of GOS
065	Kong, Yin, Wang et al. (2014)	China	Nanjing	Cfa	Su	2 days (2009)	DT	CS	Me	SUT (UCI, SC)	RS, NMS	TC-GOS	Several GOS
066	Kontoleon and Eumorfopoulou (2010)	Greece	Thessaloniki	BSk	Su	3 consecutive moths (2004-2008)	DT, NT	LN	Mi	AIRT	OS-Fx, EX, NMS	VGS	3 green facades / bare wall
067	Koyama et al. (2015)	Japan	Nagoya	Cfa	Au	3 non-consecutive days (2010)	DT	CS	Lo	SUT (ET)	OS-Fx, EX	VGS	2 green walls / control
068	Koyama et al. (2013)	Japan	Nagoya	Cfa	Wi	19 consecutive days (2008)	DT, NT	LN	Mi	AIRT/SUT (ET)	OS-Fx, EX, NMS	VGS	1 green façade / plant species
069	Lehmann et al. (2014)	Germany	Dresden	Cfb	Su	2 non-consecutive days (1999)	DT, NT	CS	Me, Lo	AIRT	RS, NMS	GOS	Several GOS / non-green site

<i>Geographic patterns</i>					<i>Investigation period</i>			<i>Methodological aspects</i>					
#	Author (year)	Country	Study area	Climate ¹	Season ²	Duration (year)	Time of day ³	Study Design ⁴	Scale ⁵	Topic (sub-topic) ⁶	Methods ⁷	GI Type ⁸	GI features / comparator
070	Leuzinger et al. (2010)	Switzerland	Basel	Cfb	Su	3 non-consecutive days (2004 & 2007)	DT	CS	Mi	SUT	OS-Fx, RS	TC	10 trees
071	Li et al. (2013)	China	Beijing	Dwa	Su, Au	3 non-consecutive days (2004 & 2008)	-	CS	Me	SUT (SC)	RS, NMS	GOS	Several GOS
072	Li et al. (2012)	China	Beijing	Dwa	Au	3 non-consecutive days (2002 & 2004)	-	CS	Me	SUT (SC)	RS, NMS	GOS	Several GOS
073	Li et al. (2011)	China	Shanghai	Cfa	Su, Wi	Several non-consecutive days (2000 and 2001)	-	CS	Me	SUT (SC)	RS, NMS	GOS	Several GOS / built-up areas
074	Li and Norford (2016)	Singapore	Singapore	Af	N/A	36 hrs of simulation (April - May 2007 & 2008)	DT, NT	LN	Me	AIRT/SUT	NMS	GOS, GR	12 simulations / real conditions
075	Lin et al. (2016)	Australia	Sydney	Cfb	Wi	1 day (2012)	DT	CS	Lo	SUT	RS, NMS	TC-GOS	5 types of LULC
076	Lin et al. (2015)	China	Beijing	Dwa	Su	1 day (2009)	DT	CS	Lo	SUT	OS-Fx, RS	GOS	30 parks / surroundings
077	Lin et al. (2013)	Taiwan	Taipei	Cfa	Su, Au, Wi, Sp	11 months (2011)	DT, NT	LN	Mi	AIRT	OS-Fx, EX	GR	2 extensive GR
078	Lin and Lin (2010)	Taiwan	Taipei	Cfa	Su	Several non-consecutive days (2007)	DT	CS	Mi	AIRT/SUT	OS-Fx	TC-GOS	12 trees within a park / unshaded
079	Lindén (2011)	Burkina Faso	Ouagadougou	BSh	Au, Wi	Several months (2003 & 2004)	DT, NT	LN	Lo	AIRT/SUT (PCI)	OS-Fx, OS-Mb, NMS	TC-GOS	18 green sites
080	Liu et al. (2015)	China	Shijiazhuang	BSk	Su	Several non-consecutive days (2006/07, 2009/10)	DT, NT	CS	Me, Mi	SUT	OS-Fx, RS	TC-GOS	5 types of LULC
081	Luo and Li (2014)	China	Chongqing	Cfa	Sp	1 day (2010)	-	CS	Me	SUT	RS	WB	Several WB / built-up areas
082	Mackey et al. (2012)	USA	Chicago	Dfa	Su	10 non-consecutive days (1995, 1996, 2007, 2009, 2010)	DT	CS	Me, Lo	SUT	RS, NMS	GOS	Several GOS / built-up areas
083	Maimaitiyiming et al. (2014)	China	Aksu	BWk	Su	1 day (2011)	-	CS	Me	SUT (SC)	RS, NMS	GOS	Several GOS
084	Mazzali et al. (2013)	Italy	Lonigo, Venice, Pisa	Cfa, Csa	Su, Au	Several consecutive months (2009, 2011-12)	-	LN	Mi	AIRT/SUT	OS-Fx, EX	VGS	3 living walls / bare wall
085	Meier and Scherer (2012)	Germany	Berlin	Cfb	Su	2 consecutive months (2010)	DT, NT	LN	Mi	SUT	OS-Fx, RS, NMS	TC	67 urban trees and 18 species
086	Milošević et al. (2017)	Serbia	Novi Sad	Cfb	Su	Several consecutive days in July (2013)	DT, NT	LjN	Mi	AIRT (HTC)	OS-Fx, NMS	TC	3 trees
087	Morakinyo et al. (2017)	HK	Hong Kong	Cwa	Su	1 day in August	DT, NT	CS	Mi	AIRT (HTC)	NMS	TC	8 tree species
088	Morakinyo et al. (2016)	Nigeria	Akure	Aw	N/A	Six consecutive months (2010-2011)	DT, NT	LN	Mi	AIRT (HTC)	OS-Fx, NMS	TC	2 sites with trees
089	Morakinyo and Lam (2016)	HK	Hong Kong	Cwa	Su	1 day in August (2015)	DT, NT	CS	Mi	AIRT (HTC)	NMS	TC	4 street scenarios with trees

<i>Geographic patterns</i>				<i>Investigation period</i>				<i>Methodological aspects</i>					
#	Author (year)	Country	Study area	Climate ¹	Season ²	Duration (year)	Time of day ³	Study Design ⁴	Scale ⁵	Topic (sub-topic) ⁶	Methods ⁷	GI Type ⁸	GI features / comparator
090	Müller et al. (2014)	Germany	Oberhausen	Cfb	Su, Au, Wi, Sp	14 consecutive months (2010-2011)		LN	Lo	AIRT (HTC)	OS-Fx, NMS	TC-GOS	4 scenarios, 8 LCZ / non-green
091	Ng et al. (2012)	HK	Hong Kong	Cwa	Su	1 day (2008)	DT	CS	Lo	AIRT	OS-Fx, NMS	GOS, GR	33 GOS and GR / built-up areas
092	Olivieri et al. (2013)	Italy	Agugliano	Cfa	Su	Several days in July and September (2008)	DT, NT	LN	Mi	AIRT/SUT	OS-Fx, EX, NMS	GR	1 extensive GR
093	Olivieri et al. (2014)	Spain	Madrid	Csa	Su	Several consecutive days (2010, 2011, 2012)	DT, NT	LN	Mi	AIRT/SUT	OS-Fx, EX, NMS	VGS	1 green façade / bare wall
094	Onishi et al. (2010)	Japan	Nagoya	Cfa	Su, Au, Wi, Sp	Five non-consecutive days (2000, 2003, 2004)	DT, NT	CS	Me	SUT	RS, NMS	TC-GOS	12 LULC
095	Ouldboukhithine et al. (2011)	France	La Rochelle	Cfb	Su	Several consecutive days (2010)	DT, NT	LN	Mi	AIRT	OS-Fx, EX, NMS	GR	1 GR (scale 1/10) / nearby
096	Parizotto and Lamberts (2011)	Brazil	Florianopolis	Cfa	Su, Wi	A couple of weeks on March and May (2008)	DT, NT	LN	Mi	AIRT/SUT	OS-Fx, EX	GR	1 GR / non-green roof
097	Pérez et al. (2011a)	Spain	Lleida	BSk	Su, Au, Wi, Sp	1 year (2008-2009)	DT	LN	Mi	AIRT/SUT	OS-Fx, EX	VGS	1 green façade / diff. orientations
098	Perini et al. (2011)	The Netherlands	Delft, Benthuisen Rotterdam	Cfb	Au	Several consecutive days (2010)	DT	CS	Mi	AIRT/SUT	OS-Fx, EX	VGS	3 types of VGS / bare wall and surroundings
099	Perini and Magliocco (2014)	Italy	Milan, Genoa, Rome	Cfa Csa	Su	3 consecutive months	DT	LN	Lo	AIRT (HTC)	NMS	TC, GOS, GR	72 configurations / non-green site
100	Peters and McFadden (2010)	USA	Minneapolis	Dfa	Su, Au, Sp	Several months (weekly) (2006)	DT	LN	Lo	SUT	OS-Fx, RS, NMS	GOS	29 sites / among
101	Qiao et al. (2013)	China	Beijing	Dwa	Su, Au, Wi, Sp	1 day per season (2008)	DT, NT	CS	Me	SUT	RS, NMS	TC-GOS	Different LULC / among
102	Rahman et al. (2017)	Germany	Munich	Cfb	Su	3 consecutive months (2015)	DT, NT	LN	Mi	AIRT (ET)	OS-Fx, NMS	TC-GOS	One plant species / 2 green squares
103	Rashid et al. (2014)	Malaysia	Shah Alam	Af	N/A	2 consecutive months	DT	LN	Mi	AIRT	OS-Fx	TC	Different tree species / among
104	Rasul et al. (2015)	Irak	Erbil	Csa	Su	Several days (2013)	DT	CS	Me	SUT (UCI, SC)	RS	TC-GOS	Different LULC / built-up area
105	Razzaghmanesh et al. (2016)	Australia	Adelaide	Csa	Su	4 days (2013)	DT, NT	CS	Me, Mi	SUT (SST)	OS-Fx, OS-Mb, EX, NMS	GR	4 intensive and extensive GR
106	Rotem-Mindali et al. (2015)	Israel	Tel Aviv	Csa	Su	3 consecutive months	NT	LN	Lo	SUT	RS, NMS	TC-GOS	20 sites / surroundings
107	Ryu et al. (2015)	Switzerland	Basel	Cfb	Su	30 consecutive days (2002) (Simulation)	DT, NT	LN	Mi	AIRT/SUT (ET)	NMS	TC	3 street canyons with trees / non-green
108	Salata et al. (2017)	Italy	Rome	Csa	Su	3 days in July (2014)	DT, NT	LN	Lo	AIRT (HTC)	OS-Fx, NMS	TC-GOS	12 scenarios / control

<i>Geographic patterns</i>				<i>Investigation period</i>			<i>Methodological aspects</i>						
#	Author (year)	Country	Study area	Climate ¹	Season ²	Duration (year)	Time of day ³	Study Design ⁴	Scale ⁵	Topic (sub-topic) ⁶	Methods ⁷	GI Type ⁸	GI features / comparator
109	Scheitlin and Dixon (2010)	USA	Stoneville	Cfa	Su, Au, Wi, Sp	10 year	DT	LN	Me	SUT	OS-Fx, RS, NMS	TC-GOS	6 LULC
110	Schwarz et al. (2012)	Germany	Leipzig	Cfb	Au	2 consecutive days (2010)	DT, NT	CS	Lo	AIRT/SUT	OS-Fx, OS-Mb, RS, NMS	WB	Different LULC / built-up area
111	Schweitzer and Erell (2014)	Israel	Tel Aviv	Csa	Su	Several consecutive months (2009)	DT, NT	LN	Mi	AIRT (ET)	OS-Fx, EX	GR	1 extensive GR & 4 plant species
112	Shahidan et al. (2012)	Malaysia	Putrajaya	Af	N/A	February-March (2009)	DT, NT	LN	Lo	AIRT (HTC)	OS-Fx, NMS	TC-GOS	12 scenarios within a GOS / control
113	Shahidan et al. (2010)	Malaysia	Selangor	Af	N/A	7 consecutive days in February (2008)	DT	LN	Mi	AIRT (HTC)	OS-Fx, NMS	TC	6 tree species
114	Shashua-Bar et al. (2012)	Greece	Athens	Csa	Su	Several days (2007)	DT, NT	CS	Mi	AIRT (HTC)	OS-Fx, NMS	TC	1 street with trees / control site
115	Shashua-Bar et al. (2011)	Israel	Beersheba	BSh	Su	Several consecutive days	DT	LN	Mi	AIRT (ET, HTC)	OS-Fx, EX	TC-GOS	1 courtyard / non-green courtyard
116	Shashua-Bar, Tsiros et al. (2010)	Greece	Athens	Csa	Su, Au	Several non-consecutive days (2006 & 2007)	DT, NT	LN	Mi	AIRT	OS-Fx, NMS	TC	2 street canyons with trees
117	Shashua-Bar, Potchter et al. (2010)	Israel	Tel Aviv	Csa	Su	-	DT	CS	Mi	AIRT	OS-Fx, OS-Mb, NMS	TC-GOS	1 street with trees / non-green site
118	Skelhorn et al. (2014)	UK	Manchester	Cfb	Su	1 day (2010)	DT	CS	Lo	AIRT/SUT	RS, NMS	GOS, GR	7 scenarios
119	Smith and Roebber (2011)	USA	Chicago	Dfa	Su	1 day (2006)	DT	CS	Me	AIRT/SUT	RS, NMS	GR	Several rooftops / urban site
120	Snir et al. (2016)	Israel	Negev desert	BWh	No data	Several consecutive months (2012-2013)	DT, NT	LN	Mi	AIRT/SUT (HTC)	OS-Fx, EX, NMS	GOS	6 species of ground cover / among
121	Song and Wang (2015)	USA	Phoenix	BWh	Su	Several consecutive days in June and July (2012)	DT, NT	LN	Me	AIRT, SUT (HTC)	NMS	GOS	30 vegetation scenarios / built-up
122	Srivaniit and Hokao (2013)	Japan	Saga	Cfa	Su	1 day (2012)	DT	CS	Mi	AIRT	OS-Mb, NMS	TC, GR	4 scenarios with TC and GR / base case & non-green
123	Steenefeld et al. (2011)	The Netherlands	Randstad region	Cfb	Su, Au, Wi, Sp	1 year (1999-2000)	DT, NT	LN	Me	AIRT	OS-Fx	GOS	Several cover fractions
124	Sternberg et al. (2011)	UK	Byland, Ramsey, Oxford, Dover, Nailsea	Cfb	Su, Au, Wi, Sp	1 year (2008-09)	DT, NT	LN	Mi	AIRT	OS-Fx	VGS	5 green facades

<i>Geographic patterns</i>				<i>Investigation period</i>			<i>Methodological aspects</i>						
#	Author (year)	Country	Study area	Climate ¹	Season ²	Duration (year)	Time of day ³	Study Design ⁴	Scale ⁵	Topic (sub-topic) ⁶	Methods ⁷	GI Type ⁸	GI features / comparator
125	Stocco et al., 2015	Argentina	Mendoza	BWk	Su	40 consecutive days (2012-2013)	DT, NT	LN	Mi	AIRT (HTC)	OS-Fx, OS-Mb	TC-GOS	3 squares
126	Su et al. (2014)	China	Nanjing	Cfa	Su, Au	3 non-consecutive days (2010)	DT, NT	CS	Mi	SUT	OS-Mb, RS, NMS	TC-GOS	5 parks
127	Sun and Chen (2012)	China	Beijing	Dwa	Su	1 day (2007)	DT	CS	Me	SUT (UCI, SC)	RS, NMS	WB	197 water bodies / nearby
128	Sun et al. (2017)	China	Beijing	Dwa	Su	1 day in August (2016)	DT, NT	CS	Lo	AIRT (HTC)	OS-Fx, NMS	GOS	18 zones within a park / built-up
129	Sun et al. (2015)	China	Beijing	Dwa	Su, Au, Wi, Sp	Several consecutive months (2009-10)	DT, NT	LN	Me	SUT	RS, NMS	TC-GOS	Several GOS / built-up area
130	Sun et al. (2012)	China	Beijing	Dwa	Su	1 day (2007)	DT	CS	Me	SUT (UCI, SC)	RS, NMS	WB	10 lakes & 5 rivers / surroundings & built-up areas
131	Sung (2013)	USA	Houston	Cfa	Su, Au, Wi, Sp	Several consecutive days (2000-10)	DT	LN	Lo	SUT	RS	TC	2 woodlands / control site
132	Susca et al. (2011)	USA	New York	Dfa	Su, Au, Wi, Sp	1 year (2008-2009)	DT, NT	LN	Mi	SUT	OS-Fx	GR	3 roofing systems / non-green
133	Susorova et al. (2014)	USA	Chicago	Dfa	Su	9 consecutive days (2013)	DT, NT	LN	Mi	AIRT/SUT	OS-Fx, EX	VGS	3 green facades / bare wall
134	Susorova et al. (2013)	USA	Chicago	Dfa	Su	4 non-consecutive days (2012)	DT, NT	CS	Mi	AIRT/SUT	OS-Fx, EX, NMS	VGS	1 experimental wall / bare wall & model
135	Taleghani et al. (2016)	USA	Los Angeles	Csa	Su	1 day in July (2014)	DT, NT	CS	Lo	AIRT (HTC)	NMS	TC, GR	5 scenarios / control
136	Taleghani et al. (2014)	USA	Portland	Csb	Su	2 consecutive months (2013)	DT, NT	LN	Lo, Mi	AIRT (PCI)	OS-Fx, NMS	TC-GOS	7 sites & 3 courtyards / non-green site
137	Tan et al. (2017)	HK	Hong Kong	Cwa	Su	Several days in July and August (2014)	DT	CS	Lo	AIRT (HTC)	OS-Fx, NMS	TC	3 Street with trees / non-green site
138	Tan et al. (2014)	Singapore	Singapore	Af	N/A	2 periods of consecutive days (2011-12)	DT, NT	LN	Mi	AIRT/SUT (HTC)	OS-Fx, EX	VGS	2 green walls / bare wall
139	Tan, C. L. et al. (2015)	Singapore	Singapore	Af	N/A	May to December (2014)	DT, NT	LN	Mi	AIRT (ET)	OS-Fx, EX, NMS	GR	3 plant settings / non-green
140	Tan, Z. et al. (2015)	HK	Hong Kong	Cwa	Su	1 day (2014)	DT	CS	Lo	AIRT	OS-Mb, NMS	TC	Several tree arrangements/ beneath & nearby
141	Tan and Li (2013)	China	Beijing	Dwa	Su	2 non-consecutive days (2009)	DT	CS	Me	SUT (PCI, SC)	RS, NMS	TC-GOS	Several GOS / nearby & built-up
142	Tayyebi and Darrel (2016)	USA	Los Angeles	Csa	Sp	1 day (2013)	DT	CS	Lo	SUT	RS, NMS	TC-GOS	3 climate zones

<i>Geographic patterns</i>				<i>Investigation period</i>			<i>Methodological aspects</i>						
#	Author (year)	Country	Study area	Climate ¹	Season ²	Duration (year)	Time of day ³	Study Design ⁴	Scale ⁵	Topic (sub-topic) ⁶	Methods ⁷	GI Type ⁸	GI features / comparator
143	Tsiros (2010)	Greece	Athens	Csa	Su	Several consecutive days (2007)	DT	LN	Mi	AIRT	OS-Fx, NMS	TC	5 street with trees
144	Tsiros and Hoffman (2014)	Greece	Athens	Csa	Su	1 month (2007)	DT, NT	LN	Mi	AIRT (HTC)	OS-Fx, NMS	GOS	1 courtyard / an urban square & wooded park
145	van Hove et al. (2015)	The Netherlands	Rotterdam	Cfb	Su, Wi, Au, Sp	3 consecutive years (2010-2012)	DT, NT	LN	Me	AIRT (HTC)	OS-Fx	GOS	14 sites / built-up
146	Vaz Monteiro et al. (2016)	UK	London	Cfb	Su, Au	Several non-consecutive days (2012)	NT	CS	Lo	AIRT (UCI)	OS-Fx, RS, NMS	TC-GOS	8 parks / nearby & control
147	Vidrih and Medved (2013)	Slovenia	Ljubljana	Cfb	Su	1 day	DT	CS	Lo	AIRT (PCI)	NMS	TC-GOS	1 park with trees / non-green site
148	Wang, Z.-H. et al. (2016)	USA	Phoenix	BWh	Su	1 year (2012)	DT, NT	LN	Mi	AIRT (ET)	OS-Fx, NMS	TC	1 street with trees (4 simulations) / base scenario
149	Wang, Y. et al. (2015)	The Netherlands	Assen	Cfb	Su, Sp	134 days (2014)	DT, NT	LN	Mi	AIRT (HTC)	OS-Fx, NMS	GOS	5 sites
150	Wong et al. (2010)	Singapore	Singapore	Af	N/A	3 non-consecutive days	DT	CS	Mi	AIRT/SUT	OS-Fx, EX	VGS	9 green facades / bare wall
151	Wong and Jusuf (2010)	Singapore	Singapore	Af	N/A	4 months (2007)	DT, NT	LN	Mi	AIRT	OS-Fx	TC	2 street with trees control
152	Xu et al. (2010)	China	Shanghai	Cfa	Su	Consecutive hours	DT	LN	Mi	AIRT/SUT (HTC)	OS-Fx, NMS	WB	3 sites near a lake / nearby, built-up
153	Yahia and Johansson (2014)	Syria	Damascus	CSb	Su, Wi	1 day in July, 1 day in January	DT, NT	CS	Mi	AIRT (HTC)	OS-Fx, NMS	TC	3 Streets with trees / non-green site
154	Yang et al. (2016)	Singapore	Singapore	Af	N/A	3 months (2012)	DT, NT	LN	Mi	AIRT (HTC)	OS-Fx, NMS	TC	1 street with trees & 11 simulations / non-green
155	Yang et al. (2011)	China	Shanghai	Cfa	Su	3 consecutive days (2008)	DT, NT	CS	Lo	AIRT (HTC)	OS-Fx, NMS	GOS	4 types of land covers
156	Zhang et al. (2013)	China	Shenzhen	Cfa	Su, Au, Wi, Sp	1 year (2010-11)	DT	LN	Mi	AIRT	OS-Fx, NMS	TC-GOS	3 parks an 15 combinations of trees & grasses / control
157	Zhao and Fong (2017)	HK	Hong Kong	Cwa	Su	3 consecutive days (2015)	DT, NT	LN	Mi	AIRT (HTC)	OS-Fx, NMS	TC-GOS	9 sites with green / built-up
158	Zheng, S. et al. (2016)	China	Tianjin	Dwa	Su, Sp	4 non-consecutive days in April, May, July & August (2015)	DT	CS	Mi	AIRT (HTC)	OS-Mb, NMS	TC-GOS	3 types of vegetation
159	Zheng et al. (2014)	USA	Phoenix	BWh	Su	3 non-consecutive days (2005)	DT, NT	CS	Me	SUT (SC)	RS	GOS	Several LULC

<i>Geographic patterns</i>				<i>Investigation period</i>			<i>Methodological aspects</i>						
#	Author (year)	Country	Study area	Climate ¹	Season ²	Duration (year)	Time of day ³	Study Design ⁴	Scale ⁵	Topic (sub-topic) ⁶	Methods ⁷	GI Type ⁸	GI features / comparator
160	Zhou, Qian et al. (2014)	USA	Baltimore	Cfa	Su, Au, Wi, Sp	4 non-consecutive days (1 days per season) (2000 & 2001)	DT	CS	Me	SUT	RS, NMS	GOS	Several LULC / built-up
161	Zhou et al. (2013)	China	Beijing	Dwa	Su, Au, Wi, Sp	8 days (2 consecutive days per season) (2005)	DT	CS	Me	SUT	OS-Fx, RS	GOS	Several LULC
162	Zhou et al. (2011)	USA	Baltimore	Cfa	Su	1 day (1999)	DT	CS	Lo	SUT (SC)	RS, NMS	TC-GOS	6 LULC types
163	Zhou and Shepherd (2010)	USA	Atlanta	Cfa	Su	Several days (1984 - 2007)	DT, NT	LN	Me	SUT	OS-Fx, NMS	GOS	Several LULC / control
164	Zinzi and Agnoli (2012)	Spain, Italy, Egypt	Barcelona, Palermo, Cairo	Csa, BWh	Su	4 days	-	CS	Mi	AIRT (ET, HTC)	NMS	GR	1 GR and 1 cool roof / conventional roof
165	Žuvela-Aloise et al. (2016)	Austria	Vienna	Cfb	Su	Several years (1981-2010)	DT, NT	LN	Me	AIRT	OS-Fx, RS, NMS	WB	4 parks and water bodies / built-up areas

¹ See the updated Köppen-Geiger climate classification (Kottek et al., 2006),

² *Su* Summer, *Au* Autumn, *Wi* Winter, *Sp* Spring.

³ *DT* Day-time, *NT* Night-time.

⁴ *LN* Longitudinal, *CS* Cross-sectional.

⁵ *Me* Meso-scale, *Lo* Local-scale, *Mi* Micro-scale.

⁶ *AIRT* Air temperature, *SUT* Surface temperature, *SST* Sub-surface temperature, *HTC* Human thermal comfort, *PCI* Park cool island, *UCI* Urban cool island, *ET* Evapotranspiration, *SC* Spatial configuration.

⁷ *OS-Fx* Fixed on-site observation, *OS-Mb* Mobile on-site observation, *RS* Remote sensing, *EX* Experimental, *NMS* Statistical modelling and simulation.

⁸ *TC* Tree canopy, *GOS* Green open spaces, *WB* Water bodies, *GR* Green roofs, *VGS* Vertical greenery systems.

Appendix C – Metadata statement of LiDAR data

General Properties	
File Identifier	3BAA0499-FD63-4D62-9405-CF1350EA659E
Hierarchy Level	series
Hierarchy Level Name	series
Standard Name	ANZLIC Metadata Profile: An Australian/New Zealand Profile of AS/NZS ISO 19115:2005, Geographic information - Metadata
Standard Version	1.1
Date Stamp	2013-06-03
Resource Title	L0106 SydneyNorth
Alternate Resource Titles	
	SydneyNorth
	Sydney
	SydneyCBD
	Parramatta
	Liverpool
Key Dates and Languages	
Date of creation	2013-06-03
Date of publication	2013-06-03
Date of revision	2013-06-03
Metadata Language	eng
Metadata Character Set	utf8
Dataset Languages	eng
Dataset Character Set	utf8
Abstract	<p>The coverage of this dataset is over the Sydney North region. The C3 LAS data set contains point data in LAS 1.2 format sourced from a LiDAR (Light Detection and Ranging) from an ALS50 (Airborne Laser Scanner) sensor. The processed data has been manually edited to achieve LPI classification level 3 whereby the ground class contains minimal non-ground points such as vegetation, water, bridges, temporary features, jetties etc. Purpose: To provide fit-for-purpose elevation data for use in applications related to coastal vulnerability assessment, natural resource management (especially water and forests), transportation and urban planning. Additional lineage information: This data has an accuracy of 0.3m (95 confidence) horizontal with a minimum point density of one laser pulse per square metre. For more information on the datasets accuracy, refer to the lineage provided in the data history.</p>
Metadata Contact Information	
Name of Individual	Shawn Ryan
Organisation Name	Land and Property Information
Position Name	Senior Spatial Technician
Role	author
Voice	02 6332 8465
Facsimile	02 6332 8466
Email Address	shawn.ryan@lpi.nsw.gov.au
Address	346 Panorama Avenue
	Bathurst NSW 2795
	Australia
Resource Contacts	
Name of Individual	Danielle Johnson
Organisation Name	Land and Property Information
Position Name	Business Development Officer (Imagery Projects)
Role	distributor
Voice	02 6332 8421

Facsimile	02 6332 8296
Email Address	Danielle.Johnson@lpi.nsw.gov.au
Address	346 Panorama Avenue, Bathurst, NSW 2975. Australia.
Lineage Statement	<p>NEDF Metadata</p> <p>Acquisition Start Date: Wednesday, 10 April 2013</p> <p>Acquisition End Date: Wednesday, 24 April 2013</p> <p>Sensor: LiDAR</p> <p>Device Name: Leica ALS50-II (S/N: 101m)</p> <p>Flying Height (AGL): 1530</p> <p>INS/IMU Used: Honeywell URIS (S/N: 56017825)</p> <p>Number of Runs: 33</p> <p>Number of Cross Runs: 3</p> <p>Swath Width: 1174.62</p> <p>Flight Direction: East - West</p> <p>Swath (side) Overlap: 12.03</p> <p>Horizontal Datum: GDA94</p> <p>Vertical Datum: AHD71 - using local Geoid model</p> <p>Map Projection: MGA56</p> <p>Description of Aerotriangulation Process Used: -</p> <p>Description of Rectification Process Used: -</p> <p>Spatial Accuracy Horizontal: 0.8</p> <p>Spatial Accuracy Vertical: 0.3</p> <p>Average Point Density (per sqm): 1.57</p> <p>Nadir Point Density: 1.03</p> <p>Laser Return Types: 4 returns (1st 2nd 3rd 4th and intensity)</p> <p>Data Thinning: N/A</p> <p>Laser Footprint Size: 0.63</p> <p>Calibration certification (Manufacturer/Cert. Company): LPI</p> <p>Limitations of the Data: Accuracy specifications (95% CI) meet ICSM guidelines for digital elevation data.</p> <p>Surface Type: N/A</p> <p>Product Type: Mass Points</p> <p>Classification Type: C3</p> <p>Grid Resolution: UNK</p> <p>Distribution Format: LAS</p> <p>Processing/Derivation Lineage: As per LPI specification</p> <p>WMS: ?</p>
Jurisdictions	
	Australia
	New South Wales
Search Words	
	CLIMATE-AND-WEATHER-Climate-change
	HAZARDS-Flood
	LAND-Topography
	PHOTOGRAPHY-AND-IMAGERY-Aerial
	PHOTOGRAPHY-AND-IMAGERY-Remote-Sensing
	WATER
Themes and Categories	
Topic Category	elevation
Topic Category	geoscientific Information
Status and Maintenance	
Status	ongoing
Maintenance and Update Frequency	As needed
Date of Next Update	
Reference system	
Reference System	GDA94 / MGA zone 56
Metadata Security Restrictions	
Classification	unclassified
Authority	LPI
Dataset Security Restrictions	

Classification	unclassified
Authority	LPI
Dataset Access Constraints	
Identifier	license
Annotation	
Identifier	Intellectual Property Rights
Annotation	
Dataset Use Constraints	
Identifier	license
Annotation	
Identifier	Intellectual Property Rights
Annotation	
Extent - Geographic Bounding Box	
North Bounding Latitude	-33.728300
South Bounding Latitude	-33.986700
West Bounding Longitude	150.899900
East Bounding Longitude	151.337629
Additional Extent - Temporal	
From Date/Time	2013-04-10
To Date/Time	2013-04-24
Distribution Information	
Name of Individual	Danielle Johnson
Organisation Name	Land and Property Information
Position Name	Business Development Officer (Imagery Projects)
Role	distributor
Voice	02 6332 8421
Facsimile	02 6332 8296
Email Address	Danielle.Johnson@lpi.nsw.gov.au
Address	346 Panorama Avenue
	Bathurst NSW 2795
	Australia

Appendix D – Data processing workflow

D.1 NDVI generation (Summer):

1. NDVI generated using the *Band 1* from CIR.tif as the Near-infrared Band and the *Band 1* from the True Colour (Aerial imagery) as the Visible or red band.
2. NDVI computed using *Raster Calculator* in ArcGIS using the following expression:

$$\text{Float (NIR-Red)}/\text{Float (NIR+Red)}$$

3. Image (.TIFF) projected to GDA 1994 MGA Zone 56 and resampled from 0.8 to 0.5m spatial resolution using *nearest* as resampling technique.

D.2 NDVI generation (Winter)

1. NDVI generated from Hyperspectral data using the *Spectral Indices* tool in ENVI 5.3.1.
2. *Saved as* (ENVI, TIFF, DTEP). Output format: .TIFF.
3. Images projected to GDA 1994 MGA Zone 56.
4. Geo-references NDVI rasters as it follows:
 - Strip S01 no-georeferenced
 - Strip S02 georeferenced to strip 1 using auto-registration and adding additional points.
5. Both strips exported as TIFF with a 1m pixel size.
6. Mosaic created using ArcGIS:
 - Layer's order define prevalent values for pixels as these were not averaged
 - Go to Windows > *Image analysis* > Choose .TIFF.
 - Go to processing choose *Blend* and tick on the icon next to it to create a mosaic.
 - Exported the mosaic as .TIFF with 1m cell size.

D.3 Thermal imagery

1. Night-/Daytime images projected using *Project raster* tool in ArcGIS to GDA 94 MGA Zone 56
2. Night-time images mosaicked using *Image analysis* tool in ArcGIS.
3. Night-/Daytime images geo-referenced to NDVI.

D.4 Aerial imagery (summer)

1. Aerial Image on *17 January 2013* resampled to 0.5m spatial resolution and projected to GDA 94 MGA Zone 56 using *Project Raster* tool in ArcGIS.
2. Downloaded mosaics from Nearmap on *01 November 2012* with a 0.597m spatial resolution.
3. Downloaded images mosaicked in ArcGIS and resampled to 0.5m spatial resolution using *Image analysis* tool.
4. Projected to GDA 94 MGA Zone 56 using *Project Raster* tool in ArcGIS.

D.5 Aerial imagery (winter)

1. Downloaded mosaics from Nearmap on 02 August 2012 with a 0.597m spatial resolution.
2. Mosaicked in ArcGIS and resampled to 0.5m spatial resolution using *Image analysis tool*.
3. Projected to GDA 94 MGA Zone 56 using *Project Raster* tool in ArcGIS.

D.6 Estimation of DSM, DEM and nDSM

1. Selection of LiDAR grids overlapping thermal and spectral imagery.
2. Added all LAS using *Add as LAS layer to the map* in LP360.
3. Choose *Export LAS files*:
 - a. Export Type: Surface
 - b. Surface method: Triangulation (TIN)
 - c. NoData: -9999
 - d. Cellsize: 1m spatial resolution
 - e. Surface Attribute(s) to export: Elevation
 - f. Export format: Binary Raster
 - g. Filter points:
 - For DSM_bld: Ground, Building, Model Key Points
 - For DSM_bld_veg: Ground, Buildings, High vegetation, Model Key Points
 - For DEM_grnd: Ground, Model Key Points
4. Exported each binary grid rasters as: .TIF with 32-bit float in ArcCatalog.
5. Resulted TIF rasters were projected to GDA 94 MGA Zone 56.
6. nDSM created using *Raster calculator* tool in ArcGIS by subtraction the ground DEM (DEM_grnd) from the building DSM (DSM_Bld).
(Expression: *Float*(DSM_Bld – DEM_grnd)) Cell size: 0.5m.

D.7 Extraction of building footprints

1. Building footprints generated by LP360 using the following parameters:
 - a. Grow window: 2.0m
 - b. Trace window: 3.0m
 - c. Minimum area: 10sqm
 - d. Dissolve overlapping polygons: 1000sqm

NOTE (for the case of large datasets):

- a. In case of large datasets, buildings were extracted in smaller segments (5-8 LAS grids per segment) to reduce long processing times. Segments had overlapping areas for future joining.
 - b. Joined different segments using *Merge (data management)* tool in ArcGIS.
 - c. The segmentation process returned incomplete polygons for overlapping areas. Segmented polygons were merged one by one using the *Editor* toolbar.
 - d. Duplicated polygons with same area were deleted using *Delete identical* tool in ArcGIS.
2. Returned shapefiles were projected to GDA 94 MGA Zone 56 using *Define projection* tool in ArcGIS.

3. Generated shapefiles contained *ZM polygons* which cannot be used in future calculations, so these were disabled using *Feature class to shapefile* tool in ArcGIS:
 - a. M Value: *Disabled*
 - b. Z Value: *Disabled*
4. Repaired geometries, and features with null geometry deleted using *Repair geometry* tool in ArcGIS.
5. Returned shapefiles were rechecked again using *Check geometry* tool in ArcGIS.
6. Shapefiles containing parcels overlapping the study area were created (only for North & South swaths in the winter case study):
 - a. All NDVI values corresponding to *1* and *NoData* were reclassified to *NoData*.
 - b. Resulting rasters (.TIF) were converted into a single polygon using *Raster to Polygon* tool in ArcGIS.
 - c. A buffer zone of 250m was created from the polygons (for each study area or strip).
 - d. Resulting polygons were used to select overlapping parcels from Cadastral datasets. Parcels were combined if necessary.
 - e. Multi-part polygons were deleted by selecting all polygons and choosing *Explode Multipart feature* tool in ArcGIS.
 - f. Duplicated polygons were deleted using *Delete Identical (Data management)*.
7. Split polygons with properties boundaries (cadastral) using *Intersect (analysis)* tool in ArcGIS to derive single buildings from continuous buildings.
 - a. Input features: cadastral properties/parcels and extracted buildings.
 - b. All returned buildings were checked against the *extracted buildings* from LP360. Buildings located in open spaces or vacant land that were not overlapping any property polygon were omitted in the results. In those cases, missing buildings were selected and copied from the *extracted buildings* dataset.
8. Multi-part polygons were deleted by selecting all polygons and choosing *Explode Multipart feature* tool in ArcGIS.
9. Duplicated polygons were deleted using *Delete Identical (Data management)* tool.
10. All irrelevant fields in attribute tables were deleted.
11. Deleted polygons small 15m² (a copy was created before this step for backup purposes).
12. Buildings were squared-up using *Feature-Analyst* software with the following settings:
 - a. Smoothing tolerance: 1m
 - b. Squaring tolerance: 5.5-6.0m (values varied depending of the dataset)
 - c. Consider all likely feature orientation when squaring: Enabled
 - d. Consider adjoining features when computing orientation: Enabled
 - e. NDVI was used as based image for rastering
13. In the case of large areas polygon shapefiles were split to reduce processing errors due to lack of memory. Squared polygons were then re-joined using *Merge* tool in ArcGIS.
14. The squaring process returned round polygons as hexagonal polygons, so these were replaced with the round polygons originally generated with LP360 (Step 1).
15. Multipart squared polygons were exploded using *Explode Multipart feature* tool in ArcGIS.
16. Duplicated polygons were deleted using *Delete Identical (Data management)* tool.
17. Deleted polygons small 12m² (a copy was created before this step for backup purposes).
18. Missing and/or wrongly generated buildings due to errors in the LiDAR datasets (low point cloud density) were added manually.

D.8 Estimation of building heights

1. Calculated average building height with *Zonal statistics as table* tool in ArcGIS using the nDSM (from Section D.6) as input value raster and the corrected *building footprints* (from Section D.7) polygons as feature zone data.
 2. Merged resulting table with the attribute table of building footprints using the unique ID of features.
 3. Deleted polygons with *Null* values (small irregular polygons overlapping bigger building footprints).
 4. Exported data as a new polygon shapefile.
- Note: some results returned very low values (<1m) when buildings were not detected due to errors in the LiDAR point tracing.

D.9 Extraction of high and medium vegetation

1. High vegetation footprints generated by LP360 using the following parameters:
 - a. Grow window: 2.0m (1.75m for areas with large patches)
 - b. Trace window; 3.0m (2.75m for areas with large patches)
 - c. Minimum area: 5.0m²
 - d. Dissolve overlapping polygons: 850m²

NOTE: In areas with very extensive and dense canopies, high vegetation was wrongly extracted. Errors include vegetated areas considered as empty spaces and buildings and open spaces extracted as vegetation. To amend this problem, erroneous areas were deleted and replaced with re-extractions covering only the affected areas. The process of combining and deleting overlapping polygons were done using the *Editor mode* in ArcGIS.

2. Returned shapefiles were projected to GDA 94 MGA Zone 56 using *Define projection* in ArcGIS.
3. Generated shapefiles contain *ZM polygons* which cannot be used in future calculations, so these were disabled using *Feature class to shapefile* tool in ArcGIS:
 - a. M Value: *Disabled*
 - b. Z Value: *Disabled*
4. Multipart squared polygons were exploded using *Explode Multipart feature* tool in ArcGIS.
5. Repaired geometries and features with *null* geometry deleted using *Repair geometry* tool in ArcGIS.
6. Duplicated polygons were deleted using *Delete Identical (Data management)* tool.
7. Deleted all high vegetation polygons completely overlapping building footprints.
8. Repeat the whole process for medium vegetation.

D.10 Surface cover classifications

1. **Initial classifications:**
 - a. Raster masks created for each study area (Parramatta, Sydney north and Sydney south) and used as a snap raster (processing extent) in the environment settings.
 - b. Classified NDVI image into different ranges representing different surface covers as per parameters below:

- *Parramatta dataset (summer)*:
 - * Water : [-1.00] – [-0.50]
 - * Total impervious : [-0.50] – [-0.15]
 - * Total pervious : [-0.15] – [1.00]
 - * Pervious Non-irrigated : [-0.15] – [0.08]
 - * Pervious Irrigated : [0.08] – [1.00]
- *Sydney North and South datasets (winter)*:
 - * Water : [-1.00] – [-0.20]
 - * Total impervious : [-0.20] – [0.25]
 - * Total pervious : [0.25] – [1.00]
 - * Pervious Non-irrigated : [0.25] – [0.60]
 - * Pervious Irrigated : [0.60] – [1.00]

- c. With *Reclassify* tool created separate rasters for each surface cover assigning a value of 1 for all cells corresponding to the respective surface cover and a value of 0 for the remaining cells. Kept *NoData* as *NoData* and assigned a cell size of 0.5m to all rasters.

2. Building surfaces:

- a. *Building footprint* features (from Section D.7) converted into a raster image with *Polygon to raster* tool with cell size of 0.5m and using the *average building heights* as the *value field*.
- b. Reclassified all pixel values corresponding to building's heights to 1, and *NoData* values to 0 to obtain a *building surface cover* raster that will be used in further raster calculations.

3. Water surfaces:

- a. Water surfaces extracted from NDVI presented errors as some pixels were misclassified as impervious surfaces.
- b. Surface water polygons obtained from cadastral data converted into a raster image with *Polygon to raster* tool with a cell size of 0.5m.
- c. With *Raster calculator* (or *Plus*) tool, added the converted water bodies based on cadastral data to the *water surface cover* raster based on NDVI classifications.
- d. Reclassified raster value 2 to 1.
- e. Some pixels corresponding to building's roofs were misclassified as water surfaces. To correct this error, the *building surface cover* raster was subtracted from the previously reclassified *water surface* raster with *Raster calculator* tool.
- f. Reclassified raster value -1 to 0.

4. Impervious surfaces:

- a. Impervious surfaces extracted from NDVI presented errors. For instance, some buildings were misclassified as pervious surfaces, and water surfaces as impervious ground. With *Raster calculator* (or *Plus*) tool, added the *building surface cover* raster to the *impervious surface cover* raster based on NDVI classifications to obtain the *total impervious surface cover*.
- b. Reclassified raster value of 2 to 1.
- c. Subtracted the *water surface cover* raster from the *total impervious surface cover* raster with *Raster calculator* (or *Minus*) tool to delete misclassified pixels.

- d. Subtracted the *building surface cover* raster from the *total impervious surface cover* raster with *Raster calculator* (or *Minus*) tool to detect only *impervious ground* surfaces.

5. Pervious surfaces and water:

- a. Converted high vegetation polygons based on LiDAR data (from Section D.9) into new raster images of 0.5m pixel resolution with *Polygon to raster* tool. Note: Use *FID* as a *value field*.
- b. Reclassified *all raster values* to *1*, and *NoData* to *0*, to be able to use it for further raster calculations.
- c. Summer case dataset: with *Times* tool created a new raster for areas overlapping high vegetation based on LiDAR data and *all pervious surfaces* based on NDVI classifications to reduce the LiDAR-based classification errors.
- d. Repeated steps a - d for medium vegetation.
- e. Winter case datasets: with *Times* tool created a new raster for areas overlapping high vegetation based on LiDAR data and *only irrigated pervious surfaces* based on NDVI classifications. This reduces the LiDAR-based classification errors and discards areas corresponding to deciduous trees as LiDAR data were not collected in winter.
- f. Discarded areas of medium vegetation that overlap building surfaces by subtracting the *building surface cover* raster from the vegetation rasters.
- g. Reclassified raster value of *-1* to *0*.
- h. Land cover classifications based on the NDVI image presented some errors, for instance, pixels corresponding to buildings and water were misclassified as pervious surfaces. To correct this issue and obtain the real low (irrigated and non-irrigated) vegetation cover, raster images corresponding to *medium and high vegetation*, *water* and *total impervious surfaces* were subtracted from both *irrigated* and *non-irrigated surface cover* rasters based on NDVI classifications. Note: reclassified *all negative raster values* to *0*.
- i. Discarded areas of water that overlap high vegetation surfaces to obtain the real *water surfaces*.
- j. Reclassified *all negative raster values* to *0*.
- k. Added *irrigated, non-irrigated, medium and high vegetation* surface cover rasters with *Raster calculator* tool to obtain the *total pervious* surface cover image.
- l. Added *irrigated and non-irrigated vegetation* surface cover rasters with *Raster calculator* tool to obtain the *total low vegetation* surface cover image.
- m. Reclassified *all positive* raster values to *1*.

D.11 FRAGSTATS calculations for high vegetation

1. Reclassified high vegetation cove raster value of *0* to *1*, *1* to *2*, and kept *NoData* as *NoData*.
2. Exported resulting image as 16-Bit Signed integer .TIF raster and reassigned *NoData* value as *-9999* for further FRAGSTATS calculations.
3. Created a grid of 50 x 50m with *Grid index features* tool using the high vegetation surface cover raster to the define the spatial extent.
4. Discarded all grids that were not completely within the raster image extent.

5. Given that FRAGSTATS was not able to process large rasters, grids were grouped in sections and merged using the *Editor mode* to generate one single polygon feature that can be used to clip the raster image in smaller sections.
6. Calculated CIRCLE_AM and nLSI using FRAGSTATS 4.3 software using the following parameters:
 - a. Input datasets: GeoTIFF grids (.TIF) corresponding to each high vegetation raster section with a *background value* of 1000.
 - b. Class descriptor file: Created a .fcd file with Notepad application with the following script:


```
ID, Name, Enabled, IsBackground
1, Nontree, false, true
2, Trees, true, false
```
 - c. Analysis parameters: Checked the following options for the sampling strategy
 - General options: Use 8 cell neighbourhood rule.
 - Uniform Tiles: Class metrics using a side length of 50.00m.
 - d. Class metrics: Selected CIRCLE Area-Weighted mean (AM) (from *Shape* tab) and Normalised LSI (nLSI) (from *Aggregation* tab).
7. Process returned a .class file and a raster image (.TIF) with tiles' IDs for each high vegetation raster section.
8. Converted raster image containing tiles' IDs into polygons with *Raster to polygon* tool using the *pixel value* as the *field*.
9. Deleted tiles (polygons) that do not overlap the study area. Resulting polygon features can be used to define the GIT grids in following steps.
10. .class files were converted into .csv file (comma delimited) by changing the file extension manually.
11. Eliminated letters and additional 0s located on the left of tiles' IDs by opening the .csv files in *Excel*:
 - a. Created a new column and typed this formula:
 =RIGHT(X, LEN(X)-Y) where
 X corresponds to the column and row value to be changed (e.g. A2)
 Y corresponds to the number of characters to be eliminated
 - b. Created a new column, copied all values from previous column and *pasted as numbers* to eliminate the formula (*paste as special > convert to number*).
 - c. In some cases, nLSI values were reported as N/A in the output files whenever the maximum class edge equalled the minimum class edge. This occurred when trees (focal class) occupied the totality of the grid. To correct this issue, N/A values were converted to 0.
 - d. Saved as .csv file.
12. Joined .csv files with FRAGSTATS indices to the attribute tables of previously generated grids (50 x 50m). Note: Keep all records when joining tables.
13. Exported joined data as new polygon shapefiles. These grids will be used for *Zonal statistics* tool calculations later.

D.12 Estimation of variables per spatial unit

1. Generation of spatial units (grids)

- a. Created unique IDs with *Create Unique IDs* (<http://ianbroad.com/arcgis-toolbox-create-unique-id-arcpy/>) tool for grids generated in previous step.
Note: Created a back-up copy first. *Runned* this tool from ArcCatalog, and feature class/table was not opened anywhere. Settings:
 - Type : Interval
 - Group by Field : NO
 - Sort by Field : NO
 - Range/interval : 1
 - Prefix or Suffix : Prefix
 - Prefix : GIT-ID_P/N/S_
P (Parramatta), N (North), S (South)
- b. Created a new *Text field* in the attribute table and copied grid ID generated by the tool with *Raster calculator*.
- c. Repeated steps 3 and 4 for grids of 50 x 50m generated as part of FRAGSTATS calculations (Section L).

2. Estimation of surface cover fractions

- a. With *Zonal Statistics as table* tool, calculated the total number of pixels (SUM) for each surface cover raster (impervious ground, impervious building, total impervious, low, medium, high vegetation and water) with grid features (both 50 x 50m and 100 x 100m) defining zones.
- b. Joined generated zonal statistics tables to attribute tables of grid features.
- c. Estimated the percentage of the grid cell occupied by each surface cover with *Field calculator* by dividing the SUM value by the total COUNT of cells per grid.
- d. Multiplied results by 100 to be expressed in percentage.

3. Estimation of average NDVI

- a. With *Zonal Statistics as table* tool, calculated average NDVI per grid by computing the mean of all pixel values within each grid from the NDVI raster image.

4. Estimation of average land surface temperature

- a. Calculated mean, maximum and minimum surface temperature values for each previously defined grid cells (GIT) with *Zonal Statistics as Table* tool using day- and night-time thermal imagery.
- b. Joined resulting tables to the attribute table of GIT using the ID of grid cells as common attribute.

D.13 Automated classification of grid into green infrastructure typologies (GIT)

1. Classified grid cells with *Field calculator* based on parameters specified in [Table 4.14](#) (Section 4.11) using the following algorithm (VB script):

Pre-logic Script code:

```
If ([Fr_Tot_Imp] >75 and [Fr_High_Ve] <=25 and [Fr_Med_Veg] <=25 and [Fr_LowIRR]
<=25 and [Fr_LowNIR] <=25 and [Fr_Tot_wat] <=25) then
```

```
[GIT_type]= "IM 1"
```

```
elseif ([Fr_Tot_Imp] >50 and [Fr_Tot_Imp] <=75 and [Fr_High_ve] <=5 and
[Fr_Med_Veg] <=25 and [Fr_LowIRR] <50 and [Fr_LowNIR] <50 and [Fr_Tot_wat] <=25)
then
```

```
[GIT_type] = "IM 2"
```

```
elseif ([Fr_Tot_Imp] >25 and [Fr_Tot_Imp] <=75 and [Fr_High_Ve] <=25 and
[Fr_Med_Veg] >25 and [Fr_Med_Veg] <=50 and [Fr_LowIRR] <40 and [Fr_LowNIR] <40
and [Fr_Tot_wat] <=25) then
```

```
[GIT_type] = "IM 3"
```

```
elseif ([Fr_Tot_Imp] >50 and [Fr_Tot_Imp] <=75 and [Fr_High_ve] >5 and
[Fr_High_Ve] <=40 and [Fr_Med_Veg] <=25 and [Fr_LowIRR] <40 and [Fr_LowNIR] <40 and
[Fr_Tot_wat] <=25 and [CIRCLE_AM] >=0.61 and [NLSI] <0.25) then
```

```
[GIT_type]= "IM 4"
```

```
elseif ([Fr_Tot_Imp] >50 and [Fr_Tot_Imp] <=75 and [Fr_High_Ve] >5 and [Fr_High_Ve]
<=25 and [Fr_Med_Veg] <=25 and [Fr_LowIRR] <40 and [Fr_LowNIR] <40 and
[Fr_Tot_wat] <=25 and [CIRCLE_AM] <0.61 and [NLSI] >0.065) then
```

```
[GIT_type]= "IM 5"
```

```
elseif ([Fr_Tot_Imp] >50 and [Fr_Tot_Imp] <=75 and [Fr_High_Ve] >5 and
[Fr_High_Ve] <=40 and [Fr_Med_Veg] <=25 and [Fr_LowIRR] <40 and [Fr_LowNIR] <40
and [Fr_Tot_wat] <=25 and [CIRCLE_AM] <0.61 and [NLSI] <=0.065) then
```

```
[GIT_type]= "IM 6"
```

```
elseif ([Fr_Tot_Imp] >25 and [Fr_Tot_Imp] <=50 and [Fr_High_Ve] <=5 and
[Fr_Med_Veg] <=25 and [Fr_LowNIR] >50 and [Fr_LowIRR] <=25 and [Fr_Tot_wat] <=25)
then
```

```
[GIT_type]= "MX 1"
```

```
elseif ([Fr_Tot_Imp] >25 and [Fr_Tot_Imp] <=50 and [Fr_High_Ve] <=5 and
[Fr_Med_Veg] <=25 and [Fr_LowNIR] <=25 and [Fr_LowIRR] >50 and [Fr_Tot_wat] <=25)
then
```

```
[GIT_type]= "MX 2"
```

```
elseif ([Fr_Tot_Imp] >25 and [Fr_Tot_Imp] <=50 and [Fr_High_Ve] <=5 and
[Fr_Med_Veg] <=25 and [Fr_LowNIR] <=50 and [Fr_LowIRR] <=50 and [Fr_Tot_wat] <=25)
then
```

```
[GIT_type]= "MX 3"
```



```
elseif ([Fr_Tot_Imp] <=25 and [Fr_High_Ve] <=5 and [Fr_Med_Veg] <=25 and
[Fr_LowNIR] <=75 and [Fr_LowIRR] <=75 and [Fr_Tot_wat] <=25) then
```

```
[GIT_type]= "MX 4"
```

```
elseif ([Fr_Tot_Imp] >25 and [Fr_Tot_Imp] <=50 and [Fr_High_Ve] >5 and
[Fr_High_Ve] <=50 and [Fr_Med_Veg] <=25 and [Fr_LowNIR] <=50 and [Fr_LowIRR] <=50
and [Fr_Tot_wat] <=25 and [CIRCLE_AM] >=0.61 and [NLSI] <0.25) then
```

```
[GIT_type]= "MX 5"
```

```
elseif ([Fr_Tot_Imp] <=25 and [Fr_High_Ve] >5 and [Fr_High_Ve] <=75 and
[Fr_Med_Veg] <=25 and [Fr_LowNIR] <=50 and [Fr_LowIRR] <=50 and [Fr_Tot_wat] <=25
and [CIRCLE_AM] >=0.61 and [NLSI] <0.25) then
```

```
[GIT_type]= "MX 6"
```

```
elseif ([Fr_Tot_Imp] >25 and [Fr_Tot_Imp] <=50 and [Fr_High_Ve] >5 and
[Fr_High_Ve] <=50 and [Fr_Med_Veg] <=25 and [Fr_LowNIR] <=50 and [Fr_LowIRR] <=50
and [Fr_Tot_wat] <=25 and [CIRCLE_AM] <0.61 and [NLSI] >0.065) then
```

```
[GIT_type]= "MX 7"
```

```
elseif ([Fr_Tot_Imp] <=25 and [Fr_High_Ve] >5 and [Fr_High_Ve] <=75 and
[Fr_Med_Veg] <=25 and [Fr_LowNIR] <=50 and [Fr_LowIRR] <=50 and [Fr_Tot_wat] <=25
and [CIRCLE_AM] <0.61 and [NLSI] >0.065) then
```

```
[GIT_type]= "MX 8"
```

```
elseif ([Fr_Tot_Imp] >25 and [Fr_Tot_Imp] <=50 and [Fr_High_Ve] >5 and
[Fr_High_Ve] <=75 and [Fr_Med_Veg] <=25 and [Fr_LowNIR] <=50 and [Fr_LowIRR] <=50
and [Fr_Tot_wat] <=25 and [CIRCLE_AM] <0.61 and [NLSI] <=0.065) then
```

```
[GIT_type]= "MX 9"
```

```
elseif ([Fr_Tot_Imp] <=25 and [Fr_High_Ve] >5 and [Fr_High_Ve] <=75 and
[Fr_Med_Veg] <=25 and [Fr_LowNIR] <=50 and [Fr_LowIRR] <=50 and [Fr_Tot_wat] <=25
and [CIRCLE_AM] <0.61 and [NLSI] <=0.065) then
```

```
[GIT_type]= "MX 10"
```

```
elseif ([Fr_Tot_Imp] <=25 and [Fr_High_Ve] <=5 and [Fr_Med_Veg] <=25 and
[Fr_LowNIR] >75 and [Fr_LowIRR] <=25 and [Fr_Tot_wat] <=25) then
```

```
[GIT_type]= "PV 1"
```

```
elseif ([Fr_Tot_Imp] <=25 and [Fr_High_Ve] <=5 and [Fr_Med_Veg] <=25 and
[Fr_LowNIR] <=25 and [Fr_LowIRR] >75 and [Fr_Tot_wat] <=25) then
```

```
[GIT_type]= "PV 2"
```

```
elseif ([Fr_Tot_Imp] <=25 and [Fr_High_Ve] <=50 and [Fr_Med_Veg] >25 and
[Fr_Med_Veg] <=50 and [Fr_LowNIR] <60 and [Fr_LowIRR] <60 and [Fr_Tot_wat] <=25)
then
```

```
[GIT_type]= "PV 3"
```



```
elseif ([Fr_Tot_Imp] <=25 and [Fr_High_Ve] <=25 and [Fr_Med_Veg] >50 and
[Fr_LowNIR] <50 and [Fr_LowIRR] <50 and [Fr_Tot_wat] <=25) then
```

```
[GIT_type]= "PV 4"
```

```
elseif ([Fr_Tot_Imp] <=25 and [Fr_High_Ve] >5 and [Fr_High_Ve] <=50 and
[Fr_Med_Veg] <=25 and [Fr_LowNIR] >50 and [Fr_LowIRR] <40 and [Fr_Tot_wat] <=25
and [CIRCLE_AM] >=0.61 and [NLSI] <0.25) then
```

```
[GIT_type]= "PV 5"
```

```
elseif ([Fr_Tot_Imp] <=25 and [Fr_High_Ve] >5 and [Fr_High_Ve] <=50 and
[Fr_Med_Veg] <=25 and [Fr_LowNIR] <40 and [Fr_LowIRR] >50 and [Fr_Tot_wat] <=25
and [CIRCLE_AM] >=0.61 and [NLSI] <0.25) then
```

```
[GIT_type]= "PV 6"
```

```
elseif ([Fr_Tot_Imp] <=25 and [Fr_High_Ve] >5 and [Fr_High_Ve] <=50 and
[Fr_Med_Veg] <=25 and [Fr_LowNIR] >50 and [Fr_LowIRR] <40 and [Fr_Tot_wat] <=25
and [CIRCLE_AM] <0.61 and [NLSI] >0.065) then
```

```
[GIT_type]= "PV 7"
```

```
elseif ([Fr_Tot_Imp] <=25 and [Fr_High_Ve] >5 and [Fr_High_Ve] <=50 and
[Fr_Med_Veg] <=25 and [Fr_LowNIR] <40 and [Fr_LowIRR] >50 and [Fr_Tot_wat] <=25and
[CIRCLE_AM] <0.61 and [NLSI] >0.065) then
```

```
[GIT_type]= "PV 8"
```

```
elseif ([Fr_Tot_Imp] <=25 and [Fr_High_Ve] >5 and [Fr_High_Ve] <=50 and
[Fr_Med_Veg] <=25 and [Fr_LowNIR] >50 and [Fr_LowIRR] <40 and [Fr_Tot_wat] <=25
and [CIRCLE_AM] <0.61 and [NLSI] <=0.065) then
```

```
[GIT_type]= "PV 9"
```

```
elseif ([Fr_Tot_Imp] <=25 and [Fr_High_Ve] >5 and [Fr_High_Ve] <=50 and
[Fr_Med_Veg] <=25 and [Fr_LowNIR] <40 and [Fr_LowIRR] >50 and [Fr_Tot_wat] <=25
and [CIRCLE_AM] <0.61 and [NLSI] <=0.065) then
```

```
[GIT_type]= "PV 10"
```

```
elseif ([Fr_Tot_Imp] <=25 and [Fr_High_Ve] >75 and [Fr_Med_Veg] >25 and
[Fr_Med_Veg] <=75 and [Fr_LowNIR] <=25 and [Fr_LowIRR] <=25 and [Fr_Tot_wat] <=25)
then
```

```
[GIT_type]= "PV 11"
```

```
elseif ([Fr_Tot_Imp] <=25 and [Fr_High_Ve] >75 and [Fr_Med_Veg] <=25 and
[Fr_LowNIR] <=25 and [Fr_LowIRR] <=25 and [Fr_Tot_wat] <=25) then
```

```
[GIT_type]= "PV 12"
```

```
elseif ([Fr_Tot_Imp] <=25 and [Fr_High_Ve] <=25 and [Fr_Med_Veg] <=25 and
[Fr_LowNIR] <=25 and [Fr_LowIRR] <=25 and [Fr_Tot_wat] >75) then
```

```
[GIT_type]= "AQ 1"
```



```
elseif ([Fr_Tot_Imp] <=25 and [Fr_High_Ve] <=5 and [Fr_Med_Veg] <=25 and
[Fr_LowNIR] <40 and [Fr_LowIRR] <40 and [Fr_Tot_wat] >50 and [Fr_Tot_wat] <=75)
then
```

```
    [GIT_type]= "AQ 2"
```

```
elseif ([Fr_Tot_Imp] <=25 and [Fr_High_Ve] <=5 and [Fr_Med_Veg] <=25 and
[Fr_LowNIR] <60 and [Fr_LowIRR] <60 and [Fr_Tot_wat] >25 and [Fr_Tot_wat] <=50)
then
```

```
    [GIT_type]= "AQ 3"
```

```
elseif ([Fr_Tot_Imp] >25 and [Fr_Tot_Imp] <=50 and [Fr_High_Ve] <=25 and
[Fr_Med_Veg] <=25 and [Fr_LowNIR] <=50 and [Fr_LowIRR] <=50 and [Fr_Tot_wat] >25
and [Fr_Tot_wat] <=75) then
```

```
    [GIT_type]= "AQ 4"
```

```
elseif ([Fr_Tot_Imp] <=25 and [Fr_High_Ve] >5 and [Fr_High_Ve] <=75 and
[Fr_Med_Veg] <=25 and [Fr_LowNIR] <40 and [Fr_LowIRR] <40 and [Fr_Tot_wat] >25
and [Fr_Tot_wat] <=75 and [CIRCLE_AM] >=0.61) then
```

```
    [GIT_type]= "AQ 5"
```

```
elseif ([Fr_Tot_Imp] <=25 and [Fr_High_Ve] >5 and [Fr_High_Ve] <=40 and
[Fr_Med_Veg] <=25 and [Fr_LowNIR] <40 and [Fr_LowIRR] <40 and [Fr_Tot_wat] >25
and [Fr_Tot_wat] <=75 and [CIRCLE_AM] <0.61) then
```

```
    [GIT_type]= "AQ 6"
```

```
elseif ([Fr_Tot_Imp] <=25 and [Fr_High_Ve] >40 and [Fr_Med_Veg] <=25 and
[Fr_LowNIR] <40 and [Fr_LowIRR] <40 and [Fr_Tot_wat] >25 and [Fr_Tot_wat] <=75
and [CIRCLE_AM] <0.61) then
```

```
    [GIT_type]= "AQ 7"
```

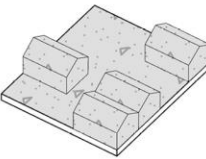




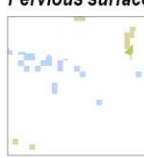
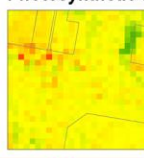
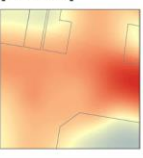

```
else
```

```
    [GIT_type]= "Unknown"
```

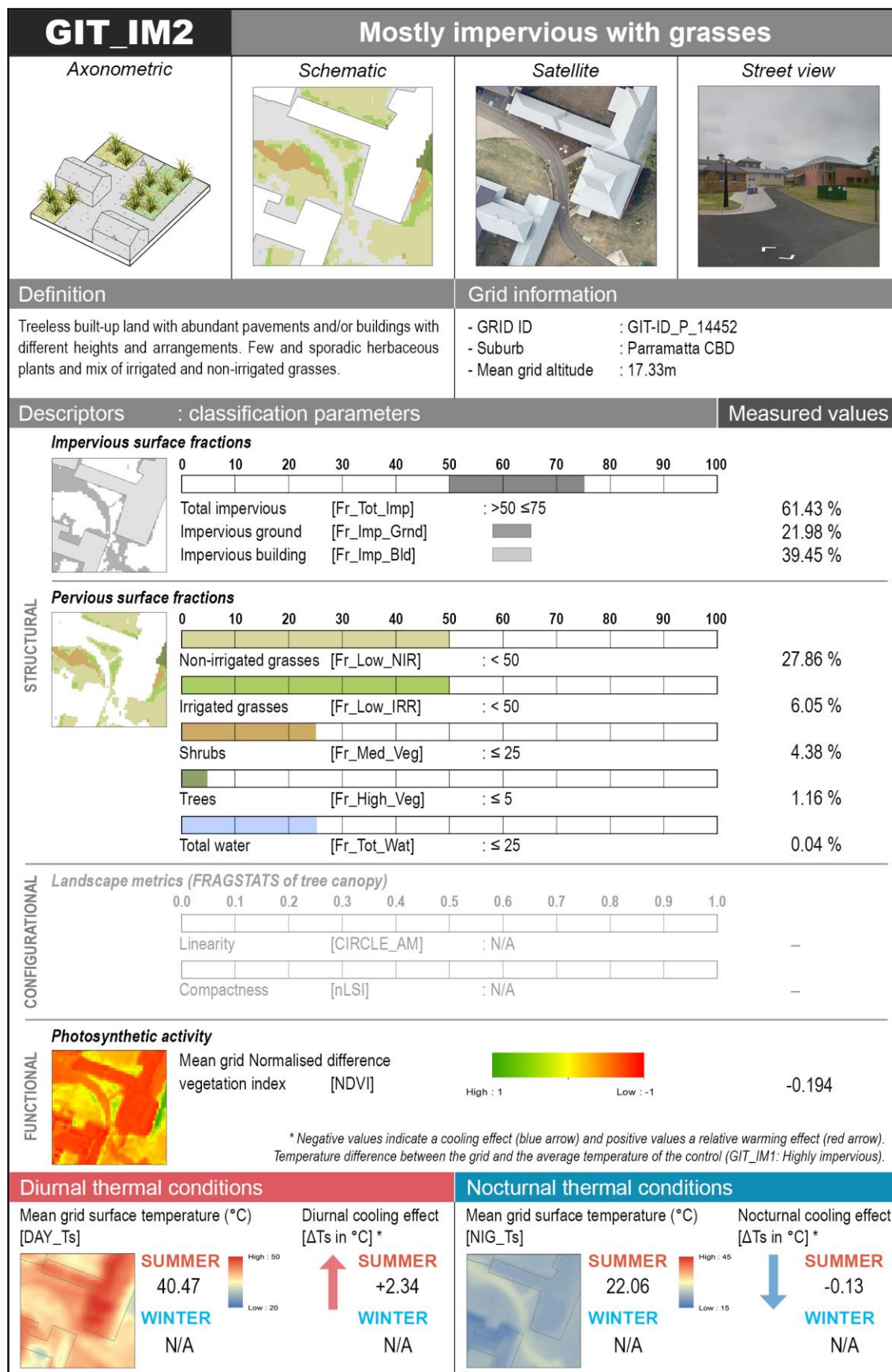
```
end if
```

```
GIT_type = [GIT_type]
```


Appendix E – Datasheets for Green Infrastructure Typologies (GITs)

GIT_IM1		Highly impervious	
<i>Axonometric</i>	<i>Schematic</i>	<i>Satellite</i>	<i>Street view</i>
			
			
Definition Extensive built-up land with little or no grasses and shrubs; few or no trees. Abundance of buildings of different heights and arrangements (open and close), paved areas, roads and bare rocks.		Grid information - GRID ID : GIT-ID_N_5422 - Suburb : Northbridge - Mean grid altitude : 88.56m	
Descriptors : classification parameters			Measured values
Impervious surface fractions			
			
0 10 20 30 40 50 60 70 80 90 100			
Total impervious [Fr_Tot_Imp] : >25 ≤50			
Impervious ground [Fr_Imp_Grnd]			
Impervious building [Fr_Imp_Bld]			
94.94 % 66.35 % 28.59 %			
Pervious surface fractions			
			
0 10 20 30 40 50 60 70 80 90 100			
Non-irrigated grasses [Fr_Low_NIR] : ≤ 25			
Irrigated grasses [Fr_Low_IRR] : ≤ 25			
Shrubs [Fr_Med_Veg] : ≤ 25			
Trees [Fr_High_Veg] : ≤ 25			
Total water [Fr_Tot_Wat] : ≤ 25			
1.43 % 0.23 % 0.00 % 0.51 % 2.89 %			
Landscape metrics (FRAGSTATS of tree canopy)			
0.0 0.1 0.2 0.3 0.4 0.5 0.6 0.7 0.8 0.9 1.0			
Linearity [CIRCLE_AM] : N/A			
Compactness [nLSI] : N/A			
– –			
Photosynthetic activity			
			
Mean grid Normalised difference vegetation index [NDVI]			
High : 1 Low : -1			
0.002			
* Negative values indicate a cooling effect (blue arrow) and positive values a relative warming effect (red arrow). Temperature difference between the grid and the average temperature of the control (GIT_IM1: Highly impervious).			
Diurnal thermal conditions		Nocturnal thermal conditions	
Mean grid surface temperature (°C) [DAY_Ts]		Mean grid surface temperature (°C) [NIG_Ts]	
			
SUMMER N/A WINTER 14.75		SUMMER N/A WINTER 3.20	
Diurnal cooling effect [ΔTs in °C] *		Nocturnal cooling effect [ΔTs in °C] *	
Control SUMMER N/A WINTER N/A		Control SUMMER N/A WINTER N/A	

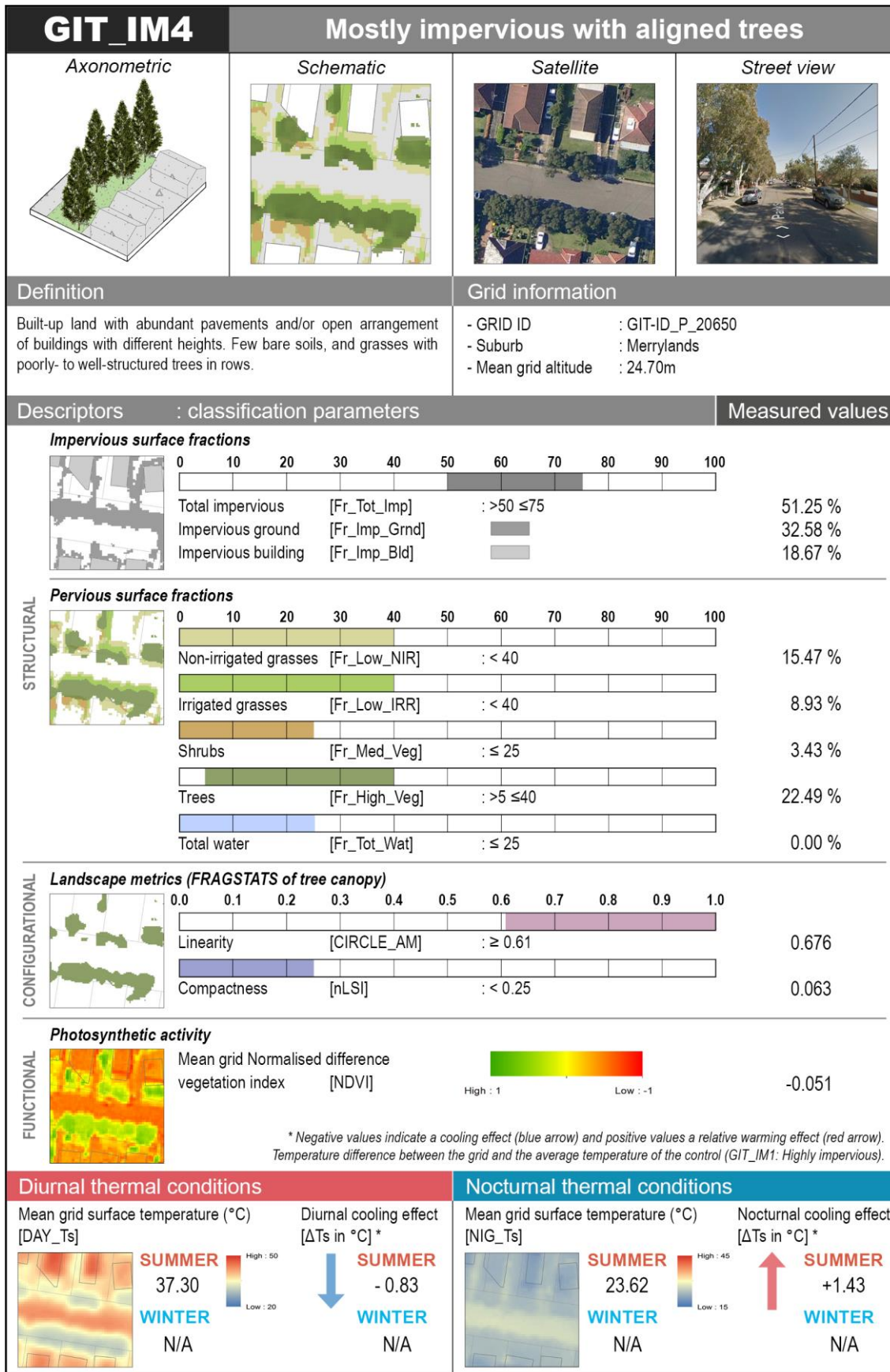
E1. Datasheet containing all variables and classification parameters calculated for the typology IM1.



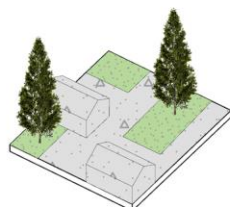
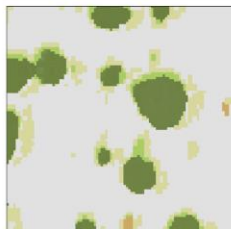
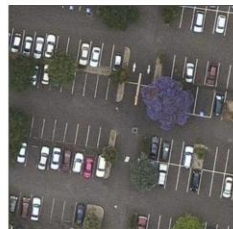

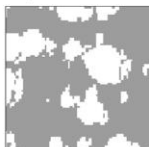









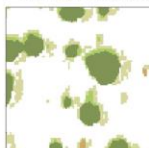







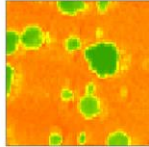

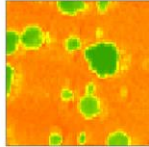

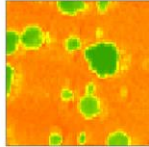

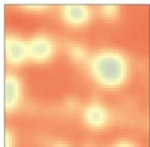



E2. Datasheet containing all variables and classification parameters calculated for the typology IM2.

GIT_IM3		Mostly impervious with shrubs			
Axonometric		Schematic	Satellite	Street view	
Definition		Grid information			
Built-up land with abundant pavements and/or buildings with different heights and arrangements. Few and sporadic bare soil, grasses, and small trees. Extensive shrubbery and hedges.		<div>- GRID ID : GIT-ID_S_9131</div> <div>- Suburb : Greenacre</div> <div>- Mean grid altitude : 26.48m</div>			
Descriptors : classification parameters		Measured values			
STRUCTURAL	Impervious surface fractions				
		<div><div></div><div></div><div></div><div></div><div></div><div></div><div></div><div></div><div></div><div></div><div></div><div></div></div>	<div>Total impervious [Fr_Tot_Imp] : >25 ≤50</div> <div>Impervious ground [Fr_Imp_Grnd]</div> <div>Impervious building [Fr_Imp_Bld]</div>	<div>38.36 %</div> <div>38.36 %</div> <div>0.00 %</div>	
	Pervious surface fractions				
		<div><div></div><div></div><div></div><div></div><div></div><div></div><div></div><div></div><div></div><div></div><div></div><div></div></div>	<div>Non-irrigated grasses [Fr_Low_NIR] : < 40</div> <div>Irrigated grasses [Fr_Low_IRR] : < 40</div> <div>Shrubs [Fr_Med_Veg] : >25 ≤50</div> <div>Trees [Fr_High_Veg] : ≤ 25</div> <div>Total water [Fr_Tot_Wat] : ≤ 25</div>	<div>18.50 %</div> <div>3.74 %</div> <div>26.48 %</div> <div>15.51 %</div> <div>0.92 %</div>	
	CONFIGURATIONAL	Landscape metrics (FRAGSTATS of tree canopy)			
		<div><div></div><div></div><div></div><div></div><div></div><div></div><div></div><div></div><div></div><div></div><div></div><div></div></div>	<div>Linearity [CIRCLE_AM] : N/A</div> <div>Compactness [nLSI] : N/A</div>	<div>—</div> <div>—</div>	
	FUNCTIONAL	Photosynthetic activity			
		<div>Mean grid Normalised difference vegetation index [NDVI]</div> <div><div></div><div></div><div></div><div></div><div></div><div></div><div></div><div></div><div></div><div></div><div></div></div> <div>High : 1Low : -1</div>			<div>0.364</div>
	<div>* Negative values indicate a cooling effect (blue arrow) and positive values a relative warming effect (red arrow). Temperature difference between the grid and the average temperature of the control (GIT_IM1: Highly impervious).</div>				
	Diurnal thermal conditions		Nocturnal thermal conditions		
<div>Mean grid surface temperature (°C) [DAY_Ts]</div> <div></div> <div><div>SUMMER N/A</div><div>WINTER 9.60</div></div>		<div>Mean grid surface temperature (°C) [NIG_Ts]</div> <div></div> <div><div>SUMMER N/A</div><div>WINTER N/A</div></div>			
<div>Diurnal cooling effect [ΔTs in °C] *</div> <div><div>SUMMER N/A</div><div>WINTER -4.65</div></div>		<div>Nocturnal cooling effect [ΔTs in °C] *</div> <div><div>SUMMER N/A</div><div>WINTER N/A</div></div>			

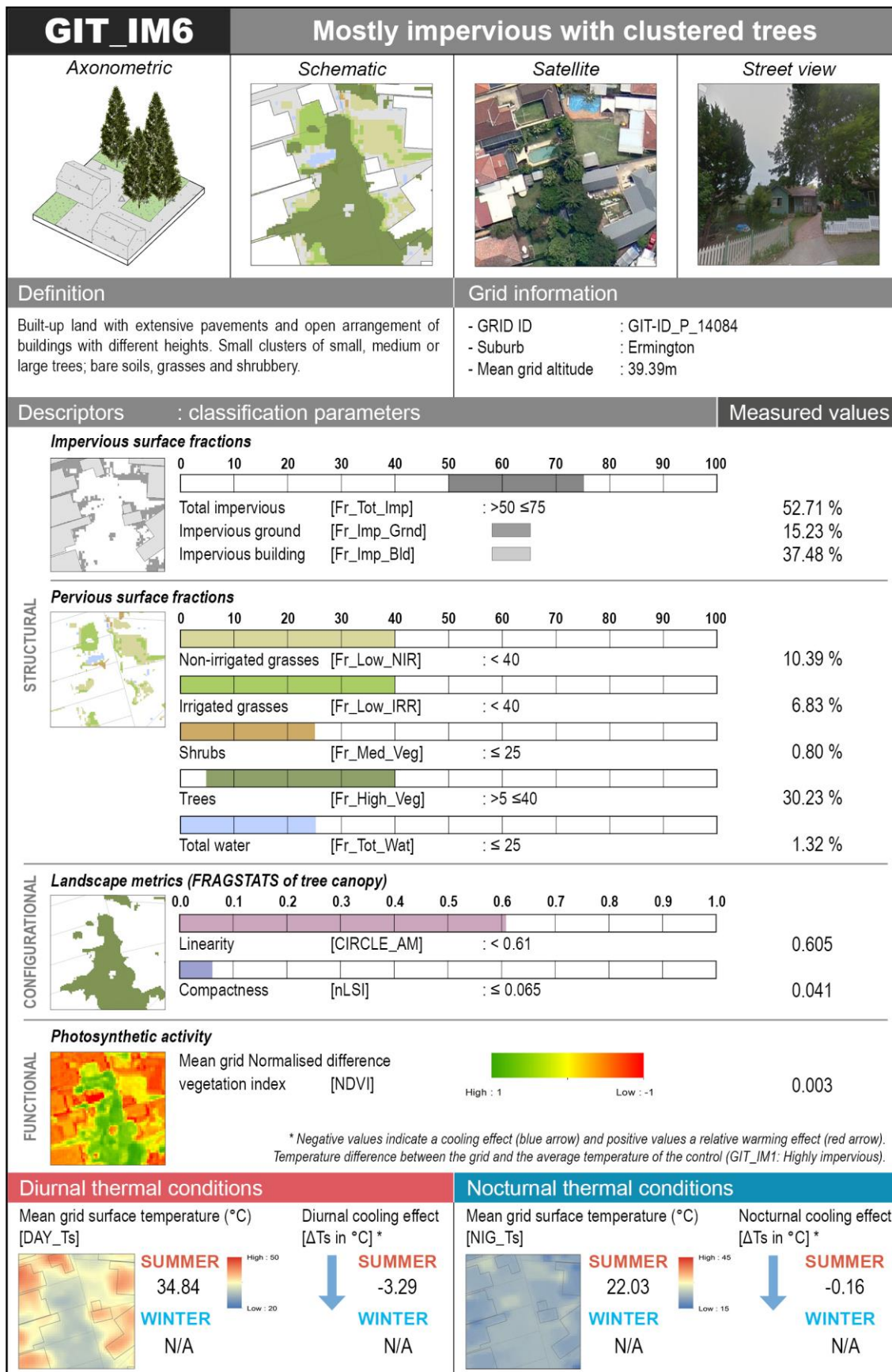
E3. Datasheet containing all variables and classification parameters calculated for the typology IM3.



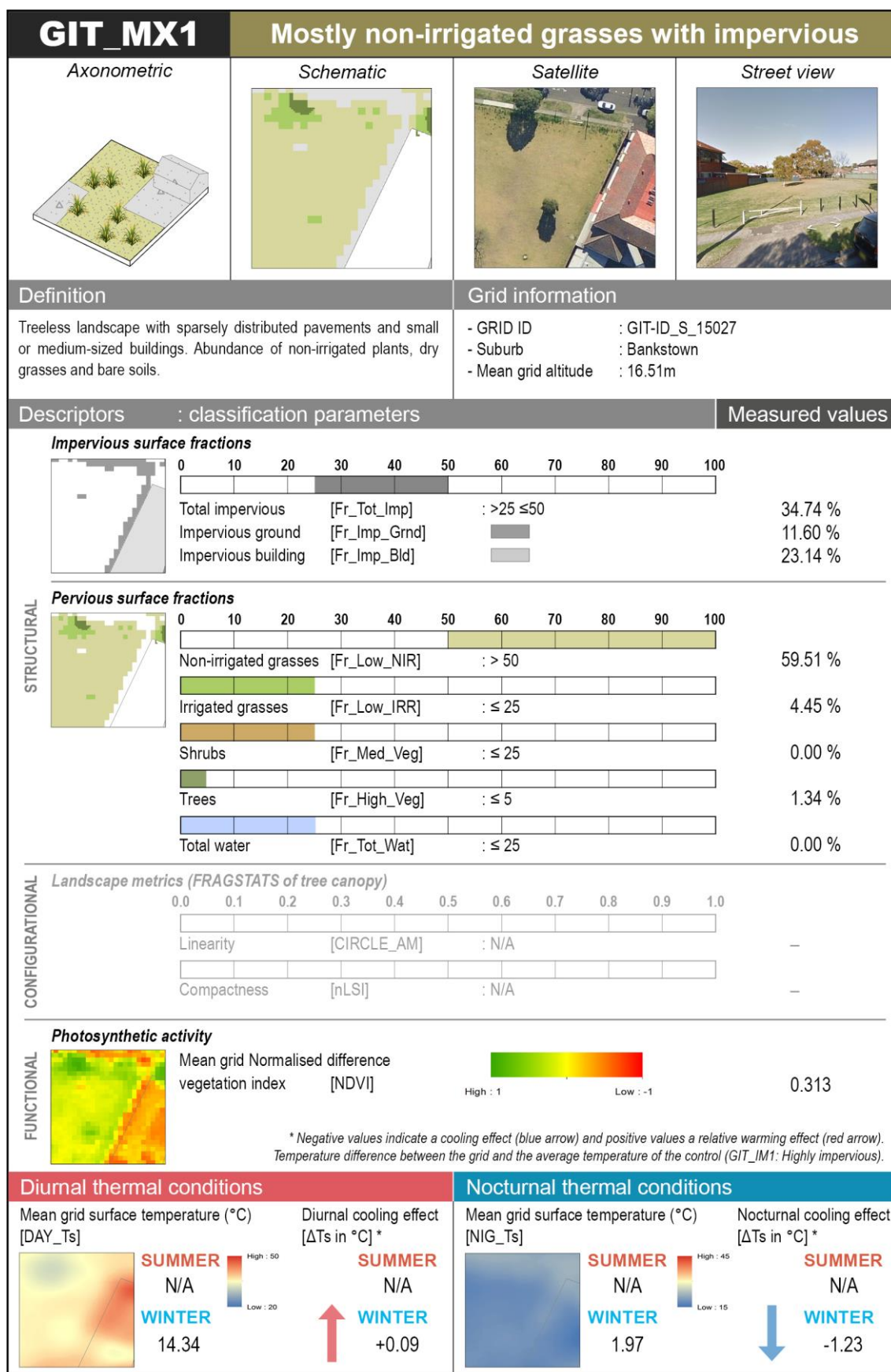
E4. Datasheet containing all variables and classification parameters calculated for the typology IM4.

GIT_IM5		Mostly impervious with scattered trees																																																																																				
Axonometric		Schematic																																																																																				
																																																																																						
Satellite		Street view																																																																																				
																																																																																						
Definition		Grid information																																																																																				
Built-up land with abundant pavements and buildings with different heights and arrangements. Individual or few dispersed trees with sporadic bare soils, grasses, and shrubbery.		- GRID ID : GIT-ID_P_19734 - Suburb : Granville - Mean grid altitude : 21.82m																																																																																				
Descriptors : classification parameters		Measured values																																																																																				
Impervious surface fractions																																																																																						
																																																																																						
<table><tr><td>0</td><td>10</td><td>20</td><td>30</td><td>40</td><td>50</td><td>60</td><td>70</td><td>80</td><td>90</td><td>100</td></tr><tr><td colspan="11"></td></tr><tr><td>Total impervious</td><td colspan="2">[Fr_Tot_Imp]</td><td colspan="2"></td><td colspan="2">: >50 ≤75</td><td colspan="4"></td><td>70.83 %</td></tr><tr><td>Impervious ground</td><td colspan="2">[Fr_Imp_Grnd]</td><td colspan="2"></td><td colspan="2"></td><td colspan="4"></td><td>70.83 %</td></tr><tr><td>Impervious building</td><td colspan="2">[Fr_Imp_Bld]</td><td colspan="2"></td><td colspan="2"></td><td colspan="4"></td><td>0.00 %</td></tr></table>				0	10	20	30	40	50	60	70	80	90	100												Total impervious	[Fr_Tot_Imp]				: >50 ≤75						70.83 %	Impervious ground	[Fr_Imp_Grnd]										70.83 %	Impervious building	[Fr_Imp_Bld]										0.00 %																									
0	10	20	30	40	50	60	70	80	90	100																																																																												
																																																																																						
Total impervious	[Fr_Tot_Imp]				: >50 ≤75						70.83 %																																																																											
Impervious ground	[Fr_Imp_Grnd]										70.83 %																																																																											
Impervious building	[Fr_Imp_Bld]										0.00 %																																																																											
STRUCTURAL	Pervious surface fractions																																																																																					
																																																																																						
	<table><tr><td>0</td><td>10</td><td>20</td><td>30</td><td>40</td><td>50</td><td>60</td><td>70</td><td>80</td><td>90</td><td>100</td></tr><tr><td colspan="11"></td></tr><tr><td>Non-irrigated grasses</td><td colspan="2">[Fr_Low_NIR]</td><td colspan="2"></td><td colspan="2">: < 40</td><td colspan="4"></td><td>11.83 %</td></tr><tr><td>Irrigated grasses</td><td colspan="2">[Fr_Low_IRR]</td><td colspan="2"></td><td colspan="2">: < 40</td><td colspan="4"></td><td>2.85 %</td></tr><tr><td>Shrubs</td><td colspan="2">[Fr_Med_Veg]</td><td colspan="2"></td><td colspan="2">: ≤ 25</td><td colspan="4"></td><td>0.40 %</td></tr><tr><td>Trees</td><td colspan="2">[Fr_High_Veg]</td><td colspan="2"></td><td colspan="2">: >5 ≤25</td><td colspan="4"></td><td>14.09 %</td></tr><tr><td>Total water</td><td colspan="2">[Fr_Tot_Wat]</td><td colspan="2"></td><td colspan="2">: ≤ 25</td><td colspan="4"></td><td>0.00 %</td></tr></table>				0	10	20	30	40	50	60	70	80	90	100												Non-irrigated grasses	[Fr_Low_NIR]				: < 40						11.83 %	Irrigated grasses	[Fr_Low_IRR]				: < 40						2.85 %	Shrubs	[Fr_Med_Veg]				: ≤ 25						0.40 %	Trees	[Fr_High_Veg]				: >5 ≤25						14.09 %	Total water	[Fr_Tot_Wat]				: ≤ 25						0.00 %
	0	10	20	30	40	50	60	70	80	90	100																																																																											
																																																																																						
	Non-irrigated grasses	[Fr_Low_NIR]				: < 40						11.83 %																																																																										
	Irrigated grasses	[Fr_Low_IRR]				: < 40						2.85 %																																																																										
Shrubs	[Fr_Med_Veg]				: ≤ 25						0.40 %																																																																											
Trees	[Fr_High_Veg]				: >5 ≤25						14.09 %																																																																											
Total water	[Fr_Tot_Wat]				: ≤ 25						0.00 %																																																																											
CONFIGURATIONAL	Landscape metrics (FRAGSTATS of tree canopy)																																																																																					
																																																																																						
	<table><tr><td>0.0</td><td>0.1</td><td>0.2</td><td>0.3</td><td>0.4</td><td>0.5</td><td>0.6</td><td>0.7</td><td>0.8</td><td>0.9</td><td>1.0</td></tr><tr><td colspan="11"></td></tr><tr><td>Linearity</td><td colspan="2">[CIRCLE_AM]</td><td colspan="2"></td><td colspan="2">: < 0.61</td><td colspan="4"></td><td>0.395</td></tr><tr><td>Compactness</td><td colspan="2">[nLSI]</td><td colspan="2"></td><td colspan="2">: > 0.065</td><td colspan="4"></td><td>0.073</td></tr></table>				0.0	0.1	0.2	0.3	0.4	0.5	0.6	0.7	0.8	0.9	1.0												Linearity	[CIRCLE_AM]				: < 0.61						0.395	Compactness	[nLSI]				: > 0.065						0.073																																				
0.0	0.1	0.2	0.3	0.4	0.5	0.6	0.7	0.8	0.9	1.0																																																																												
																																																																																						
Linearity	[CIRCLE_AM]				: < 0.61						0.395																																																																											
Compactness	[nLSI]				: > 0.065						0.073																																																																											
FUNCTIONAL	Photosynthetic activity																																																																																					
	<table><tr><td></td><td colspan="2">Mean grid Normalised difference vegetation index [NDVI]</td><td colspan="2"></td><td>-0.089</td></tr><tr><td></td><td colspan="2"></td><td colspan="2">High : 1 Low : -1</td><td></td></tr></table>					Mean grid Normalised difference vegetation index [NDVI]				-0.089				High : 1 Low : -1																																																																								
	Mean grid Normalised difference vegetation index [NDVI]				-0.089																																																																																	
			High : 1 Low : -1																																																																																			
* Negative values indicate a cooling effect (blue arrow) and positive values a relative warming effect (red arrow). Temperature difference between the grid and the average temperature of the control (GIT_IM1: Highly impervious).																																																																																						
Diurnal thermal conditions			Nocturnal thermal conditions																																																																																			
Mean grid surface temperature (°C) [DAY_Ts]			Mean grid surface temperature (°C) [NIG_Ts]																																																																																			
																																																																																						
SUMMER 40.49			SUMMER 24.85																																																																																			
WINTER N/A			WINTER N/A																																																																																			
Diurnal cooling effect [ΔTs in °C] *			Nocturnal cooling effect [ΔTs in °C] *																																																																																			
																																																																																						
SUMMER +2.36			SUMMER +2.66																																																																																			
WINTER N/A			WINTER N/A																																																																																			

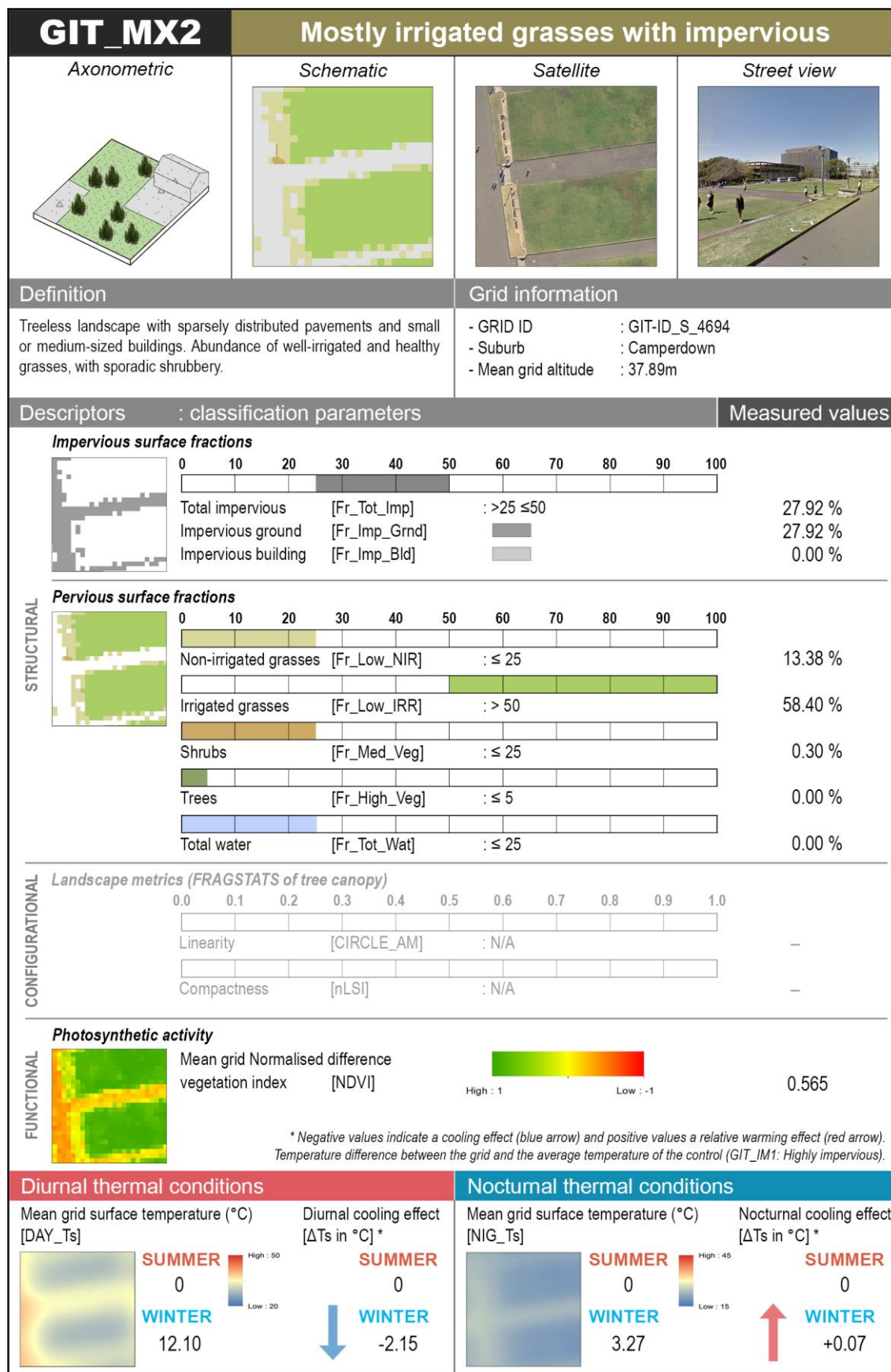
E5. Datasheet containing all variables and classification parameters calculated for the typology IM5.



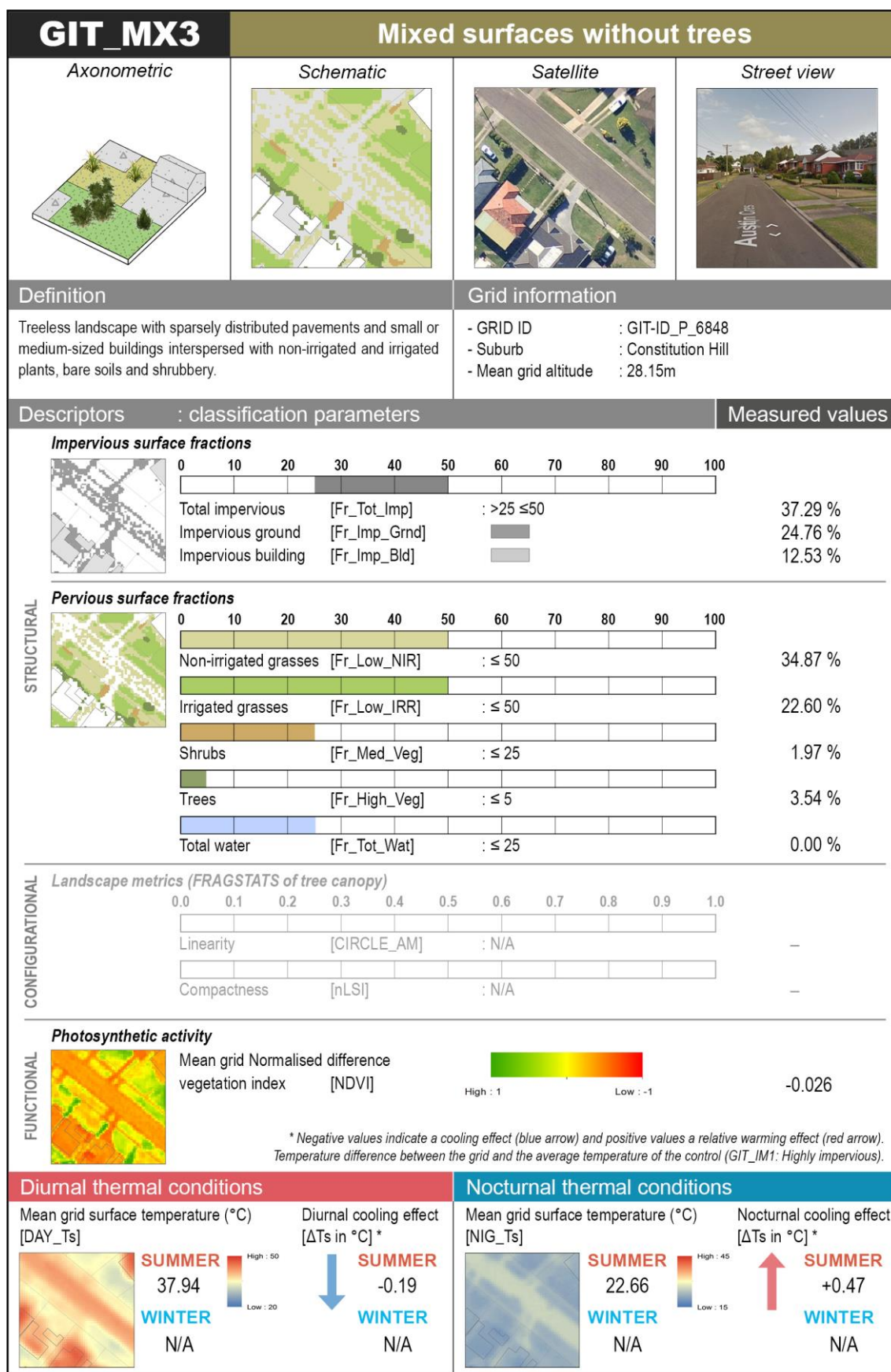
E6. Datasheet containing all variables and classification parameters calculated for the typology IM6.



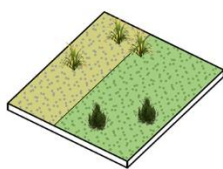

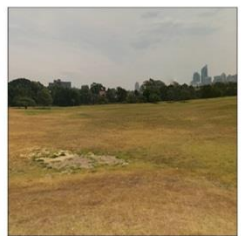

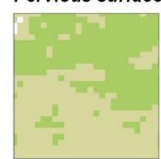
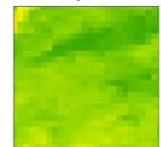


E7. Datasheet containing all variables and classification parameters calculated for the typology MX1.



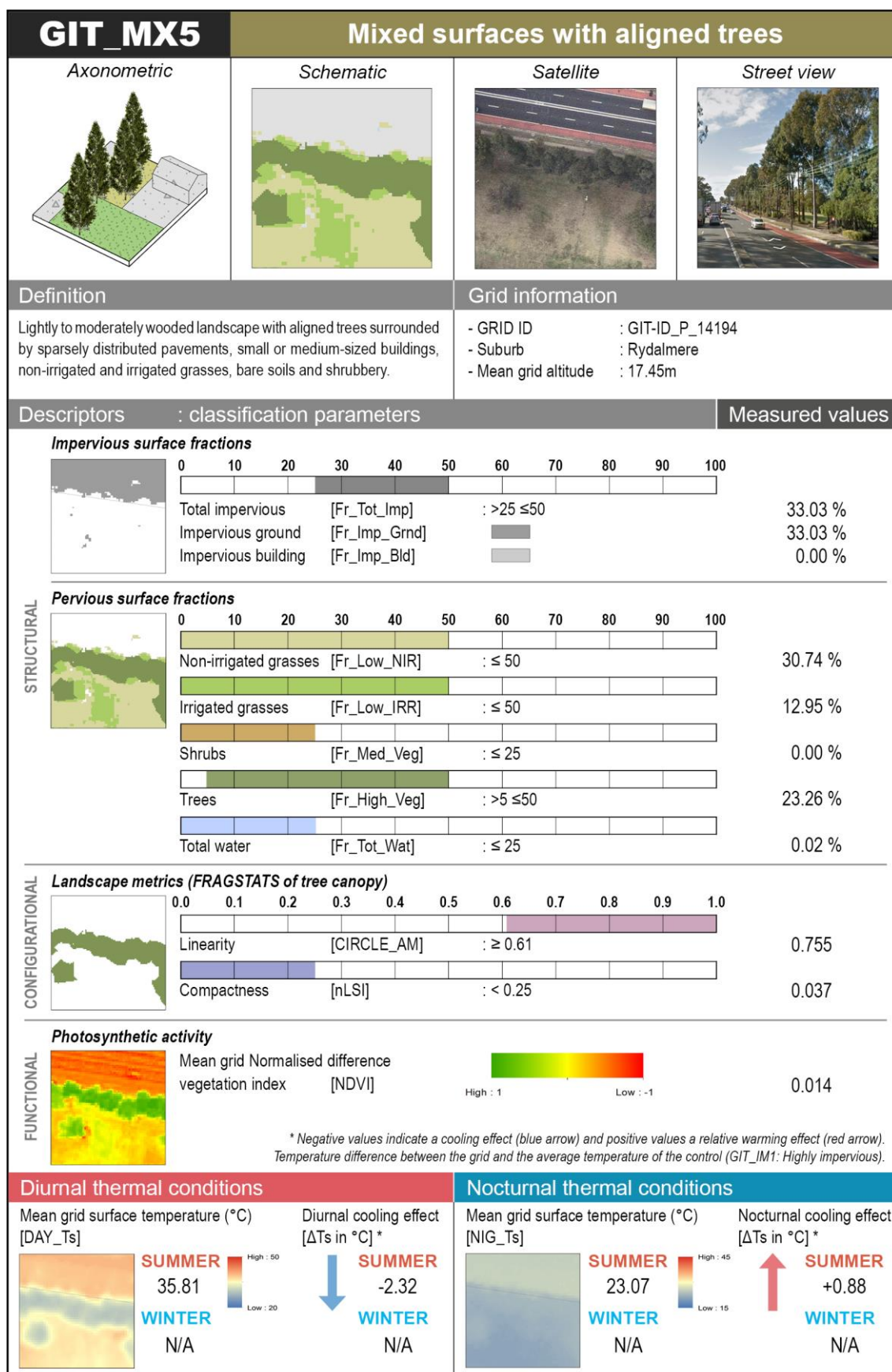
E8. Datasheet containing all variables and classification parameters calculated for the typology MX2.



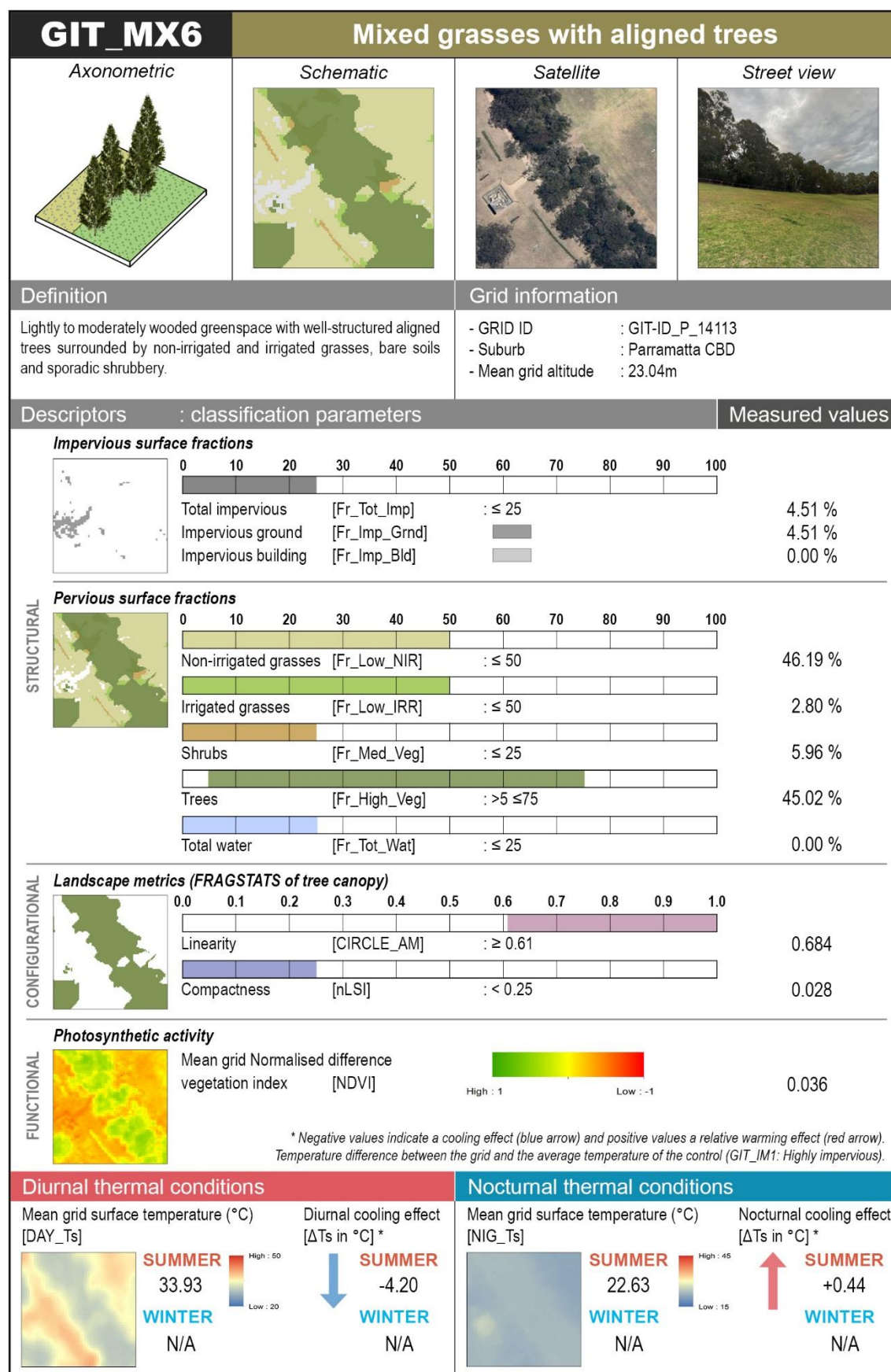
E9. Datasheet containing all variables and classification parameters calculated for the typology MX3.

GIT_MX4		Mixed grasses and bare soils	
Axonometric	Schematic	Satellite	Street view
			
Definition		Grid information	
Treeless greenspace of extensive natural covers including non-irrigated and irrigated grasses, bare soils, and shrubby is spots.		- GRID ID : GIT-ID_S_4839 - Suburb : Moore Park - Mean grid altitude : 41.07m	
Descriptors : classification parameters			Measured values
STRUCTURAL	Impervious surface fractions		
			
	0 10 20 30 40 50 60 70 80 90 100		
	Total impervious [Fr_Tot_Imp] : ≤ 25 0.40 %		
	Impervious ground [Fr_Imp_Grnd] : 0.40%		
	Impervious building [Fr_Imp_Bld] : 0.00 %		
	Pervious surface fractions		
			
	0 10 20 30 40 50 60 70 80 90 100		
	Non-irrigated grasses [Fr_Low_NIR] : ≤ 75 52.15 %		
Irrigated grasses [Fr_Low_IRR] : ≤ 75 47.45 %			
Shrubs [Fr_Med_Veg] : ≤ 25 0.00 %			
Trees [Fr_High_Veg] : ≤ 5 0.00 %			
Total water [Fr_Tot_Wat] : ≤ 25 0.00 %			
CONFIGURATIONAL	Landscape metrics (FRAGSTATS of tree canopy)		
	0.0 0.1 0.2 0.3 0.4 0.5 0.6 0.7 0.8 0.9 1.0		
	Linearity [CIRCLE_AM] : N/A —		
Compactness [nLSI] : N/A —			
FUNCTIONAL	Photosynthetic activity		
	 Mean grid Normalised difference vegetation index [NDVI] High : 1 Low : -1 0.611		
* Negative values indicate a cooling effect (blue arrow) and positive values a relative warming effect (red arrow). Temperature difference between the grid and the average temperature of the control (GIT_IM1: Highly impervious).			
Diurnal thermal conditions		Nocturnal thermal conditions	
Mean grid surface temperature (°C) [DAY_Ts]		Mean grid surface temperature (°C) [NIG_Ts]	
			
SUMMER N/A		SUMMER N/A	
WINTER 11.58		WINTER 2.50	
Diurnal cooling effect [ΔTs in °C] *		Nocturnal cooling effect [ΔTs in °C] *	
SUMMER N/A		SUMMER N/A	
WINTER -2.67		WINTER -0.70	

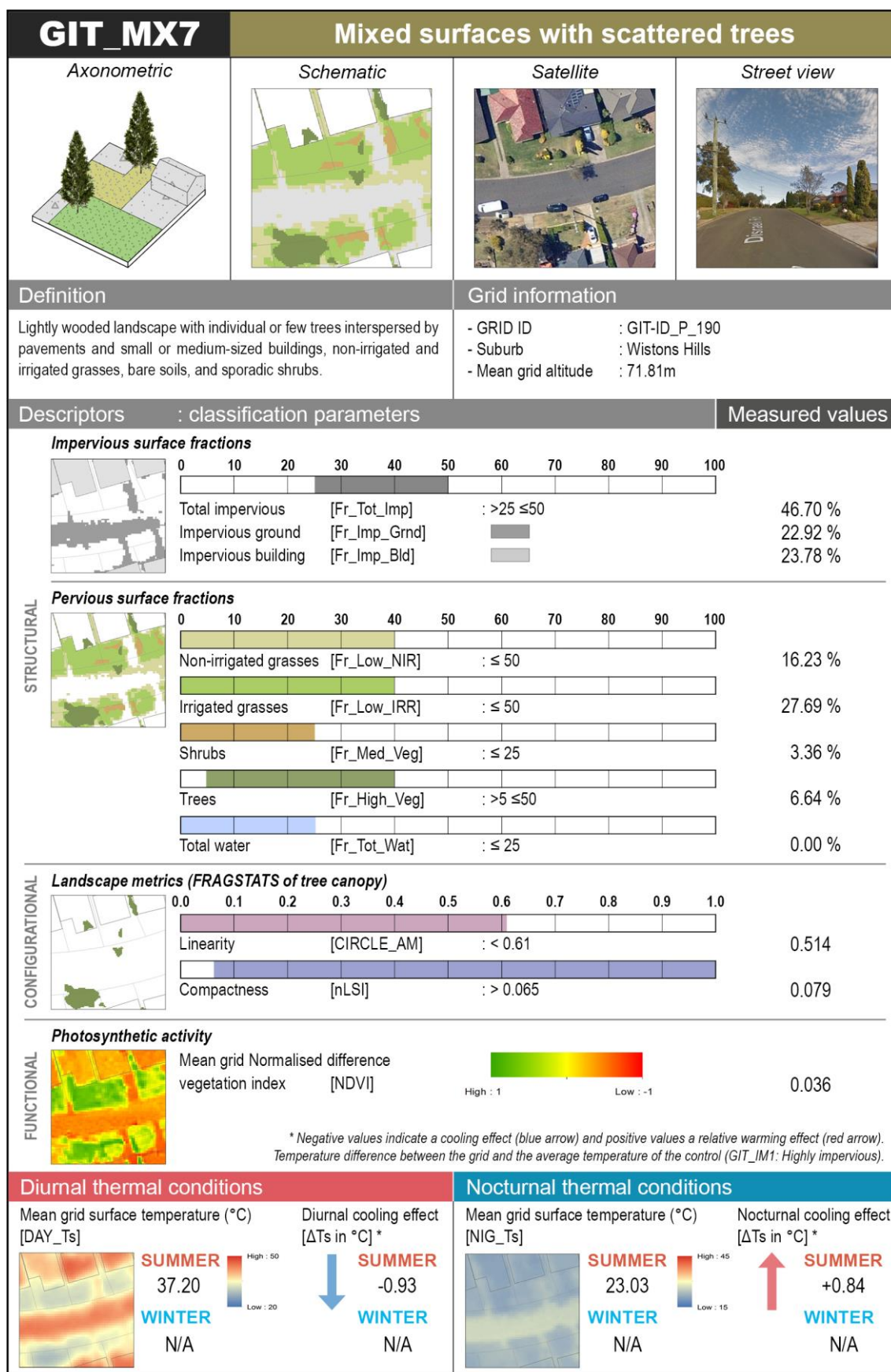
E10. Datasheet containing all variables and classification parameters calculated for the typology MX4.



E11. Datasheet containing all variables and classification parameters calculated for the typology MX5.



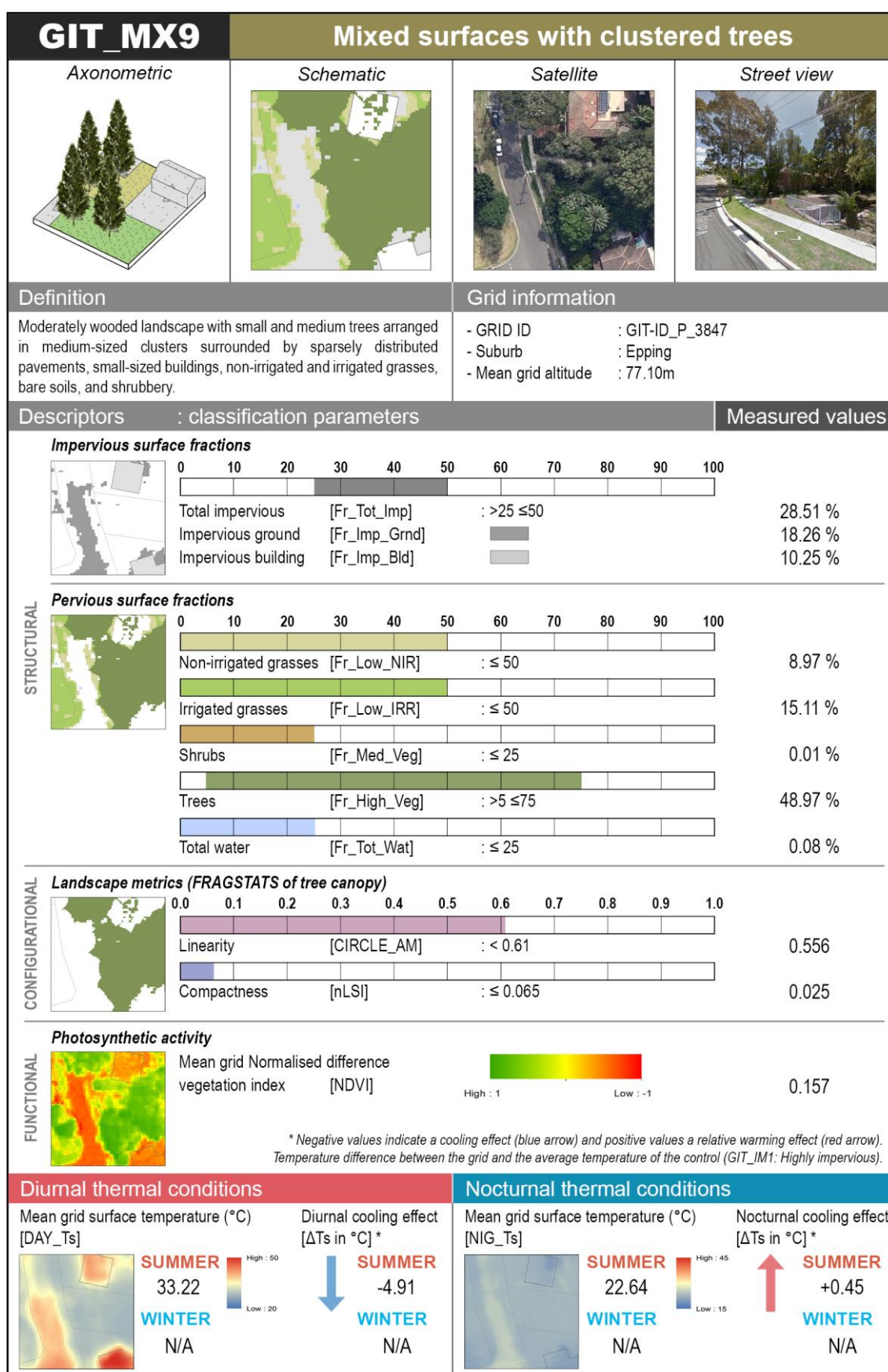
E12. Datasheet containing all variables and classification parameters calculated for the typology MX6.



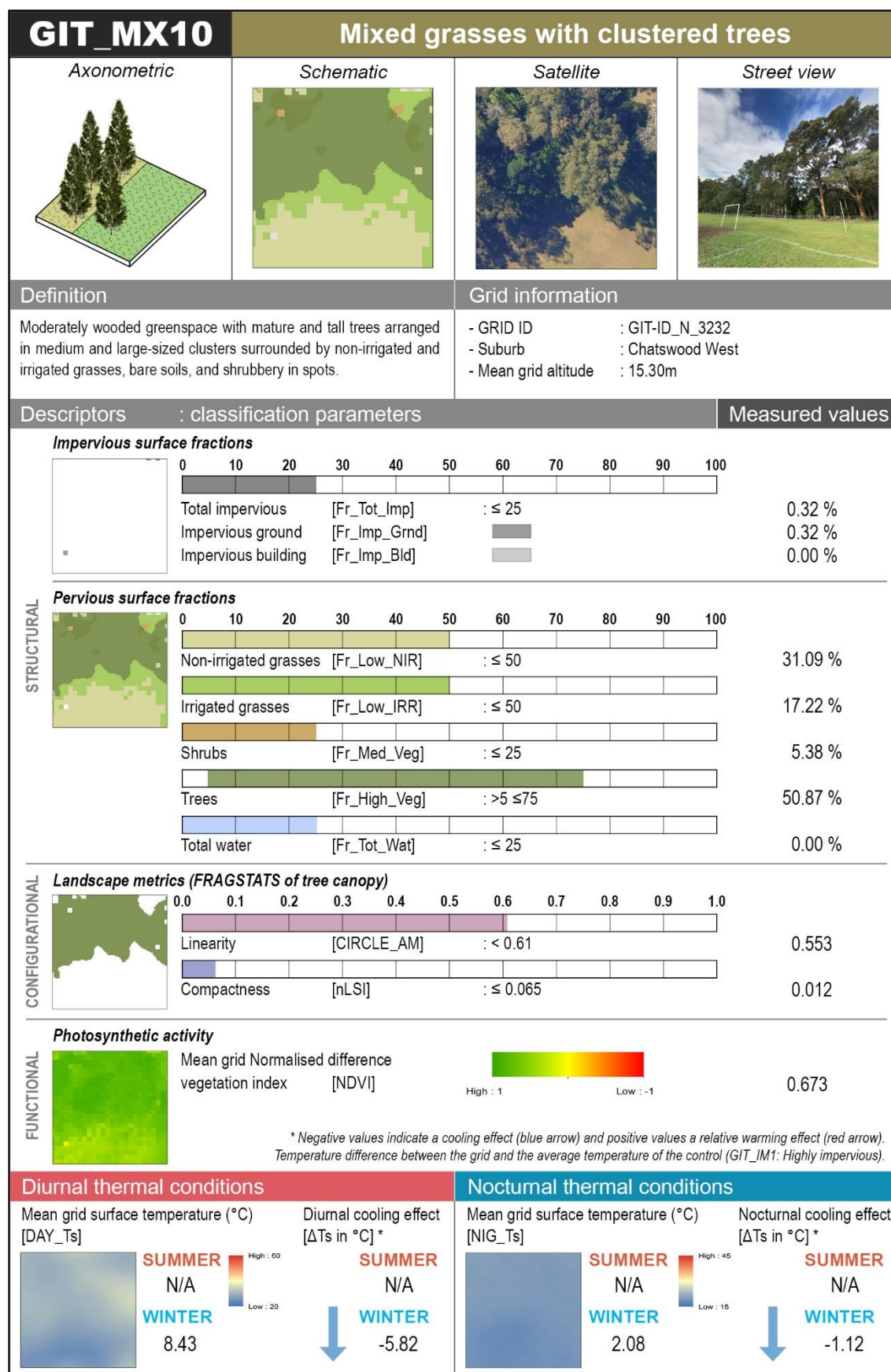
E13. Datasheet containing all variables and classification parameters calculated for the typology MX7.

GIT_MX8		Mixed grasses with scattered trees	
Axonometric	Schematic	Satellite	Street view
<div></div>		<div></div>	<div></div>
Definition		Grid information	
Lightly wooded greenspace with individual or few dispersed trees surrounded by extensive non-irrigated and irrigated grasses, and sporadic bare soils, and shrubbery.		<div>- GRID ID : GIT-ID_S_13149</div> <div>- Suburb : Bankstown</div> <div>- Mean grid altitude : 61.66m</div>	
Descriptors : classification parameters			Measured values
STRUCTURAL	Impervious surface fractions		
	<div><div></div><div>0102030405060708090100</div></div>		
	Total impervious [Fr_Tot_Imp] : ≤ 25		1.21 %
	Impervious ground [Fr_Imp_Grnd]		1.21 %
	Impervious building [Fr_Imp_Bld]		0.00 %
	Pervious surface fractions		
	<div><div></div><div>0102030405060708090100</div></div>		
	Non-irrigated grasses [Fr_Low_NIR] : ≤ 50		46.09 %
	Irrigated grasses [Fr_Low_IRR] : ≤ 50		43.91 %
	Shrubs [Fr_Med_Veg] : ≤ 25		0.00 %
Trees [Fr_High_Veg] : >5 ≤75		8.79 %	
Total water [Fr_Tot_Wat] : ≤ 25		0.00 %	
CONFIGURATIONAL	Landscape metrics (FRAGSTATS of tree canopy)		
	<div><div></div><div>0.00.10.20.30.40.50.60.70.80.91.0</div></div>		
	Linearity [CIRCLE_AM] : < 0.61		0.336
Compactness [nLSI] : > 0.065		0.065	
FUNCTIONAL	Photosynthetic activity		
	<div><div></div><div>Mean grid Normalised difference vegetation index [NDVI]</div><div><div></div><div>High : 1Low : -1</div></div><div>0.597</div></div>		
<div>* Negative values indicate a cooling effect (blue arrow) and positive values a relative warming effect (red arrow). Temperature difference between the grid and the average temperature of the control (GIT_IM1: Highly impervious).</div>			
Diurnal thermal conditions		Nocturnal thermal conditions	
Mean grid surface temperature (°C) [DAY_Ts]		Mean grid surface temperature (°C) [NIG_Ts]	
<div><div></div><div>SUMMER N/A</div><div>WINTER 11.29</div><div>High : 50Low : 20</div></div>		<div><div></div><div>SUMMER N/A</div><div>WINTER 2.43</div><div>High : 45Low : 15</div></div>	
<div><div></div><div>SUMMER N/A</div><div>WINTER -2.96</div></div>		<div><div></div><div>SUMMER N/A</div><div>WINTER -0.77</div></div>	

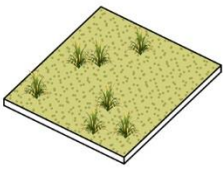



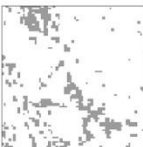

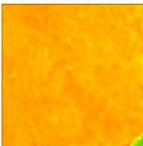


E14. Datasheet containing all variables and classification parameters calculated for the typology MX8.



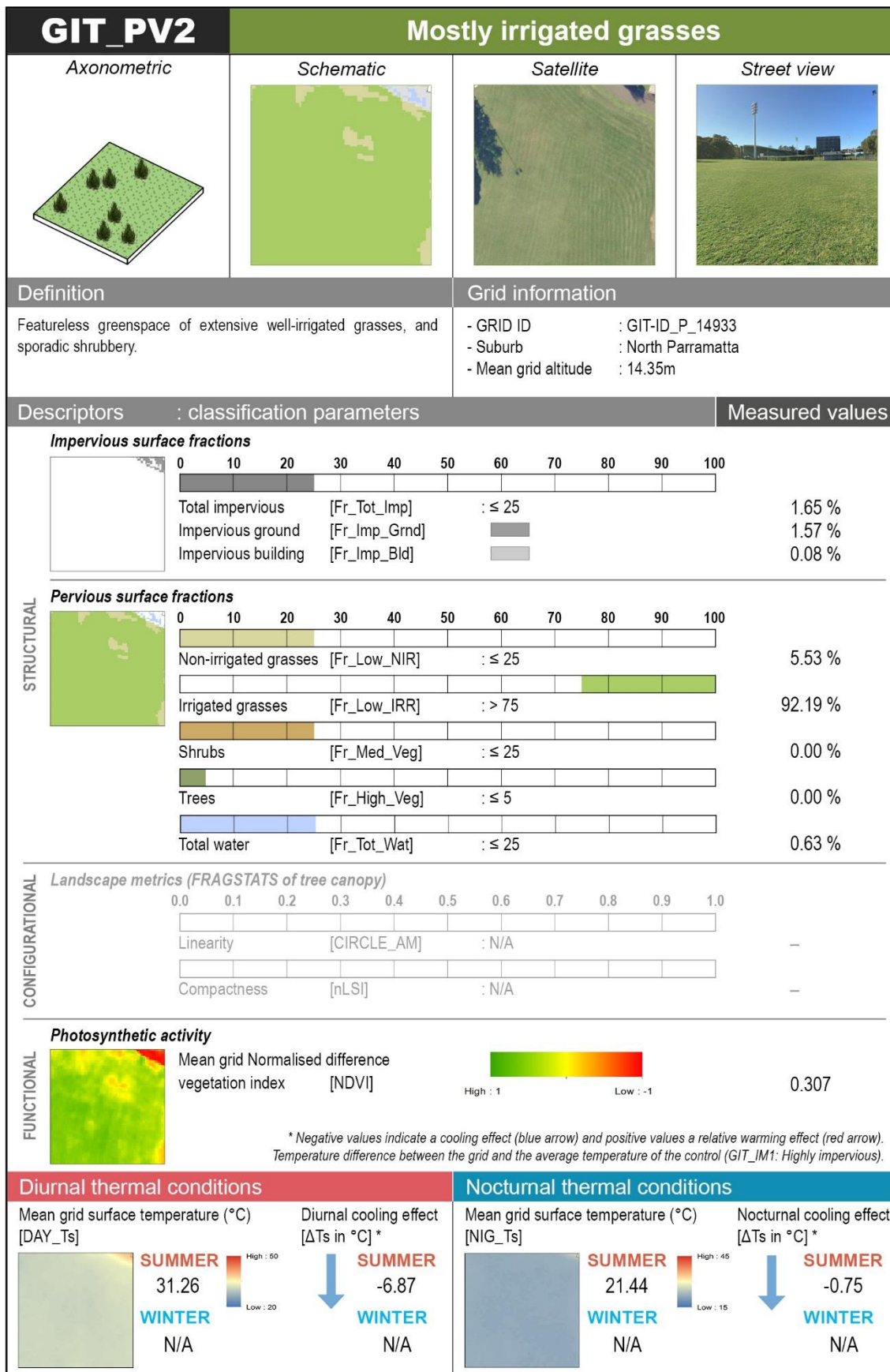
E15. Datasheet containing all variables and classification parameters calculated for the typology MX9.



E16. Datasheet containing all variables and classification parameters calculated for the typology MX10.

GIT_PV1		Mostly non-irrigated grasses	
Axonometric	Schematic	Satellite	Street view
			
Definition		Grid information	
Featureless greenspace of extensive non-irrigated plants, dry grasses, sands, bare soils and sporadic shrubbery.		- GRID ID : GIT-ID_P_7122 - Suburb : Telopea - Mean grid altitude : 62.19m	
Descriptors : classification parameters			Measured values
STRUCTURAL	Impervious surface fractions		
		0 10 20 30 40 50 60 70 80 90 100	
	Total impervious	[Fr_Tot_Imp] : ≤ 25	13.91 %
	Impervious ground	[Fr_Imp_Grnd]	13.91 %
	Impervious building	[Fr_Imp_Bld]	0.00 %
	Pervious surface fractions		
		0 10 20 30 40 50 60 70 80 90 100	
	Non-irrigated grasses	[Fr_Low_NIR] : > 75	84.61 %
	Irrigated grasses	[Fr_Low_IRR] : ≤ 25	0.00 %
	Shrubs	[Fr_Med_Veg] : ≤ 25	0.00 %
CONFIGURATIONAL	Landscape metrics (FRAGSTATS of tree canopy)		
		0.0 0.1 0.2 0.3 0.4 0.5 0.6 0.7 0.8 0.9 1.0	
	Linearity	[CIRCLE_AM] : N/A	—
	Compactness	[nLSI] : N/A	—
FUNCTIONAL	Photosynthetic activity		
		Mean grid Normalised difference vegetation index [NDVI]	-0.118
<p>* Negative values indicate a cooling effect (blue arrow) and positive values a relative warming effect (red arrow). Temperature difference between the grid and the average temperature of the control (GIT_IM1: Highly impervious).</p>			
Diurnal thermal conditions		Nocturnal thermal conditions	
Mean grid surface temperature (°C) [DAY_Ts]		Mean grid surface temperature (°C) [NIG_Ts]	
			
SUMMER 32.12		SUMMER 21.57	
WINTER N/A		WINTER N/A	
Diurnal cooling effect [ΔTs in °C] *		Nocturnal cooling effect [ΔTs in °C] *	
SUMMER -6.01		SUMMER -0.62	
WINTER N/A		WINTER N/A	

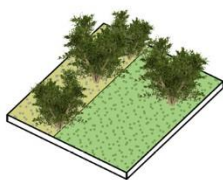





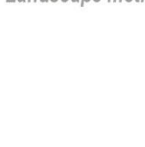
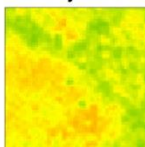





E17. Datasheet containing all variables and classification parameters calculated for the typology PV1.



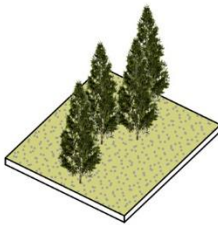






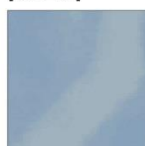
E18. Datasheet containing all variables and classification parameters calculated for the typology PV2.

GIT_PV3		Mixed grasses with shrubs and trees	
Axonometric	Schematic	Satellite	Street view
<div></div>		<div></div>	<div></div>
Definition		Grid information	
Greenspace with individual or small group of trees, sporadic shrubbery and abundance of non-irrigated and irrigated grasses, bare soils and sands.		<div>- GRID ID : GIT-ID_S_9134</div> <div>- Suburb : Strathfield South</div> <div>- Mean grid altitude : 16.84m</div>	
Descriptors : classification parameters			Measured values
STRUCTURAL	Impervious surface fractions		
	<div></div>	<div>0102030405060708090100</div>	
	Total impervious [Fr_Tot_Imp]	: ≤ 25	14.92 %
	Impervious ground [Fr_Imp_Grnd]	<div></div>	14.92 %
	Impervious building [Fr_Imp_Bld]	<div></div>	0.00 %
	Pervious surface fractions		
	<div></div>	<div>0102030405060708090100</div>	
	Non-irrigated grasses [Fr_Low_NIR]	: < 60	29.35 %
	Irrigated grasses [Fr_Low_IRR]	: < 60	9.96 %
	Shrubs [Fr_Med_Veg]	: >25 ≤50	41.85 %
Trees [Fr_High_Veg]	: ≤ 50	3.76 %	
Total water [Fr_Tot_Wat]	: ≤ 25	0.16 %	
CONFIGURATIONAL	Landscape metrics (FRAGSTATS of tree canopy)		
	<div>0.00.10.20.30.40.50.60.70.80.91.0</div>		
	Linearity [CIRCLE_AM]	: N/A	—
	<div></div>		
Compactness [nLSI]	: N/A	—	
FUNCTIONAL	Photosynthetic activity		
	<div></div>	<div>Mean grid Normalised difference vegetation index [NDVI]</div> <div>High : 1Low : -1</div>	0.418
<div>* Negative values indicate a cooling effect (blue arrow) and positive values a relative warming effect (red arrow). Temperature difference between the grid and the average temperature of the control (GIT_IM1: Highly impervious).</div>			
Diurnal thermal conditions		Nocturnal thermal conditions	
Mean grid surface temperature (°C) [DAY_Ts]		Mean grid surface temperature (°C) [NIG_Ts]	
<div></div>		<div></div>	
<div>SUMMER N/A</div> <div>WINTER 10.39</div>		<div>SUMMER N/A</div> <div>WINTER 2.46</div>	
Diurnal cooling effect [ΔTs in °C] *		Nocturnal cooling effect [ΔTs in °C] *	
<div>SUMMER N/A</div> <div>WINTER -3.85</div>		<div>SUMMER N/A</div> <div>WINTER -0.74</div>	

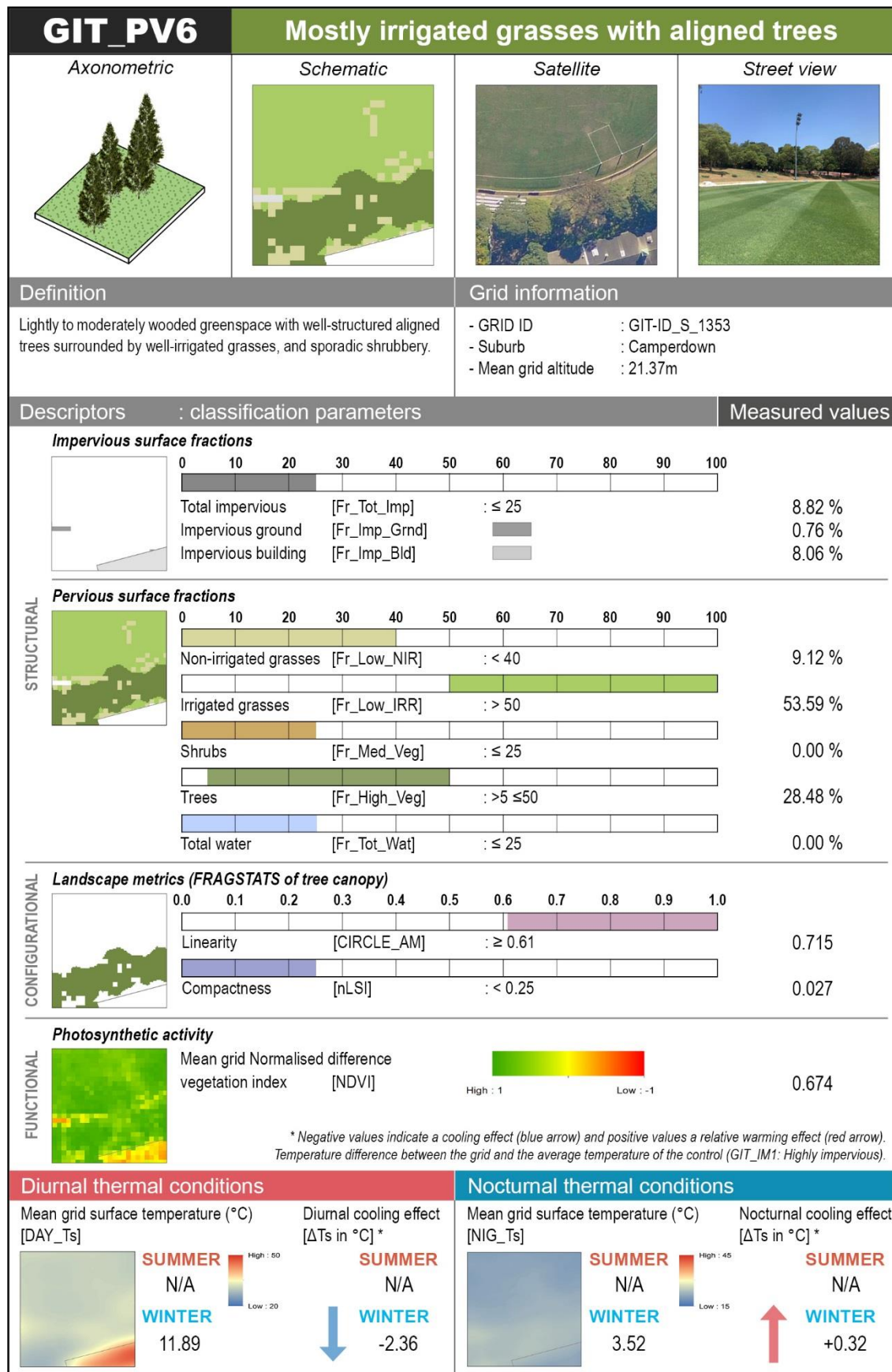
E19. Datasheet containing all variables and classification parameters calculated for the typology PV3.

GIT_PV4		Mostly shrubs		
Axonometric	Schematic	Satellite	Street view	
				
Definition		Grid information		
Greenspace with close arrangement of bushes, shrubs and small trees interspersed with grasses and bare soils. Few or no trees.		- GRID ID : GIT-ID_P_17451 - Suburb : Rosehill - Mean grid altitude : 1.70m		
Descriptors : classification parameters			Measured values	
STRUCTURAL	Impervious surface fractions			
				
	Total impervious	[Fr_Tot_Imp]	: ≤ 25	0.00 %
	Impervious ground	[Fr_Imp_Grnd]		0.00 %
	Impervious building	[Fr_Imp_Bld]		0.00 %
	Pervious surface fractions			
				
	Non-irrigated grasses	[Fr_Low_NIR]	: < 50	9.45 %
	Irrigated grasses	[Fr_Low_IRR]	: < 50	3.50 %
	Shrubs	[Fr_Med_Veg]	: > 50	85.80 %
Trees	[Fr_High_Veg]	: ≤ 25	2.25 %	
Total water	[Fr_Tot_Wat]	: ≤ 25	0.00 %	
CONFIGURATIONAL	Landscape metrics (FRAGSTATS of tree canopy)			
				
	Linearity	[CIRCLE_AM]	: N/A	—
	Compactness	[nLSI]	: N/A	—
FUNCTIONAL	Photosynthetic activity			
		Mean grid Normalised difference vegetation index [NDVI]		0.129
* Negative values indicate a cooling effect (blue arrow) and positive values a relative warming effect (red arrow). Temperature difference between the grid and the average temperature of the control (GIT_IM1: Highly impervious).				
Diurnal thermal conditions		Nocturnal thermal conditions		
Mean grid surface temperature (°C) [DAY_Ts]		Mean grid surface temperature (°C) [NIG_Ts]		
				
SUMMER 28.98 WINTER N/A		SUMMER 21.86 WINTER N/A		
Diurnal cooling effect [ΔTs in °C] *		Nocturnal cooling effect [ΔTs in °C] *		
				
SUMMER -9.15 WINTER N/A		SUMMER -0.33 WINTER N/A		

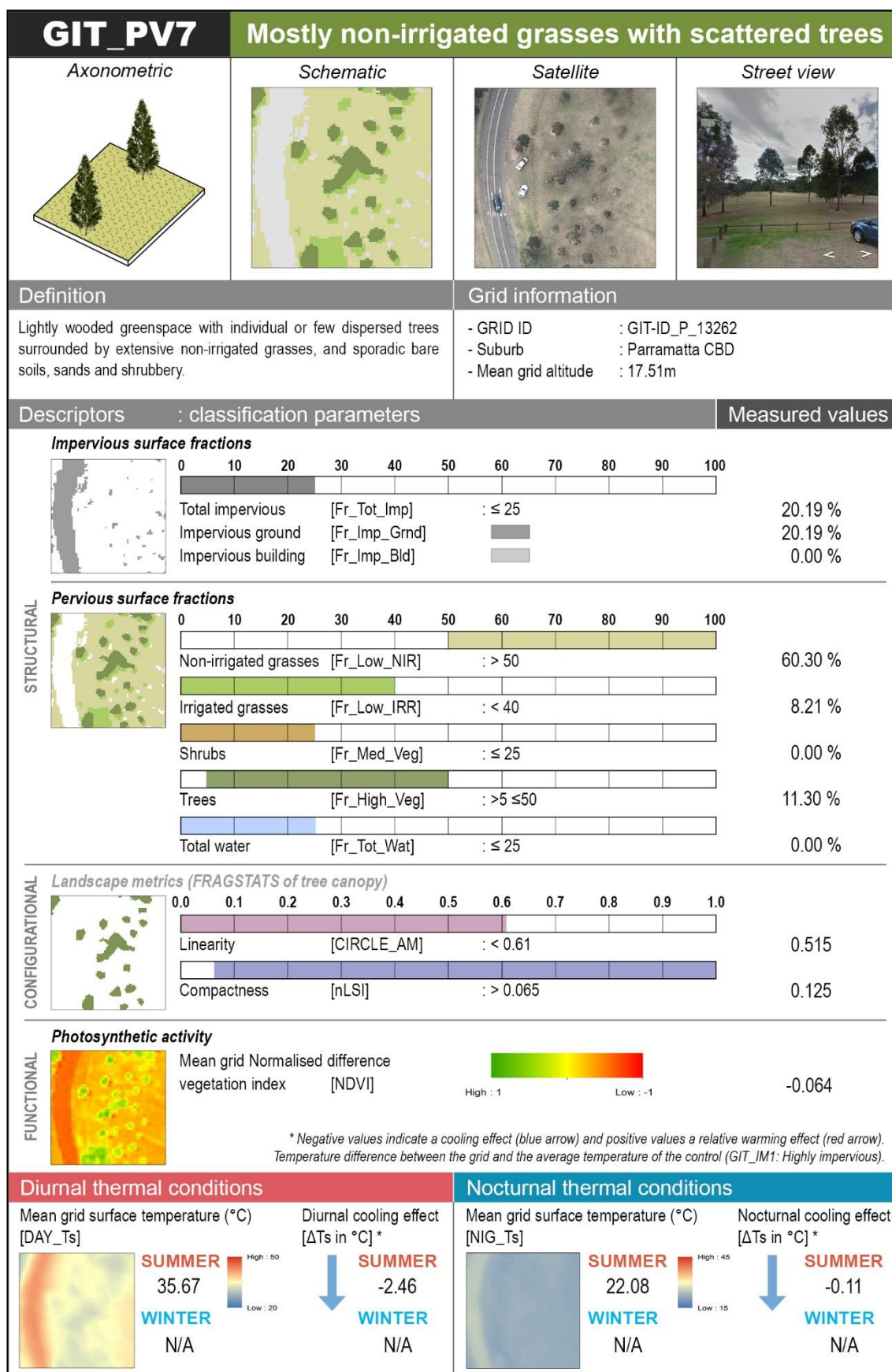
E20. Datasheet containing all variables and classification parameters calculated for the typology PV4.

GIT_PV5		Mostly non-irrigated grasses with aligned trees																																																																									
Axonometric		Schematic																																																																									
																																																																											
Satellite		Street view																																																																									
																																																																											
Definition		Grid information																																																																									
Lightly to moderately wooded greenspace with well-structured aligned trees surrounded by non-irrigated grasses, dry plants, bare soils, sands and sporadic shrubbery.		- GRID ID : GIT-ID_P_21547 - Suburb : Guildford - Mean grid altitude : 17.15m																																																																									
Descriptors : classification parameters		Measured values																																																																									
Impervious surface fractions																																																																											
																																																																											
<table><tr><td></td><td>0</td><td>10</td><td>20</td><td>30</td><td>40</td><td>50</td><td>60</td><td>70</td><td>80</td><td>90</td><td>100</td></tr><tr><td>Total impervious</td><td colspan="11">[Fr_Tot_Imp] : ≤ 25</td></tr><tr><td>Impervious ground</td><td colspan="11">[Fr_Imp_Grnd] : 0.07 %</td></tr><tr><td>Impervious building</td><td colspan="11">[Fr_Imp_Bld] : 0.00 %</td></tr></table>					0	10	20	30	40	50	60	70	80	90	100	Total impervious	[Fr_Tot_Imp] : ≤ 25											Impervious ground	[Fr_Imp_Grnd] : 0.07 %											Impervious building	[Fr_Imp_Bld] : 0.00 %																																		
	0	10	20	30	40	50	60	70	80	90	100																																																																
Total impervious	[Fr_Tot_Imp] : ≤ 25																																																																										
Impervious ground	[Fr_Imp_Grnd] : 0.07 %																																																																										
Impervious building	[Fr_Imp_Bld] : 0.00 %																																																																										
Pervious surface fractions																																																																											
																																																																											
<table><tr><td></td><td>0</td><td>10</td><td>20</td><td>30</td><td>40</td><td>50</td><td>60</td><td>70</td><td>80</td><td>90</td><td>100</td></tr><tr><td>Non-irrigated grasses</td><td colspan="11">[Fr_Low_NIR] : > 50</td></tr><tr><td>Irrigated grasses</td><td colspan="11">[Fr_Low_IRR] : < 40</td></tr><tr><td>Shrubs</td><td colspan="11">[Fr_Med_Veg] : ≤ 25</td></tr><tr><td>Trees</td><td colspan="11">[Fr_High_Veg] : >5 ≤50</td></tr><tr><td>Total water</td><td colspan="11">[Fr_Tot_Wat] : ≤ 25</td></tr></table>					0	10	20	30	40	50	60	70	80	90	100	Non-irrigated grasses	[Fr_Low_NIR] : > 50											Irrigated grasses	[Fr_Low_IRR] : < 40											Shrubs	[Fr_Med_Veg] : ≤ 25											Trees	[Fr_High_Veg] : >5 ≤50											Total water	[Fr_Tot_Wat] : ≤ 25										
	0	10	20	30	40	50	60	70	80	90	100																																																																
Non-irrigated grasses	[Fr_Low_NIR] : > 50																																																																										
Irrigated grasses	[Fr_Low_IRR] : < 40																																																																										
Shrubs	[Fr_Med_Veg] : ≤ 25																																																																										
Trees	[Fr_High_Veg] : >5 ≤50																																																																										
Total water	[Fr_Tot_Wat] : ≤ 25																																																																										
Landscape metrics (FRAGSTATS of tree canopy)																																																																											
																																																																											
<table><tr><td></td><td>0.0</td><td>0.1</td><td>0.2</td><td>0.3</td><td>0.4</td><td>0.5</td><td>0.6</td><td>0.7</td><td>0.8</td><td>0.9</td><td>1.0</td></tr><tr><td>Linearity</td><td colspan="11">[CIRCLE_AM] : ≥ 0.61</td></tr><tr><td>Compactness</td><td colspan="11">[nLSI] : < 0.25</td></tr></table>					0.0	0.1	0.2	0.3	0.4	0.5	0.6	0.7	0.8	0.9	1.0	Linearity	[CIRCLE_AM] : ≥ 0.61											Compactness	[nLSI] : < 0.25																																														
	0.0	0.1	0.2	0.3	0.4	0.5	0.6	0.7	0.8	0.9	1.0																																																																
Linearity	[CIRCLE_AM] : ≥ 0.61																																																																										
Compactness	[nLSI] : < 0.25																																																																										
Photosynthetic activity																																																																											
																																																																											
<table><tr><td>Mean grid Normalised difference vegetation index [NDVI]</td><td>High : 1</td><td>Low : -1</td><td>0.181</td></tr></table>				Mean grid Normalised difference vegetation index [NDVI]	High : 1	Low : -1	0.181																																																																				
Mean grid Normalised difference vegetation index [NDVI]	High : 1	Low : -1	0.181																																																																								
* Negative values indicate a cooling effect (blue arrow) and positive values a relative warming effect (red arrow). Temperature difference between the grid and the average temperature of the control (GIT_IM1: Highly impervious).																																																																											
Diurnal thermal conditions		Nocturnal thermal conditions																																																																									
Mean grid surface temperature (°C) [DAY_Ts]		Mean grid surface temperature (°C) [NIG_Ts]																																																																									
																																																																											
SUMMER 32.27		SUMMER 21.27																																																																									
WINTER N/A		WINTER N/A																																																																									
Diurnal cooling effect [ΔTs in °C] *		Nocturnal cooling effect [ΔTs in °C] *																																																																									
SUMMER -5.86		SUMMER -0.92																																																																									
WINTER N/A		WINTER N/A																																																																									

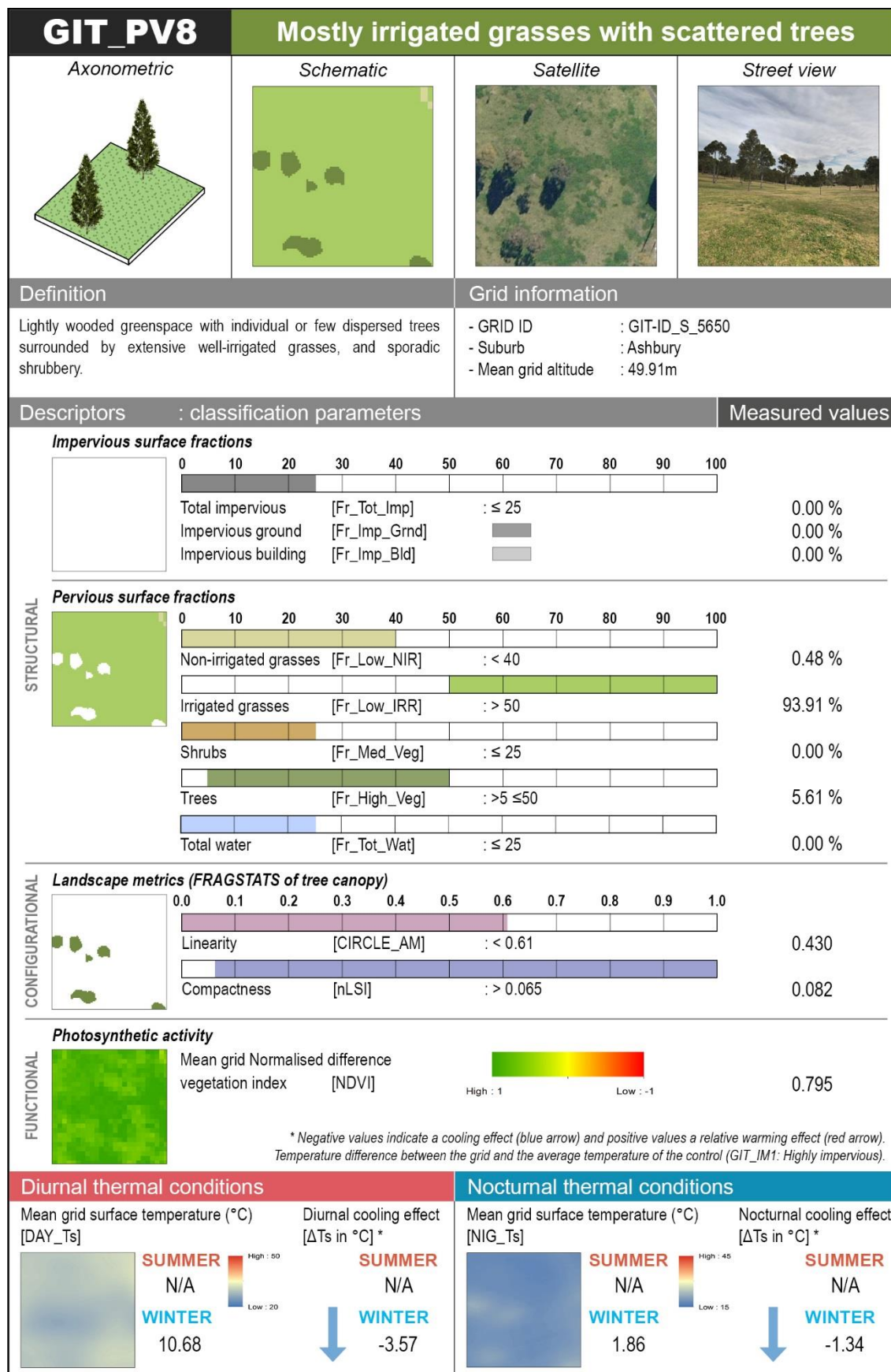
E21. Datasheet containing all variables and classification parameters calculated for the typology PV5.



E22. Datasheet containing all variables and classification parameters calculated for the typology PV6.



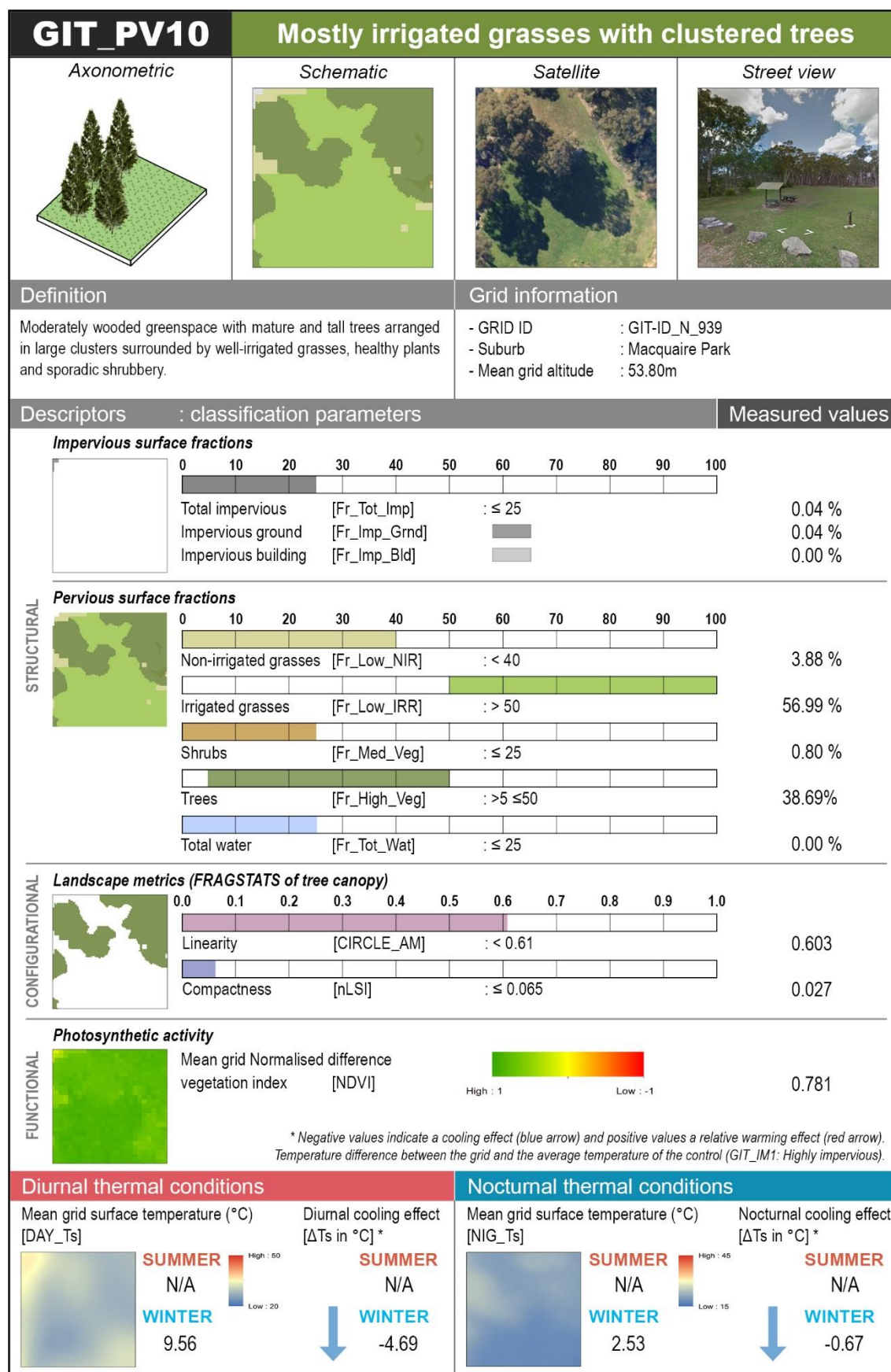
E23. Datasheet containing all variables and classification parameters calculated for the typology PV7.



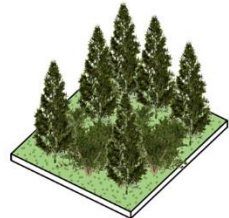





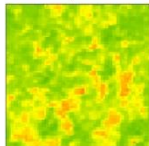


E24. Datasheet containing all variables and classification parameters calculated for the typology PV8.

GIT_PV9		Mostly non-irrigated grasses with clustered trees	
Axonometric		Schematic	
Satellite		Street view	
Definition		Grid information	
Moderately wooded greenspace with mature and tall trees arranged in large clusters surrounded by non-irrigated grasses, bare soils, and sporadic shrubbery.		- GRID ID : GRID_ID GIT-ID_N_1954 - Suburb : Macquarie Park - Mean grid altitude : 57.36m	
Descriptors : classification parameters		Measured values	
Impervious surface fractions			
0 10 20 30 40 50 60 70 80 90 100			
Total impervious [Fr_Tot_Imp] : ≤ 25		6.00 %	
Impervious ground [Fr_Imp_Grnd]		6.00 %	
Impervious building [Fr_Imp_Bld]		0.00 %	
Pervious surface fractions			
0 10 20 30 40 50 60 70 80 90 100			
Non-irrigated grasses [Fr_Low_NIR] : > 50		55.76 %	
Irrigated grasses [Fr_Low_IRR] : < 40		13.20 %	
Shrubs [Fr_Med_Veg] : ≤ 25		0.00 %	
Trees [Fr_High_Veg] : >5 ≤50		25.04 %	
Total water [Fr_Tot_Wat] : ≤ 25		0.00 %	
Landscape metrics (FRAGSTATS of tree canopy)			
0.0 0.1 0.2 0.3 0.4 0.5 0.6 0.7 0.8 0.9 1.0			
Linearity [CIRCLE_AM] : < 0.61		0.523	
Compactness [nLSI] : ≤ 0.065		0.027	
Photosynthetic activity			
Mean grid Normalised difference vegetation index [NDVI]		0.55	
High : 1 Low : -1			
* Negative values indicate a cooling effect (blue arrow) and positive values a relative warming effect (red arrow). Temperature difference between the grid and the average temperature of the control (GIT_IM1: Highly impervious).			
Diurnal thermal conditions		Nocturnal thermal conditions	
Mean grid surface temperature (°C) [DAY_Ts]		Mean grid surface temperature (°C) [NIG_Ts]	
SUMMER N/A		SUMMER N/A	
WINTER 12.84		WINTER 2.82	
High : 20 Low : 5		High : 15 Low : 0	
Diurnal cooling effect [ΔTs in °C] * SUMMER N/A WINTER -1.41		Nocturnal cooling effect [ΔTs in °C] * SUMMER N/A WINTER -0.38	

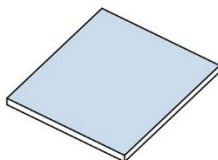

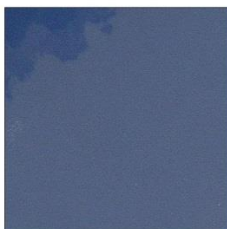
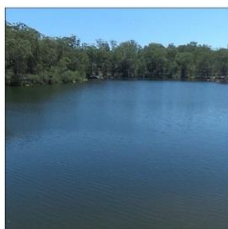
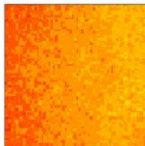


E25. Datasheet containing all variables and classification parameters calculated for the typology PV9.



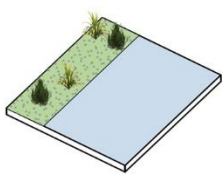



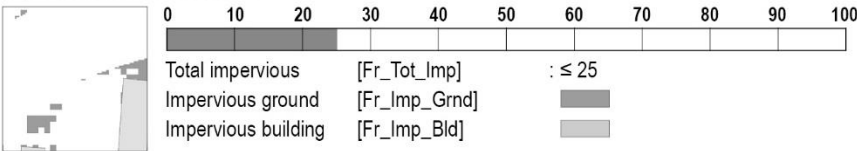
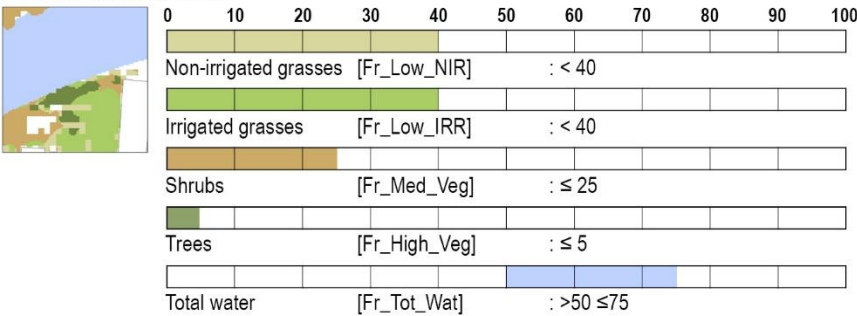
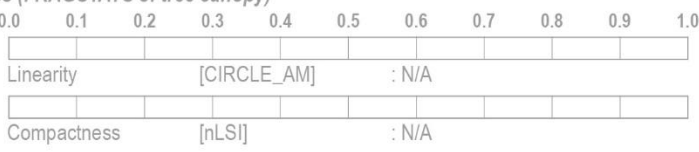
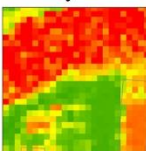
E26. Datasheet containing all variables and classification parameters calculated for the typology PV10.

GIT_PV11		Dense trees with shrubs and grasses	
Axonometric		Schematic	
			
Satellite		Street view	
			
Definition		Grid information	
Heavily wooded greenspace with mature, tall and dense trees, extensive shrubbery, and variety of grasses and bare soils.		- GRID ID : GIT-ID_P_6546 - Suburb : North Parramatta - Mean grid altitude : 36.30m	
Descriptors : classification parameters		Measured values	
STRUCTURAL	Impervious surface fractions		
			
	0 10 20 30 40 50 60 70 80 90 100		
	Total impervious [Fr_Tot_Imp] : ≤ 25		0.19 %
	Impervious ground [Fr_Imp_Grnd]		0.19 %
	Impervious building [Fr_Imp_Bld]		0.00 %
	Pervious surface fractions		
			
	0 10 20 30 40 50 60 70 80 90 100		
	Non-irrigated grasses [Fr_Low_NIR] : ≤ 25		1.54 %
Irrigated grasses [Fr_Low_IRR] : ≤ 25		2.36 %	
Shrubs [Fr_Med_Veg] : ≤ 75		5.46 %	
Trees [Fr_High_Veg] : ≤ 75		95.89 %	
Total water [Fr_Tot_Wat] : ≤ 25		0.00 %	
CONFIGURATIONAL	Landscape metrics (FRAGSTATS of tree canopy)		
	0.0 0.1 0.2 0.3 0.4 0.5 0.6 0.7 0.8 0.9 1.0		
	Linearity [CIRCLE_AM] : N/A		—
Compactness [nLSI] : N/A		—	
FUNCTIONAL	Photosynthetic activity		
	 Mean grid Normalised difference vegetation index [NDVI] High : 1 Low : -1 0.245		
* Negative values indicate a cooling effect (blue arrow) and positive values a relative warming effect (red arrow). Temperature difference between the grid and the average temperature of the control (GIT_IM1: Highly impervious).			
Diurnal thermal conditions		Nocturnal thermal conditions	
Mean grid surface temperature (°C) [DAY_Ts]		Mean grid surface temperature (°C) [NIG_Ts]	
 SUMMER 30.74 WINTER N/A High : 60 Low : 20		 SUMMER 23.02 WINTER N/A High : 45 Low : 15	
Diurnal cooling effect [ΔTs in °C] * SUMMER -7.39 WINTER N/A		Nocturnal cooling effect [ΔTs in °C] * SUMMER +0.83 WINTER N/A	

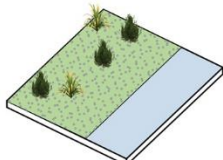





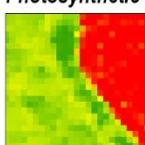




E27. Datasheet containing all variables and classification parameters calculated for the typology PV11.

GIT_AQ1		Water					
Axonometric		Schematic		Satellite		Street view	
							
Definition				Grid information			
Large open water bodies with few or no presence of vegetation.				<div>- GRID ID : GIT-ID_P_9933</div> <div>- Suburb : North Parramatta</div> <div>- Mean grid altitude : 28.25m</div>			
Descriptors : classification parameters						Measured values	
STRUCTURAL	Impervious surface fractions						
	<div><div></div><div>0102030405060708090100</div></div>						
	Total impervious		[Fr_Tot_Imp]		: ≤ 25		0.00 %
	Impervious ground		[Fr_Imp_Grnd]		<div></div>		0.00 %
	Impervious building		[Fr_Imp_Bld]		<div></div>		0.00 %
	Pervious surface fractions						
	<div><div></div><div>0102030405060708090100</div></div>						
	Non-irrigated grasses		[Fr_Low_NIR]		: ≤ 25		0.00 %
	Irrigated grasses		[Fr_Low_IRR]		: ≤ 25		0.00 %
	Shrubs		[Fr_Med_Veg]		: ≤ 25		0.00 %
Trees		[Fr_High_Veg]		: ≤ 25		0.00 %	
Total water		[Fr_Tot_Wat]		: > 75		100.0%	
CONFIGURATIONAL	Landscape metrics (FRAGSTATS of tree canopy)						
	<div><div></div><div>0.00.10.20.30.40.50.60.70.80.91.0</div></div>						
	Linearity		[CIRCLE_AM]		: N/A		—
Compactness		[nLSI]		: N/A		—	
FUNCTIONAL	Photosynthetic activity						
		Mean grid Normalised difference vegetation index [NDVI]					-0.192
<div>* Negative values indicate a cooling effect (blue arrow) and positive values a relative warming effect (red arrow).</div> <div>Temperature difference between the grid and the average temperature of the control (GIT_IM1: Highly impervious).</div>							
Diurnal thermal conditions				Nocturnal thermal conditions			
Mean grid surface temperature (°C) [DAY_Ts]		Diurnal cooling effect [ΔTs in °C] *		Mean grid surface temperature (°C) [NIG_Ts]		Nocturnal cooling effect [ΔTs in °C] *	
	<div>SUMMER25.36</div> <div>WINTERN/A</div>	<div>High : 50</div> <div>Low : 20</div>	<div>↓</div> <div>SUMMER-12.77</div> <div>WINTERN/A</div>		<div>SUMMER26.03</div> <div>WINTERN/A</div>	<div>High : 45</div> <div>Low : 15</div>	<div>↑</div> <div>SUMMER+3.84</div> <div>WINTERN/A</div>

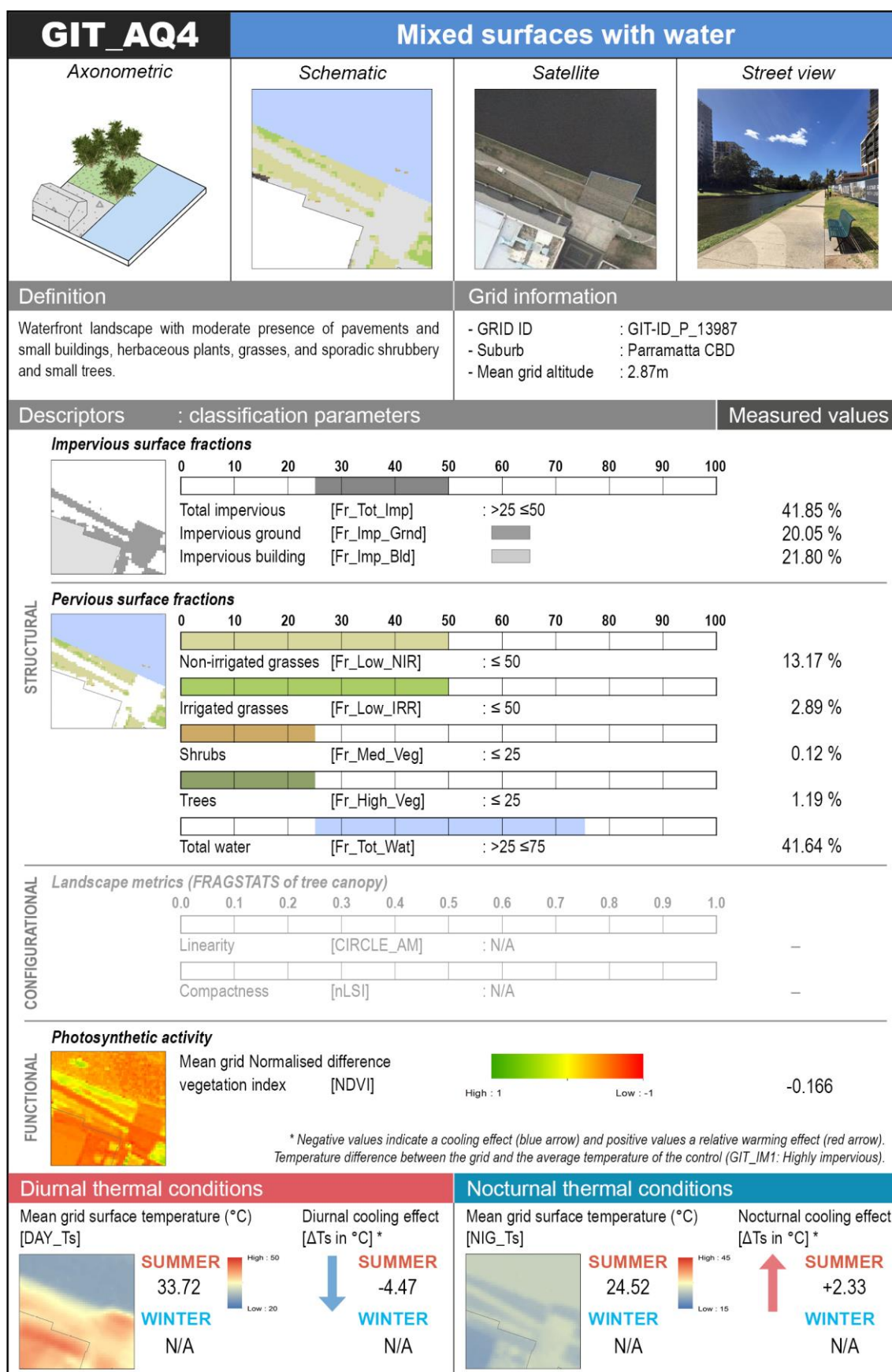
E28. Datasheet containing all variables and classification parameters calculated the typology AQ1.

GIT_AQ2		Mostly water with grasses	
Axonometric		Schematic	
			
Satellite		Street view	
			
Definition		Grid information	
Treeless waterfront landscape with minimal presence of herbaceous plants, grasses, reed-beds and shrubbery.		- GRID ID : GIT-ID_S_6923 - Suburb : Campsie - Mean grid altitude : 2.05m	
Descriptors : classification parameters		Measured values	
STRUCTURAL			
Impervious surface fractions			
			
Total impervious [Fr_Tot_Imp] : ≤ 25 14.93 %			
Impervious ground [Fr_Imp_Grnd] 5.09 %			
Impervious building [Fr_Imp_Bld] 9.84 %			
Pervious surface fractions			
			
Non-irrigated grasses [Fr_Low_NIR] : < 40 4.80 %			
Irrigated grasses [Fr_Low_IRR] : < 40 14.13 %			
Shrubs [Fr_Med_Veg] : ≤ 25 11.18 %			
Trees [Fr_High_Veg] : ≤ 5 4.96 %			
Total water [Fr_Tot_Wat] : >50 ≤75 51.34 %			
CONFIGURATIONAL			
Landscape metrics (FRAGSTATS of tree canopy)			
			
Linearity [CIRCLE_AM] : N/A —			
Compactness [nLSI] : N/A —			
FUNCTIONAL			
Photosynthetic activity			
 Mean grid Normalised difference vegetation index [NDVI] 0.161			
* Negative values indicate a cooling effect (blue arrow) and positive values a relative warming effect (red arrow). Temperature difference between the grid and the average temperature of the control (GIT_IM1: Highly impervious).			
Diurnal thermal conditions		Nocturnal thermal conditions	
Mean grid surface temperature (°C) [DAY_Ts]		Mean grid surface temperature (°C) [NIG_Ts]	
SUMMER N/A		SUMMER N/A	
WINTER 8.63		WINTER 2.82	
Diurnal cooling effect [ΔTs in °C] *		Nocturnal cooling effect [ΔTs in °C] *	
SUMMER N/A		SUMMER N/A	
WINTER -5.62		WINTER -0.38	

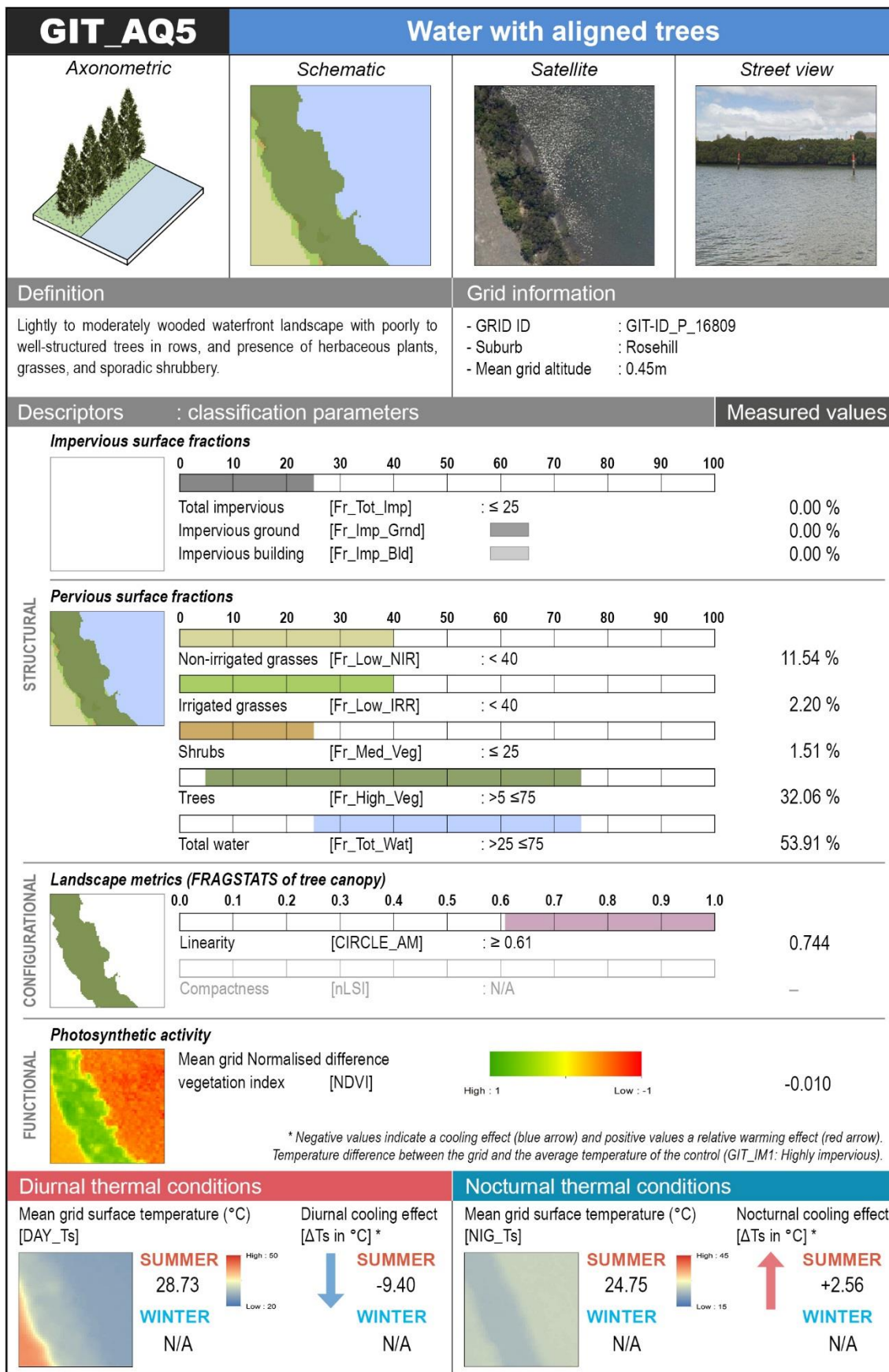
E29. Datasheet containing all variables and classification parameters calculated the typology AQ2.

GIT_AQ3		Mostly grasses with water																																																																			
Axonometric		Schematic																																																																			
																																																																					
Satellite		Street view																																																																			
																																																																					
Definition		Grid information																																																																			
Treeless waterfront landscape with moderate presence of tall herbaceous plants, grasses, reed-beds and mature shrubbery.		- GRID ID : GIT-ID_S_7843 - Suburb : Canterbury - Mean grid altitude : 4.90m																																																																			
Descriptors : classification parameters		Measured values																																																																			
Impervious surface fractions																																																																					
																																																																					
<table><tr><td>0</td><td>10</td><td>20</td><td>30</td><td>40</td><td>50</td><td>60</td><td>70</td><td>80</td><td>90</td><td>100</td></tr><tr><td colspan="11">Total impervious [Fr_Tot_Imp] : ≤ 25</td></tr><tr><td colspan="11">Impervious ground [Fr_Imp_Grnd] : 1.57 %</td></tr><tr><td colspan="11">Impervious building [Fr_Imp_Bld] : 0.00 %</td></tr></table>				0	10	20	30	40	50	60	70	80	90	100	Total impervious [Fr_Tot_Imp] : ≤ 25											Impervious ground [Fr_Imp_Grnd] : 1.57 %											Impervious building [Fr_Imp_Bld] : 0.00 %																																
0	10	20	30	40	50	60	70	80	90	100																																																											
Total impervious [Fr_Tot_Imp] : ≤ 25																																																																					
Impervious ground [Fr_Imp_Grnd] : 1.57 %																																																																					
Impervious building [Fr_Imp_Bld] : 0.00 %																																																																					
Pervious surface fractions																																																																					
																																																																					
<table><tr><td>0</td><td>10</td><td>20</td><td>30</td><td>40</td><td>50</td><td>60</td><td>70</td><td>80</td><td>90</td><td>100</td></tr><tr><td colspan="11">Non-irrigated grasses [Fr_Low_NIR] : < 60</td></tr><tr><td colspan="11">Irrigated grasses [Fr_Low_IRR] : < 60</td></tr><tr><td colspan="11">Shrubs [Fr_Med_Veg] : ≤ 25</td></tr><tr><td colspan="11">Trees [Fr_High_Veg] : ≤ 5</td></tr><tr><td colspan="11">Total water [Fr_Tot_Wat] : >25 ≤50</td></tr></table>				0	10	20	30	40	50	60	70	80	90	100	Non-irrigated grasses [Fr_Low_NIR] : < 60											Irrigated grasses [Fr_Low_IRR] : < 60											Shrubs [Fr_Med_Veg] : ≤ 25											Trees [Fr_High_Veg] : ≤ 5											Total water [Fr_Tot_Wat] : >25 ≤50										
0	10	20	30	40	50	60	70	80	90	100																																																											
Non-irrigated grasses [Fr_Low_NIR] : < 60																																																																					
Irrigated grasses [Fr_Low_IRR] : < 60																																																																					
Shrubs [Fr_Med_Veg] : ≤ 25																																																																					
Trees [Fr_High_Veg] : ≤ 5																																																																					
Total water [Fr_Tot_Wat] : >25 ≤50																																																																					
Landscape metrics (FRAGSTATS of tree canopy)																																																																					
<table><tr><td>0.0</td><td>0.1</td><td>0.2</td><td>0.3</td><td>0.4</td><td>0.5</td><td>0.6</td><td>0.7</td><td>0.8</td><td>0.9</td><td>1.0</td></tr><tr><td colspan="11">Linearity [CIRCLE_AM] : N/A</td></tr><tr><td colspan="11">Compactness [nLSI] : N/A</td></tr></table>				0.0	0.1	0.2	0.3	0.4	0.5	0.6	0.7	0.8	0.9	1.0	Linearity [CIRCLE_AM] : N/A											Compactness [nLSI] : N/A																																											
0.0	0.1	0.2	0.3	0.4	0.5	0.6	0.7	0.8	0.9	1.0																																																											
Linearity [CIRCLE_AM] : N/A																																																																					
Compactness [nLSI] : N/A																																																																					
Photosynthetic activity																																																																					
																																																																					
<table><tr><td>Mean grid Normalised difference vegetation index [NDVI]</td><td>High : 1</td><td>Low : -1</td></tr></table>				Mean grid Normalised difference vegetation index [NDVI]	High : 1	Low : -1																																																															
Mean grid Normalised difference vegetation index [NDVI]	High : 1	Low : -1																																																																			
0.209																																																																					
* Negative values indicate a cooling effect (blue arrow) and positive values a relative warming effect (red arrow). Temperature difference between the grid and the average temperature of the control (GIT_IM1: Highly impervious).																																																																					
Diurnal thermal conditions		Nocturnal thermal conditions																																																																			
Mean grid surface temperature (°C) [DAY_Ts]		Mean grid surface temperature (°C) [NIG_Ts]																																																																			
																																																																					
<table><tr><td>SUMMER</td><td>High : 50</td></tr><tr><td>N/A</td><td>Low : 20</td></tr><tr><td>WINTER</td><td>10.88</td></tr></table>		SUMMER	High : 50	N/A	Low : 20	WINTER	10.88	<table><tr><td>SUMMER</td><td>High : 45</td></tr><tr><td>N/A</td><td>Low : 15</td></tr><tr><td>WINTER</td><td>2.40</td></tr></table>		SUMMER	High : 45	N/A	Low : 15	WINTER	2.40																																																						
SUMMER	High : 50																																																																				
N/A	Low : 20																																																																				
WINTER	10.88																																																																				
SUMMER	High : 45																																																																				
N/A	Low : 15																																																																				
WINTER	2.40																																																																				
Diurnal cooling effect [ΔTs in °C] *		Nocturnal cooling effect [ΔTs in °C] *																																																																			
																																																																					
<table><tr><td>SUMMER</td><td>N/A</td></tr><tr><td>WINTER</td><td>-3.37</td></tr></table>		SUMMER	N/A	WINTER	-3.37	<table><tr><td>SUMMER</td><td>N/A</td></tr><tr><td>WINTER</td><td>-0.80</td></tr></table>		SUMMER	N/A	WINTER	-0.80																																																										
SUMMER	N/A																																																																				
WINTER	-3.37																																																																				
SUMMER	N/A																																																																				
WINTER	-0.80																																																																				

E30. Datasheet containing all variables and classification parameters calculated the typology AQ3.



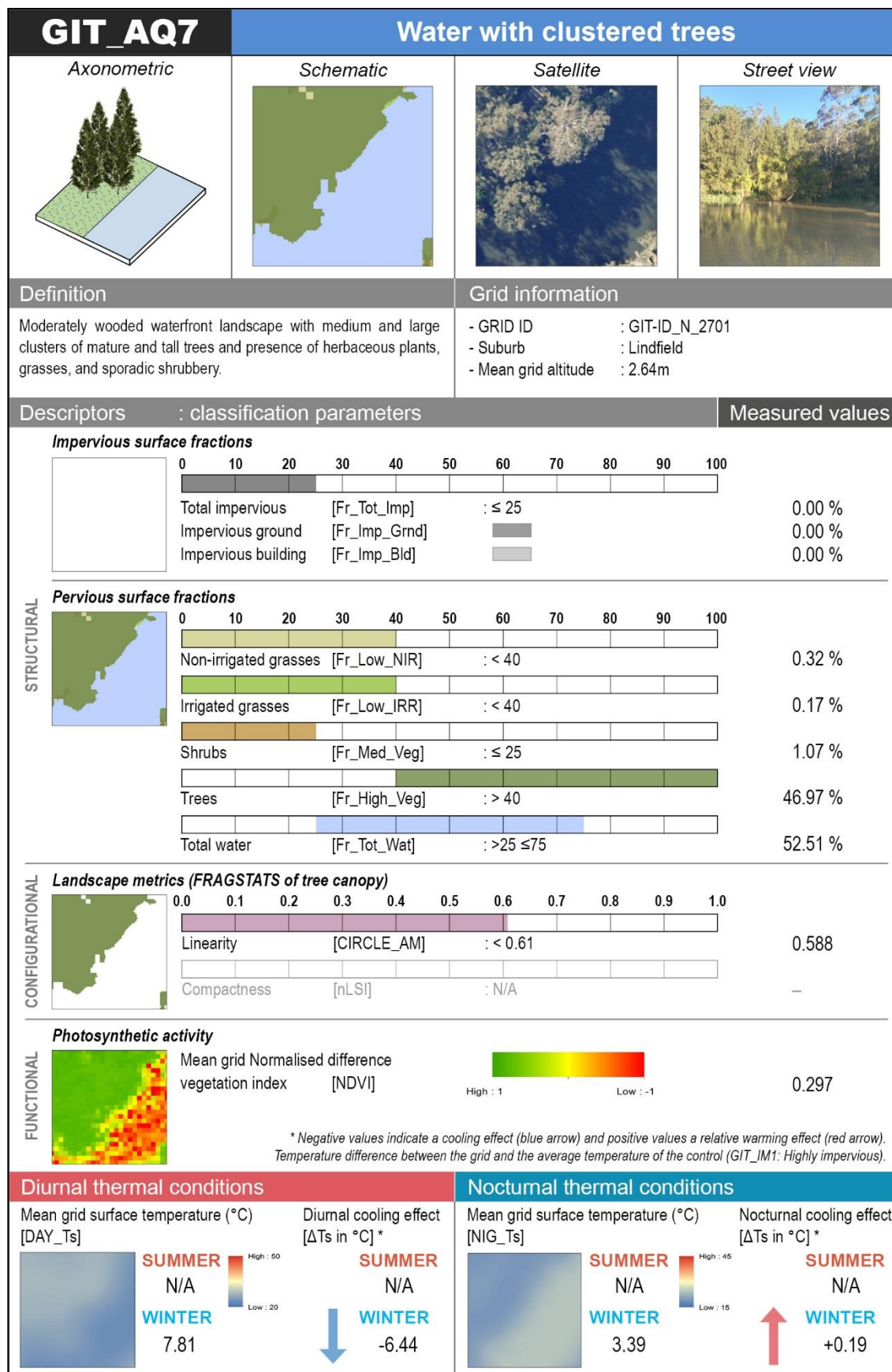
E31. Datasheet containing all variables and classification parameters calculated the typology AQ4.



E32. Datasheet containing all variables and classification parameters calculated the typology AQ5.

GIT_AQ6		Water with scattered trees	
Axonometric		Schematic	
Satellite		Street view	
Definition		Grid information	
Lightly wooded waterfront landscape with individual or few dispersed trees and moderate presence of herbaceous plants, grasses, and sporadic shrubbery.		- GRID ID : GIT-ID_P_12646 - Suburb : North Parramatta - Mean grid altitude : 4.67m	
Descriptors : classification parameters		Measured values	
Impervious surface fractions			
<div><div></div><div>0102030405060708090100</div><div>Total impervious [Fr_Tot_Imp] : ≤ 255.04 %</div><div>Impervious ground [Fr_Imp_Grnd] : 5.04 %</div><div>Impervious building [Fr_Imp_Bld] : 0.00 %</div></div>			
STRUCTURAL	Pervious surface fractions		
	<div><div></div><div>0102030405060708090100</div><div>Non-irrigated grasses [Fr_Low_NIR] : < 401.82 %</div><div>Irrigated grasses [Fr_Low_IRR] : < 409.09 %</div><div>Shrubs [Fr_Med_Veg] : ≤ 250.00 %</div><div>Trees [Fr_High_Veg] : >5 ≤4012.18 %</div><div>Total water [Fr_Tot_Wat] : >25 ≤7571.87 %</div></div>		
	Landscape metrics (FRAGSTATS of tree canopy)		
	<div><div></div><div>0.00.10.20.30.40.50.60.70.80.91.0</div><div>Linearity [CIRCLE_AM] : < 0.610.497</div><div>Compactness [nLSI] : N/A—</div></div>		
	Photosynthetic activity		
	<div><div></div><div>Mean grid Normalised difference vegetation index [NDVI]</div><div>High : 1Low : -1</div><div>-0.450</div></div>		
* Negative values indicate a cooling effect (blue arrow) and positive values a relative warming effect (red arrow). Temperature difference between the grid and the average temperature of the control (GIT_IM1: Highly impervious).			
Diurnal thermal conditions		Nocturnal thermal conditions	
Mean grid surface temperature (°C) [DAY_Ts]		Mean grid surface temperature (°C) [NIG_Ts]	
Diurnal cooling effect [ΔTs in °C] *		Nocturnal cooling effect [ΔTs in °C] *	
<div><div></div><div>SUMMER 26.61</div><div>WINTER N/A</div><div>High : 50Low : 20</div></div>		<div><div></div><div>SUMMER 25.13</div><div>WINTER N/A</div><div>High : 45Low : 15</div></div>	
<div><div></div><div>SUMMER -11.52</div><div>WINTER N/A</div></div>		<div><div></div><div>SUMMER +2.94</div><div>WINTER N/A</div></div>	

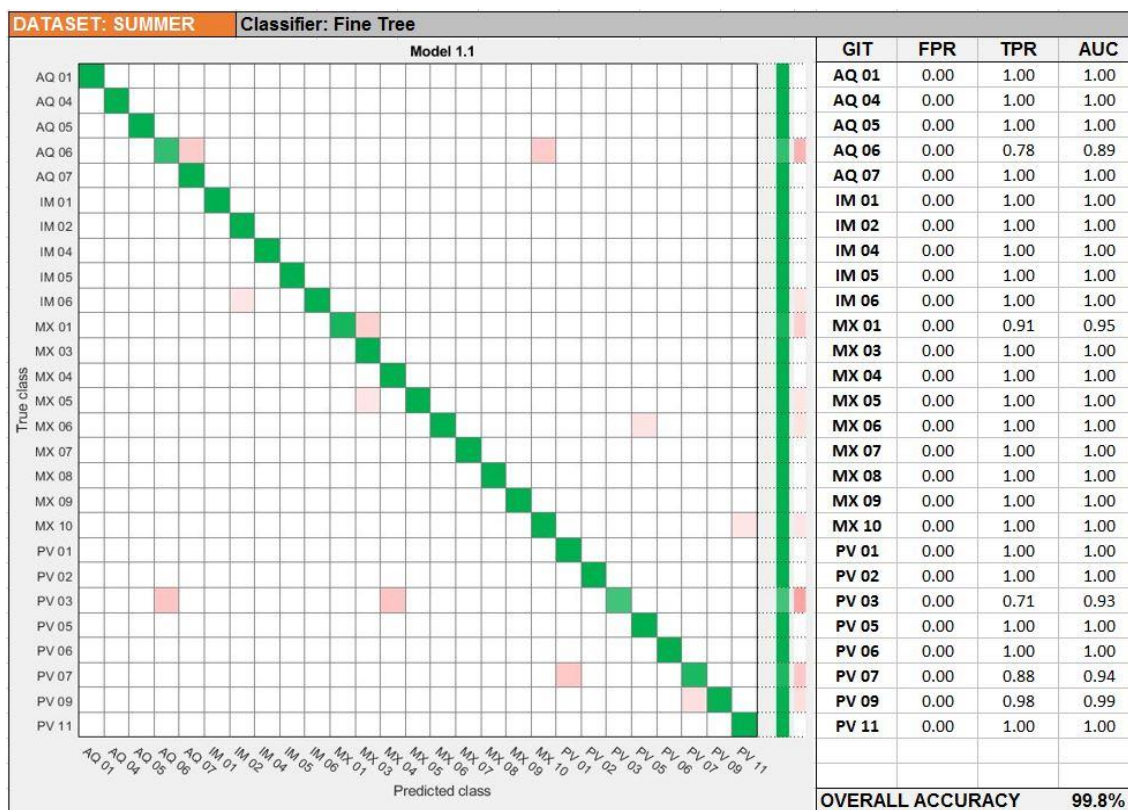
E33. Datasheet containing all variables and classification parameters calculated the typology AQ6.



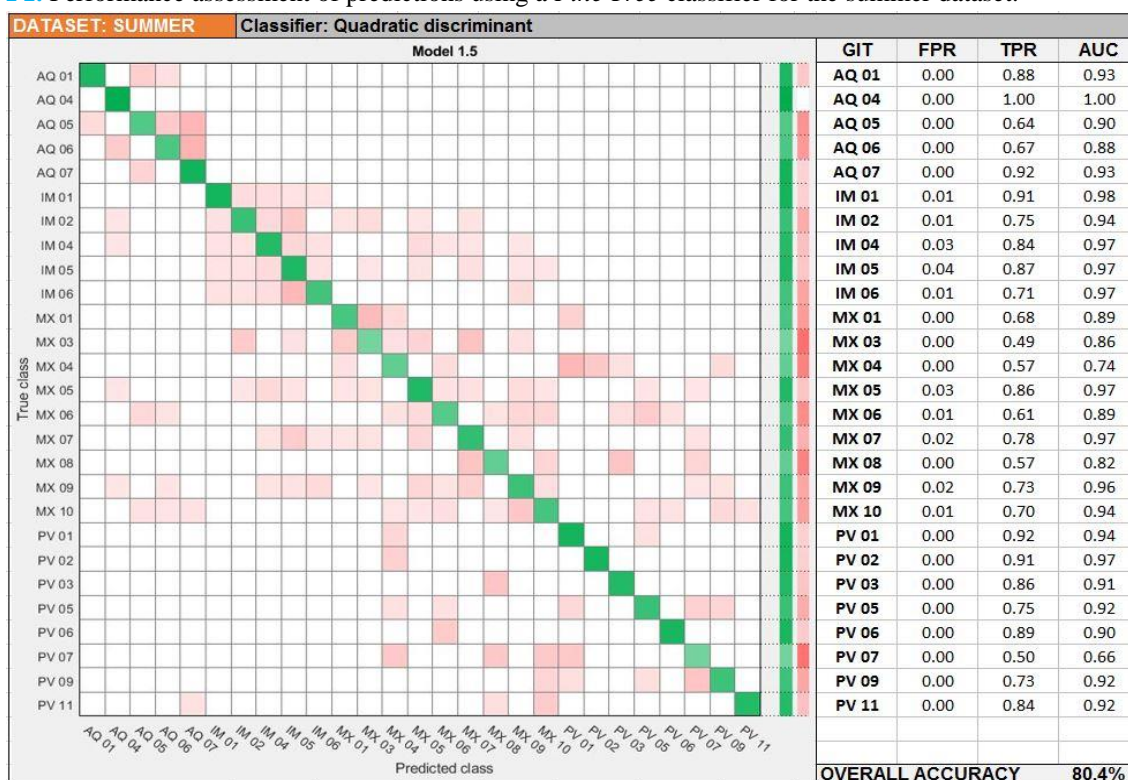
E34. Datasheet containing all variables and classification parameters calculated the typology AQ7.

Appendix F –

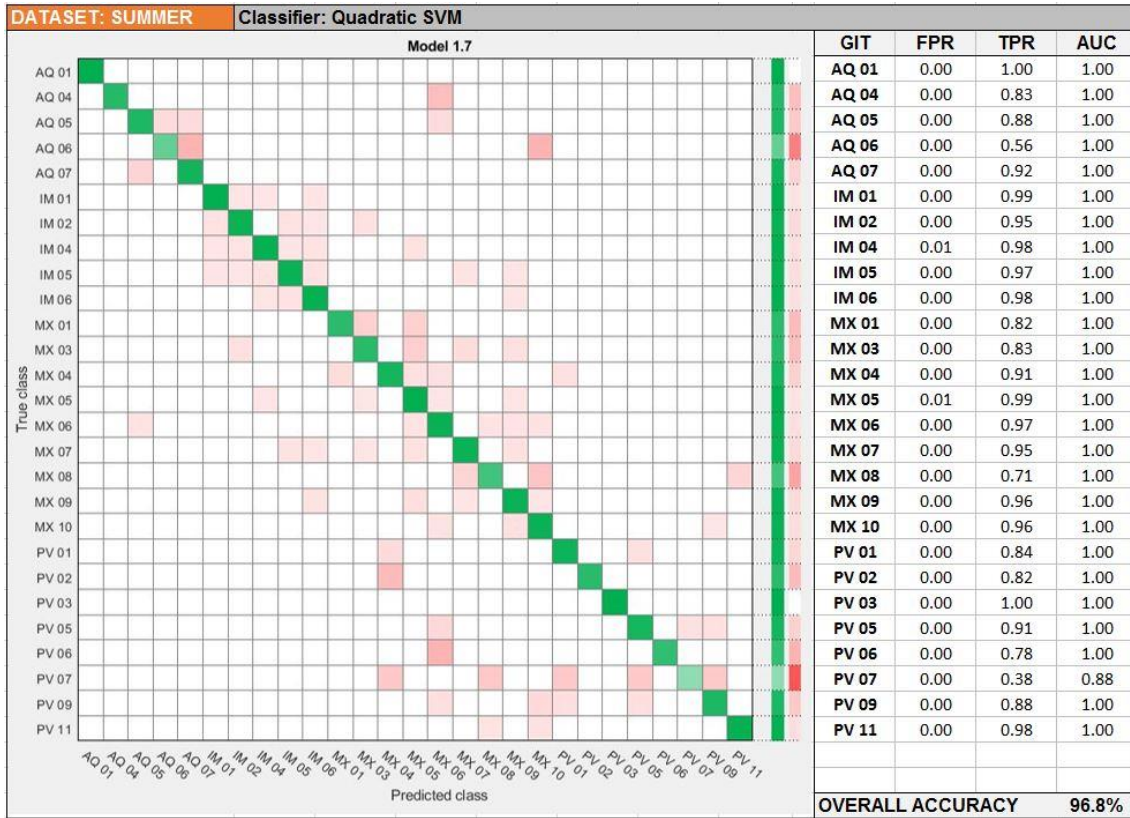
Performance assessment of selected machine learning classifiers



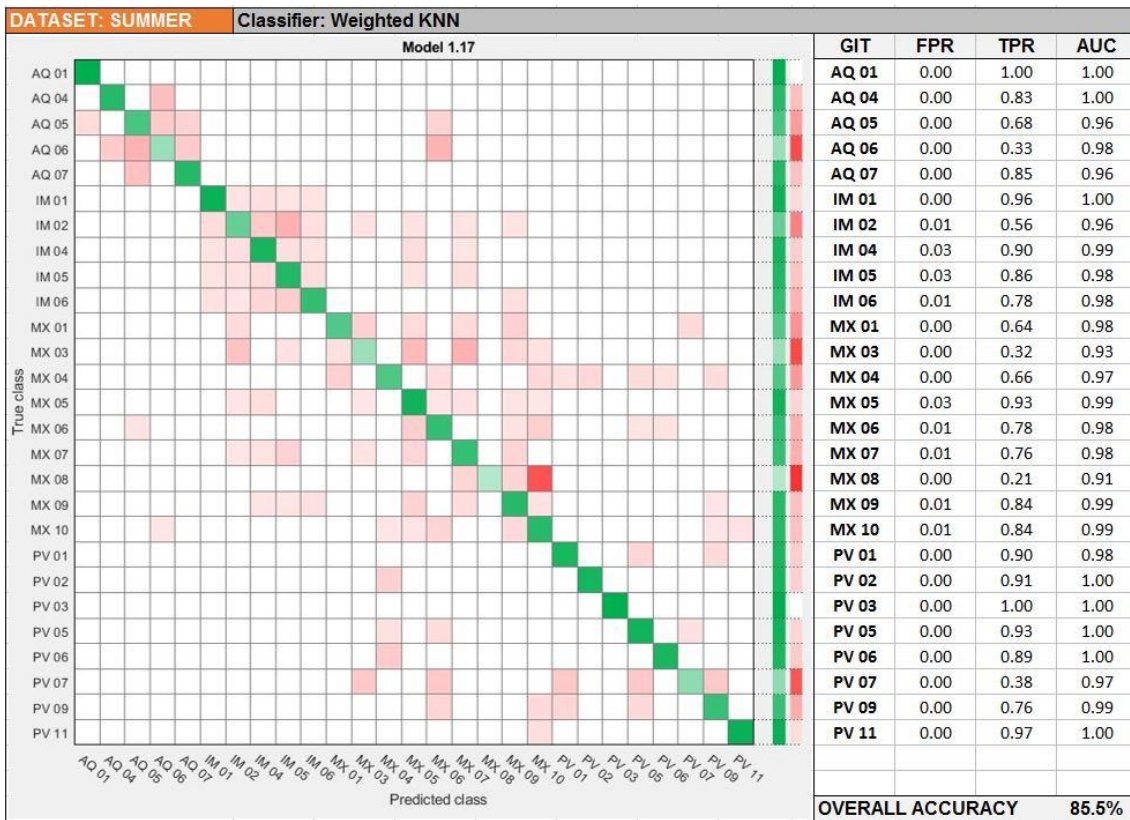
F1. Performance assessment of predictions using a *Fine Tree* classifier for the summer dataset.



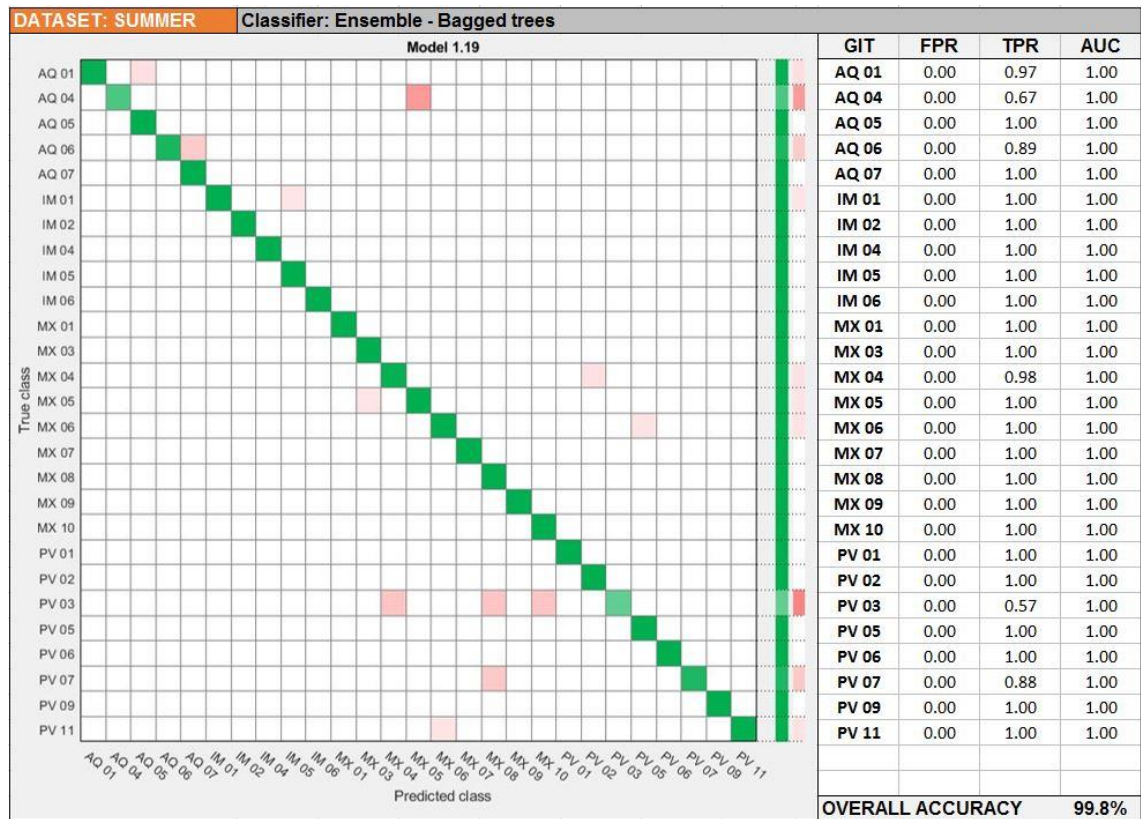
F2. Performance assessment of predictions using a *Quadratic discriminant* classifier for the summer dataset.



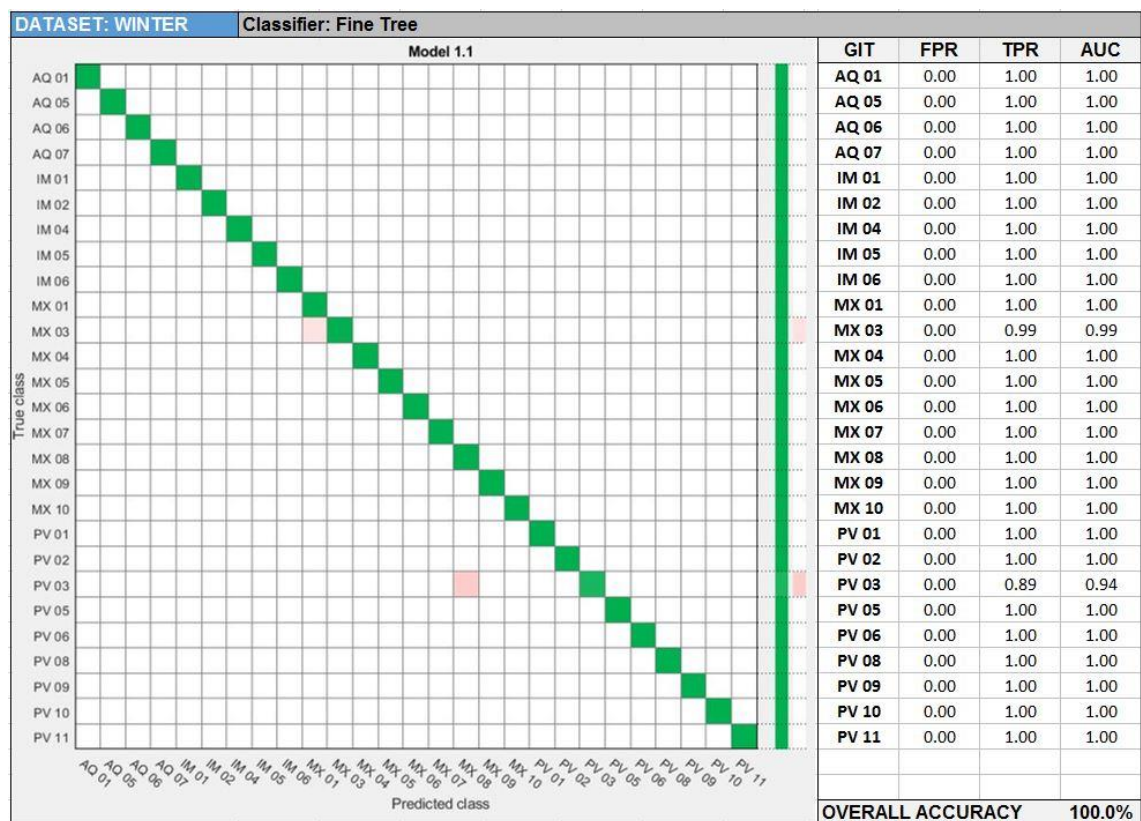
F3. Performance assessment of predictions using a *Quadratic SVM* classifier for the summer dataset.



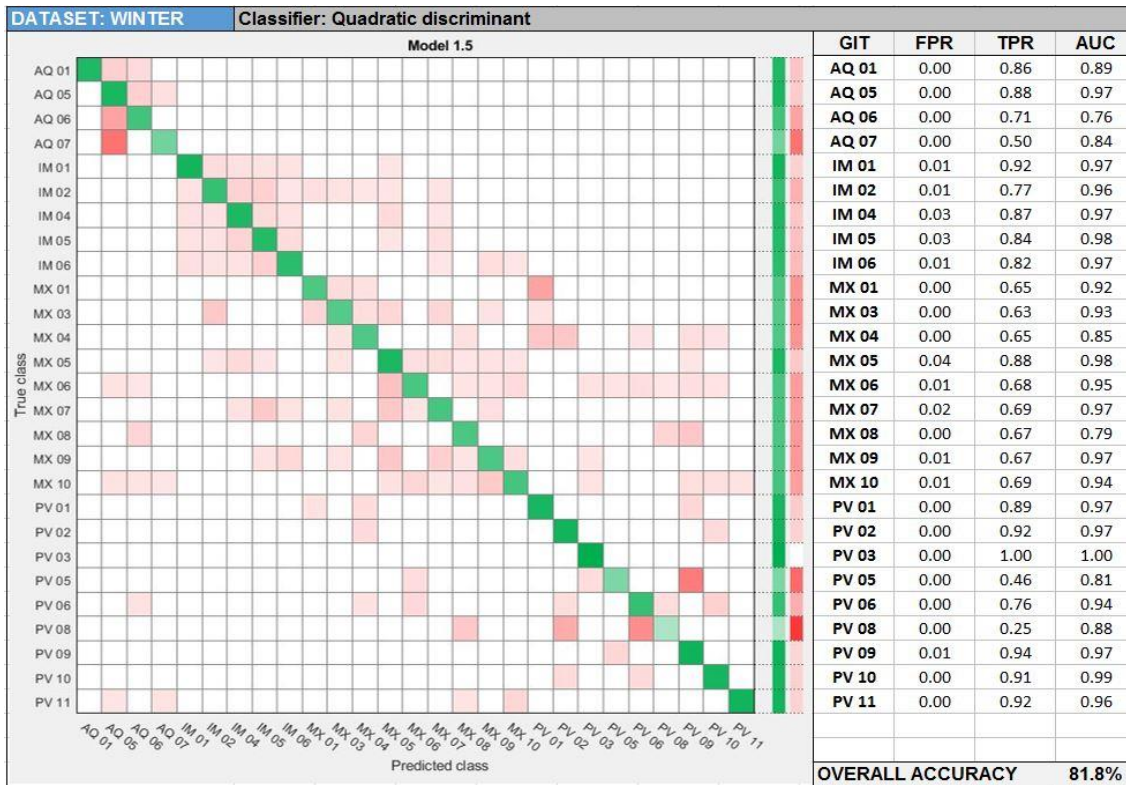
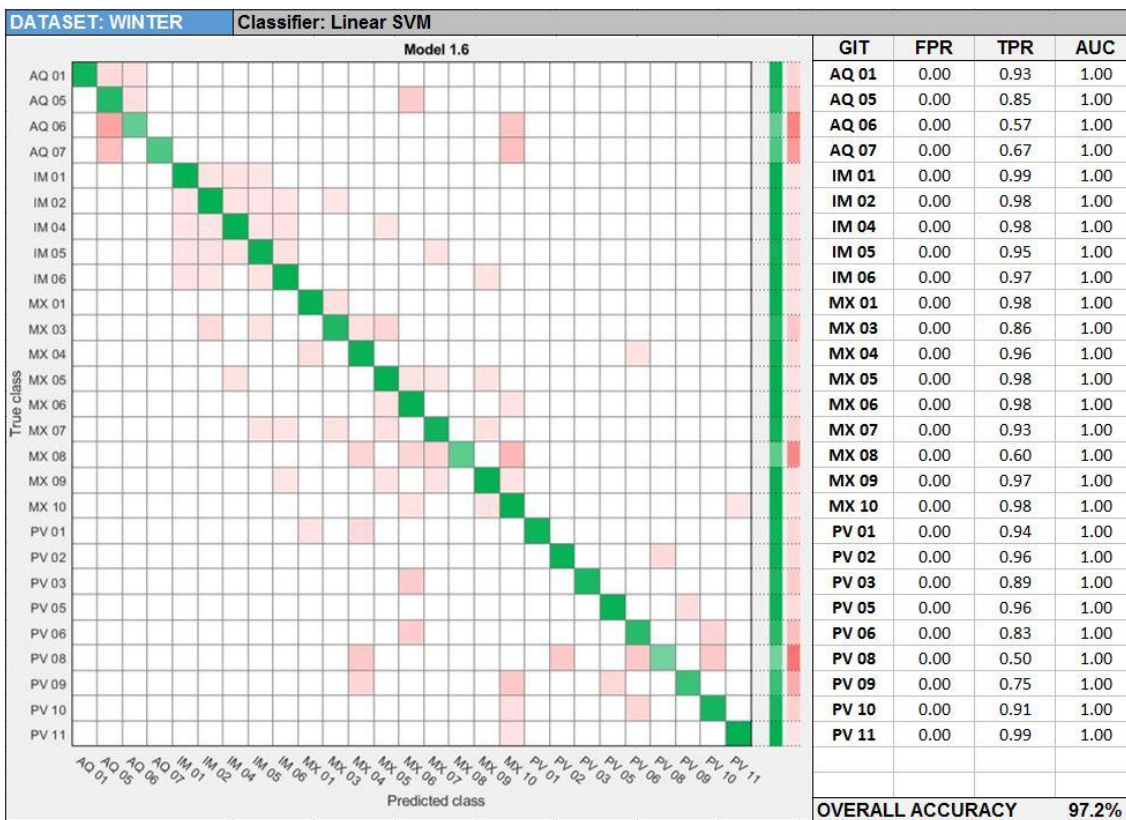
F4. Performance assessment of predictions using a *Weighted KNN* classifier for the summer dataset.

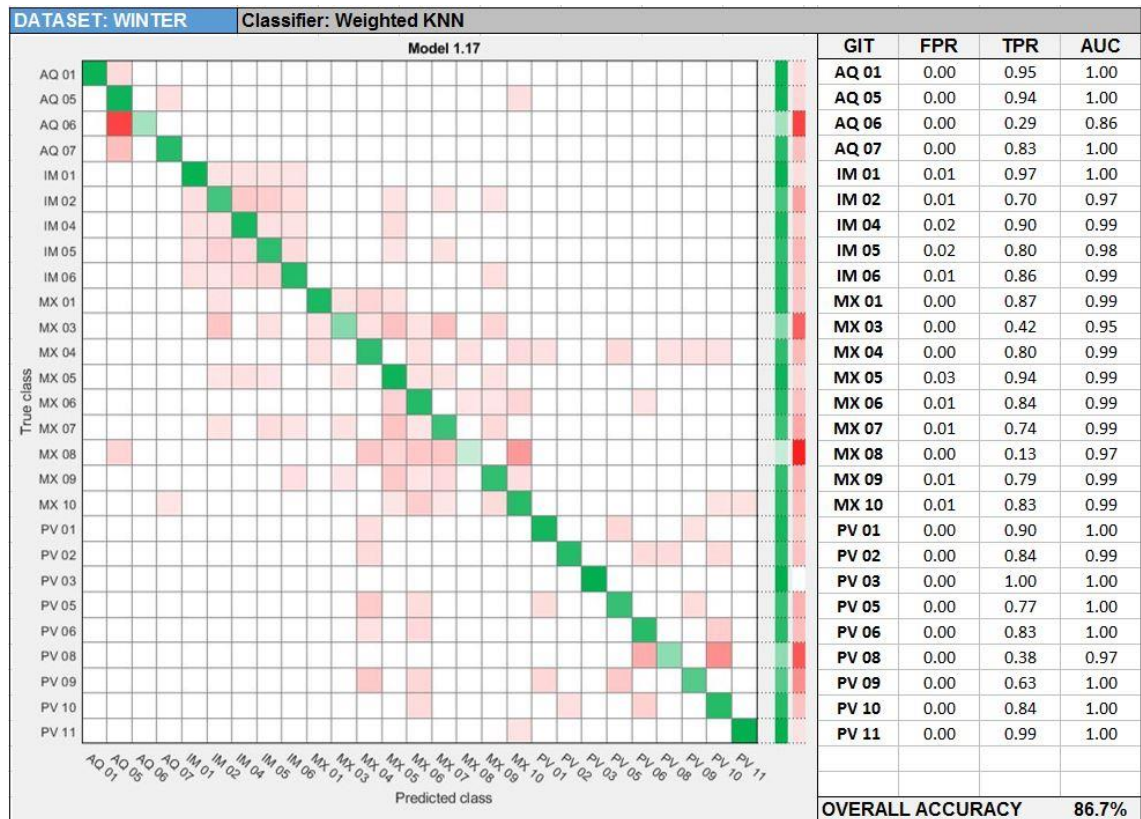


F5. Performance assessment of predictions using an *Ensemble – Bagged trees* classifier for the summer dataset.

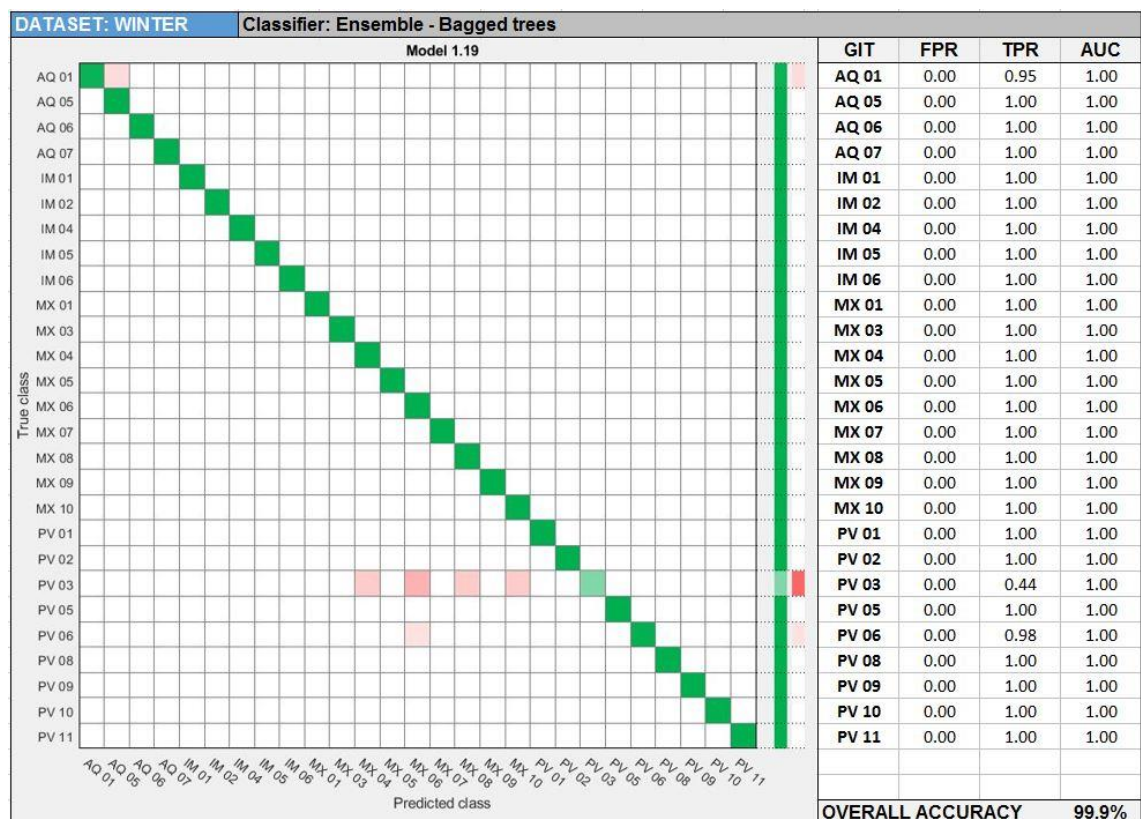


F6. Performance assessment of predictions using a *Fine Tree* classifier for the winter dataset.

F7. Performance assessment of predictions using a *Quadratic discriminant* classifier for the winter dataset.F8. Performance assessment of predictions using a *Linear SVM* classifier for the winter dataset.



F9. Performance assessment of predictions using a *Weighted KNN* classifier for the winter dataset.



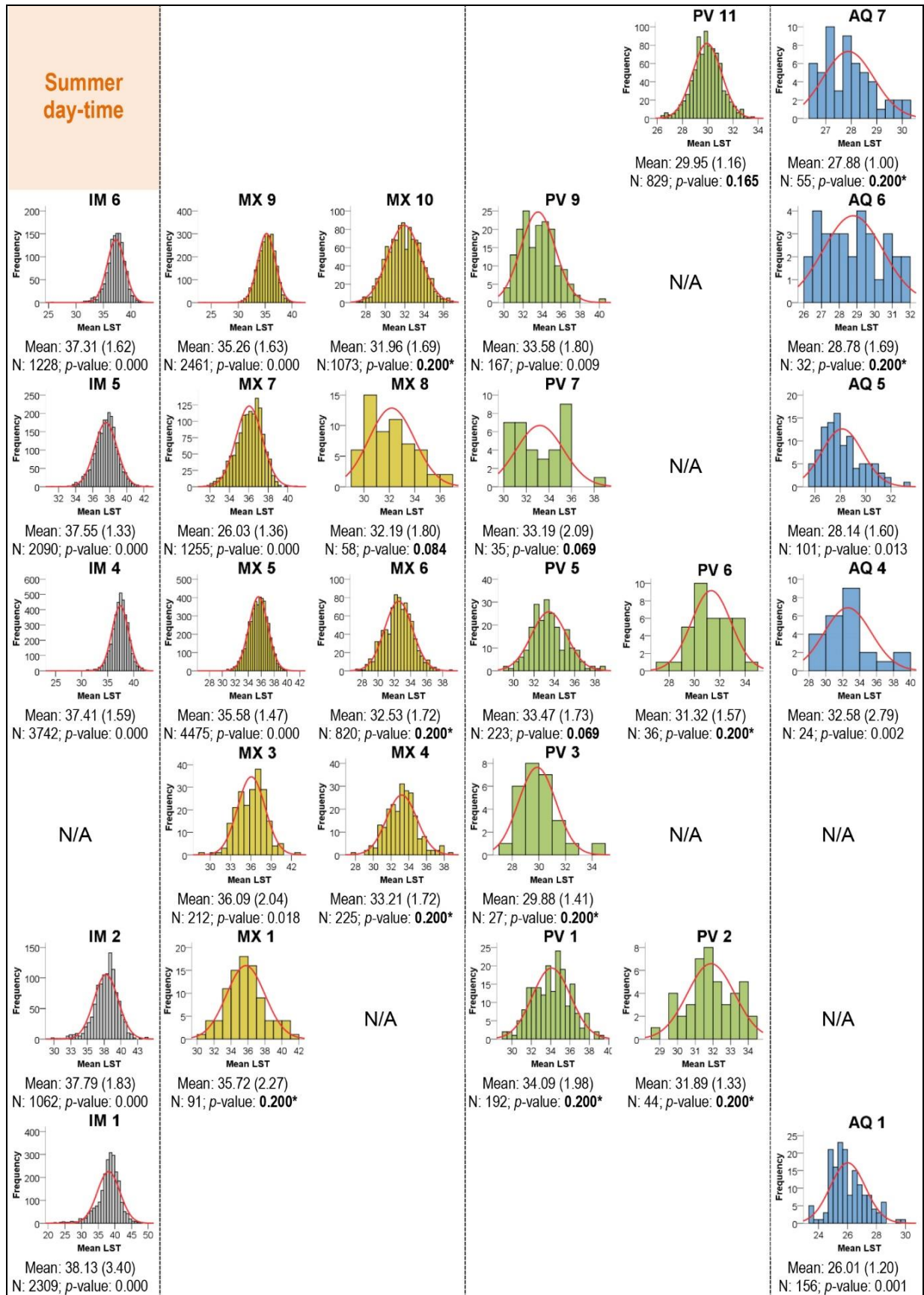
F10. Performance assessment of predictions using an *Ensemble – Bagged trees* classifier for the winter dataset.

Appendix G – Summary statistics and results of normality tests and cluster analysis of GIT classifications

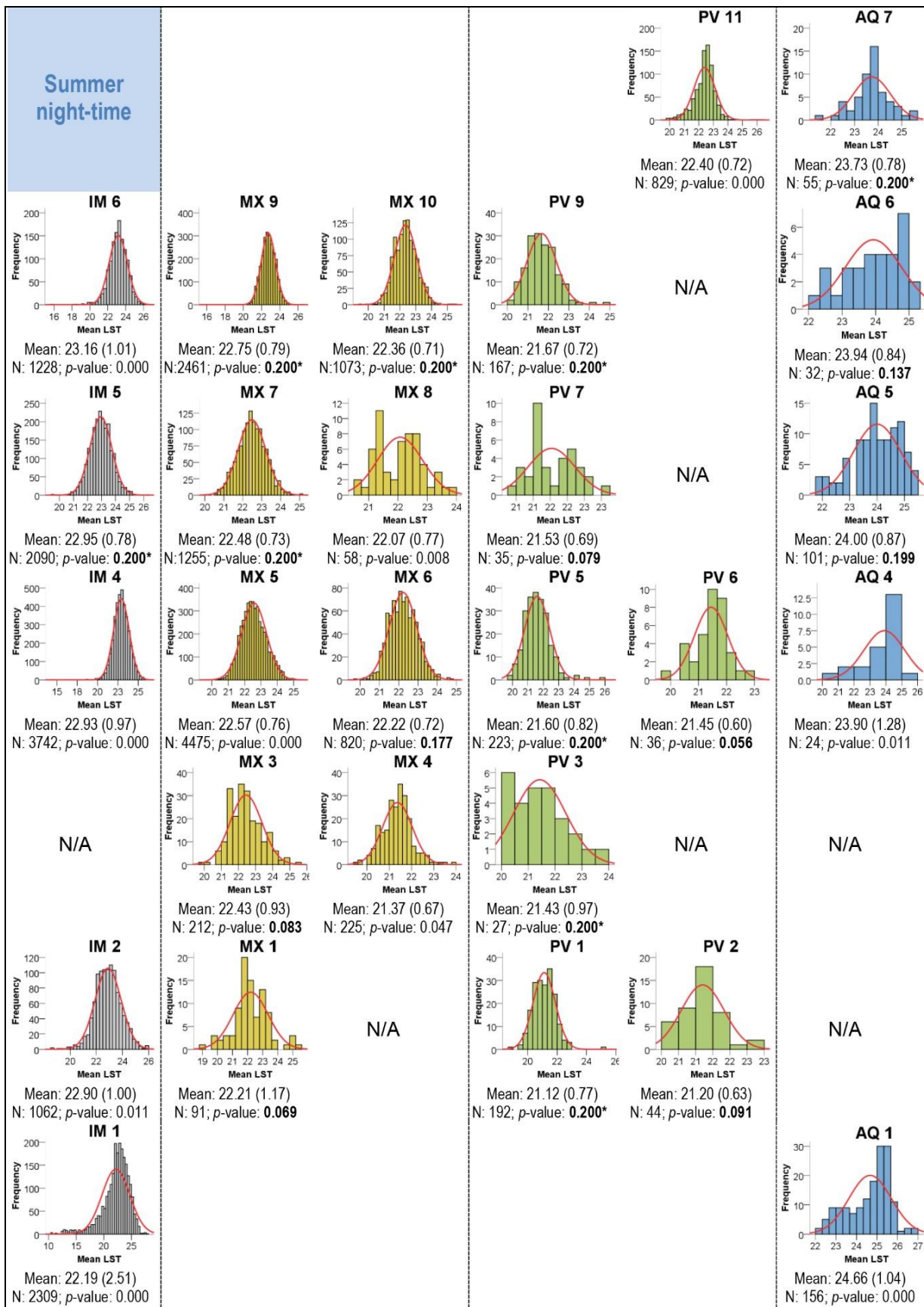
G1 Summary statistics of mean LSTs for each GIT in summer (N=sample size; Std. Dev. = standard deviations; Std. Error = Standard error; Min. = Minimum value; Max. Maximum value).

GIT	N	Summer - Daytime					Summer - Night-time				
		Mean	Std. Dev.	Std. Error	Min.	Max.	Mean	Std. Dev.	Std. Error	Min.	Max.
IM 1	2309	38.13	3.40	0.07	21.22	49.36	22.19	2.51	0.05	10.48	27.69
IM 2	1062	37.79	1.83	0.06	29.74	44.08	22.90	1.00	0.03	18.55	25.96
IM 4	3742	37.41	1.59	0.03	24.23	42.56	22.93	0.97	0.02	14.31	26.24
IM 5	2090	37.55	1.33	0.03	31.25	42.41	22.95	0.78	0.02	19.54	26.36
IM 6	1228	37.31	1.62	0.05	25.61	43.01	23.16	1.01	0.03	15.73	26.30
MX 1	91	35.72	2.27	0.24	30.21	41.35	22.21	1.17	0.12	18.84	25.55
MX 3	212	36.09	2.04	0.14	29.08	43.12	22.43	0.93	0.06	19.75	25.36
MX 4	225	33.21	1.72	0.11	27.85	38.51	21.37	0.67	0.04	19.60	23.85
MX 5	4475	35.58	1.47	0.02	27.31	41.96	22.57	0.76	0.01	19.60	25.46
MX 6	820	32.53	1.72	0.06	27.41	38.89	22.22	0.72	0.03	19.72	24.76
MX 7	1255	36.03	1.36	0.04	31.42	40.82	22.48	0.73	0.02	20.09	25.15
MX 8	58	32.19	1.80	0.24	29.80	36.70	22.07	0.77	0.10	20.59	23.88
MX 9	2461	35.26	1.63	0.03	23.91	41.33	22.75	0.79	0.02	15.80	26.45
MX 10	1073	31.96	1.69	0.05	27.24	36.90	22.36	0.71	0.02	19.49	25.50
PV 1	192	34.09	1.98	0.14	29.22	39.04	21.12	0.77	0.06	18.84	25.30
PV 2	44	31.89	1.33	0.20	28.99	34.13	21.20	0.63	0.09	20.02	23.00
PV 3	27	29.88	1.41	0.27	27.43	34.32	21.43	0.97	0.19	20.08	23.86
PV 5	223	33.47	1.73	0.12	29.08	38.64	21.60	0.82	0.05	19.75	25.77
PV 6	36	31.32	1.57	0.26	27.69	34.05	21.45	0.60	0.10	19.70	22.74
PV 7	35	33.19	2.09	0.35	30.19	38.35	21.53	0.69	0.12	20.37	23.01
PV 9	167	33.58	1.80	0.14	30.28	40.09	21.67	0.72	0.06	20.18	24.73
PV 11	829	29.95	1.16	0.04	26.44	33.56	22.40	0.72	0.03	19.79	26.34
AQ 1	156	26.01	1.20	0.10	23.39	29.80	24.66	1.04	0.08	22.23	26.88
AQ 4	24	32.58	2.79	0.57	28.73	39.02	23.90	1.28	0.26	20.34	25.33
AQ 5	101	28.14	1.60	0.16	25.53	33.19	24.00	0.87	0.09	21.80	25.35
AQ 6	32	28.78	1.69	0.30	26.10	31.60	23.94	0.84	0.15	22.21	25.13
AQ 7	55	27.88	1.00	0.14	26.39	30.26	23.73	0.78	0.11	21.40	25.60
Total	23022	35.79	2.95	0.02	21.22	49.36	22.64	1.20	0.01	10.48	27.69

G2 Frequency distribution of mean diurnal LSTs in summer for each GIT with a fitted normal distribution and results of the Kolmogorov-Smirnov test (N=sample size; standard deviations are in parenthesis, p -values <0.05 indicates a non-normal distribution, * This is a lower bound of the true significance).



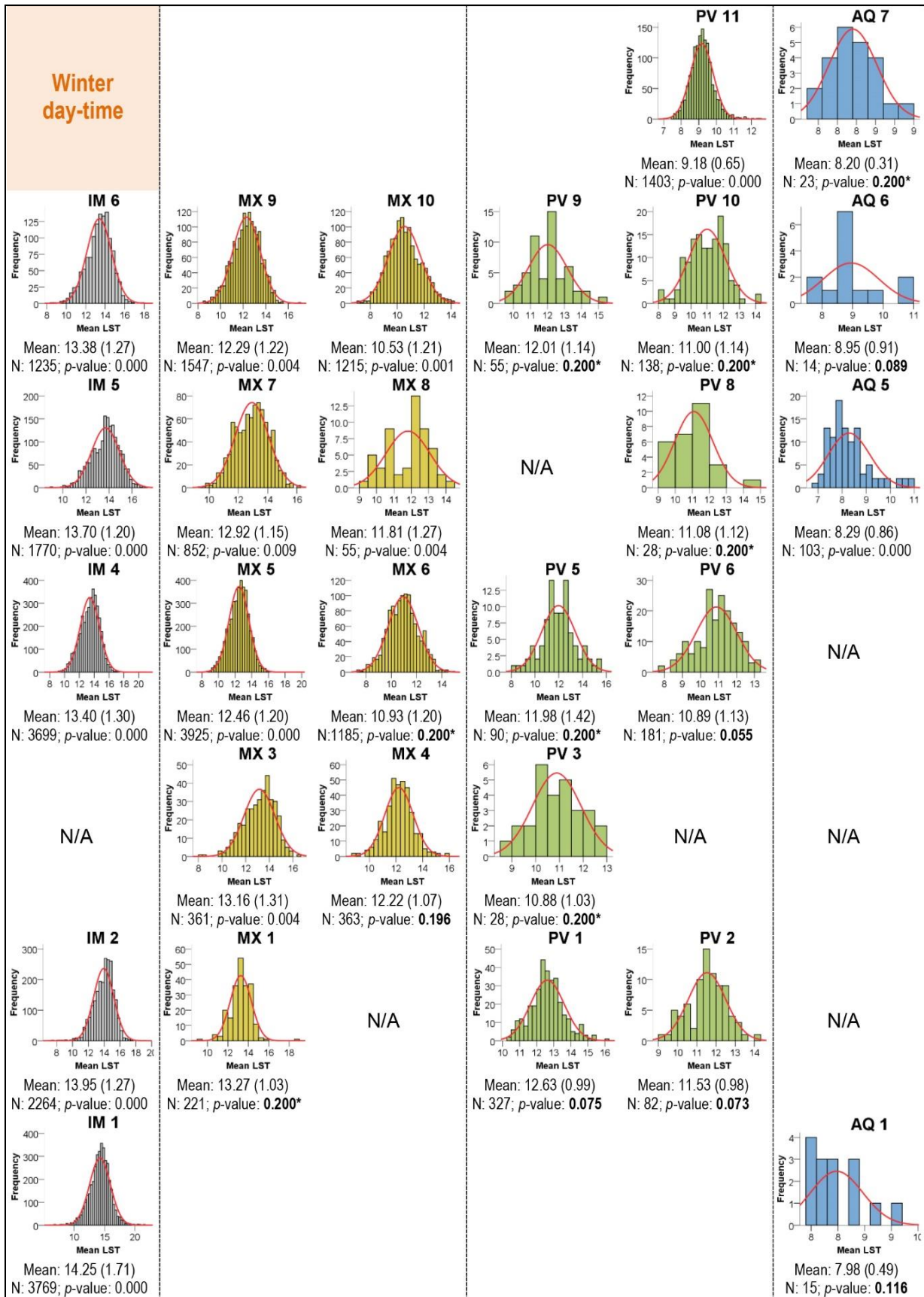
G3 Frequency distribution of mean nocturnal LSTs in summer for each GIT with a fitted normal distribution and results of the Kolmogorov-Smirnov test (N=sample size; standard deviations are in parenthesis, p -values <0.05 indicates a non-normal distribution, * This is a lower bound of the true significance).



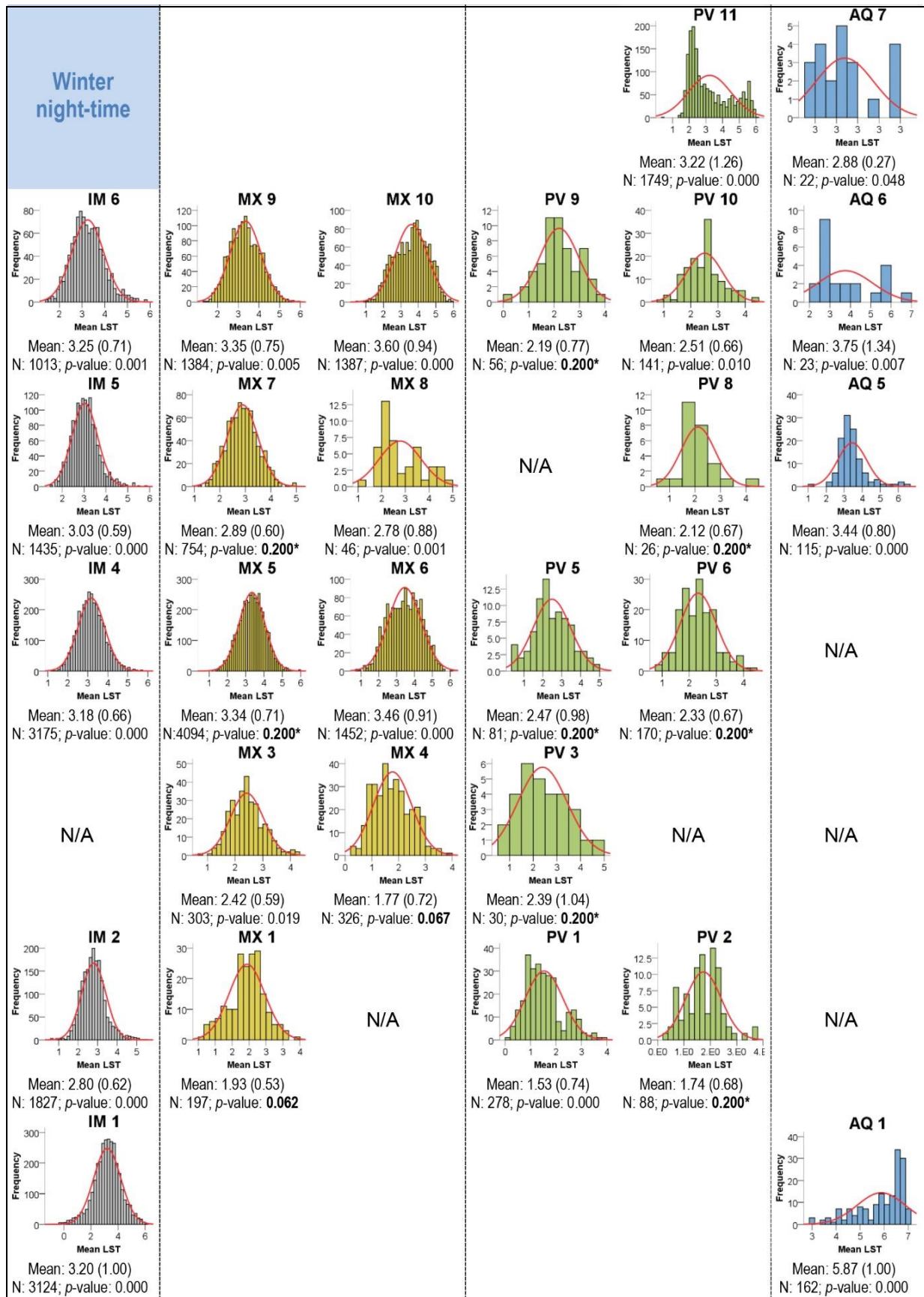
G4 Summary statistics for each GIT in winter (N=sample size; Std. Dev. = standard deviations; Std. Error = Standard error; Min. = Minimum value; Max. Maximum value).

GIT	Winter - Daytime						Winter - Night-time					
	N	Mean	Std. Dev.	Std. Error	Min.	Max.	N	Mean	Std. Dev.	Std. Error	Min.	Max.
IM 1	3769	14.25	1.71	0.03	6.04	21.78	3124	3.20	1.00	0.02	-0.97	6.20
IM 2	2264	13.95	1.27	0.03	7.32	19.06	1827	2.80	0.62	0.01	0.59	5.44
IM 4	3699	13.40	1.30	0.02	8.25	20.75	3175	3.18	0.66	0.01	1.14	5.97
IM 5	1770	13.70	1.20	0.03	8.90	17.15	1435	3.03	0.59	0.02	1.49	5.88
IM 6	1235	13.38	1.27	0.04	8.42	17.67	1013	3.25	0.71	0.02	1.38	5.81
MX 1	221	13.27	1.03	0.07	9.47	18.88	197	1.93	0.53	0.04	0.54	3.35
MX 3	361	13.16	1.31	0.07	8.30	16.39	303	2.42	0.59	0.03	0.79	4.25
MX 4	363	12.22	1.07	0.06	8.78	15.94	326	1.77	0.72	0.04	0.29	3.97
MX 5	3925	12.46	1.20	0.02	8.18	19.67	4094	3.34	0.71	0.01	0.68	5.98
MX 6	1185	10.93	1.20	0.03	7.29	14.87	1452	3.46	0.91	0.02	0.79	6.11
MX 7	852	12.92	1.15	0.04	9.42	16.16	754	2.89	0.60	0.02	1.18	4.97
MX 8	55	11.81	1.27	0.17	9.18	14.46	46	2.78	0.88	0.13	1.29	4.86
MX 9	1547	12.29	1.22	0.03	8.49	16.96	1384	3.35	0.75	0.02	1.31	5.95
MX 10	1215	10.53	1.21	0.03	7.00	14.22	1387	3.60	0.94	0.03	0.52	5.94
PV 1	327	12.63	0.99	0.05	10.41	16.11	278	1.53	0.74	0.04	0.17	3.83
PV 2	82	11.53	0.98	0.11	9.13	14.24	88	1.74	0.68	0.07	0.39	3.63
PV 3	28	10.88	1.03	0.19	8.84	12.70	30	2.39	1.04	0.19	0.63	4.58
PV 5	90	11.98	1.42	0.15	8.37	15.31	81	2.47	0.98	0.11	0.41	4.93
PV 6	181	10.89	1.13	0.08	7.84	13.25	170	2.33	0.67	0.05	0.90	4.41
PV 8	28	11.08	1.12	0.21	9.08	14.12	26	2.12	0.67	0.13	0.94	4.35
PV 9	55	12.01	1.14	0.15	9.63	15.36	56	2.19	0.77	0.10	0.22	3.73
PV 10	138	11.00	1.14	0.10	8.00	14.19	141	2.51	0.66	0.06	0.77	4.38
PV 11	1403	9.18	0.65	0.02	7.12	12.47	1749	3.22	1.26	0.03	0.36	6.12
AQ 1	15	7.98	0.49	0.13	7.46	9.12	162	5.87	1.00	0.08	2.92	7.10
AQ 5	103	8.29	0.86	0.08	6.92	10.89	115	3.44	0.80	0.08	1.22	6.56
AQ 6	14	8.95	0.91	0.24	7.76	10.82	23	3.75	1.34	0.28	2.36	6.61
AQ 7	23	8.20	0.31	0.07	7.70	8.96	22	2.88	0.27	0.06	2.51	3.39
Total	24948	12.75	1.90	0.01	6.04	21.78	23458	3.16	0.93	0.01	-0.97	7.10

G5 Frequency distribution of mean diurnal LSTs in winter for each GIT with a fitted normal distribution and results of the Kolmogorov-Smirnov test (N=sample size; standard deviations are in parenthesis, p -values <0.05 indicates a non-normal distribution, * This is a lower bound of the true significance).



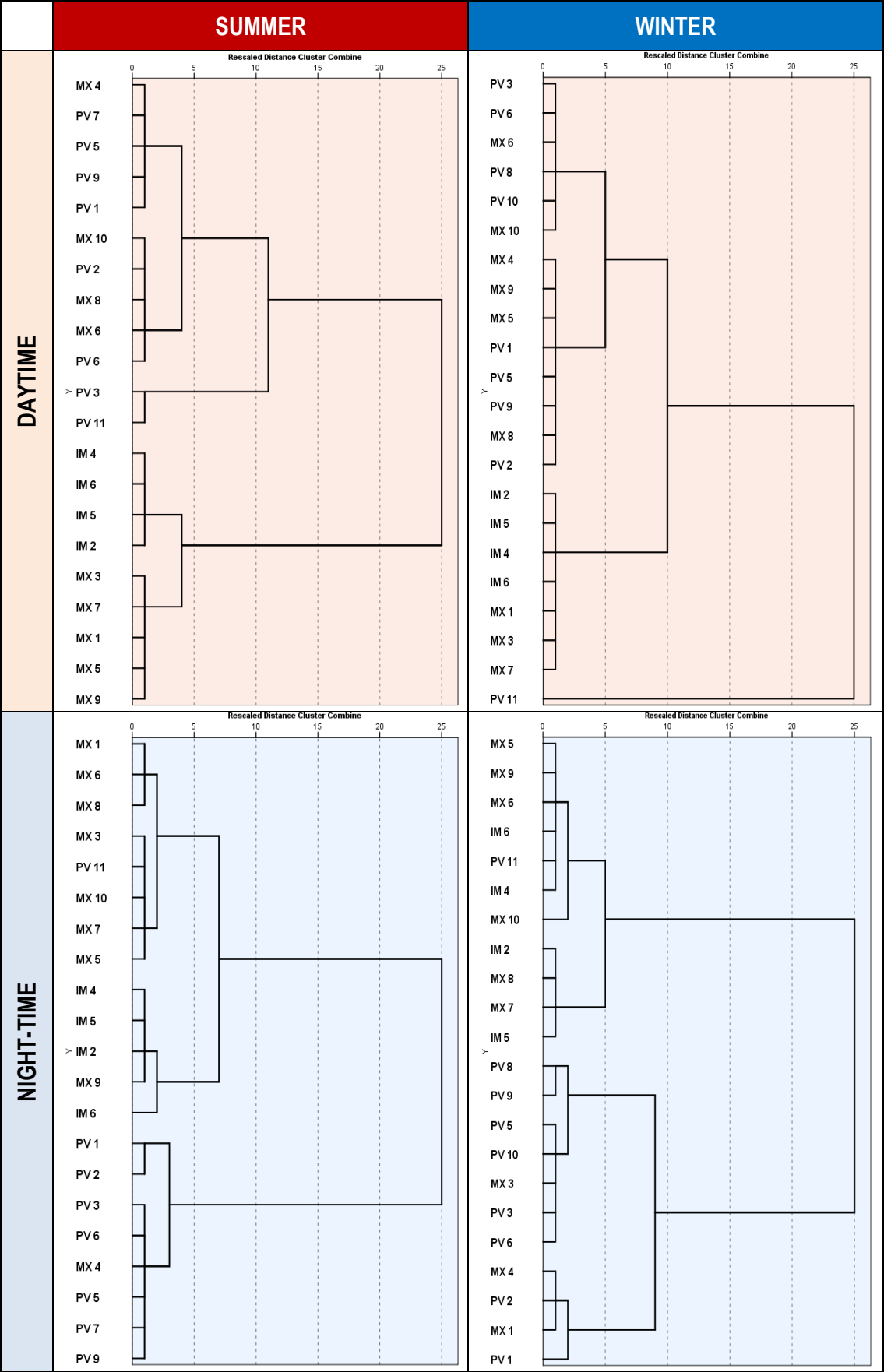
G6 Frequency distribution of mean nocturnal LSTs in winter for each GIT with a fitted normal distribution and results of the Kolmogorov-Smirnov test (N=sample size; standard deviations are in parenthesis, p -values <0.05 indicates a non-normal distribution, * This is a lower bound of the true significance).



G7 Mean and standard deviations (in parenthesis) of mean NDVI, percent of pervious surfaces, and percent of tree cover per GIT class.

GIT	SUMMER			WINTER		
	Mean NDVI	% Pervious	% Tree cover	Mean NDVI	% Pervious	% Tree cover
IM 1	-0.20 (0.06)	12.49 (8.21)	3.86 (4.41)	0.08 (0.08)	11.96 (8.14)	2.55 (3.06)
IM 2	-0.12 (0.04)	36.77 (6.79)	2.83 (1.49)	0.24 (0.05)	36.14 (6.91)	2.69 (1.53)
IM 4	-0.07 (0.05)	41.46 (6.56)	17.02 (7.60)	0.29 (0.06)	40.09 (6.85)	13.38 (6.17)
IM 5	-0.08 (0.04)	41.79 (6.17)	11.52 (4.55)	0.28 (0.05)	39.72 (6.72)	9.42 (3.49)
IM 6	-0.06 (0.05)	41.57 (6.82)	18.49 (7.16)	0.28 (0.06)	39.38 (7.02)	14.95 (5.90)
MX 1	-0.11 (0.03)	65.09 (6.64)	1.17 (1.49)	0.31 (0.04)	65.18 (6.64)	0.24 (0.79)
MX 3	-0.05 (0.06)	56.97 (6.86)	2.37 (1.72)	0.36 (0.06)	57.41 (6.25)	2.43 (1.72)
MX 4	0.08 (0.10)	87.95 (9.32)	1.12 (1.57)	0.54 (0.09)	91.06 (9.00)	1.16 (1.60)
MX 5	0.03 (0.06)	59.52 (6.55)	27.02 (10.34)	0.45 (0.06)	61.61 (7.09)	24.76 (10.07)
MX 6	0.12 (0.07)	82.68 (7.29)	39.16 (13.96)	0.61 (0.07)	85.18 (7.69)	40.86 (13.31)
MX 7	-0.01 (0.04)	57.51 (5.75)	15.69 (6.45)	0.40 (0.05)	57.95 (6.19)	12.98 (5.35)
MX 8	0.09 (0.08)	84.53 (7.16)	43.90 (27.95)	0.57 (0.09)	86.55 (8.76)	25.81 (23.87)
MX 9	0.04 (0.07)	61.44 (7.11)	31.33 (12.65)	0.46 (0.07)	62.42 (7.41)	28.28 (11.96)
MX 10	0.15 (0.08)	84.25 (7.30)	51.71 (17.16)	0.65 (0.08)	87.39 (7.76)	52.68 (16.08)
PV 1	-0.06 (0.04)	93.66 (5.93)	0.89 (1.36)	0.41 (0.06)	92.75 (7.54)	0.23 (0.72)
PV 2	0.31 (0.10)	96.13 (5.00)	0.32 (0.97)	0.72 (0.04)	98.77 (2.46)	1.24 (1.62)
PV 3	0.20 (0.12)	88.34 (10.27)	26.17 (15.75)	0.63 (0.10)	92.73 (7.96)	29.02 (15.48)
PV 5	0.01 (0.05)	89.41 (6.91)	18.11 (8.65)	0.51 (0.06)	93.18 (7.03)	15.80 (8.06)
PV 6	0.22 (0.07)	89.34 (6.80)	16.73 (7.90)	0.71 (0.06)	96.50 (5.36)	20.53 (9.76)
PV 7	-0.02 (0.04)	87.22 (7.35)	12.17 (5.50)	-	-	-
PV 8	-	-	-	0.69 (0.07)	94.71 (5.06)	9.51 (4.15)
PV 9	0.00 (0.04)	89.24 (7.01)	16.72 (8.30)	0.51 (0.06)	94.04 (6.18)	13.73 (6.90)
PV 10	-	-	-	0.71 (0.06)	96.16 (5.28)	19.82 (9.76)
PV 11	0.26 (0.08)	95.03 (4.59)	88.81 (7.21)	0.80 (0.04)	98.56 (3.15)	91.74 (7.62)
AQ 1	-0.25 (0.15)	7.02 (7.88)	5.77 (7.26)	-0.27 (0.14)	3.56 (6.35)	1.64 (3.88)
AQ 4	-0.20 (0.16)	27.01 (8.52)	8.56 (8.89)	-	-	-
AQ 5	-0.08 (0.15)	43.45 (14.72)	32.14 (12.37)	0.21 (0.18)	46.38 (12.61)	31.72 (13.42)
AQ 6	-0.10 (0.14)	42.20 (15.89)	24.34 (10.80)	0.19 (0.19)	48.42 (13.97)	20.17 (10.15)
AQ 7	0.04 (0.16)	57.20 (10.86)	53.22 (10.03)	0.46 (0.13)	64.85 (7.61)	58.73 (8.28)

G8 Dendrograms of hierarchical cluster analyses performed to terrestrial GITs using average linkage between groups.



Appendix H – Results of regression models

H1 Summary of *t*-statistic, correlation and collinearity statistics generated for the OLS models for the prediction of diurnal and nocturnal LSTs in summer and winter using all independent variables.

	Model	Variable	<i>t</i>	Sig.	Correlations			Collinearity statistics	
					Zero-order	Partial	Part	Tolerance	VIF
SUMMER	1A (DAY_T _s)	(Constant)	29.936	0.000					
		Fr_Imp_Bld	17.790	0.000	0.489	0.116	0.070	0.006	162.200
		Fr_Imp_Grnd	17.167	0.000	0.481	0.112	0.068	0.006	157.331
		Fr_Low_IRR	5.341	0.000	-0.108	0.035	0.021	0.022	45.900
		Fr_Low_NIR	10.421	0.000	-0.028	0.069	0.041	0.010	103.943
		Fr_Med_Veg	4.756	0.000	-0.222	0.031	0.019	0.319	3.138
		Fr_High_Veg	2.757	0.006	-0.582	0.018	0.011	0.005	201.445
		Fr_Tot_Wat	0.248	0.804	-0.398	0.002	0.001	0.022	45.416
		CIRCLE_AM	22.308	0.000	0.111	0.145	0.088	0.936	1.068
		nLSI	-8.360	0.000	0.222	-0.055	-0.033	0.846	1.182
		Mean_NDVI	10.620	0.000	-0.558	0.070	0.042	0.097	10.332
		Altitude	11.520	0.000	-0.032	0.076	0.045	0.897	1.115
	2A (NIG_T _s)	(Constant)	37.541	0.000					
		Fr_Imp_Bld	9.473	0.000	-0.337	0.062	0.049	0.006	162.200
		Fr_Imp_Grnd	20.942	0.000	0.431	0.137	0.108	0.006	157.331
		Fr_Low_IRR	4.477	0.000	-0.168	0.030	0.023	0.022	45.900
		Fr_Low_NIR	9.839	0.000	-0.111	0.065	0.051	0.010	103.943
		Fr_Med_Veg	2.514	0.012	-0.042	0.017	0.013	0.319	3.138
		Fr_High_Veg	7.634	0.000	0.011	0.050	0.039	0.005	201.445
		Fr_Tot_Wat	20.229	0.000	0.166	0.132	0.104	0.022	45.416
		CIRCLE_AM	25.377	0.000	0.120	0.165	0.131	0.936	1.068
		nLSI	0.849	0.396	-0.007	0.006	0.004	0.846	1.182
		Mean_NDVI	36.248	0.000	-0.062	0.232	0.186	0.097	10.332
		Altitude	-3.012	0.003	-0.077	-0.020	-0.015	0.897	1.115
WINTER	3A (DAY_T _s)	(Constant)	24.559	0.000					
		Fr_Imp_Bld	7.228	0.000	0.531	0.046	0.029	0.008	132.021
		Fr_Imp_Grnd	4.282	0.000	0.467	0.027	0.017	0.007	148.009
		Fr_Low_IRR	-4.943	0.000	-0.240	-0.031	-0.020	0.016	60.659
		Fr_Low_NIR	0.475	0.635	0.088	0.003	0.002	0.013	76.765
		Fr_Med_Veg	-2.658	0.008	-0.372	-0.017	-0.011	0.373	2.682
		Fr_High_Veg	-9.869	0.000	-0.678	-0.062	-0.039	0.005	194.767
		Fr_Tot_Wat	-10.890	0.000	-0.197	-0.069	-0.043	0.100	9.953
		CIRCLE_AM	-3.353	0.001	-0.030	-0.021	-0.013	0.729	1.372
		nLSI	4.778	0.000	0.164	0.030	0.019	0.785	1.274
		Altitude	10.864	0.000	-0.078	0.069	0.043	0.858	1.165
		Mean_NDVI	6.703	0.000	-0.676	0.042	0.027	0.025	39.899
	4A (NIG_T _s)	(Constant)	3.920	0.000					
		Fr_Imp_Bld	3.440	0.001	-0.096	0.022	0.015	0.009	114.131
		Fr_Imp_Grnd	10.373	0.000	0.068	0.068	0.046	0.008	129.240
		Fr_Low_IRR	-5.629	0.000	-0.199	-0.037	-0.025	0.018	54.967
		Fr_Low_NIR	-2.000	0.046	-0.293	-0.013	-0.009	0.015	66.359
		Fr_Med_Veg	-26.459	0.000	-0.053	-0.170	-0.117	0.378	2.643
		Fr_High_Veg	3.138	0.002	0.199	0.020	0.014	0.005	201.376
		Fr_Tot_Wat	19.519	0.000	0.237	0.126	0.086	0.030	33.354
		CIRCLE_AM	24.475	0.000	0.139	0.158	0.108	0.754	1.326
		nLSI	-15.780	0.000	-0.098	-0.103	-0.070	0.813	1.231
		Altitude	109.373	0.000	0.506	0.581	0.483	0.813	1.230
		Mean_NDVI	14.620	0.000	0.007	0.095	0.065	0.025	39.830

H2 Summary of *t*-statistic, correlation and collinearity statistics generated for revised OLS models for the prediction of diurnal and nocturnal LSTs in summer and winter using a selection of independent variables.

	Model	Variable	<i>t</i>	Sig.	Correlations			Collinearity statistics	
					Zero-order	Partial	Part	Tolerance	VIF
SUMMER	1B (DAY T_s)	(Constant)	398.696	0.000					
		Fr_Imp_Bld	61.401	0.000	0.489	0.375	0.243	0.492	2.033
		Fr_Imp_gr	48.823	0.000	0.481	0.306	0.193	0.404	2.477
		Fr_LowIRR	-15.778	0.000	-0.108	-0.103	-0.062	0.579	1.727
		Fr_Med_Veg	-4.278	0.000	-0.222	-0.028	-0.017	0.877	1.140
		Fr_High_Ve	-50.882	0.000	-0.582	-0.318	-0.201	0.36	2.776
		Fr_Tot_wat	-63.406	0.000	-0.398	-0.386	-0.251	0.757	1.322
		CIRCLE_AM	22.757	0.000	0.111	0.148	0.09	0.941	1.062
		NLSI	-8.361	0.000	0.222	-0.055	-0.033	0.858	1.166
		Altitude	10.838	0.000	-0.032	0.071	0.043	0.899	1.112
	2B (NIG T_s)	(Constant)	449.909	0.000					
		Fr_Imp_Bld	-18.788	0.000	-0.337	-0.123	-0.100	0.492	2.033
		Fr_Imp_gr	68.038	0.000	0.431	0.409	0.360	0.404	2.477
		Fr_LowIRR	3.661	0.000	-0.168	0.024	0.019	0.579	1.727
		Fr_Med_Veg	-3.409	0.001	-0.042	-0.022	-0.018	0.877	1.140
		Fr_High_Ve	25.618	0.000	0.011	0.167	0.136	0.360	2.776
		Fr_Tot_wat	42.758	0.000	0.166	0.271	0.226	0.757	1.322
		CIRCLE_AM	26.993	0.000	0.120	0.175	0.143	0.941	1.062
		NLSI	-1.263	0.207	-0.007	-0.008	-0.007	0.858	1.166
		Altitude	-4.814	0.000	-0.077	-0.032	-0.026	0.899	1.112
WINTER	3B (DAY T_s)	(Constant)	256.332	0.000					
		Fr_Imp_Bld	41.156	0.000	0.531	0.252	0.164	0.446	2.243
		Fr_Imp_gr	16.968	0.000	0.467	0.107	0.068	0.348	2.872
		Fr_LowIRR	-23.399	0.000	-0.240	-0.147	-0.093	0.464	2.154
		Fr_Med_Veg	-3.453	0.001	-0.372	-0.022	-0.014	0.660	1.515
		Fr_High_Ve	-68.622	0.000	-0.678	-0.399	-0.274	0.290	3.452
		Fr_Tot_wat	-41.550	0.000	-0.197	-0.254	-0.166	0.935	1.070
		CIRCLE_AM	-2.323	0.020	-0.030	-0.015	-0.009	0.786	1.273
		NLSI	5.236	0.000	0.164	0.033	0.021	0.790	1.266
		Altitude	11.937	0.000	-0.078	0.075	0.048	0.881	1.135
	4B (NIG T_s)	(Constant)	45.200	0.000					
		Fr_Imp_Bld	16.369	0.000	-0.096	0.106	0.073	0.427	2.343
		Fr_Imp_gr	58.899	0.000	0.068	0.359	0.261	0.325	3.078
		Fr_LowIRR	-7.573	0.000	-0.199	-0.049	-0.034	0.446	2.243
		Fr_Med_Veg	-32.024	0.000	-0.053	-0.205	-0.142	0.669	1.494
		Fr_High_Ve	55.506	0.000	0.199	0.341	0.246	0.260	3.847
		Fr_Tot_wat	81.569	0.000	0.237	0.470	0.362	0.759	1.317
		CIRCLE_AM	27.914	0.000	0.139	0.179	0.124	0.804	1.244
		NLSI	-15.185	0.000	-0.098	-0.099	-0.067	0.816	1.225
		Altitude	114.626	0.000	0.506	0.599	0.508	0.854	1.170

H3 Pearson's correlation coefficients of variables of regression model 1A with diurnal LSTs in summertime as dependent variable.

Model 1A	DAY_T _s	Fr_Imp_Bld	Fr_Imp_Grmd	Fr_Low_IRR	Fr_Low_NIR	Fr_Med_Veg	Fr_High_Veg	Fr_Tot_wat	CIRCLE_AM	nLSI	Mean_NDVI	Altitude										
DAY_T _s	1																					
Fr_Imp_Bld	.489**	1					<div>Strengths of correlations</div> <table><tr><td>0.01-0.19</td><td>No/negligible relationship</td></tr><tr><td>0.20-0.39</td><td>Weak relationship</td></tr><tr><td>0.40-0.59</td><td>Moderate relationship</td></tr><tr><td>0.60-0.79</td><td>Strong relationship</td></tr><tr><td>0.80-1.00</td><td>Very strong relationship</td></tr></table> <div>N = 23022 * Correlation is significant at the 0.05 level (1-tailed) ** Correlation is significant at the 0.01 level (1-tailed)</div>						0.01-0.19	No/negligible relationship	0.20-0.39	Weak relationship	0.40-0.59	Moderate relationship	0.60-0.79	Strong relationship	0.80-1.00	Very strong relationship
0.01-0.19	No/negligible relationship																					
0.20-0.39	Weak relationship																					
0.40-0.59	Moderate relationship																					
0.60-0.79	Strong relationship																					
0.80-1.00	Very strong relationship																					
Fr_Imp_Grmd	.481**	-.127**	1																			
Fr_Low_IRR	-.108**	-.133**	-.252**	1																		
Fr_Low_NIR	-.028**	-.349**	-.112**	.117**	1																	
Fr_Med_Veg	-.222**	-.136**	-.204**	.041**	-.167**	1																
Fr_High_Veg	-.582**	-.385**	-.461**	-.164**	-.274**	.310**	1															
Fr_Tot_Wat	-.398**	.155**	-.189**	-.111**	-.153**	-.010(.070)	.000(.497)	1														
CIRCLE_AM	.111**	.043**	-.009(.091)	.008(.119)	-.058**	.055**	.034**	-.070(.000)	1													
nLSI	.222**	.243**	.154**	-.057**	-.071**	.029**	-.221**	-.113**	.188**	1												
Mean_NDVI	-.558**	-.444**	-.587**	.348**	-.011*	.338**	.791**	-.131**	.048**	-.250**	1											
Altitude	-.032**	-.021**	-.145**	.168**	-.083**	.122**	.173**	-.121**	.130**	-.030**	.222**	1										

H4 Pearson's correlation coefficients of variables of regression model 2A with nocturnal LSTs in summertime as dependent variable.

Model 2A	NIG_T _s	Fr_Imp_Bld	Fr_Imp_Grmd	Fr_Low_IRR	Fr_Low_NIR	Fr_Med_Veg	Fr_High_Veg	Fr_Tot_wat	CIRCLE_AM	nLSI	Mean_NDVI	Altitude										
NIG_T _s	1																					
Fr_Imp_Bld	-.337**	1					<div>Strengths of correlations</div> <table><tr><td>0.01-0.19</td><td>No/negligible relationship</td></tr><tr><td>0.20-0.39</td><td>Weak relationship</td></tr><tr><td>0.40-0.59</td><td>Moderate relationship</td></tr><tr><td>0.60-0.79</td><td>Strong relationship</td></tr><tr><td>0.80-1.00</td><td>Very strong relationship</td></tr></table> <div>N = 23022 * Correlation is significant at the 0.05 level (1-tailed) ** Correlation is significant at the 0.01 level (1-tailed)</div>						0.01-0.19	No/negligible relationship	0.20-0.39	Weak relationship	0.40-0.59	Moderate relationship	0.60-0.79	Strong relationship	0.80-1.00	Very strong relationship
0.01-0.19	No/negligible relationship																					
0.20-0.39	Weak relationship																					
0.40-0.59	Moderate relationship																					
0.60-0.79	Strong relationship																					
0.80-1.00	Very strong relationship																					
Fr_Imp_Grmd	.431**	-.127**	1																			
Fr_Low_IRR	-.168**	-.133**	-.252**	1																		
Fr_Low_NIR	-.111**	-.349**	-.112**	.117**	1																	
Fr_Med_Veg	-.042**	-.136**	-.204**	.041**	-.167**	1																
Fr_High_Veg	.011*	-.385**	-.461**	-.164**	-.274**	.310**	1															
Fr_Tot_Wat	.166**	-.155**	-.189**	-.111**	-.153**	-.010(.070)	.000(.497)	1														
CIRCLE_AM	.120**	.043**	-.009(.091)	.008(.119)	-.058**	.055**	.034**	-.070**	1													
nLSI	-.007(.128)	.243**	.154**	-.057**	-.071**	.029**	-.221**	-.113**	.188**	1												
Mean_NDVI	-.062**	-.444**	-.587**	.348**	-.011*	.338**	.791**	-.131**	.048**	-.250**	1											
Altitude	-.077**	-.021**	-.145**	.168**	-.083**	.122**	.173**	-.121**	.130**	-.030**	.222**	1										

H5 Pearson's correlation coefficients of variables of regression model 3A with diurnal LSTs in wintertime as dependent variable.

Model 3A	DAY_T _s	Fr_Imp_Bld	Fr_Imp_Grmd	Fr_Low_IRR	Fr_Low_NIR	Fr_Med_Veg	Fr_High_Veg	Fr_Tot_wat	CIRCLE_AM	nLSI	Mean_NDVI	Altitude
DAY_T _s	1											
Fr_Imp_Bld	.531**	1										
Fr_Imp_Grmd	.467**	.030**	1									
Fr_Low_IRR	-.240**	-.333**	-.372**	1								
Fr_Low_NIR	.088**	-.291**	-.104**	.107**	1							
Fr_Med_Veg	-.372**	-.233**	-.316**	-.072**	-.200**	1						
Fr_High_Veg	-.678**	-.428**	-.563**	-.027**	-.325**	.546**	1					
Fr_Tot_Wat	-.197**	-.074**	-.046**	-.040**	-.120**	-.004(.242)	.000(.493)	1				
CIRCLE_AM	-.030**	.081**	-.151**	.109**	-.110**	.036**	.052**	.002(.359)	1			
nLSI	.164**	.180**	.085**	-.076**	-.050**	.092**	-.140**	-.065**	.347**	1		
Mean_NDVI	-.676**	-.609**	-.726**	.466**	.058**	.443**	.800**	-.138**	.116**	-.138**	1	
Altitude	-.078**	-.036**	-.191**	.063**	-.069**	.082**	.209**	-.125**	.231**	-.019**	.243**	1

Strengths of correlations

0.01-0.19	No/negligible relationship
0.20-0.39	Weak relationship
0.40-0.59	Moderate relationship
0.60-0.79	Strong relationship
0.80-1.00	Very strong relationship

N = 24948
** Correlation is significant at the 0.01 level (1-tailed)

H6 Pearson's correlation coefficients of variables of regression model 4A with nocturnal LSTs in wintertime as dependent variable.

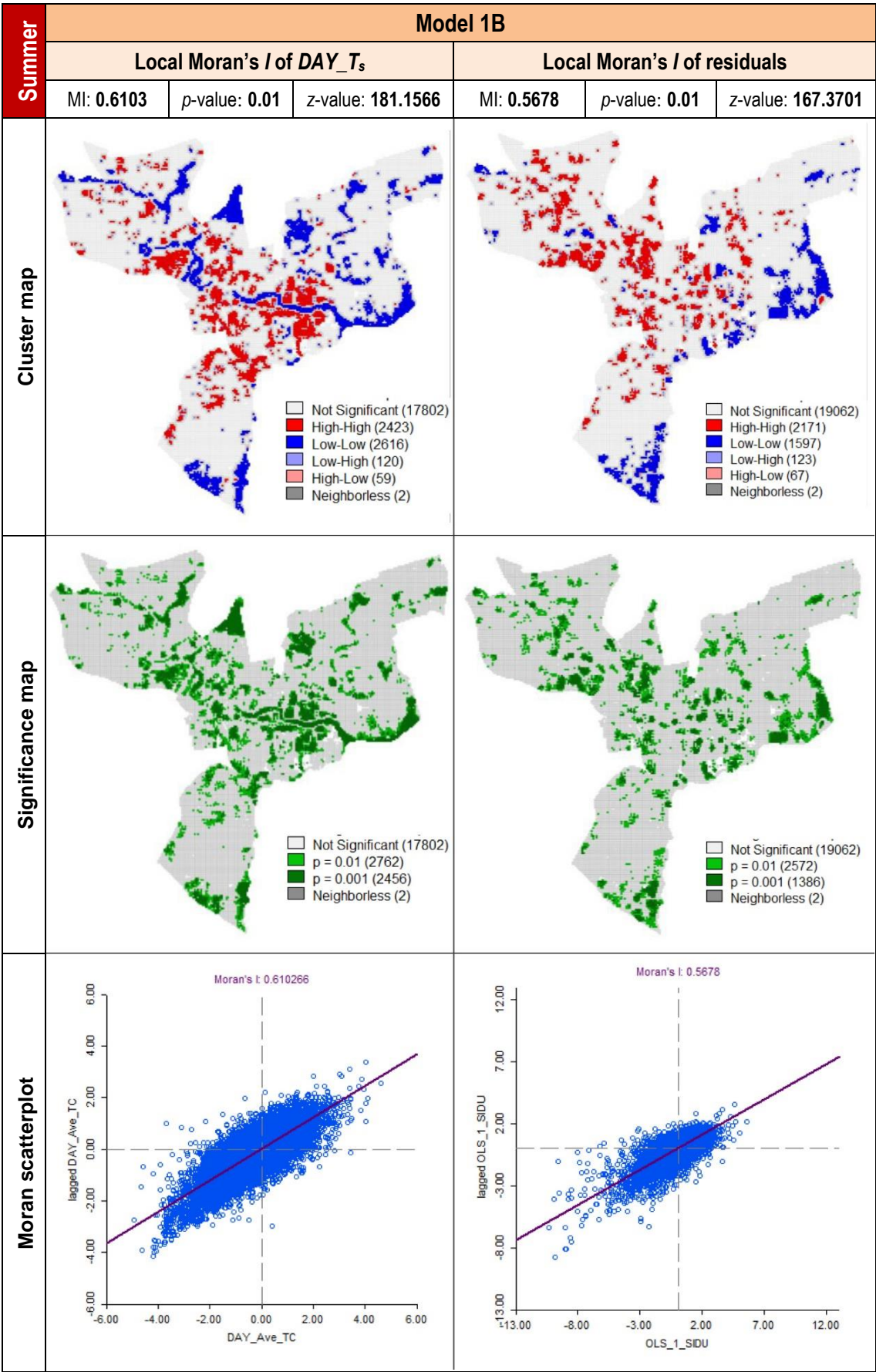
Model 4A	NIG_T _s	Fr_Imp_Bld	Fr_Imp_Grmd	Fr_Low_IRR	Fr_Low_NIR	Fr_Med_Veg	Fr_High_Veg	Fr_Tot_wat	CIRCLE_AM	nLSI	Mean_NDVI	Altitude
NIG_T _s	1											
Fr_Imp_Bld	-.096**	1										
Fr_Imp_Grmd	.068**	.089**	1									
Fr_Low_IRR	-.199**	-.310**	-.345**	1								
Fr_Low_NIR	-.293**	-.226**	-.030**	.110**	1							
Fr_Med_Veg	-.053**	-.248**	-.324**	-.077**	-.222**	1						
Fr_High_Veg	.199**	-.448**	-.577**	-.052**	-.368**	.541**	1					
Fr_Tot_Wat	.237**	-.122**	-.112**	-.083**	-.151**	-.036**	-.060**	1				
CIRCLE_AM	.139**	.091**	-.104**	.140**	-.063**	.023**	.013*	-.143**	1			
nLSI	-.098**	.175**	.101**	-.084**	-.038**	.102**	-.110**	-.110**	.321**	1		
Mean_NDVI	.007(.158)	-.579**	-.690**	.426**	.000(.482)	.448**	.807**	-.278**	.122**	-.106**	1	
Altitude	.506**	-.071**	-.230**	.118**	-.072**	.092**	.248**	-.151**	.230**	-.039**	.321**	1

Strengths of correlations

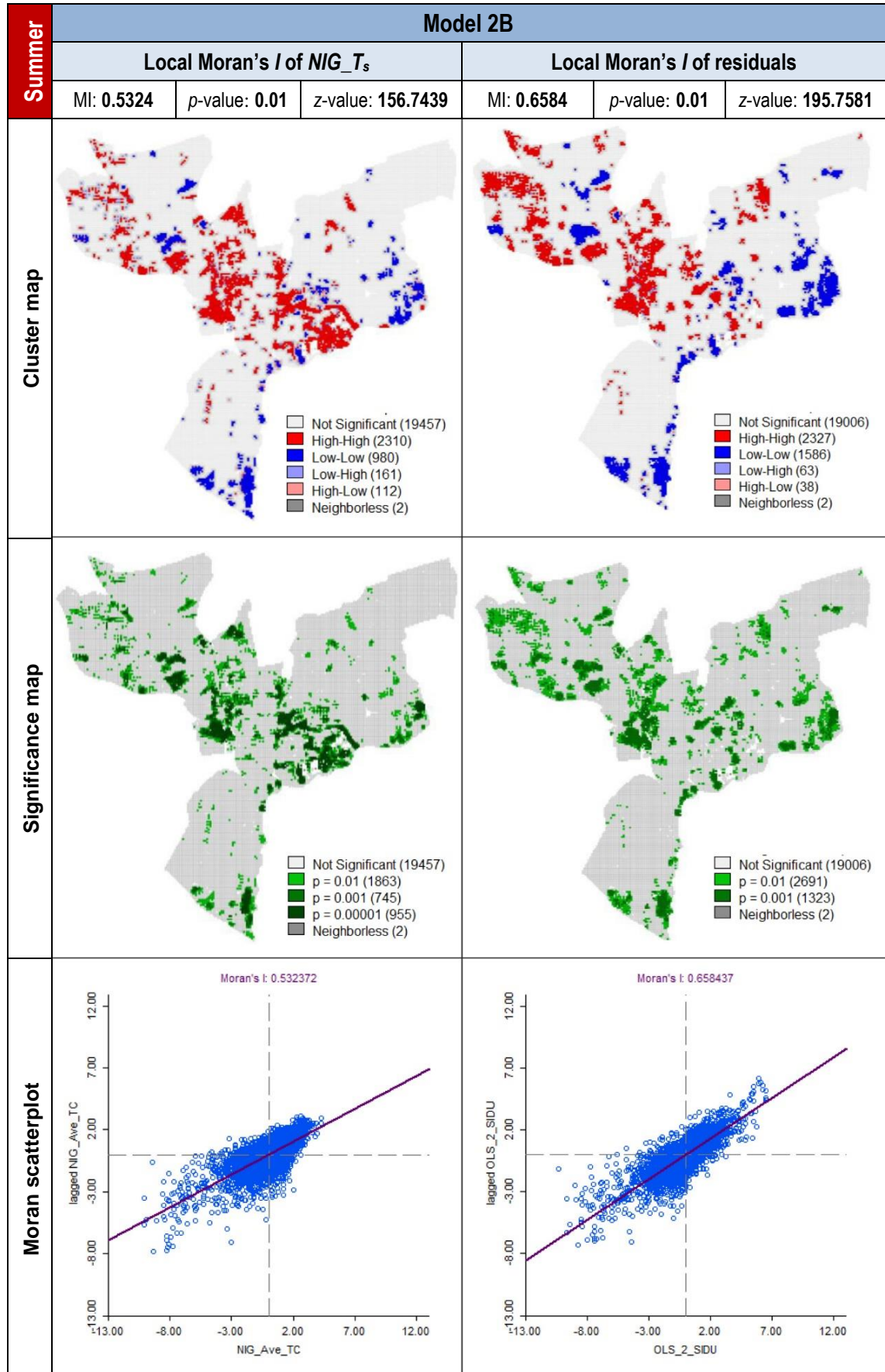
0.01-0.19	No/negligible relationship
0.20-0.39	Weak relationship
0.40-0.59	Moderate relationship
0.60-0.79	Strong relationship
0.80-1.00	Very strong relationship

N = 23022
* Correlation is significant at the 0.05 level (1-tailed)
** Correlation is significant at the 0.01 level (1-tailed)

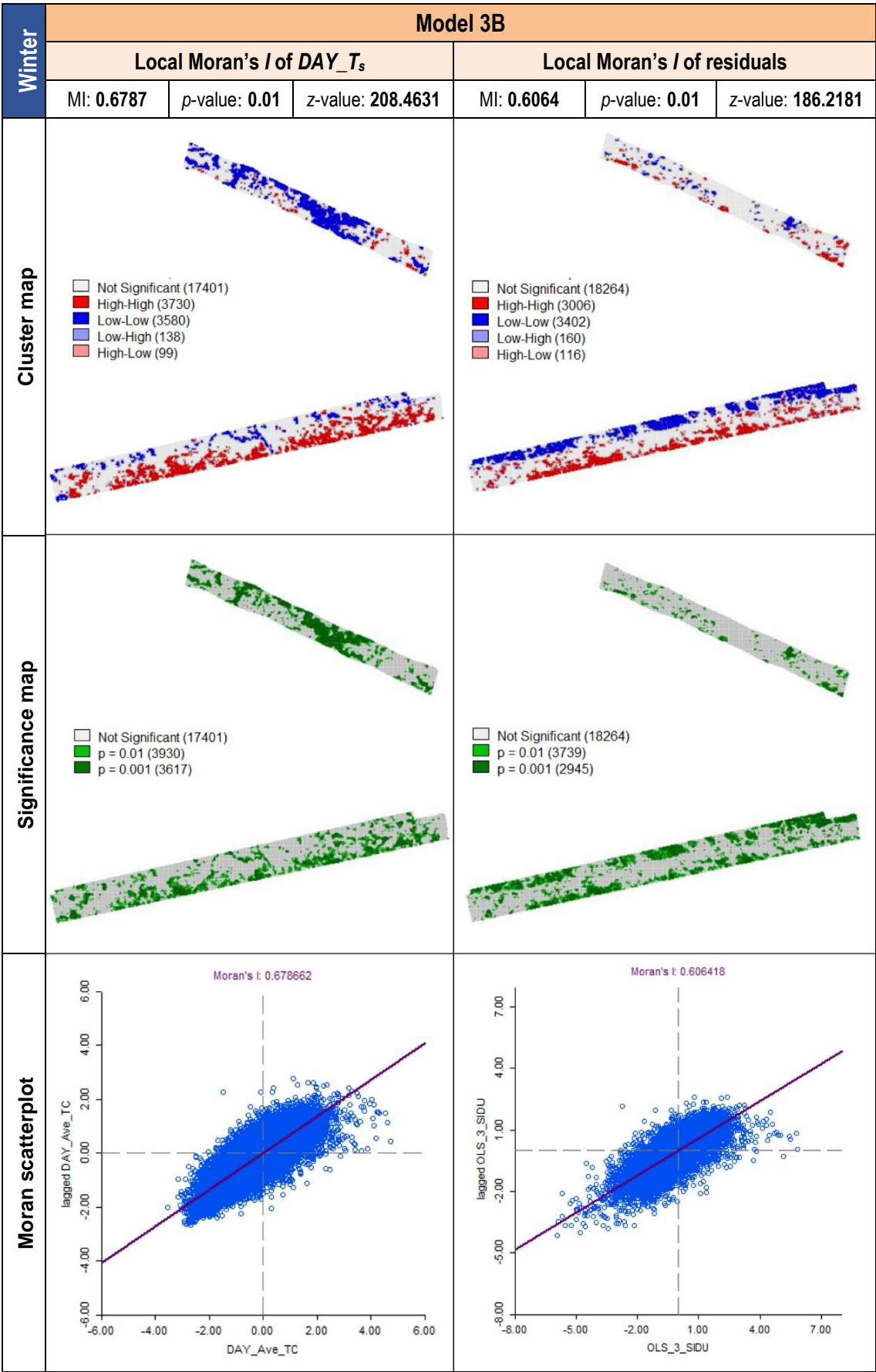
H7 LISA results (Moran scatterplot, cluster and significance maps) for the dependent variable and residuals of Model 1B showing the presence of spatial clusters (hot-/coldspots) and spatial outliers.



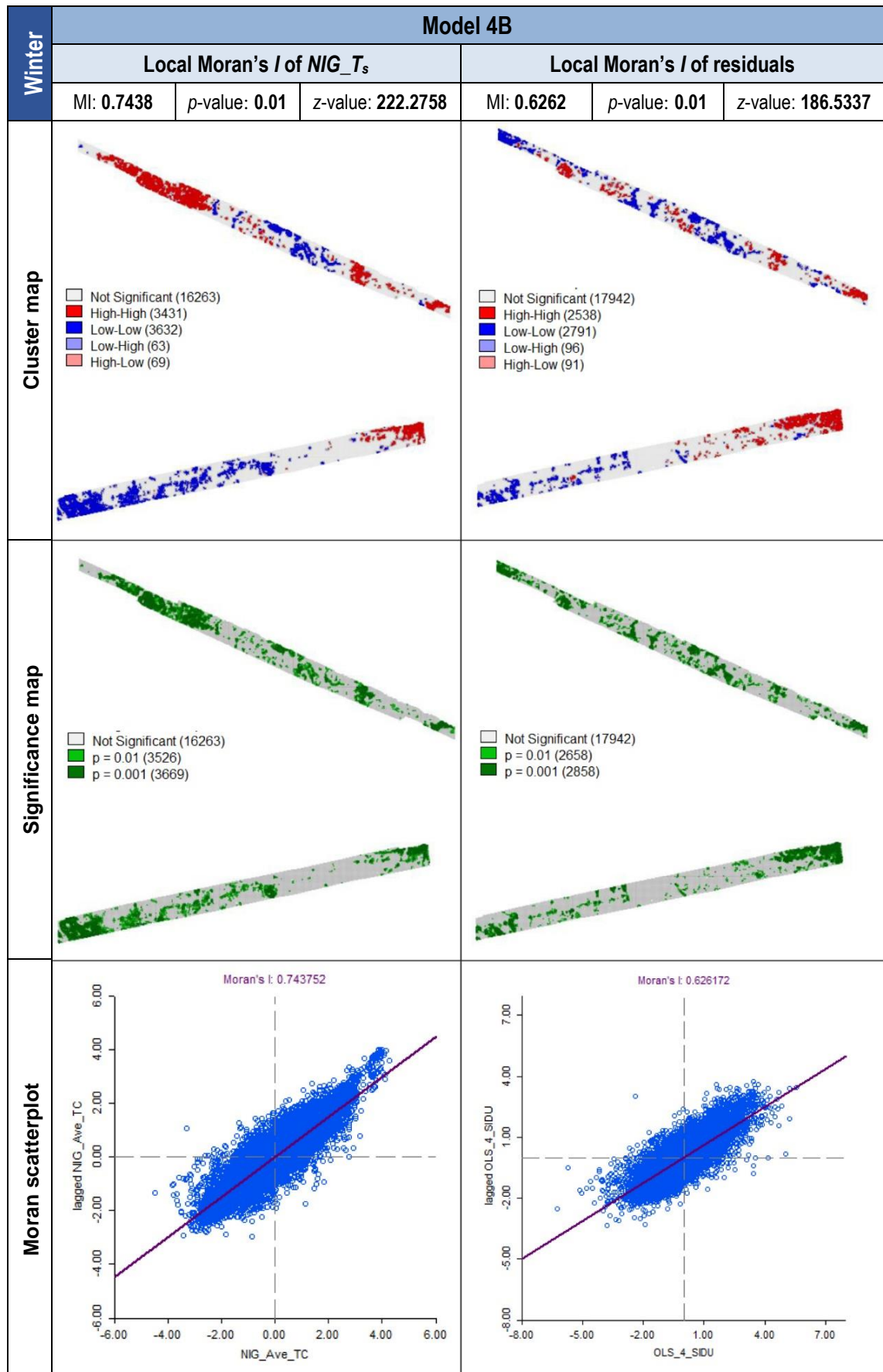
H8 LISA results (Moran scatterplot, cluster and significance maps) for the dependent variable and residuals of Model 2B showing the presence of spatial clusters (hot-/coldspots) and spatial outliers.



H9 LISA results (Moran scatterplot, cluster and significance maps) for the dependent variable and residuals of Model 3B showing the presence of spatial clusters (hot-/coldspots) and spatial outliers.



H10 LISA results (Moran scatterplot, cluster and significance maps) for the dependent variable and residuals of Model 4B showing the presence of spatial clusters (hot-/coldspots) and spatial outliers.



H11 Summary of statistics of all regression models (OLS, SEM, LAG) produced for the prediction of diurnal and nocturnal LSTs in summer and winter.

Season	SUMMER											
Time of day	Day						Night					
Model	1A	1B	1C	1D *	1E **	1F	2A	2B	2C	2D *	2E **	2F
Regression	OLS	OLS	SEM	SEM	SEM	LAG	OLS	OLS	SEM	SEM	SEM	LAG
Predictors	Fr_Imp_Bld, Fr_Imp_Grmd, Fr_Low_NIR, Fr_Low_IRR, Fr_Med_Veg, Fr_High_Veg, Fr_Tot_Wat, Mean_NDVI, CIRCLE_AM, nLSI, Altitude	Fr_Imp_Bld, Fr_Imp_Grmd, Fr_Low_IRR, Fr_Med_Veg, Fr_High_Veg, Fr_Tot_Wat, CIRCLE_AM, nLSI, Altitude	(Lambda), Fr_Imp_Bld, Fr_Imp_Gr, Fr_LowIRR, Fr_Med_Veg, Fr_High_Veg, Fr_Tot_wat, CIRCLE_AM, nLSI, Altitude	(Lambda), Fr_Imp_Bld, Fr_Imp_Gr, Fr_LowIRR, Fr_Med_Veg, Fr_High_Veg, Fr_Tot_wat, CIRCLE_AM, nLSI, Altitude	(Lambda), Fr_Imp_Bld, Fr_Imp_Gr, Fr_LowIRR, Fr_Med_Veg, Fr_High_Veg, Fr_Tot_wat, CIRCLE_AM, nLSI, Altitude	W_DAY_Ts, Fr_Imp_Bld, Fr_Imp_Gr, Fr_LowIRR, Fr_Med_Veg, Fr_High_Veg, Fr_Tot_wat, CIRCLE_AM, nLSI, Altitude	Fr_Imp_Bld, Fr_Imp_Grmd, Fr_Low_NIR, Fr_Low_IRR, Fr_Med_Veg, Fr_High_Veg, Fr_Tot_Wat, Mean_NDVI, CIRCLE_AM, nLSI, Altitude	Fr_Imp_Bld, Fr_Imp_Grmd, Fr_Low_IRR, Fr_Med_Veg, Fr_High_Veg, Fr_Tot_Wat, CIRCLE_AM, nLSI, Altitude	(Lambda), Fr_Imp_Bld, Fr_Imp_Gr, Fr_LowIRR, Fr_Med_Veg, Fr_High_Veg, Fr_Tot_wat, CIRCLE_AM, nLSI, Altitude	(Lambda), Fr_Imp_Bld, Fr_Imp_Gr, Fr_LowIRR, Fr_Med_Veg, Fr_High_Veg, Fr_Tot_wat, CIRCLE_AM, nLSI, Altitude	(Lambda), Fr_Imp_Bld, Fr_Imp_Gr, Fr_LowIRR, Fr_Med_Veg, Fr_High_Veg, Fr_Tot_wat, CIRCLE_AM, nLSI, Altitude	W_NIG_Ts, Fr_Imp_Bld, Fr_Imp_Gr, Fr_LowIRR, Fr_Med_Veg, Fr_High_Veg, Fr_Tot_wat, CIRCLE_AM, nLSI, Altitude
N cases	23022	23022	23022	368	20345	23022	23022	23022	23022	368	20345	23022
R	0.802	0.800	-	-	-	-	0.626	0.595	-	-	-	-
R ²	0.643	0.640	0.844	0.861	0.860	0.763	0.391	0.354	0.798	0.909	0.799	0.680
Adjusted R ²	0.643	0.640	-	-	-	-	0.391	0.353	-	-	-	-
S.E	1.763	1.771	1.165	0.841	0.958	1.437	0.937	0.965	0.540	0.311	0.408	0.679
F-statistic	3767.942	4538.556	-	-	-	-	1345.201	1403.516	-	-	-	-
df1	11	9	9	9	9	9	11	9	9	9	9	9
df2	23010	23012	23012	358	20335	23011	23010	23012	23012	358	20335	23011
Lag coeff. (Sig.)	-	-	0.829 (0.00)	0.551 (0.00)	0.782 (0.00)	0.5373	-	-	0.886 (0.00)	0.915 (0.00)	0.862 (0.00)	0.6953
Sig. F (p-value)	0.000	0.000	-	-	-	-	0.000	0.000	-	-	-	-
Log-Likelihood	-45720.3	-45828.6	-37792.87	-478.455	-29335.9	-41547.8	-31171.7	-31851	-20459.63	-181.203	-12429.57	-24.765.4
AIC	91464.5	91677.3	75605.7	976.911	58691.8	83117.6	62367.4	63722.1	40939.3	382.407	24879.2	49552.7
SC	91561.1	91757.7	75686.2	1015.99	58771.0	83206.1	62463.9	63802.5	41019.7	421.487	24958.4	49641.2
Durbin-Watson	1.065	1.052	-	-	-	-	0.943	0.907	-	-	-	-
Multicollinearity	218.001	20.485	-	-	-	-	218.001	20.485	-	-	-	-
Jarque-Bera (Sig.)	107148.551 (0.000)	112182.523 6 (0.000)	-	-	-	-	140438.054 (0.000)	150644.418 2 (0.000)	-	-	-	-
Breusch-Pagan (Sig.)	23670.8246 (0.000)	22177.1111 (0.000)	19069.77 (0.000)	247.4531 (0.000)	3313.721 (0.000)	18685.693 (0.000)	34768.8775 (0.000)	36322.8178 (0.000)	33816.04 (0.000)	382.9133 (0.000)	6898.934 (0.000)	35442.580 (0.000)
Koenker-Bassett (Sig.)	3934.6607 (0.000)	4149.5824 (0.000)	-	-	-	-	5033.0809 (0.000)	5113.7158 (0.000)	-	-	-	-
Likelihood ratio (Sig.)	-	-	16071.52 (0.000)	96.9575 (0.000)	12027.35 (0.000)	8561.6076 (0.000)	-	-	22782.82 (0.000)	558.6579 (0.000)	18961.35 (0.000)	14171.3502 (0.000)

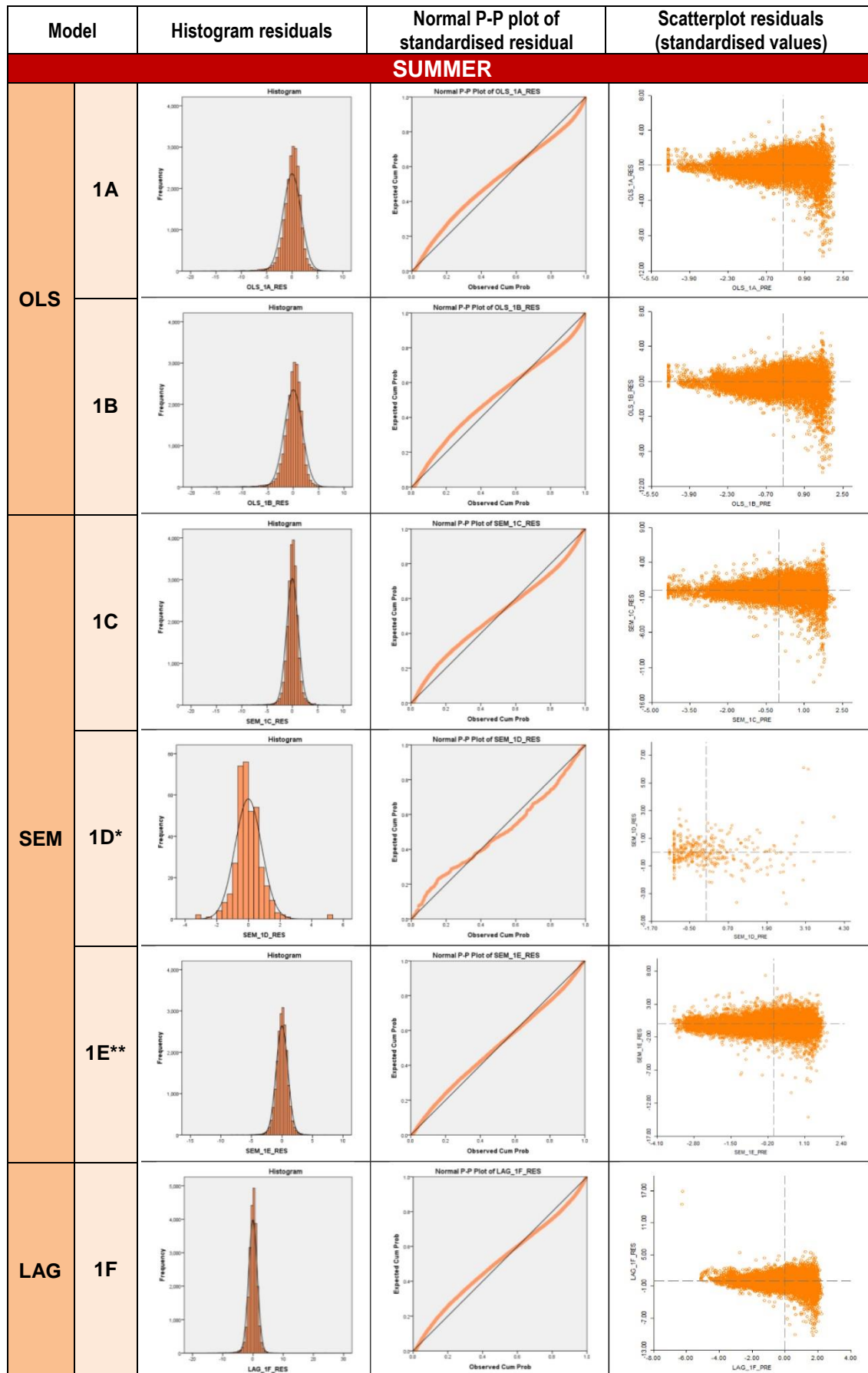
* Aquatic context; **Terrestrial context; S.E. = Spatial error; AIC = Akaike information criterion; SC = Schwarz criterion. Note: models with the best performance have been coloured.

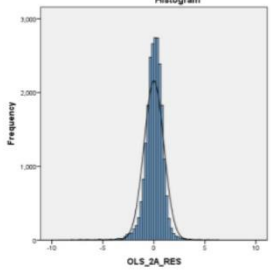
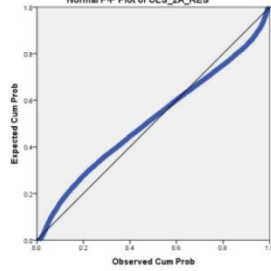
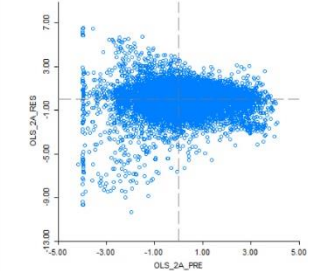
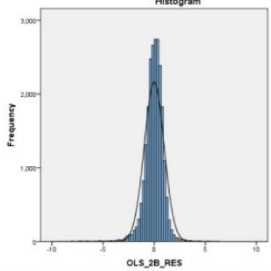
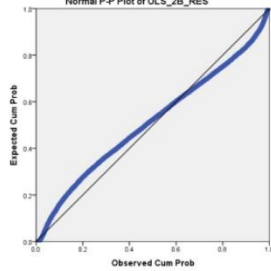
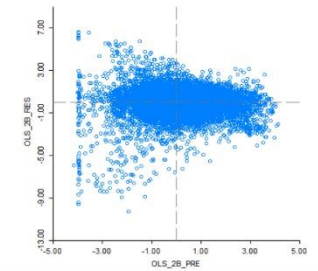
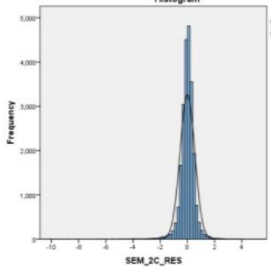
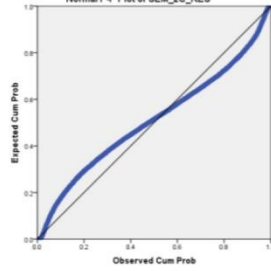
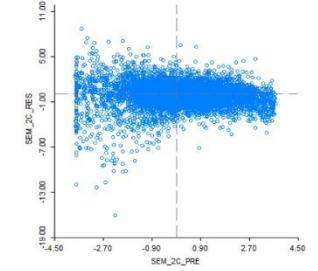
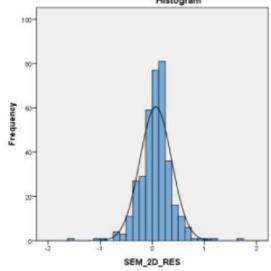
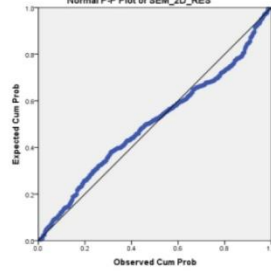
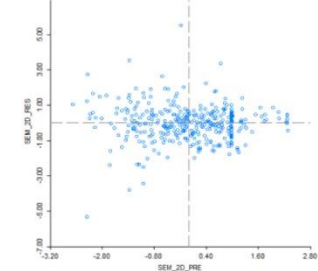
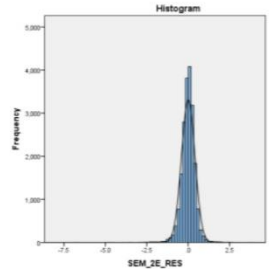
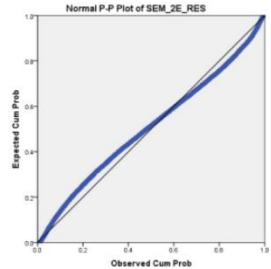
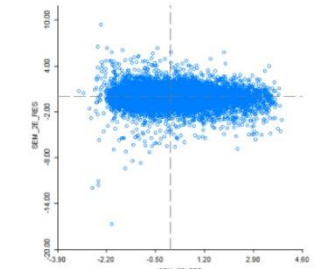
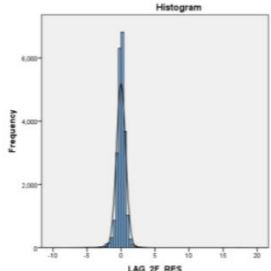
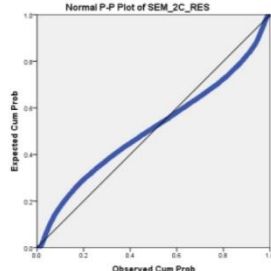
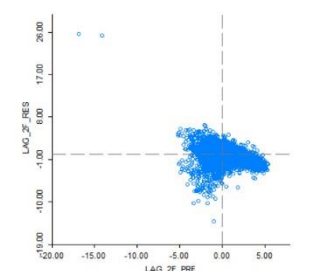
(Continued Table H11)

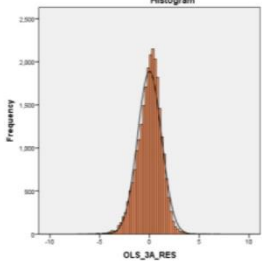
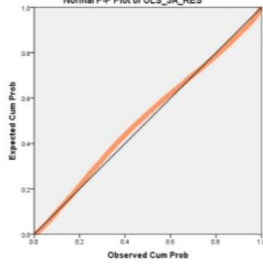
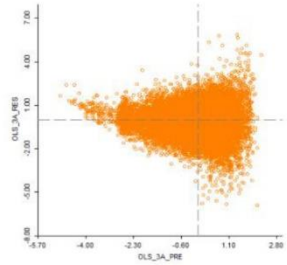
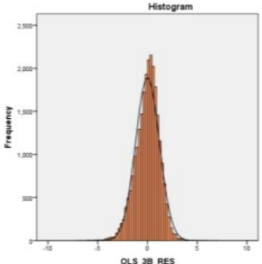
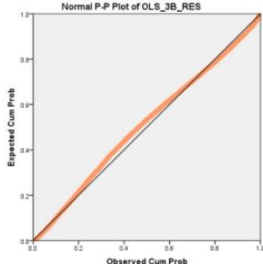
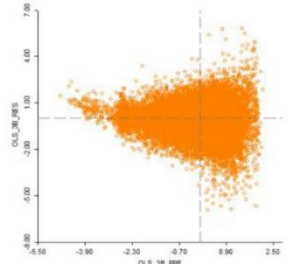
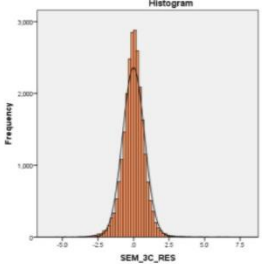
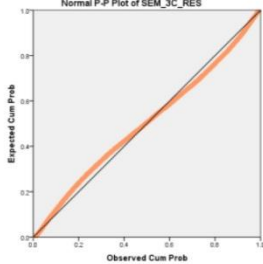
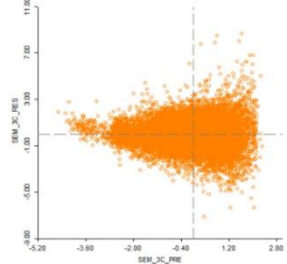
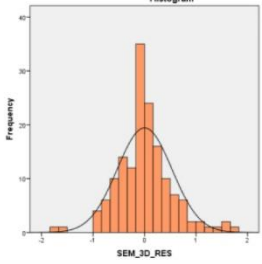
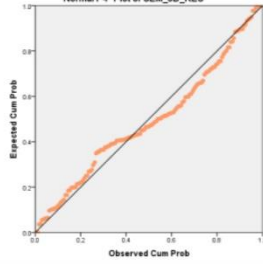
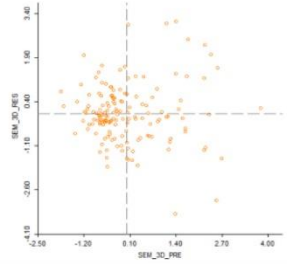
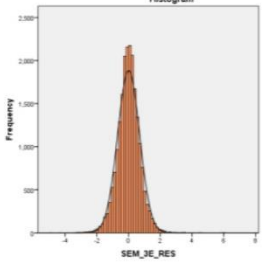
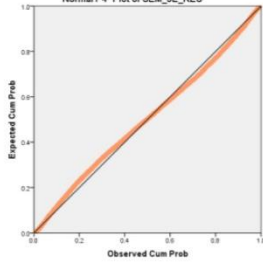
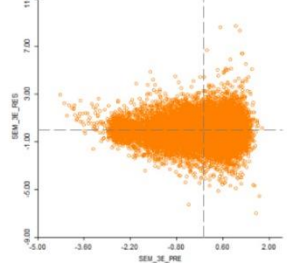
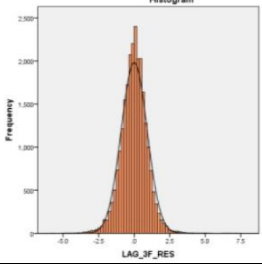
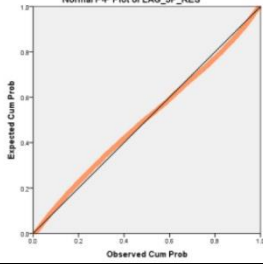
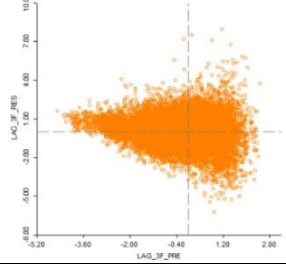
Season Time of day Model Regression	WINTER											
	Day						Night					
	3A	3B	3C	3D *	3E **	3F	4A	4B	4C	4D *	4E **	4F
	OLS	OLS	SEM	SEM	SEM	LAG	OLS	OLS	SEM	SEM	SEM	LAG
Predictors	Fr_Imp_Bld, Fr_Imp_Grnd, Fr_Low_NIR, Fr_Low_IRR, Fr_Med_Veg, Fr_High_Veg, Fr_Tot_Wat, CIRCLE_AM, Mean_NDVI, nLSI, Altitude	Fr_Imp_Bld, Fr_Imp_Grnd, Fr_Low_IRR, Fr_Med_Veg, Fr_High_Veg, Fr_Tot_Wat, CIRCLE_AM, nLSI, Altitude	(Lambda), Fr_Imp_Bld, Fr_Imp_Gr, Fr_LowIRR, Fr_Med_Veg, Fr_High_Veg, Fr_Tot_wat, CIRCLE_AM, nLSI, Altitude	(Lambda), Fr_Imp_Bld, Fr_Imp_gr, Fr_LowIRR, Fr_Med_Veg, Fr_High_Veg, Fr_Tot_wat, CIRCLE_AM, nLSI, Altitude	(Lambda), Fr_Imp_Bld, Fr_Imp_gr, Fr_LowIRR, Fr_Med_Veg, Fr_High_Veg, Fr_Tot_wat, CIRCLE_AM, nLSI, Altitude	W_DAY_Ts, Fr_Imp_Bld, Fr_Imp_gr, Fr_LowIRR, Fr_Med_Veg, Fr_High_Veg, Fr_Tot_wat, CIRCLE_AM, nLSI, Altitude	Fr_Imp_Bld, Fr_Imp_Grnd, Fr_Low_NIR, Fr_Low_IRR, Fr_Med_Veg, Fr_High_Veg, Fr_Tot_Wat, CIRCLE_AM, Mean_NDVI, CIRCLE_AM, nLSI, Altitude	Fr_Imp_Bld, Fr_Imp_Grnd, Fr_Low_IRR, Fr_Med_Veg, Fr_High_Veg, Fr_Tot_Wat, CIRCLE_AM, nLSI, Altitude	Fr_Imp_Bld, Fr_Imp_Grnd, Fr_Low_IRR, Fr_Med_Veg, Fr_High_Veg, Fr_Tot_Wat, CIRCLE_AM, nLSI, Altitude	(Lambda), Fr_Imp_Bld, Fr_Imp_gr, Fr_LowIRR, Fr_Med_Veg, Fr_High_Veg, Fr_Tot_wat, CIRCLE_AM, nLSI, Altitude	(Lambda), Fr_Imp_Bld, Fr_Imp_gr, Fr_LowIRR, Fr_Med_Veg, Fr_High_Veg, Fr_Tot_wat, CIRCLE_AM, nLSI, Altitude	W_NIG_Ts, Fr_Imp_Bld, Fr_Imp_gr, Fr_LowIRR, Fr_Med_Veg, Fr_High_Veg, Fr_Tot_wat, CIRCLE_AM, nLSI, Altitude
N cases	24948	24948	24948	155	21024	24948	23458	23458	23458	322	20012	23458
R	0.777	0.776	-	-	-	-	0.737	0.734	-	-	-	-
R ²	0.603	0.603	0.837	0.565	0.846	0.769	0.543	0.539	0.866	0.907	0.876	0.815
Adjusted R ²	0.603	0.602	-	-	-	-	0.543	0.539	-	-	-	-
S.E	1.196	1.197	0.767	0.529	0.695	0.913	0.626	0.629	0.339	0.472	0.310	0.399
F-statistic	3446.427	4200.067	-	-	-	-	2537.152	3048.077	-	-	-	-
df1	11	9	9	9	9	9	11	9	9	9	9	9
df2	24936	24938	24938	145	21014	24937	23446	23448	23448	312	20002	23447
Lag coeff. (Sig.)	-	-	0.829 (0.00)	0.383 (0.00)	0.810 (0.00)	0.6151	-	-	0.908 (0.00)	0.801 (0.00)	0.887 (0.00)	0.7839
Sig. F (p-value)	0.000	0.000	-	-	-	-	0.000	0.000	-	-	-	-
Log-Likelihood	-39856.2	-39878.6	-30496.31	-126.736	-23747.31	-33914.4	-22298.8	-22408.6	-10125.3	-262.824	-6946.26	-13137
AIC	79736.3	79777.3	61012.6	273.472	47514.6	67850.7	44621.7	44837.2	20270.6	545.649	13912.5	26296
SC	79833.8	79858.5	61093.9	303.906	47594.2	67940.1	44718.4	44917.8	20351.2	583.394	13991.6	26384.7
Durbin-Watson	1.015	1.018	-	-	-	-	1.074	1.062	-	-	-	-
Multicollinearity	199.910	18.521	-	-	-	-	185.675	18.887	-	-	-	-
Jarque-Bera (Sig.)	2452.7424 (0.000)	2571.2485 (0.000)	-	-	-	-	1964.0973 (0.000)	2019.8261 (0.000)	-	-	-	-
Breusch-Pagan (Sig.)	2438.8289 (0.000)	2445.5106 (0.000)	4467.24 (0.000)	63.8665 (0.000)	980.105 (0.000)	2869.4726 (0.000)	4684.8502 (0.000)	5013.832 (0.000)	5807.74 (0.000)	56.6246 (0.000)	568.682 (0.000)	5410.244 (0.000)
Koenker-Bassett (Sig.)	1461.0536 (0.000)	1454.5364 (0.000)	-	-	-	-	2774.7879 (0.000)	2934.3725 (0.000)	-	-	-	-
Likelihood ratio (Sig.)	-	-	18764.65 (0.000)	18.4510 (0.000)	16138.4 (0.000)	11928.56 (0.000)	-	-	24566.59 (0.000)	162.4745 (0.000)	19855.3 (0.000)	18543.159 (0.000)

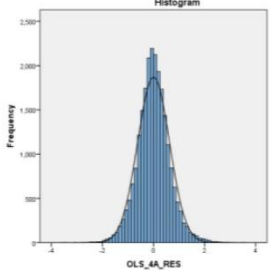
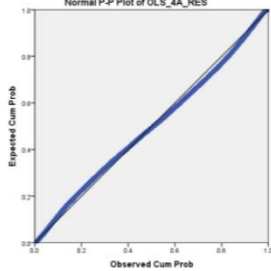
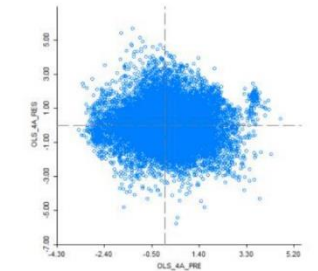
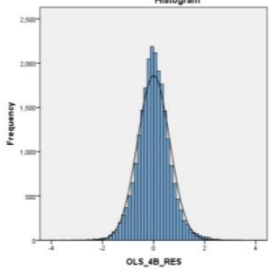
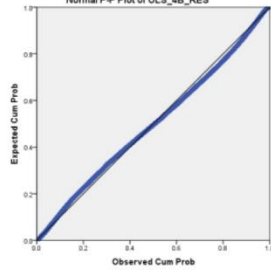
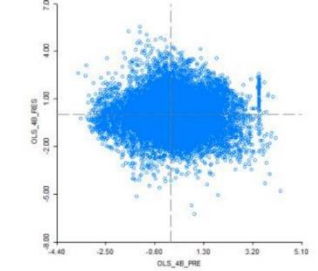
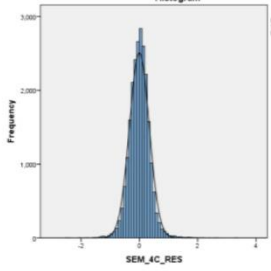
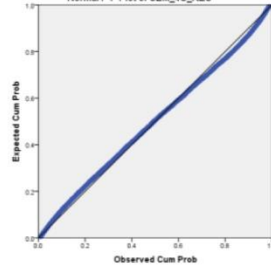
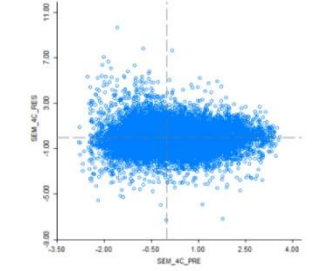
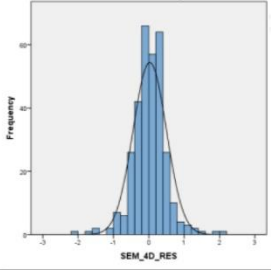
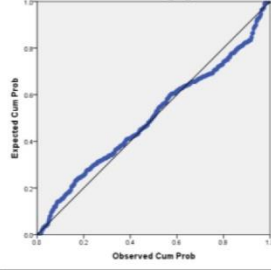
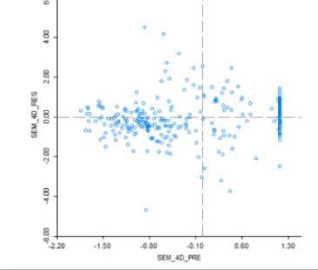
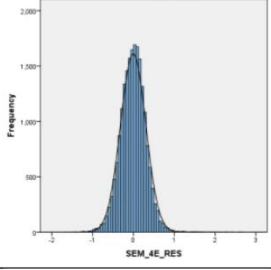
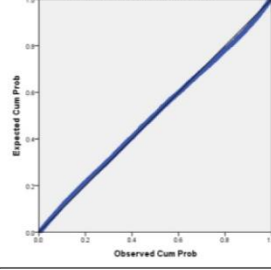
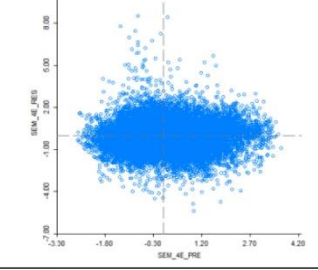
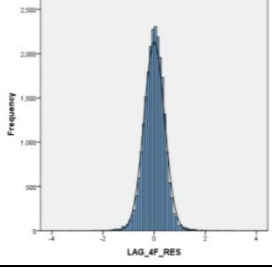
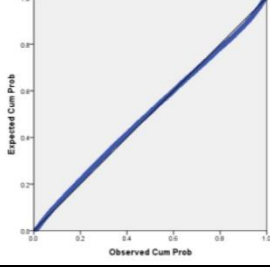
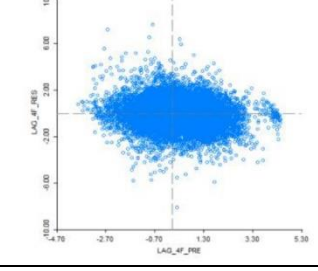
* Aquatic context; **Terrestrial context; S.E. = Spatial error; AIC = Akaike information criterion; SC = Schwarz criterion. Note: models with the best performance have been coloured.

H12 Histograms, normal P-P plots and scatterplots of residuals for all produced models (OLS, SEM, LAG).



Model		Histogram residuals	Normal P-P plot of standardised residual	Scatterplot residuals (standardised values)
OLS	2A			
	2B			
SEM	2C			
	2D*			
	2E**			
LAG	2F			

Model		Histogram residuals	Normal P-P plot of standardised residual	Scatterplot residuals (standardised values)
WINTER				
OLS	3A			
	3B			
SEM	3C			
	3D*			
	3E**			
LAG	3F			

Model		Histogram residuals	Normal P-P plot of standardised residual	Scatterplot residuals (standardised values)
OLS	4A			
	4B			
SEM	4C			
	4D*			
	4E**			
LAG	4F			

* Aquatic context; **Terrestrial context.